frontiers | Research Topics

Advances and insights in the diagnosis of viral infections and vaccines development in animals

Edited by
Jingqiang Ren, Hongliang Chai, Lihua Wang and Jianke Wang

Coordinated by
Hewei Zhang

Published in
Frontiers in Microbiology

ISSN 1664-8714
ISBN 978-2-8325-5160-8
DOI 10.3389/978-2-8325-5160-8

About Frontiers

Frontiers is more than just an open access publisher of scholarly articles: it is a pioneering approach to the world of academia, radically improving the way scholarly research is managed. The grand vision of Frontiers is a world where all people have an equal opportunity to seek, share and generate knowledge. Frontiers provides immediate and permanent online open access to all its publications, but this alone is not enough to realize our grand goals.

Frontiers journal series

The Frontiers journal series is a multi-tier and interdisciplinary set of open-access, online journals, promising a paradigm shift from the current review, selection and dissemination processes in academic publishing. All Frontiers journals are driven by researchers for researchers; therefore, they constitute a service to the scholarly community. At the same time, the *Frontiers journal series* operates on a revolutionary invention, the tiered publishing system, initially addressing specific communities of scholars, and gradually climbing up to broader public understanding, thus serving the interests of the lay society, too.

Dedication to quality

Each Frontiers article is a landmark of the highest quality, thanks to genuinely collaborative interactions between authors and review editors, who include some of the world's best academicians. Research must be certified by peers before entering a stream of knowledge that may eventually reach the public - and shape society; therefore, Frontiers only applies the most rigorous and unbiased reviews. Frontiers revolutionizes research publishing by freely delivering the most outstanding research, evaluated with no bias from both the academic and social point of view. By applying the most advanced information technologies, Frontiers is catapulting scholarly publishing into a new generation.

What are Frontiers Research Topics?

Frontiers Research Topics are very popular trademarks of the *Frontiers journals series*: they are collections of at least ten articles, all centered on a particular subject. With their unique mix of varied contributions from Original Research to Review Articles, Frontiers Research Topics unify the most influential researchers, the latest key findings and historical advances in a hot research area.

Find out more on how to host your own Frontiers Research Topic or contribute to one as an author by contacting the Frontiers editorial office: frontiersin.org/about/contact

Advances and insights in the diagnosis of viral infections and vaccines development in animals

Topic editors

Jingqiang Ren — Wenzhou University, China
Hongliang Chai — Northeast Forestry University, China
Lihua Wang — Kansas State University, United States
Jianke Wang — Hebei Agricultural University, China

Topic coordinator

Hewei Zhang — Animal Diseases and Public Health Engineering Research Center of Henan Province, China

Citation

Ren, J., Chai, H., Wang, L., Wang, J., Zhang, H., eds. (2024). *Advances and insights in the diagnosis of viral infections and vaccines development in animals*. Lausanne: Frontiers Media SA. doi: 10.3389/978-2-8325-5160-8

Table of contents

frontiers | Frontiers in Microbiology

TYPE Editorial
PUBLISHED 02 July 2024
DOI 10.3389/fmicb.2024.1443858

OPEN ACCESS

EDITED AND REVIEWED BY
Anna Kramvis,
University of the Witwatersrand, South Africa

*CORRESPONDENCE
Lihua Wang
✉ lihua@vet.k-state.edu
Jingqiang Ren
✉ rjq207@163.com
Jishu Shi
✉ jshi@vet.k-state.edu

RECEIVED 04 June 2024
ACCEPTED 19 June 2024
PUBLISHED 02 July 2024

CITATION
Wang L, Ren J, Wang J, Zhang H and Shi J (2024) Editorial: Advances and insights in the diagnosis of viral infections and vaccines development in animals.
Front. Microbiol. 15:1443858.
doi: 10.3389/fmicb.2024.1443858

Editorial: Advances and insights in the diagnosis of viral infections and vaccines development in animals

Lihua Wang[1]*, Jingqiang Ren[2]*, Jianke Wang[3], Hewei Zhang[4] and Jishu Shi[1]*

[1]Center on Biologics Development and Evaluation, Department of Anatomy and Physiology, College of Veterinary Medicine, Kansas State University, Manhattan, KS, United States, [2]Institute of Virology, Wenzhou University, Wenzhou, China, [3]Hebei Veterinary Biotechnology Innovation Center, College of Veterinary Medicine, Hebei Agricultural University, Baoding, China, [4]College of Food and Drugs, Luoyang Polytechnic, Luoyang, Henan, China

KEYWORDS

advances, insights, diagnosis, vaccine, viral infection, animal

Editorial on the Research Topic
Advances and insights in the diagnosis of viral infections and vaccines development in animals

Introduction

Animal health is vital to global wellbeing, economic development, food security, and food quality. However, animal viruses pose a significant threat, causing livestock and wildlife illnesses, economic hardship, and zoonotic diseases that can cross species barriers to endanger human health. Severe acute respiratory syndrome (SARS), avian influenza A (H5N1), and Coronavirus disease 2019 (COVID-19) serve as stark reminders of these risks (Yuen et al., 1998; Peiris et al., 2003; Zhu et al., 2020). To combat these viral foes, robust strategies are urgently needed. Accurate diagnoses of viral infections and the development of effective vaccines are critical components of such strategies. This Research Topic, "*Advances and insights in the diagnosis of viral infections and vaccines development in animals*," covered the development of novel diagnostic tools for various animal viruses and explored advancements in vaccine development utilizing diverse technologies. The Research Topic comprised 23 articles, with 11 focusing on the development, evaluation, and application of diagnostic methods. The remaining 12 articles emphasized vaccine development and evaluation.

Diagnosis of viral infections in animals

Traditionally, diagnosing viral infections in animals relied on clinical signs, pathology, antigen detection, and antibody detection. Clinical signs and pathological findings in viral infected animals are highly variable due to both viral and host factors, and often confused with other diseases of animals (Murcia et al., 2009; Wang et al., 2020). Well-established laboratory techniques like virus isolation, real-time polymerase chain reaction (RT-PCR),

and enzyme-linked immunosorbent assay (ELISA) have improved diagnostic accuracy (Wang et al., 2020, 2022; Mi et al., 2022; Azam et al., 2023). Recent advancements have taken this progress a step further by offering faster, more efficient methods. In this Research Topic, Yu et al. developed a colloidal gold immunochromatographic (GICG) strip with an enhanced signal according to the double-antibody sandwich principle and an enzyme-based signal amplification system to amplify the signal for detecting bovine parvovirus (BPV). The sensitivity of the signal-enhanced GICG strip showed 10 times higher than that of the traditional GICG strip. Liu, Sheng et al. developed a sensitive and specific TaqMan-based quantitative real-time PCR assay to detect the novel Mink Circovirus (MiCV). Li, Liu et al. generated a monoclonal antibody against duck circovirus capsid protein and investigated its potential application for native viral antigen detection. Li, Wang et al. developed propidium monoazide quantitative PCR assay for effective discrimination of infectious and inactivated African swine fever virus (ASFV). Its integration into routine diagnostics can significantly enhance the interpretation of positive ASFV results, leading to improved accuracy in identifying infected cases.

Multiplex PCR assays significantly boost diagnostic productivity by simultaneously detecting multiple pathogens from a single reaction. This approach offers several advantages: reduced costs, minimal sample requirement, and faster turnaround times (Shi et al., 2016; Dronina et al., 2021; Charlier et al., 2022). Ren, Zu et al. developed a multiplex real-time PCR assay using TaqMan probes to simultaneously detect Porcine epidemic diarrhea virus (PEDV), porcine rotavirus (PoRV), and porcine deltacoronavirus (PDCoV), the important diarrhea viruses in pig herds. This method is expected to significantly contribute to prevent and control the spread of infectious diseases, as well as aid in conducting epidemiological investigations. Yan et al. designed a dual nanoparticle-assisted polymerase chain reaction (Nano-PCR) assay for simultaneous detection of Feline calicivirus (FCV) and Feline herpesvirus type I (FHV-I). The assay showed strong specificity and high sensitivity for testing the clinical samples of feline upper respiratory tract infections.

Next-generation sequencing (NGS) has revolutionized viral diagnosis. It allows identification of previously unknown or uncultivable viruses, a significant advancement over traditional methods (Quer et al., 2022). In this Research Topic, Goraichuk et al. developed a superior method with DNase to deplete host ribosomal RNA (rRNA) before library preparation. This method significantly improves the sensitivity and accuracy of virus detection in clinical samples using NGS. Their 28S rRNA RT-qPCR assay provided a valuable foundation for the development of these host depletion strategies. Additionally, machine learning, powered by modern computing, has emerged as a powerful tool for data analysis and disease diagnosis. Liu, Zhou et al. combined machine learning with causal relationship analysis to identify shared mechanisms between COVID-19 and acute myocardial infarction (AMI). They utilized 20 mainstream machine learning algorithms to establish a powerful diagnostic predictor. This tool can estimate a specific COVID-19 patient's risk of developing AMI. These findings offer novel mechanistic insights into COVID-19 and AMI, paving the way for future advancements in preventive, personalized, and precision medicine.

Several studies of this Research Topic highlight the application of diagnostics in animal health. Sánchez-Morales et al. used a surrogate ELISA kit to analyze blood serum from randomly selected animals in a retrospective study of SARS-CoV-2. Their findings suggest a higher susceptibility to infection in cats compared to dogs. Additionally, the study revealed a significantly increased infection risk for domestic animals living in close contact with infected owners, compared to those in animal shelters with limited human interaction. Uddin et al. employed insulated isothermal PCR (iiPCR) alongside traditional PCR and virus isolation to detect Lumpy skin disease virus (LSDV) in tissue samples from affected cattle. This approach provided insights into the potential source of the circulating LSDV strain and identified the inactivated LSDV antigen as a promising vaccine candidate. Magouz et al. investigated the prevalence of canine parvovirus-2 (CPV-2) variants among dogs in Egypt. Their study utilized PCR and restriction fragment length polymorphism (RFLP) followed by VP2 sequencing on samples from clinically infected dogs. The results confirmed the widespread presence of CPV-2 in the Egyptian canine population, emphasizing the need for continuous monitoring. The data can facilitate early and accurate diagnosis of the disease, ultimately aiding in the development of new vaccination strategies for Egypt.

Vaccine development in animals

Given the absence of broad-spectrum antiviral pharmaceuticals, vaccination remains a critical tool for preventing and controlling viral infections in animals (McVey and Shi, 2010; Choudhury et al., 2021). Animal vaccines not only combat diseases in companion animals but also ensure the safety of food supplies by maintaining healthy livestock populations. Depending on the types of technologies used for antigen production and vaccine formulation, there are four types of vaccines for animal use: (i) Type I (whole virus): inactivated, killed, (ii) Type II (whole virus): modified live attenuated, reverse genetics modified, (iii) Type III (fraction/component): subunit, virus like particles, genetic DNA or RNA, killed recommitment vectors, (iv) Type IV (fraction/component): recombinant viral vectors expressing antigens (Brun, 2016). Numerous conventional Type I and Type II vaccines have been produced for companion and livestock (Coetzee et al., 2020; Lu et al., 2022; Yuan et al., 2022; Natesan et al., 2023). This Research Topic highlights advancements in Type I and Type II vaccine development. Shin et al. demonstrated that foot-and-mouth disease (FMD) inactivated vaccine with a glycyrrhizic acid adjuvant elicits potent innate and adaptive immune responses against FMD in mice and pigs. Cao et al. employed a yeast-based transformation-associated recombination (TAR) system to genetically engineer feline infectious peritonitis virus for vaccine development. Xu et al. successfully generated promising live attenuated pseudorabies virus (PRV) vaccine candidates using a codon deoptimization approach. One candidate exhibited good safety and a high level of virus neutralization in piglets, making it a potential solution against PRV variants.

An increasing number of rationally designed Type III and Type IV vaccines are developed and reaching the market (Madera et al., 2018; Shi et al., 2021; Tabynov et al., 2022). This Research

Topic showcases seven articles exploring advancements in these vaccine types. Zhang Y. et al. investigated *Bacillus subtilis* (*B. subtilis*, a gram-positive bacterium that is safe and non-toxic to humans and animals) as a vector for developing oral rabies vaccine. They constructed recombinant *B. subtilis* expressing rabies virus G proteins. Their results suggested that recombinant *B. subtilis* strains have excellent immunogenicity and are expected to be novel oral vaccine candidates for the prevention and control of wild animal rabies. Ren, Madera et al. proposed a streamlined method for isolating high-quality viral DNA from large DNA viruses and generating recombinant PRV vaccines, simplifying vaccine development. Zhang H. et al. developed a yeast-based vaccine expressing influenza hemagglutinin (HA) proteins from H5N8, H7N9, and H9N2 strains. This oral vaccine in chickens showed promise in boosting multi-systemic immune responses against H9N2 influenza. Their finding suggest that oral yeast based multivalent bird flu vaccines provide an attractive strategy to update host defense function via reshapes of multi-systemic immune homeostasis. Zhao et al. identified the PRV gD protein as a potential vaccine candidate. Their findings suggest it could be effective in protecting animals from PRV infection. Hou et al. designed a multi-epitope vaccine targeting both porcine epidemic diarrhea virus (PEDV) and porcine deltacoronavirus (PDCoV). Zhou et al. identified a B-cell epitope in Senecavirus A (SVA) that could be used to develop a marker vaccine for the disease. Fan et al. identified L11L and L7L genes in the ASFV genome as virulence factors. Deleting these genes attenuated the virus, suggesting potential targets for future vaccines.

This Research Topic also emphasizes the importance of evaluating vaccine effectiveness against circulating viruses. Mosad et al. investigated genetic diversity between Avian Orthoreovirus (ARV) strains circulating in Egypt and the current vaccine strain. They found significant genetic and protein variation, suggesting the need for a new vaccine formulated from locally isolated ARV strains. Similarly, Yang et al. studied cross-protection among different feline calicivirus genotypes. Using cross-neutralization assays and *in vivo* challenges, they identified the DL39 strain as a promising candidate with broad-spectrum protection against various FCV genotypes.

Conclusion and future perspectives

This Research Topic delves into the latest advancements in diagnosing and preventing viral infections in animals. It showcases a range of diagnostic tools, from established techniques like ELISA and PCR to cutting-edge methods like Nano-PCR, NGS, and machine learning. Vaccine development also takes center stage, with the exploration of both traditional inactivated vaccines and advanced subunit and recombinant vectored approaches. These advancements empower veterinarians and public health officials to safeguard animal and human health.

Looking ahead, the fight against animal viruses is an ongoing battle. Continuous improvement of diagnostic tools remains crucial. The future holds promise for on-site testing delivering rapid results, potentially transforming animal healthcare with faster and more targeted interventions. Similarly, research into universal vaccines with broad-spectrum protection offers immense potential, especially in the face of emerging viruses and antigenic variation. Enhancing international collaboration and information sharing can significantly accelerate vaccine development. Furthermore, improved pathogen detection in wildlife is a pressing need. We require robust tools for diagnosing emerging and re-emerging diseases that threaten endangered species or pose zoonotic risks. This includes developing innovative, non-invasive sampling methods, leveraging new technologies for comprehensive pathogen characterization, and refining data analysis and surveillance strategies (Jia et al., 2020). By staying at the forefront of scientific advancements and fostering continuous innovation, we can significantly improve the health of both animals and humans.

Author contributions

LW: Writing – original draft, Writing – review & editing. JR: Writing – review & editing. JW: Writing – review & editing. HZ: Writing – review & editing. JS: Writing – review & editing.

Funding

The author(s) declare financial support was received for the research, authorship, and/or publication of this article. This study was supported by USDA NIFA Award #2022-67015-36516, National Bio and Agro-Defense Facility Transition Fund, USDA NIFA Hatch-Multistate Project (grant number: 1021491), USDA ARS Non-Assistance Cooperative Agreements (grant numbers: 58-8064-8-011, 58-8064-9-007, 58-3020-9-020, and 59-0208-9-222), USDA NIFA Sub Award #25-6226-0633-002, and Wenzhou Basic Scientific Research Project (Y2023020).

Conflict of interest

The authors declare that the research was conducted in the absence of any commercial or financial relationships that could be construed as a potential conflict of interest.

Publisher's note

References

Azam, M. N., Khurshid, T., Gill, R. J., Ahmad, M., Haider, M. J., Rehman, A., et al. (2023). Diagnostic methods and advancements in the detection of viral infections in animals. *Biol. Clin. Sci. Res. J.*, 2023:537. doi: 10.54112/bcsrj.v2023i1.537

Brun, A. (2016). Vaccines and vaccination for veterinary viral diseases: a general overview. *Methods Mol. Biol.* 1349, 1–24. doi: 10.1007/978-1-4939-3008-1_1

Charlier, J., Barkema, H. W., Becher, P., De Benedictis, P., Hansson, I., Hennig-Pauka, I., et al. (2022). Disease control tools to secure animal and public health in a densely populated world. *Lancet Planet Health* 6, e812–e824. doi: 10.1016/S2542-5196(22)00147-4

Choudhury, S. M., Ma, X., Dang, W., Li, Y., and Zheng, H. (2021). Recent development of ruminant vaccine against viral diseases. *Front. Vet. Sci.* 8:697194. doi: 10.3389/fvets.2021.697194

Coetzee, P., Guthrie, A. J., Ebersohn, K., Maclachlan, J. N., Ismail, A., van Schalkwyk, A., et al. (2020). Complete genome sequences of virus strains isolated from bottle A of the South African live attenuated Bluetongue virus vaccine. *Microbiol. Resour. Announc.* 9, e00310–e00320. doi: 10.1128/MRA.00310-20

Dronina, J., Samukaite-Bubniene, U., and Ramanavicius, A. (2021). Advances and insights in the diagnosis of viral infections. *J. Nanobiotechnol.* 19:348. doi: 10.1186/s12951-021-01081-2

Jia, B., Colling, A., Stallknecht, D. E., Blehert, D., Bingham, J., Crossley, B., et al. (2020). Validation of laboratory tests for infectious diseases in wild mammals: review and recommendations. *J. Vet. Diagn. Invest.* 32, 776–792. doi: 10.1177/1040638720920346

Lu, Z., Yu, S., Wang, W., Chen, W., Wang, X., Wu, K., et al. (2022). Development of foot-and-mouth disease vaccines in recent years. *Vaccines* 10:1817. doi: 10.3390/vaccines10111817

Madera, R. F., Wang, L., Gong, W., Burakova, Y., Buist, S., Nietfeld, J., et al. (2018). Toward the development of a one-dose classical swine fever subunit vaccine: antigen titration, immunity onset, and duration of immunity. *J. Vet. Sci.* 19, 393–405. doi: 10.4142/jvs.2018.19.3.393

McVey, S., and Shi, J. (2010). Vaccines in veterinary medicine: a brief review of history and technology. *Vet. Clin. North. Am. Small Anim. Pract.* 40, 381–392. doi: 10.1016/j.cvsm.2010.02.001

Mi, S., Wang, L., Li, H., Bao, F., Madera, R., Shi, X., et al. (2022). Characterization of monoclonal antibodies that specifically differentiate field isolates from vaccine strains of classical swine fever virus. *Front. Immunol.* 13:930631. doi: 10.3389/fimmu.2022.930631

Murcia, P., Donachie, W., and Palmarini, M. (2009). Viral pathogens of domestic animals and their impact on biology, medicine and agriculture. *Encycl. Microbiol.* 5, 805–819. doi: 10.1016/B978-012373944-5.00368-0

Natesan, K., Isloor, S., Vinayagamurthy, B., Ramakrishnaiah, S., Doddamane, R., and Fooks, A. R. (2023). Developments in rabies vaccines: the path traversed from pasteur to the modern era of immunization. *Vaccines* 11:756. doi: 10.3390/vaccines11040756

Peiris, J. S., Yuen, K. Y., Osterhaus, A. D., and Stöhr, K. (2003). The severe acute respiratory syndrome. *N. Engl. J. Med.* 349, 2431–2441. doi: 10.1056/NEJMra032498

Quer, J., Colomer-Castell, S., Campos, C., Andrés, C., Piñana, M., Cortese, M. F., et al. (2022). Next-generation sequencing for confronting virus pandemics. *Viruses* 14:600. doi: 10.3390/v14030600

Shi, J., Wang, L., and McVey, D. S. (2021). Of pigs and men: the best-laid plans for prevention and control of swine fevers. *Anim. Front.* 11, 6–13. doi: 10.1093/af/vfaa052

Shi, X., Liu, X., Wang, Q., Das, A., Ma, G., Xu, L., et al. (2016). A multiplex real-time PCR panel assay for simultaneous detection and differentiation of 12 common swine viruses. *J. Virol. Methods.* 236, 258–265. doi: 10.1016/j.jviromet.2016.08.005

Tabynov, K., Orynbassar, M., Yelchibayeva, L., Turebekov, N., Yerubayev, T., Matikhan, N., et al. (2022). A spike protein-based subunit SARS-CoV-2 vaccine for pets: safety, immunogenicity, and protective efficacy in juvenile cats. *Front. Vet. Sci.* 9:815978. doi: 10.3389/fvets.2022.815978

Wang, L., Madera, R., Li, Y., McVey, D. S., Drolet, B. S., and Shi, J. (2020). Recent advances in the diagnosis of classical swine fever and future perspectives. *Pathogens* 9:658. doi: 10.3390/pathogens9080658

Wang, L., Mi, S., Madera, R., Li, Y., Gong, W., Tu, C., et al. (2022). A novel competitive ELISA for specifically measuring and differentiating immune responses to classical swine fever C-strain vaccine in pigs. *Viruses* 14:1544. doi: 10.3390/v14071544

Yuan, M., Yang, X., Zhang, X., Zhao, X., Abid, M., Qiu, H. J., et al. (2022). Different types of vaccines against pestiviral infections: "barriers" for "pestis". *Viruses* 15:2. doi: 10.3390/v15010002

Yuen, K. Y., Chan, P. K., Peiris, M., Tsang, D. N., Que, T. L., Shortridge, K. F., et al. (1998). Clinical features and rapid viral diagnosis of human disease associated with avian influenza A H5N1 virus. *Lancet* 351, 467–471. doi: 10.1016/S0140-6736(98)01182-9

Zhu, N., Zhang, D., Wang, W., Li, X., Yang, B., Song, J., et al. (2020). A novel coronavirus from patients with pneumonia in China, 2019. *N. Engl. J. Med.* 382, 727–733. doi: 10.1056/NEJMoa2001017

frontiers | Frontiers in Microbiology

TYPE Original Research
PUBLISHED 09 February 2023
DOI 10.3389/fmicb.2023.1126533

OPEN ACCESS

EDITED BY
Lihua Wang,
Kansas State University,
United States

REVIEWED BY
Jun Luo,
South China Agricultural University,
China
Tao Wang,
Lanzhou University,
China

*CORRESPONDENCE
Xianzhu Xia
✉ xiaxzh@cae.cn
Feihu Yan
✉ yanfh1990@163.com
Yongkun Zhao
✉ zhaoyongkun1976@126.com

SPECIALTY SECTION
This article was submitted to Virology, a section of the journal Frontiers in Microbiology

RECEIVED 18 December 2022
ACCEPTED 09 January 2023
PUBLISHED 09 February 2023

CITATION
Zhang Y, Mo R, Sun S, Cui Z, Liang B, Li E, Wang T, Feng Y, Yang S, Yan F, Zhao Y and Xia X (2023) *Bacillus subtilis* vector based oral rabies vaccines induced potent immune response and protective efficacy in mice. *Front. Microbiol.* 14:1126533. doi: 10.3389/fmicb.2023.1126533

Bacillus subtilis vector based oral rabies vaccines induced potent immune response and protective efficacy in mice

Ying Zhang[1,2], Ruo Mo[2,3], Sheng Sun[2], Zhanding Cui[4], Bo Liang[2], Entao Li[5], Tiecheng Wang[2], Ye Feng[2], Songtao Yang[2], Feihu Yan[2]*, Yongkun Zhao[2]* and Xianzhu Xia[1,2]*

[1]Northeast Forestry University College of Wildlife and Protected Area, Harbin, China, [2]Changchun Veterinary Research Institute, Chinese Academy of Agricultural Sciences, Changchun, Jilin, China, [3]College of Veterinary Medicine, Jilin Agricultural University, Changchun, Jilin, China, [4]State Key Laboratory of Veterinary Etiological Biology, Lanzhou Veterinary Research Institute, Chinese Academy of Agricultural Sciences, Lanzhou, Gansu, China, [5]Division of Life Sciences and Medicine, University of Science and Technology of China, Hefei, Anhui, China

Introduction: Rabies is a worldwide epidemic that poses a serious threat to global public health. At present, rabies in domestic dogs, cats, and some pets can be effectively prevented and controlled by intramuscular injection of rabies vaccine. But for some inaccessible animals, especially stray dogs, and wild animals, it is difficult to prevent with intramuscular injection. Therefore, it is necessary to develop a safe and effective oral rabies vaccine.

Methods: We constructed recombinant *Bacillus subtilis* (*B. subtilis*) expressing two different strains of rabies virus G protein, named CotG-E-G and CotG-C-G, immunogenicity was studied in mice.

Results: The results showed that CotG-E-G and CotG-C-G could significantly increase the specific SIgA titers in feces, serum IgG titers, and neutralizing antibodies. ELISpot experiments showed that CotG-E-G and CotG-C-G could also induce Th1 and Th2 to mediate the secretion of immune-related IFN-γ and IL-4. Collectively, our results suggested that recombinant *B. subtilis* CotG-E-G and CotG-C-G have excellent immunogenicity and are expected to be novel oral vaccine candidates for the prevention and control of wild animal rabies.

KEYWORDS

rabies, oral immunization, *Bacillus subtilis*, oral rabies vaccine, G protein

Introduction

Rabies is a natural zoonotic infectious disease, which is prevalent worldwide and poses a serious threat to global public health (Taylor and Nel, 2015). The disease is prevalent all over the world and poses a serious threat to global public health. Once clinical symptoms appear after infection, the mortality rate is almost 100% (Henle et al., 1962; Fenje, 1968). About 60,000 people die of the disease every year (Yousaf et al., 2012; Kip et al., 2018), and 95% of the cases are from developing countries such as Africa and Asia (Luo et al., 2017). Dogs, especially stray dogs, are the main source of rabies transmission in developing countries (Hampson et al., 2015; Zhao et al., 2021). In developed countries, bats and other wild animals are the main culprits in the spread of rabies. In recent years, the study of rabies in wild animals has been reported all over the world. Wild animals are the main reservoir of the Rabies virus (RABV) in nature. Human and domestic rabies deaths are frequently caused by wild animal bites (Shao et al., 2015; Ming-Yang et al., 2018; Benavides et al., 2020; Feng et al., 2022). It brings serious mental pressure and economic loss to

people. Therefore, enhanced rabies vaccination of stray dogs and wild animals is essential for global rabies control, and the most practical way to vaccinate these animals against rabies is the oral vaccine. Currently, the widely used Oral rabies vaccine (ORV) is mainly divided into the live attenuated vaccine and recombinant live rabies virus vector vaccine. Most notable are the poxvirus-vectored rabies glycoprotein recombinant virus vaccines, such as recombinant vaccinia virus and canary poxvirus expressing the rabies virus glycoprotein gene. Both vaccines are widely used for oral rabies vaccination in wild animals in North America, Canada, and Western Europe (Poulet et al., 2007; Weyer et al., 2009). At present, with the in-depth study of epidemiology, rabies in pet dogs, cats, and some domestic animals has been effectively prevented and controlled by an intramuscular rabies vaccine, but it is not suitable to prevent rabies in wild animals. Therefore, enhanced rabies vaccination of stray dogs and wild animals is essential for global rabies control, and the most practical way to vaccinate these animals against rabies is the oral vaccine. So, the development of a simple, safe and effective oral rabies vaccine for wild animals is of great significance for the prevention and control of animal rabies.

RABV, a typical neurotropic virus, is a prototypical virus in the genus *Lyssavirus* genus, family Rhabdoviridae (Wunner, 2013; Liu et al., 2017). The RABV genome is about 12 kb in length and consists of five genes encoding nucleocapsid protein (N), phosphoprotein (P), matrix protein (M), glycoprotein (G), and viral RNA polymerase (L) (Conzelmann et al., 1990). Among them, G protein is the only surface-exposed viral protein on RABV virions, and it is the only virus protein that stimulates virus neutralizing antibodies (Wiktor et al., 1973). The G protein is an important determinant for the induction of innate immune responses and of cellular and humoral immune responses required to confer complete protection in animals (Cox et al., 1977; Benjamin et al., 2015) therefore, it is a promising candidate antigen for the development of genetically engineered vaccines.

Bacillus subtilis is a Gram-positive bacterium that is safe and non-toxic to humans and animals. It has been certified as a Generally Regarded as Safe (GRAS) product and is a new type of probiotic currently widely used (Hong et al., 2005; Schumann, 2007; Elshaghabee et al., 2017). Spores have unique stress resistance and can survive high temperature, dry and acid–base invasion conditions. *B. subtilis* and its spores are widely used as antigenic protein delivery vehicles and mucosal immune enhancers and can cause a protective immune response. At present, the exogenous protein system displayed on the surface of *B. subtilis* spores is more mature and perfect, and the recombinant expression of exogenous proteins will not affect the structure of *B. subtilis* spores and the performance of survival in harsh environments. Antigens displayed on the surface of spores can also be used for immunization and can germinate in host phagocytes, resulting in an efficient antigen presentation process. Currently, in the research of vaccine against tetanus toxin and *Bacillus anthracis* protective antigens (Duc et al., 2007; Sangun et al., 2010), the spore-presenting candidate vaccine with *B. subtilis* spore as antigen display carrier has shown good immunogenicity and immune protection. In recent years, a variety of spore surface proteins, such as CotB, CotC, and CotG (Mauriello et al., 2004; Imamura et al., 2011; Mou et al., 2016), have been widely used in the system of displaying foreign proteins on the spore surface.

In this study, the results showed that both recombinant *B. subtilis* were successfully expressed. Both strains of recombinant *B. subtilis* can induce mice to produce higher levels of specific antibodies after oral immunization and improve the production and protective effect of VNA, suggesting that recombinant *B. subtilis* is a novel oral rabies vaccine candidate.

Materials and methods

Ethics statement

All BALB/c mice were purchased from Beijing Weitong Lihua Experimental Animal Technology Co., Ltd., and the animal experiments were approved by the Animal Welfare and Ethics Committee of Changchun Veterinary Research Institute under the license number JSY-DW-2018-02. All BALB/c mice were treated according to the Guidelines for the Welfare and Ethics of Laboratory Animals of China (GB 14925–2001). Experiments related to virulent strains of RABV were all carried out in the biosafety level III laboratory.

Bacterial strains, cells, viruses, and antibodies

Bacillus subtilis 168 strain (BS168) was purchased from Wuhan Pujian Biotechnology Co., Ltd. PDG1661 plasmid was purchased from BioVector Plasmid Vector Strain Cell Gene Collection Center. HuNPB3 street strain, BHK cells, and NA cells were stored in our laboratory. Reference serum from the rabies reference Laboratory of the World Organization for Animal Health. A fluorescein isothiocyanate (FITC)-conjugated monoclonal antibody (mAb) against RABV N protein was purchased from Fujirebio, an anti-RABV G protein mAb was purchased from Millipore, Horseradish peroxidase (HRP)-conjugated goat anti-mouse IgG was purchased from Abcam. HRP-conjugated goat anti-mouse IgG1, IgG2a, and IgA were purchased from Southern Biotech Company. IFN-γ and IL-4 ELISpot plates were purchased from MABTECH Company. Chemiluminescent Imaging System were purchased from Tanon Company.

Construction of recombinant *Bacillus subtilis*

Using the codon-optimized pUC57-CotG-E-G and pUC57-CotG-C-G (E-G, GenBank: J02293; C-G, GenBank: GQ918139) as templates, design primers CotG-E-G-F and CotG-E-G-R and CotG-C-G-F and CotG-C-G-R, respectively (shown in Table 1), and the CotG-E-G and CotG-C-G gene fragments were obtained after PCR amplification. The recombinant plasmids PDG1661-CotG-E-G and PDG1661-CotG-C-G were obtained by, respectively, connecting to *Bam*HI and *Eco*RI sites of the PDG1661 vector. Finally, the recombinant plasmids PDG1661-CotG-E-G and PDG1661-CotG-C-G were linearized, respectively, and transformed into BS168 through electroporation to obtain positive recombinant strains, which were named *B. subtilis* CotG-E-G and *B. subtilis* CotG-C-G.

Western blot

To detect the expression level of G protein, the recombinant *B. subtilis* CotG-E-G, CotG-C-G, and BS168 were cultured to the end logarithmic stage of bacterial growth. The bacterial solution was collected and washed three times with sterile PBS. Proteins were

TABLE 1 Primers used in this study.

Primers	Sequence (5′-3′)	Restriction enzyme site
CotG-E-G-F	CGGGATCCATGGGTCACTACTCTCACTCTGACA	*BamH I*
CotG-E-G-R	CGGAATTCTCATTTACCCCAGTTAGGTAAAC	*EcoR I*
CotG-C-G-F	CGGGATCCATGGGTCACTACTCTCACTCTGACA	*BamH I*
CotG-C-G-R	CGGAATTCTCATTTACGCAGTTAGGTCAA	*EcoR I*

Underlined nucleotides are restriction sites.

extracted from culture lysates by sonication. They were separated by 10% sodium dodecyl sulfate-polyacrylamide gel electrophoresis and then transferred to a nitrocellulose membrane. Anti-RABV G protein mAb (1:1,500) was used as the primary antibody and incubated at room temperature for 2 h. After that, HRP-conjugated goat anti-mouse IgG (1:15,000) was a secondary antibody. Electrochemiluminescence (ECL) Western Blotting Substrate was added, and the bands were captured using a Chemiluminescent Imaging System.

Immunization and challenge

6-week-old female BALB/c mice were randomly divided into 4 groups, CotG-E-G and CotG-C-G experimental groups, BS168 negative control group, and PBS control group. Mice were orally administered 1×10^{10} spore/mouse with a stainless-steel round-tip gavage cannula at days 1–3, 14–16 and 28–30. The mice were monitored daily for clinical changes, including weight, hair, body temperature, eating habits and diarrhea.

Four weeks after the last immunization, mice were challenged intramuscularly with the RABV street strain HuNPB3 (100 × IMLD50). Observe and record changes in morbidity and body weight for 21 days. When the typical rabies symptoms appeared after the challenge, the mice were anesthetized with isoflurane and then humanely killed by cervical dislocation.

Antibody detection

The mouse serum was collected at 0, 14, 28, 35 and 42 days after immunization, and the specific IgG antibody content in the serum was detected by enzyme-linked immunosorbent assay (ELISA). Antibody subtypes were detected 1 week after the last immunization. Briefly, inactivated and purified HuNPB3 was used as the coating antigen at a concentration of 1 μg/ml, loaded at 100 μl/well into 96-well microtiter plates and incubated overnight at 4°C. Incubate with 5% skim milk blocks for 2 h at 37°C. Serum to be tested was diluted 2-fold, 100 μl/well, and incubated at 37°C for 1.5 h. Then, HRP-conjugated goat anti-mouse IgG, IgG1, and IgG2a antibodies were added, at 100 μl/well, and incubated at 37°C for 1 h. Then add TMB substrate buffer to the culture dish, incubate in the dark for 10 min, stop color development with 2 M H_2SO_4, and read on OD450 microplate reader.

Fluorescent antibody virus neutralization (FAVN) (Cliquet et al., 1998) was used to detect the specific virus-neutralizing antibody (VNA) level in serum 1 week after the last immunization. Briefly, add the serum to be tested (4 replicates for each sample) in row 1, 50 μl/well, serially 3-fold serial dilutions to row 6 in a 96-well plate, and set up standard serum 0.5 IU/ml at the same time control. Then, 100 FFU of RABV CVS-11 virus was added to each well. Incubate in a 37°C 5% CO_2 incubator for 1 h, add 2×10^4 BHK cells to each well, and incubate at 37°C for 48 h, and then incubate with ice-cold 80% acetone and chamber for 30 min. and stained with FITC-labeled anti-RABV N protein antibody. The results were observed by a fluorescence microscope and calculated in IU/mL by comparison to reference serum.

Detection of specific SIgA antibodies in feces

The level of SIgA antibody in feces was detected by the indirect ELISA. Inactivated and purified HuNPB3 was used as the coating antigen. The mouse feces collected every week were resuspended in pre-cooled PBS, and the supernatant was collected by centrifugation at 4°C and added to each well of the ELISA plate. Incubate at 37°C for 1.5 h, dilute HRP-conjugated goat anti-mouse IgA with 5% skim milk, 100 μl/well, and incubate at 37°C for 1 h. TMB substrate buffer was added to the plates for 10 min in the dark, and 2 M H_2SO_4 was added to stop the reaction, then read on a microplate reader at OD450.

Splenocyte proliferation assay

One week after the last immunization, three mice in each group were euthanized, and their spleens were taken and crushed. The spleen cell suspension was filtered through a 70 μm filter, and the separated red blood cells were lysed with red blood cell lysis buffer. The splenocyte density was adjusted to 2.5×10^6 cells/ml, and purified inactivated HNPB3 antigen (10 μg/ml) was seeded in a 96-well plate for 44 h, and then removed, CCK-8 was added at 10 μl/well and incubated for 4 h, place the 96-well cell plate in a microplate reader to read the OD450 nm value. The proliferation index (PI) was calculated as (OD stimulated culture–OD unstimulated culture)/(OD unstimulated culture–OD control culture).

IFN-γ and IL-4 cytokine detection

Splenocytes were diluted to 2.5×10^6 cells/ml, co-seeded with inactivated purified HNPB3 antigen (10 μg/ml) into 96-well plates, and incubated at 37°C, 5% CO_2 for 24 h. IFN-γ and IL-4 secretion levels in splenocytes were detected using mouse enzyme-linked immunospot (ELISpot) kit. Finally, the spot-forming cells (SFCs) in each well were counted with an automated ELISpot reader.

Statistical analysis

Statistical analysis was performed using GraphPad Prism 9.0 software, and results are expressed as mean ± SD. To determine the

percent survival, Kaplan–Meier survival curves were analyzed using the log-rank test. Significance differences between groups were analyzed by one-way ANOVA or two-way ANOVA and were deemed significant at p values of 0.05 or less. Statistical significance is indicated as $^{*}p < 0.05$, $^{**}p < 0.01$, $^{***}p < 0.001$, and $^{****}p < 0.0001$.

Results

Construction of recombinant *Bacillus subtilis*

The construction strategies of recombinant *B. subtilis* CotG-E-G and CotG-C-G are shown in Figure 1A. The fusion genes CotG-E-G and CotG-C-G were, respectively, inserted into the vector PDG1661 with the promoter Pspae to obtain PDG1661-CotG-E-G and PDG1661-CotG-E-G, respectively. Then, the empty vectors PDG1661, PDG1661-CotG-E-G, and PDG1661-CotG-E-G were introduced into BS168 by electric shock transformation to obtain recombinant *B subtilis*. CotG-E-G and *B subtilis*. CotG-C-G. The lysates of *B. subtilis*. CotG-E-G and *B. subtilis*. CotG-C-G was identified by Western blotting. Two specific bands were detected with anti-RABV G protein mAb, whereas no bands were detected in the null strain (Figure 1B). The results showed that both recombinant *B. subtilis* were successfully expressed.

Serum antibody detection

To evaluate the immunogenicity of the recombinant *B. subtilis* CotG-E-G and CotG-C-G, mice were orally immunized, and serum samples were collected after each immunization, the immunization program is shown in Figure 2A. No adverse effect, such as fatality, gloomy spirit, weight loss (Figure 2B) or diarrhea, was observed in mice during the whole immunization period. Serum-specific antibody levels were determined by indirect ELISA. The results showed that both CotG-E-G and CotG-C-G in the experimental group could detect obvious IgG antibody levels. On the 14th day after immunization, the antibody level of the experimental group was significantly increased, and the difference was extremely significant compared with the control group, on the 35th day after immunization, the serum IgG antibody levels of CotG-E-G and CotG-C-G in the experimental group reached the highest level (Figure 2C). These results indicated that recombinant *B. subtilis* CotG-E-G and CotG-C-G could effectively induce a systemic humoral immune response in mice.

The production of different antibody subtypes can reflect the type of immune response to a certain extent. To further understand the antibody responses induced by CotG-E-G and CotG-C-G, 1 week after the last immunization, IgG antibody subtypes were detected in the serum of mice 1 week after the last immunization. The results showed that the value of IgG2a/IgG1 was less than 1 (Figure 2D), indicating that after oral immunization, mice developed a Th2 immune response (biased to IgG1), which could increase the level of vaccine-induced humoral immune responses to a certain extent.

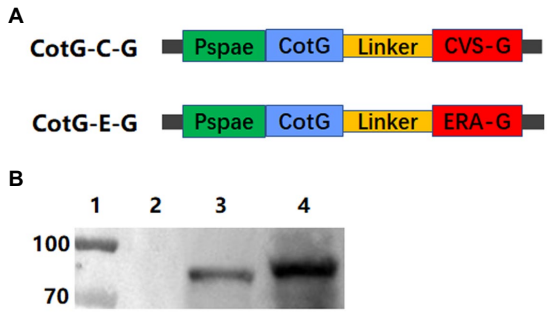

FIGURE 1
Construction and identification of recombinant *B. subtilis* expressing the immunogenic protein of RABV. **(A)** Schematic diagram of the construction of plasmids PDG1661-CotG-E-G and PDG1661-CotG-C-G expressing CotG-E-G fusion gene and CotG-C-G fusion gene, respectively. The Pspae represents promoter and the CotG represents spore capsid protein. **(B)** The expression of the G fusion protein in recombinant *B. subtilis* was detected by Western blotting. lane1: Maker; lane 2: *B. subtilis* BS168; lane 3: *B. subtilis* CotG-C-G; lane 4: *B. subtilis* CotG-E-G.

Neutralizing antibody detection

To further determine whether recombinant *B. subtilis* CotG-E-G and CotG-C-G could induce the production of VNA, serum samples were obtained after the last immunization. No specific VNA was detected in the serum of mice in the control group, while the VNA titers of CotG-E-G and CotG-C-G in the experimental group were higher than 0.5 IU/ml, as shown in Figure 2E, according to the WHO that the RABV neutralizing antibody titer greater than 0.5 IU/ml has a protective effect on the body. The results showed that both recombinant *B. subtilis* have good immunogenicity.

Detection of specific SIgA levels in feces

The specific SIgA antibody level was detected in the feces of mice after oral immunization. Significant SIgA antibody level could be detected in the feces of the experimental group from the 14th day after immunization, which is significantly higher than that of the control group, and the specific SIgA antibody level reaches the highest level on the 35th day after immunization (Figure 3), indicating that recombinant *B. subtilis* CotG-E-G and CotG-C-G could effectively induce mucosal immune response after oral immunization.

Splenocyte proliferation assay

To evaluate the effects of CotG-E-G and CotG-C-G on splenocyte proliferation in mice, *in vitro* splenocyte proliferation assay was performed 1 week after the last immunization. The splenocyte proliferation ability of CotG-E-G and CotG-C-G mice immunized with inactivated and purified HNPB3 protein was significantly higher than that of control mice (Figure 4A). The results showed that recombinant *B. subtilis* could promote the proliferation of immune cells and stimulate a strong antigen-specific immune response.

Detection of splenic lymphocyte cytokines

To further investigate the antigen-specific cellular immune response, the levels of secreted IFN-γ and IL-4 in mouse splenocytes were detected

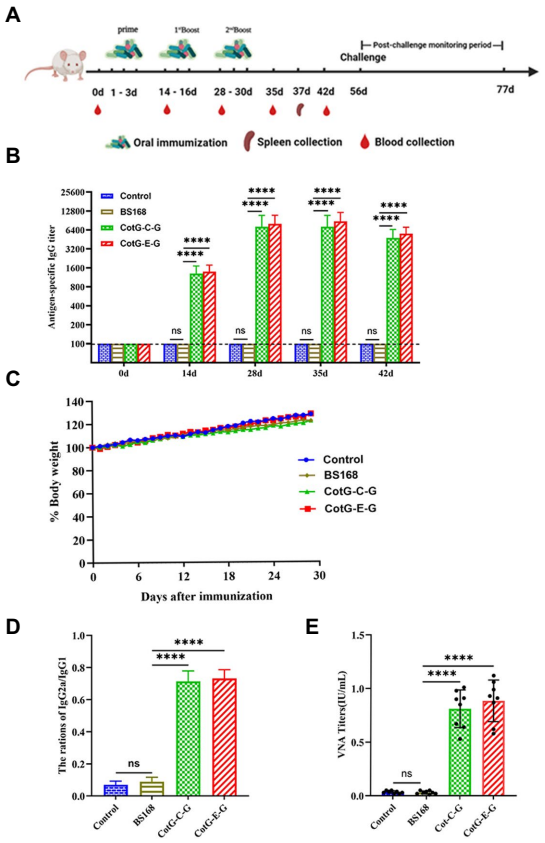

FIGURE 2
Specific anti-RABV antibody detection. **(A)** Immune scheme, BALB/c mice were randomly divided into 4 group, which were CotG-E-G, CotG-C-G, BS168 and PBS control group. Serum samples were collected at 0, 14, 28, 35 and 42days (n=8/ group). Spleens were collected from mice on day 37 (n=3/group). **(B)** Changes of body weight in mice during immune period. **(C)** The levels of specific IgG (Serum dilution multiples start from 100 times, sequentially doubling dilution) antibodies in mouse serum were detected by indirect ELISA. **(D)** One week after the last immunization, the IgG2a/IgG1 ratio was determined by indirect ELISA. **(E)** One week after the last immunization, VNA titers were determined by the FAVN method. The mean and standard deviation of each group were analyzed using one-way or multi-way ANOVA (*p<0.05, **p<0.01, ***p<0.001, **** p<0.0001).

by ELISpot assay. As shown in Figures 4B,C, the amounts of IFN-γ and IL-4 secreted in the splenocytes of CotG-E-G and CotG-C-G mice in the immunized group were significantly higher than those in the control groups, it is suggested that recombinant *B. subtilis* could enhance cytokine production, indicating that both Th1 and Th2 of acquired immunity were activated.

Protection after the challenge of orally immunized mice

To determine the protective efficacy of recombinant *B. subtilis* CotG-E-G and CotG-C-G. Four weeks after the last immunization, mice were challenged with a lethal dose of HNPB3 of 100×IMLD50 and were monitored continuously for 21 days to observe their clinical symptoms and mortality. As shown in Figure 5, the control group mice all died within 10 days after the challenge. In contrast, individual mice in the experimental group CotG-E-G began to develop rabies symptoms such as convulsions and paralysis on the 8th day and were humanely sacrificed. After the 21-day observation period, the survival rate of CotG-E-G in the experimental group was 50%, and the survival rate of CotG-C-G was 40%. These results indicated that recombinant *B. subtilis* had good immunogenicity and a certain protective effect against lethal RABV attacks.

Discussion

Stray animals and wild animals live in no fixed place and have a wide range of activities, so it is difficult to vaccinate against rabies through intramuscular injection. Therefore, the large-scale application of oral rabies vaccine (ORV) is the best way to solve the problem of rabies vaccination in stray animals and wild animals. The earliest oral immunization applied to wild animals is the attenuated live vaccine, mainly including ERA, SAD B19 and SAG-2 strains. ERA strain was the first to immunize red foxes as ORV in Europe, and achieved good immune effect (Baer et al., 1971; Steck et al., 1982). ERA strains were widely used to control fox rabies in North America between 1989 and 2009, greatly reducing the risk of human exposure to rabies (Rosatte et al., 2007, 2008). Wild animal ORVs prepared from attenuated rabies virus strains such as SAG2 and SAD B19 has been successfully used to control rabies in European foxes and raccoons in the United States and Canada, greatly reducing the spread of wild animal rabies (Wallace et al., 2020). Currently, the World Organization for Animal Health (WOAH) recommends two oral rabies vaccines, SAG2 and VR-G, for oral vaccination of dogs (Jackson, 2013). In 2021, Thailand will carry out the first large-scale application of ORV, and 83.0% (1,485/1789) of stray dogs will be immunized through ORV, significantly improving the vaccination coverage of stray dogs (Chanachai et al., 2021). Therefore, the oral rabies vaccine plays an important role in the global elimination of human rabies deaths from dog transmission.

Oral administration is simple and safe and has received more and more attention in vaccine development. In recent years, many oral rabies vaccines have been developed and evaluated, including recombinant live vector vaccines, attenuated vaccines, and recombinant virus vaccines. Given the safety and efficacy of the recombinant live vector vaccine, it can be used as a candidate vaccine for oral rabies vaccines. One of the current challenges in developing oral vaccines is that low pH in the gastric environment can destroy vaccine immunity. So, *B. subtilis* was selected as the oral vaccine delivery carrier in this study. *B. subtilis* has strong stress resistance, can resist the erosion of gastric acid in the gastrointestinal tract, and can effectively survive in the low-acid environment in the stomach and complex intestinal conditions (Zhou et al., 2008a,b; Li et al., 2022). *B. subtilis* exerts immune adjuvant activity and is effective against most oral antigens (Tanasienko et al., 2005). *B. subtilis* can germinate in intestinal antigen-presenting cells, where antigens can be processed and presented to downstream immune cells, inducing a strong mucosal immune response in the intestine (Duc le et al., 2004; Mauriello et al., 2007). In addition, the production cost of *B. subtilis* is low, the production process is simple, and it is easy to store, which reduces the cost of vaccine transportation. It is safe and non-toxic to humans and animals, and is certified as a GRAS product. Therefore, it can be used as an efficient delivery vehicle.

Isticato et al. (2001) first established a spore surface display system, using CotB as the anchor gene, the 459 amino acid fragment of the C-terminal of tetanus toxin (TTFC) was successfully displayed on the surface of *B. subtilis* by budding surface display technology.

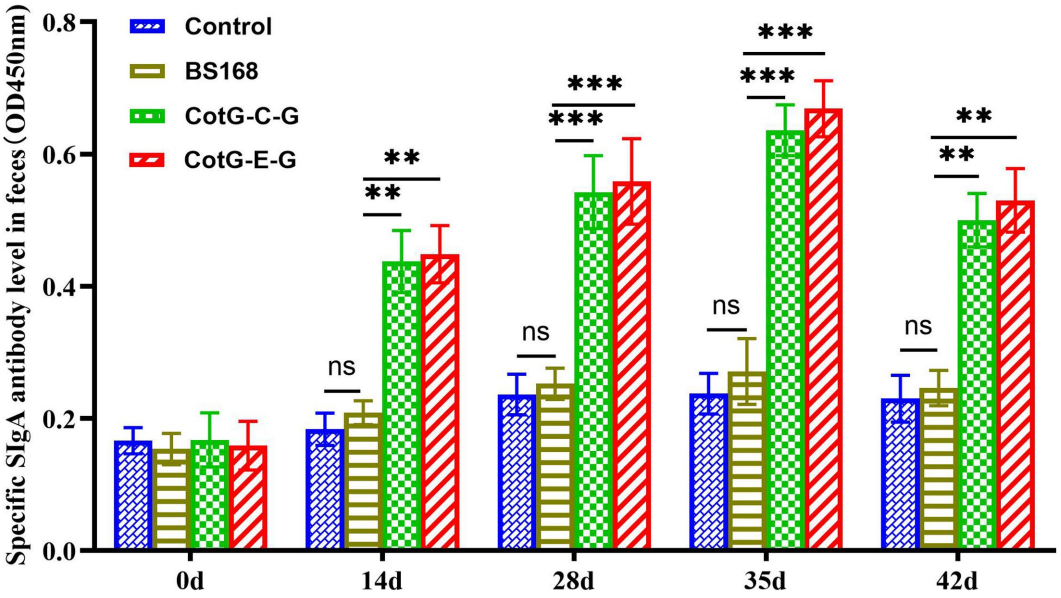

FIGURE 3
Detection of specific SIgA mucosal levels. The feces of mice (n=8) were collected at 0, 14, 28, 35 and 42days after the first vaccination, and the specific SIgA (the value of OD450 nm was calculated) level was detected by indirect ELISA. Data are presented as mean±SD for each group (*p<0.05, **p<0.01, ***p<0.001, ****p<0.0001).

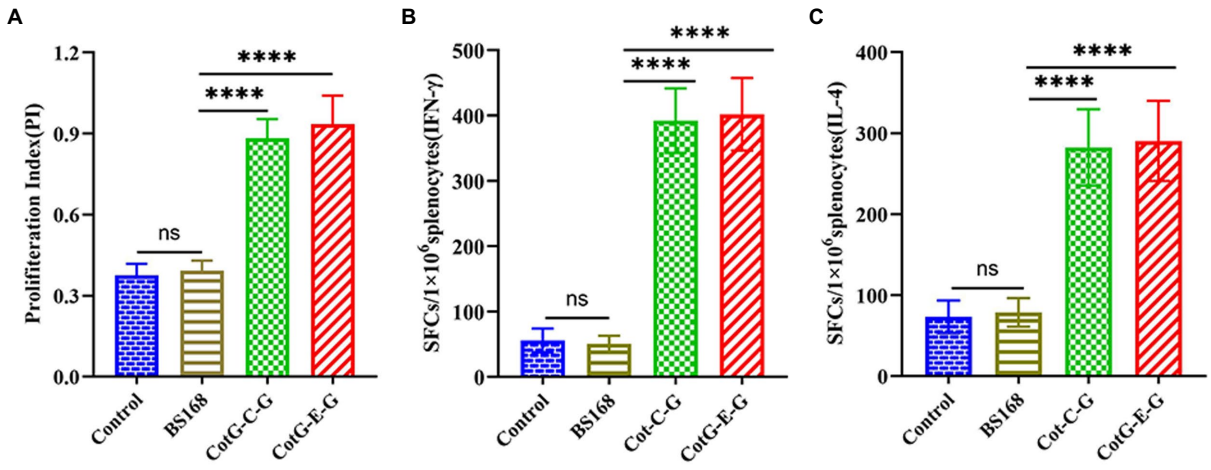

FIGURE 4
Splenocyte proliferation. On the 37th day after immunization, the spleens of mice were taken (n=3/group), Splenocytes were stimulated with inactivated purified HNPB3 protein. **(A)** CCK-8 colorimetric assay for cell proliferation index. **(B,C)** The levels of IFN-γ and IL-4 secreted by splenocytes were measured by ELISpot method (The ordinate represents the number of spot-forming cells per well). Data are presented as mean±SD of each group (*p<0.05, **p<0.01, *** p<0.001, ****p<0.0001).

Using the fusion protein Cot B-TTFC of TTFC and CotB to immunize mice by oral and intranasal methods, the mice can produce mucosal IgA and systemic IgG immune responses. Kwon (Kwon et al., 2007) used the CotG gene of capsid protein as a fusion vector and successfully demonstrated galactosidase on the surface of *B. subtilis* bud hug. The recombinant bud hug had galactosidase catalytic activity in the water-organic reaction system. In addition, related studies have proved that *B. subtilis* probiotic strains did not cause significant adverse effects in acute toxicity tests (Yuan et al., 2012; Zhang et al., 2013), organs such as the heart and liver, indicating that *B. subtilis* is safe and non-toxic to mammals (Mingmongkolchai and Panbangred, 2018).

Serum-neutralizing antibodies reflect the neutralizing ability of the body to the virus, to a certain extent, it could replace the challenge study. RABV-neutralizing antibody assays are considered the gold standard for evaluating the rabies vaccine. The WHO and WOAH suggest that the RABV-VNA titer of 0.5 IU/ml has a protective effect on the body (Chen and Emergency, 2019). This standard has been applied in many reports (Tanisaro et al., 2010; Mittal, 2013). In this study, 1 week after the last immunization, the RABV VNA titers of

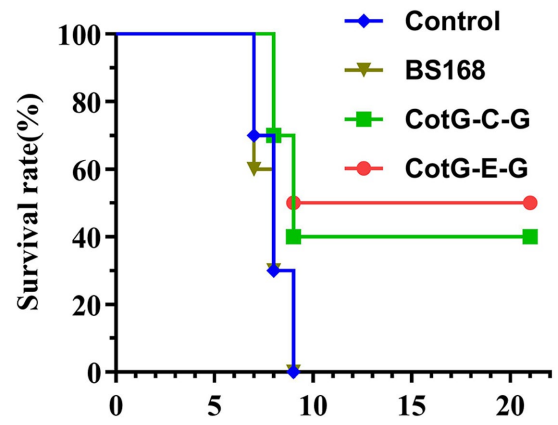

FIGURE 5
Protection of recombinant *B. subtilis* against lethal RABV challenge. Groups of mice (n=10) were challenged with 100×IMLD50 of RABV street strain 4weeks after the last immunization. Observed for 21days. The survival of mice in each group at different times after the challenge was recorded. The p value between BS168 and CotG-E-G group was 0.071, and BS168 and CotG-C-G group was 0.144.

CotG-E-G and CotG-C-G in the experimental group were higher than 0.5 IU/ml (Figure 2D). These results indicated that both recombinant *B. subtilis* strains had certain protective effects against RABV. Studies have shown that SIgA is the main antibody subtype and effector for body defense. SIgA antibody in intestinal mucosa has the function of neutralizing the virus, inhibiting virus invasion, and regulating the dynamic balance of mucosal surface (Liu et al., 2009; Kamada and Núñez, 2014). Serum immunoglobulin IgG antibody is an important indicator of the systemic immune response. In this study, after oral immunization of mice with recombinant *B. subtilis* CotG-E-G and CotG-C-G, the levels of RABV-specific SIgA in feces and IgG antibody in serum were detected. The results showed that the RABV specific SIgA and IgG antibody levels were significantly increased. These results indicated that the mice developed efficient humoral immune responses after oral immunization. Notably, specific antibodies induced by recombinant *B. subtilis* persisted for more than 35 days with high antibody levels, this may be related to the spores resisting digestion and germinating in the gut (Casula, 2002; Duc Le et al., 2004). In terms of cellular immune responses, the results showed that recombinant *B. subtilis* could induce spleen cell antigen-specific cell proliferation (Figure 4A), and effectively stimulate splenocytes to secrete IFN-γ and IL-4. IFN-γ is a Th1 cytokine involved in cellular immune responses, IFN-γ plays an antiviral role by promoting the lysis and clearance of virus-infected cells and inhibiting the expression and replication of viral genes (Venkataswamy et al., 2015). IL-4 is a Th2 cytokine associated with humoral immune responses, which drives the maturation of B cells into plasma cells, resulting in antibody production (Fang et al., 2007). This indicates that recombinant *B. subtilis* can effectively stimulate the production of Th1 and Th2 cytokines in mice, thereby enhancing cellular and humoral immune responses.

In conclusion, our results showed that immunization of mice with recombinant *B. subtilis* significantly increased the fecal-specific SIgA titers, serum specific IgG antibody levels, and serum neutralizing antibodies, it can induce the body to produce strong cellular and humoral immune responses, which is helpful to better resist the invasion of RABV. These data suggest that recombinant *B. subtilis* is expected to be a new and promising oral rabies vaccine candidate to prevent and control rabies in wild animals.

Data availability statement

The datasets presented in this study can be found in online repositories. The names of the repository/repositories and accession number(s) can be found at: https://www.ncbi.nlm.nih.gov/genbank/, E-G: J02293. https://www.ncbi.nlm.nih.gov/genbank/, C-G: GQ918139.

Ethics statement

The animal experiments were approved by the Animal Welfare and Ethics Committee of Changchun Veterinary Research Institute under the license number JSY-DW-2018-02. All BALB/c mice were treated according to the Guidelines for the Welfare and Ethics of Laboratory Animals of China (GB 14925–2001).

Author contributions

YiZ and XX conceived and designed the experiments. YiZ, RM, SS, BL, and EL performed the experiments. YiZ and ZC analyzed the data. TW, YF, and SY contributed reagents, materials, and analysis tools. YiZ wrote the manuscript. XX, YoZ, and FY reviewed the manuscript. XX and YiZ requested financial support. All authors read and approved the final manuscript.

Funding

This research was supported by the Jilin Provincial Science and Technology Development Program (20210202052NC).

Acknowledgments

We thank Jilin Provincial Science and Technology Development Project Fund for funding the project.

Conflict of interest

The authors declare that the research was conducted in the absence of any commercial or financial relationships that could be construed as a potential conflict of interest.

Publisher's note

References

Baer, G. M., Abelseth, M. K., and Debbie, J. G. (1971). Oral vaccination of foxes against rabies. *Am. J. Epidemiol.* 93, 487–490. doi: 10.1093/oxfordjournals.aje.a121283

Benavides, J. A., Megid, J., Campos, A., and Hampson, K. (2020). Using surveillance of animal bite patients to decipher potential risks of rabies exposure from domestic animals and wildlife in Brazil. *Front. Public Health* 8:318. doi: 10.3389/fpubh.2020.00318

Benjamin, D., Glenn, R., and Matthias, S. (2015). Everything you always wanted to know about rabies virus (but were afraid to ask). *Ann. Rev. Virol.* 2, 451–471. doi: 10.1146/annurev-virology-100114-055157

Casula, G. (2002). *Evaluation of Bacillus subtilis Spores as a Probiotic and a Delivery System for Heterologous Antigens*. London: Royal Holloway University of London,

Chanachai, K., Wongphruksasoong, V., Vos, A., Leelahapongsathon, K., Tangwangvivat, R., Sagarasaeranee, O., et al. (2021). Feasibility and effectiveness studies with oral vaccination of free-roaming dogs against rabies in Thailand. *Viruses* 13:571. doi: 10.3390/v13040571

Chen, R., and Emergency, D. O. (2019). Updates and interpretation on third report of WHO expert consultation on rabies. *Transl. Med. J.* Available at: https://apps.who.int/iris/handle/10665/272364

Cliquet, F., Aubert, M., and Sagné, L. (1998). Development of a fluorescent antibody virus neutralisation test (FAVN test) for the quantitation of rabies-neutralising antibody. *J. Immunol. Methods* 212, 79–87. doi: 10.1016/S0022-1759(97)00212-3

Conzelmann, K. K., Cox, J. H., Schneider, L. G., and Thiel, H. J. (1990). Molecular cloning and complete nucleotide sequence of the attenuated rabies virus SAD B19. *Virology* 175, 485–499. doi: 10.1016/0042-6822(90)90433-R

Cox, J. H., Dietzschold, B. A., and Schneider, L. G. (1977). Rabies virus glycoprotein. II. Biological and serological characterization. *Infect. Immun.* 16, 754–759. doi: 10.1128/iai.16.3.754-759.1977

Duc, L. H., Hong, H., Atkins, H., Flick-Smith, H., Durrani, Z., Rijpkema, S., et al. (2007). Immunization against anthrax using *Bacillus subtilis* spores expressing the anthrax protective antigen. *Vaccine* 25, 346–355. doi: 10.1016/j.vaccine.2006.07.037

Duc Le, H., Hong, H. A., Uyen, N. Q., and Cutting, S. M. (2004). Intracellular fate and immunogenicity of *B. subtilis* spores. *Vaccine* 22, 1873–1885. doi: 10.1016/j.vaccine.2003.11.021

Elshaghabee, F., Rokana, N., Gulhane, R., Sharma, C., and Panwar, H. (2017). *Bacillus* as potential probiotics: status, concerns, and future perspectives. *Front. Microbiol.* 8:1490. doi: 10.3389/fmicb.2017.01490

Fang, T. C., Yashiro-Ohtani, Y., Bianco, C. D., Knoblock, D. M., Blacklow, S. C., and Pear, W. S. (2007). Notch directly regulates Gata3 expression during T helper 2 cell differentiation. *Immunity* 27, 100–110. doi: 10.1016/j.immuni.2007.04.018

Feng, Y., Wang, Y., Hada, D., Gaosuyilatu, L. X., Xu, Z., Hasibagen, B. A., et al. (2022). Diversity of rabies virus detected in Inner Mongolia, China, 2019-2021. *Transbound. Emerg. Dis.* 69, 249–253. doi: 10.1111/tbed.14451

Fenje, P. (1968). Advances in rabies research. *Can. J. Public Health* 59, 217–228.

Hampson, K., Coudeville, L., Lembo, T., Sambo, M., Kieffer, A., Attlan, M., et al. (2015). Estimating the global burden of endemic canine rabies. *PLoS Negl. Trop. Dis.* 9:e0003709. doi: 10.1371/journal.pntd.0003709

Henle, W., Kikuth, W., Meyer, K. F., Nauck, E. G., and Tomcsik, J. (1962). Ergebnisse der mikrobiologie immunittsforschung und experimentellen therapie: fortsetzung der ergebnisse der hygiene bakteriologie immunittsforschung und experimentellen therapie. *Curr. Top. Microbiol. Immunol.* 32, 1–22.

Hong, H. A., Le, H. D., and Cutting, S. M. (2005). *The use of bacterial spore formers as probiotics*. *FEMS Microbiol. Rev.* 29: 813–835.

Imamura, D., Kuwana, R., Takamatsu, H., and Watabe, K. (2011). Proteins involved in formation of the outermost layer of *Bacillus subtilis* spores. *J. Bacteriol.* 193, 4075–4080. doi: 10.1128/JB.05310-11

Isticato, R., Cangiano, G., Tran, H. T., Ciabattini, A., Medaglini, D., Oggioni, M. R., et al. (2001). Surface display of recombinant proteins on *Bacillus subtilis* spores. *J. Bacteriol.* 183, 6294–6301. doi: 10.1128/JB.183.21.6294-6301.2001

Jackson, A. C. (2013). Rabies: Scientific Basis of the Disease and its Management. *New Zealand Laboratory News*.

Kamada, N., and Núñez, G. (2014). Regulation of the immune system by the resident intestinal bacteria. *Gastroenterology* 146, 1477–1488. doi: 10.1053/j.gastro.2014.01.060

Kip, E., Staal, J., Verstrepen, L., Tima, H. G., and Terryn, S. (2018). MALT1 controls attenuated rabies virus by inducing early inflammation and T cell activation in the brain. *J. Virol.* 92:17. doi: 10.1128/JVI.02029-17

Kwon, S. J., Jung, H. C., and Pan, J. G. (2007). Transgalactosylation in a water-solvent biphasic reaction system with beta-galactosidase displayed on the surfaces of *Bacillus subtilis* spores. *Appl. Environ. Microbiol.* 73, 2251–2256. doi: 10.1128/AEM.01489-06

Li, W., Li, J., Dai, X., Liu, M., Khalique, A., Wang, Z., et al. (2022). Porcine circovirus surface display of type 2 antigen protein cap on the spores of: an effective mucosal vaccine candidate. *Front. Immunol.* 13:1007202. doi: 10.3389/fimmu.2022.1007202

Liu, J. K., Hou, X. L., Wei, C. H., Yu, L. Y., He, X. J., Wang, G. H., et al. (2009). Induction of immune responses in mice after oral immunization with recombinant *Lactobacillus casei* strains expressing enterotoxigenic *Escherichia coli* F41 fimbrial protein. *Appl. Environ. Microbiol.* 75, 4491–4497. doi: 10.1128/AEM.02672-08

Liu, J., Wang, H., Gu, J., Deng, T., Yuan, Z., Hu, B., et al. (2017). BECN1-dependent CASP2 incomplete autophagy induction by binding to rabies virus phosphoprotein. *Autophagy* 13, 739–753. doi: 10.1080/15548627.2017.1280220

Luo, J., Zhang, B., Wu, Y., Tian, Q., Zhao, J., Lyu, Z., et al. (2017). Expression of interleukin-6 by a recombinant rabies virus enhances its immunogenicity as a potential vaccine. *Vaccine* 35, 938–944. doi: 10.1016/j.vaccine.2016.12.069

Mauriello, E. M., Cangiano, G., Maurano, F., Saggese, V., De Felice, M., Rossi, M., et al. (2007). Germination-independent induction of cellular immune response by *Bacillus subtilis* spores displaying the C fragment of the tetanus toxin. *Vaccine* 25, 788–793. doi: 10.1016/j.vaccine.2006.09.013

Mauriello, E., Le, H. D., Isticato, R., Cangiano, G., Hong, H. A., Felice, M., et al. (2004). Display of heterologous antigens on the *Bacillus subtilis* spore coat using cot C as a fusion partner. *Vaccine* 22, 1177–1187. doi: 10.1016/j.vaccine.2003.09.031

Mingmongkolchai, S., and Panbangred, W. (2018). *Bacillus* probiotics: an alternative to antibiotics for livestock production. *J. Appl. Microbiol.* 124, 1334–1346. doi: 10.1111/jam.13690

Ming-Yang, Y. U., Wang, G. Y., Alatengheli, W. W. X., Gui, J. Y., Zhang, Q. W., Wei, Y. H., et al. (2018). Epidemiology of animal rabies in Inner Mongolia. *Chin. J. Vet. Sci.*

Mittal, M. K. (2013). Revised 4-dose vaccine schedule as part of postexposure prophylaxis to prevent human rabies. *Pediatr. Emerg. Care* 29, 1119–1121. doi: 10.1097/PEC.0b013e3182a63125

Mou, C., Zhu, L., Xing, X., Lin, J., and Yang, Q. (2016). Immune responses induced by recombinant *Bacillus subtilis* expressing the spike protein of transmissible gastroenteritis virus in pigs. *Antivir. Res.* 131, 74–84. doi: 10.1016/j.antiviral.2016.02.003

Poulet, H., Minke, J., Pardo, M. C., Juillard, V., and Audonnet, J. C. (2007). Development and registration of recombinant veterinary vaccines. The example of the canarypox vector platform. *Vaccine* 25, 5606–5612. doi: 10.1016/j.vaccine.2006.11.066

Rosatte, R., Allan, M., Bachmann, P., Sobey, K., and Schumacher, C. (2008). Prevalence of tetracycline and rabies virus antibody in raccoons, skunks, and foxes following aerial distribution of V-RG baits to control raccoon rabies in Ontario. *Can. J. Wildl. Dis.* 44, 946–964. doi: 10.7589/0090-3558-44.4.946

Rosatte, R. C., Power, M. J., Donovan, D., and Davies, J. (2007). Elimination of arctic variant rabies in red foxes, metropolitan Toronto. *Emerg. Infect. Dis.* 13, 25–27. doi: 10.3201/eid1301.060622

Sangun, L., Belitsky, B. R., Brinker, J. P., Kerstein, K. O., Brown, D. W., et al. (2010). Clements development of a *Bacillus subtilis*-based rotavirus vaccine. *Clin. Vaccine Immunol.* 17:10. doi: 10.1128/CVI.00135-10

Schumann, W. (2007). Production of recombinant proteins in *Bacillus subtilis*. *Adv. Appl. Microbiol.* 62, 137–189. doi: 10.1016/S0065-2164(07)62006-1

Shao, X., Ren, J., Wen, Y., Yang, Y., and Chen, X. (2015). Characterization of a virulent dog-originated rabies virus affecting more than twenty fallow deer (*Dama dama*) in Inner Mongolia, China. *Infect. Genet. Evol.* 31, 127–134. doi: 10.1016/j.meegid.2014.12.024

Steck, F., Wandeler, A., Bichsel, P., Capt, S., and Schneider, L. (1982). Oral immunisation of foxes against rabies: a field study. *Zoonoses Public Health* 29, 372–396. doi: 10.1111/j.1439-0450.1982.tb01237.x

Tanasienko, O. A., Cheremshenko, N. L., Titova, G. P., Potebnya, M. G., Gavrilenko, M. M., Nagorna, S. S., et al. (2005). Elevation of the efficacy of antitumor vaccine prepared on the base of lectines from *B. subtilis* B-7025 upon its combined application with probiotics *in vivo*. *Exp. Oncol.* 27, 336–338. PMID: 16404358

Tanisaro, T., Tantawichien, T., Tiranathanagul, K., Susantitaphong, P., Chirananthavat, T., Praditpornsilpa, K., et al. (2010). Neutralizing antibody response after intradermal rabies vaccination in hemodialysis patients. *Vaccine* 28, 2385–2387. doi: 10.1016/j.vaccine.2010.01.003

Taylor, L. H., and Nel, L. H. (2015). Global epidemiology of canine rabies: past, present, and future prospects. *Vet. Med. (Auckl)* 6, 361–371. doi: 10.2147/VMRR.S51147

Venkataswamy, M. M., Madhusudana, S. N., Sanyal, S. S., Taj, S., Belludi, A. Y., Mani, R. S., et al. (2015). Cellular immune response following pre-exposure and postexposure rabies vaccination by intradermal and intramuscular routes. *Clin. Exp. Vaccine Res.* 4, 68–74. doi: 10.7774/cevr.2015.4.1.68

Wallace, R. M., Cliquet, F., Fehlner-Gardiner, C., Fooks, A. R., and Muller, T. (2020). Role of oral rabies vaccines in the elimination of dog-mediated human rabies deaths. *Emerg. Infect. Dis.* 26, 1–9. doi: 10.3201/eid2612.201266

Weyer, J., Rupprecht, C. E., and Nel, L. H. (2009). Poxvirus-vectored vaccines for rabies--a review. *Vaccine* 27, 7198–7201. doi: 10.1016/j.vaccine.2009.09.033

Wiktor, T. J., Gyrgy, E., Schlumberger, D., Sokol, F., and Koprowski, H. (1973). Antigenic properties of rabies virus components. *J. Immunol.* 110, 269–276. doi: 10.4049/jimmunol.110.1.269

Wunner, J. (2013). *Rabies: Scientific Basis of the Disease and its Management*. Cambridge, Massachusetts: Academic Press

Yousaf, M. Z., Qasim, M., Zia, S., Khan, M., and Khan, S. (2012). Rabies molecular virology, diagnosis, prevention and treatment. *Virol. J.* 9:50. doi: 10.1186/1743-422X-9-50

Yuan, J., Yang, J., Zhuang, Z., Yang, Y., Lin, L., and Wang, S. (2012). Thrombolytic effects of Douchi fibrinolytic enzyme from Bacillus subtilis LD-8547 in vitro and in vivo. *BMC Biotechnol.* 12:36. doi: 10.1186/1472-6750-12-36

Zhang, Y., Gao, J., Zhang, C., Kong, F., Wang, J., and Feng, C. (2013). Toxicological and safety evaluation of *Bacillus subtilis* strain Tpb55. *Chin. J. Biol. Control*.

Zhao, J., Zhang, Y., Chen, Y., Zhang, J., Pei, J., Cui, M., et al. (2021). A novel oral rabies vaccine enhances the immunogenicity through increasing dendritic cells activation and germinal center formation by expressing U-OMP19 in a mouse model. *Emerg. Microbes Infect.* 10, 913–928. doi: 10.1080/22221751.2021.1923341

Zhou, Z., Xia, H., Hu, X., Huang, Y., Li, Y., Li, L., et al. (2008a). Oral administration of a *Bacillus subtilis* spore-based vaccine expressing *Clonorchis sinensis* tegumental protein 22.3 kDa confers protection against *Clonorchis sinensis*. *Vaccine* 26, 1817–1825. doi: 10.1016/j.vaccine.2008.02.015

Zhou, Z., Xia, H., Hu, X., Huang, Y., Ma, C., Chen, X., et al. (2008b). Immunogenicity of recombinant *Bacillus subtilis* spores expressing *Clonorchis sinensis* tegumental protein. *Parasitol. Res.* 102, 293–297. doi: 10.1007/s00436-007-0762-x

frontiers | Frontiers in Microbiology

TYPE Original Research
PUBLISHED 23 March 2023
DOI 10.3389/fmicb.2023.1141101

OPEN ACCESS

EDITED BY
Jianke Wang,
Hebei Agricultural University,
China

REVIEWED BY
Makoto Ujike,
Nippon Veterinary and Life Science University,
Japan
Jianjun Zhao,
Heilongjiang Bayi Agricultural University,
China
Hualei Wang,
Jilin University,
China

*CORRESPONDENCE
Hongtao Kang
✉ kanghongtao@caas.cn
Honglin Jia
✉ jiahonglin@caas.cn

†These authors have contributed equally to this work

SPECIALTY SECTION
This article was submitted to Virology, a section of the journal Frontiers in Microbiology

RECEIVED 10 January 2023
ACCEPTED 01 March 2023
PUBLISHED 23 March 2023

CITATION
Cao H, Gu H, Kang H and Jia H (2023) Development of a rapid reverse genetics system for feline coronavirus based on TAR cloning in yeast.
Front. Microbiol. 14:1141101.
doi: 10.3389/fmicb.2023.1141101

Development of a rapid reverse genetics system for feline coronavirus based on TAR cloning in yeast

Hongmin Cao†, Haorong Gu†, Hongtao Kang* and Honglin Jia*

State Key Laboratory of Veterinary Biotechnology, Harbin Veterinary Research Institute, Chinese Academy of Agricultural Sciences, Harbin, China

Introduction: Reverse genetics has become an indispensable tool to gain insight into the pathogenesis of viruses and the development of vaccines. The yeast-based synthetic genomics platform has demonstrated the novel capabilities to genetically reconstruct different viruses.

Methods: In this study, a transformation-associated recombination (TAR) system in yeast was used to rapidly rescue different strains of feline infectious peritonitis virus, which causes a deadly disease of cats for which there is no effective vaccine.

Results and discussion: Using this system, the viruses could be rescued rapidly and stably without multiple cloning steps. Considering its speed and ease of manipulation in virus genome assembly, the reverse genetics system developed in this study will facilitate the research of the feline coronaviruses pathogenetic mechanism and the vaccine development.

KEYWORDS

FCoV, FIPV, reverse genetics, transformation-associated recombination, yeast

1. Introduction

Feline infectious peritonitis (FIP), caused by feline infectious peritonitis virus (FIPV), is a severe and lethal systemic infection of cats. Clinically, FIP can be divided into exudate type and nonexudate type based on whether or not peritoneal effusion is observed. Once exudative FIP symptoms appear, the mortality rate can be as high as 100%. Currently, there is still no effective vaccine available for this deadly disease. Accurate diagnosis of this disease is also difficult due to poor understanding of the pathogenetic mechanisms of FIPV. There are two pathogenic types of feline coronaviruses (FCoV): feline enteric coronavirus (FECV) and feline infectious peritoniitis virus (FIPV). The prevalence of FCoV infection in feline populations is generally high and may exceed 90% in multicat environments. The incidence of FIP, however, is very low and rarely affects more than 5% of infected cats (Pedersen, 2009; Drechsler et al., 2011). FECV is generally considered a mild, nonpathogenic form of FCoV. Oral FECV infection either is subclinical or causes very mild, nonspecific clinical symptoms, such as transient anorexia, in older cats (Vogel et al., 2010). However, in young (Specific Pathogen Free) SPF kittens, oral FECV infection causes severe enteritis (Pedersen et al., 1981; Addie and Jarrett, 1992).

FCoV belong to the genus *Alphacoronavirus* within the family *Coronaviridae* of the order *Nidovirales* (Tekes and Thiel, 2016). FCoV is single-stranded, positive-sense RNA virus. Their genomes are about 28 kb in size and encode at least 11 open reading frames

(ORFs), with two of the major ORFs encoding a replicase. ORF1a and ORF1b encode 16 nonstructural proteins (NSPs); four ORFs encode structural proteins (spike protein S, envelope protein E, membrane protein M, and nucleocapsid protein N); and five ORFs encode the nonstructural proteins 3a, 3b, 3c, 7a, and 7b (Ziebuhr et al., 2000; Dye and Siddell, 2005; Tekes et al., 2008). It is believed that FIPV evolved from FECV. Based on extensive sequence analysis of FECV and FIPV isolates, it was believed that mutations in S and accessory genes are involved in the development of FIP (Herrewegh et al., 1995; Vennema et al., 1998; Kennedy et al., 2001; Pedersen et al., 2009; Chang et al., 2012; Licitra et al., 2013; Bank-Wolf et al., 2014; Lewis et al., 2015). However, substituting FIPV S gene into the FECV skeleton did not induce FIP biotype transformation (Ehmann et al., 2018; Wang et al., 2021). Therefore, the pathogenic mechanisms it has evolved that distinguish from FECV is still unclear. FCoVs can be divided into serotypes I and II according to the spike gene. Both FECV and FIPV contains the two serotypes. There is consistent evidence indicating that type II FCoVs were evolved from the recombination of partial RNA sequences containing the speak genes of type I FCoVs and canine coronavirus (CCoVs; Herrewegh et al., 1998; Shiba et al., 2007; Terada et al., 2014). Although type II FCoV is easily propagated in cell culture, type I FCoV isolates generally grow poorly in cell culture. The vast majority (70 to 98%) of natural infections occurring worldwide are caused by serotype I FCoVs, which serotype II FCoVs are less common (Hohdatsu et al., 1992; Addie et al., 2003; Benetka et al., 2004; Kummrow et al., 2005; Shiba et al., 2007; Duarte et al., 2009; Lin et al., 2009; Amer et al., 2012; Li et al., 2019).

Currently, reverse genetic systems for coronaviruses have been developed based on various cloning platforms including bacterial artificial chromosome (BAC) vectors (Almazan et al., 2000), vaccinia virus vector (Thiel and Siddell, 2005), transformation-associated recombination (TAR) system in yeast (Thao et al., 2020), circular polymerase extension reaction strategy (CPER; Torii et al., 2021), and infectious subgenomic amplicons (ISA) (Melade et al., 2022). The successful establishment of reverse genetics systems for FCoVs based on BAC vector (Balint et al., 2012) and vaccinia virus (Ehmann et al., 2018) have also been reported. However, coronaviruses are often difficult to clone and manipulate in Escherichia coli due to the large size of the genomes. Meanwhile, occasional instability occurred in the genomes assembled by the BAC vector (Almazan et al., 2000; Yount et al., 2000). The major drawback of the vaccinia virus-based rescuing system is that it required multiple cloning steps, and inconvenient screening processes. Although infectious viruses could be generated by the ISA method, viral populations rescued through this system are often more diverse than that derived from an infectious clone (Mohamed Ali et al., 2018; Driouich et al., 2019). Therefore, generation of a more infectious clone is still necessary for studying the pathogenic mechanism of FIPV. In this study, we have further improved yeast-based TAR system by shorting the construction steps, and the construction of infective cDNA of FCoV could be completed in 1 week. Overall, we provide a rapid, reverse genetics system for assembling an infectious clone of FCoV *via* a yeast-based TAR which would benefit for the FCoV vaccine development and pathogenetic mechanism research.

2. Materials and methods

2.1. Cells and virus general culture conditions

Crandell-Rees feline kidney (CRFK) cells were available in our laboratory. Baby Hamster Kidney cell clone (BSR-T7/5), which stably expresses T7 RNA polymerase (T7 pol), was kindly provided by Zhigao Bu (Harbin Veterinary Research Institute, Chinese Academy of Agricultural Sciences). Felis catus whole-fetus 4 (FCWF-4) cells were purchased from the ATCC. All cells were maintained in Dulbecco's modified Eagle's medium (DMEM; Sigma Aldrich, D6429) with 10% FBS (Clark, FB25015) at 37°C in an atmosphere of humidified air containing 5% (v/v) CO_2.

2.2. Bacterial and yeast strains

TransforMax Epi300 cells (Lucigen) were used to propagate the plasmid. All yeast transformation experiments were performed using *Saccharomyces cerevisiae* VL6-48N (MATα trp1-Δ1 ura3-Δ1 ade2-101 his3-Δ200 lys2 met14 cir°), which was provided by Vladimir Larionov (Laboratory of Biosystems and Cancer, National Cancer Institute, Bethesda, Maryland, 20,892, USA; Wach et al., 1994; Kouprina et al., 1998; Noskov et al., 2002). Yeast cells were first cultured in YPDA broth (Takara Bio, 630,306), then transformed cells were placed on a minimum synthetic definition (SD) agar without histidine (SD-His; Takara Bio, Clontech, 630,415,630,411).

2.3. Virus strains

Full-length nucleotide (nt) sequences of FIPV I Black, FIPV II DF-2, and FECV I MG893511 (GenBank accession numbers EU186072.1, JQ408981.1, and MG893511.1, respectively) were independently used for the construction of each infectious cDNA clone using the TAR system. The FIPV II DF-2 were purchased from the ATCC. FIPV Black is a culture-adapted serotype virus (Black, 1980). But the ability to induce Symptomatic FIP is lost in cats (Thiel et al., 2014). FIPV DF-2 is a culture-adapted type II strain and has a strong pathogenic ability to cats (Balint et al., 2014). Serotype I FECV (FECV I MG89351) cannot be propagated in standard cell culture and causes an asymptomatic but persistent infection in cats (Ehmann et al., 2018).

2.4. Viral genome assembly in yeast

The plasmid of pCC1BAC-His3 was used for TAR cloning. The sequence of yeast centromere (CEN6), yeast replication origin (autonomously replicating sequence (ARS)), and yeast selectable marker (His3) shown in Supplementary Table 3 were synthesized by Comate Bioscience Company Limited (Gibson et al., 2010) and cloned into the pCC1BAC vector to produce the pCC1BAC-His3 vector. The cDNA fragments were amplified by PCR, using primers that overlapped at least 50 bp with segments containing the 5′ or 3′ ends of different viral genomes (Supplementary Table 1). Amplification was performed using KOD DNA polymerase (TOYOBO, KOD-401)

according to the manufacturer's instructions. The template used to generate the cloned TAR fragment is shown in Table 1.

Yeast conversion was performed using a high-efficiency lithium acetate/SS vector DNA/PEG method. Briefly, yeast cells were grown with agitation in a YPDA-rich medium at 30°C and activated twice until the optical density reached 1.0 at 600 nm before 3 ml of the culture was used for each transformation event. Transformation was carried out using a DNA mixture with a total concentration of 1 μg for all fragments. The following transformation yeast cells were plated on SD-His plates and incubated at 30°C for 48 h. Transformants were picked and suspended in 3 ml SD-His liquid medium and incubated overnight at 30°C, with shaking. For the preparation of crude, genomic DNA from transformants, aliquots (1 ml) of each culture were centrifuged, and the resulting cells pellets were resuspended in 200 μL TE Buffer (10 mM Tris–HCl, 1 mM EDTA. pH 8.0 [Amresco; Solarbio Life Sciences]) before being heated to 100°C for 10 min and then placed on an ice bath for 10 min. These genome preparations were used as templates for the identification by PCR of yeast transformants containing appropriately assembled FCoV DNA fragments using primers designed to amplify all fragment junctions (Supplementary Table 2). Clones harboring plasmids shown to contain all the expected overlapping junctions were identified, and plasmids were extracted from 20 ml cultures of those clones using the Yeast Plasmid Kit (OMEGA) according to the manufacturer's instructions but with the following modifications: (1) buffer YP I (500 μL) was supplemented with 40 μL of enzymolysis solution (10 mg/ml enzymolysis 20-T; 50 mM Tris–HCl pH 7.5; 50% (v/v) glycerol) and 100 μL β-mercaptoethanol, and (2) the mixture was incubated at 37°C for 1 h prior to the addition of buffer YP II. Then the plasmids were purified according to the instructions.

2.5. Transformation of yeast plasmids into *Escherichia coli*

Purified recombinant yeast plasmids containing the appropriately assembled, full-length viral genome were transformed into *E. coli* Epi300 cells. Yeast plasmid (30 ng) was transferred into EPI300 cells. After shaking, copycontrol inducer (1:1000) was added to the bacteria and the recombinant plasmid was purified from 200 ml bacterial culture using the QIAfilter Plasmid Midi Kit (QIAGEN).

2.6. Recovery of viruses

T7 or CMV promoters were added to the 5′ end of the viral genome, and the hepatitis delta virus ribozyme (HDVrz) and bovine growth hormone (BGH) transcription terminal signals were added after poly (A) sequences. In short, the recombinant plasmids were transfected into BSR-T7/5 cells or CRFK cells. The rescued viruses were passaged once in CRFK cells and harvested by freezing and thawing three times. Specific-genome sequencing of the recombinant viruses was performed before viruses were titrated and stored at −80°C.

2.7. Virus growth kinetics

Virus titration were conducted in 96-well plates. The viruses were serially diluted tenfold, and 100 μL of each dilution was added to separate wells and incubated for 2 h at room temperature. After incubation, the serum-free culture medium was replaced with 2% (v/v) FBS DMEM culture medium, and wells containing visible cytolytic lesions were recorded. Viral titers were expressed as the median tissue culture infective dose Log10 ($TCID_{50}$/ml) according to the method of Reed and Muënch (Pizzi, 1950). The growth kinetic of rCMV-Black-S was determined with FCWF-4 cells and the CRFK cells were used for the growth evaluation of the remaining viruses. The cells were infected with the virus at an MOI of 0.01, and the supernatant containing virus was collected and titrated at 6 h, 12 h, 24 h, 36 h, and 48 h post-infection, respectively. The growth curve of the virus was generated using GraphPad Prism 8.

2.8. Immunofluorescence assay

CRFK cells were mock infected or infected with rFCoV at an MOI of 0.1 for 12 h and then washed three times with PBS. After washing, CRFK cells were fixed with 4% (v/v) paraformaldehyde (Biosharp, BL302A) in PBS for 15 min and then permeabilized with 0.3% (v/v) Triton X-100 (Solarbio Life Sciences, T8200) in PBS for 15 min. After washing, the CRFK cells were incubated with mouse anti-FIPV N antibody at a dilution of 1:2, 000 at 4°C overnight. Subsequently, Alexa Fluor 488 (1;10,000)-conjugated Goat Antimouse IgG (Invitrogen, A11001) was added as a secondary antibody. After washing three times with PBS, DAPI (SIGMA, D9542-5MG) was added for 15 min. After washing three times with PBS, fluorescence was observed under an inverted fluorescence microscope (Zeiss).

2.9. Purification of recombinant FCoV

The cell culture supernatants (100 ml) were harvested on day 4 post-infection and centrifuged (4,000 × g for 30 min at 4°C) to remove cell debris. The recombinant FCoV were then pelleted by ultracentrifugation at 60,000 × g for 2 h at 4°C. The pellets were resuspended in Hepes-saline buffer at 4°C overnight and then purified through a 10–20-30% discontinuous sucrose gradient at 60,000 × g for 4 h at 4°C. The FCoV at the bottom of the tube was

TABLE 1 Cloning RNA virus genome using synthetic genomics platform.

Virus	Size (kb)	Template	Fragment generation	Number of fragments	Virus rescue
rT7-Black-S_{DF-2}	29.2	Synthetic DNA plasmid	PCR	8	Yes
rCMV-Black-S_{DF-2}	29.2	Synthetic DNA plasmid	PCR	9	Yes
rCMV-MG893511-S_{DF-2}	32.9	Synthetic DNA plasmid	PCR	10	Yes
rCMV-Black-S	29.3	Synthetic DNA plasmid	PCR	9	Yes

collected. The highly purified virus particles obtained were resuspended in 100 μL of Hepes-saline buffer.

2.10. Western blotting

For the western blot analysis, rescued viruses were mixed with 4 × SDS loading buffer and boiled for 10 min. The samples were analyzed using 12% SDS-PAGE and transferred onto a PVDF membrane. The membrane was blocked with a blocking buffer (Thermo Fisher Scientific, Waltham, USA) and incubated with a mouse anti-FIPV N antibody, at a dilution of 1:2,000, at room temperature for 2 h. After incubation, the membranes were washed five times with TBST buffer and incubated with DyLight 800-labeled anti-mouse IgG at a dilution of 1:10,000 for 1 h at room temperature.

3. Results

3.1. Design of FCoV genome assembly

The full process for constructing an infectious clone of feline coronaviruses is shown in Figure 1. The design of different FCoV fragments and the assembly of a complete genome are indicated in the individual figures. Each fragment overlaps its neighbor by at least 50 base pairs. The TAR clone vector and FCoV genomic fragments were co-transferred into yeast cells to assemble the whole virus genome and the shuttle vector, and the recombinant plasmids in yeast were transformed into *E. coli*. Finally, the plasmids were extracted from the *E. coli* to rescue recombinant viruses.

3.2. Rescue of an infectious FIPV Black-S_{DF-2} virus strain driven by a T7 promoter

First, we tried to rescue a chimeric virus with a type II S protein in the FIPV Black backbone, using a T7 promoter and a stable cell line expressing T7 RNA polymerase (BSR-T7/5). The strategy diagram of constructing a full-length FIPV T7-Black-S_{DF-2} clone in the pCC1BAC-His3 vector was shown in Figure 2A. PCR was used to confirm the presence of viral genome segments and segment junctions in DNA isolated from yeast clones. Plasmids from positive clones were transferred into *E. coli*, and the presence of a plasmid harboring the entire FCoV genome was verified by PCR (Figure 2B), restriction enzyme analysis (Figure 2C), and sequencing. The results indicated that this chimeric sequence contained only one nucleotide mutation, which might have arisen as a result of DNA polymerase infidelity during the PCR amplification step. Transfection of the purified plasmid into CRFK cells resulted in the visible cytopathic effect of syncytial fusion about 24 h after transfection (Figure 2D).

The first three generations of the rescued rT7-Black-S_{DF-2} strain were extracted for reverse transcription to give cDNAs, the specific sequences of which were confirmed by PCR (Figure 2E). Expression of the N protein of rT7-Black-S_{DF-2} was verified by IFA using a monoclonal antibody. The cytoplasm of typical syncytic cells showed obvious staining of N protein (Figure 2F). Moreover, western blot analysis revealed a band that reacted with the monoclonal antibody against N protein, in rFCoV particles released by transfected cells (Figure 2G). As shown in Figure 2H, electron microscopy revealed the presence of virus particles with coronavirus-like morphological characteristics, including typical spike structures, in the supernatant of cells. Next generation sequencing verified that the sequence of the rescued virus was 100% identical to the sequence cloned in the assembled recombinant plasmid.

3.3. Rescue of virus strain FIPV Black-S_{DF}-2, FECV MG893511-SDF-2, and FIPV Black with a CMV promoter

A rescued virus harboring a CMV promoter would not need to be transcribed *in vitro* or assisted by T7 pol expression cell lines, which would make rescuing the virus faster and more convenient. Thus, we replaced the T7 promoter with the CMV promoter in the pCC1BAC-His3 as described above and used it to assemble several FCoV genomes. The strategy for constructing these clones in the pCC1BAC-His3 vector were shown in the Figure 3A (FIPV Black-S_{DF-2}), Figure 4A (FECV MG893511-S_{DF-2}) and Figure 5A (FIPV Black wild type). Correct assembly of the viral genome were screened and identified by PCR (Figure 3B: FIPV Black-S_{DF-2}; Figure 4B: FECV MG893511-S_{DF-2}; Figure 5B: FIPV Black wild type) and restriction enzyme analyses (Figure 3C: FIPV Black-S_{DF-2}; Figure 4C: FECV

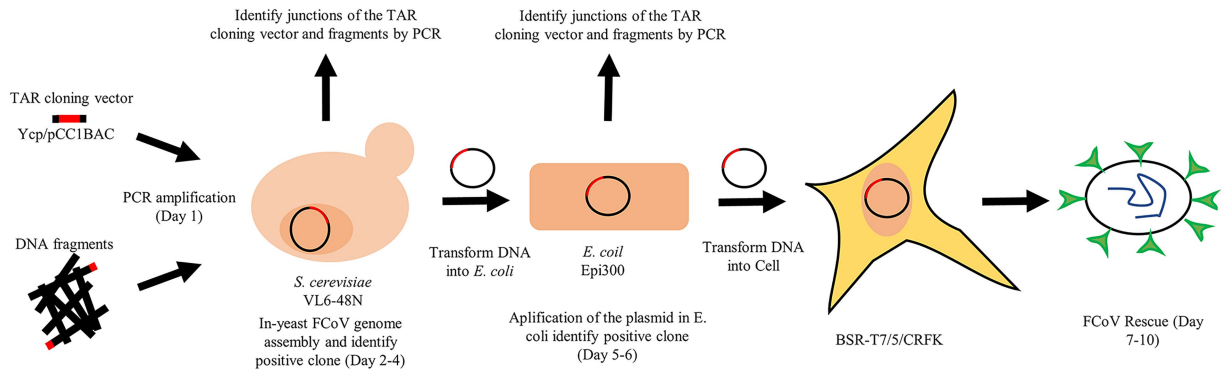

FIGURE 1
The full process of viral genome assembly and virus rescue.

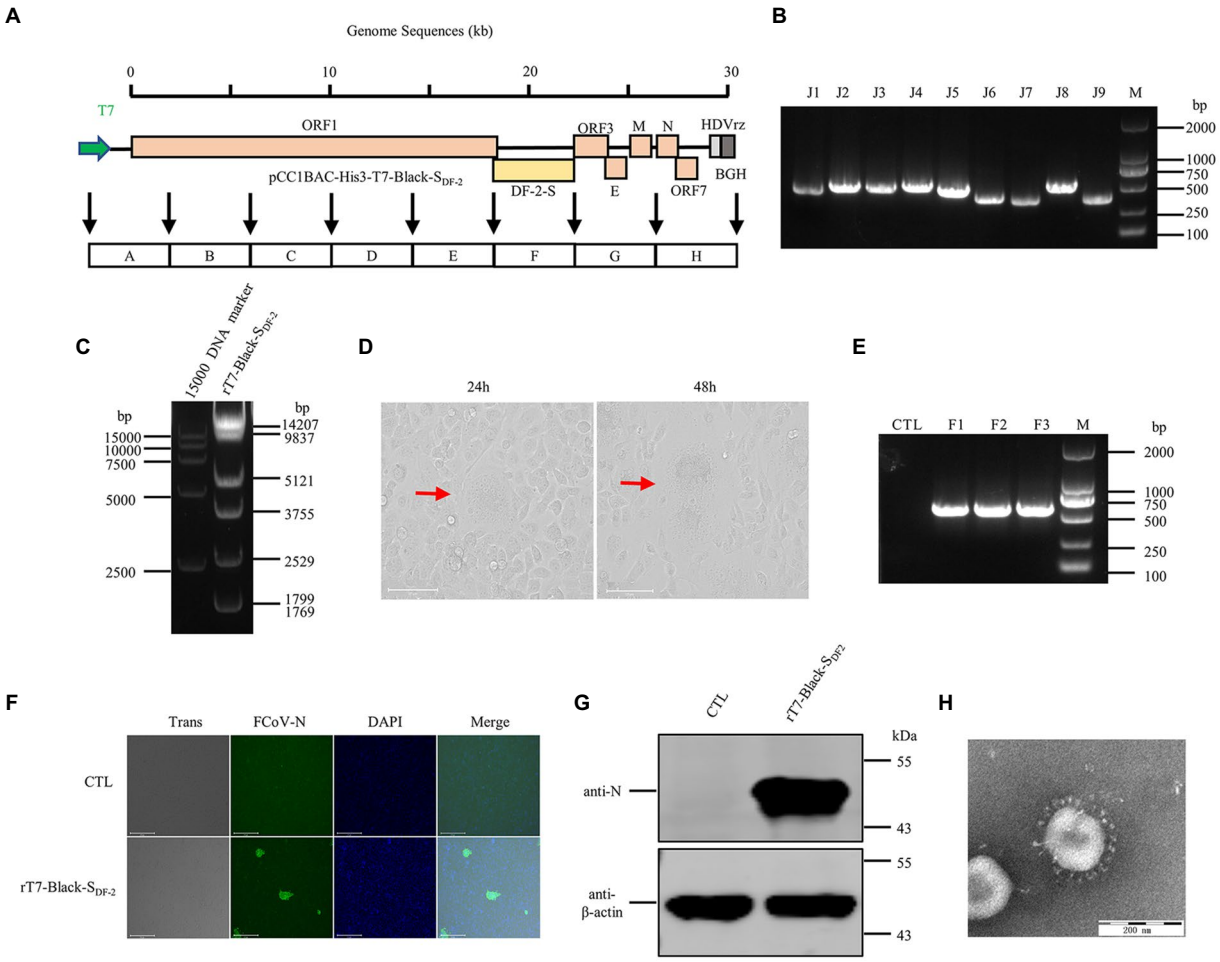

FIGURE 2
The recovery and identification of chimeric FIPV strain Black-SDF-2 driven by a T7 promoter. **(A)** Strategy diagram for the construction of pCC1BAC-His3-T7-Black-SDF-2. **(B)** Identification of fragment interfaces of the plasmids recovered from bacteria. **(C)** Enzyme digestion of pCC1BAC-His3-T7-Black-SDF-2 plasmid (NotI and NheI). **(D)** Significant cytopathic effects (CPE) were observed at 24 and 48h after infection with CRFK cells. **(E)** PCR identification of the rescued recombinant virus. **(F)** and **(G)** rT7-Black-SDF-2 virus infected CRFK cells for 12h was identified by IFA (Scale Bar, 275μm) and WB. **(H)** Electron microscopy examination of the purified virus.

MG893511-S$_{DF-2}$; Figure 5C: FIPV Black wild type). The plasmids were then transfected into CRFK cells using PEI transfection reagent. After 48 h, the cells were freeze-thawed once. The resulting supernatant was placed on CRFK cells and cultured for 24 h. Cytopathic effects could be observed for all the three viruses (Figure 3D: FIPV Black-S$_{DF-2}$; Figure 4D: FECV MG893511-S$_{DF-2}$; Figure 5D: FIPV Black wild type). The rescued virus was further identified by PCR (Figure 3E: FIPV Black-S$_{DF-2}$; Figure 4E: FECV MG893511-S$_{DF-2}$; Figure 5E: FIPV Black wild type), western blotting (Figure 3F: FIPV Black-S$_{DF-2}$; Figure 4F: FECV MG893511-S$_{DF-2}$; Figure 5F: FIPV Black wild type), IFAT (Figure 3G: FIPV Black-S$_{DF-2}$; Figure 4G: FECV MG893511-S$_{DF-2}$; Figure 5G: FIPV Black wild type), and electron microscopy (Figure 3H: FIPV Black-S$_{DF-2}$; Figure 4H: FECV MG893511-S$_{DF-2}$; Figure 5H: FIPV Black wild type). All recombinant viruses with serotype II S protein could replicate properly, the rescued viruses displayed growth characteristics similar to those displayed by serotype II FCoV strain DF2 and reached peak titers at 24 h after infection (Figure 3I: FIPV Black-S$_{DF-2}$; Figure 4I: FECV MG893511-S$_{DF-2}$). There is no significant difference in the titer of rescued viruses with either a T7 promoter or a CMV promoter. The recombinant FIPV Black with wild type S protein could replicate in FCWF-4 cells with high MOI which was similar to previous study as shown in Figure 5I (Tekes et al., 2008).

4. Discussion

The emergence of FIPV poses a serious global threat to cat health. Consequently, research is required to improve our understanding of the biology and pathogenesis of this virus, and this should provide a basis for the development of intervention strategies. Currently, there is no definitive test to diagnose FIP. Although antibody levels or titers of coronaviruses can be measured, they cannot clearly distinguish FECV from FIPV. A positive result simply means the cat has previously been exposed to coronavirus but not necessarily to FIPV. FCoV infection usually causes mild or asymptomatic infection in cats, but mutants with increased pathogenicity may emerge during infection (Chang et al., 2011; Kipar and Meli, 2014; Pedersen, 2014;

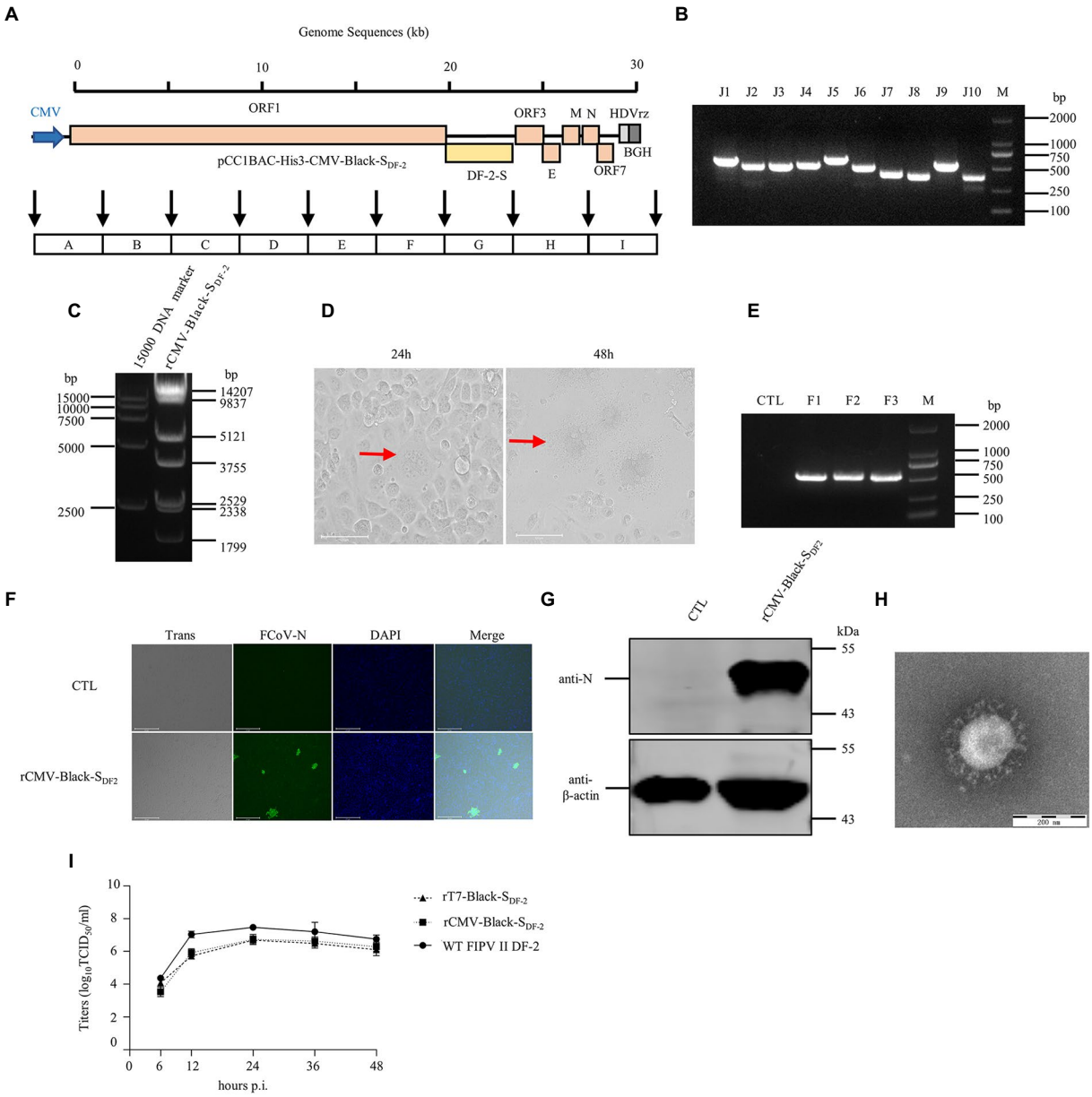

FIGURE 3
The recovery and identification of the chimeric FIPV strain Black-S$_{DF-2}$ driven by a CMV promoter. **(A)** Strategy diagram for the construction of pCC1BAC-His3-CMV-Black-S$_{DF-2}$. **(B)** Identification of fragment interfaces in bacteria. **(C)** Enzyme digestion of pCC1BAC-His3-CMV-Black-S$_{DF-2}$ plasmid (*Not*I and *Nhe*I). **(D)** Significant cytopathic effects (CPE) were observed at 24 and 48h after infection with CRFK cells. **(E)** PCR identification of the recombinant virus. **(F)** and **(G)** rCMV-Black-S$_{DF-2}$ virus infected CRFK cells for 12h was identified by IFA (Scale Bar, 275μm) and WB. **(H)** Electron microscopy examination of the purified virus. **(I)** Growth kinetics of rT7-Black-S$_{DF-2}$, rCMV-Black-S$_{DF-2}$, and WT FIPV II DF-2 after infection of CRFK cells at an MOI of 0.01. wt, wild type.

Tekes and Thiel, 2016). It is estimated that FIPV conversion occurs in about 5% of cats persistently infected with FECV (Chang et al., 2011; Felten and Hartmann, 2019). FIPV is thought to be a mutation of FECV that is prevalent in individual cats (Vennema et al., 1998). However, the nature of the mutation that results in the switch from FECV to FIPV is currently unknown (Kipar and Meli, 2014). To address this core problem, a reverse genetics system for both highly and weakly virulent FCoV is urgently needed.

The yeast-based TAR system has been used to construct coronaviruses (Thao et al., 2020). The system could further improve because the large quantities of yeast extraction is costly and complex, it also requires *in vitro* transcription, and the effect of RNA electrotransfer is not as good as that of DNA transfection. In this study, we assembled infective cDNA clones of FCoV using a pCC1BAC-His3 vector and amplified them through a copy-controlled system in *E. coli*. In addition, T7 promoter was replaced by CMV promoter which does not require *in vitro* transcription, and thus the experimental process is short and convenient. Consistent with previous reports, without the need for tedious cloning processes, the construction of infective cDNA of FCoV could be completed in 1 week.

Type I FCoV causes about 80% of the natural infections of cats worldwide, while the other 20% are due to type II FCoV. To

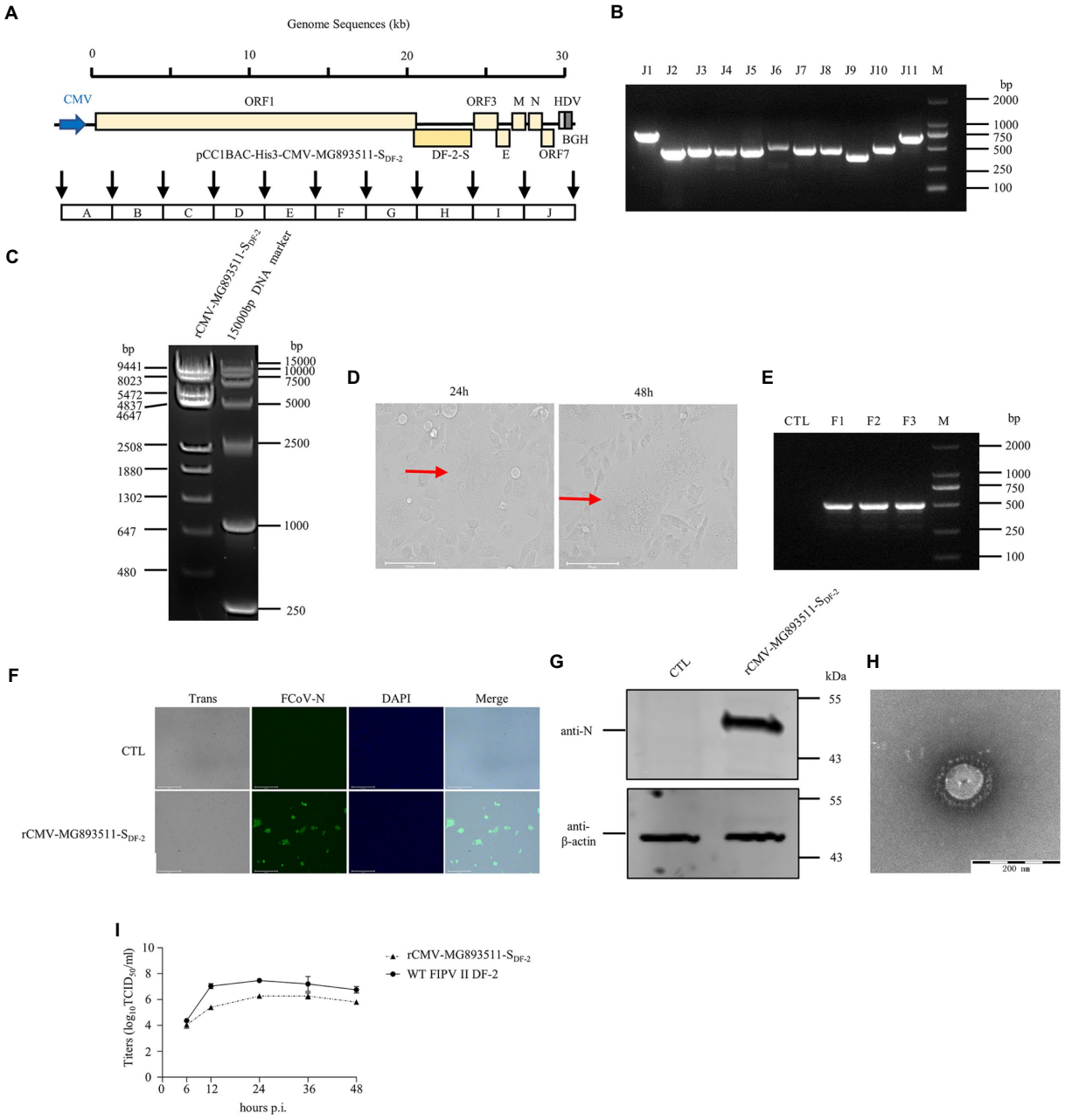

FIGURE 4
The recovery and identification of the chimeric FECV strain of MG893511-S$_{DF-2}$. **(A)** Strategy diagram for the construction of pCC1BAC-His3-CMV-Black-S$_{DF-2}$. **(B)** Identification of fragment interfaces of the plasmids recovered from bacteria. **(C)** Enzyme digestion of pCC1BAC-His3-CMV-MG893511-S$_{DF-2}$ plasmid (*Bgl*II). **(D)** Significant cytopathic effects (CPE) were observed at 24 and 48h after infection with CRFK cells. **(E)** PCR identification of the rescued recombinant FCoV virus. **(F)** and **(G)** rCMV-MG893511-S$_{DF-2}$ virus infected CRFK cells for 12h was identified by IFA (Scale Bar, 275μm) and WB. **(H)** Electron microscopy of the purified virus. **(I)** Growth kinetics of rCMV-MG893511-S$_{DF-2}$ and WT FIPV II DF-2 after infection of CRFK cells at an MOI of 0.01. wt, wild type.

date, most research on FCoV has focused on type II viruses, mainly because they can be easily grown in cell culture compared to type I FCoV. Here, a culture-adapted type I Black strain was also rescued through this system. The type I Black strain is one of the few strains that can grow in cells. Although we have not introduced Black strain successfully due to the COVID-19 epidemic, but the recombinant FIPV Black with wild type S protein in our study displayed growth characteristics similar to previous study (Tekes et al., 2008). The successful establishment of reverse genetics of this strain based on our TAR system will further facilitate the study of the pathogenesis of type I FCoV. In addition, the S gene used in the previous reverse genetic systems was derived from the type II strain 79–1,146. The author found that substituting S gene of this strain could not induce biotype conversion of avirulent viruses to pathogenic ones. Therefore, it will be interesting to evaluate the pathogenesis of a virus carrying a S gene from a different type II FIPV, for example, the viruses carrying S gene of DF II strain rescued in this study.

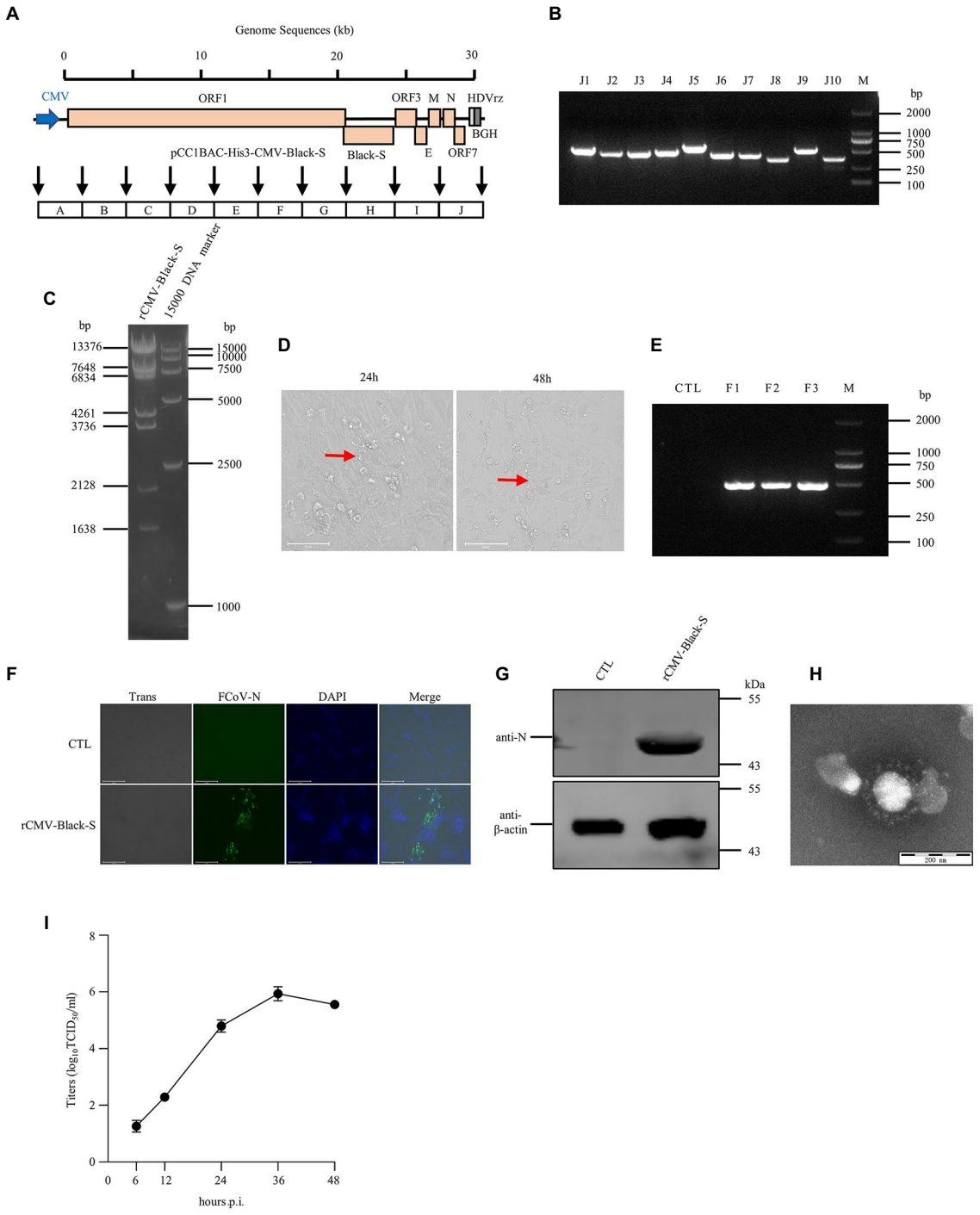

FIGURE 5
The recovery and identification of culture-adapted wild-type I FIPV Black strain. **(A)** Strategy diagram for the construction of pCC1BAC-His3-CMV-Black-S. **(B)** Identification of fragment interfaces of the plasmid recovered from bacteria. **(C)** Restriction enzyme digestion of the positive plasmid (*Nco*I) purified from *E. coli*. **(D)** Significant cytopathic effects (CPE) were observed at 24 and 48h after infection with FCWF-4 cells. **(E)** PCR identification of the rescued virus. **(F)** and **(G)** rCMV-Black-S virus infected FCWF-4 cells for 12h was identified by IFA (Scale Bar, 275μm) and WB. Electron microscopy of the purified virus. **(H)** Electron microscopy examination of the purified virus. **(I)** Growth curve of rescued rCMV-Black-S virus on FCWF-4 cells with original MOI of 0.1.

The ability to systematically exchange genome fragments from FECV with matching fragments from FIPV, as described in this study, will enable mapping of the genetic changes required to convert a FECV biotype into a FIPV biotype. Such a reverse genetic system would be helpful not only in the study of culture-adapted coronaviruses but also in that of wild-type I coronaviruses, for which there are currently no suitable cell culture systems. In conclusion, the virulent and attenuated full-length cDNA clones of FCoV described here provide a powerful tool for studying the transmission and pathogenesis of FCoV, and evaluating FIP vaccines and therapeutics.

Data availability statement

The original contributions presented in the study are included in the article/Supplementary material, further inquiries can be directed to the corresponding authors.

Author contributions

HK and HJ: conceptualization. HC and HG: investigation. HK and HC: original draft preparation. HK and HJ: review and editing. All authors have read and agreed to publish the version of manuscript. Author order was determined based on workload.

Acknowledgments

The authors thank Vladimir Larionov at Laboratory of Biosystems and Cancer, National Cancer Institute, Bethesda, Maryland, 20892, USA for providing *Saccharomyces cerevisiae* VL6-48 N.

Conflict of interest

The authors declare that the research was conducted in the absence of any commercial or financial relationships that could be construed as a potential conflict of interest.

Publisher's note

Supplementary material

The Supplementary material for this article can be found online at: https://www.frontiersin.org/articles/10.3389/fmicb.2023.1141101/full#supplementary-material

References

Addie, D. D., and Jarrett, O. (1992). A study of naturally occurring feline coronavirus infections in kittens. *Vet. Rec.* 130, 133–137. doi: 10.1136/vr.130.7.133

Addie, D. D., Schaap, I. A. T., Nicolson, L., and Jarrett, O. (2003). Persistence and transmission of natural type I feline coronavirus infection. *J. Gen. Virol.* 84, 2735–2744. doi: 10.1099/vir.0.19129-0

Almazan, F., Gonzalez, J. M., Penzes, Z., Izeta, A., Calvo, E., Plana-Duran, J., et al. (2000). Engineering the largest RNA virus genome as an infectious bacterial artificial chromosome. *Proc. Natl. Acad. Sci. U. S. A.* 97, 5516–5521. doi: 10.1073/pnas.97.10.5516

Amer, A., Siti Suri, A., Abdul Rahman, O., Mohd, H. B., Faruku, B., Saeed, S., et al. (2012). Isolation and molecular characterization of type I and type II feline coronavirus in Malaysia. *Virol. J.* 9:278. doi: 10.1186/1743-422X-9-278

Balint, A., Farsang, A., Zadori, Z., and Belak, S. (2014). Comparative in vivo analysis of recombinant type II feline coronaviruses with truncated and completed ORF3 region. *PLoS One* 9:e88758. doi: 10.1371/journal.pone.0088758

Balint, A., Farsang, A., Zadori, Z., Hornyak, A., Dencso, L., Almazan, F., et al. (2012). Molecular characterization of feline infectious peritonitis virus strain DF-2 and studies of the role of ORF3abc in viral cell tropism. *J. Virol.* 86, 6258–6267. doi: 10.1128/JVI.00189-12

Bank-Wolf, B. R., Stallkamp, I., Wiese, S., Moritz, A., Tekes, G., and Thiel, H. J. (2014). Mutations of 3c and spike protein genes correlate with the occurrence of feline infectious peritonitis. *Vet. Microbiol.* 173, 177–188. doi: 10.1016/j.vetmic.2014.07.020

Benetka, V., Kubber-Heiss, A., Kolodziejek, J., Nowotny, N., Hofmann-Parisot, M., and Mostl, K. (2004). Prevalence of feline coronavirus types I and II in cats with histopathologically verified feline infectious peritonitis. *Vet. Microbiol.* 99, 31–42. doi: 10.1016/j.vetmic.2003.07.010

Black, J. W. (1980). Recovery and in vitro cultivation of a coronavirus from laboratory-induced cases of feline infectious peritonitis (FIP). *Vet. Med. Small Anim. Clin.* 75, 811–814. PMID: 6247809

Chang, H. W., Egberink, H. F., Halpin, R., Spiro, D. J., and Rottier, P. J. (2012). Spike protein fusion peptide and feline coronavirus virulence. *Emerg. Infect. Dis.* 18, 1089–1095. doi: 10.3201/eid1807.120143

Chang, H. W., Egberink, H. F., and Rottier, P. J. (2011). Sequence analysis of feline coronaviruses and the circulating virulent/avirulent theory. *Emerg. Infect. Dis.* 17, 744–746. doi: 10.3201/eid1706.102027

Drechsler, Y., Alcaraz, A., Bossong, F. J., Collisson, E. W., and Diniz, P. P. (2011). Feline coronavirus in multicat environments. *Vet. Clin. North Am. Small Anim. Pract.* 41, 1133–1169. doi: 10.1016/j.cvsm.2011.08.004

Driouich, J. S., Moureau, G., de Lamballerie, X., and Nougairede, A. (2019). Reverse genetics of RNA viruses: ISA-based approach to control viral population diversity without modifying virus phenotype. *Viruses* 11:666. doi: 10.3390/v11070666

Duarte, A., Veiga, I., and Tavares, L. (2009). Genetic diversity and phylogenetic analysis of feline coronavirus sequences from Portugal. *Vet. Microbiol.* 138, 163–168. doi: 10.1016/j.vetmic.2009.03.009

Dye, C., and Siddell, S. G. (2005). Genomic RNA sequence of feline coronavirus strain FIPV WSU-79/1146. *J. Gen. Virol.* 86, 2249–2253. doi: 10.1099/vir.0.80985-0

Ehmann, R., Kristen-Burmann, C., Bank-Wolf, B. R., Konig, M., Herden, C., Hain, T., et al. (2018). Reverse genetics for type I feline coronavirus field isolate to study the molecular pathogenesis of feline infectious peritonitis. *MBio* 9:e01422-18. doi: 10.1128/mBio.01422-18

Felten, S., and Hartmann, K. (2019). Diagnosis of feline infectious peritonitis: a review of the current literature. *Viruses* 11:1068 doi: 10.3390/v11111068

Gibson, D. G., Glass, J. I., Lartigue, C., Noskov, V. N., Chuang, R. Y., Algire, M. A., et al. (2010). Creation of a bacterial cell controlled by a chemically synthesized genome. *Science* 329, 52–56. doi: 10.1126/science.1190719

Herrewegh, A. A., Smeenk, I., Horzinek, M. C., Rottier, P. J., and de Groot, R. J. (1998). Feline coronavirus type II strains 79-1683 and 79-1146 originate from a double recombination between feline coronavirus type I and canine coronavirus. *J. Virol.* 72, 4508–4514. doi: 10.1128/JVI.72.5.4508-4514.1998

Herrewegh, A. A., Vennema, H., Horzinek, M. C., Rottier, P. J., and de Groot, R. J. (1995). The molecular genetics of feline coronaviruses: comparative sequence analysis of the ORF7a/7b transcription unit of different biotypes. *Virology* 212, 622–631. doi: 10.1006/viro.1995.1520

Hohdatsu, T., Okada, S., Ishizuka, Y., Yamada, H., and Koyama, H. (1992). The prevalence of types I and II feline coronavirus infections in cats. *J. Vet. Med. Sci.* 54, 557–562. doi: 10.1292/jvms.54.557

Kennedy, M., Boedeker, N., Gibbs, P., and Kania, S. (2001). Deletions in the 7a ORF of feline coronavirus associated with an epidemic of feline infectious peritonitis. *Vet. Microbiol.* 81, 227–234. doi: 10.1016/s0378-1135(01)00354-6

Kipar, A., and Meli, M. L. (2014). Feline infectious peritonitis: still an enigma? *Vet. Pathol.* 51, 505–526. doi: 10.1177/0300985814522077

Kouprina, N., Annab, L., Graves, J., Afshari, C., Barrett, J. C., Resnick, M. A., et al. (1998). Functional copies of a human gene can be directly isolated by transformation-associated recombination cloning with a small 3′ end target sequence. *Proc. Natl. Acad. Sci. U. S. A.* 95, 4469–4474. doi: 10.1073/pnas.95.8.4469

Kummrow, M., Meli, M. L., Haessig, M., Goenczi, E., Poland, A., Pedersen, N. C., et al. (2005). Feline coronavirus serotypes 1 and 2: seroprevalence and association with disease in Switzerland. *Clin. Diagn. Lab. Immunol.* 12, 1209–1215. doi: 10.1128/CDLI.12.10.1209-1215.2005

Lewis, C. S., Porter, E., Matthews, D., Kipar, A., Tasker, S., Helps, C. R., et al. (2015). Genotyping coronaviruses associated with feline infectious peritonitis. *J. Gen. Virol.* 96, 1358–1368. doi: 10.1099/vir.0.000084

Li, C., Liu, Q., Kong, F., Guo, D., Zhai, J., Su, M., et al. (2019). Circulation and genetic diversity of feline coronavirus type I and II from clinically healthy and FIP-suspected cats in China. *Transbound. Emerg. Dis.* 66, 763–775. doi: 10.1111/tbed.13081

Licitra, B. N., Millet, J. K., Regan, A. D., Hamilton, B. S., Rinaldi, V. D., Duhamel, G. E., et al. (2013). Mutation in spike protein cleavage site and pathogenesis of feline coronavirus. *Emerg. Infect. Dis.* 19, 1066–1073. doi: 10.3201/eid1907.121094

Lin, C. N., Su, B. L., Wang, C. H., Hsieh, M. W., Chueh, T. J., and Chueh, L. L. (2009). Genetic diversity and correlation with feline infectious peritonitis of feline coronavirus type I and II: a 5-year study in Taiwan. *Vet. Microbiol.* 136, 233–239. doi: 10.1016/j.vetmic.2008.11.010

Melade, J., Piorkowski, G., Touret, F., Fourie, T., Driouich, J. S., Cochin, M., et al. (2022). A simple reverse genetics method to generate recombinant coronaviruses. *EMBO Rep.* 23:e53820. doi: 10.15252/embr.202153820

Mohamed Ali, S., Vega-Rua, A., Driouich, J. S., de Lamballerie, X., Failloux, A. B., and Nougairede, A. (2018). Comparison of chikungunya viruses generated using infectious clone or the infectious subgenomic amplicons (ISA) method in Aedes mosquitoes. *PLoS One* 13:e0199494. doi: 10.1371/journal.pone.0199494

Noskov, V., Kouprina, N., Leem, S. H., Koriabine, M., Barrett, J. C., and Larionov, V. (2002). A genetic system for direct selection of gene-positive clones during recombinational cloning in yeast. *Nucleic Acids Res.* 30, 8e–88e. doi: 10.1093/nar/30.2.e8

Pedersen, N. C. (2009). A review of feline infectious peritonitis virus infection: 1963-2008. *J. Feline Med. Surg.* 11, 225–258. doi: 10.1016/j.jfms.2008.09.008

Pedersen, N. C. (2014). An update on feline infectious peritonitis: virology and immunopathogenesis. *Vet. J.* 201, 123–132. doi: 10.1016/j.tvjl.2014.04.017

Pedersen, N. C., Boyle, J. F., Floyd, K., Fudge, A., and Barker, J. (1981). An enteric coronavirus infection of cats and its relationship to feline infectious peritonitis. *Am. J. Vet. Res.* 42, 368–377.

Pedersen, N. C., Liu, H., Dodd, K. A., and Pesavento, P. A. (2009). Significance of coronavirus mutants in feces and diseased tissues of cats suffering from feline infectious peritonitis. *Viruses* 1, 166–184. doi: 10.3390/v1020166

Pizzi, M. (1950). Sampling variation of the fifty percent end-point, determined by the reed-Muench (Behrens) method. *Hum. Biol.* 22, 151–190. PMID: 14778593

Shiba, N., Maeda, K., Kato, H., Mochizuki, M., and Iwata, H. (2007). Differentiation of feline coronavirus type I and II infections by virus neutralization test. *Vet. Microbiol.* 124, 348–352. doi: 10.1016/j.vetmic.2007.04.031

Tekes, G., Hofmann-Lehmann, R., Stallkamp, I., Thiel, V., and Thiel, H. J. (2008). Genome organization and reverse genetic analysis of a type I feline coronavirus. *J. Virol.* 82, 1851–1859. doi: 10.1128/JVI.02339-07

Tekes, G., and Thiel, H. J. (2016). Feline coronaviruses: pathogenesis of feline infectious peritonitis. *Adv. Virus Res.* 96, 193–218. doi: 10.1016/bs.aivir.2016.08.002

Terada, Y., Matsui, N., Noguchi, K., Kuwata, R., Shimoda, H., Soma, T., et al. (2014). Emergence of pathogenic coronaviruses in cats by homologous recombination between feline and canine coronaviruses. *PLoS One* 9:e106534. doi: 10.1371/journal.pone.0106534

Thao, T. N., Labroussaa, F., Ebert, N., V'Kovski, P., Stalder, H., Portmann, J., et al. (2020). Rapid reconstruction of SARS-CoV-2 using a synthetic genomics platform. *Nature* 582, 561–565. doi: 10.1038/s41586-020-2294-9

Thiel, V., and Siddell, S. G. (2005). Reverse genetics of coronaviruses using vaccinia virus vectors. *Curr. Top. Microbiol. Immunol.* 287, 199–227. doi: 10.1007/3-540-26765-4_7

Thiel, V., Thiel, H. J., and Tekes, G. (2014). Tackling feline infectious peritonitis via reverse genetics. *Bioengineered* 5, 396–400. doi: 10.4161/bioe.32133

Torii, S., Ono, C., Suzuki, R., Morioka, Y., Anzai, I., Fauzyah, Y., et al. (2021). Establishment of a reverse genetics system for SARS-CoV-2 using circular polymerase extension reaction. *Cell Rep.* 35:109014. doi: 10.1016/j.celrep.2021.109014

Vennema, H., Poland, A., Foley, J., and Pedersen, N. C. (1998). Feline infectious peritonitis viruses arise by mutation from endemic feline enteric coronaviruses. *Virology* 243, 150–157. doi: 10.1006/viro.1998.9045

Vogel, L., Van der Lubben, M., te Lintelo, E. G., Bekker, C. P., Geerts, T., Schuijff, L. S., et al. (2010). Pathogenic characteristics of persistent feline enteric coronavirus infection in cats. *Vet. Res.* 41:71. doi: 10.1051/vetres/2010043

Wach, A., Brachat, A., Pohlmann, R., and Philippsen, P. (1994). New heterologous modules for classical or PCR-based gene disruptions in Saccharomyces cerevisiae. *Yeast* 10, 1793–1808. doi: 10.1002/yea.320101310

Wang, G., Hu, G., Liang, R., Shi, J., Qiu, X., Yang, Y., et al. (2021). Establishment of full-length cDNA clones and an efficient Oral infection model for feline coronavirus in cats. *J. Virol.* 95:e0074521. doi: 10.1128/JVI.00745-21

Yount, B., Curtis, K. M., and Baric, R. S. (2000). Strategy for systematic assembly of large RNA and DNA genomes: transmissible gastroenteritis virus model. *J. Virol.* 74, 10600–10611. doi: 10.1128/jvi.74.22.10600-10611.2000

Ziebuhr, J., Snijder, E. J., and Gorbalenya, A. E. (2000). Virus-encoded proteinases and proteolytic processing in the Nidovirales. *J. Gen. Virol.* 81, 853–879. doi: 10.1099/0022-1317-81-4-853

frontiers | Frontiers in Microbiology

TYPE Original Research
PUBLISHED 29 March 2023
DOI 10.3389/fmicb.2023.1153106

OPEN ACCESS

EDITED BY
Hongliang Chai,
Northeast Forestry University,
China

REVIEWED BY
Yutian Zou,
Sun Yat-sen University Cancer Center (SYSUCC),
China
Yunfeng Wang,
Université Paris-Saclay,
France

*CORRESPONDENCE
Andras Hajdu
✉ hajdu.andras@inf.unideb.hu
Ling Zhang
✉ topgun1128@163.com

†These authors have contributed equally to this work

SPECIALTY SECTION
This article was submitted to Virology, a section of the journal Frontiers in Microbiology

RECEIVED 28 January 2023
ACCEPTED 27 February 2023
PUBLISHED 29 March 2023

CITATION
Liu Y, Zhou S, Wang L, Xu M, Huang X, Li Z, Hajdu A and Zhang L (2023) Machine learning approach combined with causal relationship inferring unlocks the shared pathomechanism between COVID-19 and acute myocardial infarction.
Front. Microbiol. 14:1153106.
doi: 10.3389/fmicb.2023.1153106

Machine learning approach combined with causal relationship inferring unlocks the shared pathomechanism between COVID-19 and acute myocardial infarction

Ying Liu[1†], Shujing Zhou[2,3†], Longbin Wang[4†], Ming Xu[4], Xufeng Huang[2,3], Zhengrui Li[5,6,7,8,9,10], Andras Hajdu[2*] and Ling Zhang[5,6,7,8,9,10*]

[1]Department of Cardiology, Sixth Medical Center, PLA General Hospital, Beijing, China, [2]Department of Data Science and Visualization, Faculty of Informatics, University of Debrecen, Debrecen, Hungary, [3]Faculty of Medicine, University of Debrecen, Debrecen, Hungary, [4]Department of Clinical Veterinary Medicine, Huazhong Agricultural University, Wuhan, China, [5]Department of Oral and Maxillofacial-Head and Neck Oncology, Shanghai Ninth People's Hospital, Shanghai Jiao Tong University School of Medicine, Shanghai, China, [6]College of Stomatology, Shanghai Jiao Tong University, Shanghai, China, [7]National Center for Stomatology, Shanghai, China, [8]National Clinical Research Center for Oral Diseases, Shanghai, China, [9]Shanghai Key Laboratory of Stomatology, Shanghai, China, [10]Shanghai Research Institute of Stomatology, Shanghai, China

Background: Increasing evidence suggests that people with Coronavirus Disease 2019 (COVID-19) have a much higher prevalence of Acute Myocardial Infarction (AMI) than the general population. However, the underlying mechanism is not yet comprehended. Therefore, our study aims to explore the potential secret behind this complication.

Materials and methods: The gene expression profiles of COVID-19 and AMI were acquired from the Gene Expression Omnibus (GEO) database. After identifying the differentially expressed genes (DEGs) shared by COVID-19 and AMI, we conducted a series of bioinformatics analytics to enhance our understanding of this issue.

Results: Overall, 61 common DEGs were filtered out, based on which we established a powerful diagnostic predictor through 20 mainstream machine-learning algorithms, by utilizing which we could estimate if there is any risk in a specific COVID-19 patient to develop AMI. Moreover, we explored their shared implications of immunology. Most remarkably, through the Bayesian network, we inferred the causal relationships of the essential biological processes through which the underlying mechanism of co-pathogenesis between COVID-19 and AMI was identified.

Conclusion: For the first time, the approach of causal relationship inferring was applied to analyzing shared pathomechanism between two relevant diseases, COVID-19 and AMI. Our findings showcase a novel mechanistic insight into COVID-19 and AMI, which may benefit future preventive, personalized, and precision medicine.

KEYWORDS

COVID-19, acute myocardial infarction, diagnostic biomarkers, machine learning, causal relationship, bioinformatics

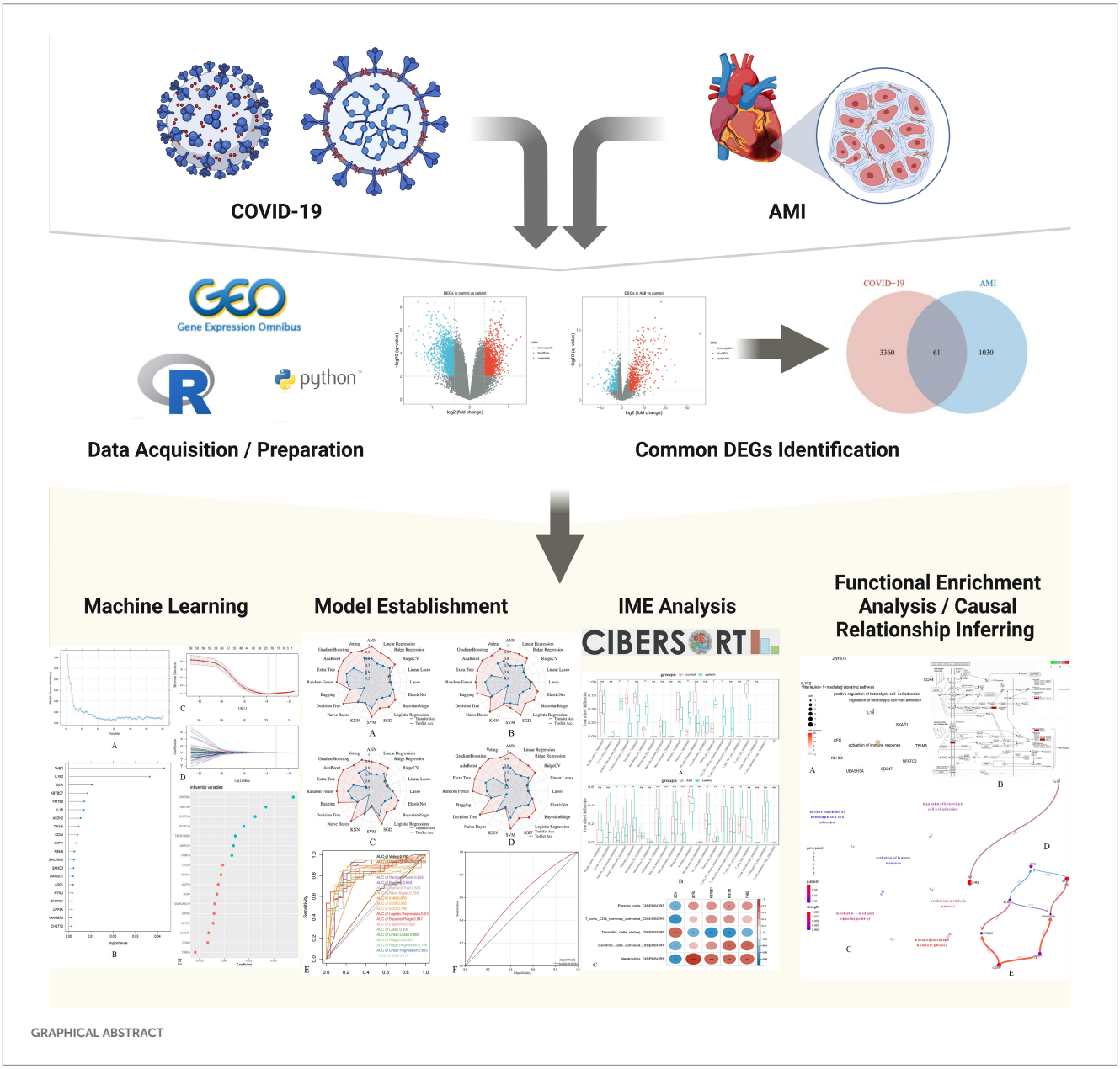

GRAPHICAL ABSTRACT

Introduction

The emergence of the novel coronavirus 2019 (COVID-19) has triggered a global pandemic and posed unprecedented pressure on healthcare systems worldwide (Haldane et al., 2021; Lal et al., 2021). Today, it is well-realized that the severe acute respiratory syndrome coronavirus 2 (SARS-CoV-2) is the pathogen virus that causes COVID-19 and can further worsen it into severe lower respiratory tract infections in many mammals. Recently, many studies have pointed out that since the main target of the SARS-CoV-2 virus is the ACE receptor, a broadly existing surface receptor on diverse cell types across the whole human body, patients with COVID-19 infection are seemingly at a much higher risk of various life-threatening disease onset, such as cardiomyopathy, neuropathy, etc. (Kuderer et al., 2020; Lee et al., 2020; Rugge et al., 2020; Grivas et al., 2021; Li F. et al., 2021; Safiabadi Tali et al., 2021). However, although increasing evidence has shown that COVID-19 patients have an increased risk of sudden heart attacks, its connections with acute myocardial infarction (AMI) have not yet been identified to date. In fact, myocardial infarction, a heart muscle's inability to receive enough oxygen and nutrients due to sudden blockage of the arteries, is one of the significant invisible hands of such heart diseases (Roth et al., 2017; Tsao et al., 2022). Statistically speaking, it is estimated that up to 8.3% of COVID-19-infected individuals may develop acute myocardial infarction, which is more than twice the incidence in the general population (Kumar et al., 2021; Toscano et al., 2021). Given the potential risk of AMI onset in the COVID-19-positive population, understanding such mechanisms is crucial. Hence, we investigated the shared pathomechanism between COVID-19 and AMI in the present study. We obtained gene expression profiles from the Gene Expression Omnibus (GEO). Having identified differentially expressed genes (DEGs) shared by COVID-19 and AMI, we performed a series of

bioinformatics analyses to enhance the current understanding of this issue. We even developed a strong AMI diagnostic predictor for COVID-19-positive patients. From this end, we first attempted to identify the in-depth causal relationship between the two diseases based on their shared pathomechanism. As a result, our findings may provide further insight into future research and clinical practice regarding COVID-19 and AMI.

The general design of the present study is visualized in Graphical abstract.

Materials and methods

Data acquisition, preparation, and statistic management

GEO[1] is an extensive gene expression database for various diseases that is freely available in the public domain. For COVID-19, we used the GSE164805 for analytics (Zhang et al., 2021). For AMI, we integrated GSE29111, GSE60993, GSE109048, GSE29532, GSE19339, GSE48060, GSE66360, and GSE97320 as a merged dataset (Silbiger et al., 2013; Suresh et al., 2014; Park et al., 2015; Muse et al., 2017; Gobbi et al., 2019). The normalization and calibration were done through the "normalizeBetweenArrays" function of the R package, "limma," for both COVID-19 and AMI datasets (Supplementary Data S1). The analyses above were conducted by different R software packages and the integrative Python package "sklearn" (Pedregosa et al., 2011). If not specifically mentioned, the statistic test used in the analytics is the Wilcoxon rank sum test. Notably, within some figures, *, **, and *** may occur, indicative of a p-value < 0.05, 0.01, and 0.001, respectively.

Identification of common DEGs between COVID-19 and AMI

In the present study, differential expression analysis was performed using the R package, "limma" (Ritchie et al., 2015). To avoid omission, DEGs were screened at a threshold of p-value < 0.05 and Log2 |fold change| > 1.00. After screening out the DEGs for COVID-19 and AMI, we crossed them to find common DEGs.

Machine learning

The selection of feature genes to build the diagnostic predictor is crucial. In the present study, we first used the "RFE" algorithm to determine the ideal number of genes for formal modeling. Then we combined the linear algorithm, "LASSO," with the non-linear algorithm, "Random Forest," to narrow the list of potential genes of interest. As a result, the selected feature genes would be processed to construct the formal model (i.e., the AMI diagnostic predictor for COVID-19 patients).

For formal modeling, the whole AMI merged dataset was randomized and then separated into a training set and a test set at a ratio of 7.5:2.5. According to the "no-free-lunch" theorem, if one machine learning algorithm outperforms the others on a specific assessment, it should sacrifice certain points on the other assessment measurements (Wolpert and Macready, 1997). In short, nothing is perfect. However, through the exhaustive try-in of the mainstream machine learning algorithms and elucidation of different algorithms, we were able to choose the best one in general. Therefore, in the present study, 20 machine-learning algorithms, including Linear Regression, Ridge Regression, RidgeCV, Linear LASSO, LASSO, ElasticNet, BayesianRidge, Logistic Regression, SGD, SVM, KNN, Naive Bayes, Decision Tree, Bagging, Random Forest, Extra Tree, AdaBoost, GradientBoosting, Voting, and ANN, were compared and evaluated.

Decision curve analysis

Usually, clinical models are absolutely and mathematically evaluated by the values of ROC-AUC, Accuracy, Precision, Recall, and F1-score without considering clinical outcomes. To overcome this disadvantage, Decision curve analysis (DCA) is used to compare the clinical benefits gained by employing different diagnostic predictors (Vickers and Elkin, 2006; Vickers et al., 2019). The more superior the curve localizes, the better prediction it outputs from the clinical aspect.

Analysis of the immune microenvironment

CIBERSORT[2] was used to assess the abundance of various infiltrating immune cells (Chen et al., 2018; Craven et al., 2021). Overall, 22 immune cell types were quantified. Correlation analysis between the immune cell types and GLS and SLC31A1 was done by the Pearson method. The visualization was created by the R package "ggplot2."

Functional enrichment analysis

Functional enrichment analysis included Gene Ontology (GO) terms and Kyoto Encyclopedia of Genes and Genomes (KEGG) pathways. The R package, "clusterprofiler" was used to carry out the functional enrichment analysis based on the common DEGs (Wu et al., 2021). The borderline criteria for selecting top enriched GO terms and KEGG pathways was with a significant adjusted p-value < 0.05.

Causal relationship inferring

When studying gene expression profiling, inferring gene regulatory networks' causality is crucial for investigating underlying molecular mechanisms. Herein, based on functional enrichment,

1 www.ncbi.nlm.nih.gov/geo

2 https://cibersort.stanford.edu/

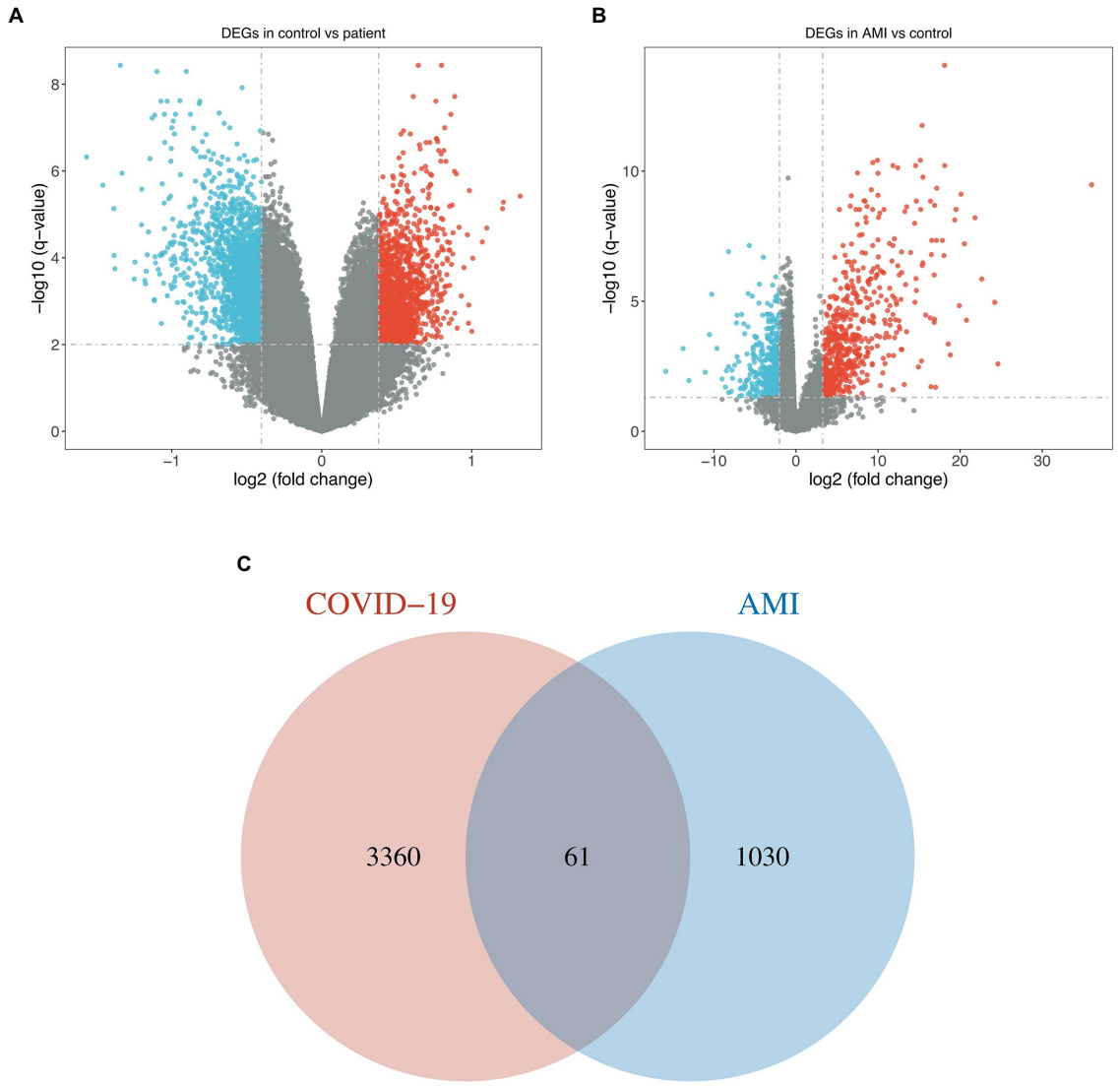

FIGURE 1
Identification of common DEGs between COVID-19 and AMI. **(A,B)** Volcano plots demonstrated the upregulated and downregulated DEGs of the COVID-19 dataset and merged AMI dataset. **(C)** Venn diagram shows the 61 common DEGs.

we leveraged an advanced AI-essential R package, "CBNplot" to uncover the hidden secrets between COVID-19 and AMI (Sato et al., 2022).

Results

Identification of common DEGs between COVID-19 and AMI

For the GSE164805 dataset, 3,421 DEGs were found, among which there were 1,527 genes upregulated and 1,894 genes downregulated (Figure 1A). For the merged AMI dataset, we identified 1,091 DEGs, including 483 upregulated genes and 608 downregulated genes (Figure 1B). By taking the intersection of DEGs of the GSE164805 dataset and the merged AMI dataset, there were 61 common DEGs found, which were visualized by Venn diagrams (Figure 1C; Supplementary Figure S1).

Pre-modeling: Integrative approach for feature genes selection

Since the mathematical relationship between the predictors and the outcome was unknown, we combined both linear (i.e., LASSO) and non-linear (i.e., Random Forest) methods to filter out the most promising genes for formal modeling after determining the ideal number of genes that the RFE algorithm should use. As a result, 5 genes were believed to be the best option since, after this point, the RMSE-value fluctuated on a tiny scale, suggesting only little changes in the predictive powerfulness occurred (Figure 2A). On the other hand, the Random Forest algorithm ranked the importance of each top 20 genes, in which

10.3389/fmicb.2023.1153106

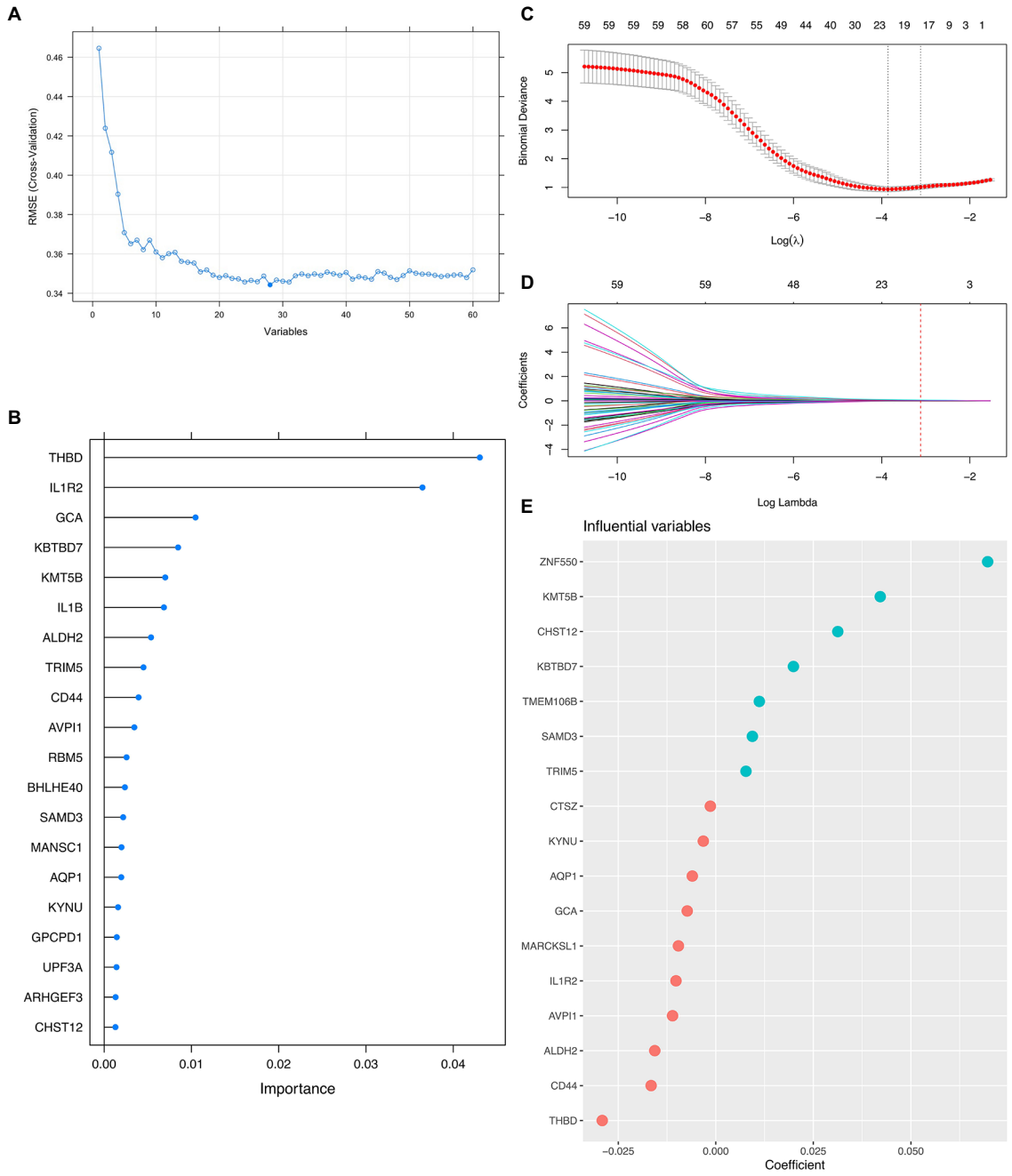

FIGURE 2
Integrative Approach for Feature Genes Selection. **(A)** Scree plot demonstrating the fluctuation of the RMSE value against the number of variants (i.e., feature genes) involved in formal modeling. **(B)** Lollipop plot shows each top 20 feature gene's importance by the Random Forest algorithm. **(C,D)** Dot plots and curves demonstrate the binormal deviance changes and coefficient allocation process against the value of Log Lambda, respectively. **(E)** Bubble plot showing the importance of each top 20 feature genes by LASSO.

THBD, IL1R2, GCA, KBTBD7, and KMT5B were the uppermost (Figure 2B). Furthermore, the LASSO narrowed down the binormal deviance to the minimum (Figure 2C) and allocated a coefficient to each gene (Figure 2D), also showing the top 20 most weighted genes (Figure 2E). After that, we selected the overlapping genes from the top 20 genes given by the Random Forest algorithm and the LASSO for formal modeling.

Formal modeling: Establishing an AMI diagnostic predictor for COVID-19 patients

Herein, we attempted 20 different machine learning methods currently under service in the field so that the data, in terms of the predictive performance and property, could be fit as optimally as possible. Consequently, Extra Tree exerted the maximum performance

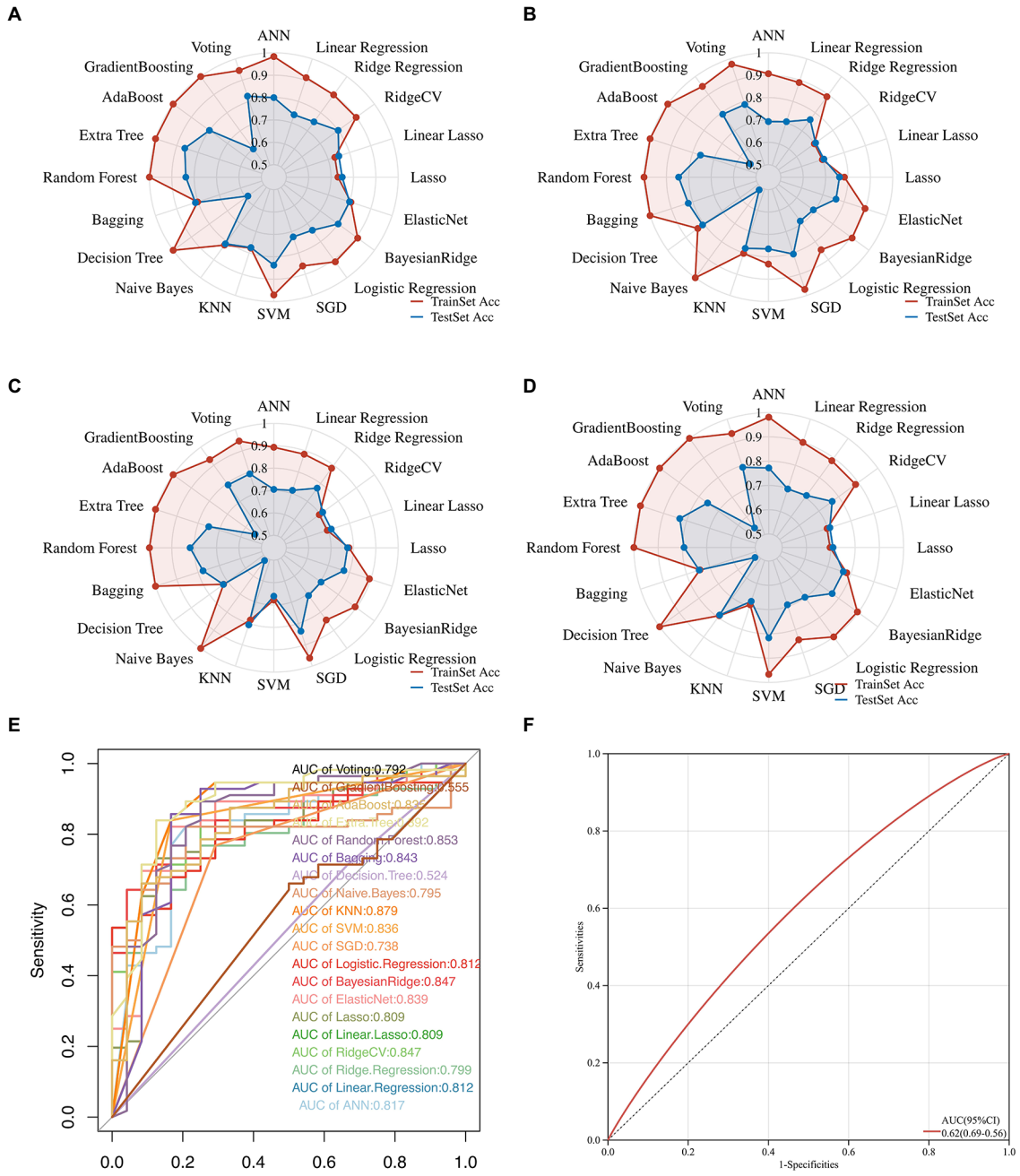

FIGURE 3
Multifaceted evaluation of 20 mainstream machine-learning diagnostic predictors. **(A–D)** The Radar plot demonstrates accuracy, recall, and F1-score measurement in the train and test sets, respectively. **(E)** Receiver Operative Curve (ROC), in which each predictor's Area Under Curve (AUC) value was compared. Generally, an AUC value over 0.7 was considered a good predictive performance. **(F)** ROC of the cardiac troponin.

regarding the Accuracy, Precision, Recall, and F1-score, followed immediately by Random Forest, and then SVM (Figures 3A–D; Supplementary Figure S2). In addition, the value of ROC-AUC of Extra Tree was the highest among the candidates, up to 0.892 in the test dataset (Figure 3E). Meanwhile, cardiac troponin, a gold standard biomarker for AMI, only possessed a ROC-AUC value of 0.62. Therefore, it was deemed that the Extra Tree algorithm was much superior (Figure 3F).

Exploration of the feature genes' implications in immunology

With the help of the CIBERSORT platform, it was observed that in COVID-19-positive patients, Plasma Cells, Activated CD4 Memory T Cells, CD8 T Cells, both Activated and Resting Dendritic Cells, M0 Macrophages, and Neutrophils were statistically different from that in COVID-19-negative patients (Figure 4A). Interestingly, besides

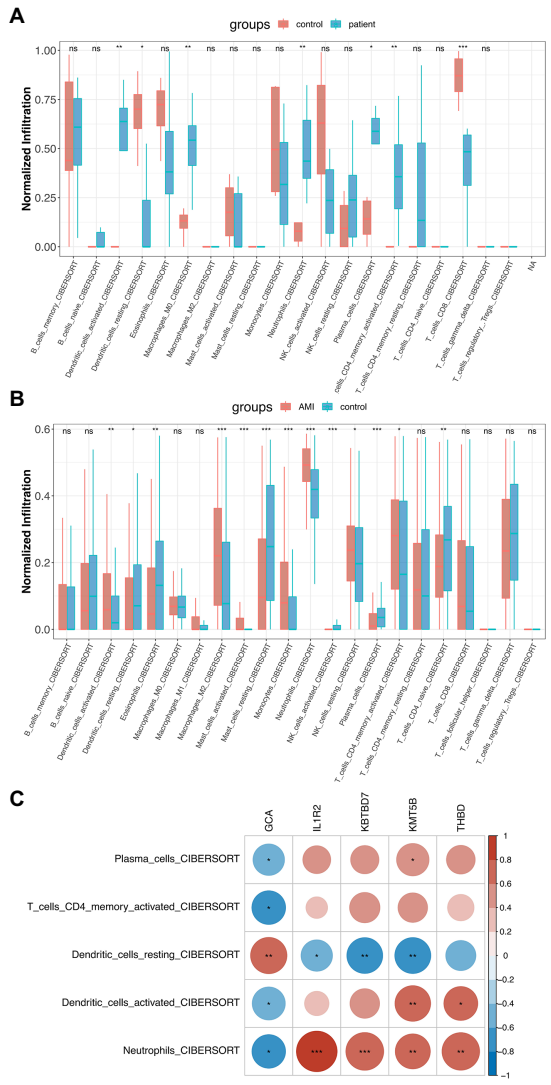

FIGURE 4
Immunological implications of the feature genes. **(A)** Comparison of infiltrating immune cells in patients who were COVID-19-positive and-negative. **(B)** Comparison of infiltrating immune cells in patients with AMI and healthy controls. **(C)** Correlation analysis of feature genes and the 5 shared differentially regulated immune cells.

Resting Dendritic Cells, CD8 T Cells were less abundant in COVID-19-positive patients. For AMI, Plasma Cells, Activated CD4 Memory T Cells, CD4 Naïve Cells, both Activated and Resting Dendritic Cells, both Activated and Resting Mast Cells, both Activated and Resting NK Cells, Macrophage M2, Eosinophils, and Neutrophils were statistically different from that in healthy controls (Figure 4B). Then, the 5 shared differentially regulated immune cells (i.e., Plasma Cells, Activated CD4 Memory T Cells, both Activated and Resting Dendritic Cells, and Neutrophils) were screened out. They underwent a correlation analysis with the feature genes (Figure 4C). Subsequently, it was found that the GCA gene was statistically associated with all 5 shared differentially regulated immune cells, and Neutrophils were statistically associated with all the feature genes. However, except for Resting Dendritic Cells, the GCA gene was negatively correlated with the other shared differentially regulated immune cells, hindering it might serve as an inhibitor in the immune system activation in the shared pathomechanism of COVID-19 and AMI.

Functional enrichment analysis and causal relationship inferring

First, a traditional functional enrichment analysis was performed, in which we identified 6 statistically significant GO terms and 1 KEGG pathway. The enriched GO terms included "hyaluronan metabolic process," "interleukin-1-mediated signaling pathway," "regulation of heterotypic cell–cell adhesion," "activation of immune response," and "positive regulation of heterotypic cell–cell adhesion" (Figure 5A). The KEGG pathway was "Fluid shear stress and atherosclerosis" from which the more precise subpathway was "Atherogenesis" (Figure 5B). Then, we employed the R package "CBNplot" to infer the causal relationships between them, the results of which could be verified through probabilistic inferring and classification according to the explanation of Sato et al. (Figure 5C). Herein, we found that "activation of immune response" served as a core within the interactive network and exhibited the most robust causal relationship with the "interleukin-1-mediated signaling pathway," indicative of their significance in the co-pathogenesis of COVID-19 and AMI. The direction was from "activation of immune response" to "interleukin-1-mediated signaling pathway." The details are visualized in Figures 5D,E. By observing the genes involved and the directions of the vectors, it was thought that IL1B seemingly played the most critical role.

Discussion

Cardiovascular disease is an essential cause of the global burden of death, far exceeding cancer. Most of these deaths were due to acute myocardial infarction (AMI; Roth et al., 2017; Tsao et al., 2022). At the same time, with the gradual severity of the epidemic, like similar epidemic diseases, COVID-19 has also brought more adverse complications (Anastasiou et al., 2012; Del Sole et al., 2020; Li et al., 2020, 2022; Lippi et al., 2020; Li X. et al., 2021; Ramphul et al., 2021a,b; Chai et al., 2022). Accumulating evidence shows that the prevalence of AMI in COVID-19 patients is much higher than that in the uninfected population (Kumar et al., 2021; Toscano et al., 2021). This compels us to look for the mechanisms underlying the interaction between these two diseases and to explore the potential behind this complication. As a result, we found potential drug targets for COVID-19 and its related AMI, leaving a theoretical basis for diagnosing and treating related diseases.

We obtained gene expression data for COVID-19 and AMI from the GEO database. On this basis, 61 shared differentially expressed genes (DEGs) were screened out, and a series of systematic and bioinformatics analyzes were performed. We also developed a robust predictor from 20 mainstream machine-learning algorithms to estimate the risk of AMI in COVID-19 patients. Most notably, we infer causal relationships among the most important biological processes through Bayesian networks. Through these processes, we identified mechanisms underlying the co-pathogenesis of COVID-19 and AMI.

Among all DEGs, THBD, IL1R2, GCA, KBTBD7, and KMT5B were found to be most important in the LASSO and the Random

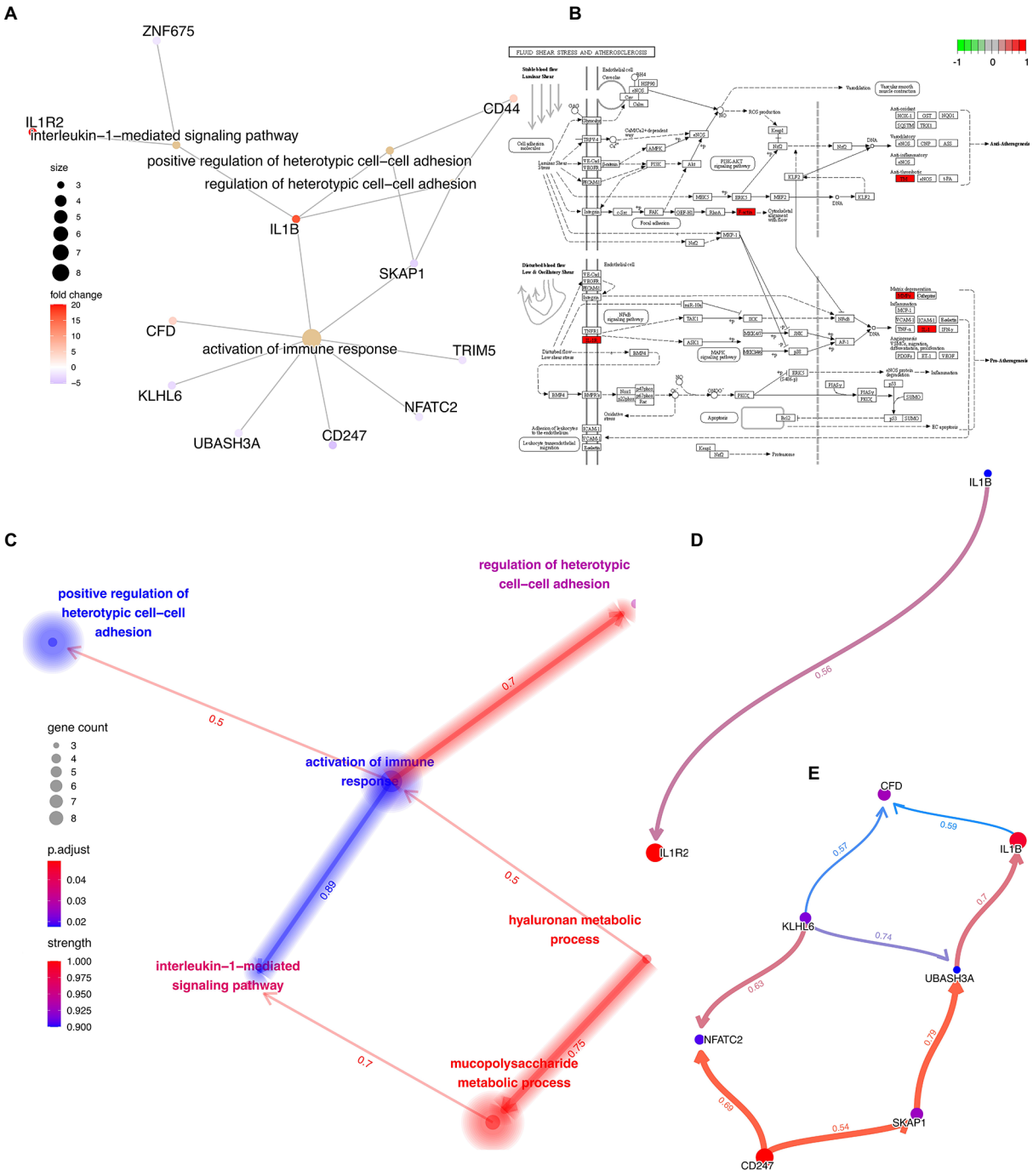

FIGURE 5
Functional Enrichment Analysis and Causal Relationship Inferring. **(A)** Interactive network demonstrating the interactions between the feature genes and the enriched GO terms and KEGG pathways. **(B)** Detailed KEGG pathway, "Fluid shear stress and atherosclerosis," activated genes are marked in red. **(C)** Interactive network demonstrating the interactions between the different GO terms and KEGG pathways with directions. The directions of the arrows indicate the causal relationship. **(D,E)** Complex causal relationship inferred within the enriched GO terms, "activation of immune response" and "interleukin-1-mediated signaling pathway."

Forest algorithm. THBD and its encoded thrombomodulin play an important role in forming venous thrombosis and vascular inflammation (Ireland et al., 1997; Doggen et al., 1998; Anastasiou et al., 2012). They also have unique roles in other non-thrombotic cardiovascular diseases such as AMI. Zhao et al. have reasoned that IL1R2 is a common marker gene of myocardial infarction, especially closely related to immune infiltration in AMI patients (Zhao et al., 2020). GCA drives coronary ischemia and promotes the development of immune cell arterial inflammation (Akiyama et al., 2021). KBTBD7 is now one of the most promising targets in the AMI. The researchers targeted and regulated KBTBD7 through various measures to inhibit inflammation, cardiac dysfunction, and maladaptive remodeling after

myocardial infarction with weak downstream p28 and NF-κB signaling. One example of such a complex network is the work of Yang et al. in 2018, in which they found that MiR-21 suppressed AMI by targeting KBTBD7 and controlling p38 and NF-κB signaling pathways (Qian et al., 2011; Liu et al., 2015; Yang et al., 2015). Interestingly, KMT5B is considered in traditional biological science to be a key gene regulating stem cell and neurological development (Chen et al., 2022; Hulen et al., 2022). Only recently has it been discovered that it plays a vital role in vascular endothelial cell inflammation and angiogenesis (Guo et al., 2015). The above-mentioned key DEGs reveal the disease characteristics of AMI caused by COVID-19 to a certain extent. They may prove that COVID-19 can induce thrombosis and even AMI formation through vascular inflammation triggered by cell inflammation.

Inspired by the latest advancement in artificial intelligence, we traversed 20 mainstream machine learning algorithms to fit the data and improve performance (Wolpert and Macready, 1997; Xie et al., 2023). We found that Extra Tree had the highest predictive performance. For further validation, we compared it to cardiac troponin, a recognized gold standard biomarker for AMI. Interestingly, we found that the predictive power of Extra Tree (AUC = 0.892) was much higher than that of cardiac markers such as cardiac troponin (AUC = 0.62). This indicates that the Extra Tree predictor has a very high accuracy for AMI diagnosis in COVID-19 patients, posing a challenge to traditional biomarkers and inspiring us to mine out more potential but promising novel biomarkers in the future.

In addition, we explored the immunological association between these two diseases. We found that the highly active immune cells were nearly identical in both diseases. Plasma Cells, Activated CD4 Memory T Cells, Activated and Resting Dendritic Cells, and Neutrophils are key secretory cells of cellular immune factors. It is believed that the excessive inflammatory response and cytokine storm induced by the virus can lead to myocardial injury, which may be one of the key factors in the occurrence of AMI after COVID-19.

The highly active "activated immune response" and "interleukin-1-mediated signaling pathway" verified our previous findings to a certain extent. Both DEGs and immunoassays confirmed that the disease of COVID-19 and AMI is immune-focused and can even be specific to the activation of IL1-related immune pathways. In the post-coronavirus epidemic era or the long coronavirus era, we can start from this immune pathway to explore the key damage pathways of COVID-19 in the circulatory system and then find new preventive measures.

A limitation of this study is that we could not model COVID-19 and AMI disease in animals due to the level of laboratory safety required by COVID-19. However, as an exploratory pioneer study, for the first time in history, we have applied a causal inference approach to studying the shared pathogenesis of COVID-19 and AMI. Our findings demonstrate novel mechanistic insights into COVID-19 and AMI that may aid future prevention, personalized and precision medicine.

Data availability statement

The original contributions presented in the study are included in the article/Supplementary material, further inquiries can be directed to the corresponding authors.

Author contributions

YL and SZ: conceptualization and methodology. YL, SZ, LW, MX, XH, and AH: software and validation. YL, SZ, AH, and ZL: formal analysis and writing - original draft preparation. LW, MX, and XH: data curation. AH, ZL, and LZ: supervision, funding acquisition and writing - review and editing. SZ, XH, AH, and ZL: visualization. XH and LZ: project administration. All authors have read and agreed to the published version of the manuscript.

Funding

The work was supported by the National Natural Science Foundation of China (81771127), the Seed Foundation of the Ninth People's Hospital, Shanghai Jiao Tong University School of Medicine (JYZZ196), and by the project TKP2021-NKTA-34, implemented with the support provided by the National Research, Development, and Innovation Fund of Hungary under the TKP2021-NKTA funding scheme.

Acknowledgments

We want to express our deep gratitude to the public databases, including GEO, TCGA, GeneCards, OMIM, HPA, CTD, Swiss, and more, for providing open-accessible and high-quality research resources. We also sincerely thank the National Natural Science Foundation of China and the Seed Foundation of the Ninth People's Hospital, Shanghai Jiao Tong University School of Medicine for their generosity to financialize the present study.

Conflict of interest

The authors declare that the research was conducted in the absence of any commercial or financial relationships that could be construed as a potential conflict of interest.

Publisher's note

Supplementary material

The Supplementary material for this article can be found online at: https://www.frontiersin.org/articles/10.3389/fmicb.2023.1153106/full#supplementary-material

References

Akiyama, M., Ohtsuki, S., Berry, G. J., Liang, D. H., Goronzy, J. J., and Weyand, C. M. (2021). Innate and adaptive immunity in Giant cell arteritis. *Front. Immunol.* 11:25. doi: 10.3389/fimmu.2020.621098

Anastasiou, G., Gialeraki, A., Merkouri, E., Politou, M., and Travlou, A. (2012). Thrombomodulin as a regulator of the anticoagulant pathway: implication in the development of thrombosis. *Blood Coagul. Fibrinolysis* 23, 1–10. doi: 10.1097/MBC.0b013e32834cb271

Chai, H., Li, X., Li, M., Lv, X., Yu, W., Li, Y., et al. (2022). Emergence, evolution, and pathogenicity of influenza a(H7N4) virus in shorebirds in China. *J. Virol.* 96:e0171721. doi: 10.1128/JVI.01717-21

Chen, G., Han, L., Tan, S., Jia, X., Wu, H., Quan, Y., et al. (2022). Loss-of-function of KMT5B leads to neurodevelopmental disorder and impairs neuronal development and neurogenesis. *J. Genet. Genomics* 49, 881–890. doi: 10.1016/j.jgg.2022.03.004

Chen, B., Khodadoust, M. S., Liu, C. L., Newman, A. M., and Alizadeh, A. A. (2018). Profiling tumor infiltrating immune cells with CIBERSORT. *Methods Mol. Biol.* 1711, 243–259. doi: 10.1007/978-1-4939-7493-1_12

Craven, K. E., Gökmen-Polar, Y., and Badve, S. S. (2021). CIBERSORT analysis of TCGA and METABRIC identifies subgroups with better outcomes in triple negative breast cancer. *Sci. Rep.* 11:4691. doi: 10.1038/s41598-021-83913-7

Del Sole, F., Farcomeni, A., Loffredo, L., Carnevale, R., and Menichelli, D. (2020). Features of severe COVID-19: a systematic review and meta-analysis. *Eur. J. Clin. Invest.* 50:e13378

Doggen, C. J., Kunz, G., Rosendaal, F. R., Lane, D. A., Vos, H. L., Stubbs, P. J., et al. (1998). A mutation in the thrombomodulin gene, 127G to a coding for Ala25Thr, and the risk of myocardial infarction in men. *Thromb. Haemost.* 80, 743–748. doi: 10.1055/s-0037-1615352

Gobbi, G., Carubbi, C., Tagliazucchi, G. M., Masselli, E., Mirandola, P., Pigazzani, F., et al. (2019). Sighting acute myocardial infarction through platelet gene expression. *Sci. Rep.* 9:19574. doi: 10.1038/s41598-019-56047-0

Grivas, P., Khaki, A. R., Wise-Draper, T. M., French, B., Hennessy, C., Hsu, C. Y., et al. (2021). Association of clinical factors and recent anticancer therapy with COVID-19 severity among patients with cancer: a report from the COVID-19 and cancer consortium. *Ann. Oncol.* 32, 787–800. doi: 10.1016/j.annonc.2021.02.024

Guo, X., Xue, H., Guo, X., Gao, X., Xu, S., Yan, S., et al. (2015). MiR224-3p inhibits hypoxia-induced autophagy by targeting autophagy-related genes in human glioblastoma cells. *Oncotarget* 6, 41620–41637. doi: 10.18632/oncotarget.5871

Haldane, V., De Foo, C., Abdalla, S. M., Jung, A.-S., Tan, M., Wu, S., et al. (2021). Health systems resilience in managing the COVID-19 pandemic: lessons from 28 countries. *Nat. Med.* 27, 964–980. doi: 10.1038/s41591-021-01381-y

Hulen, J., Kenny, D., Black, R., Hallgren, J., Hammond, K. G., Bredahl, E. C., et al. (2022). KMT5B is required for early motor development. *Front. Genet.* 13:901228. doi: 10.3389/fgene.2022.901228

Ireland, H., Kunz, G., Kyriakoulis, K., Stubbs, P. J., and Lane, D. A. (1997). Thrombomodulin gene mutations associated with myocardial infarction. *Circulation* 96, 15–18. doi: 10.1161/01.cir.96.1.15

Kuderer, N. M., Choueiri, T. K., Shah, D. P., Shyr, Y., Rubinstein, S. M., Rivera, D. R., et al. (2020). Clinical impact of COVID-19 on patients with cancer (CCC19): a cohort study. *Lancet* 395, 1907–1918. doi: 10.1016/S0140-6736(20)31187-9

Kumar, N., Verma, R., Lohana, P., Lohana, A., and Ramphul, K. (2021). Acute myocardial infarction in COVID-19 patients. A review of cases in the literature. *Arch. Med. Sci.* 6, e169–e175. doi: 10.5114/amsad.2021.109287

Lal, A., Erondu, N. A., Heymann, D. L., Gitahi, G., and Yates, R. (2021). Fragmented health systems in COVID-19: rectifying the misalignment between global health security and universal health coverage. *Lancet* 397, 61–67. doi: 10.1016/S0140-6736(20)32228-5

Lee, L. Y. W., Cazier, J.-B., Starkey, T., Briggs, S. E. W., Arnold, R., Bisht, V., et al. (2020). COVID-19 prevalence and mortality in patients with cancer and the effect of primary tumour subtype and patient demographics: a prospective cohort study. *Lancet Oncol.* 21, 1309–1316. doi: 10.1016/S1470-2045(20)30442-3

Li, F., Li, Y.-Y., Liu, M.-J., Fang, L.-Q., Dean, N. E., Wong, G. W. K., et al. (2021). Household transmission of SARS-CoV-2 and risk factors for susceptibility and infectivity in Wuhan: a retrospective observational study. *Lancet Infect. Dis.* 21, 617–628. doi: 10.1016/S1473-3099(20)30981-6

Li, X., Lv, X., Li, Y., Peng, P., Zhou, R., Qin, S., et al. (2021). Highly pathogenic avian influenza a(H5N8) virus in swans, China, 2020. *Emerg. Infect. Dis.* 27, 1732–1734. doi: 10.3201/eid2706.204727

Li, X., Lv, X., Li, Y., Xie, L., Peng, P., An, Q., et al. (2022). Emergence, prevalence, and evolution of H5N8 avian influenza viruses in Central China, 2020. *Emerg. Microb. Infect.* 11, 73–82. doi: 10.1080/22221751.2021.2011622

Li, X., Sun, J., Lv, X., Wang, Y., Li, Y., Li, M., et al. (2020). Novel Reassortant avian influenza a(H9N2) virus isolate in migratory waterfowl in Hubei Province, China. *Front. Microbiol.* 11:13. doi: 10.3389/fmicb.2020.00220

Lippi, G., Sanchis-Gomar, F., and Henry, B. M. (2020). Active smoking and COVID-19: a double-edged sword. *Eur. J. Intern. Med.* 77, 123–124. doi: 10.1016/j.ejim.2020.04.060

Liu, Z., Ye, P., Wang, S., Wu, J., Sun, Y., Zhang, A., et al. (2015). MicroRNA-150 protects the heart from injury by inhibiting monocyte accumulation in a mouse model of acute myocardial infarction. *Circ. Cardiovasc. Genet.* 8, 11–20. doi: 10.1161/CIRCGENETICS.114.000598

Muse, E. D., Kramer, E. R., Wang, H., Barrett, P., Parviz, F., Novotny, M. A., et al. (2017). A whole blood molecular signature for acute myocardial infarction. *Sci. Rep.* 7:12268. doi: 10.1038/s41598-017-12166-0

Park, H.-J., Noh, J. H., Eun, J. W., Koh, Y.-S., Seo, S. M., Park, W. S., et al. (2015). Assessment and diagnostic relevance of novel serum biomarkers for early decision of ST-elevation myocardial infarction. *Oncotarget* 6, 12970–12983. doi: 10.18632/oncotarget.4001

Pedregosa, F., Varoquaux, G., Gramfort, A., Michel, V., Thirion, B., Grisel, O., et al. (2011). Scikit-learn: machine learning in python. *J. Mach. Learn. Res.* 12, 2825–2830.

Qian, L., van Laake, L. W., Huang, Y., Liu, S., Wendland, M. F., and Srivastava, D. (2011). miR-24 inhibits apoptosis and represses Bim in mouse cardiomyocytes. *J. Exp. Med.* 208, 549–560. doi: 10.1084/jem.20101547

Ramphul, K., Ramphul, Y., Park, Y., Lohana, P., Kaur Dhillon, B., and Sombans, S. (2021b). A comprehensive review and update on severe acute respiratory syndrome coronavirus 2 (SARS-CoV-2) and coronavirus disease 2019 (COVID-19): what do we know now in 2021? *Arch. Med. Sci.* 6, 5–e13. doi: 10.5114/amsad.2021.105065

Ramphul, K., Lohana, P., Ramphul, Y., Park, Y., Mejias, S., Dhillon, B. K., et al. (2021a). Hypertension, diabetes mellitus, and cerebrovascular disease predispose to a more severe outcome of COVID-19. *Arch. Med. Sci.* 6:e30–e39. doi: 10.5114/amsad.2021.105255

Ritchie, M. E., Phipson, B., Wu, D., Hu, Y., Law, C. W., Shi, W., et al. (2015). Limma powers differential expression analyses for RNA-sequencing and microarray studies. *Nucleic Acids Res.* 43:e47. doi: 10.1093/nar/gkv007

Roth, G. A., Johnson, C., Abajobir, A., Abd-Allah, F., Abera, S. F., Abyu, G., et al. (2017). Global, regional, and national burden of cardiovascular diseases for 10 causes, 1990 to 2015. *J. Am. Coll. Cardiol.* 70, 1–25. doi: 10.1016/j.jacc.2017.04.052

Rugge, M., Zorzi, M., and Guzzinati, S. (2020). SARS-CoV-2 infection in the Italian Veneto region: adverse outcomes in patients with cancer. *Nat. Cancer* 1, 784–788. doi: 10.1038/s43018-020-0104-9

Safiabadi Tali, S. H., LeBlanc, J. J., Sadiq, Z., Oyewunmi, O. D., Camargo, C., Nikpour, B., et al. (2021). Tools and techniques for severe acute respiratory syndrome coronavirus 2 (SARS-CoV-2)/COVID-19 detection. *Clin. Microbiol. Rev.* 34:e00228-20. doi: 10.1128/CMR.00228-20

Sato, N., Tamada, Y., Yu, G., and Okuno, Y. (2022). CBNplot: Bayesian network plots for enrichment analysis. *Bioinformatics* 38, 2959–2960. doi: 10.1093/bioinformatics/btac175

Silbiger, V. N., Luchessi, A. D., Hirata, R. D. C., Lima-Neto, L. G., Cavichioli, D., Carracedo, A., et al. (2013). Novel genes detected by transcriptional profiling from whole-blood cells in patients with early onset of acute coronary syndrome. *Clin. Chim. Acta Int. J. Clin. Chem.* 421, 184–190. doi: 10.1016/j.cca.2013.03.011

Suresh, R., Li, X., Chiriac, A., Goel, K., Terzic, A., Perez-Terzic, C., et al. (2014). Transcriptome from circulating cells suggests dysregulated pathways associated with long-term recurrent events following first-time myocardial infarction. *J. Mol. Cell. Cardiol.* 74, 13–21. doi: 10.1016/j.yjmcc.2014.04.017

Toscano, O., Cosentino, N., Campodonico, J., Bartorelli, A. L., and Marenzi, G. (2021). Acute myocardial infarction during the COVID-19 pandemic: An update on clinical characteristics and outcomes. *Front. Cardiovasc. Med.* 8:648290. doi: 10.3389/fcvm.2021.648290

Tsao, C. W., Aday, A. W., Almarzooq, Z. I., Alonso, A., Beaton, A. Z., Bittencourt, M. S., et al. (2022). Heart disease and stroke statistics-2022 update: a report from the American heart association. *Circulation* 145, e153–e639. doi: 10.1161/CIR.0000000000001052

Vickers, A. J., and Elkin, E. B. (2006). Decision curve analysis: a novel method for evaluating prediction models. *Med. Decis. Making* 26, 565–574. doi: 10.1177/0272989X06295361

Vickers, A. J., van Calster, B., and Steyerberg, E. W. (2019). A simple, step-by-step guide to interpreting decision curve analysis. *Diagn Progn Res* 3:18. doi: 10.1186/s41512-019-0064-7

Wolpert, D. H., and Macready, W. G. (1997). No free lunch theorems for optimization. *IEEE Trans. Evol. Comput.* 1, 67–82. doi: 10.1109/4235.585893

Wu, T., Hu, E., Xu, S., Chen, M., Guo, P., Dai, Z., et al. (2021). Cluster profiler 4.0: a universal enrichment tool for interpreting omics data. *Innovation* 2, 3:100141. doi: 10.1016/j.xinn.2021.100141

Xie, J., Luo, X., Deng, X., Tang, Y., Tian, W., Cheng, H., et al. (2023). Advances in artificial intelligence to predict cancer immunotherapy efficacy. *Front. Immunol.* 13:4. doi: 10.3389/fimmu.2022.1076883

Yang, Y., Cheng, H.-W., Qiu, Y., Dupee, D., Noonan, M., Lin, Y.-D., et al. (2015). MicroRNA-34a plays a key role in cardiac repair and regeneration following myocardial infarction. *Circ. Res.* 117, 450–459. doi: 10.1161/CIRCRESAHA.117.305962

Zhang, Q., Meng, Y., Wang, K., Zhang, X., Chen, W., Sheng, J., et al. (2021). Inflammation and antiviral immune response associated with severe progression of COVID-19. *Front. Immunol.* 12:631226. doi: 10.3389/fimmu.2021.631226

Zhao, E., Xie, H., and Zhang, Y. (2020). Predicting diagnostic gene biomarkers associated with immune infiltration in patients with acute myocardial infarction. *Front. Cardiovasc. Med.* 7:23. doi: 10.3389/fcvm.2020.586871

frontiers | Frontiers in Microbiology

TYPE Original Research
PUBLISHED 17 April 2023
DOI 10.3389/fmicb.2023.1156251

OPEN ACCESS

EDITED BY
Hongliang Chai,
Northeast Forestry University, China

REVIEWED BY
Van Giap Nguyen,
Vietnam National University of Agriculture, Vietnam
Sofia Egana Labrin,
University of Maryland, United States

*CORRESPONDENCE
Ehab Kotb Elmahallawy
✉ eehaa@unileon.es
Walied Abdo
✉ waliedsobhy40@gmail.com

†These authors have contributed equally to this work

RECEIVED 01 February 2023
ACCEPTED 28 March 2023
PUBLISHED 17 April 2023

CITATION
Mosad SM, Elmahallawy EK, Alghamdi AM, El-Khayat F, El-Khadragy MF, Ali LA and Abdo W (2023) Molecular and pathological investigation of avian reovirus (ARV) in Egypt with the assessment of the genetic variability of field strains compared to vaccine strains. *Front. Microbiol.* 14:1156251. doi: 10.3389/fmicb.2023.1156251

Molecular and pathological investigation of avian reovirus (ARV) in Egypt with the assessment of the genetic variability of field strains compared to vaccine strains

Samah M. Mosad[1†], Ehab Kotb Elmahallawy[2*†], Abeer M. Alghamdi[3], Fares El-Khayat[4], Manal F. El-Khadragy[5], Lobna A. Ali[6] and Walied Abdo[7*]

[1]Department of Virology, Faculty of Veterinary Medicine, Mansoura University, Mansoura, Egypt, [2]Department of Zoonoses, Faculty of Veterinary Medicine, Sohag University, Sohag, Egypt, [3]Department of Biology, Faculty of Science, Al-Baha University, Al-Baha, Saudi Arabia, [4]Department of Poultry Diseases, Faculty of Veterinary Medicine, Kafrelsheikh University, Kafrelsheikh, Egypt, [5]Department of Biology, College of Science, Princess Nourah bint Abdulrahman University, Riyadh, Saudi Arabia, [6]Cell Biology and Histochemistry, Zoology Department, Faculty of Science, South Valley University, Qena, Egypt, [7]Department of Pathology, Faculty of Veterinary Medicine, Kafrelsheikh University, Kafrelsheikh, Egypt

Avian orthoreovirus (ARV) is among the important viruses that cause drastic economic losses in the Egyptian poultry industry. Despite regular vaccination of breeder birds, a high prevalence of ARV infection in broilers has been noted in recent years. However, no reports have revealed the genetic and antigenic characteristics of Egyptian field ARV and vaccines used against it. Thus, this study was conducted to detect the molecular nature of emerging ARV strains in broiler chickens suffering from arthritis and tenosynovitis in comparison to vaccine strains. Synovial fluid samples ($n = 400$) were collected from 40 commercial broiler flocks in the Gharbia governorate, Egypt, and then pooled to obtain 40 samples, which were then used to screen ARV using reverse transcriptase polymerase chain reaction (RT-PCR) with the partial amplification of ARV sigma C gene. The obtained RT-PCR products were then sequenced, and their nucleotide and deduced amino acid sequences were analyzed together with other ARV field and vaccine strains from GenBank. RT-PCR successfully amplified the predicted 940 bp PCR products from all tested samples. The phylogenetic tree revealed that the analyzed ARV strains were clustered into six genotypic clusters and six protein clusters, with high antigenic diversity between the genotypic clusters. Surprisingly, our isolates were genetically different from vaccine strains, which aligned in genotypic cluster I/protein cluster I, while our strains were aligned in genotypic cluster V/protein cluster V. More importantly, our strains were highly divergent from vaccine strains used in Egypt, with 55.09–56.23% diversity. Sequence analysis using BioEdit software revealed high genetic and protein diversity between our isolates and vaccine strains (397/797 nucleotide substitutions and 148-149/265 amino acid substitutions). This high genetic diversity explains the vaccination failure and recurrent circulation of ARV in Egypt. The present data highlight the need to formulate a new effective vaccine from locally isolated ARV strains after a thorough screening of the molecular nature of circulating ARV in Egypt.

KEYWORDS

avian orthoreovirus, ARV, sigma C, vaccine, phylogenetic analysis, histopathology

1. Introduction

Avian orthoreovirus is a member of the genus *Orthoreovirus*, which belongs to the *Spinareoviridae* family and Reovirales order, as classified by the International Committee on Taxonomy of Viruses[1]. With regard to its structure, ARV has a unique double-layered icosahedral capsid that measures about 70–80 nm in diameter without the envelope (Spandidos and Graham, 1976). The ARV particle has 10 double-stranded genomic RNA segments (1–4 kbp). The genomic segments are classified by polyacrylamide gel electrophoresis according to their size into three classes: small (S1–S4), medium (M1–M3), and large (L1–L3) (Spandidos and Graham, 1976). Segment S1 encodes three proteins, while each of the other nine segments translates into a single protein. S1 possesses three open reading frames (ORFs): ORF1 and ORF2 encode P10 and P17 non-structural proteins, respectively, whereas ORF3 encodes sigma C (δC) structural protein, which is located on the surface of the viral capsid and acts as a viral attachment protein and apoptosis inducer, selects specific neutralizing antibodies, and is considered the major antigenic determinant of ARV (Martínez-Costas et al., 1997; Shih et al., 2004; Benavente and Martínez-Costas, 2007). Based on the molecular characterization of sigma C protein sequences, six ARV genotypes have been identified (Kant et al., 2003; Ayalew et al., 2017; Palomino-Tapia et al., 2018). Most reports have stated that there are only six genotypic clusters of ARV isolated from chickens, while the seventh genotypic cluster is from wild birds (Kim et al., 2022). However, De la Torre et al. (2021) detected a new variant strain from poultry and classified ARV into seven genotypic clusters.

With regard to its evolution, the first report of avian reovirus being isolated from birds was in 1954 (Fahey and Crawley, 1954). Consequently, several ARV variants were isolated worldwide with high antigenic diversity. Most ARV infections are asymptomatic, and the virus can infect various avian species, causing a wide range of disease conditions, but broiler and broiler breeder chickens are the most clinically affected (Rosenberger et al., 1989; Jones, 2000; Davis et al., 2012). ARV is the principal cause of hock joint and footpad arthritis and tenosynovitis in young broiler chickens. The affected birds are usually unable to reach food and water, so their growth can be reduced and their production slow, and even death can occur with severe ARV infection (Gouvea and Schnitzer, 1982; Lee et al., 1992; Liu et al., 2003). Other disease conditions are also caused by ARV infection, including runting–stunting syndrome, malabsorption syndrome, hepatitis, myocarditis, pericarditis, enteritis, pneumonia, encephalitis, and immunosuppression (Robertson, 1986; Van der Heide, 2000). With regard to the impact, ARV infections in poultry cause extreme economic losses from increased mortality rates (up to 10%), low feed conversion rate, reduced weight gain, lack of performance, uneven growth rate, viral arthritis/tenosynovitis, diminished marketability of diseased birds, condemnation of affected carcasses, and secondary viral or bacterial infections (Van der Heide, 2000).

In Egypt, both live attenuated and inactivated ARV vaccines are available. Attenuated vaccines contain the S1133 or 2177 strain, while inactivated vaccines contain strains S1133, 1733, 2408, and SS412. Protection against reovirus mainly depends on the transfer of maternal antibodies through the yolk to the progeny, thus, breeding birds are vaccinated three to four times (Rekik and Silim, 1992; Van der Heide, 2000; Zhang et al., 2005). Despite the use of an integrated vaccination program for breeder birds in Egypt using both inactivated and modified live virus vaccines, offspring are not fully protected. ARV was first detected in Egypt in 1984 (Tantawi et al., 1984), then was identified serologically in several Egyptian governorates (Zaher and Mohamed, 2009; Abd El-Samie, 2014). It was then identified by RT-PCR from proventriculitis, tenosynovitis, and malabsorption syndromes (Kutkat et al., 2010; Ramzy et al., 2016; Mansour et al., 2018). Then, molecular characterization of ARV was performed based on the σA-encoding gene (Al-Ebshahy et al., 2020). It is important to mention that ARV has extreme inherent genetic variability because of the segmented RNA genome, which increases recombination and reassortment mutation events (Liu et al., 2003; Bányai et al., 2011).

The poultry industry worldwide has faced the consequences of ARV variant emergence since 2011 (Lu et al., 2015; Zhong et al., 2016; Gallardo, 2017; Sellers, 2017; Egaña-Labrin et al., 2019; Ayalew et al., 2020). The new variants have accompanied acute tenosynovitis, arthritis, and pericarditis even in broilers and breeders vaccinated against ARV (Van der Heide, 2000; Davis et al., 2012). As ARV is unaffected by certain disinfection methods and can survive for long periods in the environment, variants can be easily transferred between countries through imported chickens, processed chicken products, and eggs (Ayalew et al., 2020). In addition, because ARV is unaffected by pH, heat, certain disinfectants, and proteolytic enzymes, it is difficult to keep the virus away from chicken farms (Jones, 2000). Consequently, the best sustainable decision is to control ARV by using proper genetic and antigenic vaccines. Despite the high prevalence of ARV infection in Egypt, the genetic and antigenic nature of ARV is not clear, as no previous studies investigated the ARV sigma C gene in Egypt. Therefore, the current study aimed to detect the genotypic properties of emerging ARV strains in broiler chickens suffering from arthritis and tenosynovitis. To the authors' knowledge, this is the first study to carry out a molecular investigation of ARV based on the sigma C protein to assess genetic variability in comparison to the vaccine strains used in Egypt.

2. Materials and methods

2.1. Ethical considerations

This study was revised and approved by the Kafrelsheikh University Animal Care and Use Committee, Kafrelsheikh University, Egypt (code number KFS-2020/3).

2.2. Clinical samples

Samples ($n = 400$) were collected from 40 commercial broiler flocks located in Gharbia governorate, Egypt, during 2020–2021.

1 ICTV. Available online at: https://ictv.global/taxonomy (accessed 9 September 2022).

FIGURE 1
Clinical signs of ARV infections in broiler chickens. Broiler chicken with unilateral arthritis, hock joint swelling, and ruffled wing's feather.

Synovial fluid was collected from 10 diseased birds per farm and pooled, and this was considered one working sample. The diseased birds thought to be infected with ARV were 10–25 days old. For histopathological examination, samples from the heart, liver, spleen, and tendons, including synovial membranes, were freshly collected and fixed in formalin (10%). The studied flocks were not vaccinated against ARV, but their breeders were vaccinated at 6 weeks of age and again at 10 weeks of age using a modified live virus vaccine, then with inactivated reovirus vaccine at 17 weeks of age. Other pathogens causing arthritis and other systemic macroscopic and microscopic lesions as *Escherichia coli*, *Staphylococcus aureus*, and *Pseudomonas aeruginosa* were excluded from tested samples by multiplex PCR according to Ammara et al. (2014). Meanwhile, *Mycoplasma synoviae* and *Salmonella* sp. were also excluded by PCR as described elsewhere (Bencina et al., 2001; Shanmugasamy et al., 2011; Ammar et al., 2019).

2.3. Histopathological examination

Samples from the heart, liver, spleen, and tendons, including synovial membranes, were immersed in 10% buffered neutral formalin for fixation. Then, samples were subjected to routine tissue techniques, including dehydration,

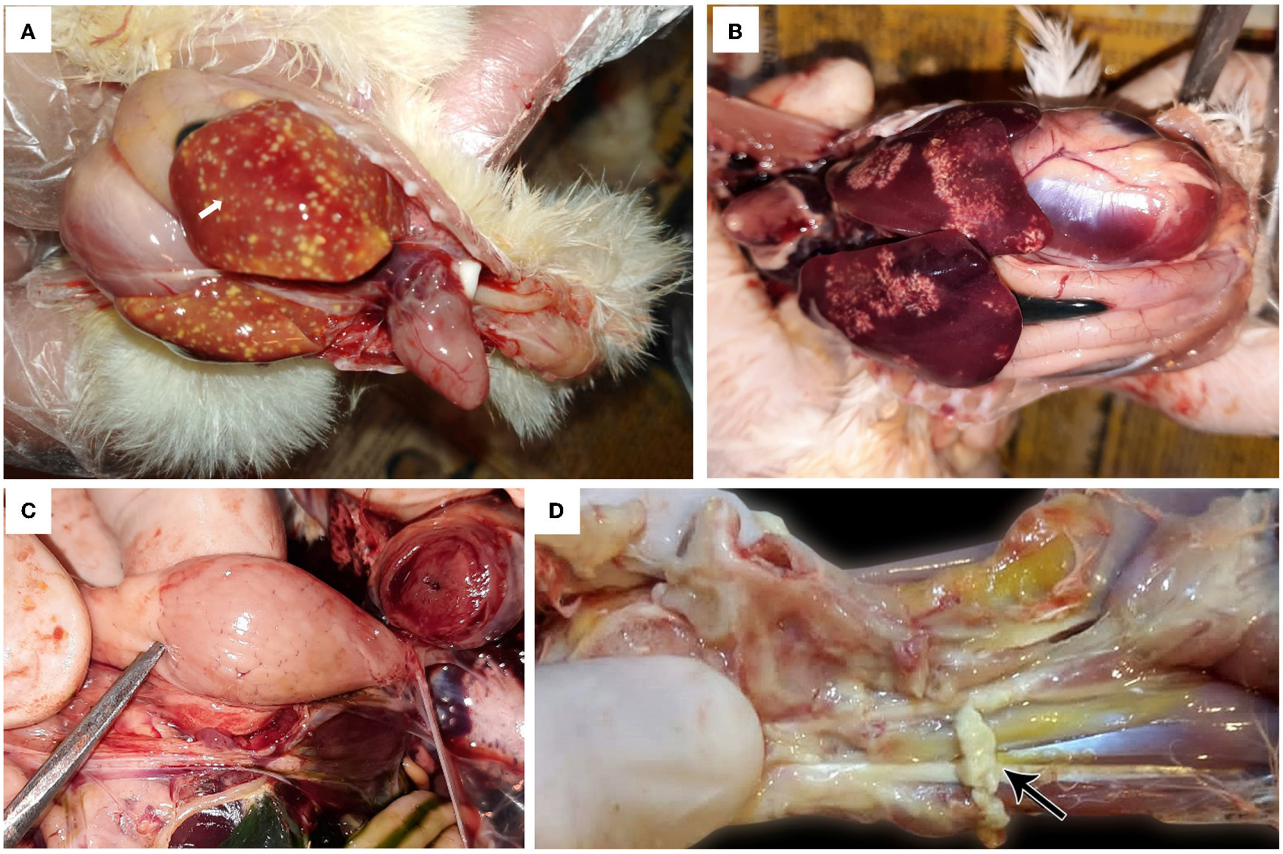

FIGURE 2
Avian orthoreovirus postmortem lesions in broiler chickens. **(A)** Broiler chicks show enlarged orange liver with numerous necrotic pale hepatic foci and hemorrhagic pericarditis (arrow). **(B)** Broiler chickens show hepatic necrosis. **(C)** Broiler chick with enlarged lemon-shaped proventriculus. **(D)** Broiler chicken with swelling, edema in the tendon, and full thickness tendon rupture (arrow).

clearance, embedding, and casting. The paraffin blocks were cut *via* microtome into 4–5 μm sections, which were fixed on glass slides for further staining with hematoxylin and eosin.

2.4. Molecular identification of ARV

2.4.1. Viral RNA extraction

Synovial fluid was used for the extraction of viral RNAs using a QIAamp® Min Elut® Virus Spin Kit (Qiagen, Hilden, Germany) according to the manufacturer's directions. The extracted RNA was then frozen at −80 °C until use in sigma C gene amplification.

2.4.2. Reverse transcriptase polymerase chain reaction

A total of pooled 40 synovial fluids samples were tested for ARV by the RT-PCR partial amplification of the sigma C gene. RT-PCR was performed for the partial amplification of the ORF3 of genomic segment S1, which encodes ARV sigma C protein using a previously constructed primer set (Goldenberg et al., 2010). The oligonucleotide primer sequences were ARV δC F: 5′-TCMRTCRCAGCGAAGAGARGTCG-3′ and ARV δC R: 5′-TCRRTGCCSGTACGCAMGG-3′. These primers were synthesized by Metabion International AG (Steinkirchen, Germany). Qiagen one-step RT-PCR kit (Qiagen, Hilden, Germany) was used for RT-PCR according to the manufacturer's instructions. A Thermal cycler (T Gradient, Biometra, Germany) was set at an individual cycle of two steps: 50°C for 30 min and 94°C for 2 min; followed by 35 triple-step cycles: 94°C for 1 min, 50°C for 1 min, and 72°C for 1 min; with a single terminal elongation cycle of 72°C for 10 min. The 940 bp PCR products were then examined by agarose gel (1.5%) electrophoresis and an ultraviolet transilluminator (Biometra, Germany).

2.4.3. Sequencing and phylogenetic analysis

The PCR products of positive samples with the strongest bands were selected, and their DNA was agarose gel purified with QIAquick PCR gel purification kits (Qiagen, Valencia, CA, USA), following the manufacturer's guidelines. The obtained DNA was submitted to Macrogen laboratory, South Korea, for forward and reverse sequencing. Direct nucleotide analysis was done according to several previous studies (Ayalew et al., 2017; Palomino-Tapia et al., 2018; Chen et al., 2019; Egaña-Labrin et al., 2019). The UniProt blast was also used for protein

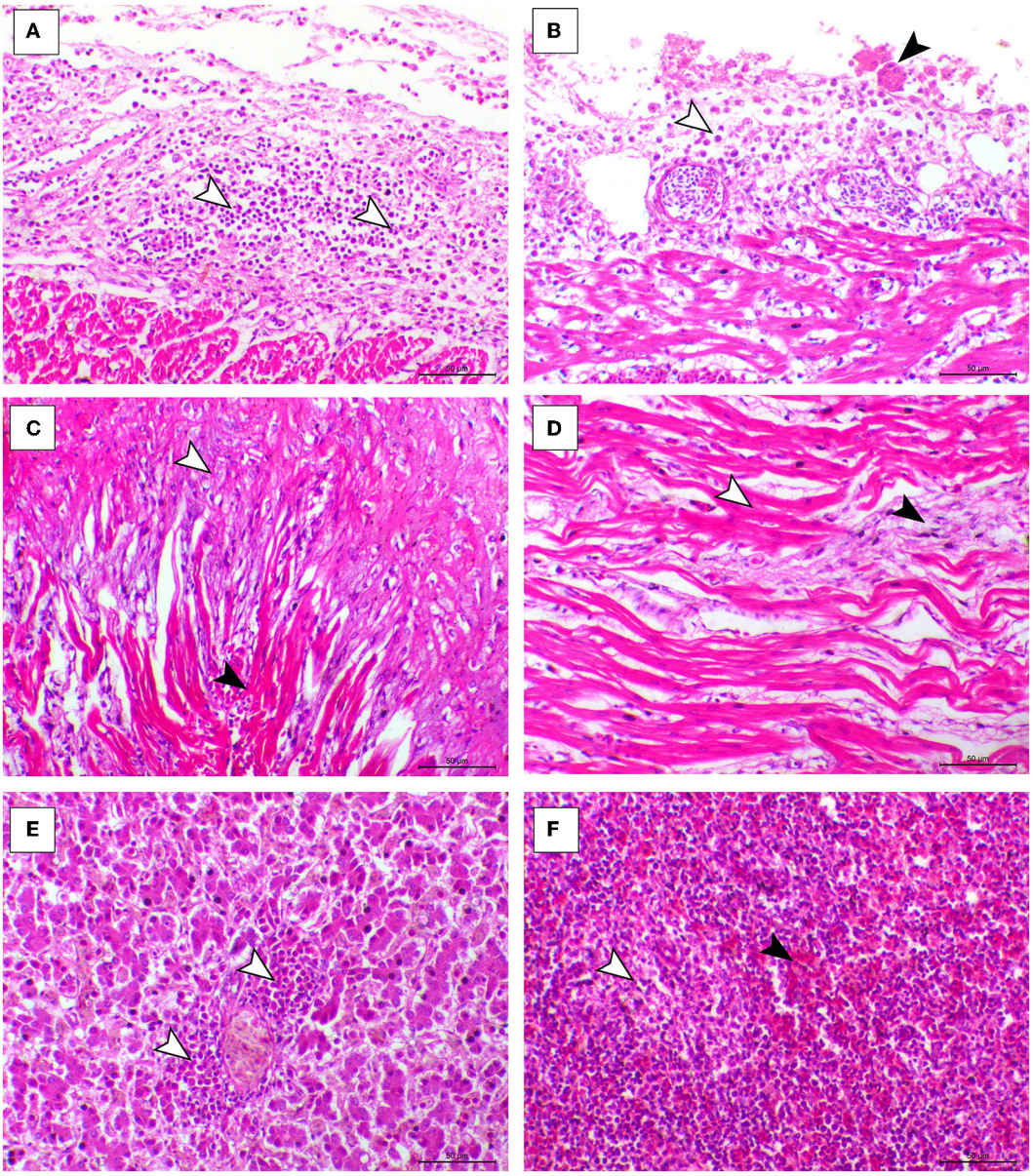

FIGURE 3
Cardiac, hepatic, and splenic histopathological lesions in the ARV-infected broiler chickens. **(A, B)** The pericardium of broiler chicks shows pericarditis associated with intense inflammatory cells infiltration (arrowheads). **(C)** Myocardium of broiler chicks shows marked atrophy of the myocardial cells (white arrowheads) and interstitial fibrosis (black arrowhead). **(D)** Myocardium of broiler chicks show myxomatous changes (white arrowhead) and severe eosinophilic sarcoplasmic degeneration (black arrowhead). **(F)** Liver of broiler chicks show periportal heterophilic infiltration (white arrowheads). **(E)** Liver of broiler chicks show the congestion of red pulp (black arrowhead) and moderate degree of lymphoid depletion (white arrowhead), H&E, bar = 50 μm.

alignment to detect vaccine strain sigma C protein due to its divergence from our sequence. The protein sequences of the vaccines were also tracked and get their nucleotide sequence accession numbers then used in the NCBI nucleotide blast. The resulting sequences of the nucleotides of selected samples were then aligned using the BLAST tool in NCBI and then deposited in GenBank (http://www.ncbi.nlm.nih.gov/Genbank) with accession numbers OL741460 (Gharbia/1-20) and OL741461 (Gharbia/2-20). The sequences were then analyzed by ClustalW2 (https://www.ebi.ac.uk/Tools/msa/clustalw2/). The resulting files were analyzed to construct the phylogenetic tree with other reference sequences using MEGA X software (http://www.megasoftware.net/) for neighbor-joining phylogenic tree construction with a 1,000 repeat bootstrap test, p-distance substitution model, and pairwise deletion gap treatment together with other GenBank reference ARV sequences. BioEdit software version 7.1 was used for nucleotide and deduced amino acid sequence alignment using ClustalW (Hall, 1999).

10.3389/fmicb.2023.1156251

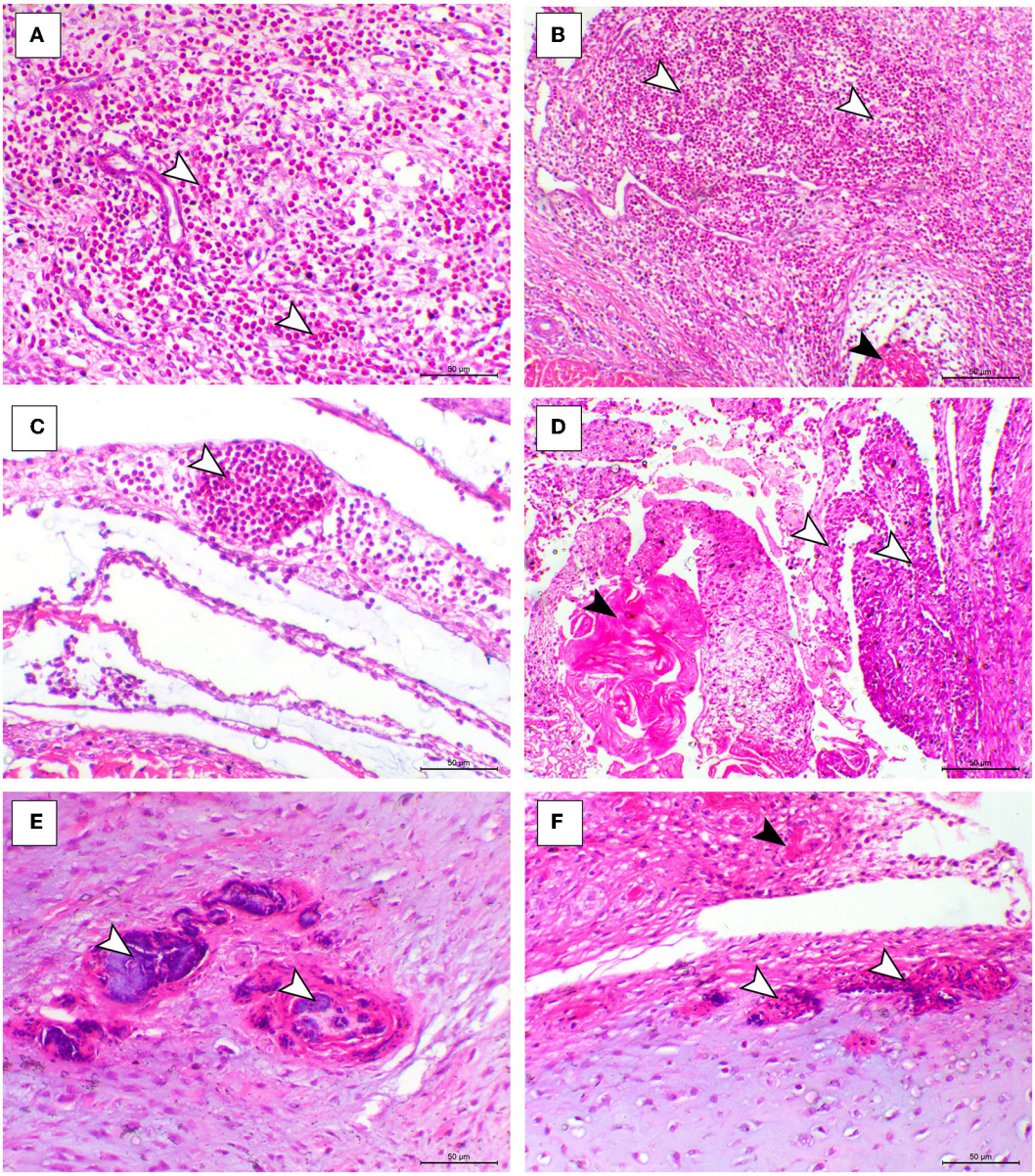

FIGURE 4
Synovial, tendon, and articular cartilaginous histopathological lesions in the ARV-infected broiler chickens. **(A–C)** Fibrin foci (black arrowhead) and marked heterophilic cell infiltration (white arrowheads) within the synovial membrane. **(D)** Necrosis o the synovial membrane (black arrowhead) and hypertrophy of synovial cells (white arrowhead). **(E, F)** Articular tissues showing multifocal necrosis on the surface or within the cartilage (white arrowhead), H&E, bar= 50 μm.

3. Results

3.1. Clinical picture, postmortem lesions, and histopathological examination

The affected birds suffered from severe arthritis/tenosynovitis, which led to lameness and splay-leg with swelling of the hock joint and bumble foot (Figure 1). In some cases, the inflammation spread into the adjacent musculature. Uneven growth and growth retardation were also recorded, with 6% mortality and 50% culling rates. Upon the gross examination of affected carcasses, tendons and tendon sheaths showed marked edema, with tendon rupture (Figure 2D) and severe hemorrhage; pericarditis (Figure 2A), and myocarditis were also recorded in some cases. An enlarged lemon-shaped proventriculus (Figure 2C) with enlarged liver was reported, along with the orange discoloration of the hepatic parenchyma and miliary distribution of numerous pale tan necrotic hepatic foci (Figures 2A, B).

The histopathological features of infected birds are illustrated in Figures 3, 4. The examined heart sections showed pericarditis features extending to the myocardium. The pericardial sac showed massive fibrinous exudation with marked granulation tissue formation and capillary congestion, associated with severe inflammatory cell infiltration, including heterophils,

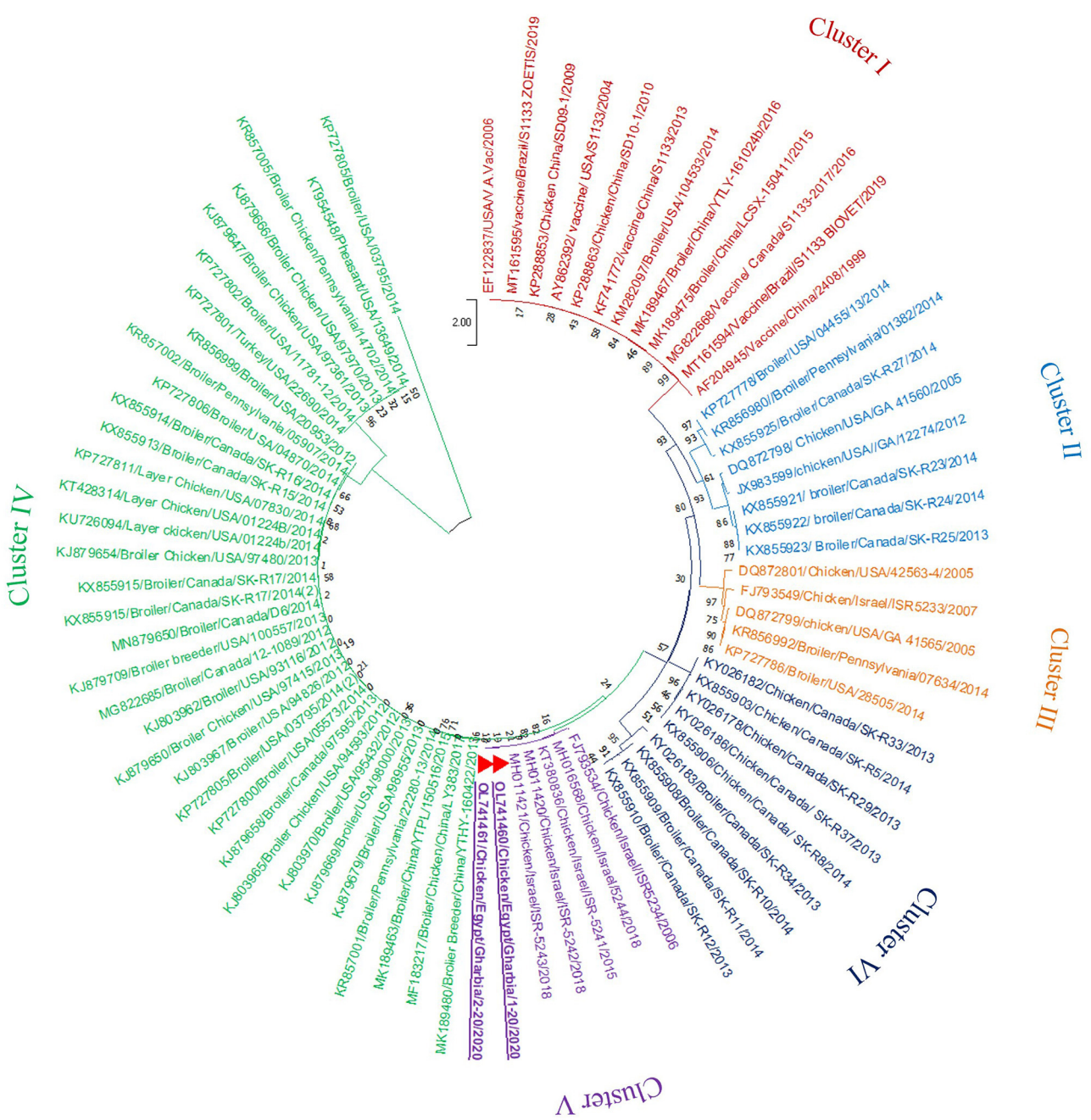

FIGURE 5
Phylogenetic tree of ARV sigma C gene nucleotide sequences constructed with MEGA X software in which the analyzed sequences are clustered into six genotyping clusters (genotypic cluster I–VI) according to Ayalew et al. (2017) ARV classification. Our isolates (red triangles) are clustered in genotypic cluster V away from all vaccine strains which are clustered in genotypic cluster I.

lymphocytes, macrophages, and occasional syncytial cells. The myocardium revealed marked atrophy and degeneration rather than myocarditis. The inflammatory cells within the muscle layers were extended from pericardial lesions. There was marked interstitial cell proliferation. The endocardium showed severe degenerative changes ranging from sarcoplasmic eosinophilia to myxomatous changes. The liver of diseased birds showed marked sinusoidal congestion, hepatic degeneration, and periportal heterophilic cell infiltration. The spleen showed moderate to severe lymphoid depletion associated with histocytic cell infiltration. The synovial membranes showed severe synovitis, associated with necrosis of the synovial membranes admixed with fibrin within a granulation matrix and accompanied by severe heterophil infiltration. The tendons showed necrotic tendonitis associated with multifocal necrotic foci, with marked infiltration of inflammatory cells consisting of heterophils, lymphocytes, and macrophages. The articular surface showed multifocal necrotic changes in dystrophic calcification lesions.

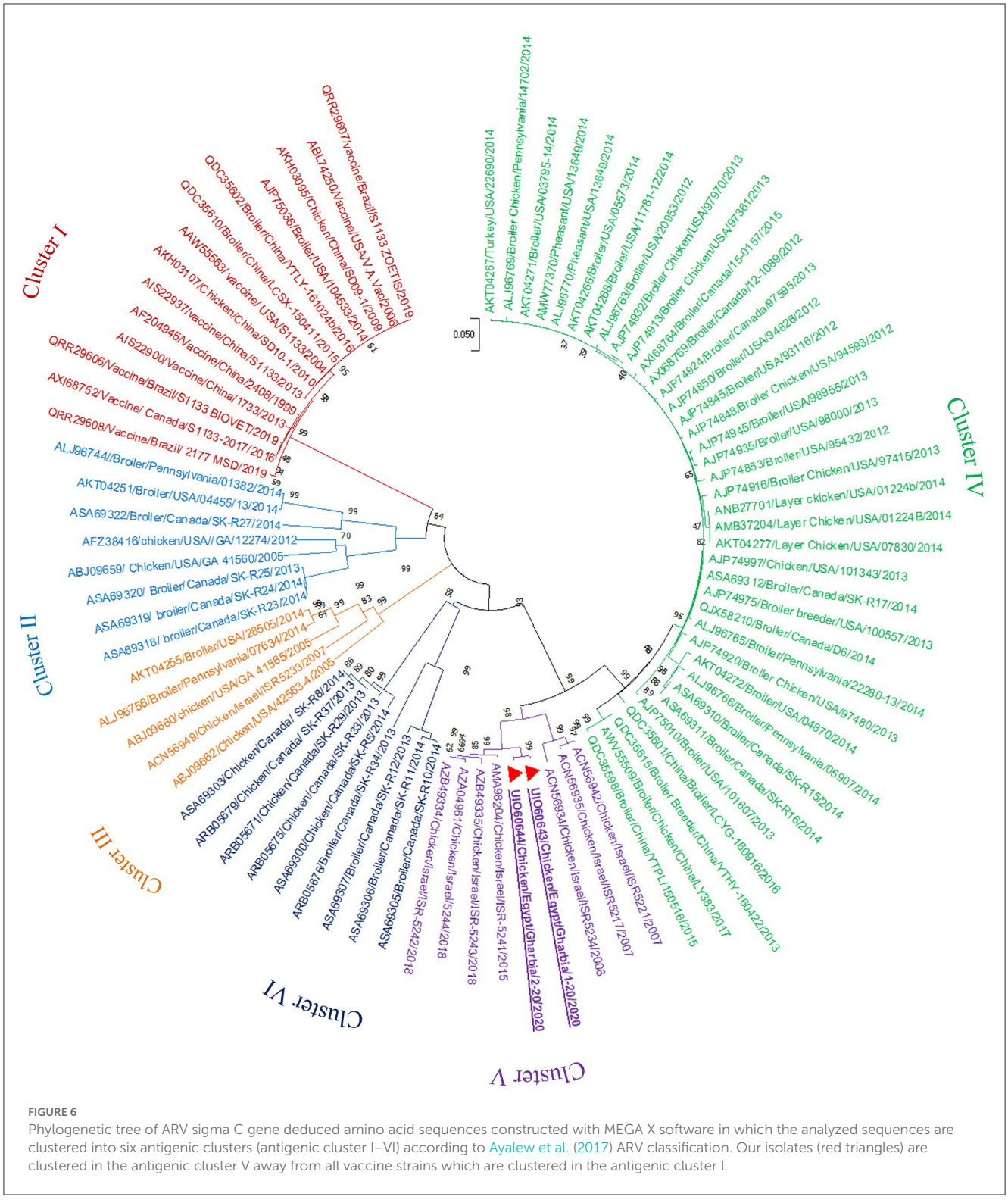

FIGURE 6
Phylogenetic tree of ARV sigma C gene deduced amino acid sequences constructed with MEGA X software in which the analyzed sequences are clustered into six antigenic clusters (antigenic cluster I–VI) according to Ayalew et al. (2017) ARV classification. Our isolates (red triangles) are clustered in the antigenic cluster V away from all vaccine strains which are clustered in the antigenic cluster I.

3.2. RT-PCR, sequencing, and phylogenetic analysis

In the present study, RT-PCR successfully amplified the 940 bp fragment of the ARV sigma C gene from the 40 tested samples (100%). The Sigma C gene is usually used for genotyping and classifying ARV into protein clusters, as it is considered to be positioned in an extremely variable genomic region (Attoui, 2011; Kim et al., 2022). To study the genotypic properties of ARV, phylogenetic analysis of sigma C gene nucleotide sequences from our two selected isolates was performed together with 83 other sequences of reference field and vaccine strains retrieved from

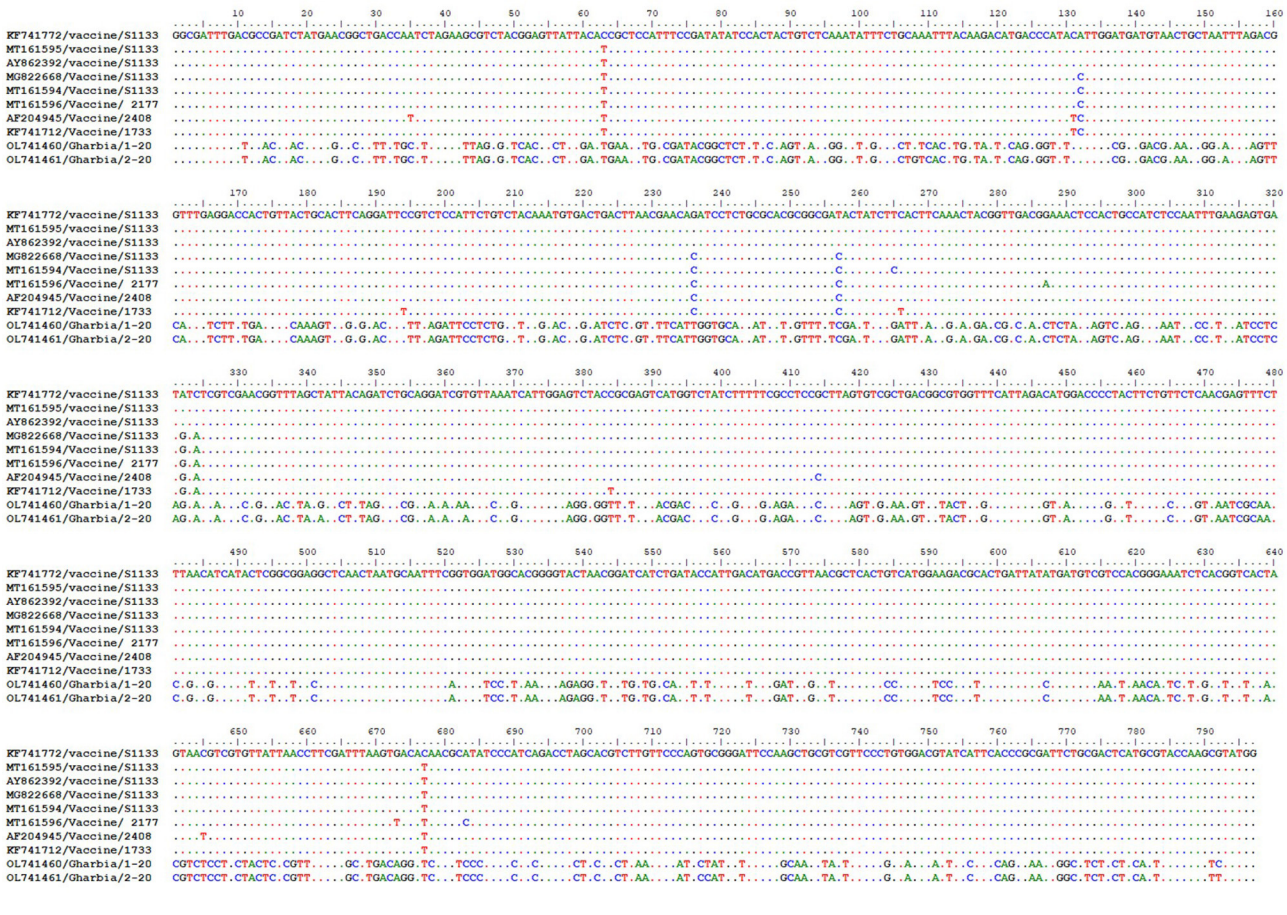

FIGURE 7
Avian orthoreovirus sigma C gene nucleotide sequences analysis using BioEdit software showing 397 nucleotide substitutions (out of 797 aligned nucleotides) in our isolates in comparison to vaccine strains used in Egypt.

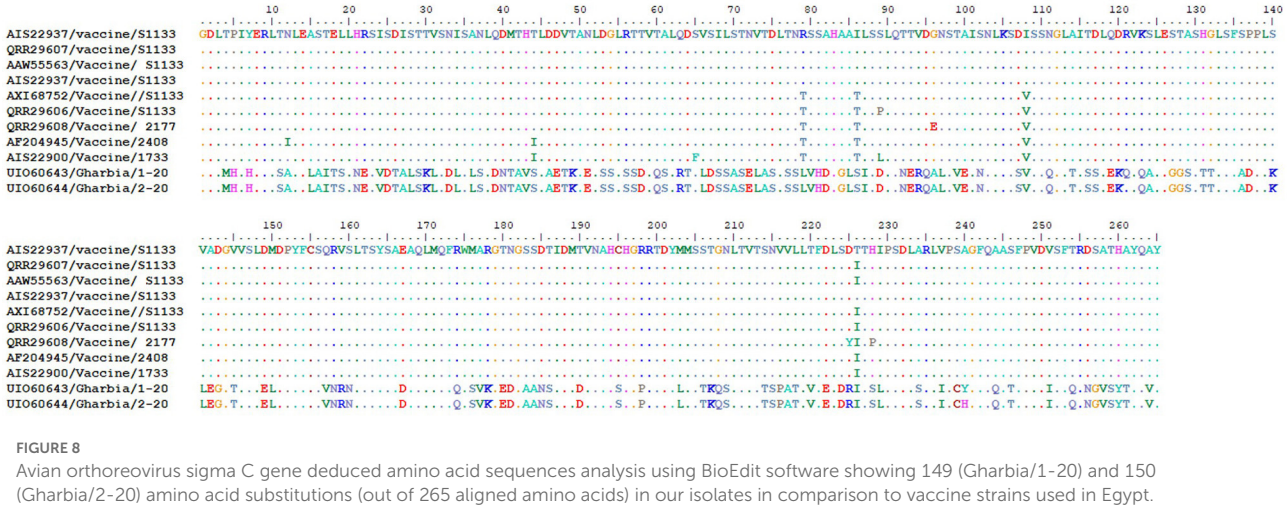

FIGURE 8
Avian orthoreovirus sigma C gene deduced amino acid sequences analysis using BioEdit software showing 149 (Gharbia/1-20) and 150 (Gharbia/2-20) amino acid substitutions (out of 265 aligned amino acids) in our isolates in comparison to vaccine strains used in Egypt.

GenBank. Generally, the phylogenetic tree revealed that all 85 strains involved in the phylogenetic analysis were classified into six genotypic clusters (I–VI) (Figure 5). Based on ARV classification (Ayalew et al., 2017), all vaccine strains were clustered in cluster I. Surprisingly, our isolates were genetically different from vaccine strains and were clustered in genotypic cluster V with other

isolates from Israel (the same geographic location). In addition, phylogenetic analysis of the deduced amino acid sequences from the sigma C gene of our two selected ARV isolates and the 83 reference strains from GenBank (the same strains used in nucleotide sequence analysis) was performed to study the deduced sigma C protein relatedness. All ARV strains were clustered into six clusters (I–VI) (Figure 6); the vaccine strains were in cluster I, while our isolates differed from those and were in cluster V with other isolates from Israel.

The diversity among the six deduced sigma C protein clusters was calculated with MEGA X software, which revealed high protein diversity among the six genotypic clusters. The lowest detected diversity was 13.21% between cluster V (ISR-5241) and cluster IV (LCYG-160916). Shockingly, the highest deduced protein diversity (57.65%) was between cluster V (including our strains) and cluster I (including the vaccine strains). The highest deduced protein diversity was between the ISR-5242 and S1133 vaccine strains. The diversity within clusters ranged from 0 to 39.62%; specifically, the ranges for clusters I–VI were 0.0–2.64%, 0.0–34.72%, 2.26–20.38%, 0.0–7.92%, 0.38–13.64%, and 0.0–39.62%, respectively (Supplementary Table 1). Surprisingly, our strains were highly divergent from vaccine strains used in Egypt: 55.47–56.23% between Gharbia/1-20 and vaccine strains, and 55.09–55.85% between Gharbia/2-20 and vaccine strains.

To detect the genetic and deduced sigma C protein diversity between our two isolates and vaccine strains used in Egypt, the nucleotide sequences of the sigma C gene and its deduced amino acid sequences were analyzed with BioEdit software using vaccine strain S1133 (KF741772) as a reference. Nucleotide sequence analysis revealed high genetic diversity between our isolates and vaccine strains, with a substitution of 397 out of 797 aligned nucleotides (49.81%), as shown in Figure 7. Amino acid sequence analysis revealed high diversity between our isolates and vaccine strains, with a substitution of 149 (Gharbia/1-20) and 148 (Gharbia/2-20) out of 265 aligned amino acids (55.85 and 56.23%, respectively), as shown in Figure 8. On the other hand, there were few or no substitutions in nucleotide and amino acid sequences between vaccine strains and reference strain S1133 (Figures 7, 8). Our two isolates (Gharbia/1-20 and Gharbia/2-20) are genetically similar, with five nucleotide substitutions (A191G, G425A, A445G, T801C, and C875T) leading to two amino acid substitutions (Q148R and Y267H).

4. Discussion

Despite regular vaccination of breeder chickens against ARV in Egypt, pathogenic ARV infection remains a great challenge to the poultry industry, causing severe economic losses. The ineffectiveness of conventional vaccines and the recurrence of emergent pathogenic strains are alarming and threaten the broiler poultry industry. Moreover, ARV infection in broiler chickens at poultry farms that use uncommon ARV vaccinations has been increasingly observed in Egypt. As there are scarce studies on such an important disease in Egypt, genetic and antigenic characterization of emerging ARV strains is essential.

In the present study, 40 pooled synovial fluid samples were collected from 40 unvaccinated commercial broiler flocks, but their breeders were vaccinated (three doses of ARV vaccine). However, ARV is included in many pathological syndromes; the only major ARV-related clinical presentations are viral arthritis and runting–stunting syndrome (Jones and Guneratne, 1984; Rosenberger et al., 1989). Our samples were collected from birds suffering from arthritis/tenosynovitis and runting–stunting syndrome, which commonly affects broiler chickens infected with ARV (Robertson, 1986; Benavente and Martínez-Costas, 2007; Ayalew et al., 2017). In the present study, we observed bilateral arthritis in most studied chickens with marked swelling in both hock joints, while in previous studies (Jones and Guneratne, 1984) either unilateral or bilateral arthritis could be observed in ARV infection. The most characteristic clinical signs and postmortem evidence of runting–stunting syndrome observed in this study were stunted growth and enlarged lemon-shaped proventriculus with reduced gizzard size, as described elsewhere (Page et al., 1982; Hieronymus et al., 1983). In relation to microscopic lesions, as shown in our study, tenosynovitis, myocarditis, and hepatitis were the most common pathological lesions associated with ARV in the affected birds. The noticed lesions were consistent with previously reported data (Souza et al., 2018; Choi et al., 2022). Similarly, the experimental infection of ARV showed an interesting finding regarding the appearance of the ARV lesions, and footpad infection demonstrated earlier hock lesions mostly after 2 days of infection (Chen et al., 2015). In relation to systemic infection, it was accompanied by pericarditis, hepatitis, pancreatitis, and bursal atrophy. Lymphocytes and macrophages were the most components of the infiltrate. Taken into consideration, the bursa and intestinal mucosa may be a site for the initial replication of ARV, while the joints were the most serious consequence of viral replication (Jones, 2000). Importantly, the macrophages play a key role in viral replication and transmission (Mills and Wilcox, 1993). In the present study, the hepatic lesion showed multifocal yellowish foci, which is consistent with several previous reports (Choi et al., 2022). The foci consisted mostly of mononuclear cells consisting of lymphocytes and macrophages. In certain cases, lympho-histocytic infiltration and polykaryocytes appearance were reported (Mandelli et al., 1978). Interestingly, the main sites of the lesions as the hock joint, tendon, and lymphoid organs were the most organs used for viral isolation (Choi et al., 2022).

Along with the observed clinical signs, microscopic findings, and postmortem changes, the RT-PCR results confirmed the presence of ARV in all studied chickens, indicating that the arthritis was almost certainly ARV related. RT-PCR partial amplification of the sigma C gene was sensitive, and detected the virus in 100% of tested samples, while another study (Tang and Lu, 2016) concluded that some false-negative results could occur with sigma C gene amplification, as the sigma C sequence is highly variable. Even though the sigma C protein is within the most hypervariable region of ARV proteins (Liu et al., 2003), some other conserved sequences were identified within the sigma C protein (Goldenberg et al., 2010). Molecular characterization and genotypic correlation studies contribute to our understanding of the epidemiology, source, and evolution of emergent viral variants (Kant et al., 2003; Kort et al., 2015). Such studies mainly depend on the sequence of the extremely variable sequence in the ARV genome (sigma C gene), which is usually used to genotype ARV and classify it into antigenic clusters (Liu et al., 2003; Calvo et al., 2005; Goldenberg et al., 2010;

Kort et al., 2015; Lu et al., 2015; Ayalew et al., 2017). As the efficacy of a vaccine mainly relies on its genetic and antigenic relatedness to field strains, an analysis of the genetic variability of Egyptian field ARV strains in comparison to vaccine strains depending on the sigma C protein sequence was performed to gain a better understanding of the antigenic variability among circulating ARV strains in Egypt.

Phylogenetic analysis of the sigma C gene nucleotide and deduced amino acid sequences from our two selected isolates was performed, together with sequences of reference field and vaccine strains retrieved from GenBank. Generally, the phylogenetic trees revealed that all strains included in the phylogenetic analysis were genetically diverse and clustered into six genotypic clusters and six sigma C protein-based clusters, as described elsewhere (Liu et al., 2003; Kort et al., 2015; Lu et al., 2015; Sellers, 2017; Palomino-Tapia et al., 2018). De la Torre et al. (2021) detected seven genotypic clusters from poultry, and Kim et al. (2022) characterized six genotypic clusters from poultry and an additional seventh genotypic cluster from wild birds. The genetic diversity between established ARV strains and new variant strains may be due to accumulated mutations and numerous reassortment actions (Ayalew et al., 2020). Surprisingly, all vaccine strains were clustered in genotype I and deduced protein cluster I, and our isolates were genetically different, clustered in genotype V and deduced protein cluster V with other isolates from Israel (the same geographic location), suggesting that the genotype V and deduced protein cluster V strains might have the same epidemiological origin. Several studies (Kant et al., 2003; Liu et al., 2003; Goldenberg et al., 2010) reported that it was not possible to relate ARV infection to geographic location, but another study (Ayalew et al., 2020) reported that there was widespread geographic intermixing of ARV, with the non-specific distribution of the six ARV genotypes in different countries around the world, which suggests that effective ARV prevention cannot be achieved without a vaccine formulation that contains the proper antigens from all ARV genotypes.

Our results revealed high genetic diversity among the six clusters (13.21 to 57.65%), similar to a previous report (Goldenberg et al., 2010) that recorded 50% diversity among studied isolates. Despite the regular vaccination of breeder chickens against ARV, there have been recurrent ARV outbreaks in different localities in Egypt, and the vaccines are based on strains isolated in the USA. The parent strains of these vaccines (S1133, 2177, 2035, 2408, and 1733 vaccine strains) were developed in the late 1970s and early 1980s (Van der Heide et al., 1983; Rosenberger et al., 1989). Therefore, the failure of ARV vaccination together with the increased incidence of ARV infections may be due to the newly emerging strains, which are genetically divergent from the vaccine strains. This may explain the observed vaccination failure associated with traditional vaccines, and it significantly increases the complication and difficulty of controlling and preventing ARV infections effectively. These suggestions were supported in previous studies (Ayalew et al., 2017). The vaccine strains have been shown to be ineffective at protecting against ARV infection because the RNA nature of this virus causes different mutation events, generating new variant strains that are incompletely neutralized by the antibodies produced against classical vaccine strains. Therefore, prompt characterization and genotyping of the strains causing disease in the field is needed, then autogenous vaccines based on the field strains can be formulated (Goldenberg et al., 2010; Lublin et al., 2011; Sellers et al., 2013; Troxler et al., 2013).

Our results revealed up to 39.62% diversity within the deduced sigma C protein clusters, while another study (Chen et al., 2019) recorded 45.7–51.4% amino acid diversity between their field isolate and vaccine strains. Surprisingly, our strains were highly divergent from vaccine strains used in Egypt, showing 55.09–56.23% diversity, which explains the vaccination failure and recurrent circulation of ARV. These results were confirmed by a study (Palomino-Tapia et al., 2018) that stated that an effective autogenous vaccine program would require at least 95% amino acid similarity between this vaccine strain and the circulating field strains. Some countries have begun to formulate autogenous ARV vaccines from local field strains, such as in Israel, where an autogenous inactivated ARV vaccine was formulated from local field strain 641 to achieve a better immune response (Goldenberg et al., 2010). The present study has some limitations which include the limited number of sequenced samples and the use of degenerated primer set targeting the sigma C protein coding ORF which is a high variable gene.

5. Conclusion

Our results suggest that ARV variants can evade the immunity of commonly used vaccine strains, as our field strains highly diverged from the vaccine strains used in Egypt. These findings reflect the necessity of formulating a new effective vaccine from locally isolated ARV strains, following a thorough screening of the molecular nature of circulating ARV strains in Egypt. These findings provide novel baseline information about the genetic information of the virus.

Data availability statement

The original contributions presented in the study are included in the article/Supplementary material, further inquiries can be directed to the corresponding authors.

Ethics statement

The animal study was reviewed and approved by the Ethics Committee of the Kafrelsheikh University Animal Care and Use Committee, Kafrelsheikh University, Egypt with code number; KFS-2020/3.

Author contributions

SM, EE, AA, and WA were involved in the conception of the idea and methodology design and performed data analysis and interpretation. SM, EE, AA, FE-K, ME-K, LA, and WA participated in the methodology design, sampling and laboratory work, and data analysis. SM, EE, and WA contributed their scientific advice, prepared the manuscript for publication, and completed revisions. All authors have read and agreed to the published version of the manuscript.

Funding

This study was supported by Princess Nourah bint Abdulrahman University Researchers Supporting Project number (PNURSP2023R23), Princess Nourah bint Abdulrahman University, Riyadh, Saudi Arabia.

Conflict of interest

The authors declare that the research was conducted in the absence of any commercial or financial relationships that could be construed as a potential conflict of interest.

Publisher's note

All claims expressed in this article are solely those of the authors and do not necessarily represent those of their affiliated organizations, or those of the publisher, the editors and the reviewers. Any product that may be evaluated in this article, or claim that may be made by its manufacturer, is not guaranteed or endorsed by the publisher.

Supplementary material

The Supplementary Material for this article can be found online at: https://www.frontiersin.org/articles/10.3389/fmicb.2023.1156251/full#supplementary-material

References

Abd El-Samie, L. (2014). Some causes of chicken's growth retardation in sharkia, Egypt. *Assiut. Vet. Med. J.* 61, 32–37. doi: 10.21608/avmj.2014.169747

Al-Ebshahy, E., Mohamed, S., and Abas, O. (2020). First report of seroprevalence and genetic characterization of avian orthoreovirus in Egypt. *Trop. Anim. Health Prod.* 52, 1049–1054. doi: 10.1007/s11250-019-02100-z

Ammar, A. M., Abdeen, E. E., Abo-Shama, U. H., Fekry, E., and Kotb Elmahallawy, E. (2019). Molecular characterization of virulence and antibiotic resistance genes among *Salmonella* serovars isolated from broilers in Egypt. *Lett. Appl. Microbiol.* 68, 188–195. doi: 10.1111/lam.13106

Ammara, M. A., Abd El-Aziz, N. K., Nasef, S. A., Bakry, N. R., El Atfehy, N. M., Erfan, A. M., et al. (2014). Use of Multiplex PCR for detection of bacterial respiratory infections in poultry. *Zagazig Veter. J.* 42, 133–144. doi: 10.21608/zvjz.2014.60059

Attoui, H. (2011). "Family reoviridae in virus taxonomy: classification and nomenclature of viruses," in Ninth *Report of the International Committee on Taxonomy of Viruses* 541–54.

Ayalew, L. E., Ahmed, K. A., Mekuria, Z. H., Lockerbie, B., Popowich, S., Tikoo, S. K., et al. (2020). The dynamics of molecular evolution of emerging avian reoviruses through accumulation of point mutations and genetic re-assortment. *Virus Evol.* 6, veaa025. doi: 10.1093/ve/veaa025

Ayalew, L. E., Gupta, A., Fricke, J., Ahmed, K. A., Popowich, S., Lockerbie, B., et al. (2017). Phenotypic, genotypic and antigenic characterization of emerging avian reoviruses isolated from clinical cases of arthritis in broilers in Saskatchewan, Canada. *Sci. Rep.* 7, 1–13. doi: 10.1038/s41598-017-02743-8

Bányai, K., Dandár, E., Dorsey, K. M., Mató, T., and Palya, V. (2011). The genomic constellation of a novel avian orthoreovirus strain associated with runting-stunting syndrome in broilers. *Virus Genes.* 42, 82–89. doi: 10.1007/s11262-010-0550-z

Benavente, J., and Martínez-Costas, J. (2007). Avian reovirus: structure and biology. *Virus Res.* 123, 105–119. doi: 10.1016/j.virusres.2006.09.005

Bencina, D., Drobnic-Valic, M., Horvat, S., Narat, M., Kleven, S. H., Dovc, P., et al. (2001). Molecular basis of the length variation in the N-terminal part of *Mycoplasma synoviae* hemagglutinin. *FEMS Microbiol. Lett.* 203, 115–123. doi: 10.1111/j.1574-6968.2001.tb10829.x

Calvo, P. G., Fox, G. C., Parrado, X. L. H., Llamas-Saiz, A. L., Costas, C., Martínez-Costas, J., et al. (2005). Structure of the carboxy-terminal receptor-binding domain of avian reovirus fibre sigmaC. *J. Mol. Biol.* 354, 137–149. doi: 10.1016/j.jmb.2005.09.034

Chen, H., Yan, M., Tang, Y., and Diao, Y. (2019). Pathogenicity and genomic characterization of a novel avian orthoreovius variant isolated from a vaccinated broiler flock in China. *Avian Pathol.* 48, 334–342. doi: 10.1080/03079457.2019.1600656

Chen, Y. S., Shen, P. C., Su, B. S., Liu, T. C., Lin, C. C., Lee, L. H., et al. (2015). Avian reovirus replication in mononuclear phagocytes in chicken footpad and spleen after footpad inoculation. *Can. J. Vet. Res.* 79, 87–94.

Choi, Y. R., Kim, S. W., Shang, K., Park, J. Y., Zhang, J., Jang, H. K., et al. (2022). Avian reoviruses from wild birds exhibit pathogenicity to specific pathogen free chickens by footpad route. *Front. Veter. Sci.* 9, 844903. doi: 10.3389/fvets.2022.844903

Davis, J. F., Kulkarni, A., and Fletcher, O. (2012). Myocarditis in 9-and 11-day-old broiler breeder chicks associated with a reovirus infection. *Avian Dis.* 56, 786–790. doi: 10.1637/10267-060712-Case.1

De la Torre, D., Astolfi-Ferreira, C. S., Chacón, R. D., Puga, B., and Piantino Ferreira, A. J. (2021). Emerging new avian reovirus variants from cases of enteric disorders and arthritis/tenosynovitis in Brazilian poultry flocks. *Br. Poultry Sci.* 62, 361–372. doi: 10.1080/00071668.2020.1864808

Egaña-Labrin, S., Hauck, R., Figueroa, A., Stoute, S., Shivaprasad, H., Crispo, M., et al. (2019). Genotypic characterization of emerging avian reovirus genetic variants in California. *Sci. Rep.* 9, 1–10. doi: 10.1038/s41598-019-45494-4

Fahey, J., and Crawley, J. (1954). Studies on chronic respiratory disease of chickens II. Isolation of a virus. *Canad. J. Compar. Med. Veter. Sci.* 18, 13.

Gallardo, R. A. (2017). "Molecular epidemiology of reoviruses in California," in *Proceedings of the 66th of the Western Poultry Disease Conference* (Sacramento, California) 54–5.

Goldenberg, D., Pasmanik-Chor, M., Pirak, M., Kass, N., Lublin, A., Yeheskel, A., et al. (2010). Genetic and antigenic characterization of sigma C protein from avian reovirus. *Avian Pathol.* 39, 189–199. doi: 10.1080/03079457.2010.480969

Gouvea, V., and Schnitzer, T. J. (1982). Pathogenicity of avian reoviruses: examination of six isolates and a vaccine strain. *Infect. Immun.* 38, 731–738. doi: 10.1128/iai.38.2.731-738.1982

Hall, T. A. (1999). "BioEdit: a user-friendly biological sequence alignment editor and analysis program for Windows 95/98/NT," in *Nucleic acids symposium series* (London: Information Retrieval Ltd.) c1979–c2000.

Hieronymus, D. R., Villegas, P., and Kleven, S. (1983). Identification and serological differentiation of several reovirus strains isolated from chickens with suspected malabsorption syndrome. *Avian Dis.* 27, 246–254. doi: 10.2307/1590390

Jones, R. (2000). Avian reovirus infections. *Rev. Scientif. Tech.* 19, 614–619. doi: 10.20506/rst.19.2.1237

Jones, R., and Guneratne, J. (1984). The pathogenicity of some avian reoviruses with particular reference to tenosynovitis. *Avian Pathol.* 13, 173–189. doi: 10.1080/03079458408418522

Kant, A., Balk, F., Born, L., van Roozelaar, D., Heijmans, J., Gielkens, A., et al. (2003). Classification of Dutch and German avian reoviruses by sequencing the $ sigma $ C protein. *Vet. Res.* 34, 203–212. doi: 10.1051/vetres:2002067

Kim, S. W., Choi, Y. R., Park, J. Y., Wei, B., Shang, K., Zhang, J. F., et al. (2022). Isolation and genomic characterization of avian reovirus from wild birds in South Korea. *Front. Vet. Sci.* 9, 794934. doi: 10.3389/fvets.2022.794934

Kort, Y. H., Bourogâa, H., Gribaa, L., Hassen, J., and Ghram, A. (2015). Genotyping and classification of Tunisian strains of avian reovirus using RT-PCR and RFLP analysis. *Avian Dis.* 59, 14–19. doi: 10.1637/10879-060414-Reg.1

Kutkat, M., Hoda, M., Khalil, S., El-Fatah, M., and Torky, H. (2010). Studies on proventriculitis in broilers with molecular characterization of its viral causes. *J. Am. Sc.* 6, 582–592.

Lee, L., Wang, Y., and Shien, J. (1992). Serological characterization of reoviruses isolated from avian species in Taiwan. *J. Chin. Soc. Vet. Sci.* 18, 69–72.

Liu, H. J., Lee, L. H., Hsu, H. W., Kuo, L. C., and Liao, M. H. (2003). Molecular evolution of avian reovirus:: evidence for genetic diversity and reassortment of the S-class genome segments and multiple cocirculating lineages. *Virology.* 314, 336–349. doi: 10.1016/S0042-6822(03)00415-X

Lu, H., Tang, Y., Dunn, P. A., Wallner-Pendleton, E. A., Lin, L., Knoll, E. A., et al. (2015). Isolation and molecular characterization of newly emerging avian reovirus variants and novel strains in Pennsylvania, USA, 2011–2014. *Sci. Rep.* 5, 1–11. doi: 10.1038/srep14727

Lublin, A., Goldenberg, D., Rosenbluth, E., Heller, E. D., and Pitcovski, J. (2011). Wide-range protection against avian reovirus conferred by vaccination with representatives of four defined genotypes. *Vaccine.* 29, 8683–8688. doi: 10.1016/j.vaccine.2011.08.114

Mandelli, G., Rampin, T., and Finazzi, M. (1978). Experimental reovirus hepatitis in newborn chicks. *Vet. Pathol.* 15, 531–543. doi: 10.1177/030098587801500411

Mansour, S. M., ElBakrey, R. M., Orabi, A., Ali, H., and Eid, A. A. (2018). Isolation and detection of avian reovirus from tenosynovitis and malabsorption affected broiler chickens with involvement of vertical transmission. *J. Virol. Sci.* 4, 24–32.

Martínez-Costas, J., Grande, A., Varela, R., García-Martínez, C., and Benavente, J. (1997). Protein architecture of avian reovirus S1133 and identification of the cell attachment protein. *J. Virol.* 71, 59–64. doi: 10.1128/jvi.71.1.59-64.1997

Mills, J. N., and Wilcox, G. E. (1993). Replication of four antigenic types of avian reovirus in subpopulations of chicken leukocytes. *Avian Pathol.* 22, 353–361. doi: 10.1080/03079459308418926

Page, R., Fletcher, O., Rowland, G. N., Gaudry, D., and Villegas, P. (1982). Malabsorption syndrome in broiler chickens. *Avian Dis.* 26, 618–624. doi: 10.2307/1589910

Palomino-Tapia, V., Mitevski, D., Inglis, T., van der Meer, F., and Abdul-Careem, M. F. (2018). Molecular characterization of emerging avian reovirus variants isolated from viral arthritis cases in Western Canada 2012–2017 based on partial sigma (σ) C gene. *Virology.* 522, 138–146. doi: 10.1016/j.virol.2018.06.006

Ramzy, N. M., and Ibrahim, H. N., ElHadad, S. F. (2016). Molecular Characterization and Hemato Biochemical Studies of Reovirus in Ismailia Farms. *Egyptian J. Chem. Environ. Health.* 2, 167–182. doi: 10.21608/ejceh.2016.247635

Rekik, M. R., and Silim, A. (1992). Comparison of a vaccine strain and field isolates of avian reovirus by T1-oligonucleotide mapping. *Avian Dis.* 36, 237–246. doi: 10.2307/1591496

Robertson, M. D. (1986). Avian reovirus. *Vet. Bull.* 56, 155–174.

Rosenberger, J., Sterner, F., Botts, S., Lee, K., and Margolin, A. (1989). *In vitro* and *in vivo* characterization of avian reoviruses. I. Pathogenicity and antigenic relatedness of several avian reovirus isolates. *Avian Dis.* 33, 535–544. doi: 10.2307/1591118

Sellers, H., Linneman, E., Gauthiersloan, V., and Collet, T. (2013). "Isolation and characterization of reovirus field isolates from clinical cases of viral arthritis," in *Proceedings of the 62nd of the Western Poultry Disease Conference* (Sacramento, California).

Sellers, H. S. (2017). Current limitations in control of viral arthritis and tenosynovitis caused by avian reoviruses in commercial poultry. *Vet. Microbiol.* 206, 152–156. doi: 10.1016/j.vetmic.2016.12.014

Shanmugasamy, M., Velayutham, T., and Rajeswar, J. (2011). Inv A gene specific PCR for detection of *Salmonella* from broilers. *Veter. World.* 4, 562. doi: 10.5455/vetworld.2011.562-564

Shih, W. L., Hsu, H. W., Liao, M. H., Lee, L. H., and Liu, H. J. (2004). Avian reovirus σC protein induces apoptosis in cultured cells. *Virology.* 321, 65–74. doi: 10.1016/j.virol.2003.12.004

Souza, S. O., De Carli, S., Lunge, V. R., Ikuta, N., Canal, C. W., Pavarini, S. P., et al. (2018). Pathological and molecular findings of avian reoviruses from clinical cases of tenosynovitis in poultry flocks from Brazil. *Poult. Sci.* 97, 3550–3555. doi: 10.3382/ps/pey239

Spandidos, D., and Graham, A. (1976). Physical and chemical characterization of an avian reovirus. *J. Virol.* 19, 968–976. doi: 10.1128/jvi.19.3.968-976.1976

Tang, Y., and Lu, H. (2016). Whole genome alignment based one-step real-time RT-PCR for universal detection of avian orthoreoviruses of chicken, pheasant and turkey origins. *Infect. Genet. Evolut.* 39, 120–126. doi: 10.1016/j.meegid.2016.01.018

Tantawi, H., Amina, N., Youssef, Y., Fawzia, M., Al-Abdulla, J., El-Batrawi, A., et al. (1984). Infectious tenosynovitis in broilers and broiler breeders in Egypt. *Vet. Res. Commun.* 8, 229–235. doi: 10.1007/BF02214716

Troxler, S., Rigomier, P., Bilic, I., Liebhart, D., Prokofieva, I., Robineau, B., et al. (2013). Identification of a new reovirus causing substantial losses in broiler production in France, despite routine vaccination of breeders. *Veter. Rec.* 172, 556. doi: 10.1136/vr.101262

Van der Heide, L. (2000). The history of avian reovirus. *Avian Dis.* 44, 638–641. doi: 10.2307/1593104

Van der Heide, L., Kalbac, M., and Brustolon, M. (1983). Development of an attenuated apathogenic reovirus vaccine against viral arthritis/tenosynovitis. *Avian Dis.* 27, 698–706. doi: 10.2307/1590312

Zaher, K., and Mohamed, S. (2009). Diagnosis of avian reovirus infection in local Egyptian chicks. *Global Veter.* 3, 227–231.

Zhang, X., Ji, Y., Zhang, L., Harrison, S. C., Marinescu, D. C., Nibert, M. L., et al. (2005). Features of reovirus outer capsid protein μ1 revealed by electron cryomicroscopy and image reconstruction of the virion at 7.0 Å resolution. *Structure.* 13, 1545–1557. doi: 10.1016/j.str.2005.07.012

Zhong, L., Gao, L., Liu, Y., Li, K., Wang, M., Qi, X., et al. (2016). Genetic and pathogenic characterisation of 11 avian reovirus isolates from northern China suggests continued evolution of virulence. *Sci. Rep.* 6, 1–10. doi: 10.1038/srep 35271

frontiers | Frontiers in Microbiology

TYPE Original Research
PUBLISHED 09 May 2023
DOI 10.3389/fmicb.2023.1174737

OPEN ACCESS

EDITED BY
Lihua Wang,
Kansas State University, United States

REVIEWED BY
Dhinakar Raj Gopal,
Tamil Nadu Veterinary and Animal Sciences University, India
Niu Mingfu,
Henan University of Science and Technology, China

*CORRESPONDENCE
Xinyuan Qiao
✉ qiaoxinyuan@126.com

†These authors have contributed equally to this work and share first authorship

RECEIVED 27 February 2023
ACCEPTED 14 April 2023
PUBLISHED 09 May 2023

CITATION
Yu X, Jiang Y, Zhang S, Wang C, Wang R, Zhang L, Tao S, Cui W, Li J and Qiao X (2023) Development of a colloidal gold immunochromatographic strip with enhanced signal for the detection of bovine parvovirus. *Front. Microbiol.* 14:1174737. doi: 10.3389/fmicb.2023.1174737

Development of a colloidal gold immunochromatographic strip with enhanced signal for the detection of bovine parvovirus

Xiaoli Yu[1†], Yanping Jiang[1†], Songsong Zhang[1], Caihong Wang[1], Ruichong Wang[2], Lanlan Zhang[3], Siming Tao[1], Wen Cui[1], Jiaxuan Li[1] and Xinyuan Qiao[1*]

[1]Heilongjiang Key Laboratory for Animal Disease Control and Pharmaceutical Development, Department of Preventive Veterinary Medicine, College of Veterinary Medicine, Northeast Agricultural University, Harbin, China, [2]Department for Radiological Protection, Heilongjiang Province Center for Disease Control and Prevention, Harbin, China, [3]Promotion Demonstration Department of Heilongjiang Fishery Technology Extension Station, Harbin, China

Bovine parvovirus (BPV) is a pathogen responsible for respiratory and digestive tract symptoms in calves and abortion and stillbirth in pregnant cows. In this study, we developed a colloidal gold immunochromatographic (GICG) strip with an enhanced signal for detecting BPV according to the double-antibody sandwich principle and an enzyme-based signal amplification system to amplify the signal. This system utilizes horseradish peroxidase reacting with a substrate solution containing 3,3′,5,5′-tetramethylbenzidine and dextran sulfate to obtain insoluble blue products on the test and control lines. We optimized different reaction conditions, including the amount of monoclonal antibodies (mAbs), pH of the colloidal gold solution, coating solution, blocking solution, sample pad treatment solution, antibody concentration in the control line, and antibody concentration in the detection line. The sensitivity of the signal-enhanced GICG strip showed that the minimum amount for detecting BPV was 10^2 $TCID_{50}$, 10 times higher than that of the traditional GICG strip. The results of the specificity test showed that the signal-enhanced GICG strip had no cross-reactivity with BRV, BVDV, or BRSV. The results of the repeatability test showed that the coefficient of variation between and within batches was less than 5%, showing good repeatability. Moreover, for validation, PCR and the signal-enhanced GICG strip were used to detect 280 clinical bovine fecal samples. The concordance rate compared with PCR was 99.29%. Hence, the developed strip exhibited high sensitivity and specificity for the detection of BPV. Therefore, this strip could be a rapid, convenient, and effective method for the diagnosis of BPV infection in the field.

KEYWORDS

bovine parvovirus, monoclonal antibody, signal enhancement, colloidal gold immunochromatography, antigen dectection

1. Introduction

Bovine parvovirus (BPV) is a member of the genus Bocaparvovirus of the family Parvoviridae (Qiu et al., 2017). It is the smallest icosahedral virus, with no envelope and a diameter of approximately 23 nm. The BPV genome consists of single-stranded DNA with a length of 5,491 nt (Kailasan et al., 2015), with three open reading frames (ORFs). ORF1 encodes a

729-amino-acid-long protein, the non-structural protein NS1. ORF2 encodes a 255-amino-acid-long protein, the non-structural protein NP1. The viral structural proteins VP1 and VP2 are encoded by ORF3. The molecular weights of VP1 and VP2 are 75 and 61 kDa, respectively. At the same time, VP3 is produced after the hydrolysis of the VP2 protein, which is involved in BPV DNA replication and virion assembly. BPV infection mainly causes reproductive dysfunction in pregnant cows and respiratory and gastrointestinal diseases in newborn calves. BPV can be transmitted in several ways, and the initial clinical symptoms of infection are not obvious (Zhang et al., 2020), making it difficult to diagnose and prevent infections. Traditionally, BPV detection is mainly based on serological, etiological, and molecular methods. Most traditional methods require a long time and special laboratory diagnosis equipment (Wang et al., 2019a; Gong et al., 2020). Therefore, a rapid, specific, and convenient method for field detection is of practical significance for the prevention and control of BPV infections.

Since colloidal gold has been introduced into the field of immunochemistry, this technology has developed and matured. Specifically, the colloidal gold immunochromatographic (GICG) strip is a fast and convenient detection method that is especially suitable for on-site detection. The reaction of gold-labeled antibodies with their corresponding antigens can result in a visible color reaction (Vilela et al., 2012). The distinctive advantages of colloidal gold particles are that they can be directly observed, and visible results can be obtained. Therefore, GICG strips have been widely used in various applications, Iing the diagnosis of viral infections and the detection of bacteria and drug residues in food (Wu et al., 2017; Lin et al., 2020; Pan et al., 2020). Their rapid analysis and simplicity of operation provide promising diagnostic methods for various applications. However, their detection sensitivity is low, limiting their application in clinical diagnosis. Hence, improving the sensitivity of GICG is an important research direction (Guo et al., 2019, 2021).

Currently, strategies to improve immunochromatographic technologies mainly focus on developing new solid-phase carriers or the addition of novel labeling molecules. Some studies combined newer technologies with strip detection, such as photoelectric sensing and microchip technologies. One strategy to improve sensitivity is to combine an enzyme signal amplification system with colloidal gold-labeled antibodies. Colloidal Au particles can be used to combine antibodies and enzymes. Moreover, horseradish peroxidase (HRP) can be conjugated to colloidal gold-labeled antibodies and improve the color depth of the strip (Parolo et al., 2013; Cho et al., 2015). Hence, enzyme signal amplification systems can effectively improve the detection sensitivity of GICG strips.

In this study, a signal-enhanced GICG strip for detecting BPV was developed using purified monoclonal antibodies (mAbs) and polyclonal antibodies (pAbs) against BPV. This method is specific, rapid, and sensitive for the detection of BPV, which is suitable for pathogen diagnosis in the field.

2. Materials and methods

2.1. Ethics statement

All animal experiments and animal maintenance procedures were performed according to the Ethical Committee for Animal Sciences of Heilongjiang Province and international recommendations for animal welfare. This trial was conducted in accordance with the regulations governing laboratory animals and the Charter of the Ethics Committee for Laboratory Animals of Northeast Agricultural University (Protocol code NEAU2018024).

2.2. Cells and virus strains

The myeloma (SP2/0) cells line was purchased from the China Center for Type Culture Collection (Wuhan, China). Bovine parvovirus(BPV; ATCC strain VR-767), Bovine rotavirus (BRV; strain NCDV), Bovine viral diarrhea virus (BVDV; strain BA), and Bovine respiratory syncytial virus (BRSV; strain 391–2), were stored in our lab. Bovine turbinate (BT) cell lines.

2.3. Animals

Specific pathogen-free BALB/c mice and New Zealand rabbits were purchased from Changsheng Biotechnology Limited (Liaoning, China).

2.4. The culture and purification of BPV

Maintain BT cells in culture flasks containing cell maintenance medium in an incubator at 37°C with 5% CO_2. Trypsinize a confluent flask of BT cells, and then trypsin was discarded. After adding 3% v/v serum cell maintenance solution, and cultured it in an incubator for 6–12 h. After that, BPV was inoculated into BT cells. When the cytopathic effect reached 80%, the virus culture was collected, which was centrifuged at 4°C and 10,000 r/min for 2 min. The supernatant fluid containing virus was collected and used to immunize animals.

2.5. Preparation of pAbs and mAbs

New Zealand rabbits were administered with purified BPV (500 μg) after emulsification in complete Freunds' adjuvant (Sigma, St. Louis, MO, United States) for the first injection and the same dose after emulsification in incomplete Freunds' adjuvant (Sigma) given as two boosters every 2 weeks. Sera were collected 7 days after the last booster. Immunoglobulins were precipitated using standard ammonium sulfate precipitation. Briefly, an equal amount of saturated ammonium persulfate solution was dropped into the mixed serum, stirring on ice until a precipitate was formed. The mixture was centrifuged at 12,000 × *g* for 30 min. The deposits were dissolved in PBS, dialyzed against PBS, and the protein concentration was determined. The pAbs were analyzed using sodium dodecyl sulfate-polyacrylamide gel electrophoresis (SDS-PAGE) and an indirect immunofluorescence assay (IFA). In the IFA test, monoclonal or polyclonal antibodies were used as primary antibodies, and FITC-labeled goat anti-rabbit IgG (Sigma) or FITC-goat anti-mouse IgG (Sigma) were used as the secondary antibody.

BALB/c mice were administered purified BPV (100 ng) after emulsification in complete Freund's adjuvant for the first injection and the same dose after emulsification in incomplete Freund's adjuvant for two boosters every 2 weeks. After BALB/c mice were immunized with BPV, the splenocytes were harvested and fused with SP2/0 myeloma

cells. After fusion, hybridoma cells were screened using an indirect enzyme-linked immunosorbent assay (ELISA).

BALB/c mice were pretreated with liquid paraffin and then injected intraperitoneally with hybridoma cells secreting antibodies against BPV. Ascites were collected after 2 weeks. A double-antibody sandwich ELISA was used to detect ascites titers. Hybridoma cells with the highest titers and affinities were selected to prepare ascites and purify mAbs for use in subsequent experiments. Ascites were purified using a HiTrap Protein G HP (GE Healthcare, Milwaukee, United States) according to the manufacturer's instructions. The activity of the mAbs was analyzed *via* SDS-PAGE and IFA identification. MAbs isotype was detected by using an Monoclonal antibody isotyping kit (Sigma). Bovine Parvovirus protein reacting against mAbs was detected by Western blotting. The BT cell culture was as negative control.

2.6. Preparation of colloidal gold

Gold particles with an average diameter of 20 nm were prepared according to the method described by Wang et al. (2014). In brief, a suspension of gold particles was prepared under reflux conditions where 100 mL of a gold chloride solution (0.01%) was heated to boiling. Approximately, 1.0 mL of trisodium citrate solution (1%) was then added rapidly to the gold chloride solution while stirring. The resulting solution was boiled for another 5–10 min until the color of the mixture changed to wine red. The gold particles were detected using transmission electron microscopy (TEM) after cooling. Finally, 0.05% sodium azide (as a preservative) was added to the gold particle solution and then stored at 4°C.

2.7. Conjugation of anti-BPV mAbs with colloidal gold

Complexes of mAbs conjugated with colloidal gold were prepared according to a previous method (Shukla et al., 2011). In brief, the pH of the colloidal gold solution was adjusted to 8.0–9.0 with 0.2 M K_2CO_3. The following procedure was conducted to estimate the minimal amount of mAbs required to stabilize colloidal gold particles. First, 1 mL of colloidal gold solution was added quickly to 100 μL of serial dilutions of mAbs at increasing concentrations (10–100 μg/mL). After 5 min, 100 μL of 10% NaCl solution was added to the mixture and was left to stand for another 2 h. When the amount of mAbs added exceeded the minimum required to stabilize colloidal gold particles, the color was unchanged or changed from reddish to blue. The optimum concentration of mAbs added was 130% of the lowest concentration needed for labeling. One hundred microliters of mAbs at the optimum concentration were then added to each tube and mixed. After 5 min, 100 μL of a 10% NaCl solution was added to the mixture. After 2 h, the color of the solution was observed. The optimum pH of the colloidal gold solution was the minimum pH at which the solution remained reddish.

To conjugate anti-BPV mAbs with colloidal gold, the optimum concentration of mAbs which determined by the above method was rapidly added to 20 mL of the colloidal gold solution and incubated for 30 min after rapid stirring. The mixture was then stabilized with a 5% BSA solution (the final concentration of BSA was 1%) and stirred for 30 min. After incubation for 1 h, the supernatant was discarded *via* centrifugation at 10,000 × g for 30 min at 4°C. Twenty milliliters of a 2% BSA solution (containing 0.01 M sodium borate) was then used to resuspend the precipitate, which was centrifuged again at 10,000 × *g* for 30 min at 4°C to clean off the unlabeled mAbs. Finally, 4 mL of a TB solution (containing 3% sucrose, 3% BSA, 0.05% sodium azide, and 0.01 M sodium borate) was used to resuspend the precipitate. The solution of colloidal gold-labeled mAbs was stored at 4°C. The conjugation of colloidal gold with mAbs was confirmed using UV–visible (UV/Vis) spectroscopy (Ultropec 2100 pro UV; Amersham Pharmacia, Sydney). The gold-labeled mAb solutions were stored at 4°C until use.

2.8. Preparation of colloidal gold and enzyme-labeled antibody conjugates

Horseradish peroxidase was used as the labeling enzyme. HRP-labeled mAbs were prepared by diluting the mAbs to 1 mg/mL following the instructions of an antibody-conjugated HRP kit (Abcam, Shanghai, China). ELISA was used to identify the effect of antibody conjugation with HRP. Briefly, the plates were coated with BPV, incubated overnight at 4°C, and blocked with PBS containing 2% BSA. Then, 100 μL of a 1:100 dilution of the enzyme was added to label the mAbs, which were incubated for 1.5 h at 37°C. After washing, 100 μl diluted HRP-labeled goat anti-mouse secondary antibodies (Sigma-Aldrich, United States) were added to the plates and incubated at 37°C for 1.5 h. The plates were washed by deionized water and 100 μL of 3,3′,5,5′-tetramethylbenzidine (TMB) color development solution (Sigma) was added. After incubating at 37°C in the dark for 10 min, 50 μL of a 10% of sulfuric acid was added, and the absorbance was measured at 490 nm using a microplate reader.

Complexes of enzyme-labeled mAbs conjugated with colloidal gold were prepared according to a previous method (Shukla et al., 2011). The prepared HRP enzyme-labeled mAbs were conjugated with colloidal gold particles under the same conditions as previously described, which was placed in the conjugate pad. The conjugation of colloidal gold with mAbs was examined using UV/Vis spectroscopy.

2.9. Optimizing the reaction reagents

It is necessary to optimize the reaction reagents to improve the performance of signal-enhanced test strips. Here, 0.01 M phosphate buffer (PB, containing 0.6% $NaH_2PO_4{\cdot}2H_2O$ and 2.2% $Na_2HPO_4{\cdot}12H_2O$), PBS, and 20 mM Tris-Cl were used as coating solutions to treat the antibodies. Control and test lines were used to analyze the effects of these coating solutions. Moreover, 3% BSA, 5% BSA, 3% skim milk, and 5% skim milk were used as blocking solutions, respectively. The background color and sample chromatography time were determined to analyze the effects of blocking. The sample pads were soaked in solution A (0.05% Tween-20, 5% sucrose, 0.3% Triton X-100, and 1% BSA), solution B (0.05% Tween-20, 5% sucrose, 0.5% Triton X-100, and 0.5% BSA), solution C (5% sucrose, 0.3% Triton X-100, and 1% BSA), and solution D (5% sucrose, 0.5% Triton X-100, and 0.5% BSA) at 25°C for 30 min. Afterward, the sample pads were dried at 37°C for 3 h and stored at room temperature. Test lines were used to analyze the effects of the

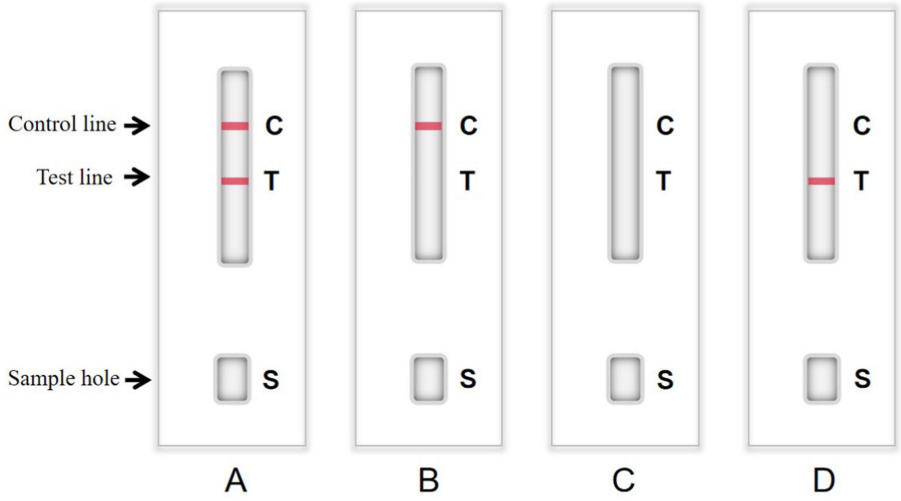

FIGURE 1
Structure chart of colloidal gold immunochromatographic (GICG) strip. **(A)** The test result is positive when both the test line and the control line are red. **(B)** When only the control line is red, the test result is negative. **(C)** The test result is invalid when there is no strip color. **(D)** The detection result is invalid only when the test line is red.

different treatment solutions. The detection procedure was as follows. First, 50 μL of a sample was added to the sample pad. TMB substrate was added to the sample pad, and the NC membranes were rinsed with deionized water. After 10 min, the result was judged using the naked eye. If the sample contained detectable particles, they formed complexes with the enzyme-labeled mAbs conjugated with colloidal gold. If the test line showed a weak color or color, the test result was weakly positive or positive, respectively. If the sample did not contain detectable particles, the test line would be colorless, indicating that the test result was negative. The color of the control line was used as a standard to evaluate whether the prepared strip was valid (color) or invalid (colorless; Figure 1). The goat anti-mouse IgG with a concentration of 1 mg/mL g was coated on the control line. The mAb in the conjugate pad bound with the colloidal gold and HRP conjugate to color the control line during testing.

2.10. Sensitivity and specificity of the prepared signal-enhanced test strips

Under the optimized conditions, enzyme-labeled signal-enhanced test strips and conventional test strips without enzyme labeling were prepared simultaneously. The sensitivity of the two test strips was also tested. Samples containing different concentrations of BPV (10^5 $TCID_{50}$/0.1 mL) were diluted in a series of 1, 1:10, 1:100, 1:1,000, and 1:10,000. The sensitivity of the signal-enhanced test strip was evaluated by detecting BPV at different concentrations, and the results were evaluated using the naked eye. The procedure was repeated thrice.

The specificity test was conducted with standard negative samples, standard positive samples, and samples containing bovine rotavirus (BRV), bovine viral diarrhea virus (BVDV), or bovine respiratory syncytial virus (BRSV) under optimized conditions to evaluate the specificity of the signal-enhanced test strip. Briefly, 50 μL of the samples were added to the sample pad and the results were observed after 10 min using the naked eye. The procedure was repeated thrice.

2.11. Detection of clinical samples

A total of 280 fecal samples from different farms where diarrheal disease occurred (Jilin Province, Liaoning Province, and Heilongjiang Province in China) were collected, placed in sterile polyethylene tubes, numbered, and transported to the laboratory using a car freezer (4°C). The fecal sample of 2 g was dissolved in 0.5 mL of sterile PBS solution, which was centrifuged for 10 min at 1,000 r/min, and then the supernatant was dropped in the sample hole of the developed strip. The results were observed after 10 min using the naked eye. The samples were then analyzed *via* PCR, conventional strip test, and the developed strips. We use a DNA extraction kit (Sigma-Aldrich, United States) to extract DNA from fecal samples. Specific primers were designed based on the conserved regions of the BPV VP2 gene in GenBank. The primers for PCR were designed using the Oligo6.0 software based on the conserved regions of VP2 gene. The amplicon sizes were 206 bp. The forward primer sequence is 5′-GCTGGCACTGCCGGGT-3′, and the reverse primer sequence is 5′-CTCCCTCTATTCCTCGGCTCT-3′. The reaction conditions were as follows: 95°C for 5 min followed by 30 cycles of 94°C for 30 s, 45°C for 30 s, and 72°C for 30 s and a final extension at 72°C for 10 min. Products were visualized on 2% agarose gels. The detection results of the signal-enhanced test strips were compared with those obtained using PCR.

3. Results

3.1. Quality evaluation of purified polyclonal antibodies and monoclonal antibodies

Mouse sera were collected 7 days after the last immunization. After purification using standard ammonium sulfate precipitation, aliquots were analyzed *via* SDS-PAGE. The results showed that the IgG protein was effectively purified. The light and heavy chains of

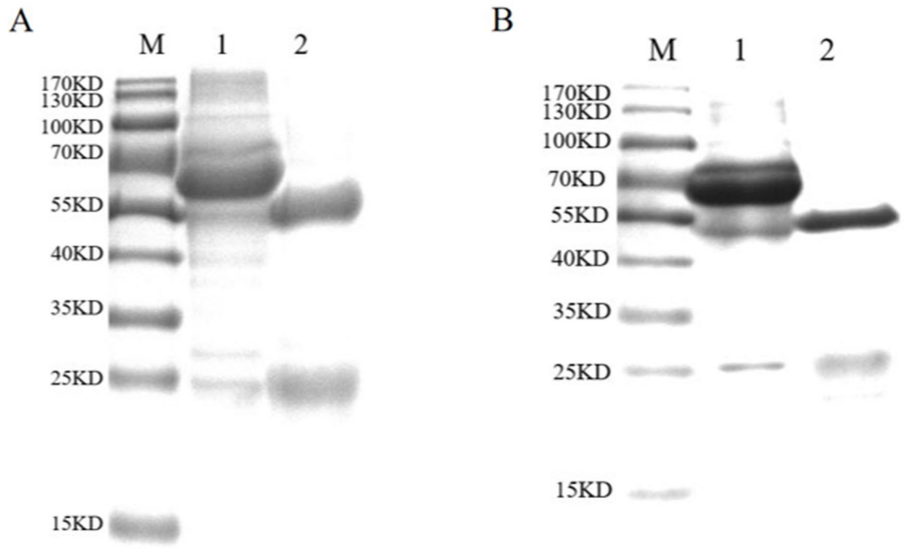

FIGURE 2
SDS-PAGE analysis of purified antibodies. **(A)** SDS-PAGE analysis of purified pAbs. Lane M: standard protein marker; Lane 1: unpurified pAbs; Lane 2: purified pAbs. The IgG protein was purified effectively. The light chain and heavy chain of IgG were clear and visible, and the sizes of them were 54 and 24kDa, respectively. **(B)** SDS-PAGE analysis of purified mAbs. Lane M: standard protein marker; Lane 1: unpurified mAbs; Lane 2: purified mAbs; the mAbs were purified effectively. The light chain and heavy chain were clear and visible, and the sizes of them were 55 and 25kDa, respectively.

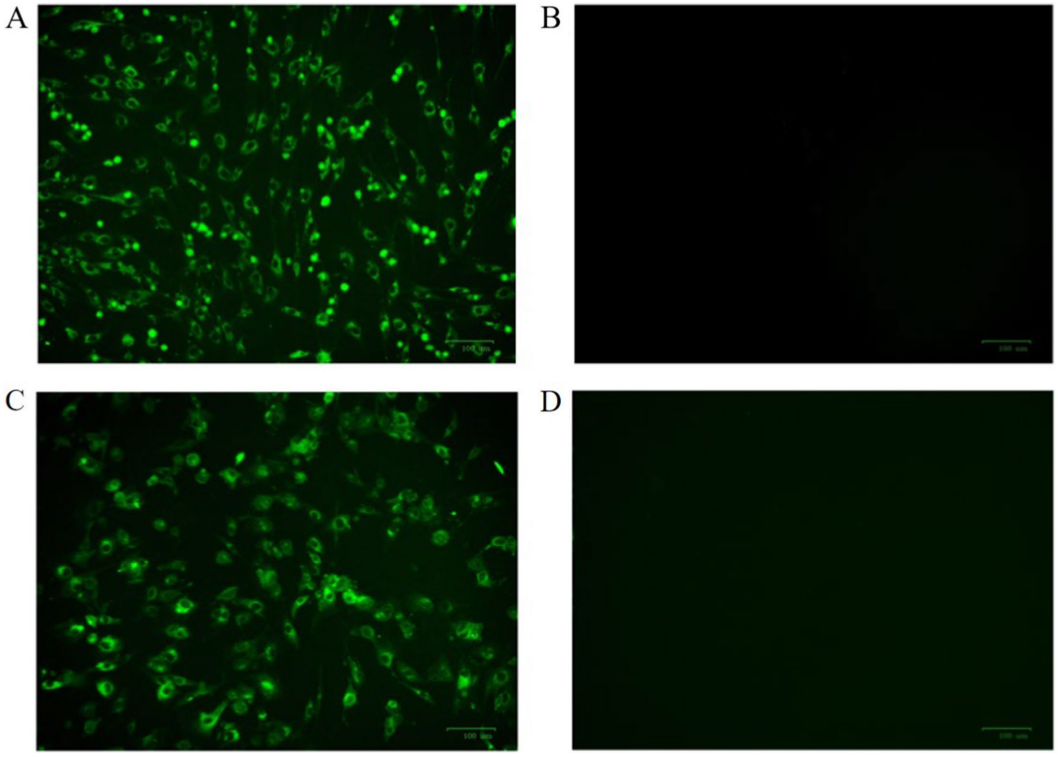

FIGURE 3
The indirect immunofluorescence identification results of antibodies were observed by fluorescence microscope. **(A)** BPV polyclonal antibody as primary antibody; **(B)** negative serum for primary antibody; **(C)** BPV monoclonal antibody as primary antibody; and **(D)** SP2/0 cell culture supernatant as primary antibody.

IgG were both clear and visible (Figure 2A). The purified BPV pAbs were identified using IFA (Figure 3). The results showed that green fluorescence could be detected in cells treated with BPV pAbs (Figure 3A), while no fluorescence was observed in the negative control (Figure 3B). The protein concentration was measured to be 10.52 mg/mL using a trace protein concentration meter. The pAbs against BPV was coated on the test line as a capture antibody. The pAbs coated on the test line was 10.52 mg/mL.

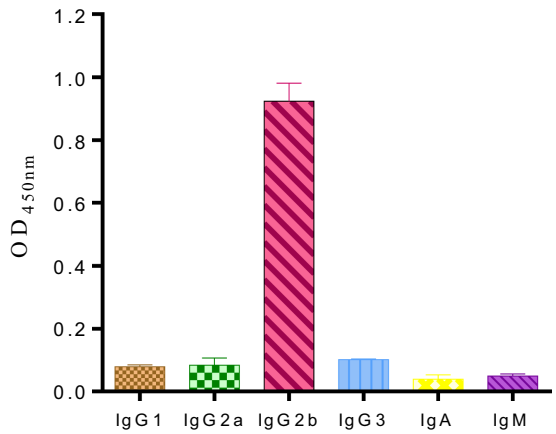

FIGURE 4
Subclass determination of the monoclonal antibody cells. The results showed that the subtype of monoclonal antibody was IgG2b subtype.

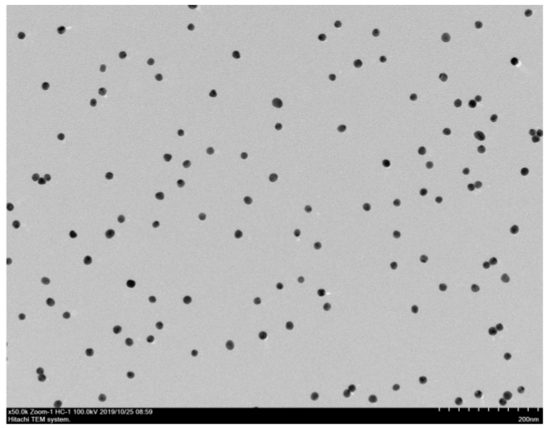

FIGURE 6
Transmission electron microscopy image of gold nanoparticles. Transmission electron microscope observation showed that particles had varying sizes and shapes with an average diameter of 25–15nm.

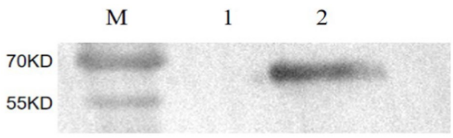

FIGURE 5
The identification of mAbs by Western blot. M: Protein molecular weight marker; 1: Negative control; 2: Purified BPV.

The purified mAbs were further analyzed using SDS-PAGE and IFA. The results showed that mAbs were effectively purified as both light and heavy chains were clear and visible (Figure 2B). The purified BPV mAbs were further evaluated using IFA. Specific green fluorescence was observed in cells treated with mAbs (Figure 3C), while no fluorescence was observed in the negative control (Figure 3D). The protein concentration was determined to be 3.12 mg/mL as measured using a trace protein concentration meter. The results showed that the subtype of mAbs was IgG2b (Figure 4). Western blot analysis showed that the band size was about 61 kDa, which was consistent with the size of the VP2 protein of BPV (Figure 5).

3.2. Characterization of colloidal gold particles

The results showed that the prepared colloidal gold particles were well-dispersed and uniform in size (Figure 6). Colloidal gold particles were spherical, with an average diameter of 18.8–22.5 nm. No aggregation of colloidal gold particles occurred, indicating that colloidal gold particles were stable in the solution. Colloidal gold particles exhibited good stability, and no precipitation occurred within 2 months. The absorption peak was at 520 nm according to the UV/Vis spectra because of the surface resonance of the colloidal gold particles. The peak width was narrow (Figure 7), meeting the standard for using colloidal gold as a probe.

3.3. Optimization and characterization of antibody-gold conjugates

The optimum pH value of the colloidal gold solution was the minimum pH value at which the solution remained reddish, which was 8.5 (Figure 8A). At pH 8.5, the optimum concentration of the purified antibody was determined. The result showed that the minimum concentration of purified mAbs to maintain the reddish color of the solution was 39.06 μg/mL (Figure 8B). The optimum concentration of mAbs to be added was 130% of this minimum to stabilize the solution. Hence, the optimum concentration of purified mAbs for conjugation was 50.78 μg/mL.

3.4. Characterization of colloidal gold and enzyme-labeled antibody conjugates

Horseradish peroxidase-labeled mAbs against BPV were detected *via* direct ELISA, and their OD_{450} values were determined (Figure 9). The results showed that HRP-labeled BPV mAbs were successfully prepared. Similarly, the UV/Vis absorption peak was at 520 nm because of the surface resonance of the colloidal gold particles (Figure 10).

3.5. Optimization of reaction reagents

According to the hybridization method mentioned above, the results showed that 0.01 M PB was the most effective coating solution in treating antibodies. The bands of the control line and the test line were more clearly visible after treating the antibodies with 0.01 M PB (Figure 11A). Furthermore, 3% BSA, 5% BSA, 3% skim milk, and 5% skim milk solution were used as blocking solutions (Figure 11B). The background was lighter when 3% BSA and 5% BSA solutions were used for blocking compared to the other solutions. Furthermore, the blocking time was shorter when using 3% BSA compared to 5% BSA, which was more suitable for rapid testing. The sample pads were soaked in different treatment solutions. The results showed that the test line was most

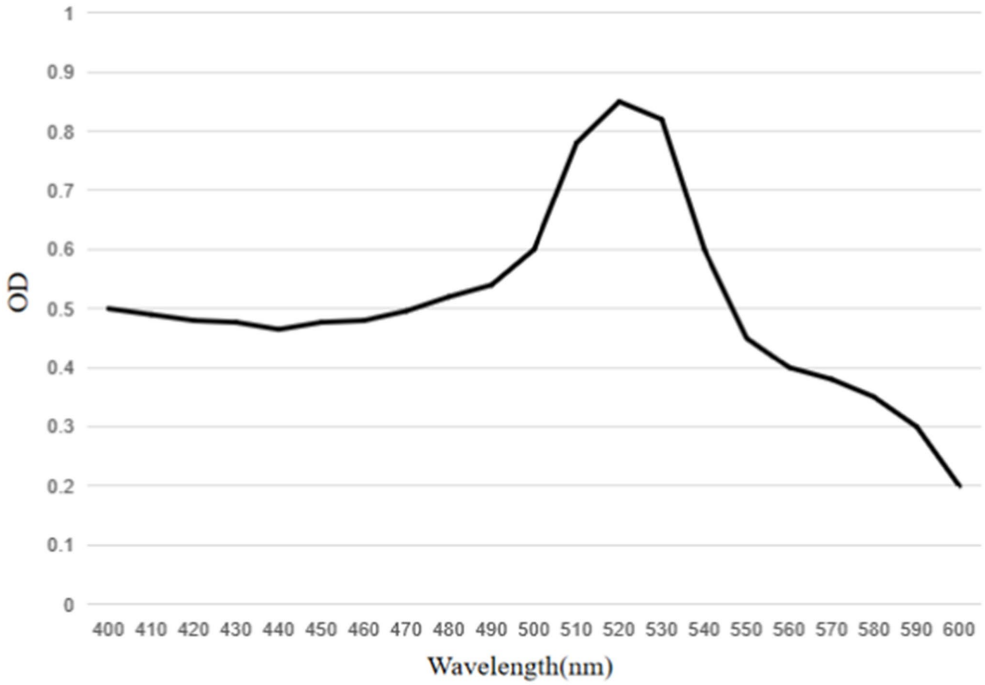

FIGURE 7
UV–visible spectra of mAbs labeled colloidal gold particles. The peak of the colloidal gold curve was at 520nm due to surface resonance of the colloidal gold particles. The peak width was narrow and met the standard of colloidal gold to use as probes.

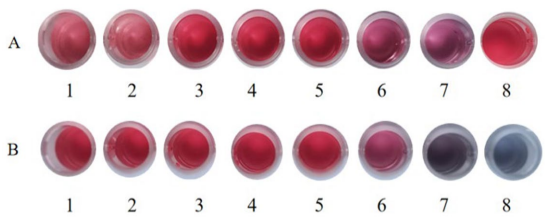

FIGURE 8
The optional pH of colloidal gold in labeling. **(A)** The colloidal gold solution was added into different tubes (1,000μL/tube) and the pH values of the colloidal gold solution were adjusted to (1) 7.0, (2) 7.5, (3) 8.0, (4) 8.5, (5) 9.0, (6) 9.5, and (7) 10.0 with 0.2M K2CO3, respectively. (8) Colloid gold solution without pH adjustment. **(B)** The optimum amount of gold-labeled antibodies. (1) Colloid gold solution. The 1mL of colloidal gold solution was added quickly into 100μL of (2) 312.5μg/mL, (3) 156.25μg/mL, (4) 78.13μg/mL, (5) 39.06μg/mL, (6) 19.53μg/mL, (7) 9.77μg/mL, and (8) 0μg/mL of mAbs, respectively.

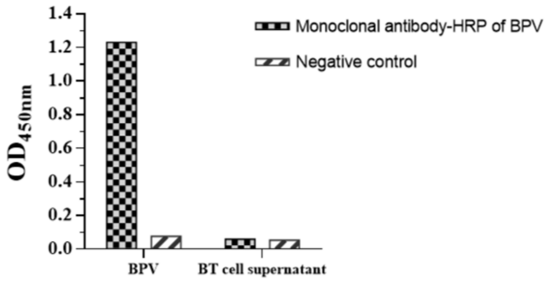

FIGURE 9
Identification of HRP labeled mAbs against BPV by direct ELISA.

clearly visible when the sample pad was soaked in solution A (0.05% Tween-20, 5% sucrose, 0.3% Triton X-100, and 1% BSA; Figure 11C). Based on these results, solution A was used to soak the sample pads.

3.6. Sensitivity and specificity evaluation

After preparing the conventional test strips, the sensitivity test results showed that the minimum amount of BPV they detected was approximately 10^3 $TCID_{50}$ (Figure 12A). In contrast, the sensitivity test results of the signal-enhanced test strips showed that the minimum amount of BPV they detected was approximately 10^2 $TCID_{50}$ (Figure 12B). These results indicate that the sensitivity of the signal-enhanced test strip was 10 times higher than that of an conventional test strip.

The specificity test results showed no cross-reaction when detecting BRV, BVDV, and BRSV using signal-enhanced test strips, showing good specificity (Figure 13). These results suggest that the signal-enhanced test strips showed good reactivity and specificity in detecting BPV.

3.7. Clinical sample testing

Two hundred and eighty fecal samples were collected from different farms (Jilin, Liaoning, and Heilongjiang provinces). Each sample was detected using the signal-enhanced GICG strip

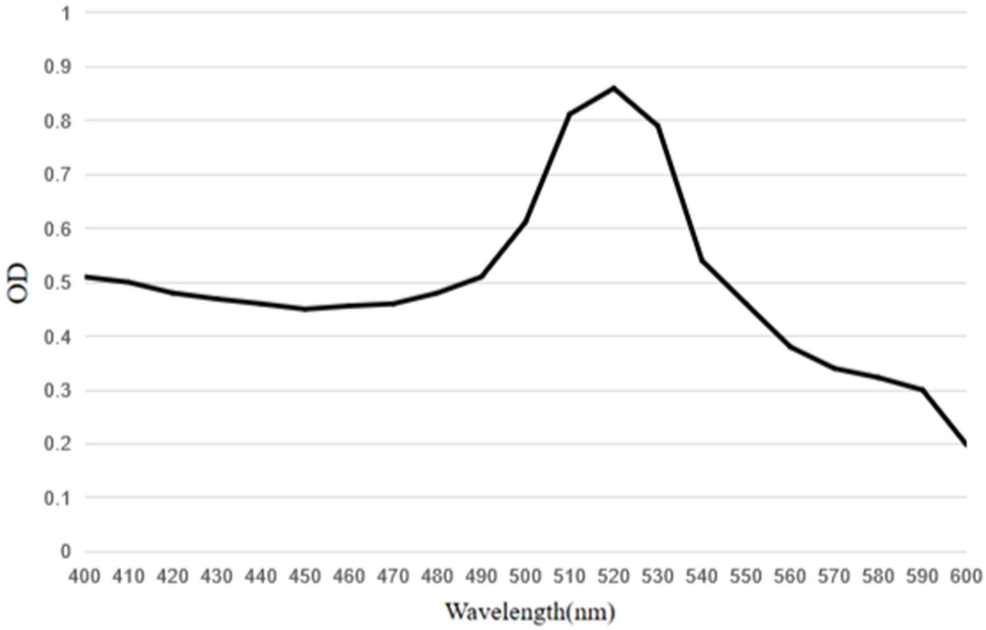

FIGURE 10
UV–visible spectra of conjugate of mAbs with HRP labeled colloidal gold particles. The peak of the colloidal gold curve was at 520nm due to surface resonance of the colloidal gold particles. The peak width was narrow and met the standard of colloidal gold to use as probes.

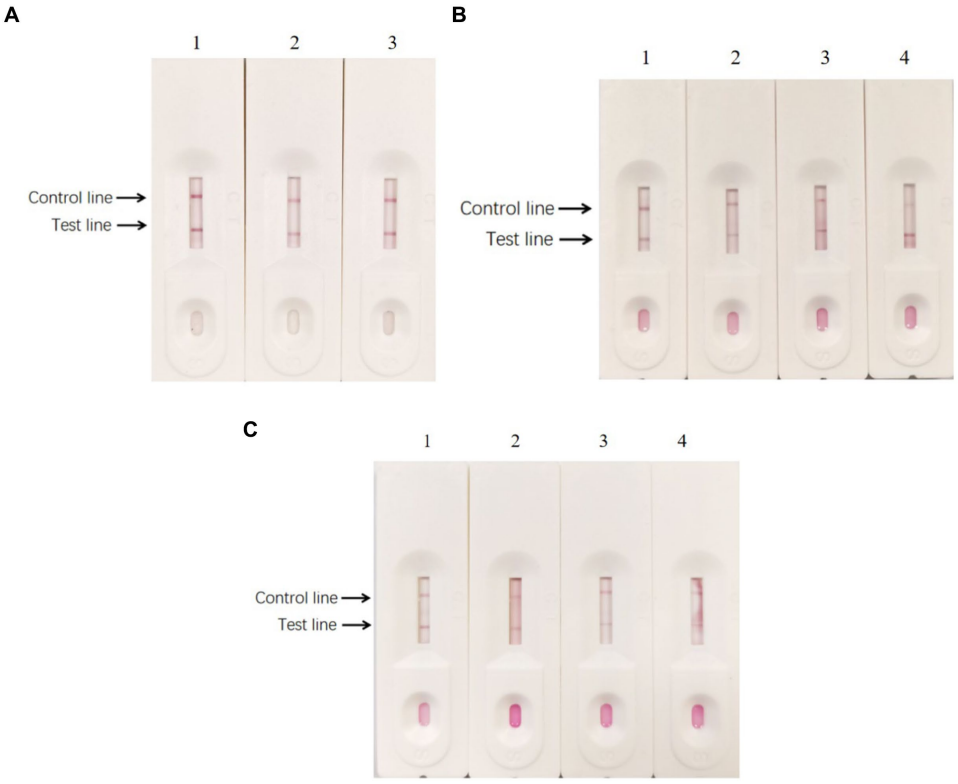

FIGURE 11
Optimization of reaction reagents. **(A)** Different coating solutions were used to treat the antibodies. (1) 0.01MPB; (2) PBS, and (3) 20mM Tris-Cl in treating the antibodies. **(B)** Different blocking solution. (1) 3% BSA; (2) 5% BSA; (3) 3% skim milk, and (d) 5% skim milk. **(C)** The sample pads were soaked in different solutions, respectively. (1) Containing 0.05% Tween-20, 5% sucrose, 0.3% Triton X-100, and 1% BSA; (2) containing 0.05% Tween-20, 5% sucrose, 0.5% Triton X-100, and 0.5% BSA; (3) containing 5% sucrose, 0.3% Triton X-100, and 1% BSA; (4) containing 5% sucrose, 0.5% Triton X-100, and 0.5% BSA.

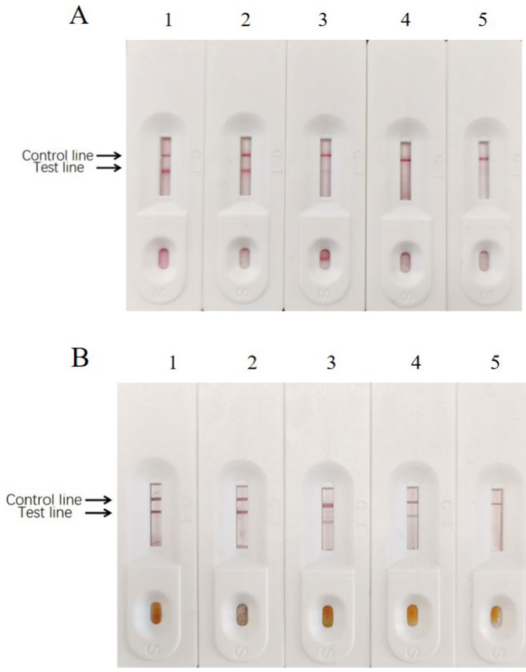

FIGURE 12
Sensitivity of enzyme-labeled signal-enhanced test strips. **(A)** Sensitivity of traditional GICG test strip. **(B)** Sensitivity of signal enhanced GICG test strip. BPV of 10^5 $TCID_{50}$/0.1ml was diluted in (1) 1, (2) 10, (3) 100, (4) 1000 and (5) 10000 fold, respectively.

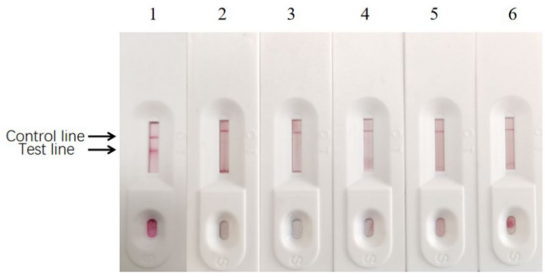

FIGURE 13
Results of specificity test of enzyme-labeled signal-enhanced test strips. (1) BPV; (2) BRV; (3) BVDV; (4) BRSV; (5) BT cell culture; (6) PB buffer solution.

(Figure 14A) and PCR (Figure 14B). Fourteen positive samples were detected using the signal-enhanced GICG strip. Twelve positive samples were detected using the conventional GICG strip, while 16 positive samples were detected by PCR. The test results for the signal-enhanced GICG strip and PCR were then compared (Table 1), showing that the concordance rate between the signal-enhanced GICG strip and PCR was 99.29%.The test results for the conventional GICG strip and PCR were then compared (Table 1), showing that the concordance rate between the conventional GICG strip and PCR was 98.57%. These results indicate that the sensitivity of the signal-enhanced test strip was higher than that of an conventional test strip.

4. Discussion

Bovine parvovirus infections can cause abortions in pregnant cows and affect herd reproduction rates (Barnes et al., 1982). Calves infected with BPV show respiratory and digestive symptoms such as dyspnea, cough, and diarrhea. After pathological examination of their respiratory and digestive tracts, lesions of different degrees were observed. BPV infection can be transmitted vertically and horizontally. Pregnant cows can directly infect fetal cattle during pregnancy (Liggitt et al., 1982). The seroprevalence of BPV in cattle herds is high owing to multiple transmission routes. Moreover, the initial clinical signs are not obvious as recessive infections (Storz et al., 1978), making early diagnosis and prevention difficult.

Some etiological and serological techniques have been developed for detecting BPV infections, such as virus isolation and identification, electron microscopy, PCR, fluorescence quantitative PCR (FQ-PCR), serum neutralization tests, IFA, and ELISA. Most of these methods need to be performed in the laboratory and require technicians or special instruments (Mengeling et al., 1986; Joon et al., 2019; Wang et al., 2019b). Therefore, these methods are unsuitable for field testing.

As a rapid and simple detection method, GICG technology has been increasingly used to detect various infectious pathogens (Song et al., 2016; Yu et al., 2019). BPV-infected cattle can shed viral particles in their feces; therefore, it is possible to detect antigens in fecal samples. In the present study, we developed a signal-enhanced GICG containing mAbs and pAbs against BPV to detect fecal antigens. Colloidal gold particles can initially adsorb protein antibodies (Pollitt et al., 2015). Many studies have shown that colloidal gold particles approximately 20 nm in diameter are suitable for mAb labeling. Hence, colloidal gold particles of approximately 20 nm in diameter were prepared in this study, which were dispersed and uniform in size. The dispersed colloidal gold particles flowed easily through the membrane. Moreover, the prepared colloidal gold particles had good stability, and no precipitation occurred within 2 months. The reaction conditions of the immunochromatographic test strip are important parameters affecting its quality (Ge et al., 2018; Li et al., 2020). Here, we optimized different reaction conditions, including the amount of mAbs, pH of the colloidal gold solution, coating solution, blocking solution, sample pad treatment solution, antibody concentration in the control line, and antibody concentration in the detection line. The method we developed is based on the double-antibody sandwich ELISA principle. Polyclonal antibodies, as capture antibodies, can recognize a variety of antigen epitopes. The mAbs against BPV are conjugated to HRP as the detection antibody, which can amplify the detection signal.

Most GICG tools for pathogen detection are based on the generation of color signals from colloidal gold tracers that are visible to the naked eye. These methods often exhibit low sensitivity. New materials have been introduced to improve the sensitivity of these test strips. Parolo et al. (2013) developed a GICG with a detection antibody modified with HRP, which amplified the detection signal. Cho et al. (2015) developed an enhanced enzyme-labeled GICG system. The detection limit of this system for *Escherichia coli* O157:H7 was 100 CFU/mL, which increased approximately 1,000-fold due to signal amplification (Cho et al., 2015). In this study, enzyme-labeled mAbs were used instead of mAbs on the test line to improve the sensitivity of the strip test. We used mAbs and enzyme-labeled mAbs

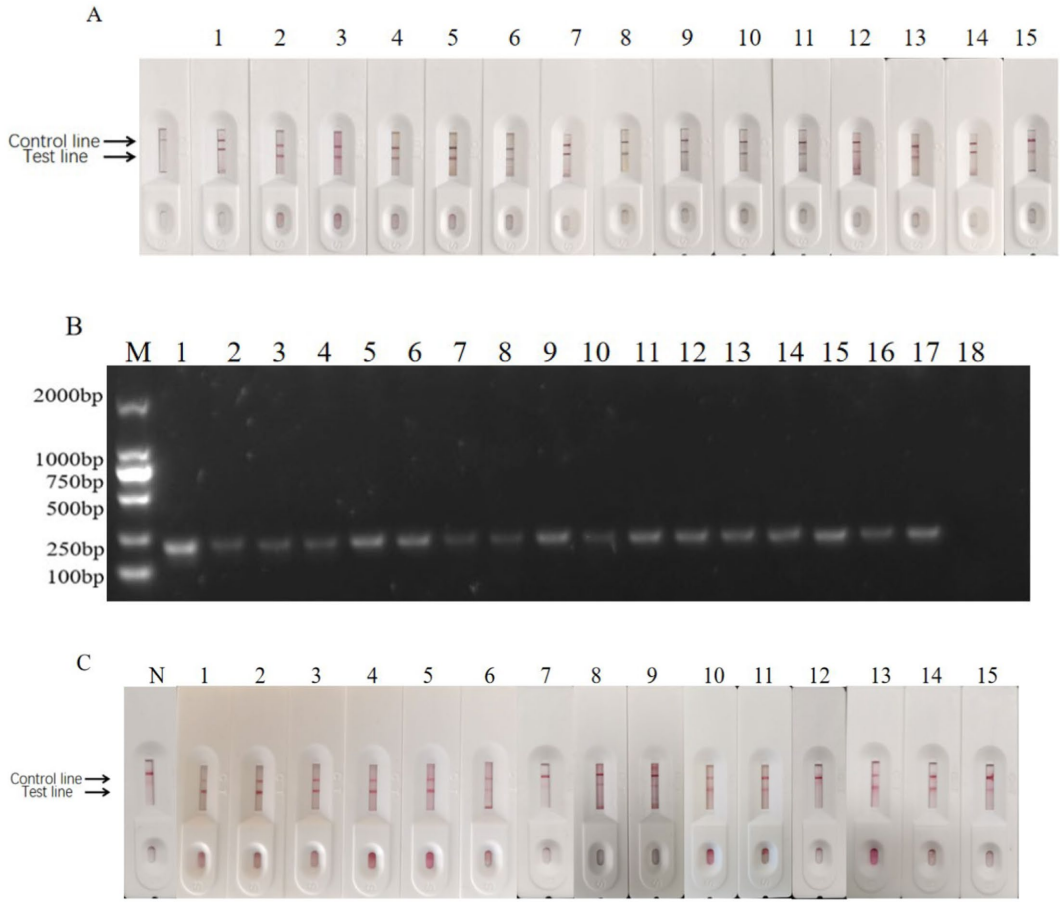

FIGURE 14
Clinical sample test results. **(A)** Positive sample test results of enzyme-labeled signal-enhanced test strips. N: Negative control; 1: Heilongjiang No.10; 2: Heilongjiang No.41; 3: Heilongjiang No.36; 4: Heilongjiang No.52; 5: Heilongjiang No.6; 6: Heilongjiang No.5; 7: Heilongjiang No.66; 8: Heilongjiang No.50; 9: Neimenggu No. 36; 10: Jilin No.8; 11: Jilin No.6; 12: Jilin No.22; 13: Heilongjiang No.235; 14: Heilongjiang No.231; and 15: Positive control. **(B)** The detection result of positive samples by PCR. M: DNA Marker; 1: Positive control; 2: Heilongjiang No.41; 3: Heilongjiang No.61; 4: Heilongjiang No.36; 5: Heilongjiang No.52; 6: Heilongjiang No.6; 7: Heilongjiang No.5; 8: Heilongjiang No.3; 9: Heilongjiang No. 66; 10: Heilongjiang No.50; 11: Neimenggu No.36. 12: Jilin No.8. 13: Jilin No.6. 14: Heilongjiang No.10; 15: Jilin No.22; 16: Heilongjiang No.235; 17: Heilongjiang No.231; and 18: Negative control. **(C)** Positive sample test results of enzyme-labeled signal-enhanced test strips. N: Negative control; 1: Heilongjiang No.10; 2: Heilongjiang No.41; 3: Heilongjiang No.36; 4: Heilongjiang No.52; 5: Heilongjiang No.6; 6: Heilongjiang No.5; 7: Heilongjiang No.66; 8: Heilongjiang No.50; 9: Neimenggu No. 36; 10: Jilin No.8; 11: Jilin No.6; 12: Jilin No.22; 13: Heilongjiang No.235; 14: Heilongjiang No.231; and 15: Positive control.

TABLE 1 Test results of clinical samples by signal-enhanced GICG strips and PCR.

Test method	Number of samples	Detection result (negative/positive)	Compliance rate of signal enhanced GICG strip	Positive sample compliance rate of signal enhanced GICG strip	Negative samples conformity rate of signal enhanced GICG strip
The signal enhanced GICG strip	280	266/14			
PCR	280	264/16	99.29%	87.5%	100%
The conventional GICG strip	280	268/12	99.29%	85.71%	100%

to prepare the signal-enhanced colloidal gold test strips. The limit of detection for BPV was 10^2 $TCID_{50}$/0.1 mL using the developed test strip. These results indicate that the sensitivity of the signal-enhanced test strip was 10 times higher than that of an ordinary test strip. TMB was used as an insoluble blue-violet chromogen, which was deposited in the control and test lines. The TMB introduced in this test did not require the use of a professional luminescence analyzer, and the improvement in sensitivity could be observed with the naked eye.

The validation assay revealed that the prepared test strip showed high specificity and no cross-reactivity with other clinical pathogens. To detect clinical samples, we compared the results of the test strip and PCR. The two methods showed good correspondence. Moreover, the test strips exhibited good specificity. Although PCR has a higher sensitivity and lower detection limit, the test strip is both simple and rapid. Unlike conventional detection methods, colloidal gold-based immunochromatographic strips can be easily used without special

equipment and only require simple visual judgment. Therefore, the colloidal gold immunochromatographic method established in this study not only improves the sensitivity of test strips but also does not require special detection instruments for diagnosing BPV infections. In the future, the GICG strip developed in this study may be more suitable for practical production, particularly for large-scale field analyses.

Data availability statement

The original contributions presented in the study are included in the article/supplementary material, further inquiries can be directed to the corresponding author.

Ethics statement

The animal study was reviewed and approved by Ethical Committee for Animal Sciences of Heilongjiang Province Ethics Committee for Laboratory Animals of Northeast Agricultural University.

Author contributions

XY, SZ, and CW performed the experiments. RW and LZ analyzed the experimental data. ST, WC, and JL collected the clinical samples. YJ collected the clinical samples and contributed to manuscript revision. XQ conceived and designed the study. All authors contributed to the article and approved the submitted version.

Funding

This research was funded by Key Research and Development Program of Heilongjiang Province (Grant no: GA21B004), the Natural Science Foundation of Heilongjiang Province (Grant no: LH2020C022), and the National Natural Science Foundation of China (NSFC; No. 32072876).

Conflict of interest

The authors declare that the research was conducted in the absence of any commercial or financial relationships that could be construed as a potential conflict of interest.

Publisher's note

All claims expressed in this article are solely those of the authors and do not necessarily represent those of their affiliated organizations, or those of the publisher, the editors and the reviewers. Any product that may be evaluated in this article, or claim that may be made by its manufacturer, is not guaranteed or endorsed by the publisher.

References

Barnes, M. A., Wright, R. E., Bodine, A. B., and Alberty, C. F. (1982). Frequency of bluetongue and bovine parvovirus infection in cattle in South Carolina dairy herds. *Am. J. Vet. Res.* 6, 1078–1080.

Cho, I. H., Bhunia, A., and Irudayaraj, J. (2015). Rapidpathogendetectionbylateral-flowimmunochromatographicassaywith gold nanoparticle-assisted enzyme signal amplification. *Int. J. Food Microbiol.* 206, 60–66. doi: 10.1016/j.ijfoodmicro.2015.04.032

Ge, W. L., Suryoprabowo, S., Wu, X. L., Zheng, Q. K., and Kuang, H. (2018). Rapid immunochromatographic test strip detection of mabuterol and its cross-reactivity with mapenterol. *Food Agric. Immunol.* 29, 1028–1040. doi: 10.1080/09540105.2018.1499709

Gong, Z. D., Shen, X. Y., Liang, H. Q., Geng, J. J., and Wei, S. C. (2020). Taq Manprobeq RT-PCRdetectsbovineparvovirus and appliesclinically. *Turk. J. Vet. Anim. Sci.* 44, 364–369. doi: 10.3906/vet-1907-80

Guo, J. C., Chen, S. Q., Guo, J. H., and Ma, X. (2021). Nanomaterial Labelsin LateralFlowImmunoassaysforPoint-of-care-testing. *J. Mater. Sci. Technol.* 60, 90–104. doi: 10.1016/j.jmst.2020.06.003

Guo, W. S., Zhang, Y., Hu, X. Y., Zhang, T., Liang, M., Yang, X. L., et al. (2019). Region growing AlgorithmCombinedWithFastPeakDetectionforSegmentingColloidal GoldImmunochromatographicStripImages. *IEEE Access* 7, 169715–169723. doi: 10.1109/ACCESS.2019.2955510

Joon, D., Nimesh, M., Gupta, S., Kumar, C., Varma-Basil, M., and Saluja, D. (2019). Development and evaluation of rapid and specific sdaA LAMP-LFD assay with Xpert MTB/RIF assay for diagnosis of tuberculosis. *J. Microbiol. Methods* 159, 161–166. doi: 10.1016/j.mimet.2019.03.002

Kailasan, S., Halder, S., Gurda, B., Bladek, H., Chipman, P. R., McKenna, R., et al. (2015). Structure of an enteric pathogen, bovine parvovirus. *J. Virol.* 89, 2603–2614. doi: 10.1128/JVI.03157-14

Li, G. Q., Rong, Z., Wang, S. Q., Zhao, H. Y., Piao, D. R., Yang, X. W., et al. (2020). Rapid detection of brucellosis using a quantum dot-based immunochromatographic test strip. *PLos Neglect Trop.* 14:e0008557. doi: 10.1371/journal.pntd.0008557

Liggitt, H. D., DeMartini, J. C., and Pearson, L. D. (1982). Immunologic responses of the bovine fetus to parvovirus infection. *Am. J. Vet. Res.* 8, 1355–1359.

Lin, L., Wu, X. L., Cui, G., Song, S. S., Kuang, H., and Xu, C. L. (2020). Colloidal gold ImmunochromatographicStripAssayfortheDetectionofAzaperoneinPork and pork liver. *ACS Omega* 5, 1346–1351. doi: 10.1021/acsomega.9b01841

Mengeling, W. L., Paul, P. S., Bunn, T. O., and Ridpath, J. F. (1986). Antigenic relationships among autonomous parvoviruses. *J. Gen. Virol.* 67, 2839–2844. doi: 10.1099/0022-1317-67-12-2839

Pan, Y. B., Li, X. R., Yang, G., Fan, J. L., Tang, Y. T., Zhao, J., et al. (2020). Serologicalimmunochromatographicapproachindiagnosiswith SARS-CoV-2infectedCOVID-19patients. *J. Inf. Secur.* 81, E28–E32. doi: 10.1016/j.jinf.2020.03.051

Parolo, C., de la Escosura-Muniz, A., and Merkoci, A. (2013). Enhancedlateralflowimmunoassayusinggoldnanoparticles loaded with enzymes. *Biosens. Bioelectron.* 40, 412–416. doi: 10.1016/j.bios.2012.06.049

Pollitt, M. J., Buckton, G., Piper, R., and Brocchini, S. (2015). Measuring antibody coatings on gold nanoparticles by optical spectroscopy. *RSC Adv.* 5, 24521–24527. doi: 10.1039/c4ra15661g

Qiu, J. M., Soderlund-Venermo, M., and Young, N. S. (2017). Human Parvoviruses. *Clin. Microbiol. Rev.* 30, 43–113. doi: 10.1128/CMR.00040-16

Shukla, S., Leem, H., and Kim, M. (2011). Development of a liposome-based immunochromatographic strip assay for the detection of Salmonella. *Anal. Bioanal. Chem.* 401, 2581–2590. doi: 10.1007/s00216-011-5327-2

Song, C. M., Liu, C., Wu, S. Y., Li, H. L., Guo, H. Q., Yang, B., et al. (2016). Development of a lateral flow colloidal gold immunoassay strip for the simultaneous detection of Shigella boydii and Escherichia coli O157:H7 in bread, milk and jelly samples. *Food Control* 59, 345–351. doi: 10.1016/j.foodcont.2015.06.012

Storz, J., Young, S., Carroll, E. J., Bates, R. C., Bowen, R. A., and Keney, D. A. (1978). Parvovirus infection of the bovine fetus:distribution of infection, antibody response，and age-related susceptibility. *Am. J. Vet. Res.* 7, 1099–1102.

Vilela, D., Gonzalez, M. C., and Escarpa, A. (2012). Sensingcolorimetricapproachesbasedongold and silvernanoparticlesaggregation: Chemicalcreativitybehindtheassay. *Anal. Chim. Acta* 751, 24–43. doi: 10.1016/j.aca.2012.08.043

Wang, Y., Wang, L. F., Zhang, J. W., Wang, G. X., Chen, W. B., Chen, L., et al. (2014). Preparation of colloidal gold immunochromatographic strip for detection of paragonimiasis skrjabini. *PLoS One* 9:e092034. doi: 10.1371/journal.pone.0092034

Wang, M. M., Yan, Y., Wang, R. C., Wang, L., Zhou, H., Li, Y. J., et al. (2019b). Simultaneous detection of bovine rotavirus, bovine parvovirus, and bovine viral

diarrhea virus using a gold nanoparticle-assisted PCR assay with a dual-priming oligonucleotide system. *Front. Microbiol.* 10:2884. doi: 10.3389/fmicb.2019.02884

Wang, M. M., Yan, Y., Wang, R. C., Wang, L., Zhou, H., Li, Y. J., et al. (2019a). Simultaneous Detectionof BovineRotavirus, bovine parvovirus, and bovine viral DiarrheaVirusUsingaGoldNanoparticle-assisted PCRAssayWithaDual-priming oligonucleotide system. *Front. Microbiol.* 10:2884. doi: 10.3389/fmicb.2019.02884

Wu, W. D., Li, M., Chen, M., Li, L. P., Wang, R., Chen, H. L., et al. (2017). Developmentofacolloidalgoldimmunochromatographicstripforrapiddetectionof Streptococcusagalactiaeintilapia. *Biosens. Bioelectron.* 91, 66–69. doi: 10.1016/j.bios.2016.11.038

Yu, M. M., Bao, Y. L., Wang, M. P., Zhu, H. B., Wang, X. Y., Xing, L. X., et al. (2019). Development and application of a colloidal gold test strip for detection of avian leukosis virus. *Appl. Microbiol. Biotechnol.* 103, 427–435. doi: 10.1007/s00253-018-9461-z

Zhang, M. D., Hill, J. E., Godson, D. L., Ngeleka, M., Fernando, C., and Huang, Y. Y. (2020). Thepulmonaryvirome, bacteriological and histopathologicalfindingsinbovine respiratorydiseasefromwestern Canada. *Transbound. Emerg. Dis.* 67, 924–934. doi: 10.1111/tbed.13419

frontiers | Frontiers in Microbiology

TYPE Original Research
PUBLISHED 31 May 2023
DOI 10.3389/fmicb.2023.1206021

OPEN ACCESS

EDITED BY
Peng Lin,
Bohai University, China

REVIEWED BY
Shichong Han,
Henan Agricultural University, China
Yajun Wang,
Northeast Forestry University, China

*CORRESPONDENCE
Lihua Wang
✉ lihua@vet.k-state.edu
Jingqiang Ren
✉ rjq207@163.com

RECEIVED 14 April 2023
ACCEPTED 08 May 2023
PUBLISHED 31 May 2023

CITATION
Ren J, Madera R, Cunningham C, Shi J and Wang L (2023) An easy method to generate recombinant pseudorabies virus expressing the capsid protein of Porcine circovirus type 2d. *Front. Microbiol.* 14:1206021. doi: 10.3389/fmicb.2023.1206021

An easy method to generate recombinant pseudorabies virus expressing the capsid protein of Porcine circovirus type 2d

Jingqiang Ren[1,2,3]*, Rachel Madera[1], Chase Cunningham[1], Jishu Shi[1] and Lihua Wang[1]*

[1]Department of Anatomy and Physiology, College of Veterinary Medicine, Kansas State University, Manhattan, KS, United States, [2]Institute of Virology, Wenzhou University, Chashan University Town, Wenzhou, China, [3]Key Laboratory of Special Animal Epidemic Disease, Ministry of Agriculture, Institute of Special Economic Animal and Plant Sciences, Chinese Academy of Agricultural Sciences, Changchun, China

Introduction: Homologous recombination is an effective way to generate recombinant viruses for vaccine research such as pseudorabies virus (PRV) and adenovirus. Its efficiency can be affected by the integrity of viral genome and the linearization sites.

Methods: In the study, we described a simple approach to isolate the viral DNA with high genomic integrity for large DNA viruses and a time-saving method to generate recombinant PRVs. Several cleavage sites in the PRV genome were investigated by using the EGFP as a reporter gene for identification of PRV recombination.

Results: Our study showed that cleavage sites of XbaI and AvrII are ideal for PRV recombination which showed higher recombinant efficiency than others. The recombinant PRV-EGFP virus can be easily plaque purified in 1–2 weeks after the transfection. By using PRV-EGFP virus as the template and XbaI as the linearizing enzyme, we successfully constructed the PRV-PCV2d_ORF2 recombiant virus within a short period by simply transfecting the linearized PRV-EGFP genome and PCV2d_ORF2 donor vector into BHK-21 cells. This easy and efficient method for producing recombinant PRV might be adapted in other DNA viruses for the generation of recombinant viruses.

KEYWORDS

pseudorabies virus, homologous recombination, linearization, efficient, PCV2d

Introduction

Pseudorabies virus (PRV) is a causative agent of Aujeszky's disease or pseudorabies that can cause reproductive failure characterized by abortion, embryonic death, mummification, and stillbirths. It also causes central nervous system problems, respiratory distress, and weight loss in pigs (Card et al., 1995; Guerin and Pozzi, 2005; Yin et al., 2012; Deng et al., 2022; Zheng et al., 2022). The virus belongs to the Herpesviridae family and has a double-stranded linear DNA genome. The genome of PRV is approximately 141–145 kb long which encodes at least 70 different proteins. A total of 11 different envelope glycoproteins of PRV have been identified, namely, gB, gC, gD, gE, gG, gH, gI, gK, gL, gM, and gN (Dietz et al., 2000; Klupp et al., 2004). The glycoproteins gB gD, gH, gL, and gK were identified as the essential proteins of PRV that are necessary for virus attachment to the host cell surface. The other glycoproteins such as gC, gE, gG, gI, gM, and gN are considered non-essential for viral entry and replication in which foreign genes can be inserted stably (Schmidt et al., 2001; Vallbracht et al., 2018).

It has been reported how attenuated PRV can be a useful vector to develop recombinant vaccines for protection against both pseudorabies and other diseases (Thomsen et al., 1987; Freuling et al., 2017; Feng et al., 2020; Tong et al., 2020; Zheng et al., 2020).

PRV Bartha-K61 is an attenuated PRV vaccine strain in which complete gE and partial gI genes have been deleted. The vaccine strain was developed in Hungary and produced by extensive passage *in vitro*. It can grow well in pig kidney cells (PK-15 cells), baby hamster kidney fibroblast cells (BHK-21 cells), chicken eggs, and chicken embryo fibroblast cells (CEF cells) (Dong et al., 2014). As a marker vaccine, the Bartha-K61 vaccine has played a significant role in the prevention of PRV and differential diagnosis of wild-type viruses from vaccine strain due to its safety and immunogenicity in pig vaccination (An et al., 2013; Wang et al., 2014; Delva et al., 2020). It is still widely used in many countries, including China. To date, there are several ways to generate recombinant PRV, co-transfection of plasmid DNA containing homologous arms and virus or viral genome directly (Tong et al., 2020; Zheng et al., 2020; Tan et al., 2022) and CRISPR/Cas9-mediated homologous recombination (Tang et al., 2016; Feng et al., 2020). Although conventional homologous recombination methods provide a convenient way to produce recombinant viruses and recombinant vaccines, the efficiency of recombination including the plaque purification of the recombinant virus requires several rounds of screening and will likely consume valuable time. In the present study, we described an easy and efficient method for the isolation of PRV genome DNA intact and the construction of recombinant PRV Bartha-K61 virus. To demonstrate the application of the established method, the capsid protein gene (ORF2) of PCV2d (a variant strain of porcine circovirus type 2, characterized by severe respiratory disease complex in pigs, which has become a predominant genotype circulating in swine herds in many countries) was amplified and inserted into the genome of PRV Bartha-K61.

Materials and methods

Cells and virus

PK-15 and BHK-21 cells were purchased from the American Type Culture Collection (ATCC, VA, United States) and cultured in Minimum Essential Medium (MEM; Gibco, MA, United States) or Dulbecco's modified Eagle's medium (DMEM; Gibco, MA, United States), supplemented with 10% fetal bovine serum (FBS; Atlanta Biologicals, GA, United States) and 1x antibiotic-antimycotic (Gibco, MA, United States) at 37 °C within a 5% CO_2 incubator. PRV Bartha-K61 strain was kindly provided by Professor Enquist (Princeton University). It was propagated in PK-15 cells and kept in liquid nitrogen until use.

Extraction of viral DNA

To obtain a complete viral genome, PK-15 cells were plated in a T75-mm flask at a concentration of 5×10^5 cells/flask and grown overnight to a confluence of 80–90%. The growth medium was replaced with 12 ml of fresh maintenance medium (MEM containing 2% FBS), and the cells were infected with PRV at a multiplicity of infection (MOI) of 0.5 PFU/cell. At 24 h post-infection, the culture medium was removed, and the cells were washed three times with 10 mL phosphate buffered saline (PBS). An additional 5 mL of PBS was added to the flask, and the cells were scraped into a 15-ml tube. After centrifugation at 2,000 x *g* for 20 min at 4°C, the cell pellet was resuspended in 1 ml lysis buffer solution (0.5% SDS, 10 mmol/L Tris-HCl pH 7.8, 5 mmol/L EDTA, 10 μg/ml RNase, and 50 μg/ml proteinase K) and incubated at 37°C in a water bath for 2–3 h. After centrifugation at 2,000 x *g* for 20 min at 4°C, the supernatant was collected in a new tube. The viral DNA in the supernatant was extracted with equal volumes of the UltraPure™ phenol:chloroform:isoamyl alcohol solution (25:24:1, v/v/v, Thermo Fisher Scientific, MA, United States) three times. The clear upper phase was transferred to a new 5-mL tube. In total, 2 volumes of ice-cold 100% ethanol and 1/10 volume of 3M sodium acetate (NaAc) at pH 5.2 were added to the tube, which was mixed by inverting the tube gently 8–10 times. The tube was then placed on ice for 10 min to separate the genomic DNA. A white floccule was obviously observed in the tube, which was the viral DNA. We carefully took the DNA using a sterile pipette tip or disposable inoculation loop and blotted the excess liquid, allowing it to dry for 5–10 min at room temperature. The viral DNA was resuspended in 200–500 μl TE buffer and maintained at 4°C for later use.

Construction of plasmids

The pUC-gG-MCS (pUG) vector was constructed by Jens B. Bosse (Professor Enquist Lab, Princeton University). It was derived from pUC57 plasmid by inserting 850 bp of homology into the surroundings of the PstI site in the gG gene locus of the PRV Becker strain. For convenient insertion of exogenous genes, a pCMV-IE-MCS-SV40pA cassette was inserted between the two recombinant arms (Figure 1A). To verify the recombinant plasmid system and facilitate plaque visualization, the EGFP gene was cloned into pUG between the restriction sites of AgeI and KpnI to generate the plasmid pUG-EGFP. To further confirm the system and generate the recombinant virus, another plasmid pUG-PCV2d_ORF2 holding the PCV2d ORF2 gene was constructed. The PCV2d ORF2 gene was inserted into the same sites as the EGFP gene.

Generation of recombinant virus

To investigate the efficiency of generation recombinant viruses and the chances of productive integration, different restriction enzymes were used to linearize the viral DNA according to the analysis of the viral genome (Figure 1B). Six groups with different transfection strategies were compared separately (Table 1). All linearized viral DNA and plasmids were precipitated with ethanol/NaAc as per the above description before the transfection step.

For transfection, BHK-21 cells were seeded into 6-well plates at 5×10^5 cells/well so that the monolayers could be 80–90% confluent on the following day. In total, 3 μg of digested plasmid

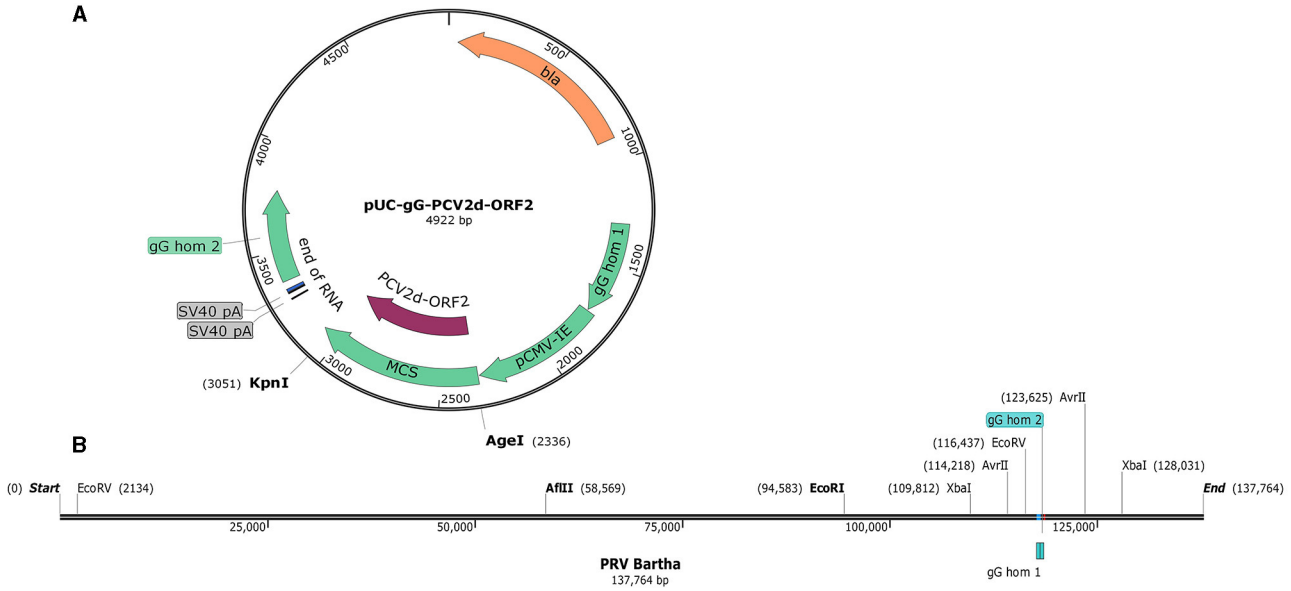

FIGURE 1
The map of the pUC-gG-MCS vector and the genome of PRV Bartha. **(A)** gG hom1 and gG hom2 are the two recombinant arms in the gG locus of PRV Becker. **(B)** Restriction enzyme analysis of the PRV Bartha genome, unique and dual cutters were listed and used in this study.

TABLE 1 Different groups of the transfection.

Groups	Linearization of viral DNA	Linearization of plasmid	Transfection complex mixture
A	EcoRI	HindIII	Linearized viral DNA + linearized plasmid
B	EcoRV	HindIII	Linearized viral DNA + linearized plasmid
C	XbaI	HindIII	Linearized viral DNA + linearized plasmid
D	AvrII	HindIII	Linearized viral DNA + linearized plasmid
E	XbaI	___	Linearized viral DNA + plasmid
F	___	HindIII	Virus + linearized plasmid

Viral genomes and plasmids were treated or non-treated with different restriction enzymes.

pUG-EGFP was co-transfected with 1.5 μg of linearized PRV genomic DNA using Lipofectamine 3000 (Thermo Fisher Scientific, MA, United States), according to the manufacturer's instructions. Fluorescent EGFP and CPE of the cells were checked daily under a fluorescent microscope with an objective lens of 20× magnification.

Plaque purification

After 1 or 2 days of incubation at 37°C, the single plaques were marked on the underside of the 6-well plate using a fine-tip marker pen under a fluorescence microscope. For the generation of the recombinant PRV, either viral plaques with fluorescence were selected (PRV-EGFP) or viral plaques without fluorescence signals were selected (PRV-PCV2d_ORF2). All marked plaques were picked separately from a 1.5-ml tube containing 200 μl DMEM using a sterile Pasteur pipette, and then the viral plaques were labeled and stored at −80 °C as stocks for the next passage. After 2 to 3 rounds of plaque purification, the selected plaques were passaged on PK-15 cells, and the cultured recombinant viruses were subjected to further analysis.

RT-PCR

Total cellular RNA of different plaque isolates was extracted using the commercially available viral nucleic acid extraction kit (IBI Scientific, IA, United States). The first-strand cDNA was prepared using a ProtoScript® first strand cDNA synthesis kit (New England Biolabs, MA, United States), according to the manufacturer's instructions. To confirm the recombinant virus PRV-PCV2d_ORF2, the inserted fragment of ORF2 was verified using PCR with the PCV2d ORF2 special primers (Forward primer: 5′-ACCGGTGCCACCATGACGTATCCAAGGAGGCG-3′, reverse primers 5′-GGTACCTCACTTAGGGTTAAGTGGGG-3′).

Immunofluorescence assay

PK-15 cells were dispensed into a 96-well plate and infected with PRV-PCV2d_ORF2 at an MOI of 1 in a final volume of 200 μl for 24 h. The cells were washed three times with PBS and fixed in cold methanol for 20 min at −20 °C. After fixation, the cells were permeated with 0.1% Triton X-100 at room temperature for 15 min

and incubated with 5% FBS for 1 h at 37 °C. The cells were then incubated with anti-PCV2 capsid MAb (RTI, PA, United States) for 2 h at 4°C. After three washes with PBS, the cells were subjected to immunofluorescence staining with Alexa Fluor 488 goat anti-mouse IgG secondary antibody (Thermo Fisher Scientific, MA, United States) for 1 h at room temperature. Following three washes with PBS, the fluorescence signal was detected under a fluorescent microscope.

Western blot

PK-15 cells were inoculated with PRV-PCV2d_ORF2 for 24 h in a 6-well plate. Cell lysates were separated using SDS-polyacrylamide gel electrophoresis (SDS-PAGE) with a gradient concentration of acrylamide (12%) followed by transfer onto nitrocellulose membranes. The membrane was blocked with 5% non-fat milk in PBS for 1 h and incubated with a mouse anti-PCV2 capsid MAb (RTI, PA, United States) overnight at 4°C. The following day, the membrane was incubated with a solution of horseradish peroxidase-conjugated rabbit anti-mouse IgG (Thermo Fisher Scientific, MA, United States) in PBS containing 1% non-fat milk for 1 h at room temperature. After incubation with SuperSignal West Pico chemiluminescent substrate (Thermo Fisher Scientific, MA, United States) for 5 min, the blots were analyzed with an imaging system.

Results

Generation of recombinant virus PRV-EGFP

Viral DNA was extracted from PRV Bartha-K61 strain-infected PK-15 cells. To facilitate plaque visualization, we cloned the EGFP gene into the pUC-gG-MCS (pUG) vector between the restriction sites of AgeI and KpnI to generate the plasmid pUG-EGFP. Co-transfection of the XbaI/AvrII linearized viral DNA and HindIII linearized pUG-EGFP into BHK-21 cells can produce obvious CPE and fluorescence signal at 24 h post-transfection (Figure 2G). The plaque purification of the recombinant viruses can be performed directly after the transfection. After two or three rounds of plaque picking, we successfully obtained the recombinant virus PRV-EGFP.

Selection of cleavage sites significantly affects the efficiency of recombination

To investigate the impact of cleavage sites on the efficiency of recombination, we linearized the viral DNA by different restriction enzymes. Co-transfection of linearized viral DNA with non-linearized plasmid pUG-EGFP caused an observable EGFP signal after transfection (Figure 2E). However, most of the fluorescence disappeared after the second round passage. When co-transfecting linearized viral DNA with linearized plasmid pUG-EGFP, expression of EGFP in cells can be observed in the EcoRI or EcoRV-treated viral DNA group. However, CPE or viral plaques were not easily detected after transfection (Figures 2A, B). Most interestingly, only the viral genome that was digested by XbaI or AvrII can cause obvious CPE and plaques after co-transfection with the linearized plasmid pUG-EGFP (Figures 2C, D). The recombinant efficiency of the AvrII-treated viral genome is higher than that of the XbaI-treated viral genome, which can produce more viral plaques. This indicates that the closer the linearized incision is to the ends of the recombination arm, the higher the recombination efficiency that will be generated.

Generation of the recombinant virus PRV-PCV2d_ORF2

The strategy to efficiently construct recombinant virus PRV-PCV2d_ORF2 is using the genome of the PRV-EGFP virus as the template and replacing the EGFP gene with PCV2d_ORF2 using the homologous recombination approach. We inserted the PCV2d ORF2 gene into the vector pUG to generate plasmid pUG-PCV2d_ORF2. As expected, plaques formed 24 h post-transfection by co-transfecting of XbaI-treated (compared with AvrII, XbaI is an economical site) genome DNA of PRV-EGFP virus and HindIII-treated plasmid pUG-PCV2d_ORF2 into BHK-21 cells. After two rounds of viral plaque purification (Figure 3A), the purified viruses without bring fluorescence were passaged on PK-15 cells (Figure 3B). RT-PCR (Figure 3C), sequencing, IFA, and Western blot (Figures 3D–F) results showed that we successfully obtained the recombinant virus PRV-PCV2d_ORF2.

Discussion

Homologous recombination is a type of genetic recombination in which the genetic material of the virus, eukaryote, or bacteria is exchanged naturally between two molecules of DNA that contain similar recombinant arms. Over the past few decades, it has been used extensively in the construction of recombinant adeno-associated virus (Fisher et al., 1997; Jacob et al., 2020), poxvirus (Fisher et al., 1997; Wyatt et al., 2015), and herpesvirus (Wilkinson and Weller, 2003; Boscheinen et al., 2019). It is a powerful tool to precisely manipulate the genome for producing a new gene or virus according to the experimental need. There were a variety of ways to produce recombinant PRV according to the previous reports (Takashima et al., 2002; Lin et al., 2005; Lerma et al., 2016; Tang et al., 2016). However, it is very time consuming to generate recombinant PRVs by using the limited dilution method. The strategy mentioned in this report, i.e., makes the plaque purification possible by monitoring EGFP which can be replaced in the future, significantly shortening the time for constructing recombinant PRVs.

Previous studies have reported that linearizing viral DNA at the desired insertion site before transfection can enforce homology-directed repair (HDR) by recombination with the co-transfected plasmids. To achieve this, a transfer virus expressing EGFP must be generated first by co-transfecting plasmid with PRV or PRV genome. Two unique restriction sites were designed and flanked

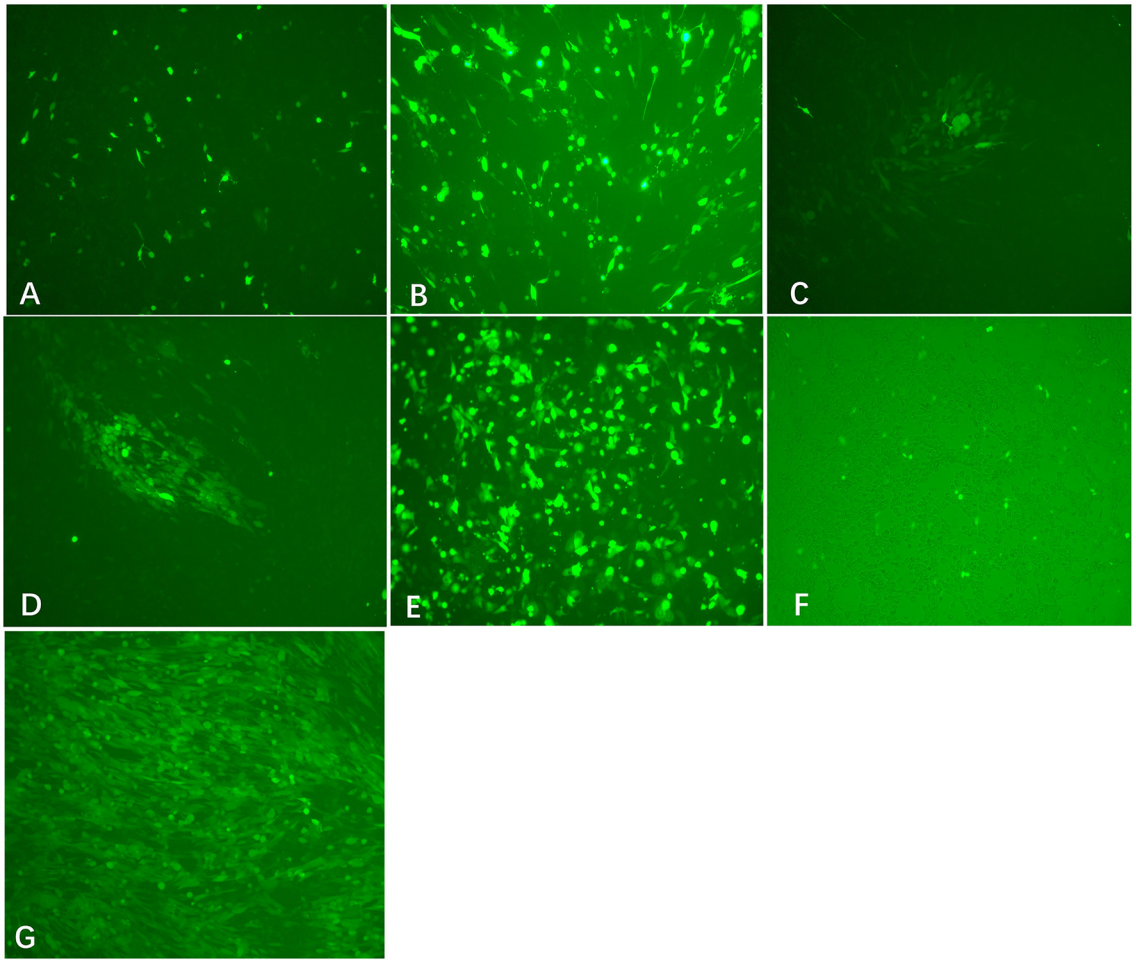

FIGURE 2
Transfection results of different treated viral DNA and plasmids (200×). Co-transfection of EcoRI-treated viral DNA + HindIII-treated pUG-EGFP **(A)**, EcoRV-treated viral DNA + HindIII-treated pUG-EGFP **(B)**, XbaI-treated viral DNA+ HindIII-treated pUG-EGFP **(C)**, AvrII-treated viral DNA + HindIII-treated pUG-EGFP **(D)**, XbaI-treated viral DNA + pUG-EGFP plasmid **(E)**, and virus + HindIII-treated pUG-EGFP **(F)** into BHK-21 cells, respectively. At 24 h after transfection, the expression of EGFP was observed in each group, but virus plaques were detected only in groups C and D. **(G)** The recombinant virus PRV-EGFP was obtained by plaque purification (200×).

on both sides of the EGFP-coding sequence, then the unique restriction sites could be used between the plasmid expressing a gene of interest and the PRV-EGFP genome (Klingbeil et al., 2014). However, the step for preparing recombinant virus PRV-EGFP may require several rounds and weeks of plaque purification (Zhao et al., 2020). In recent years, the CRISPR/Cas9 system has also been widely used in homology-directed repair (HDR), this approach can be used to introduce desired sequences by homologous recombination (Hirohata et al., 2019). Undeniably, the CRISPR/Cas9 technology has emerged as a powerful tool that enables ready modification of the mammalian genome and accelerates biological and medical research *in vivo*. However, the efficiencies of CRISPR/Cas9-mediated homologous recombination are still limited by the sizes of targeted chromosomal regions and donor DNAs. DNA repair may cause deletion, insertion and mutation in CRISPR/Cas9 target sites for homologous recombination, and to avoid this, sgRNA should be designed at uncritical regions, such as introns (Zhang et al., 2020). In addition, promiscuous cleavage of off-target sites remains a major concern in the application of the CRISPR/Cas9 technology (Lin et al., 2016; Rose et al., 2020). In this study, the viral DNA was digested with restriction enzymes cleaving at one (EcoRI) or more sites (AvrII, EcoRV, and XbaI) in the genome. After transfection, we can restore the infectious full-length genome, which is quite efficient.

Previous studies have found that the topology of DNA can affect transfection efficiency. Although linearized DNA may have a lower efficiency of transfection compared with the circular DNA, it can improve the efficiency of generating stable transfected cells and enhance the recovery of recombinant viruses (Kitts et al., 1990; von Groll et al., 2006; Hsu and Uludag, 2008; Stuchbury and Munch, 2010). The efficiency of the recombination was up to 10-fold higher than that of co-transfections with circular DNA when using linearized plasmids to produce recombinant baculovirus (Kitts et al., 1990). However, the site of cleavage also played an important role in both transient and stable transfection efficiency (Stuchbury and Munch, 2010). In the present study, we compared the effects of cleavage sites on recombination efficiency. The sites of XbaI and AvrII were close to the recombinant arms and had

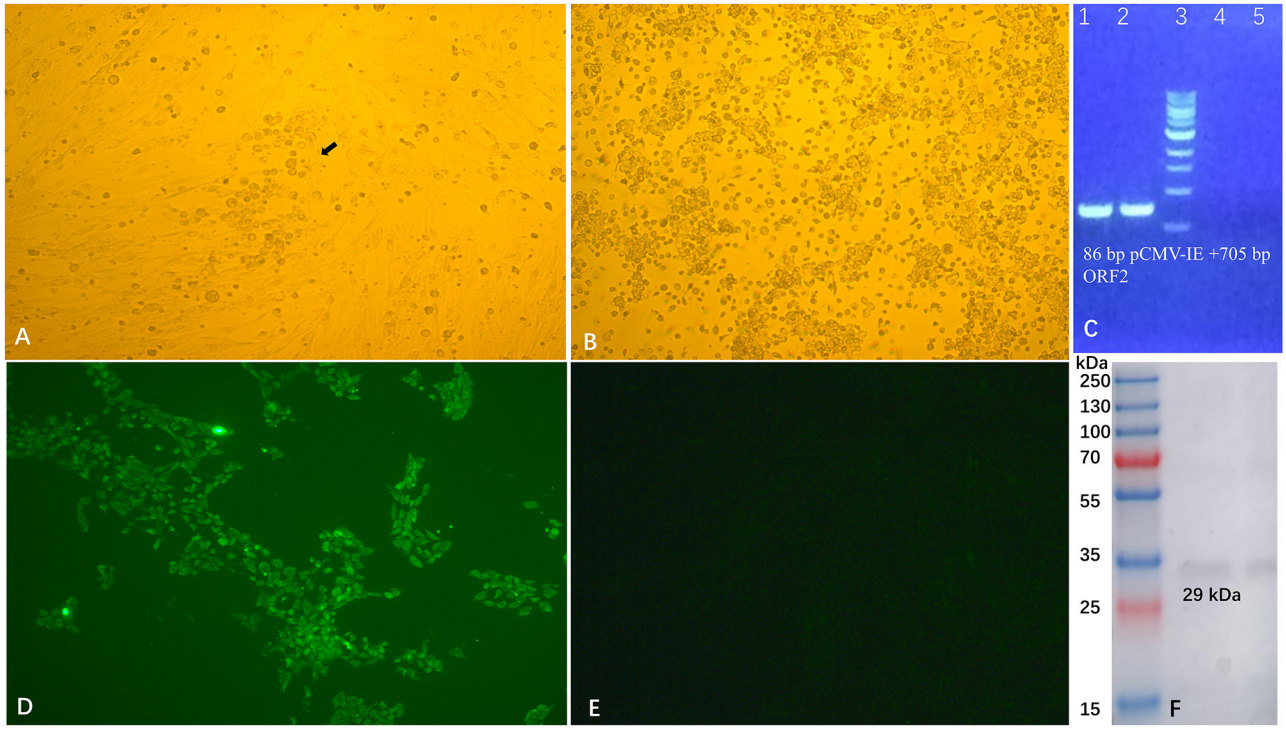

FIGURE 3
Generation and identification of recombinant PRV-PCV2d_ORF2. The recombinant PRV-ORF2 was purified by plaque picking from BHK-21 cells (200 ×) **(A)**, and the purified virus was then propagated in PK-15 cells **(B)**. RT-PCR **(C)**, IFA **(D)**, and Western blot **(F)** were used to confirm the expression of PCV2d capsid protein. Cells infected with PRV-PCV2d_ORF2 developed immunofluorescence and the expression of capsid protein could be detected by PCV monoclonal antibody, and cells infected with Bartha did not show immunofluorescence **(E)**.

high recombination efficiency when using these sites to cut the viral genome, which suggests that the closer to the recombinant arm, the higher the obtained efficiency will be. The different outcomes of transfection experiments with EcoRI, EcoRV, XbaI, and AvrII-digested PRV DNA might be due to the different relevance of the affected genome positions and their sensitivity to erroneous NHEJ (non-homologous end joining) repair. XbaI and AvrII cut sites within the inverted repeat regions (IR-S and TR-S) of the genome and possibly correct repair of one copy might be sufficient to restore infectivity.

Furthermore, the integrity of the viral genome is crucial for producing recombinant viruses. We have tried multiple methods to isolate the whole viral genome including commercially available viral nucleic acid extraction kits (IBI Scientific, IA, United States) and different ways to precipitate the virus particles including the PEG precipitation. None of them was able to obtain an intact viral DNA genome. The method described here was the most convenient and did not require a special reagent or instrument. We also provide insight that this method can be used for adenovirus, poxvirus, and other herpesviruses for large viral DNA genome isolation.

Data availability statement

The original contributions presented in the study are included in the article/supplementary material, further inquiries can be directed to the corresponding authors.

Author contributions

LW and JS designed and supervised the project. JR, LW, and JS collected literature, drafted the original manuscript, and analyzed the data. JR, RM, and CC performed the experiment. All authors contributed to the article and approved the submitted version.

Funding

This work is supported by awards from the National Bio and Agro-Defense Facility Transition Fund, the USDA National Institute of Food and Agriculture, Hatch-Multistate project, grant number (1021491), USDA ARS Non-Assistance Cooperative Agreements, grant numbers (58-8064-8-011, 58-8064-9-007, 58-3020-9-020, and 59-0208-9-222), National Pork Board Grant, grant number (18-059), and the China Scholarship Council (Grant no. 201703250028).

Acknowledgments

We thank Abbey Pentz and Jay Henry for their assistance in the laboratory. We also thank Prof. Lynn W. Enquist (Princeton University) for kindly providing the PRV Bartha strain and pUC-gG-MCS vector (NIH Virus Center grant no. OD010996). JR is

grateful for financial support from the China Scholarship Council (Grant no. 201703250028).

Conflict of interest

The authors declare that the research was conducted in the absence of any commercial or financial relationships that could be construed as a potential conflict of interest.

Publisher's note

All claims expressed in this article are solely those of the authors and do not necessarily represent those of their affiliated organizations, or those of the publisher, the editors and the reviewers. Any product that may be evaluated in this article, or claim that may be made by its manufacturer, is not guaranteed or endorsed by the publisher.

References

An, T. Q., Peng, J. M., Tian, Z. J., Zhao, H. Y., Li, N., Liu, Y. M., et al. (2013). Pseudorabies virus variant in bartha-k61-vaccinated pigs, China, 2012. *Emerg. Inf. Dis.* 19, 1749–1755. doi: 10.3201/eid1911.130177

Boscheinen, J. B., Thomann, S., Knipe, D. M., DeLuca, N., Schuler-Thurner, B., Gross, S., et al. (2019). Generation of an oncolytic herpes simplex virus 1 expressing human melanA. *Front. Immunol.* 10, 2. doi: 10.3389/fimmu.2019.00002

Card, J. P., Dubin, J. R., Whealy, M. E., and Enquist, L. W. (1995). Influence of infectious dose upon productive replication and transynaptic passage of pseudorabies virus in rat central nervous system. *J. Neurovirol.* 1, 349–358. doi: 10.3109/13550289509111024

Delva, J. L., Nauwynck, H. J., Mettenleiter, T. C., and Favoreel, H. W. (2020). The attenuated pseudorabies virus vaccine strain bartha k61: a brief review on the knowledge gathered during 60 years of research. *Pathogens* 9, 11. doi: 10.3390/pathogens9110897

Deng, J., Wu, Z., Liu, J., Ji, Q., and Ju, C. (2022). The role of latency-associated transcripts in the latent infection of pseudorabies virus. *Viruses* 14, 7. doi: 10.3390/v14071379

Dietz, P., Klupp, B. G., Fuchs, W., Kollner, B., Weiland, E., Mettenleiter, T. C., et al. (2000). Pseudorabies virus glycoprotein K requires the UL20 gene product for processing. *J. Virol.* 74, 5083–5090. doi: 10.1128/JVI.74.11.5083-5090.2000

Dong, B., Zarlenga, D. S., and Ren, X. F. (2014). An overview of live attenuated recombinant pseudorabies viruses for use as novel vaccines. *J. Immunol. Res.* 2014, 824630. doi: 10.1155/2014/824630

Feng, Z., Chen, J., Liang, W., Chen, W., Li, Z., Chen, Q., et al. (2020). The recombinant pseudorabies virus expressing African swine fever virus CD2v protein is safe and effective in mice. *Virol. J.* 17, 180. doi: 10.1186/s12985-020-01450-7

Fisher, K. J., Jooss, K., Alston, J., Yang, Y., Haecker, S. E., High, K., et al. (1997). Recombinant adeno-associated virus for muscle directed gene therapy. *Nat. Med* 3, 306–312. doi: 10.1038/nm0397-306

Freuling, C. M., Muller, T. F., and Mettenleiter, T. C. (2017). Vaccines against pseudorabies virus (PrV). *Vet. Microbiol.* 206, 3–9. doi: 10.1016/j.vetmic.2016.11.019

Guerin, B., and Pozzi, N. (2005). Viruses in boar semen: detection and clinical as well as epidemiological consequences regarding disease transmission by artificial insemination. *Theriogenology* 63, 556–572. doi: 10.1016/j.theriogenology.2004.09.030

Hirohata, A., Sato, I., Kaino, K., Iwata, Y., Koizumi, N., Mishiba, K. I., et al. (2019). CRISPR/Cas9-mediated homologous recombination in tobacco. *Plant Cell Rep* 38, 463–473. doi: 10.1007/s00299-018-2320-7

Hsu, C. Y. M., and Uludag, H. (2008). Effects of size and topology of DNA molecules on intracellular delivery with non-viral gene carriers. *BMC Biotechnol.* 8, 23. doi: 10.1186/1472-6750-8-23

Jacob, A., Brun, L., Jimenez Gil, P., Menard, L., Bouzelha, M., Broucque, F., et al. (2020). Homologous recombination offers advantages over transposition-based systems to generate recombinant baculovirus for adeno-associated viral vector production. *Biotechnol J.* 8, e2000014. doi: 10.1002/biot.202000014

Kitts, P. A., Ayres, M. D., and Possee, R. D. (1990). Linearization of baculovirus DNA enhances the recovery of recombinant virus expression vectors. *Nucleic Acids Res.* 18, 5667–5672. doi: 10.1093/nar/18.19.5667

Klingbeil, K., Lange, E., Teifke, J. P., Mettenleiter, T. C., and Fuchs, W. (2014). Immunization of pigs with an attenuated pseudorabies virus recombinant expressing the haemagglutinin of pandemic swine origin H1N1 influenza A virus. *J. Gen Virol.* 95, 948–959. doi: 10.1099/vir.0.059253-0

Klupp, B. G., Hengartner, C. J., Mettenleiter, T. C., and Enquist, L. W. (2004). Complete, annotated sequence of the pseudorabies virus genome. *J. Virol.* 78, 2166–2166. doi: 10.1128/JVI.78.4.2166.2004

Lerma, L., Munoz, A. L., Wagner, S., Dinu, M., Martin, B., Tabares, E., et al. (2016). Construction of recombinant pseudorabies viruses by using PRV BACs deficient in IE180 or pac sequences: application of vBAC90D recombinant virus to production of PRV amplicons. *Virus Res.* 213, 274–282. doi: 10.1016/j.virusres.2015.11.028

Lin, C., Li, H., Hao, M., Xiong, D., Luo, Y., Huang, C., et al. (2016). Increasing the efficiency of CRISPR/Cas9-mediated precise genome editing of HSV-1 virus in human cells. *Sci. Rep.* 6, 34531. doi: 10.1038/srep34531

Lin, Y., Qigai, H., Xiaolan, Y., Weicheng, B., and Huanchun, C. (2005). The co-administrating of recombinant porcine IL-2 could enhance protective immune responses to PRV inactivated vaccine in pigs. *Vaccine* 23, 4436–4441. doi: 10.1016/j.vaccine.2005.03.034

Rose, J. C., Popp, N. A., Richardson, C. D., Stephany, J. J., Mathieu, J., Wei, C. T., et al. (2020). Suppression of unwanted CRISPR-Cas9 editing by co-administration of catalytically inactivating truncated guide RNAs. *Nat. Commun.* 11, 2697. doi: 10.1038/s41467-020-16542-9

Schmidt, J., Gerdts, V., Beyer, J., Klupp, B. G., and Mettenleiter, T. C. (2001). Glycoprotein D-independent infectivity of pseudorabies virus results in an alteration of in vivo host range and correlates with mutations in glycoproteins B and H. *J. Virol.* 75, 10054–10064. doi: 10.1128/JVI.75.21.10054-10064.2001

Stuchbury, G., and Munch, G. (2010). Optimizing the generation of stable neuronal cell lines via pre-transfection restriction enzyme digestion of plasmid DNA. *Cytotechnology* 62, 189–194. doi: 10.1007/s10616-010-9273-1

Takashima, Y., Nagane, N., Hushur, O., Matsumoto, Y., and Otsuka, H. (2002). Bovine herpesvirus-1 (BHV-1) recombinant expressing pseudorabies virus (PrV) glycoproteins B and C induces type 1 immune response in BALB/c mice. *J Vet Med. Sci.* 64, 589–596. doi: 10.1292/jvms.64.589

Tan, L., Shu, X., Xu, K., Liao, F., Song, C., Duan, D., et al. (2022). Homologous recombination technology generated recombinant pseudorabies virus expressing EGFP facilitates to evaluate its susceptibility to different cells and screen antiviral compounds. *Res. Vet. Sci.* 145, 125–134. doi: 10.1016/j.rvsc.2022.02.005

Tang, Y. D., Liu, J. T., Fang, Q. Q., Wang, T. Y., Sun, M. X., An, T. Q., et al. (2016). Recombinant pseudorabies virus (prv) expressing firefly luciferase effectively screened for CRISPR/Cas9 single guide RNAs and antiviral compounds. *Viruses* 8, 90. doi: 10.3390/v8040090

Thomsen, D. R., Marotti, K. R., Palermo, D. P., and Post, L. E. (1987). Pseudorabies virus as a live virus vector for expression of foreign genes. *Gene* 57, 261–265. doi: 10.1016/0378-1119(87)90130-2

Tong, W., Zheng, H., Li, G. X., Gao, F., Shan, T. L., Zhou, Y. J., et al. (2020). Recombinant pseudorabies virus expressing E2 of classical swine fever virus (CSFV) protects against both virulent pseudorabies virus and CSFV. *Antiviral Res.* 173, 104652. doi: 10.1016/j.antiviral.2019.104652

Vallbracht, M., Rehwaldt, S., Klupp, B. G., Mettenleiter, T. C., and Fuchs, W. (2018). Functional role of n-linked glycosylation in pseudorabies virus glycoprotein gH. *J. Virol.* 92, 9. doi: 10.1128/JVI.00084-18

von Groll, A., Levin, Y., Barbosa, M. C., and Ravazzolo, A. P. (2006). Linear DNA low efficiency transfection by liposome can be improved by the use of cationic lipid as charge neutralizer. *Biotechnol. Prog.* 22, 1220–1224. doi: 10.1021/bp060029s

Wang, C. H., Yuan, J., Qin, H. Y., Luo, Y., Cong, X., Li, Y. F., et al. (2014). A novel gE-deleted pseudorabies virus (PRV) provides rapid and complete protection from lethal challenge with the PRV variant emerging in Bartha-K61-vaccinated swine population in China. *Vaccine* 32, 3379–3385. doi: 10.1016/j.vaccine.2014.04.035

Wilkinson, D. E., and Weller, S. K. (2003). The role of DNA recombination in herpes simplex virus DNA replication. *IUBMB Life* 55, 451–458. doi: 10.1080/1521654031000161223 7

Wyatt, L. S., Earl, P. L., and Moss, B. (2015). Generation of recombinant vaccinia viruses. *Curr. Protoc. Microbiol.* 39, 14118. doi: 10.1002/9780471729259.mc14a04s39

Yin, S. H., Yang, S. L., Shang, Y. J., Cai, X. P., and Liu, X. T. (2012). Development and optimization of multiplex- pcr for simultaneous detection of porcine pseudorabies virus, porcine parvovirus, and porcine circovirus type 2. *Int. J. Appl. Res. Vet. Med.* 10, 273–279. Available online at: http://www.jarvm.com/articles/Vol10Iss3/Vol10%20Iss3%20Shuanghui.pdf

Zhang, F., Cheng, W.ang, S., and Zhu, J. (2020). Crispr/Cas9-mediated cleavages facilitate homologous recombination during genetic engineering of a large chromosomal region. *Biotechnol Bioeng* 117, 2816–2826. doi: 10.1002/bit.27441

Zhao, Y., Wang, L. Q., Zheng, H. H., Yang, Y. R., Liu, F., Zheng, L. L., et al. (2020). Construction and immunogenicity of a gE/gI/TK-deleted PRV based on porcine pseudorabies virus variant. *Mol. Cell Probes* 53, 101605. doi: 10.1016/j.mcp.2020.101605

Zheng, H. H., Fu, P. F., Chen, H. Y., and Wang, Z. Y. (2022). Pseudorabies Virus: From Pathogenesis to Prevention Strategies. *Viruses* 14, 8. doi: 10.3390/v14081638

Zheng, H. H., Wang, L. Q., Fu, P. F., Zheng, L. L., Chen, H. Y., Liu, F., et al. (2020). Characterization of a recombinant pseudorabies virus expressing porcine parvovirus VP2 protein and porcine IL-6. *Virology J.* 17, 1. doi: 10.1186/s12985-020-1292-8

frontiers | Frontiers in Microbiology

TYPE Original Research
PUBLISHED 31 May 2023
DOI 10.3389/fmicb.2023.1153922

OPEN ACCESS

EDITED BY
Lihua Wang,
Kansas State University, United States

REVIEWED BY
Sujuan Chen,
Yangzhou University, China
Victor Manuel Petrone-García,
National Autonomous University of Mexico, Mexico

*CORRESPONDENCE
Yongqing Li
✉ chuanyudady@sina.com
Jinhai Huang
✉ jinhaih@tju.edu.cn

†These authors have contributed equally to this work

RECEIVED 30 January 2023
ACCEPTED 25 April 2023
PUBLISHED 31 May 2023

CITATION
Zhang H, Li Z, Zhang H, Guo Y, Zhang X, Zhang L, Yang L, Li S, Li C, Cui D, Xie R, Li Y and Huang J (2023) Recombinant hemagglutinin displaying on yeast reshapes congenital lymphocyte subsets to prompt optimized systemic immune protection against avian influenza infection.
Front. Microbiol. 14:1153922.
doi: 10.3389/fmicb.2023.1153922

Recombinant hemagglutinin displaying on yeast reshapes congenital lymphocyte subsets to prompt optimized systemic immune protection against avian influenza infection

Han Zhang[1†], Zexing Li[1†], Huixia Zhang[1], Yanyu Guo[1], Xinyi Zhang[1], Lilin Zhang[1], Liu Yang[1], Shujun Li[1], Changyan Li[1], Daqing Cui[1], Ruyu Xie[1], Yongqing Li[2]* and Jinhai Huang[1]*

[1]School of Life Sciences, Tianjin University, Tianjin, China, [2]Institute of Animal Husbandry and Veterinary Medicine, Beijing Academy of Agricultural and Forestry Sciences, Beijing, China

Introduction: Prophylactic vaccination is regarded as the most effective means to control avian flu infection. Currently, there is a need for a universal vaccine that provides broad and long-lasting protection against influenza virus. Meanwhile, although yeast-based vaccines have been used in clinic, studies are still required to further understand the molecular mechanism of yeast-based vaccines under physiological conditions.

Methods: We generated a yeast-based vaccine against influenza hemagglutinin (HA) of H5, H7 and H9 using surface displaying technology and evaluated the protective efficacy of chickens after exposure to H9N2 influenza virus.

Results: Oral yeast vaccine provided less clinical syndrome, reduced viral loading and alleviated airway damage significantly. Compared to the commercial inactivated vaccine, yeast vaccine stimulated the activation of splenic NK and APCs cells and boosted TLR7-IRF7-IFN signaling in spleen. Meanwhile, γδ T cells in the bursa of Fabricius were activated and the innate lymphoid cells (ILCs) in the bursa of Fabricius promoted the CILPs to differentiate to ILC3 cells in oral yeast birds. Moreover, the reshaped gut microbiota and a suppressed Th17-IL17-mediated inflammation in intestine was observed in oral yeast chickens, which might facilitate the recovery of intestinal mucosal immunity upon virus infection. Collectively, our findings suggest that oral yeast based multivalent bird flu vaccines provide an attractive strategy to update host defense function via reshapes of multi-systemic immune homeostasis.

KEYWORDS

avian influenza virus, *Saccharomyces cerevisiae*, innate immunity, vaccine, chicken

Introduction

Avian influenza virus (AIV) is an acute and highly contagious zoonotic pathogen that poses a serious threat to public health and the poultry industry. Avian influenza virus subtypes H5N8 and H7N9 are highly pathogenic avian influenza (HPAI) and can cause severe mortality, while H9N2 is a low pathogenic avian influenza (LPAI), which does the

same. The first epidemic of HPAI occurred in Guangxi province and quickly spread to 16 provinces of China in 2004, and it resulted in great economic losses and was accompanied by a high mortality rate from human influenza in China (Swayne et al., 2014; Chen et al., 2018). Vaccination is considered an efficient strategy to control AIV infection, and massive vaccination programs were launched to fight against bird flu infection since then. Usually, combined H5N8, H7N9, and H9N2 inactivated vaccines were widely used in poultry (Allen et al., 2019; Christensen et al., 2019). However, the commercial inactivated influenza vaccines offer little protection against pandemic influenza virus strains (Bajic et al., 2019). Meanwhile, the vaccination procedures of inactivated vaccines were time-consuming and relied on hand labor.

Hemagglutinin protein (HA) of influenza A viruses, a homotrimeric glycoprotein in architecture, is the only antigen present on the viral surface and contains several glycosylation sites (Bangaru et al., 2019; Vahey and Fletcher, 2019). Crystallographic studies have shown that HA forms a trimer embedded on the viral envelope surface, and each monomer consists of a globular head (HA1) and a rod-like stalk region (HA2). Moreover, the latter HA2 region is more conserved among different HA subtypes, and it is considered the primary target for universal vaccines (Xuan et al., 2011). Recombinant HA protein subunit vaccines were evaluated for their safety and efficacy in humans and chickens in previous studies (Wu et al., 2010; Kim et al., 2017; Lei et al., 2020). Several universal influenza vaccines including a limited number of antigens that have epitopes that are conserved across different influenza virus subtypes are in development to provide protection against diverse influenza virus subtypes (Arevalo et al., 2022). Continued efforts to further characterize the phenotype and function of these vaccines will guide the development of more effective vaccines, which provide long-lasting protective efficacy against both seasonal and pandemic influenza viruses (Cho and Wrammert, 2016).

Recently, gut microbiota (GM) modulation approaches are considered one of the most promising strategies to improve animal health and welfare in commercial poultry production. The immune system of avian species, such as chickens, is thought to be very different from mammalian species (Kaiser, 2010). Unique features, such as cecum tonsils (the largest lymphoid aggregates in the bird's gut) and the bursa of *Fabricius* (a B-cell powerhouse), both of which are located in the distal region of the intestinal mucosa, make the avian gut-associated immune system a very specific anatomical and immunological landscape compared to that of mammals. Therefore, modulation of the chicken gut microbiota might provide a stronger positive effect on chicken health, and there is a great need to understand the influence of GM modulation on the chicken gut-associated immune system.

Yeast is considered to be a simple and cost-effective protein expression host, and yeast-based vaccines have gained popularity due to their rapidly engineered and manipulated characteristics to express foreign antigens and viral epitopes (Kiflmariam et al., 2013; Jiang et al., 2014; Guan et al., 2015; Sen and Mansell, 2020). A yeast displaying influenza H7N9 oral vaccine provides protection against the lethal H7N9 virus challenge in mice (Lei et al., 2020). Recent studies demonstrated that oral recombinant *Saccharomyces cerevisiae* successfully introduced recombinant protein and DNA into rabbit dendritic cells (Franzusoff et al., 2005). Meanwhile, yeast is preferred in GM modulation approaches because of its multiple effects as a probiotic, including anti-toxin, resistance to intestinal pathogens, and maintenance of the integrity of the intestinal epithelial mucosa. However, the influence of yeast-based vaccines on gut-associated immune systems and GM modulation of chickens were not fully understood.

In this study, we try to present an alternative strategy for inducing universal immunity against distinct influenza virus strains. Instead of focusing on immunogens to elicit antibodies against epitopes that are conserved among many different influenza virus strains, we designed a novel trivalent recombinant protein yeast surface display-based vaccine, which simultaneously expressed the HA regions of H5N8, H7N9, and H9N2 subtypes and lineages. The immunogenicity and protective efficacy of this vaccine were tested by using the chicken model, and our experimental results demonstrated that the yeast vaccine is safe, efficient, and inexpensive for commercial production. Further studies revealed that our triple yeast vaccine can selectively activate immune organs (bursa of *Fabricius* and spleen), suppress parenchymal organ inflammatory responses, promote tissue-resident ILC3 cell proliferation, exert protective functions in bursa, and lead to differentiation of ILCs, NKs, and γδT cells in different tissues, all of which collectively contributed to the defense response against influenza virus infection of vaccinated chickens.

Results

Construction of a trivalent recombinant *S. cerevisiae* strain expressing HA proteins of subtypes H5N8, H7N9, and H9N2

To meet the requirements of developing safe and effective influenza oral vaccines, we developed a trivalent recombinant HA protein vaccine by yeast surface display manner using *Saccharomyces Cerevisiae* strain (MATa aga1 his3Δ200 leu2Δ0 lys2Δ0 trp1Δ63 ura3Δ0 met15Δ0) as shown in Figure 1A. The positive transformed yeast clones were further confirmed by analyzing yeast genomic DNA for correct insertion. The recombinant *S. Cerevisiae* strain expressing H9/HA was named ST1814G/Aga2-H9, and the recombinant *S. Cerevisiae* strains expressing HA proteins of H5N8, H7N9, and H9N2 were named ST1814G/Aga2-H579 in this study. The Western blot results indicated that the HA proteins of H5N8, H7N9, and H9N2 strains were all expressed successfully in our engineered yeast strains (Figure 1B). Immunofluorescence assay and flow cytometry assay demonstrated that HA proteins from both ST1814G/Aga2-H9 and ST1814G/Aga2-H579 were expressed on the yeast surface successfully (Figures 1C, D). Overall, these results indicate that the trivalent HA proteins were successfully expressed and located on the cell surface of our engineered yeast vaccine cells.

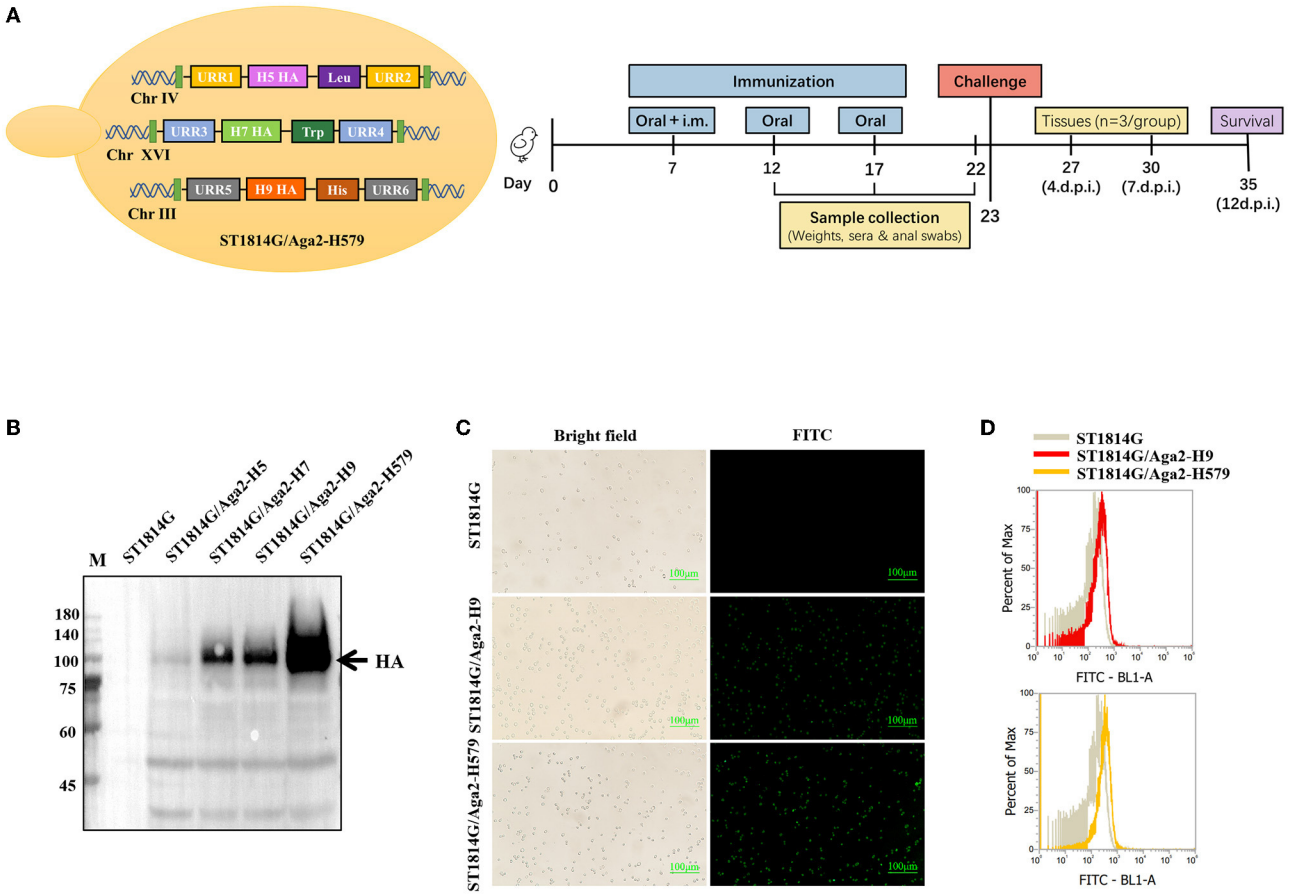

FIGURE 1
Analysis of HA protein expression in recombinant Saccharomyces cerevisiae strains. **(A)** Schematic diagram of yeast construction (Left) and animal evaluation experiments (right). **(B)** The Western blot analysis of HA expression in recombinant S. cerevisiae. Lane M. Blue Plus IV Protein Maker (10–180 kDa); Lane 1. ST1814G; Lane 2. ST1814G/Aga2-H5; Lane 3. ST1814G/Aga2-H7; Lane 4. ST1814G/Aga2-H9; Lane 5. ST1814G/Aga2-H579. **(C)** ST1814G/Aga2-H9 cells and ST1814G/Aga2-H579 cells were incubated with mouse anti-His-tag antibody followed by fluorescein isothiocyanate (FITC)-conjugated anti-mouse IgG. Treated yeast cells were fixed on glass slides, and the localization of HA was analyzed by fluorescence microscope. **(D)** The expression profile of recombinant protein was also determined by flow cytometry. The gray lines (dark shades) represent ST1814G cells, the red line stands for ST1814G/Aga2-H9 cells, and the yellow line stands for ST1814G/Aga2-H579 cells.

Effects of oral yeast vaccines on body weight, organ indices, specific antibody production, and virus challenge of chickens

To monitor the safety of our engineered yeast vaccines, the weight of the whole body and different organs was recorded during the three immunization procedures. As shown in Figures 2A, B, oral-engineered yeast vaccines had no negative effect on the growth of the chickens but rather tend to mildly increase the weight of chickens. The organ index results showed a considerable disturbance of the liver by the inactivated vaccine, which may trigger a strong inflammatory response or macrophage infiltration that leads to relative liver enlargement. In contrast, the oral yeast vaccine group, including ST1814G/Aga2-H9 and ST1814G/Aga2-H579, did not cause liver enlargement, suggesting that the oral yeast vaccine could reduce the potential for further damage to the organism.

To detect the special antibodies production of HA protein by ST1814G/Aga2-H9 and ST1814G/Aga2-H579, the levels of IgG in sera and IgA in anal swabs were determined by the ELISA assay (Figures 2C, D). The levels of specific IgG and IgA were significantly higher in oral yeast vaccine and inactivated vaccine groups than those in the ST1814G or YPD groups as early as 5 days after the first immunization, and the specific antibody levels were increased progressively with the immunization times. The results indicated that, in comparison with the control group, both the oral yeast vaccine and the traditional inactivated vaccine were able to stimulate a strong humoral immune response against the antigen HA protein in chickens.

At 5 days after the third immunization, the chickens were challenged with H9N2 (A/Hebei/218/2010), and the survival rate was recorded as in Figure 2E. Only 53% of chickens survived in the YPD and ST1814G groups, and 71% of chickens survived in the inactivated vaccine group; the ST1814G/Aga2-H579 group had a high survival rate of 86%, and the ST1814G/Aga2-H9 group was able to provide 100% protection for the chickens. It indicated that oral administration of ST1814G/Aga2-H9 yeast or ST1814G/Aga2-H579 yeast provided better protection for chickens after H9N2

10.3389/fmicb.2023.1153922

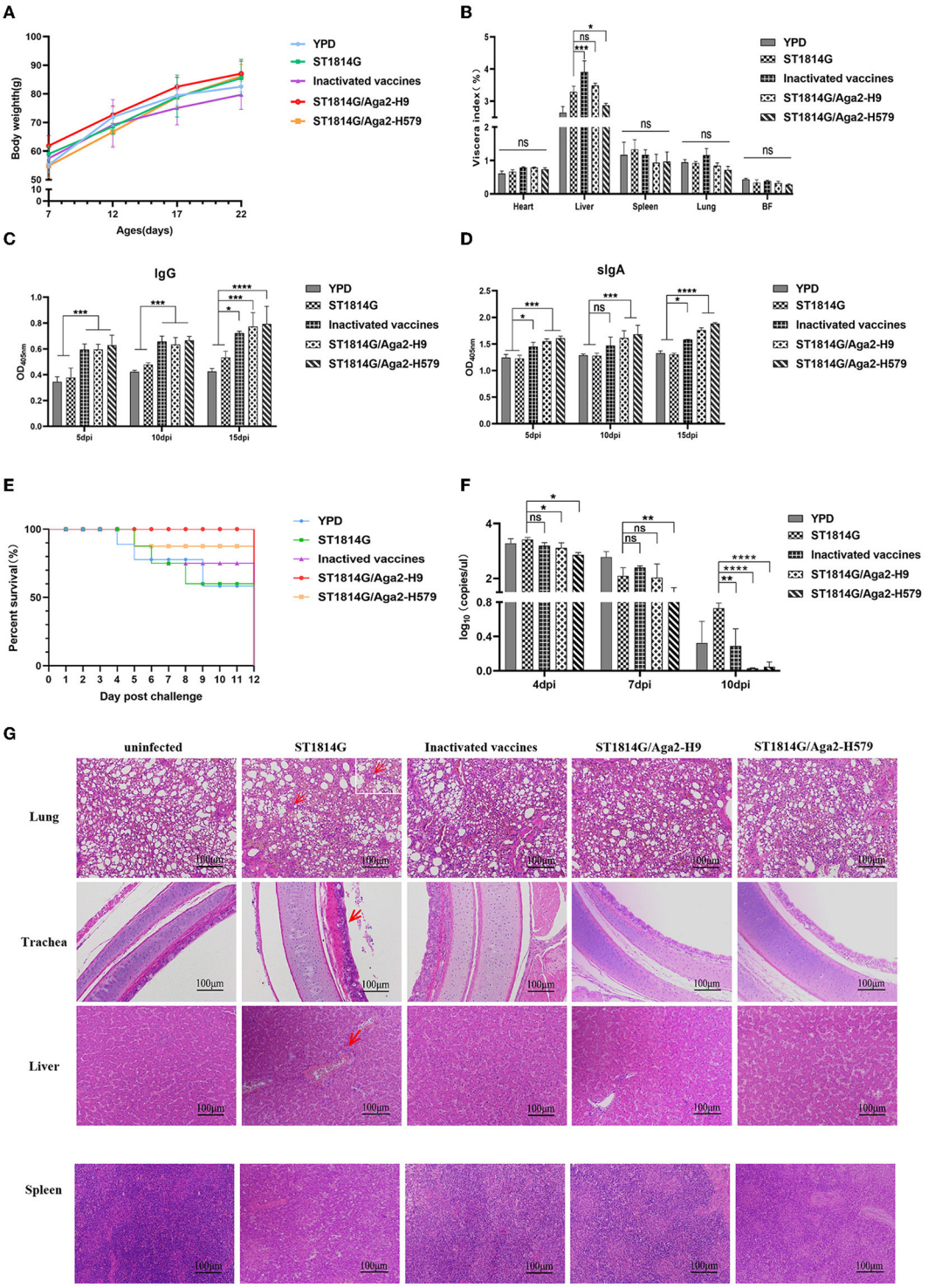

FIGURE 2
Effects of oral recombinant yeast vaccine on growth, viscera index, special antibody production, survival curve, virus titer, and histopathological sections after viral challenge. **(A)** The weight of chickens was measured at 5 days intervals, and three chickens were randomly selected from each group to graph the change in weight. **(B)** 5 days after the third immunization, the organ index (wet weight of viscera/body weight) for each chicken in each group was recorded, including the heart, liver, spleen (×10), lungs, and bursa of *Fabricius*. **(C, D)** The secretion levels of H9N2 HA-specific IgG in serum and sIgA in anal swabs of vaccinated chickens were determined by ELISA, and the differences were compared among groups, respectively. **(E)** The survival curve was recorded after the H9N2 virus was injected into seven chickens in each group, and the percentage of survival was calculated. **(F)** Virus titers in blood were measured by absolute qPCR assay on days 4, 7, and 10 after virus infection (dpi: day post-infection). **(G)** Microscopic lesions of tracheal epithelial cells, alveolar cells and hepatocytes, and spleen cells in experimentally infected birds were demonstrated by hematoxylin and eosin staining (HE). Left to right: uninfected group; ST1814G group, inactivated vaccine group, ST1814G/Aga2-H9 group, and ST1814G/Aga2-H579 group after being infected. The data in the figures were obtained from three independent experiments and represent the averages ± SD. The significance of differences was determined by a two-way analysis of variance (*$p < 0.05$; **$p < 0.01$; ***$p < 0.001$; ****$p < 0.0001$ or ns, no significance). The red arrow indicates massive infiltration of lymphocytes in tissues.

10.3389/fmicb.2023.1153922

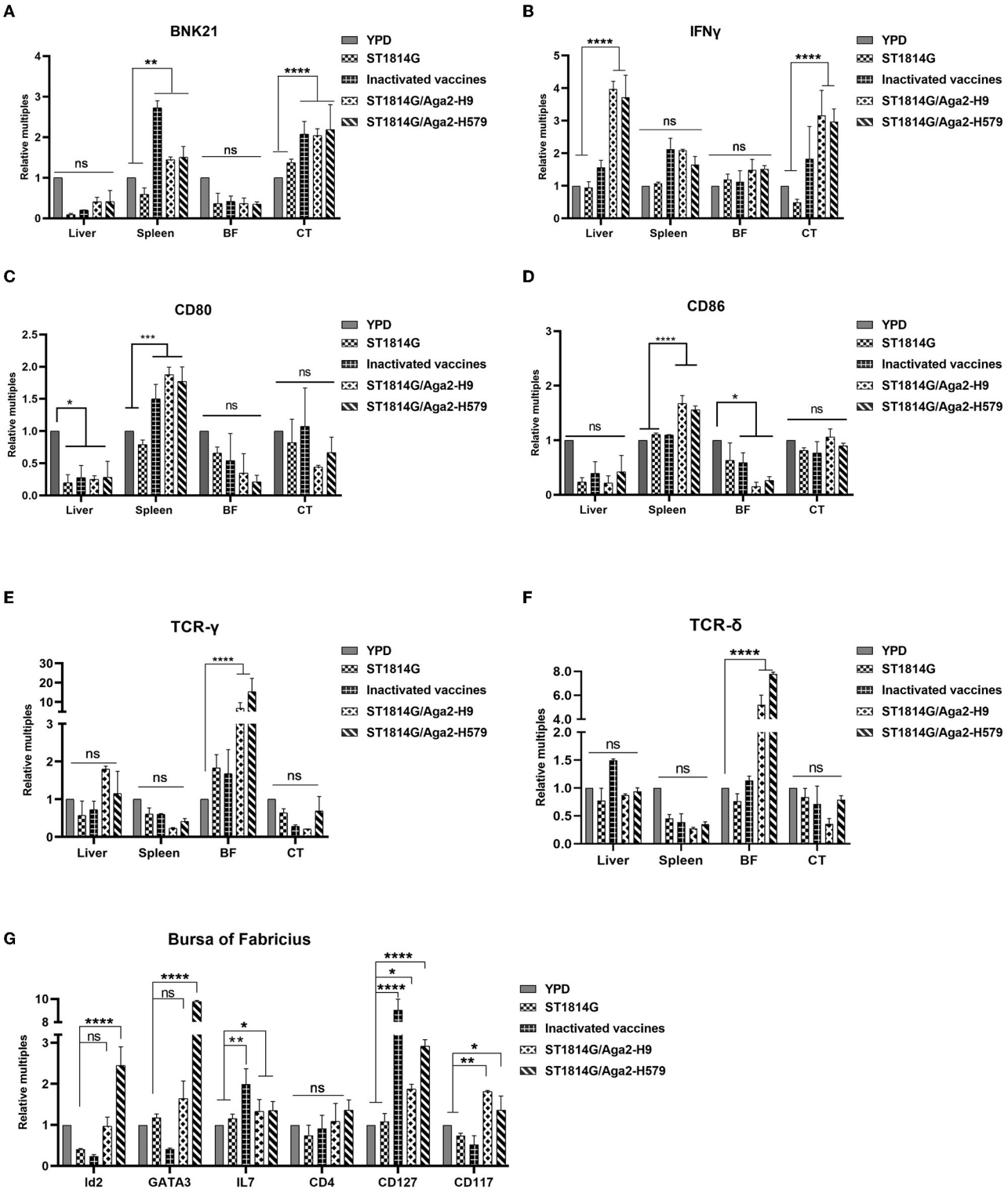

FIGURE 3
Effect of oral yeast vaccine on the relative mRNA expression of cell factors associated with NK cells, γδT cells, and ILCs. **(A, B)** The mRNA expression of the NK cell surface receptor BNK21 and its secreted IFNG in the five groups of the liver, spleen, bursa of *Fabricius* (BF), and cecum tonsils (CF). **(C, D)** The mRNA expression of the APC cell surface receptor CD80 and CD86 in five groups of the liver, spleen, bursa of *Fabricius* (BF), and cecum tonsils (CF). **(E, F)** The mRNA expression of the gamma and delta chains of T-cell TCR in the five groups of the liver, spleen, bursa of *Fabricius* (BF), and cecum tonsils (CF). **(G)** Transcript levels of ILCs-related factors in the five groups of the bursa of *Fabricius*, including marker molecules, transcription factors, and secreted cytokines. The differences were compared among groups, respectively, and the data in the figures were obtained from three independent experiments and represent the averages ± SD. The significance of differences was determined by a two-way analysis of variance (*$p < 0.05$; **$p < 0.01$; ***$p < 0.001$; ****$p < 0.0001$ or ns, no significance).

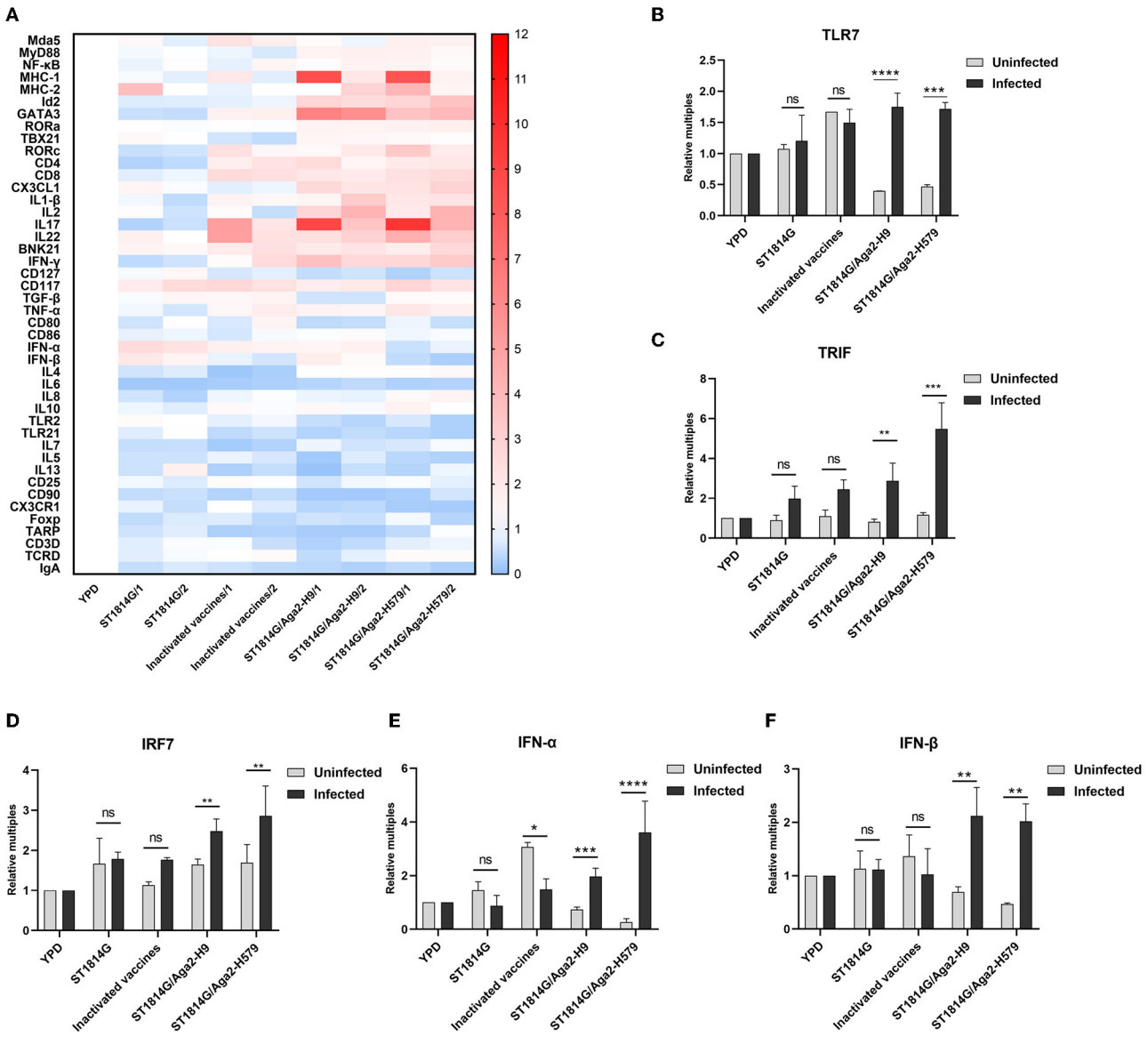

FIGURE 4
Effect of oral yeast vaccine on the relative mRNA expression of immune-related cytokines in cecum tonsils and signaling molecules of the TLR7 pathway. **(A)** The heat map on transcript levels of five groups of immune-related cytokines in the cecum tonsils (CF). Transcript levels of TLR7 **(B)**, TRIF **(C)**, IRF7 **(D)**, IFNα **(E)**, and IFNβ **(F)** in the spleen of uninfected (gray) and infected (black) chickens in the five groups. The differences were compared among groups, respectively, and the data in the figures were obtained from three independent experiments and represent the averages ± SD. The significance of differences was determined by a two-way analysis of variance (*$p < 0.05$; **$p < 0.01$; ***$p < 0.001$; ****$p < 0.0001$ or ns, no significance).

virus infection. Consistent with the survival rate experiments, virus titer experiments, which were measured in the blood of each group at 4, 7, and 10 days after the H9N2 infection, also indicated that oral administration of ST1814G/Aga2-H9 yeast or ST1814G/Aga2-H579 yeast could additionally decrease the virus titer of chickens (Figure 2F).

We further checked the histopathological lesions of each group (Figure 2G). Compared to the group without virus infection, the ST1814G group showed significantly higher airway lesions and pneumonia symptoms that are characterized by interstitial lung congestion with hemorrhage and massive infiltration of lymphocytes, macrophages, and granulocytes. In contrast, the lung tissue of the other three immunization groups had only scattered lymphocyte infiltrates. Meanwhile, the main liver lesions were characterized by intrahepatic erythrocytosis with lymphocytic infiltration around the vessels in the ST1814G group, whereas the immunized groups showed only scattered lymphocytic infiltration or no symptom in the liver tissue. Spleen histology showed blurred boundaries between the red and white marrow in the ST1814G group and the inactivated vaccine group, suggesting that an inflammatory response occurred in the spleen, whereas the red and white marrow were more clearly defined in the oral yeast

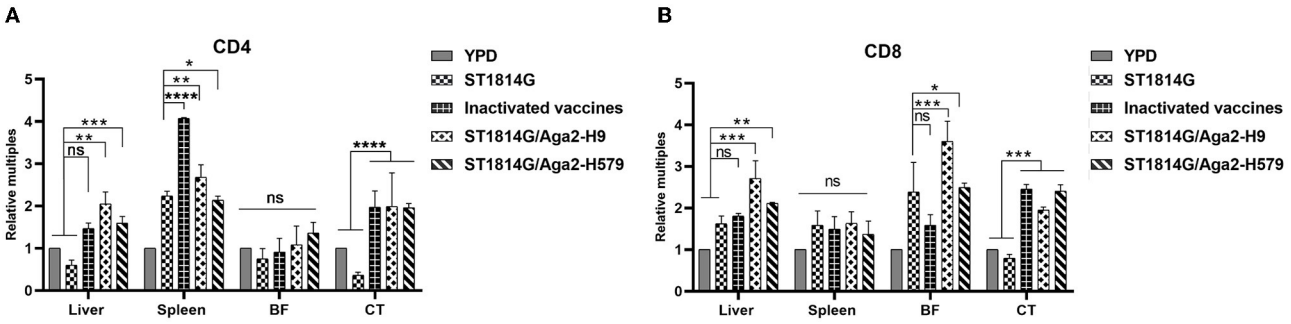

FIGURE 5
Evaluation of CD4$^+$T-cell and CD8$^+$T-cell levels after three immunizations. The mRNA expression levels of the five groups of CD4 **(A)** and CD8 **(B)** in the liver, spleen, bursa of Fabricius (BF), and cecum tonsils (CT). The data in the figures were obtained from three independent experiments and represent the averages ± SD. The significance of differences was determined by a two-way analysis of variance (*$p < 0.05$; **$p < 0.01$; ***$p < 0.001$; ****$p < 0.0001$ or ns, no significance).

immunization groups. Taken together, these results showed that the oral yeast vaccines were effective in defending against and clearing viruses and hence protecting immunized chickens from deadly injuries.

Oral yeast vaccine regulates tissue-resident innate immune cell abundance to protect chickens from lethal viral damage

Previous studies reported that the oral yeast vaccination was able to activate innate immune cells, such as macrophage and NK cells (Jensen et al., 2007; Liu et al., 2021; Walachowski et al., 2022). To test whether our engineered yeast vaccines could influence innate immune cell abundance, we determined the expression level of molecule markers of important innate immune cells in different groups.

BNK21 is an important molecule marker of natural killer (NK) cells, and IFNγ is the main product of the NK cells, so the expression level of both of them indicated the NK cell abundance to some extent (Yang et al., 2014; Neulen et al., 2015). Our experimental results suggested that both BNK21 (Figure 3A) and IFNγ (Figure 3B) were upregulated in the spleen and cecum tonsils after immunization by inactivated vaccine and oral yeast vaccine, suggesting that NK cells might accumulate in the spleen and cecum tonsils and produce IFNγ in large quantities after immunization with oral yeast vaccine, which are immediately effective in fighting against virus invasion and removing damaged cells.

To monitor the abundance of antigen-presenting cells (APCs), such as macrophage and dendritic cells, we checked macrophage-specific protein CD80 and CD86 and dendritic cell-related chemokine ligand (CX3CL1) and receptor (CX3CR1). Our experimental results suggested that both CD80/CD86 (Figure 3C) and CX3CL1/CX3CR1 (Supplementary Figure 1A) were upregulated in the spleen after immunization by oral yeast vaccine, suggesting that antigen-presenting cells might accumulate in the spleen, which potently activated the NK cells, NKT cells, and T cells, facilitating cytotoxic T-cell responses.

γδ T cells, as tissue-resident T cells, also serve as the first line of defense for immunity and are capable of generating a rapid response to pathogen invasion. To monitor the γδ T-cell abundance, we analyzed the transcription levels of genes encoding the gamma and delta chains of the T-cell receptor (TCR) in different organs of chickens. As shown in Figures 3D, E, the genes were increased in the bursa of *Fabricius*, suggesting that γδ T cells might accumulate in the bursa of *Fabricius* as a primary immune organ.

Innate lymphoid cells (ILCs) are reported to regulate tissue immune homeostasis, resist pathogenic infection, and enhance T- and B-cell-mediated acquired immune responses in humans and mice, however, chicken ILC-like cells have not been fully verified right now. To explore the possibility, we first analyzed and selected the critical and specific homologous genes for human and mouse ILCs and we found that 92.3% of them were cloned successfully (primers for cloning genes showed in Supplementary Table 1), suggesting that chickens, as evolutionarily original animals, are likely to have ILCs. Meanwhile, the transcription factors (GATA3 and Id2), the differentiation-dependent factor IL7, and specific surface markers (CD127 and CD117) of the oral yeast group were all upregulated (Figure 3F, Supplementary Figure 2B) compared to those in the ST1814G group. These are critical factors that regulate the transformation of common ILC precursors (CILPs) to ILCs (Zhong and Zhu, 2017; Zhu, 2017), suggesting that oral yeast-immunized chickens were likely to stimulate more ILC formation by the differentiation of CILPs in the bursa of *Fabricius*.

Oral yeast vaccine promotes innate immune signaling pathway in the spleen

In addition to innate immune cells, there are also some important innate immune signaling pathways that constitute the first line of defense against pathogen invasion and mediate the activation of immune cells. To further analyze the protective mechanisms of yeast vaccine-elicited innate immunity, we first examined the transcript levels of factors involved in intracellular innate immunity in different groups (Figure 4A). We found that,

10.3389/fmicb.2023.1153922

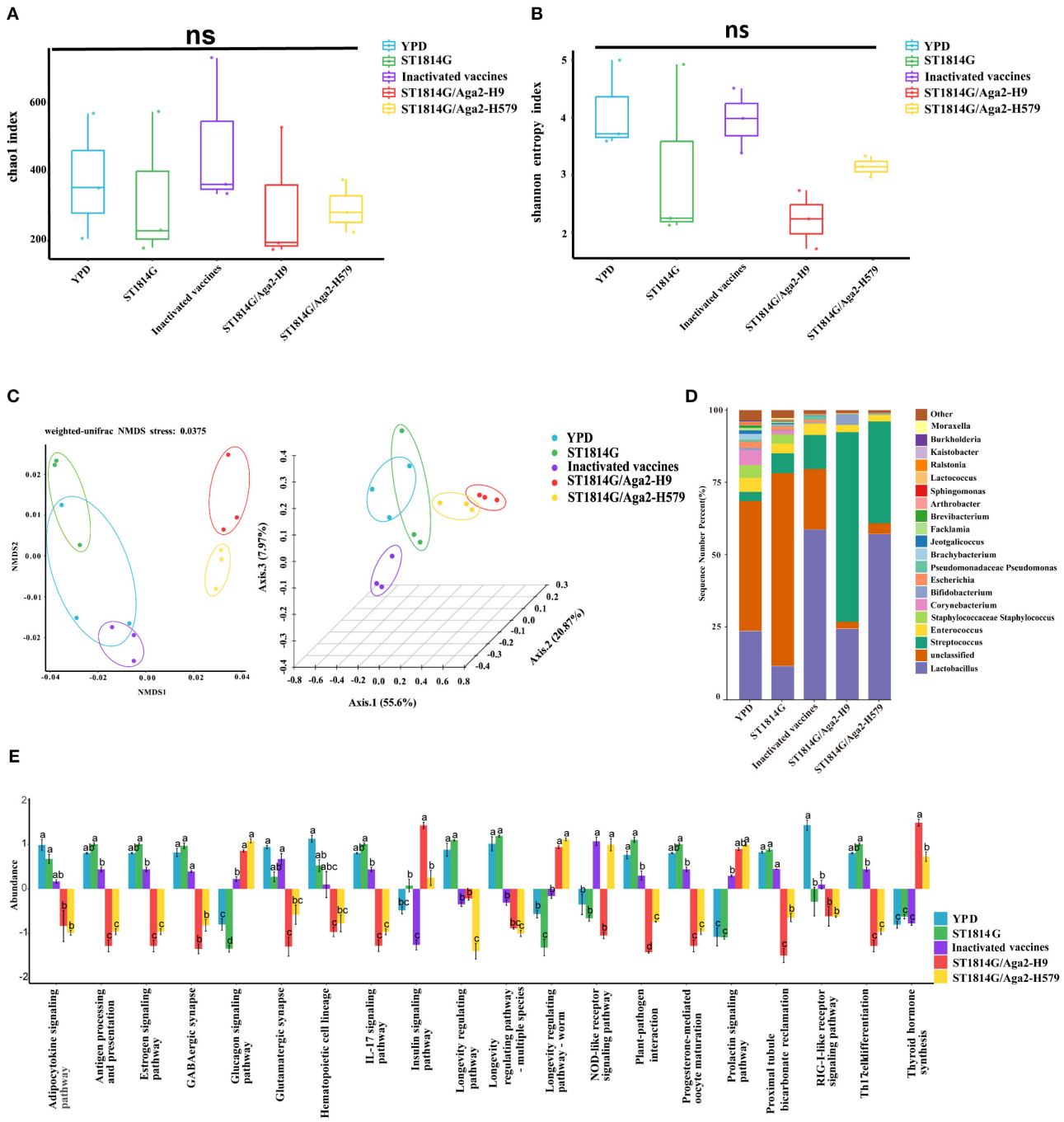

FIGURE 6
Relative abundance and intergroup diversity of gut microbiota in chickens post-immunization. The alpha diversity index reflects species diversity in the five groups of samples, **(A)** the Chao1 index reflects the species abundance of the 5 groups, **(B)** the Shannon index assesses the species diversity of the 5 groups, **(C)** beta diversity, including NMDS analysis and PCoA analysis, assesses differences in microbial community structure in the five groups of samples. **(D)** Species distribution histogram of chicken gut microbiota in each group at the genus level. **(E)** Analysis of functional differences between groups in the KEGG pathways: Twenty signaling pathways including antigen processing and presentation, estrogen signaling pathway, and GABAergic synapse. The data in the figures were obtained from three independent experiments and represent the averages ± SD. The significance of differences was determined by a two-way analysis of variance or Dunnett's test (*$p < 0.05$; **$p < 0.01$; ***$p < 0.001$; ****$p < 0.0001$ or ns, no significance).

compared to the ST1814G group, the factor expression levels were mostly upregulated in cecum tonsils in oral yeast vaccine groups, suggesting that cecum tonsils play an important role in the efficacy of yeast vaccine in chickens. The spleen plays an important role in immune function in the organism, and we found that oral administration of yeast vaccine stimulated

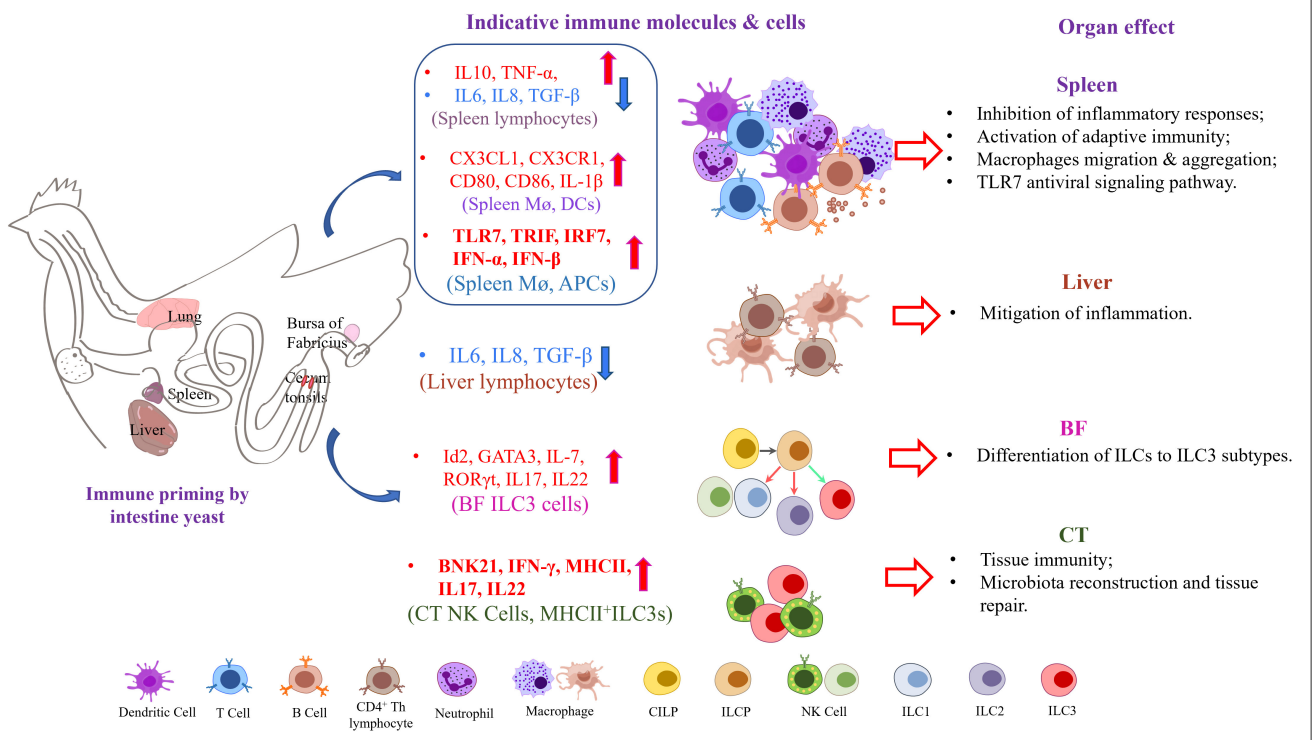

FIGURE 7
Oral yeast vaccine caused alterations of primary immune cytokines in several immune organs and lymph nodes in chickens.

TLR7-TRIF-IRF7-dependent interferon signaling pathway in the situation of H9N2 influenza virus infection in the spleen (Figures 4B–F; Supplementary Figure 2A), whereas the expression level of MyD88 was not influenced (Supplementary Figure 1B). Therefore, we concluded that the innate immune signaling pathway might be activated after oral administration of yeast vaccine in the cecum tonsil, which is an important immune organ for fighting against pathogen invasion. Especially, the interferon signaling pathway was triggered a in TLR7-TRIF-IRF7-dependent manner upon virus infection in the oral yeast-immunized chickens.

Oral yeast vaccine has various effects on different tissue-resident T cell

As mentioned above, the oral yeast vaccine might cause the accumulation of APCs, such as macrophages and dendritic cells, in the spleen, which implied that the function of T cells might be influenced in the oral yeast vaccination group. Both CD4 and CD8 are characteristic molecule markers of T cells. $CD4^+$ T cells mainly perform cellular regulatory functions, promote downstream T helper (Th) cell and regulatory T (TREG) cell differentiation, and achieve a regulatory effective immune response to pathogens. $CD8^+$ T cells mainly exert cellular immune functions and secrete perforin and granzyme through MHC-I-dependent processes to protect the organism against intracellular threats such as viruses and bacteria, as well as neoplasms. To explore whether the function of T cells is influenced by the oral yeast vaccine, we next checked the expression levels of CD4 and CD8 in different immune organs and lymph nodes. As shown in Figure 5, the expression levels of both CD4 and CD8 are upregulated in the liver and cecum tonsils. In particular, CD4 is significantly upregulated in the spleen while CD8 is significantly upregulated in the bursa of *Fabricius*. These results indicated that both $CD4^+$ T cells and $CD8^+$ T cells might play important roles in the liver and cecum tonsils, which was consistent with our above results that the cecum tonsils might be a primary influenced immune organ in the situation of oral yeast vaccination (Figure 4A). In addition, $CD4^+$ T cells might dominate immune regulatory responses in the spleen, and $CD8^+$ T cells might dominate cytotoxic T-cell responses in the bursa of *Fabricius*.

Oral yeast vaccine improves the gut microbiota and suppresses the Th17 cell differentiation and IL17-mediated cellular inflammation

It is known that yeast is probiotic to colonize the intestinal microenvironment, and thus, gut microbiota and intestinal mucosal immunity might be changed due to the influence of oral yeast (Zhang et al., 2022b). To further explore the protective mechanism of oral yeast vaccine, we next performed 16S rRNA-amplicon sequencing to analyze the change of gut microbiota in different groups.

The alpha diversity index indicates species diversity, namely the abundance and evenness of species composition, of the sample.

TABLE 1 Experiment design of chicken immunization.

Groups	Number of chickens	Dosage per chicken	Immunization	
			Times	Route
YPD	13	1 mL	3	Oral administration
ST1814G	13	1×10^9 CFU	3	Oral administration
Inactivated vaccines	13	0.2 mL	1	i.m.
ST1814/Aga2-H9	13	1×10^9 CFU	3	Oral administration
ST1814/Aga2-H579	13	1×10^9 CFU	3	Oral administration

The Chao1 index and Shannon index analysis reflected that there were no significant differences in species abundance and diversity between the oral yeast vaccine groups and the other groups (Figures 6A, B). The beta diversity index is used to compare species composition between different samples using statistical methods, such as non-metric multidimensional scaling (NMDS) and principal coordinate analysis (PCoA). As shown in Figure 6C, the two oral yeast vaccine groups were much closer to each other, whereas the inactivated vaccine group was closer to the YPD group and ST1814G group, suggesting our oral yeast vaccine indeed had different species composition compared to the yeast vehicle group and the inactivated vaccine group, which might stand for the protective function of oral yeast vaccine in chickens.

Next, we analyzed the relative abundance of species at the genus level of gut microbiota, using the species abundance table from the operational taxonomic unit (OUT) clustering analysis (Figure 6D). Among the eight high abundance genera, compared to the yeast vehicle group and inactivated vaccine group, oral administration of yeast vaccines could increase the abundance of probiotic bacteria (*Bifidobacterium* and *Lactobacillus*), decrease the abundance of pathogenic bacteria (*Escherichia*, *Corynebacterium*, *and Staphylococcus*), and maintain normal intestinal bacteria (*Enterococcus* and *Streptococcus*). These changes in gut microbiota indicated that oral administration of yeast vaccines improved the intestinal microenvironment, which might further influence intestinal mucosal immunity through the adjustment of microbial metabolic product.

The different species abundance lists of different groups were further processed for an enrichment analysis based on the KEGG Ontology databases to obtain functional annotations. Notably, among the many different signaling pathways between the oral yeast vaccine group and ST1814G group, the IL17 signaling pathway and T helper 17 (Th17) cell differentiation signaling pathway attracted our attention. The Th17 cells are essential for controlling extracellular bacterial and fungal infections, and they also trigger autoimmune responses by secreting pro-inflammatory cytokine IL17 (Sandner et al., 2021). It is reported that the dynamic balance of the gut microbiome is critical for maintaining Treg/Th17 homeostasis in the intestine, which is important for the susceptibility to inflammatory bowel disease (Omenetti and Pizarro, 2015). The relative abundance of microbiota involved in regulating these two signaling pathways was lower in the oral yeast vaccine group than those in the ST1814G group, suggesting that oral yeast immunization could suppress the Th17 cell differentiation and IL17-mediated cellular inflammation (Figure 6E).

Discussion

Current strategies for developing and manufacturing the avian influenza vaccine have safety and production issues, are time-consuming, and are somewhat limited in the ability to quickly generate a vaccine matched with mutate virus (Lei et al., 2020). In this study, we successfully developed an oral yeast vaccine candidate that expressed three HA proteins simultaneously for preventing different avian influenza virus subtype infections. Our experimental results suggested that it provided desired protective effect without side effects for chickens. To better understand the protective molecular mechanisms of oral yeast vaccines, we detected the effects of oral yeast vaccine on congenital lymphocyte subsets of different tissues and gut microbiota in different treated groups, such as ST1814G yeast vehicle, traditional inactivated vaccine, and our engineered oral yeast vaccines.

The *S. cerevisiae* surface display system successfully expressed HA proteins, but the measured protein molecular weights were larger than predicted (H5 74.5 kDa, H7 71.5 kDa, and H9 69 kDa). Based on studies reporting that glycosylation in yeast increases the molecular weight of the protein (Liu et al., 2022), we presume that glycosylation occurred during post-translational modification in yeast in this study. It has been proposed that glycosylation can enhance immunogenicity and thermal stability (Maciola et al., 2017) and also can lead to a decrease in protein expression (Peraino et al., 2012). We consider that protein glycosylation in yeast is very complex cellular engineering, and whether it affects various aspects of the biological activity of HA proteins remains to be explored.

The oral yeast vaccine alters the activation dynamics of congenital lymphocyte subsets in different tissues. *S. cerevisiae* is an ideal vehicle for delivering protein subunit and nucleic acid vaccines. β-glucan (Torosantucci et al., 2000) and mannans (Liu Y. N. et al., 2021) from yeast cell walls are the main active components, and the diameter of yeast further facilitates the recognition by antigen-presenting cells of organisms (Silva et al., 2021; Feng et al., 2022). In our study, we found that, compared to the ST1814G yeast vehicle group, oral administration of HA present on the surface of *S. cerevisiae* could upregulate chemokines and the abundance of tissue-resident NK cell, APCs, γδ T cell, and ILCs. In particular, the NK cells might mainly accumulate in the spleen and cecum tonsils while the APCs mainly accumulate in the spleen. In contrast, γδ T cells and ILCs might mainly accumulate in the bursa of *Fabricius* (Supplementary Figure 2B). Those changes in several immune organs and the predominant immune cells in oral yeast birds indicated that the spleen and cecum tonsils could recognize the signaling of HA-displaying yeasty and then continue

TABLE 2 Primers for qRT-PCR.

Gene name (chicken)	Primer sequence(5′-3′)	Size (bp)	References
H9-HA	F:CAGAACAAGAAGGCAGCAA R:AATGTGATGACCATTGCATGG	199	GenBank: KC296446.1
CD4	F:AGGATTGTGGAACTGTCACCTC R:CTGCCACCTCATACCAGTGATT	174	GenBank: DQ202315.1
CD8	F:AGCCACAACAACAGCAGCAC R:TACAAGGAGCACGAGGCAGA	177	GenBank: AY519197.1
CD80	F:CAGCAAGCCGAACATAGAAAGA R:AGCAAACTGGTGGACCTGAGA	270	NM_001079739.2
CD86	F:AAGGATACCAGATACCCTCCCT R:AGGGTGATTGCCAGAAAGCC	189	XM_046908563.1
CX3CL1	F:TCTCCAGATCCCGTTTGCAC R:CACGATCTTCTCCACCCACG	241	GenBank: AM398231.1
CX3CR1	F:ACCACAGGGAGTCGCATTTA R:TCCAGCAAGTGCGGTTACTTT	198	XM_040696048.2
IL1-β	F:CCAGAAAGTGAGGCTCAACATTG R:GACATGTAGAGCTTGTAGCCCTT	114	GenBank: HQ329098.1
IL10	F:TTCTTCCCGTAACCACGTCC R:AGGCAGTCATGCGTTGTTTG	193	NM_001004414.4
IL6	F:CCTGTTCGCCTTTCAGACCT R:GGGATGACCACTTCATCGGG	171	GenBank: HM179640.1
IL8	F:ATTCAAGATGTGAAGCTGAC R:AGGATCTGCAATTAACATGAGG	196	GenBank: DQ393272.2
TNF-A	F:CCGCCCAGTTCAGATGAGTT R:GCAACAACCAGCTATGCACC	130	GenBank: AY765397.1
TGF-B	F:GGTGCCCCATCGGAGTTATT R:TTGCTGAGGATTTGACCCCG	186	XM_040694846.2
BNK21	F:GGGAAGGCAAAGAGCATCCA R:CTCCAGAAATGCTCCCGAGG	138	XM_046928526.1
TARP	F:TGCCTACTGGGAGTCACGAT R:TCATCGGTCCATTTCACCCG	195	NM_001318455.1
TCRD	F:GGTACCGTCAGACACTCGAT R:TACAGGGCACGTAGAGACAGA	154	GenBank: AF175433.1
Id2	F:CTGACCACGCTCAACACAGA R:GTTAGCGTGGATTCCTCCCC	272	NM_205002.2
GATA3	F:GTTCGGGTGCAAATCACGAC R:GATCGCCGTTGGCATTTCTC	272	XM_046908458.1
IL7	F:GGACCATGTCCCATGCCTT R:GCTCTTCGATGTCATGGCTG	156	GenBank: AJ852017.1
CD127	F:AGGATCAAGCCTGTCGTGTG R:TCGGCTTTTGCTTGAATGCC	158	NM_001080106.1
CD117	F:GTTGAAACCAAGCGCCCATT R:AATGAATCTCGCTTCCGCCT	195	NM_204361.1
TBX21	F:GACCTCTACGACAAGGAGCC R:CTCAGCTCCAGCCCCAGG	153	XM_040692014.2
RORα	F: AGCTCGCATCCCATCTGGA R:CGGAGCGGACTCCATGTTTT	144	XM_046899012.1
RORγt	F:CCACAGACCGCCATGCGAG R:GGACATGCGGCCAAACTTGA	270	XM_025143434.2
IL5	F:CAGTGCTGGCTCACATTCAG R:CTGTATCCACCCTTCTGCGG	203	NM_001007084.2

(Continued)

TABLE 2 (Continued)

Gene name (chicken)	Primer sequence(5′-3′)	Size (bp)	References
IL13	F:AGTCCCTGAGCATTTGGGTG R:CAACTGTGGGGATGAAGGCA	230	NM_001007085.3
IL17	F:GATGCTGGATGCCTAACCCA R:TGTTTGATGGGCACGGAGTT	257	GenBank: AY744450.1
IL22	F:AGCCCTACATCAGGAATCGC R:CAGGGATGCCAGGAACTGTG	230	NM_001199614.1
IFNα	F: CACCTTCCTCCAAGACAACGATT R:GGCATCCAGCATCTCCTTTC	130	GenBank: GU119896.1
IFNβ	F: CCTCAACCAGATCCAGCATT R:GGATGAGGCTGTGAGAGGAG	180	GenBank: KF741874.1
IFNγ	F: CTGACAAGTCAAAGCCGCAC R:GCATCTCCTCTGAGACTGGC	230	GenBank: AH009942.2
TLR7	F:TGTGATGTGGAAGCCTTTGA R:ATTATCTTTGGGCCCCAGTC	219	NM_001011688.3
TRIF	F:GGTGCCACATTCTGTGAGGA R:GAAGGTCGCTGGATGGACTC	173	NM_001081506.1
MyD88	F:GAAAGAAGGTGTCGGAGGATG R:AATTGTAATGAACCGCAAGATACT	183	NM_001030962.5
IRF-7	F:AAGTGCAAGGTCTTCTGGGC R:GGAAGATGGTGAAGTCGGGG	172	NM_205372.2
β-actin	F:ATGAAGCCCAGAGCAAAAGA R:GGGGTGTTGAAGGTCTCAAA	120	GenBank: L08165.1

to trigger signaling pathway of the TLR7-TRIF-IRF7-denpendent interferon signaling pathway after yeast vaccination in the spleen (Figure 4). As the primary immune organ in birds, the activation of innate lymphocytes, such as γδ T cells and ILCs, was observed in the bursa of *Fabricius*, which hints at a possible origin of them from the bursa. The TLR7 can recognize viral single-stranded ribonucleic acid (ssRNA) and promote IL-1β and iNOS production in macrophages of H4N6 LPAIV-infected chicken (Annamalai et al., 2015; Abdul-Cader et al., 2018). The boosted TLR7-TRIF-IRF7-dependent interferon pathway and IL-1β production after the virus challenge maybe contribute to the deducing viral loading and good protection observed in our oral yeast vaccine. The existence of a memory response by oral immunity in birds and how they work is still a challenging problem.

The oral yeast vaccine prompts ILC3 cell differentiation in the bursa of *Fabricius*. The enhanced CILPs differentiated into ILCs were deduced in the bursa of *Fabricius in* oral yeast-immunized chickens and were supported by the upregulation of the specific transcription factors (GATA3, ID2), essential regulatory cytokine (IL7), and surface molecule markers (CD127, CD117) (Figure 3G). To understand which type of ILC cells contributes to it, the mRNA levels of three subtype-specific molecular markers of ILCs in the bursa tissues were detected. Both ILC1- and ILC2-related transcription factors and cytokines (T-bet and IFNγ for ILC1; RORα, IL5, and IL13 for ILC2) (Vivier et al., 2018; De Pasquale et al., 2021) were suppressed or detected no difference among the groups. In contrast, ILC3-related transcription factors RORγt were significantly upregulated (Supplementary Figure 1C). Meanwhile, IL22 secreted by ILC3 was also significantly increased in the bursa of *Fabricius*. These results suggested that the oral yeast vaccine elicits ILC3 proliferation to promote the innate immune response, mucosal repair, and barrier establishment against extracellular pathogen infection. Certainly, there is an urgent need for the successful sorting and identification of ILC cells in chickens to further verify their functions.

Oral HA-present *S. cerevisiae* is a potent alternative vaccine causing ideal protective responses and mild inflammatory responses. Usually, the inactivated vaccine triggers a strong inflammatory response or macrophage infiltration that leads to a relatively big liver index. However, this phenomenon was not induced in the groups of oral yeast vaccine (Figure 2B). To understand the contribution of the engineered yeast vaccines in the inflammatory response, the major pro-inflammatory factors, including IL6, IL8, TNF-α, and TGF-β, and the suppressing inflammatory cytokine IL10 (Liu Z. et al., 2019) were measured. The downregulation of all pro-inflammatory factors was observed in the organs of oral yeast groups compared with those in the inactivated vaccine group, which was consistent with the above organ index experiments (Supplementary Figures 3A–D). Interestingly, IL10 was significantly upregulated in the spleen after immunization. Considering the accumulation of APCs in the spleen, we speculated that specific APCs, such as macrophages, might be dynamically regulated by IL10 to perform the inhibition role of the inflammation response *in vivo*. Yeast is able to colonize the mouse intestine and become the predominant species further reshaping the microbiota and intestinal microenvironment (Dong et al., 2022). The functional prediction of gut microbiota demonstrated a reduced Th17 cell/IL17 signaling pathway in

the yeast vaccine group, which also decreased the intestinal inflammation response (Zhang et al., 2022a). Taken together, these results indicated that oral administration of yeast vaccine might facilitate the repairmen of gut mucosa damage caused by pathogen invasion, which elicit the innate intestinal mucosal immunity to protect the organism from fatal influenza virus infection (Ravindran and Thornton, 2022; Serafini et al., 2022).

Generally, the roles of oral yeast vaccine in defending avian influenza virus infection may be performed by altering immune response in different immune organs or lymph node tissues (Figure 7). 1. The activation of the APC-indicated chemokines and TLR7-TRIF-IRF7-dependent interferon signaling in the spleen indicates the crucial roles of the spleen in response process of oral yeast immunity. 2. The NK cells, γδ T cells, and ILC3 cells derived from CILPs from the bursa change the cytokine spectrum and trigger the activation of some immune cells, such as CD4+ T cells in the spleen and CD8+ T cells in the bursa of *Fabricius*. 3. The oral administration of yeast vaccine alters the structure of gut microbiota and their metabolites and stimulates a mild inflammatory response, which is important to the contribution of their good immune protection.

Further studies will be required to fully elucidate the mechanisms by which the HA yeast vaccine provides protection. In most cases, symptoms and severity are greatly reduced, and the virus is cleared faster in yeast-feeding birds. Our present findings suggest that protection against IAV infection may be provided through non-neutralizing mechanisms, such as innate immune cell function regulation and immune microenvironment homeostasis remodeling. The deficiency in our study is that, in order to construct a multivalent yeast vaccine, we constructed an *S. cerevisiae* strain of H579, but limited by the existing laboratory conditions, we only did the attack protection experiment for H9. We believe that H5 and H7 are also expressed, so they can be resistant to all three viruses to some extent, but this needs further testing. Our overall approach will likely be useful for infectious diseases other than influenza viruses. Multivalent yeast vaccines may be applied against other variable pathogens. Additional studies will be required to reveal the function of those novel innate lymphocytes, such as macrophages, NK cells, γδ T cells, and ILC3 cells, which participated in immune protection and understand their underlying immunological mechanisms in detail.

Materials and methods

Virus, vaccine, yeast, and plasmids

The H9N2 subtype avian influenza virus strain (GenBank: KC296446.1) was isolated and stored in our laboratory. The avian influenza-inactivated vaccine was bought from YEBIO Bioengineering Co., Ltd., Qingdao (Qingdao, China). In this study, yeast strain ST1814G constructed in our laboratory (MATa aga1 his3Δ200 leu2Δ0 lys2Δ0 trp1Δ63 ura3Δ0 met15Δ0) was utilized as the host cell for the surface display system. Plasmids for constructing recombinant yeast strains include nutrient-deficient screening markers: PMV- LEU2, PMV- TRP, PMV-HIS, and homologs chromosome armsPMV-URR1, PMV-URR2 and performed the element assembly as previously described (Guo et al., 2015). The POT-GPD-RFP-ADH1 plasmid containing 667 bp GAPDH promoter sequences, 187 bp ADH1 terminator sequences, and RFP selective marker sequence was from our laboratory.

Construction of transcription units

The chimeric H5/7/9 HA (hemagglutinin) recombinant yeast vaccine was constructed, the 1404bp sequences of the H5N8 HPAI virus strain (A/goose/Hebei/HG12/2021), the 1515bp sequences of the H7N9 HPAI virus strain (A/duck/Jiangxi/3096/2009), and the 1344bp sequences of the H9N2 LPAI virus strain (A/Hebei/218/2010) were selected. HA-optimized genes (with the transmembrane domain and the signal peptide removed) (H5N8 subtype and H7N9 subtype) were cloned from laboratory strains, and the HA gene sequence of the H9N2 subtype of AIV was obtained from the NCBI website and optimized for synthesis by GENEWIZ (Beijing, China). Three HA genes were subcloned into three yeast expression vectors (pGPD-ADH1-POT with His-tag at the C terminal and Aga2 signal peptide at the N terminal), respectively by using a One-step Cloning kit (Vazyme, Nanjing). These strategies would anchor the recombinant proteins to the yeast surface and allow tracking of expression by anti-His-tag specific antibodies. The recombinant plasmids were named pGPD-H5-ADH1-POT, pGPD-H7-ADH1-POT, and pGPD-H9-ADH1-POT, respectively.

Construction of yeast

Using yeast that had completed the construction of the H5-Leu module on chromosome IV as a substrate, the H7 gene was constructed into chromosome XVI using the filter tag Trp and the H9 gene was constructed into chromosome III using the filter tag His (Figure 1A). Our transcriptional construction unit refers to a previously published article, briefly described as follows: Construct pGPD-HA-ADH1-POT vector, *Bsa*I enzyme cleavage plasmid to obtain linearized transcript; perform *Bsm*BI enzyme cleavage with screening marker plasmid, URR1, URR2; then T4 ligation, transformation into yeast in LiAc, screen positive clones corresponding to nutrient-deficient plates, and extract genome for identification. H5/H7/H9 are all using the same method.

Western blotting

The expression of HA protein in trivalent recombinant yeast was identified by the Western blotting technique. In total, 2 ml of yeast cultured overnight at 30°C was taken at 10,000 rpm for 1 min, which was then collected. The pellets were broken with an equal amount of silica beads of 60 μL protein extraction buffer (2 % SDS, 100 mmol/L DTT, 125 mmol/L Tris-HCl, pH 6.8). Next, the mixture was centrifuged at 12,000 rpm for 10 min at 4°C, and the supernatant was carefully obtained into a new EP tube by adding 5× loading buffer and boiled for 10 min. Treated samples were resolved on a precast 12% polyacrylamide

gel and then electrophoretically transferred to the methanol-activated polyvinylidene fluoride membrane (PVDF) (PALL, USA), after blocking with TBS-Tween containing 5% skim milk at room temperature for 2 h and then incubated with a rabbit anti-His antibody (1:5,000 diluted, Yeasen Biotech, Shanghai, China) at room temperature for 1 h. Following three 5-min washes with TBS-Tween, the membrane was followed by 1:5000 diluted horseradish peroxidase (HRP)-conjugated goat anti-rabbit IgG, (Yeasen Biotech, Shanghai, China) for 1 h and then treated with three final washes. Specific proteins were visualized with Western lightning chemiluminescence reagent plus substrate mixture (Bio-Rad, USA) and imaged using the ChemiDoc imaging system (Gel DocTM XR + imaging system, Bio-Rad, USA).

Immunofluorescence and flow cytometry

The yeast cells containing the target genes were harvested and centrifuged. The blank strain of ST1814G was used as a negative control during this experiment. First, the yeast cells were centrifuged at 6000 rpm for 1 min at 4°C. The cells were treated with a mouse anti-His-tag and followed by FITC-conjugated rabbit anti-mouse IgG antibody at 4°C for 1 h and re-suspended with 500 μL of sterile PBS. Finally, 5 μL of *S. cerevisiae* pellets were used for immunofluorescence assay under an inverted fluorescence microscope. For flow cytometry analysis, 500 μL pellets were analyzed by flow cytometry analysis (BD FACSCalibur, BD Bioscience, San Jose, CA, USA).

Oral immunization and virus challenge

The animal study was performed following the guidelines and regulations of the Laboratory Animal Ethical and Welfare Committee of Tianjin University (permit number, TJUE-2021–051). A total of 65 (mixed sex) egg-laying chickens (White Laiheng) were obtained and housed in specific pathogen-free (SPF) facilities. All birds were given free feed and free access to drinking water. The chickens were divided into five groups (13 birds per group) named YPD group, ST1814G group, inactivated vaccine group, ST1814G/Aga2-H9 group, and ST1814G/Aga2-H579 group. Immunization methods are presented in Table 1.

At 5 days after each immunization, the weight of three randomly selected poultry was taken, and blood and anal swab samples were taken for ELISA assays to detect changes in antibody titers in each group. On day 5 after the third immunization, three chicks were randomly euthanized for tissue sampling (liver, spleen, lung, bursa of *Fabricius*, and cecum tonsils) to detect the changes occurring in the different tissues. On day 6 after the third immunization, seven birds per group (mixed sex) were randomly selected and challenged intranasally with 100 μL A/Hebei/218/2010 (H9N2) virus ($TCID_{50} = 10^{-4.8}$/0.1 mL) and observed for 12 days to record the mortality rate, while blood was collected on the 4th, 7th, and 10th days to determine the virus titer in blood. The animal immunization and the virus challenge process are shown in Figure 1B. At the end of the experimental trials, the birds were humanly euthanized and adequately disposed of.

Analysis of gut microbiota

Sampling was performed on the 5th day after the end of immunization, and the intestinal contents were taken from 10 cm above the junction of the small intestine and the cecum of three chickens in each group. Samples were sent to Wekemo Tech Group Co., Ltd. (Shenzhen, China) for 16 S rRNA sequencing. The pair of primers (Forward: 5′ -ACTCCTACGGGAGGCAGCA-3′ and Reverse: 5′ -GGACTACHVGGGTWTCTA AT- 3′) were obtained according to the V3–V4 conserved region. The amplicon analysis process is based on Qiime2 software, and amplicon second-generation sequencing data are de-noised to generate ASV, taxonomic annotation, species screening, basic statistics, significant difference comparison, alpha diversity analysis, beta diversity analysis, correlation analysis, PICRUSt2 functional prediction, functional statistics, functional difference comparison, etc. Among Dunnett's multiple comparison tests, the KEGG Orthology (KO) abundance table was selected for functional difference comparison, and the Organismal Systems was selected among the seven classes of biometabolic pathways. All data were processed using the online platform of Wekemo Bioincloud (https://www.bioincloud.tech).

Enzyme-linked immunosorbent assay (ELISA)

HA-specific serum IgG and mucosal IgA antibody levels were separately determined by ELISA. In brief, 96-well ELISA plates were coated overnight at 4°C using 0.1 μg of recombinant HA protein of A/Hebei/218/2010 (H9N2) as the antigen. The wells were washed three times with PBS containing 0.05% Tween 20 (PBS-T) and blocked with PBS-T containing 1% BSA for 2 h at room temperature. To the reaction add serum at 1:40 dilution (select optimal dilution after serial dilutions) or the anal swab in PBS to the plate and incubate at 37°C for 1 h, followed by incubation with HRP-goat anti-chicken IgG conjugate (Solarbio, Beijing, China) or goat anti-chicken IgA conjugate (Abcam, USA) at 37°C for 1 h, respectively. After incubation with TMB substrate solution (Solarbio, Beijing, China) for 12 min in the dark, the reaction was blocked by 2 M H_2SO_4, and the optical density (OD405) of each well was measured using a microplate spectrometer.

Quantitative real-time PCR (qRT-PCR)

The expressions of chicken immune-related cytokine genes in the inactivated vaccine group, the oral yeast vaccine group (ST1814G/Aga2-H9 and ST1814G/Aga2-H579), the control ST1814G group, and the blank control YPD group were detected by quantitative PCR (qPCR). For each group of three, RNA was extracted from the tissues using the TRIzol reagent (Yeasen Biotech, Shanghai, China), reverse transcription was performed using the Hifair®III 1st Strand cDNA Synthesis SuperMix (Yeasen Biotech, Shanghai, China), and the concentration of cDNA generated was ensured at 2,000 ng/ul. For qPCR, primers for CD4, CD8, CD127, CD117, GATA3, etc., were designed using the Primer-Blast tool (Table 2). The absolute fluorescence quantitative

PCR assay was used to quantify the viral titer of H9N2, detecting primers in Table 2. qPCR was performed in a total volume of 20 μL per well, using the Hieff® qPCR SYBR Green Master Mix (Yeasen Biotech, Shanghai, China) and the amplification step consisted of 40 cycles of pre-denaturation at 94°C for 5 min, followed by denaturation at 94°C for 10 s and extension at 60°C for 30 s, followed by melting curve analysis. CT values were determined in triplicate for each sample using an ABI 7500 real-time quantitative fluorescence PCR instrument. Data were calculated based on the 2-ΔΔCT method. β-actin was used as an internal reference for the normalization of relative mRNA expression, and the error lines indicated the standard.

Statistical analysis

A pairwise comparison between treatment and control groups was performed using statistical tools analysis of variance (ANOVA) using SPSS software, version 18.0 (SPSS, Chicago, IL, USA). All the graphs were generated using GraphPad Prism 5.0. (GraphPad Software, La Jolla, CA, USA) "ns" indicates no significant difference ($P > 0.05$). "*," "**," and "***" indicate statistically significant differences with values of $P < 0.05$, $P < 0.01$, and $P < 0.001$, respectively.

Data availability statement

The datasets presented in this study can be found in online repositories. The names of the repository/repositories and accession number(s) can be found in the article/Supplementary material.

Ethics statement

The animal study was reviewed and approved by the Laboratory Animal Ethical and Welfare Committee of Tianjin University. Written informed consent was obtained from the owners for the participation of their animals in this study.

Author contributions

JH conceived and designed the experiments, HanZ, ZL, HuiZ, YG, XZ, LZ, LY, SL, CL, DC, RX, and YL performed the experiments, HanZ, ZL, and JH analyzed the data and wrote the study. All authors contributed to the article and approved the submitted version.

Funding

This work was supported by the Tianjin Synthetic Biotechnology Innovation Capability Improvement Project in China (TSBICIP-KJGG-014) and the Key Underprop Project of Tianjin Municipal Science and Technology Bureau (20YFZCSN00340).

Conflict of interest

The authors declare that the research was conducted in the absence of any commercial or financial relationships that could be construed as a potential conflict of interest.

Publisher's note

Supplementary material

The Supplementary Material for this article can be found online at: https://www.frontiersin.org/articles/10.3389/fmicb.2023.1153922/full#supplementary-material

References

Abdul-Cader, M. S., De Silva Senapathi, U., Nagy, E., Sharif, S., and Abdul-Careem, M. F. (2018). Antiviral response elicited against avian influenza virus infection following activation of toll-like receptor (TLR)7 signaling pathway is attributable to interleukin (IL)-1beta production. *BMC Res. Notes.* 11, 859. doi: 10.1186/s13104-018-3975-4

Allen, J. D., Jang, H., DiNapoli, J., Kleanthous, H., and Ross, T. M. (2019). Elicitation of protective antibodies against 20 years of future H3N2 cocirculating influenza virus variants in ferrets preimmune to historical H3N2 influenza viruses. *J. Virol.* 93, e00946–18. doi: 10.1128/JVI.00946-18

Annamalai, A., Ramakrishnan, S., Sachan, S., Sharma, B. K., Anand Kumar, B. S., Kumar, V., et al. (2015). Administration of TLR7 agonist, resiquimod, in different types of chicken induces a mixed Th1 and Th2 response in the peripheral blood mononuclear cells. *Res. Vet. Sci.* 100, 105–108. doi: 10.1016/j.rvsc.2015.04.007

Arevalo, C. P., Bolton, M. J., Le Sage, V., Ye, N., Furey, C., Muramatsu, H., et al. (2022). A multivalent nucleoside-modified mRNA vaccine against all known influenza virus subtypes. *Science* . 378, 899–904. doi: 10.1126/science.abm0271

Bajic, G., Maron, M. J., Adachi, Y., Onodera, T., McCarthy, K. R., McGee, C. E., et al. (2019). Influenza antigen engineering focuses immune responses to a subdominant but broadly protective viral epitope. *Cell Host Microbe.* 25, 827–835. doi: 10.1016/j.chom.2019.04.003

Bangaru, S., Lang, S. S., Schotsaert, M., Vanderven, H. A., Zhu, X. Y., Kose, N., et al. (2019). A site of vulnerability on the influenza virus hemagglutinin head domain trimer interface. *Cell.* 177, 1136. doi: 10.1016/j.cell.2019.04.011

Chen, C., Fan, W. H., Li, J., Zheng, W. N., Zhang, S., Yang, L. M., et al. (2018). A promising IFN-deficient system to manufacture IFN-sensitive influenza vaccine virus. *Front Cell Infect Mi.* 8, 00127. doi: 10.3389/fcimb.2018.00127

Cho, A., and Wrammert, J. (2016). Implications of broadly neutralizing antibodies in the development of a universal influenza vaccine. *Curr. Opin. Virol.* 17, 110–115. doi: 10.1016/j.coviro.2016.03.002

Christensen, S. R., Toulmin, S. A., Griesman, T., Lamerato, L. E., Petrie, J. G., Martin, E. T., et al. (2019). Assessing the protective potential of h1n1 influenza virus hemagglutinin head and stalk antibodies in humans. *J. Virol.* 93, 2019. doi: 10.1128/JVI.02134-18

De Pasquale, C., Campana, S., Bonaccorsi, I., Carrega, P., and Ferlazzo, G. I. L. C. (2021). in chronic inflammation, cancer and targeting with biologicals. *Mol. Aspects Med*. 80, 100963. doi: 10.1016/j.mam.2021.100963

Dong, Z. R., Mu, Q. J., Kong, W. G., Qin, D. C., Zhou, Y., Wang, X. Y., et al. (2022). Gut mucosal immune responses and protective efficacy of oral yeast Cyprinid herpesvirus 2 (CyHV-2) vaccine in Carassius auratus gibelio. *Front. Immunol.* 13, 932722. doi: 10.3389/fimmu.2022.932722

Feng, X. X., Xie, Q., Xu, H. B., Zhang, T. T., Li, X. A., Tian, Y. M., et al. (2022). Yeast microcapsule mediated natural products delivery for treating ulcerative colitis through anti-inflammatory and regulation of macrophage polarization. *Acs Appl Mater Inter*. 14, 31085–31098. doi: 10.1021/acsami.2c05642

Franzusoff, A., Duke, P. C., King, T. H., Lu, Y. N., and Rodell, T. C. (2005). Yeasts encoding tumour antigens in cancer immunotherapy. *Expert. Opin. Biol. Th*. 5, 565–575. doi: 10.1517/14712598.5.4.565

Guan, J., Deng, Y., Chen, H., Yin, X., Yang, Y., Tan, W. J., et al. (2015). Priming with two DNA vaccines expressing hepatitis C virus NS3 protein targeting dendritic cells elicits superior heterologous protective potential in mice. *Arch. Virol*. 160, 2517–2524. doi: 10.1007/s00705-015-2535-7

Guo, Y., Dong, J., Zhou, T., Auxillos, J., Li, T., Zhang, W., et al. (2015). YeastFab: the design and construction of standard biological parts for metabolic engineering in Saccharomyces cerevisiae. *Nucleic Acids Res*. 43, e88. doi: 10.1093/nar/gkv464

Jensen, G. S., Hart, A. N., and Schauss, A. G. (2007). An antiinflammatory immunogen from yeast culture induces activation and alters chemokine receptor expression on human natural killer cells and B lymphocytes in vitro. *Nutr. Res*. 27, 327–335. doi: 10.1016/j.nutres.2007.04.008

Jiang, W. M., Wang, S. C., Liu, H. L., Yu, J. M., Du, X., Hou, G. Y., et al. (2014). Evaluation of avian influenza virus isolated from ducks as a potential live vaccine candidate against novel H7N9 viruses. *Vaccine*. 32, 6433–6439. doi: 10.1016/j.vaccine.2014.09.050

Kaiser, P. (2010). Advances in avian immunology–prospects for disease control: a review. *Avian Pathol*. 39, 309–324. doi: 10.1080/03079457.2010.508777

Kiflmariam, M. G., Yang, H. J., and Zhang, Z. Y. (2013). Gene delivery to dendritic cells by orally administered recombinant Saccharomyces cerevisiae in mice. *Vaccine*. 31, 1360–1363. doi: 10.1016/j.vaccine.2012.11.048

Kim, S. M., Kim, Y. I., Park, S. J., Kim, E. H., Kwon, H. I., Si, Y. J., et al. (2017). Vaccine efficacy of inactivated, chimeric hemagglutinin H9/H5N2 avian influenza virus and its suitability for the marker vaccine strategy. *J. Virol*. 91, e01693–16. doi: 10.1128/JVI.01693-16

Lei, H., Xie, B., Gao, T., Cen, Q., and Ren, Y. (2020). Yeast display platform technology to prepare oral vaccine against lethal H7N9 virus challenge in mice. *Microb. Cell Fact*. 19, 53. doi: 10.1186/s12934-020-01316-1

Liu, B., Yin, Y., Liu, Y. X., Wang, T. T., Sun, P., Ou, Y. Q., et al. (2022). A vaccine based on the receptor-binding domain of the spike protein expressed in glycoengineered pichia pastoris targeting SARS-CoV-2 stimulates neutralizing and protective antibody responses. *Engineering-Prc*. 13, 107–115. doi: 10.1016/j.eng.2021.06.012

Liu, H., Meng, Z., Wang, H., Zhang, S., Huang, Z., Geng, X., et al. (2021). Robust immune responses elicited by a hybrid adjuvant based on beta-glucan particles from yeast for the hepatitis B vaccine. *ACS Appl Bio Mater*. 4, 3614–3622. doi: 10.1021/acsabm.1c00111

Liu, Y. N., Wu, Q., Wu, X. Y., Algharib, S. A., Gong, F. Y., Hu, J. P., et al. (2021). Structure, preparation, modification, and bioactivities of beta-glucan and mannan from yeast cell wall: A review. *Int. J. Biological Macromolecules*. 173, 445–456. doi: 10.1016/j.ijbiomac.2021.01.125

Liu, Z., Zhang, F., Lu, P., Zhao, R., Zhang, H., Song, B., et al. (2019). Selenium-yeast alleviated inflammatory damage caused by lead via inhibiting ras/ERK pathway and inflammatory factors in chicken skeletal muscles. *Biol. Trace Elem. Res*. 190, 493–500. doi: 10.1007/s12011-018-1558-9

Maciola, A. K., Pietrzak, M. A., Kosson, P., Czarnocki-Cieciura, M., Smietanka, K., Minta, Z., et al. (2017). The length of N-glycans of recombinant H5N1 hemagglutinin influences the oligomerization and immunogenicity of vaccine antigen. *Front. Immunol*. 8, 00444. doi: 10.3389/fimmu.2017.00444

Neulen, M. L., Viertlboeck, B. C., Straub, C., and Gobel, T. W. (2015). Identification of novel chicken CD4(+) CD3(-) blood population with NK cell like features. *Dev. Comp. Immunol*. 49, 72–78. doi: 10.1016/j.dci.2014.11.012

Omenetti, S., and Pizarro, T. T. (2015). The Treg/Th17 axis: a dynamic balance regulated by the gut microbiome. *Front. Immunol*. 6, 00639. doi: 10.3389/fimmu.2015.00639

Peraino, J., Zhang, H. P., Hermanrud, C. E., Li, G. Y., Sachs, D. H., Huang, C. A., et al. (2012). Expression and purification of soluble porcine CTLA-4 in yeast Pichia pastoris. *Protein Expres Purif*. 82, 270–278. doi: 10.1016/j.pep.2012.01.012

Ravindran, R., and Thornton, E. (2022). ILC3-induced regulatory T cells are directed by gut microorganisms. *Nat. Rev. Immunol*. 22, 207. doi: 10.1038/s41577-022-00697-1

Sandner, L., Alteneder, M., Zhu, C., Hladik, A., Hoegler, S., Rica, R., et al. (2021). The tyrosine kinase tec regulates effector Th17 differentiation, pathogenicity, and plasticity in T-cell-driven intestinal inflammation. *Front. Immunol*. 12, 750466. doi: 10.3389/fimmu.2021.750466

Sen, S., and Mansell, T. J. (2020). Yeasts as probiotics: Mechanisms, outcomes, and future potential. *Fungal Genet. Biol*. 137, (2020). doi: 10.1016/j.fgb.2020.103333

Serafini, N., Jarade, A., Surace, L., Goncalves, P., Sismeiro, O., Varet, H., et al. (2022). Trained ILC3 responses promote intestinal defense. *Science* . 375, 859–863. doi: 10.1126/science.aaz8777

Silva, A. J. D., de Macedo, L. S., Leal, L. R. S., de Jesus, A. L. S., and Freitas, A. C. (2021). Yeasts as a promising delivery platform for DNA and RNA vaccines. *FEMS Yeast Res*. 21, (2021). doi: 10.1093/femsyr/foab018

Swayne, D. E., Spackman, E., and Pantin-Jackwood, M. (2014). Success factors for avian influenza vaccine use in poultry and potential impact at the wild bird-agricultural interface. *Ecohealth*. 11, 94–108. doi: 10.1007/s10393-013-0861-3

Torosantucci, A., Chiani, P., and Cassone, A. (2000). Differential chemokine response of human monocytes to yeast and hyphal forms of Candida albicans and its relation to the beta-1,6 glucan of the fungal cell wall. *J Leukocyte Biol*. 68, 923–932. doi: 10.1189/jlb.68.6.923

Vahey, M. D., and Fletcher, D. A. (2019). Low-fidelity assembly of influenza a virus promotes escape from host cells. *Cell*. 176, 678–678. doi: 10.1016/j.cell.2019.01.009

Vivier, E., Artis, D., Colonna, M., Diefenbach, A., Di Santo, J. P., Eberl, G., et al. (2018). Innate lymphoid cells: 10 years on. *Cell*. 174, 1054–1066. doi: 10.1016/j.cell.2018.07.017

Walachowski, S., Breyne, K., Secher, T., Cougoule, C., Guzylack-Piriou, L., Meyer, E., et al. (2022). Oral supplementation with yeast beta-glucans improves the resolution of Escherichia coli-associated inflammatory responses independently of monocyte/macrophage immune training. *Front. Immunol*. 13, 1086413. doi: 10.3389/fimmu.2022.1086413

Wu, J. A., Liu, S. Z., Dong, S. S., Dong, X. P., Zhang, W. L., Lu, M., et al. (2010). Safety and immunogenicity of adjuvanted inactivated split-virion and whole-virion influenza A (H5N1) vaccines in children: a phase I-II randomized trial. *Vaccine*. 28, 6221–6227. doi: 10.1016/j.vaccine.2010.07.008

Xuan, C., Shi, Y., Qi, J., Zhang, W., Xiao, H., Gao, G. F., et al. (2011). Structural vaccinology: structure-based design of influenza A virus hemagglutinin subtype-specific subunit vaccines. *Protein Cell*. 2, 997–1005. doi: 10.1007/s13238-011-1134-y

Yang, C., Zhang, X., Xu, F., Wen, H., Lian, C., Chen, H., et al. (2014). [Preparation and characterization of polyclonal antibodies against haplotype chicken natural killer cell receptor B-NK19 and B-NK21]. *Xi Bao Yu Fen Zi Mian Yi Xue Za Zhi*. 30, 1274–1277.

Zhang, L., Lin, Q., Jiang, L., Wu, M., Huang, L., Quan, W., et al. (2022a). Increased circulating innate lymphoid cell (ILC)1 and decreased circulating ILC3 are involved in the pathogenesis of Henoch-Schonlein purpura. *BMC Pediatr*. 22, 201. doi: 10.1186/s12887-022-03262-w

Zhang, L., Yao, L., Guo, Y., Li, X., Ma, L., Sun, R., et al. (2022b). Oral SARS-CoV-2 spike protein recombinant yeast candidate prompts specific antibody and gut microbiota reconstruction in mice. *Front. Microbiol*. 13, 792532. doi: 10.3389/fmicb.2022.792532

Zhong, C., and Zhu, J. F. (2017). Transcriptional regulators dictate innate lymphoid cell fates. *Protein Cell*. 8, 242–254. doi: 10.1007/s13238-017-0369-7

Zhu, J. F. (2017). GATA3 regulates the development and functions of innate lymphoid cell subsets at multiple stages. *Front. Immunol*. 8, (2017). doi: 10.3389/fimmu.2017.01571

frontiers | Frontiers in Microbiology

TYPE Original Research
PUBLISHED 23 June 2023
DOI 10.3389/fmicb.2023.1206038

OPEN ACCESS

EDITED BY
Jianke Wang,
Hebei Agricultural University, China

REVIEWED BY
Naidong Wang,
Hunan Agricultural University, China
Jue Liu,
Yangzhou University, China

*CORRESPONDENCE
Jingliang Su
✉ suzhang@cau.edu.cn
Yu Huang
✉ huangyu_815@163.com

RECEIVED 14 April 2023
ACCEPTED 05 June 2023
PUBLISHED 23 June 2023

CITATION
Li J, Liu F, Ren Z, Fu G, Shi J, Zhao N, Huang Y and Su J (2023) Generation of a monoclonal antibody against duck circovirus capsid protein and its potential application for native viral antigen detection.
Front. Microbiol. 14:1206038.
doi: 10.3389/fmicb.2023.1206038

Generation of a monoclonal antibody against duck circovirus capsid protein and its potential application for native viral antigen detection

Jinxin Li[1], Fengli Liu[1], Zhihao Ren[1], Guanghua Fu[2], Jizhen Shi[1], Naiyu Zhao[1], Yu Huang[2]* and Jingliang Su[1]*

[1]Key Laboratory of Animal Epidemiology and Zoonosis of the Ministry of Agriculture, College of Veterinary Medicine, China Agricultural University, Beijing, China, [2]Institute of Animal Husbandry and Veterinary Medicine, Fujian Academy of Agricultural Sciences, Fuzhou, China

Introduction: Duck circovirus (DuCV) infection is currently recognized as an important immunosuppressive disease in commercial duck flocks in China. Specific antibodies against DuCV viral proteins are required to improve diagnostic assays and understand the pathogenesis of DuCV infection.

Methods and results: To generate DuCV-specific monoclonal antibodies (mAbs), a recombinant DuCV capsid protein without the first 36 N-terminal amino acids was produced in *Escherichia coli*. Using the recombinant protein as an immunogen, a mAb was developed that reacted specifically with the DuCV capsid protein, expressed in *E. coli* and baculovirus systems. Using homology modeling and recombinant truncated capsid proteins, the antibody-binding epitope was mapped within the region of ^{144}IDKDGQIV^{151}, which is exposed to solvent in the virion capsid model structure. To assess the applicability of the mAb to probe the native virus antigen, the murine macrophage cell line RAW267.4 was tested for DuCV replicative permissiveness. Immunofluorescence and Western blot analysis revealed that the mAb recognized the virus in infected cells and the viral antigen in tissue samples collected from clinically infected ducks.

Discussion: This mAb, combined with the *in vitro* culturing method, would have widespread applications in diagnosing and investigating DuCV pathogenesis.

KEYWORDS

duck, circovirus, DuCV, capsid protein, monoclonal antibody, *in vitro* culturing

1. Introduction

Duck circovirus (DuCV) was first discovered by Hattermann et al. in 2003 from a Mulard duck exhibiting feathering disorder, poor body condition, and low weight (Hattermann et al., 2003). Genomic analysis assigned the isolate to the genus *Circovirus* of the family Circoviridae. Subsequent DuCV infections have been detected in commercial duck flocks in the United States, Europe, and Asia (Banda et al., 2007; Cha et al., 2013; Matczuk et al., 2015; Neale et al., 2022; Tran et al., 2022). DuCV is an important co-factor in duck enteritis virus, goose parvovirus, and *Riemerella anatipestifer* infections (Neale et al., 2022), but the mechanism by which the virus causes the disease is not fully understood. DuCV infection combined with goose parvovirus increases the prevalence of short beak and dwarfism syndrome in meat-type ducks (Liu et al., 2020). The disease induced by DuCV may result

from virus-induced immunopathological disorders. In experimentally infected ducks, DuCV targeted the bursa of Fabricius, thymus, and spleen, causing extensive damage to immune organs, and viral DNA was also detected in the liver and intestines (Hong et al., 2018). In the last decade, high rates of DuCV infection in Chinese commercial duck populations have been detected by PCR, with a prevalence of 10–81.6% (Liu et al., 2009; Wang et al., 2011). This high prevalence and the easy circulation of DuCV are a problem for commercial duck flocks. Currently, there is no commercially available vaccine or specific measures to prevent the spread of the disease. Routine diagnostics of DuCV are required to monitor infection numbers in duck flocks and advance our understanding of the pathogenesis of virus infection.

DuCV is a non-enveloped virus with a circular single-stranded genomic DNA that ranges from 1987 to 1996 nucleotides (nt) in length (Breitbart et al., 2017; Liao et al., 2022). The DuCV genome contains at least two major open reading frames (ORFs) encoding the replication-associated protein (Rep) and capsid protein (Cap). Initial structural insights detailing the three-dimensional (3D) structures of circovirus virions used electron microscopy (EM). These EM images revealed that the members of the genus *Circovirus* adopt a similar capsid structure that forms multisubunit virions with T = 1 icosahedral symmetry (Crowther et al., 2003). The first high-resolution atomic structure of PCV2 Cap was solved using X-ray crystallography, showing that the Cap subunits comprise a single canonical jelly roll domain. The jelly roll domain comprises two β-sheets, each containing four β-strands. Shorter loops that connect the β-strands decorate the surface of the capsid, whereas the longer loops predominantly mediate interactions between capsids (Khayat et al., 2011, 2019). Cap is the major structural protein that self-associates to form the capsid of the virus and represents the primary target for antibodies in infected individuals. Thus, Cap is the most frequently used antigen for developing serological diagnostic tests (Liu et al., 2010; Yang et al., 2017).

Monoclonal antibodies (mAbs) against porcine circovirus and psittacine beak and feather disease virus and mAb-based assays have been described (Ritchie et al., 1992; McNeilly et al., 2001). The reported use of mAbs to detect the PCV antigen in cryostat sections from a pig experimentally infected with the virus enabled the identification of the sites of replication of PCV. The mAbs for the psittacine beak and feather disease virus were used to detect PBFDV by immunohistochemistry in related studies (Allan et al., 1994). However, no report has yet described the use of a mAb against DuCV. In this study, a mAb against *Escherichia coli*-expressed DuCV Cap was generated and characterized. Furthermore, *in vitro* culturing of DuCV using the murine macrophage cell line RAW267.4 was investigated. The reactivity of the mAb with native viral Cap in DuCV-infected RAW cells and tissues from clinically diseased ducks was evaluated.

2. Materials and methods

2.1. Detection of the DuCV genome by PCR

DNA was extracted from duck spleen tissues using a virus DNA kit (Tiangen Co., Ltd, Beijing, China). The PCR detection primers and thermal cycling were performed as described previously (Li et al., 2014). One of the DuCV-positive spleen samples from a Pekin duckling was used to amplify the full-length genome with overlapping primers DuCV-CX-F (5′-TGGCTCTCTCGTGCCCGGGGATCT-3′) and DuCV-CX-R (5′-AGGCTCTTCCTCCCAGCGACT-3′). The sequenced genome of the strain SXD1 was deposited in GenBank.

2.2. Generation and purification of recombinant DuCV capsid protein in *E. coli*

There are two reports on the *in vitro* culturing of DuCV (Mészáros et al., 2014; Li et al., 2020), both of which employed methods that require specialized cell lines or techniques. The yield using either of these methods is low. In contrast, the high-level expression of full and truncated fragments of DuCV Cap has been achieved using *E. coli* and baculovirus-based expression systems (Xiang et al., 2013; Lu et al., 2014). In this study, a 684-bp DNA fragment of the Cap encoding gene was amplified with the primers (DuCVorf2-F1: 5′-CGC*GGATCCTTTTCCGTAGTGACATATAA*-3′; DuCVorf2-R1: 5′-CCC*AAGCTT*CTAGAAGCCCGTGAACTGTCC-3′; underlined text shows the restriction endonuclease sequences), using viral DNA as the template. The PCR product was digested with *Bam*HI/*Hin*dIII and cloned into pMAL-C5x and pET-32a vectors. The recombinant plasmids, designated as pMAL-CapΔNLS and pET-CapΔNLS, were confirmed by sequencing and transformed into *E. coli* BL21 cells for protein expression. The recombinant bacteria were propagated in Luria–Bertani (LB) medium containing 100 μg/ml of ampicillin at 37°C with orbital rotation until an OD_{600} of 0.6 was reached. Recombinant protein expression was induced by the addition of 1.0 mM isopropyl-b-D-thiogalactopyranoside (IPTG). Cells were grown for a further 5 h at 37°C. Target protein expression was analyzed by sodium dodecyl sulfate-polyacrylamide gel electrophoresis (SDS-PAGE) and Coomassie brilliant blue gel staining and Western blotting with a monoclonal antibody against the His-tag. His-tagged recombinant proteins were purified by immobilized metal affinity chromatography (Ni-NTA Sepharose) under denaturing conditions and according to the manufacturer's instructions (Solarbio, Beijing, China).

2.3. Generation of a eukaryotic expression vector of the DuCV capsid protein

The eukaryotic expression system was constructed by amplifying the 724-bp DNA fragment of the Cap encoding gene using the primers DuCVorf2-F2 (5′-AAAAC TGCAGGTGGCGGACCGAAATAAAATGTTTTCCGTAGTGAC ATATAAGG-3′) and DuCVorf2-R2 (5′-CCGCTCGAGTCAGTG ATGATGATGATGATGGAAGCCCGTGAACTGTCCAAATT-3′), as described above. The amplified fragment was cloned into the *Pst*I/*Xho*I site of the pFastBac baculovirus transfer vector, as described previously (Liu et al., 2021). After confirming the sequence, the pFastBac-CapΔNLS construct was transformed into

DH10Bac competent *E. coli* cells (Thermo Fisher Scientific Inc., MA, United States) to produce a recombinant bacmid, according to the manufacturer's instructions. The recombinant bacmid was then purified and transfected into Sf9 cells to produce a recombinant baculovirus containing the DuCV *cap*Δ*NLS* gene.

2.4. Generation and screening of DuCV capsid protein-specific hybridoma

Five BALB/c mice (6–8 weeks old; Beijing Vital River Laboratory Animal Technology Co., Ltd., Beijing, China) were immunized subcutaneously with 100 μg of purified *E. coli*-expressing capsid protein pMAL-CapΔNLS with Freund's complete adjuvant. The mice were boosted twice at 2-week intervals with the recombinant capsid protein with Freund's incomplete adjuvant. Two weeks after the third immunization, sera were collected and assessed by indirect ELISA using the following approach. Mice were injected intraperitoneally with 110 μg of the purified recombinant capsid protein. After 3 days, mice were euthanized, and spleen cells were fused with SP2/0 myeloma cells by adding polyethylene glycol 2000. The fused cells were cultured in DMEM containing HAT and 15% fetal bovine serum (FBS), with a layer of macrophage feeder cells collected from a mouse peritoneal cavity. After 10 days of incubation, the hybridoma supernatants were screened by ELISA. ELISA-positive hybridoma cells were then subcloned by limiting dilution. The positive hybridoma clone was expended in a 6-well plate, and the supernatant of the culture was collected for immunoglobulin isotyping using the Mouse Monoclonal Antibody Isotyping Kit (Sigma–Aldrich, St Louis, MO, USA), according to the manufacturer's instructions. The selected hybridoma was inoculated into adult female BALB/c mice to produce an ascitic fluid antibody.

2.5. Western blotting

Protein samples were first separated by 12% denaturing SDS-PAGE and visualized by Coomassie brilliant blue staining. The separated proteins were transferred to a polyvinylidene fluoride (PVDF) membrane for Western blotting. Membranes were incubated overnight in blocking solution [1× phosphate-buffered saline, 0.05% (v/v) Tween-20 (PBST), 5% (w/v) skim milk powder] at 4°C with gentle rocking. After removal of the blocking solution, the mouse monoclonal antibody was diluted in PBST and incubated for 1 h at room temperature. The membrane was then washed three times with PBST, and HRP-conjugated goat anti-mouse IgG was added at a dilution of 1:5000. After incubation at room temperature for 1 h, the membrane was washed, and the signal was developed using the chemiluminescence substrate (ECL reagent; Cwbiotech, Beijing, China).

2.6. Indirect enzyme-linked immunosorbent assay (ELISA)

An indirect ELISA was developed to screen the specific antibodies in the immunized mouse sera and hybridoma supernatants. In brief, 96-well ELISA plates were coated with 2 μg/ml purified *E. coli*-expressed DuCV capsid protein pET-CapΔNLS overnight at 4°C. The plate was blocked with blocking solution at 37°C for 2 h and washed three times with PBST. The hybridoma supernatants were added to each well and incubated at 37°C for 1 h. Mouse sera collected before fusion were serially diluted two-fold from the initial dilution of 1:1250. After washing three times with PBST, 100 μl HRP-conjugated goat anti-mouse IgG (1:5000 in PBST) was added and incubated at 37°C for 1 h. After washing, the substrate TMB (3,3′,5,5′-tetramethylbenzidine) was added (100 μl/well), and the reaction was incubated in darkness for 10 min. The reaction was stopped by the addition of 50 μl 2M H_2SO_4, and the absorbance was measured at 450 nm.

2.7. Indirect immunofluorescence assay (IFA)

mAb binding to recombinant DuCV capsid protein expressed in baculovirus was examined by the seeding of Sf9 cells (ATCC CRL-1711) in a 96-well culture plate in DMEM/F12 (Hyclone) containing 10% FBS and incubating the cells at 28°C. Cells were infected at 80% confluence with the recombinant baculovirus containing the DuCV *cap*-Δ*NLS* gene at a multiplicity of infection (MOI) of 0.1. After 72 h of incubation at 28°C, cells were fixed with pre-chilled acetone/methanol (1:1) for 20 min at room temperature, followed by saponin permeabilization for 10 min. The plate was washed three times with PBST and incubated with a blocking buffer at 37°C for 30 min. Cell wells were washed, and the diluted murine ascitic mAb was added. After incubation at 37°C for 1 h, cell wells were washed, and DyLight 488 AffiniPure Goat Anti-Mouse IgG (H+L; Earthox, CA, USA) was added at a dilution of 1:1000. After incubation at 37°C for 1 h, cells were washed three times and mounted with DAPI. Fluorescence was recorded under a fluorescence microscope (Olympus Corporation, Japan).

2.8. *In vitro* culturing of DuCV

The mouse macrophage cell line RAW267.4 (ATCC TIB-71) was cultured in DMEM supplemented with 10% FBS and 1% penicillin-streptomycin at 37°C in the presence of 5% CO_2 to develop a convenient *in vitro* DuCV culturing method. The original DuCV-positive spleen tissue was homogenized in DMEM, clarified by centrifugation at 8,000 × *g* for 10 min, and filtered through a 0.22-μm membrane filter. The filtered suspension was inoculated to the cell monolayers with ∼80% confluence, and DMEM containing 1% FBS was added after 1 h of incubation at 37°C. At 96 h post-infection, the supernatant was transferred to freshly cultured cell monolayers. This step was repeated three times, and the infectivity of DuCV was assessed by real-time PCR with primers qDuCV-F (5′-TTACAAACCACGCGGGAAGT-3′) and qDuCV-R (5′-CTGGGCGGGTTCATACTTGT-5′), which are based on the conservative region of the Rep gene of DuCV SXD1 (GenBank accession No.: OQ759610). qPCR reactions were performed in a CFX Connect™ Real-time PCR Detect System (Bio-Rad, Hercules, CA, USA) reaction solution (20 μl) containing 8.0 μl ddH_2O, 10 μl 2×RealStar Fast SYBR qPCR Mix (GenStar, Beijing, China), 1.0 μl template DNA (extracted from RAW cell lysate), and 0.5 μl of each primer, qDuCV-F and qDuCV-R.

10.3389/fmicb.2023.1206038

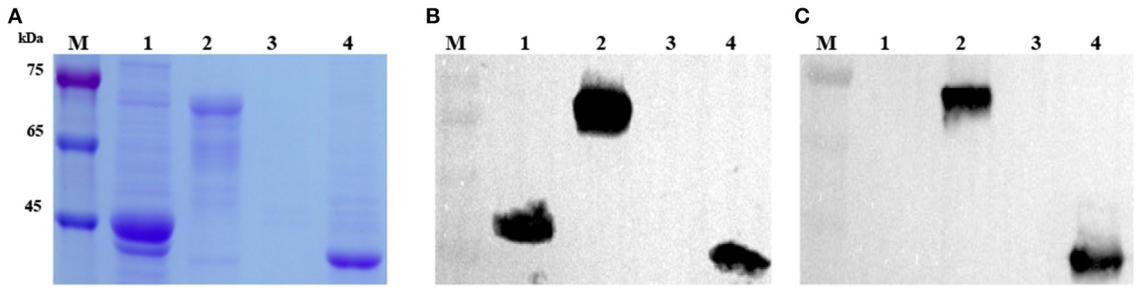

FIGURE 1
Analysis and identification of recombinant DuCV capsid proteins expressed in *E. coli*. **(A)** SDS-PAGE analysis of recombinant CapΔNLS protein (CP) of DuCV expressed in *E. coli*. **(B)** Western blotting identified the recombinant capsid protein with a monoclonal antibody against the His-tag. **(C)** Western blotting identified the recombinant capsid protein with the monoclonal antibody 4A2. M: protein marker; Lanes 1 and 2: lysates of *E. coli* with the pMAL-C5x vector and pMAL-CapΔNLS; Lanes 3 and 4: lysates of *E. coli* with the pET-32a vector and pET-CapΔNLS.

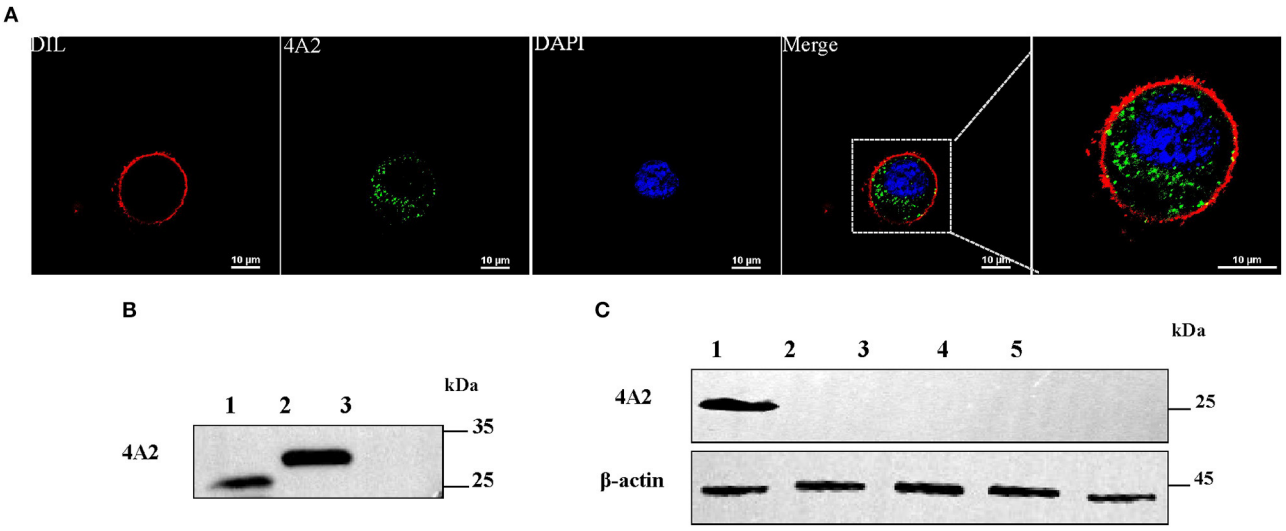

FIGURE 2
Detection of the reactivity of mAb 4A2 with baculovirus-expressed DuCV capsid protein and different viral proteins by Western blotting. **(A)** IFA staining of Sf9 cells infected with recombinant baculovirus. Cells were infected with recombinant baculovirus containing the DuCV capsid gene. After 72 h post-infection, cells were fixed and labeled with mAb 4A2 and then by the DyLight 488-labeled secondary mAb (green). Nuclei were stained with DAPI (blue), and cytomembranes were stained with DIL (red). **(B)** Western blot analysis of mAb 4A2 with baculovirus-expressed DuCV capsid protein. Lane 1: positive control of recombinant DuCV Cap expressed in duck enteritis virus; Lane 2: protein from the eukaryotic expression of duck circular capsid; Lane 3: protein from Sf9 cells. **(C)** Western blot analysis of mAb 4A2 with different viral proteins. Lane 1: positive control of recombinant DuCV Cap expressed in duck enteritis virus; Lanes 2 to 5: cell lysates of proteins from duck enteritis virus, goose parvovirus, Tembusu virus, and duck astrovirus.

Thermal cycler conditions were as follows: 95°C for 2 min at stage 1; 40 cycles of 95°C for 15 s, 60°C for 30 s, and 72°C for 30 s. DuCV-infected RAW267.4 cells were also treated for capsid protein detection by IFA and Western blotting using the mAb and following the abovementioned steps.

3. Results

3.1. Expression of recombinant DuCV capsid protein

The target DNA fragment encoding the truncated Cap protein of DuCV was amplified successfully using the DNA template extracted from the DuCV-positive spleen sample. After cloning and transformation, single colonies were selected, and DNA sequence fidelity was confirmed by Sanger sequencing. Constructs transformed into *E. coli* BL21 and protein expression induced by IPTG were assessed by SDS-PAGE. Protein bands in the SDS-PAGE gel corresponding to the expected size (~68.2 kDa for pMAL-CapΔNLS and 40.9 kDa for pET-CapΔNLS) were observed in the cell lysates (Figure 1A). Western blotting showed the recombinant capsid protein reacted with a monoclonal antibody against the His-tag (Figure 1B). His-tagged proteins, pMAL-CapΔNLS and pET-CapΔNLS, were purified using Ni-NTA affinity chromatography and used for mouse immunization and plate-coating antigen in ELISA screening of the monoclonal antibody, respectively.

10.3389/fmicb.2023.1206038

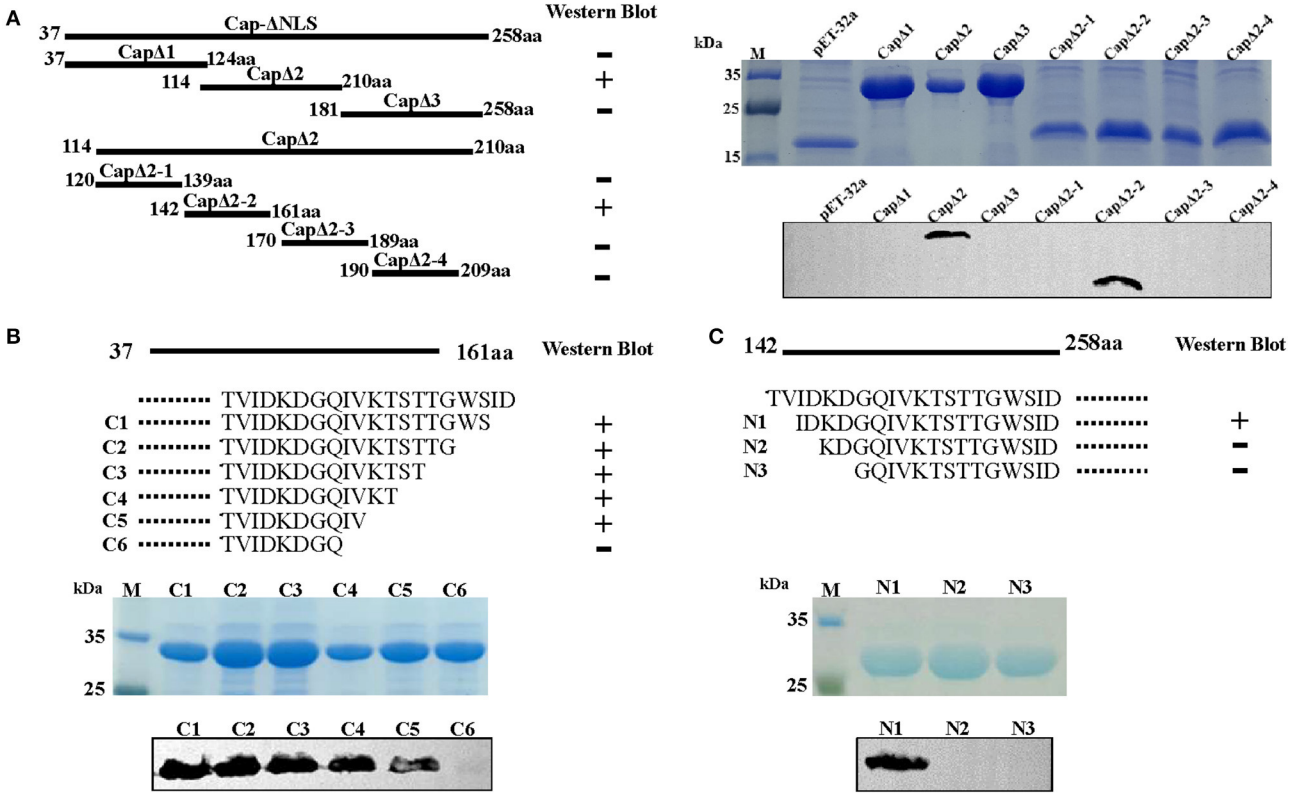

FIGURE 3
Epitope mapping of mAb 4A2 by Western blot analysis. **(A)** A series of seven overlapping recombinant truncated capsid proteins were synthesized to identify the linear epitope of the mAb. Three N-terminal **(B)** and six C-terminal **(C)** truncated fragments of DuCV capsid were constructed as described in the methods. Western blot analysis indicated that mAb 4A2 specifically reacted with CapΔ2, CapΔ2-2, C1, C2, C3, C4, C5, and N1, of which, the overlapping sequence was ^{144}IDKDGQIV^{151}.

3.2. Generation of a monoclonal antibody against the DuCV capsid protein

MAbs were generated by immunization of mice with recombinant DuCV capsid protein and then tested for the presence of specific serum antibodies. Spleen cells from an immunized mouse were fused with Sp2/0 myeloma cells, and hybridoma supernatants were screened by ELISA using purified pET-CapΔNLS as the plate-coating antigen. After four rounds of sub-cloning, hybridoma 4A2 was eventually established as a monoclonal cell line and chosen for further investigation. The isotype of mAb 4A2 was determined as IgG2a with a kappa light chain. Western blotting showed that the mAb reacted with recombinant DuCV Cap produced in *E. coli* (Figure 1C).

In IFA, mAb 4A2 recognized the DuCV capsid protein, expressed in the recombinant baculovirus-infected Sf9 cells, mainly in the cytoplasm (Figure 2A). Western blot analysis of the infected Sf9 cell lysate using the mAb gave a prominent band with a molecular weight of ~29.1 kDa (Figure 2B). No band was detected in non-infected cells (Figure 2B) or lysates of duck fibroblast cells infected with duck enteritis virus, goose parvovirus, Tembusu virus, or duck astrovirus (Figure 2C). As expected, the cellular marker was detected by an anti-mouse β-actin antibody (Beyotime, Beijing, China). The results indicated that the mAb binds specifically to the DuCV capsid protein.

3.3. Recognition epitope of mAb 4A2

The epitope region recognized by 4A2 mAb was analyzed by constructing pET-32a-derived recombinant plasmids containing a series of truncated DuCV capsid gene fragments and transformed into *E. coli* BL21. As shown in Figure 3A, truncated Cap proteins were expressed in *E. coli*, and Western blotting analysis showed that CapΔ2 (114–210 aa) and CapΔ2-2 (142–161 aa) reacted with mAb 4A2, presenting a strong signal for the sequence ^{142}TVIDKDGQIVKTSTTGWSID^{161}. Further omission of amino acid residues from the N- and C-termini of the peptides revealed the sequence ^{144}IDKDGQIV^{151} to be essential for 4A2 mAb binding (Figures 3B, C).

Multiple protein sequence alignment of capsid proteins from DuCV, goose circovirus, and pigeon circoviruses indicated that the mapped epitope region ^{144}IDKDGQIV^{151} is conserved among DuCV strains, except for strain the TC2 (GenBank: DQ166836), which displays one amino acid substitution, i.e., G148R (Table 1). Amino sequences in the epitope region were noted to be highly divergent between circoviruses from different birds. This divergence was also supported by mAb 4A2 not cross-reacting with the Cap of goose circovirus expressed in *E. coli* (Supplementary Figure 1).

Structural modeling based on the bat circovirus Cap structure (PDB ID: 6rpo.1.A https://swissmodel.expasy.org) indicated that

10.3389/fmicb.2023.1206038

TABLE 1 Multiple protein sequence alignments of the epitope of mAb 4A2 in capsid proteins of DuCV, GoCV, and CoCV (the strains isolated in our laboratory are shown in red).

Strain name (accession no.)	Cap protein							
	144	145	146	147	148	149	150	151
DuCV I-SXD1 (OQ759610)	I	D	K	D	G	Q	I	V
DuCV I-JZ22	.	.	.	.	.	.	.	.
DuCV I-YS22	.	.	.	.	.	.	.	.
DuCV I-MH11 (EU344805)	.	.	.	.	.	.	.	.
DuCV I-TC2 (DQ166836)	.	.	.	.	R	.	.	.
DuCV I-LY0701 (EU022374)	.	.	.	.	.	.	.	.
DuCV I-WF0804 (GU131343)	.	.	.	.	.	.	.	.
DuCV II-MH25 (EF451157)	.	.	.	.	.	.	.	.
DuCV II-Germany (AY228555)	.	.	.	.	.	.	.	.
DuCV II-AQ0901 (GU014543)	.	.	.	.	.	.	.	.
DuCV II-WF0801 (GU131340)	.	.	.	.	.	.	.	.
DuCV II-3753-52 (DQ100076)	.	.	.	.	.	.	.	.
DuCV II-ZHEJIANG (GQ334371)	.	.	.	.	.	.	.	.
GoCV-SDJN21-1	I	D	K	E	G	N	I	T
GoCV-DG1 (KT808650)	.	.	.	E	.	N	.	T
GoCV-Hun3 (MG254880)	.	.	.	E	.	N	.	T
GoCV-Anhui15 (MF581299)	.	.	.	E	.	N	.	T
CoCV-Germany (NC002361.1)	P	M	Y	D	A	R	L	K
CoCV-RS0120 (KY114965.1)	P	M	Y	D	A	R	L	K
CoCV-PG-14-844 (KU.593626.1)	P	I	Y	D	A	R	L	K
CoCV-PL14 (MK994769.1)	P	M	Y	D	A	R	L	K
CoCV-TJ62 (MW0253.1)	P	I	Y	D	A	R	L	K

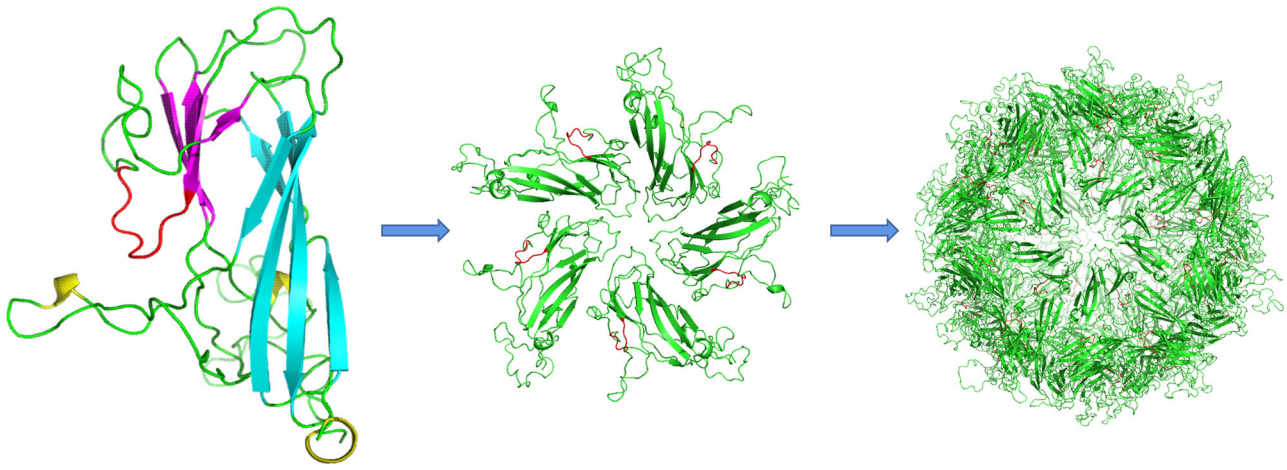

FIGURE 4
Structural modeling of DuCV Cap. The monomeric unit of the capsid protein comprises two β-sheets composed of five (cyan) and four strands (magenta). The epitope of mAb 4A2 is shown in red, whereas loops are shown in green. One pentamer is shown in the center of each VLP. The epitope region (red) is located immediately after the fifth β-strand and solvent-exposed.

10.3389/fmicb.2023.1206038

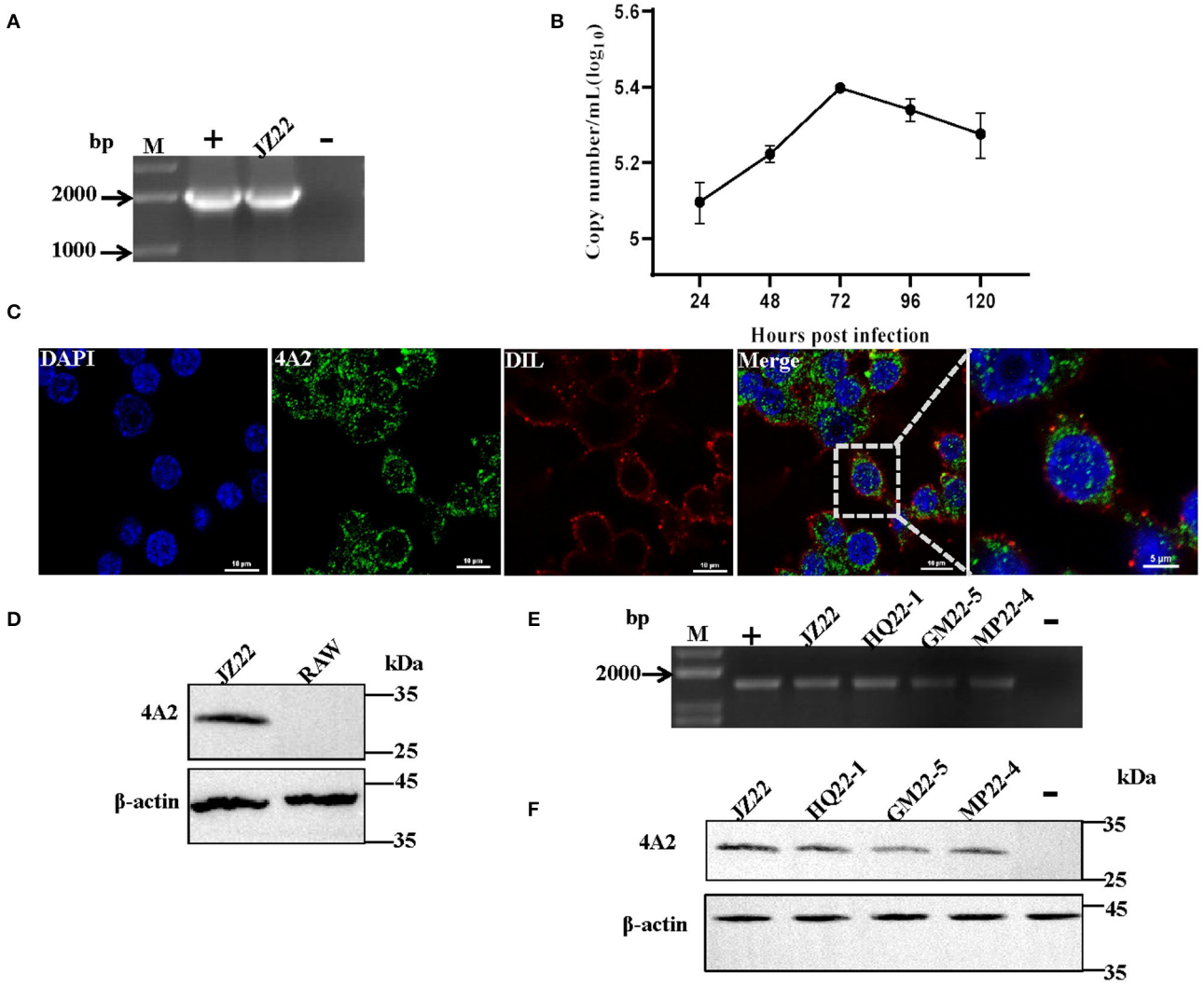

FIGURE 5
Detection of the native viral antigen of DuCV with mAb 4A2. **(A)** Detection of DuCV strain JZ22 by PCR. **(B)** Growth kinetics of DuCV in RAW cells. **(C)** Immunofluorescence detection of DuCV in RAW cell culture. RAW264.7 inoculated with DuCV strain JZ22 and monolayers were fixed for 72 h post-infection. IFA analysis was performed by probing with mAb 4A2 (green). The nucleus of each cell was stained with DAPI (blue), and the cytomembrane was stained with DIL (red). **(D)** Western blot analysis of a DuCV-infected RAW cell lysate. **(E)** PCR detection of DuCV in clinical duck spleen samples. **(F)** Western blot analysis of the DuCV antigen in clinical duck spleen samples.

DuCV Cap comprises two β-sheets, one containing five β-strands and the other containing four β-strands, with 12 loops connecting the β-strands. The epitope region was predicted to be positioned immediately after the fifth β-strand and exposed to solvent (Figure 4).

3.4. Application of mAb 4A2 for native DuCV antigen detection

To investigate whether the mAb 4A2 can be used for immunological diagnostic methods, IFA was performed on a RAW264.7 cell monolayer infected with DuCV strain JZ22. Replication of DuCV in the cell culture after three sequential passages was detected by PCR (Figure 5A). The kinetic change in the viral DNA copies revealed by real-time PCR indicated modest replication of DuCV in RAW cells (Figure 5B). IFA confirmed the PCR results, with green fluorescence intracytoplasmic foci observed in DuCV JZ22-infected cells (Figure 5C). Further detection of DuCV-infected RAW cell lysates by Western blotting gave a prominent band of ~30 kDa in a dilution of 1:1000 of mAb 4A2 (Figure 5D). No band was detected in the non-infected cell lysate.

Next, we evaluated the diagnostic potential of the generated mAb 4A2. Clinically collected duck spleen samples were detected by Western blotting. Consistent with PCR detection (Figure 5E), the monoclonal antibody detection of the PCR-positive spleen samples at a dilution of 1:100 resulted in a positive band with a molecular weight of ~30 kDa (Figure 5F).

4. Discussion

Recent studies have highlighted that the widespread distribution of DuCV infection and its immunosuppressive effects are a problem for commercial duck flocks in China. However, the limited laboratory host system for DuCV propagation hampers the investigation of this virus. More sensitive, specific, and readily standardized diagnostic assays are urgently needed. Applications of mAbs to porcine circoviruses and the beak and feather disease virus have been presented (Ritchie et al., 1992; McNeilly et al., 2001). These applications include using mAbs for immunostaining cell cultures and tissue sections and detecting a virus-specific antibody by ELISA and HI (Shearer et al., 2008). In this study, we reported the generation of a mAb against the DuCV capsid protein in combination with the propagation of a DuCV strain in a RAW cell line. The results should enable further development of standardized immune diagnostic methods.

Only one report has described the *in vitro* culturing of DuCV using continuous cell lines created from primary Muscovy duck retina and somite cells (Mészáros et al., 2014). The relatively low viral productivity and restricted availability of avian cell lines hamper the production of whole DuCV virus particles in large quantities. In this study, a fragment of the DuCV capsid protein that omits the N-terminal NLS region was produced in *E. coli* and baculovirus expression systems. Using the recombinant protein as an immunogen, the mAb 4A2 against DuCV was produced. The antibody-binding epitope was determined to be ^{144}IDKDGQIV^{151} of the capsid protein, whose surface is exposed in the capsid protein model and thus accessible for antibody binding (Figure 4). This result was supported by mAb, recognizing the recombinant capsid protein expressed in baculovirus and the native capsid protein in DuCV-infected RAW267.4 cells in IFA and Western blotting analysis. The specific infectivity detected by qRT-PCR and characterized by IFA indicated that DuCV replicated effectively in RAW267.4 cells, providing an option for developing a more convenient *in vitro* culturing approach for DuCV isolates. Given that it detected viral antigens in the spleen tissues from clinically infected ducks, the mAb 4A2 should have widespread applications in both diagnostic detection and research work.

In summary, our study presents the generation of a monoclonal antibody against the DuCV capsid protein and its potential application in viral antigen detection. The successful *in vitro* culturing of DuCV using RAW267.4 cells and the detection of the viral antigen in infected cells are effective alternative approaches to investigate the replication properties of DuCV.

Data availability statement

The datasets presented in this study can be found in online repositories. The names of the repository/repositories and accession number(s) can be found at: https://www.ncbi.nlm.nih.gov/nuccore/OQ759610.1/.

Ethics statement

The animal study was reviewed and approved by the China Agricultural University Animal Ethics Committee and it was conducted in accordance with the guidelines of the Beijing Municipality on the Review of Welfare and Ethics of Laboratory Animals, approved by the Beijing Municipality Administration Office of Laboratory Animals and the Regulations for the Administration of Affairs Concerning Experimental Animals, approved by the State Council of China.

Author contributions

JL and JSu conceived and designed the experiments and wrote the manuscript. JL, FL, ZR, JSh, and NZ performed the experiments. JL, FL, and JSu analyzed the data. GF and YH contributed to reagents/materials. All authors contributed to the article and approved the submitted version.

Funding

This research was funded by National Key R&D Program under Grant: 2016YFD0500800 and CAU-Grant for the Prevention and Control of Immunosuppressive Diseases in Animals (CAU-GPCIDA).

Acknowledgments

The authors thank Liwen Bianji (https://www.liwenbianji.cn) for editing the English text of a draft of this manuscript.

Conflict of interest

The authors declare that the research was conducted in the absence of any commercial or financial relationships that could be construed as a potential conflict of interest.

Publisher's note

Supplementary material

The Supplementary Material for this article can be found online at: https://www.frontiersin.org/articles/10.3389/fmicb.2023.1206038/full#supplementary-material

References

Allan, G. M., Mackie, D. P., Mcnair, J., Adair, B. M., and McNulty, M. S. (1994). Production, preliminary characterisation and applications of monoclonal antibodies to porcine circovirus. *Vet. Immunol. Immunop.* 43, 357–371. doi: 10.1016/0165-2427(94)90157-0

Banda, A., Galloway-Haskins, R. I., Sandhu, T. S., and Schat, K. A. (2007). Genetic analysis of a duck circovirus detected in commercial Pekin ducks in New York. *Avian Dis.* 51, 90–95. doi: 10.1637/0005-2086(2007)051[0090:GAOADC]2.0.CO;2

Breitbart, M., Delwart, E., Rosario, K., Segalés, J., Varsani, A., Consortium, I. R., et al. (2017). ICTV virus taxonomy profile: circoviridae. *J. Gen. Virol.* 98, 1997–1998. doi: 10.1099/jgv.0.000871

Cha, S. Y., Kang, M., Cho, J. G., and Jang, H. K. (2013). Genetic analysis of duck circovirus in Pekin ducks from South Korea. *Poult. Sci.* 92, 2886–2891. doi: 10.3382/ps.2013-03331

Crowther, R. A., Berriman, J. A., Curran, W. L., Allan, G. M., and Todd, D. (2003). Comparison of the structures of three circoviruses: chicken anemia virus, porcine circovirus type 2, and beak and feather disease virus. *J. Virol.* 77, 13036–13041. doi: 10.1128/JVI.77.24.13036-13041.2003

Hattermann, K., Schmitt, C., Soike, D., and Mankertz, A. (2003). Cloning and sequencing of Duck circovirus (DuCV). *Arch. Virol.* 148, 2471–2480. doi: 10.1007/s00705-003-0181-y

Hong, Y. T., Kang, M., and Jang, H. K. (2018). Pathogenesis of duck circovirus genotype 1 in experimentally infected Pekin ducks. *Poult. Sci.* 97, 3050–3057. doi: 10.3382/ps/pey177

Khayat, R., Brunn, N., Speir, J. A., Hardham, J. M., Ankenbauer, R. G., Schneemann, A., et al. (2011). The 2.3-angstrom structure of porcine circovirus 2. *J. Virol.* 85, 7856–7862. doi: 10.1128/JVI.00737-11

Khayat, R., Wen, K., Alimova, A., Gavrilov, B., Katz, A., Galarza, J. M., et al. (2019). Structural characterization of the PCV2d virus-like particle at 3.3 Å resolution reveals differences to PCV2a and PCV2b capsids, a tetranucleotide, and an N-terminus near the icosahedral 3-fold axes. *Virology* 537, 186–197. doi: 10.1016/j.virol.2019.09.001

Li, Z., Fu, G., Feng, Z., Chen, J., Shi, S., Liu, R., et al. (2020). Evaluation of a novel inactivated vaccine against duck circovirus in muscovy ducks. *Vet. Microbiol.* 241, 108574. doi: 10.1016/j.vetmic.2019.108574

Li, Z., Wang, X., Zhang, R., Chen, J., Xia, L., Lin, S., et al. (2014). Evidence of possible vertical transmission of duck circovirus. *Vet. Microbiol.* 174, 229–232. doi: 10.1016/j.vetmic.2014.09.001

Liao, J. Y., Xiong, W. J., Tang, H., and Xiao, C. T. (2022). Identification and characterization of a novel circovirus species in domestic laying ducks designated as duck circovirus 3 (DuCV3) from Hunan province, China. *Vet. Microbiol.* 275, 109598. doi: 10.1016/j.vetmic.2022.109598

Liu, F., Cao, Y., Yan, M., Sun, M., Zhang, Q., Wang, J., et al. (2021). Development of a colloidal gold immunochromatographic assay for duck enteritis virus detection using monoclonal antibodies. *Pathogens* 10, 365. doi: 10.3390/pathogens10030365

Liu, J., Yang, X., Hao, X., Feng, Y., Zhang, Y., Cheng, Z., et al. (2020). Effect of goose parvovirus and duck circovirus coinfection in ducks. *J. Vet. Res.* 64, 355–361. doi: 10.2478/jvetres-2020-0048

Liu, S., Zhang, X., Chen, Z., Gao, J., Wei, X., Kong, Y., et al. (2009). Epidemic investigation of duck circovirus in spontaneous diseased duck flocks in China. *Chin. J. Vet. Sci.* 29, 1402–1405.

Liu, S. N., Zhang, X. X., Zou, J. F., Xie, Z. J., Zhu, Y. L., Zhao, Q., et al. (2010). Development of an indirect ELISA for the detection of duck circovirus infection in duck flocks. *Vet. Microbiol.* 145, 41–46. doi: 10.1016/j.vetmic.2010.03.010

Lu, Y., Jia, R., Zhang, Z., Wang, M., Xu, Y., Zhu, D., et al. (2014). *In vitro* expression and development of indirect ELISA for Capsid protein of duck circovirus without nuclear localization signal. *Int. J. Clin. Exp. Pathol.* 7, 4938–4944.

Matczuk, A. K., Krawiec, M., and Wieliczko, A. (2015). A new duck circovirus sequence, detected in velvet scoter (*Melanitta fusca*) supports great diversity among this species of virus. *Virol. J.* 12, 121. doi: 10.1186/s12985-015-0352-y

McNeilly, F., McNair, I., Mackie, D. P., Meehan, B. M., Kennedy, S., Moffett, D., et al. (2001). Production, characterisation and applications of monoclonal antibodies to porcine circovirus 2. *Arch. Virol.* 146, 909–922. doi: 10.1007/s007050170124

Mészáros, I., Tóth, R., Bálint, A., Dán, A., Jordan, I., Zádori, Z., et al. (2014). Propagation of viruses infecting waterfowl on continuous cell lines of Muscovy duck (*Cairina moschata*) origin. *Avian Pathol.* 43, 379–386. doi: 10.1080/03079457.2014.939941

Neale, S., Welchman, D., Garcia-Rueda, C., Grierson, S., and Pearson, A. (2022). Detection of duck circovirus in Great Britain. *Vet. Rec.* 191, 424. doi: 10.1002/vetr.2463

Ritchie, B. W., Niagro, F. D., Latimer, K. S., Steffens, W. L., Pesti, D., Aron, L., et al. (1992). Production and characterization of monoclonal antibodies to psittacine beak and feather disease virus. *J. Vet. Diagn. Invest.* 4, 13–18. doi: 10.1177/104063879200400104

Shearer, P. L., Bonne, N., Clark, P., Sharp, M., and Raidal, S. R. (2008). Development and applications of a monoclonal antibody to a recombinant beak and feather disease virus (BFDV) capsid protein. *J. Virol. Methods* 147, 206–212. doi: 10.1016/j.jviromet.2007.08.029

Tran, G. T. H., Mai, N. T., Bui, V. N., Dao, T. D., Trinh, D. Q., Vu, T. T. T., et al. (2022). Duck circovirus in northern Vietnam: genetic characterization and epidemiological analysis. *Arch. Virol.* 167, 1871–1877. doi: 10.1007/s00705-022-05501-y

Wang, D., Xie, X., Zhang, D., Ma, G., Wang, X., Zhang, D., et al. (2011). Detection of duck circovirus in China: a proposal on genotype classification. *Vet. Microbiol.* 147, 410–415. doi: 10.1016/j.vetmic.2010.07.014

Xiang, Q. W., Zou, J. F., Wang, X., Sun, Y. N., Gao, J. M., Xie, Z. J., et al. (2013). Identification of two functional nuclear localization signals in the capsid protein of duck circovirus. *Virology* 436, 112–117. doi: 10.1016/j.virol.2012.10.035

Yang, C., Xu, Y., Jia, R., Li, P., Zhang, L., Wang, M., et al. (2017). Prokaryotic expression of a codon-optimized capsid gene from duck circovirus and its application to an indirect ELISA. *J. Virol. Methods* 247, 1–5. doi: 10.1016/j.jviromet.2017.05.003

frontiers | Frontiers in Microbiology

TYPE Original Research
PUBLISHED 31 July 2023
DOI 10.3389/fmicb.2023.1205297

OPEN ACCESS

EDITED BY
Jingqiang Ren,
Wenzhou University, China

REVIEWED BY
Xiaobo Wen,
Hainan University, China
Yongsheng Liu,
Hebei Normal University of Science and Technology, China

*CORRESPONDENCE
Xue Leng
✉ xuel@jlau.edu.cn
Rui Du
✉ durui197101@sina.com

†These authors have contributed equally to this work

RECEIVED 13 April 2023
ACCEPTED 10 July 2023
PUBLISHED 31 July 2023

CITATION
Liu Y, Sheng C, Zhou Y, Li J, Gong Q, Shi K, Liu F, Xu L, Cui Z, Leng X and Du R (2023) Application of quantitative real-time PCR to detect *Mink Circovirus* in minks, foxes and raccoon dogs in northern China. *Front. Microbiol.* 14:1205297. doi: 10.3389/fmicb.2023.1205297

Application of quantitative real-time PCR to detect *Mink Circovirus* in minks, foxes and raccoon dogs in northern China

Yingyu Liu[1†], Chenyan Sheng[1†], Yu Zhou[2], Jianming Li[3], Qinglong Gong[1], Kun Shi[3], Fei Liu[1], Lihui Xu[1], Zhenzhen Cui[3], Xue Leng[3*] and Rui Du[3*]

[1]College of Animal Science and Technology, Jilin Agricultural University, Changchun, China, [2]Huizhou Customs District P.R. China, Huizhou, China, [3]College of Chinese Medicine Materials, Jilin Agricultural University, Changchun, China

Mink circovirus disease caused by *Mink Circovirus* (MiCV) is a serious infectious disease of mink that has become prevalent in recent years in China, severely affecting the reproductive performance of mink and causing significant economic losses to farms. To date, there have been few studies on MiCV, its pathogenic mechanism is not clear, and there is no effective vaccine or drug to prevent and control the disease. Therefore, it is necessary to establish a rapid and reliable molecular diagnostic method, which would aid future studies of this novel virus. In our study, we developed a sensitive and specific TaqMan-based quantitative real-time PCR assay targeting the MiCV Cap gene. The assay showed no cross-reaction with other tested animal viruses. The assay is highly sensitive, with a detection limit of as low as 10 plasmid DNA copies and 2.38×10^{-2} pg of viral DNA. The intra and inter--assay coefficients of variation were both low. The positive detection rate of MiCV in clinical samples from minks, foxes, and raccoon dogs were 58.8% (133/226), 50.7% (72/142), and 42.2% (54/128), respectively, giving a total positive detection rate of 52.2% (259/496). Higher contamination levels were observed in samples from the environment in direct or indirect contact with animals, with a total positive detection rate of 75.1% (220/293). These epidemiological results showed that minks, foxes, and raccoon dogs had high infection rates of MiCV. This was also the first study to detect MiCV on the ground and equipment of fur-bearing animal farms. Our assay is highly sensitive and specific for the diagnosis and quantification of MiCV, and should provide a reliable real-time tool for epidemiological and pathogenetic study of MiCV infection.

KEYWORDS

***Mink Circovirus*, quantitative real-time PCR, epidemiological investigation, detection, fur-bearing animals**

1. Introduction

Circoviruses have various hosts among mammals and birds (Li et al., 2010; Decaro et al., 2014). In recent years, in addition to the well-known *Porcine Circovirus*, *Circoviruses* that can infect canines, penguins, bats, and other animals have been reported (Piewbang et al., 2018; Matsumoto et al., 2019; Morandini et al., 2019; Canuti et al., 2022). Mink circovirus disease,

caused by a new *Circovirus* member, *Mink Circovirus* (MiCV), has only been discovered in China and is reported to be able to infect foxes and raccoon dogs (Yang et al., 2018). Taxonomically, MiCV belongs to the genus *Circovirus* in the family *Circoviridae*. *Circoviruses* are small envelope-free icosahedral viruses, with a diameter of 15–25 nm, and a circular single-stranded DNA genome, which is the smallest known auto replicating viral genome (Breitbart et al., 2017; Rosario et al., 2017). The genome of MiCV comprises about 1700 nucleotides, including two main open reading frames (ORFs), one encoding the replication-related protein (Rep) and the other encoding viral capsid protein (Cap; Ge et al., 2018a). In *Circovirus*, the ORF encoding Rep is on the sense strand of the genome, while the Rep of *Cyclovirus* is encoded by the complementary strand of double-stranded DNA (Breitbart et al., 2017; Rosario et al., 2017; Shulman and Davidson, 2017; Zhao et al., 2019). The Rep protein (35.8 kDa) is mainly involved in virus replication and plays an important role in virus proliferation, while Cap, is the main structural protein (27.8 kDa) and has good immunogenicity (Rosario et al., 2017).

Mink circovirus disease has a wide epidemic range in China. Existing epidemiological research results showed that the positive rate of MiCV was 30.30% in Heilongjiang Province, 38.46% in Jilin Province, 52.88% in Shandong Province, 58.46% in Liaoning Province and 67.90% in Hebei Province (Ge et al., 2018a). MiCV has caused great economic losses to the mink breeding industry. Minks infected with the virus showed poor appetite, mental fatigue, rough fur, diarrhea, and even death, and the virus easily causes mixed infection with Aleutian mink disease virus, Canine distemper virus and other viruses (Ge et al., 2018b). Most minks recovered spontaneously, however, their growth was poor, their fur quality was significantly reduced, and the reproductive capacity of females was lower than before infection. MiCV can be transmitted between minks of different ages.

In many places in China, minks, foxes, and raccoon dogs are kept on the same fur-bearing animal farms. A study showed that MiCV can infect not only minks, but also foxes and raccoon dogs，accompanied by similar clinical symptoms such as drowsiness, anorexia, pale mouth and unkempt fur (Yang et al., 2018). Besides, the persistence of the virus in the environment is also an important factor in the spread of the disease. To date, no large-scale MiCV prevalence studies in minks, foxes and raccoon dogs have been carried out. Viral contamination in the environment is also unknown. There have been few studies on MiCV, its pathogenic mechanism is not clear, and there is no effective vaccine and drug to treat the disease. Therefore, it is important to establish a rapid and effective detection method for disease prevention and control. Quantitative real-time PCR (qPCR) detection has the advantages of strong specificity, high sensitivity and relatively low cost (Abdel-Moneim et al., 2017; Tong et al., 2020; de Oliveira Lopes et al., 2021; Gong et al., 2021). It can quickly determine viruses in different tissue samples and has become an important tool in veterinary virology and disease control (Varga and James, 2006; Vázquez et al., 2017; Cui et al., 2018).

In this study, a TaqMan-based qPCR method was established to detect MiCV DNA. Subsequently, we detected MiCV DNA in clinical samples from minks, foxes, raccoon dogs and farm environments in China.

2. Materials and methods

2.1. Viruses and samples

MiCV strain HB3 (GenBank accession No. MK561562.1), Aleutian mink disease virus (AMDV) DL125 strain (Isolated by Dr. Liu of the Economic Animal Infectious Diseases Laboratory of Jilin Agricultural University in 2015 citation), Pseudorabies virus (PRV) JL03 strain, and Porcine circovirus 2 (PCV-2) were stored in the Economic Animal Infectious Diseases Laboratory of Jilin Agricultural University. The vaccine strains mink enteritis virus (MEV), canine distemper virus (CDV), and canine adenovirus type 2 (CAdV-2) were purchased from Teyan Biotechnology, Ltd., (Jilin, China) and QiLu Animal Health Products, Ltd., (Shandong, China), respectively.

Two hundred and twenty-six mink anal swab samples, 142 fox anal swab samples, 128 raccoon dog anal swab samples, and 293 environmental swab samples were collected from 6 farms in Jilin, Heilongjiang, and Shandong provinces in China from 2021 to 2022.

2.2. Primer design and synthesis

According to the MiCV genome sequences obtained in the laboratory in recent years and all 13 of MiCV genome sequences deposited in GenBank, DNAMAN (LynnonBiosoft, USA) was used to perform multiple comparisons to obtain a highly conserved region in the Cap region of the genome. Primer 5.0 (PREMIER Biosoft International, Palo Alto, California, USA) was used to design the required primers (real-time quantitative PCR primers and common PCR primers) and probes (Table 1). The primers and probes were synthesized by Comate Bioscience Co. Ltd., (Changchun, China).

2.3. DNA extraction

All swab samples were repeatedly frozen and thawed three times and centrifuged. According to the manufacturer's protocol, a Viral DNA Kit (Omega Biotek, Winooski, VT, USA) was used to extract DNA from 200 μl of the supernatant. After the DNA samples were eluted into 100 μl of Elution Buffer, they were stored at − 20°C until required.

2.4. Preparation of the standard plasmid

The 684 bp fragment of the Cap gene was amplified from the DNA of MiCV strain HB3 using PCR with the MiCV-Cap-F and MiCV-Cap-R primers. A Midi Purification Kit (Tiangen Biotech, Beijing, China) was used to purify the amplification products from the agarose gel, which were then ligated into the vector pMD18-T (Takara Biotechnology, Dalian, China) to construct recombinant plasmid pMD-MiCV. pMD-MiCV was transformed into *Escherichia coli* DH5α cells (TransGen Biotech, Beijing, China), purified. Using a plasmid miniprep Kit (Axygen A Corning Brand, Suzhou, China), and verified by sequencing (carried out by Comate Bioscience, Changchun, China). The target plasmid pMD-MiCV had an original concentration of 210.47 ng/μl, as measured using a Nanodrop One spectrophotometer (Thermo Scientific, Wilmington, DE, USA). Ten-fold serial dilutions

TABLE 1 Primers and probes used in this study.

Name	Sequence (5′ to 3′)	Length (bp)	Position[a]
MiCV-F	AGGGCCTTTGGGCATCATTG	107	1,473-1,579
MiCV-R	CCCGCCTGCAAACTGAAGAA		
MiCV-Cap-F	TTAAGTTTGCTTTGGGAAATTGACT	684	1,020–1703
MiCV-Cap-R	ATGCCCGTAAGATCGCGATACTCGC		
MiCV-Probe	FAM-ACGGAGTTGCTGCAGATGCCACGGT-TAMR	-	1,529–1,553

[a]Nucleotide positions are designated according to the gene of MiCV strain HB3 (GenBank accession No. MK561562.1).

of plasmid DNA in elution buffer were created and stored at −20°C until further testing. According to the following formula: the copy number of the plasmid (copies/μl) = [concentration of plasmid (ng/μl) × (6.02×10^{23})]/[(plasmid length × 660×10^{9})], the copy number of the plasmid was 5.68×10^{10} copies/μl. The original plasmid was diluted using elution buffer to 1.0×10^{10} copies/μl, stored as the standard plasmid-20°C until required.

2.5. Establishment of a standard curve for qPCR

The standard plasmid pMD-MiCV was serially diluted 10 times with elution buffer, 1.0×10^{6} copies/μl to 1.0×10^{1} copies/μl as templates to establish the standard curve, created by plotting the logarithm of the plasmid copy number against the measured cycle threshold (Ct) values. The standard curve, the correlation coefficient of the standard curve, and the qPCR efficiencies were calculated using the GraphPad Prism 7 software (GraphPad Inc., La Jolla, CA, USA). The amount of DNA quantified in each sample was expressed as number of copies per reaction. The final volume was 20 μl including 10 μl of TB Green® Premix Ex Taq™ II (Takara Biomedical Technology, Beijing, China), 0.8 μl each of the MiCV-F and MiCV-R primers (10 μmol/L), 0.4 μl of the probe MiCV-P (10 μmol/L), 1 μl of template, and 6 μl of ddH_2O. The qPCR reaction was carried out in eight tubes by fluorescence quantitative PCR in qTOWER3 G instrument (Analytik Jena AG, Jena, Germany). The procedure comprised incubation at 95°C for 3 min, followed by 45 cycles of 95°C for 10 s and 57°C for 40 s.

2.6. Specificity, sensitivity, and repeatability analysis

To exclude qPCR cross-reactivities between MiCV and other pathogens, six viruses, namely, AMDV, PRV (PRV has occurred in mink in recent years, and might be related to eating pigs' viscera), PCV-2, MEV, CDV and CAdV-2 were subjected to qPCR to confirm the specificity of the technique. MiCV strain HB3 was used as the positive control and ddH_2O was used as the negative control, and each sample was repeated 3 times.

To compare the sensitivity of qPCR and conventional PCR, dilutions of plasmid pMD-MiCV (1.0×10^{5} copies/μl to1.0×10^{0} copies/μl) and DNA of MiCV strain HB3 (2.38×10^{2} pg/μl to 2.38×10^{-3} pg/μl) were used as templates for qPCR and conventional PCR. The conventional PCR reaction was performed using the primer pair MiCV-cap-F and MiCV-cap-R. Besides, the diagnostic sensitivity of the qPCR was tested by the positive clinical samples verified by sequencing.

Three different dilutions of standard plasmid (1.0×10^{2} copies/μl, 1.0×10^{4} copies/μl, and 1.0×10^{6} copies/μl) were used for amplification in three parallel assays under the same conditions. The coefficient of variation (CV) was calculated according to the formula CV = (SD [Ct value]/overall average [Ct value]) × 100, to evaluate the intra-and inter-assay repeatability and stability in the qPCR method.

2.7. Clinical samples

A total of 789 clinical samples were collected from different fur-bearing animal farms in China. The samples included anal swab samples and environmental swab samples. The anal swab samples were collected by inserting sterile cotton swab into the anus about 2 to 3 cm, gently rotating it, and pulling it out. The anal swab samples were then placed into sampling tubes that contained 2 ml of sterile phosphate-buffered saline. The environmental swab samples were collected using a sterile cotton swab to clean each sampling area including cages, troughs, soil under the cages, sewage under the cages, aisle floors, breeder's clothes, and equipment, for 20 to 30 s, then placing it into the sample tubes holding 2 ml of sterile phosphate-buffered saline. All samples were stored at −80°C immediately after being transported back to the laboratory at low temperature. The qPCR assays were performed on these samples for MiCV detection.

3. Results

3.1. Establishment of the standard curve for qPCR

Ten-fold serial dilutions of plasmids were used to construct a standard curve by plotting the logarithm of the plasmid copy number against the measured Ct values (Figure 1). The standard curve had a wide dynamic range of 10^{1} to10^{6} copies/μl with a linear correlation (R^2) of 0.996 between the Ct value and the logarithm of the plasmid copy number. The amplification efficiency of the obtained qPCR was 93%.

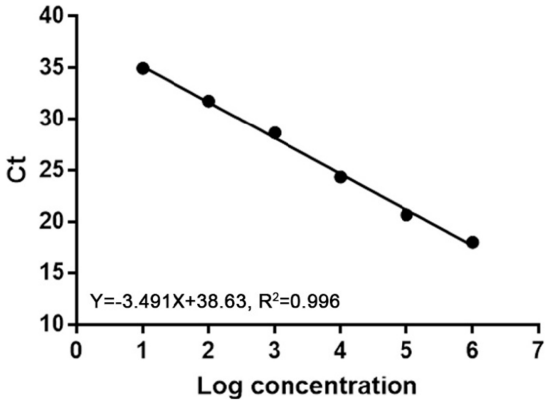

FIGURE 1
Standard curve of real-time PCR to detect MiCV. The correlation coefficient (R^2) was 0.996 and the slope was −3.491.

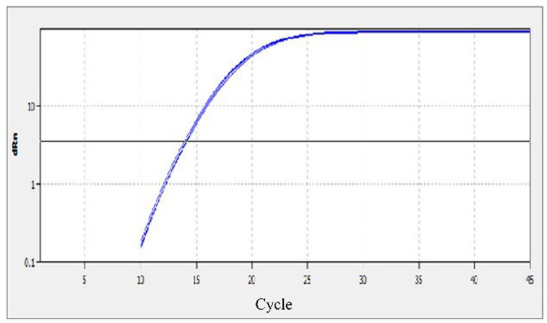

FIGURE 2
Specificity of the qPCR assay. The templates included DNA or cDNA of MiCV, AMDV, PRV, PCV-2, MEV, CDV, CAdV2 and the water control.

3.2. Specificity, sensitivity, and repeatability of the qPCR

The specificity of the qPCR assay was evaluated using eight different reactions, which included, MiCV, AMDV, PRV, PCV-2, MEV, CDV, CAdV2 and a negative water control. Strong fluorescent signals were obtained from reactions with MiCV in three replications; while no signals were obtained from the other six virus samples and the water control (Figure 2). The results demonstrated that the MiCV assay specifically detected the target virus without cross detection of any non-target pathogens.

The sensitivity of the qPCR assays were evaluated by testing 10-fold serial dilutions of the DNA standards and the positive clinical samples. For the standard plasmid DNA of pMD-MiCV, the detection limit of qPCR was 1.0×10^1 copies/μl, while the detection limit of conventional PCR was 1.0×10^3 copies/μl (Figures 3A,B). For the virus DNA of MiCV strain HB3, the detection limit of qPCR was 2.38×10^{-2} pg/μl, while the detection limit of conventional PCR was 2.38×10^1 pg/μl (Figures 4A,B). For the positive clinical samples, 35 of 35 positive samples were verified as positive by qPCR assay. Thus, the diagnostic sensitivity of the qPCR was 100%.

The intra-and inter-assay reproducibility was assessed using three dilutions of the standard plasmid pMD-MiCV DNA (1.0×10^2 copies/μl, 1.0×10^4 copies/μl, and 1.0×10^6 copies/μl). The values of the intra-assay co-efficient of variation (CV) ranged from 0.46 to 0.96%, and the values of the inter-assay CV ranged from 1.37 to 1.98%, indicating that the qPCR method was highly reproducible.

3.3. Detection of the clinical samples

The application of qPCR was evaluated by detecting 226 mink anal swabs, 142 fox anal swabs and 128 raccoon dog anal swabs. The positive detection rates of MiCV in minks, foxes and raccoon dogs were 58.8, 50.7, and 42.2%, respectively (Table 2). The total positive detection rate was 52.2%. The positive detection rate of MiCV in minks was higher than that in foxes and raccoon dogs. The positive detection rate of MiCV in fur-bearing animals ≥1 year old was 55.1%, and was 49.6% in fur-bearing animals <1 year old. The positive detection rate in male fur-bearing animals was 51.0%, and was 53.5% in female fur-bearing animals (Table 3). Environmental samples from fur-bearing animal farms had a higher positive detection rate of 75.1%. Among them, the positive rates were higher in samples from cages, troughs, soil under the cages and sewage under the cages than in samples from floors, breeder's clothes, and equipment (Table 4).

4. Discussion

For MiCV, there is no cell culture system for virus isolation and identification, and there is no effective vaccine or specific drug to prevent and control the disease. Some farmers used homemade inactivated vaccines (tissue supernatants of diseased mink inactivated using formalin) to prevent the disease and reduce morbidity; however, after a period of application, some minks developed symptoms of Aleutian disease. There are serious safety concerns with this type of vaccine; therefore, it has been discontinued (Wang et al., 2021). In view of this situation, the effective way to prevent the disease is to detect and eliminate the positive animals gradually in China. The recombinase polymerase amplification method had a minimum detection limit of 10 copies, but requires purification of amplification products and agarose gel electrophoresis to analyze the results (Ge et al., 2018c). The SYBR Green-based real-time PCR detection method for MiCV established by Cui could detect a minimum of 10^1 copies/μl, in which the specific primers referred to the Cap gene sequences of eight different MiCV strains (Cui et al., 2018).

In this study, a quantitative real-time PCR technology based on TaqMan was established. The standard curve of the qPCR was established as shown in Figure 1. The correlation coefficient (R^2) was 0.996 and the amplification efficiency was 93%, which indicated that the method established in this study is highly efficient, and mighty be a suitable approach for MiCV diagnosis. The primers and probes were designed according to the whole genome sequences of MiCV obtained in the laboratory in recent years and all 13 of MiCV genome sequences deposited in GenBank. Besides, six viruses that could cause potential cross-reactivity in qPCR assays were assessed. The qPCR method could successfully detect MiCV and without any cross reaction with other viral pathogens, including AMDV, MEV, CDV,

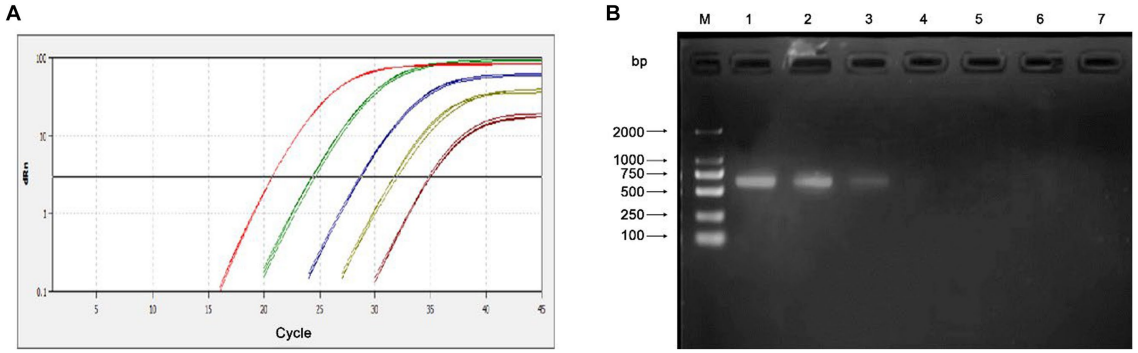

FIGURE 3
Sensitivity of the qPCR assay for the plasmid DNA of pMD-MiCV. **(A)** The qPCR amplification curve. **(B)** Electrophoresis of conventional PCR reactions. The template concentrations of plasmid DNA ranged from 1.0×10^5 copies/μl to 1.0×10^0 copies/μl. A negative control was included.

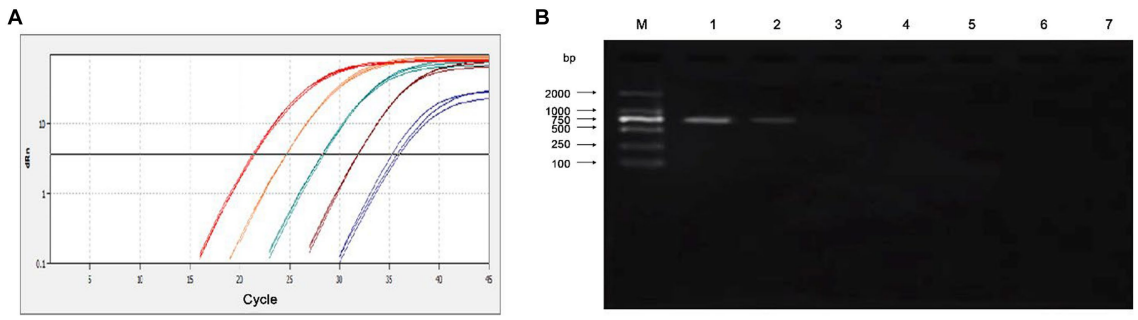

FIGURE 4
Sensitivity of the qPCR assay for the virus DNA of MiCV strain HB3. **(A)** The qPCR amplification curve. **(B)** Electrophoresis of conventional PCR reactions. The template concentrations of virus DNA ranged from 2.38×10^2 pg/μl to 2.38×10^{-3} pg/μl. A negative control was included.

CAdV-2, PRV, and PCV-2, indicating the high specificity and reliability of this method for MiCV detection. For the plasmid DNA, the minimum detection limit of the established qPCR method was 1.0×10^1 copies/μl, whereas that for conventional PCR was 1.0×10^3 copies/μl. For the virus DNA of MiCV, the minimum detection limit of the established qPCR method was 2.38×10^{-2} pg/μl, the conventional PCR was 2.38×10^1 pg/μl. The results showed that the sensitivity of qPCR was higher than that of conventional PCR to detect MiCV. Moreover, the minimum detection limit of the qPCR method established in this study was lower than that of the previously established conventional PCR method and qPCR method (Wang et al., 2021). The values of the intra-assay CV ranged from 0.46 to 0.96%, and the values of the inter-assay CV ranged from 1.37 to 1.98%, which indicated that the qPCR method is highly reproducible.

MiCV infective rates in minks are high in some fur-bearing animal farms in China (Cui et al., 2018; Wang et al., 2021). In this study, we also detected a high positive detection rate of MiCV in minks, with positive detection rates exceeding 55% in Heilongjiang Province, Jilin Province, and Shandong Province. In clinical samples, the positive detection rate of MiCV in foxes was 52.4% in Heilongjiang Province, 50.9% in Jilin Province, and 48.9% in Shandong Province; in raccoon dogs it was 43.9% in Heilongjiang Province, 39.6% in Jilin Province, and 43.6% in Shandong Province. The total positive detection rate of MiCV in minks was higher (58.8%) than that in foxes (50.7%) and raccoon dogs (42.2%). However, the positive detection rates were lower than the 93% (40/43), 95.5% (21/22), and 69.2% (9/13) reported by Yang (Yang et al., 2018). We also found that the positive detection rate of MiCV in fur-bearing animals ≥ 1 year old was higher than that in animals <1 year old. The positive detection rate in male fur-bearing animals was lower than that in female fur-bearing animals. Usually when an infectious disease occurs on a farm, its pathogen can persist in the environment for a long time (Prieto et al., 2017). In this study we tested some environmental samples from cages, sinks, soil and sewage under cages. We found that the environmental samples of these fur-bearing animal farms have high positive detection rates. Among them, the samples from cages, troughs, soil under the cages, and sewage under cages had higher positive detection rates than the samples from aisle floors, breeder's clothes and equipment. It is worth noting that these elements are frequently moved within the farm and in some exceptional cases are even transferred to other farms, which poses a significant risk to biosecurity. As far as we know, these results are the first application of the qPCR method to detect MiCV infection in environmental samples from fur-bearing animal farms. Unlike bacteria, there is no accepted standard culture method to quantify viruses in environmental samples; therefore, qPCR detection is a useful tool to study the epidemiology of viral diseases (Rodríguez-Lázaro et al., 2012). Although the presence of viral DNA cannot

TABLE 2 The prevalence of MiCV in the clinical samples used in this study.

Province	Mink			Fox			Raccoon dog		
	Number	Positive number	Positive rate (%)	Number	Positive number	Positive rate (%)	Number	Positive number	Positive rate (%)
Heilongjiang	75	42	56.0	42	22	52.4	41	18	43.9
Jilin	83	46	55.4	55	28	50.9	48	19	39.6
Shandong	68	45	66.2	45	22	48.9	39	17	43.6
Total	226	133	58.8	142	72	50.7	128	54	42.2

TABLE 3 MiCV positivity in fur-bearing animals of different ages and sexes.

Groups		Number	Positive number	Positive rate (%)
Ages	≥1 year old	234	129	55.1
	<1 year old	262	130	49.6
	Total	496	259	52.2
Gender	Male	251	128	51.0
	Female	245	131	53.5
	Total	496	259	52.2

TABLE 4 Detection rate of MiCV in the environment of fur-bearing animal farms.

Source	Number	Positive number	Positive rate (%)
Cages	68	55	80.9
Troughs	53	44	83.0
Soil under the cages	56	43	76.8
Sewage under the cages	37	27	73.0
Aisle floors	21	14	66.7
Breeder's clothes	32	22	68.8
Equipment	26	15	57.7
Total	293	220	75.1

be interpreted as "infection" because its detection cannot determine infectivity, it might increase the risk of reinfection or transmission of the disease in the farms. These results focus attention on the role of environmental contamination in farms in the maintenance and transmission of this disease.

5. Conclusion

In this study, a highly sensitive, specific, repeatable and quantitative real-time PCR method for MiCV DNA detection was developed. The results showed that the positive detection rate of MiCV in minks was higher than that in foxes and raccoon dogs. The samples taken from the environment of the fur-bearing animal farms had high positive rates, and the positive detection rates in samples from cages, troughs, soil under the cages, and sewage under the cages were higher than those in the samples from the aisle floor, breeder clothes, and equipment. This study could contribute to control the spread of MiCV disease.

Data availability statement

The original contributions presented in the study are included in the article/supplementary material, further inquiries can be directed to the corresponding authors.

Ethics statement

The animal study was reviewed and approved by Animal Welffare and Research Ethics Committee of Jinlin Agricultural University (JLAU08201409).

Author contributions

YL and CS: conceived of the study, carried out the experiment and drafted the manuscript, conducting a research and investigation process, specifically performing the experiments, or data/evidence

collection YZ and JL: provision of study materials, reagents, materials, patients, laboratory samples, animals, instrumentation, computing resources, or other analysis tools. QG, KS, and FL: management and coordination responsibility for the research activity and execution, including mentorship external to the core team. LX and ZC: application of statistical, mathematical, computational, or other formal techniques to analyze or synthesize study data, preparation, creation and/or presentation of the published work, specifically visualization/data presentation. XL: conceived of the study and revising the manuscript critically. RD: acquisition of the financial support for the project leading to this publication. All authors contributed to the article and approved the submitted version.

Funding

This research was supported by the Science and Technology Development Project of Jilin Province (grant numbers 20220101332JC and YDZJ202301ZYTS334) and the Science and Technology Research Project of Jilin Provincial Department of Education (grant number JJKH20210366KJ).

Acknowledgments

The authors grateful to all study participants for their contributions.

Conflict of interest

The authors declare that the research was conducted in the absence of any commercial or financial relationships that could be construed as a potential conflict of interest.

Publisher's note

References

Abdel-Moneim, A. S., Shehab, G. M., Alsulaimani, A. A., and Al-Malky, M. I. R. (2017). Development of Taq Man RT-qPCR for the detection of type a human respiratory syncytial virus. *Mol. Cell. Probes* 33, 16–19. doi: 10.1016/j.mcp.2017.02.006

Breitbart, M., Delwart, E., Rosario, K., Segalés, J., Varsani, A., and Ictv Report, C. (2017). ICTV virus taxonomy profile: Circoviridae. *J. Gen. Virol.* 98, 1997–1998. doi: 10.1099/jgv.0.000871

Canuti, M., Rodrigues, B., Bouchard, É., Whitney, H. G., Lang, A. S., Dufour, S. C., et al. (2022). Distinct epidemiological profiles of porcine circovirus 3 and fox circovirus in Canadian foxes (Vulpes spp.). *Curr. Res. Micro. Sci.* 3:100161. doi: 10.1016/j.crmicr.2022.100161

Cui, X., Shi, Y., Zhao, L., Gu, S., Wei, C., Yang, Y., et al. (2018). Application of real-time quantitative PCR to detect mink circovirus in naturally and experimentally infected minks. *Front. Microbiol.* 9:937. doi: 10.3389/fmicb.2018.00937

de Oliveira Lopes, G. A., Ferreira, L. R., de Souza Trindade, G., Fonseca, A. A. Jr., and Dos Reis, J. K. P. (2021). qPCR assay for the detection of Pseudocowpox virus. *Arch. Virol.* 166, 243–247. doi: 10.1007/s00705-020-04872-4

Decaro, N., Martella, V., Desario, C., Lanave, G., Circella, E., Cavalli, A., et al. (2014). Genomic characterization of a circovirus associated with fatal hemorrhagic enteritis in dog, Italy. *PLoS One* 9:e105909. doi: 10.1371/journal.pone.0105909

Ge, J., Cui, X., Shi, Y., Zhao, L., Wei, C., Wen, S., et al. (2018a). Development and application of an indirect enzyme-linked immunosorbent assay based on recombinant capsid protein for the detection of mink circovirus infection. *BMC Vet. Res.* 14:29. doi: 10.1186/s12917-018-1337-z

Ge, J., Gu, S., Cui, X., Zhao, L., Ma, D., Shi, Y., et al. (2018b). Genomic characterization of circoviruses associated with acute gastroenteritis in minks in northeastern China. *Arch. Virol.* 163, 2727–2735. doi: 10.1007/s00705-018-3908-5

Ge, J., Shi, Y., Cui, X., Gu, S., Zhao, L., and Chen, H. (2018c). Rapid and sensitive detection of mink circovirus by recombinase polymerase amplification. *J. Virol. Methods* 256, 1–5. doi: 10.1016/j.jviromet.2018.02.022

Gong, H. Y., Li, Q. Y., Zhang, H., Ye, L., Shi, L., and Feng, Y. H. (2021). Development and comparison of qPCR and qLAMP for rapid detection of the decapod iridescent virus 1 (DIV1). *J. Invertebr. Pathol.* 182:107567. doi: 10.1016/j.jip.2021.107567

Li, L., Kapoor, A., Slikas, B., Bamidele, O. S., Wang, C., Shaukat, S., et al. (2010). Multiple diverse circoviruses infect farm animals and are commonly found in human and chimpanzee feces. *J. Virol.* 84, 1674–1682. doi: 10.1128/jvi.02109-09

Matsumoto, T., Sato, M., Nishizono, A., and Ahmed, K. (2019). A novel bat-associated circovirus identified in northern Hokkaido, Japan. *Arch. Virol.* 164, 2179–2182. doi: 10.1007/s00705-019-04286-x

Morandini, V., Dugger, K. M., Ballard, G., Elrod, M., Schmidt, A., Ruoppolo, V., et al. (2019). Identification of a novel Adélie penguin circovirus at cape crozier (Ross Island, Antarctica). *Viruses* 11:1088. doi: 10.3390/v11121088

Piewbang, C., Jo, W. K., Puff, C., van der Vries, E., Kesdangsakonwut, S., Rungsipipat, A., et al. (2018). Novel canine circovirus strains from Thailand: evidence for genetic recombination. *Sci. Rep.* 8:7524. doi: 10.1038/s41598-018-25936-1

Prieto, A., Fernández-Antonio, R., Díaz-Cao, J. M., López, G., Díaz, P., Alonso, J. M., et al. (2017). Distribution of Aleutian mink disease virus contamination in the environment of infected mink farms. *Vet. Microbiol.* 204, 59–63. doi: 10.1016/j.vetmic.2017.04.013

Rodríguez-Lázaro, D., Cook, N., Ruggeri, F. M., Sellwood, J., Nasser, A., Nascimento, M. S., et al. (2012). Virus hazards from food, water and other contaminated environments. *FEMS Microbiol. Rev.* 36, 786–814. doi: 10.1111/j.1574-6976.2011.00306.x

Rosario, K., Breitbart, M., Harrach, B., Segalés, J., Delwart, E., Biagini, P., et al. (2017). Revisiting the taxonomy of the family Circoviridae: establishment of the genus Cyclovirus and removal of the genus Gyrovirus. *Arch. Virol.* 162, 1447–1463. doi: 10.1007/s00705-017-3247-y

Shulman, L. M., and Davidson, I. (2017). Viruses with circular single-stranded DNA genomes are everywhere! *Ann. Rev. Virol.* 4, 159–180. doi: 10.1146/annurev-virology-101416-041953

Tong, M., Sun, N., Cao, Z., Cheng, Y., Zhang, M., Cheng, S., et al. (2020). Molecular epidemiology of Aleutian mink disease virus from fecal swab of mink in Northeast China. *BMC Microbiol.* 20:234. doi: 10.1186/s12866-020-01910-8

Varga, A., and James, D. (2006). Real-time RT-PCR and SYBR green I melting curve analysis for the identification of plum pox virus strains C, EA, and W: effect of amplicon size, melt rate, and dye translocation. *J. Virol. Methods* 132, 146–153. doi: 10.1016/j.jviromet.2005.10.004

Vázquez, L., Guadamuro, L., Giganto, F., Mayo, B., and Flórez, A. B. (2017). Development and use of a real-time quantitative PCR method for detecting and quantifying Equol-producing bacteria in human Faecal samples and slurry cultures. *Front. Microbiol.* 8:1155. doi: 10.3389/fmicb.2017.01155

Wang, L., Zhang, Y., Chen, T., Mi, L., Sun, X., Zhou, X., et al. (2021). The mink circovirus capsid subunit expressed by recombinant baculovirus protects minks against refractory diarrhea in field. *Viruses* 13:606. doi: 10.3390/v13040606

Yang, Y., Cheng, Y., Li, N., Cheng, S., Guo, L., Zhou, Y., et al. (2018). Mink circovirus can infect minks, foxes and raccoon dogs. *Virol. Sin.* 33, 561–564. doi: 10.1007/s12250-018-0059-5

Zhao, L., Rosario, K., Breitbart, M., and Duffy, S. (2019). Eukaryotic circular rep-encoding single-stranded DNA (CRESS DNA) viruses: ubiquitous viruses with small genomes and a diverse host range. *Adv. Virus Res.* 103, 71–133. doi: 10.1016/bs.aivir.2018.10.001

frontiers | Frontiers in Microbiology

TYPE Original Research
PUBLISHED 08 August 2023
DOI 10.3389/fmicb.2023.1226877

OPEN ACCESS

EDITED BY
Hongliang Chai,
Northeast Forestry University, China

REVIEWED BY
Xiaobo Wen,
Hainan University, China
Liu Sidang,
Shandong Agricultural University, China

*CORRESPONDENCE
Liandong Qu
✉ quliandong@caas.cn
Jiasen Liu
✉ neauljs@163.com

RECEIVED 22 May 2023
ACCEPTED 24 July 2023
PUBLISHED 08 August 2023

CITATION
Yang Y, Liu Z, Chen M, Feng K, Qi R, Zheng Y, Wang Y, Kang H, Jiang Q, Yang M, Qu L and Liu J (2023) Classification of genotypes based on the VP1 gene of feline calicivirus and study of cross-protection between different genotypes.
Front. Microbiol. 14:1226877.
doi: 10.3389/fmicb.2023.1226877

Classification of genotypes based on the VP1 gene of feline calicivirus and study of cross-protection between different genotypes

Yupeng Yang[1], Zhe Liu[1], Mengru Chen[2], Kexin Feng[1], Ruibin Qi[1], Yating Zheng[1], Ying Wang[2], Hongtao Kang[1], Qian Jiang[1], Mingfa Yang[1], Liandong Qu[1]* and Jiasen Liu[1]*

[1]State Key Laboratory for Animal Disease Control and Prevention, Harbin Veterinary Research Institute, Chinese Academy of Agricultural Sciences, Harbin, China, [2]College of Veterinary Medicine, Northeast Agricultural University, Harbin, China

Feline calicivirus (FCV) causes upper respiratory tract diseases and even death in cats, thereby acting as a great threat to feline animals. Currently, FCV prevention is mainly achieved through vaccination, but the effectiveness of vaccination is limited. In this study, 105 FCV strain VP1 sequences with clear backgrounds were downloaded from the NCBI and subjected to a maximum likelihood method for systematic evolutionary analysis. Based on the genetic analysis results, FCV-positive sera were prepared using SPF mice and Chinese field cats as target animals, followed by a cross-neutralization assay conducted on the different genotype strains and *in vivo* challenge tests were carried out to further verify with the strain with best cross-protection effect. The results revealed that FCV was mainly divided into two genotypes: GI and GII. The GI genotype strains are prevalent worldwide, but all GII genotype strains were isolated from Asia, indicating a clear geographical feature. This may form resistance to FCV prevention in Asia. The *in vitro* neutralization assay conducted using murine serum demonstrated that the cross-protection effect varied among strains. A strain with broad-spectrum neutralization properties, DL39, was screened. This strain could produce neutralizing titers ($10 \times 2^{3.08}$–$10 \times 2^{0.25}$) against all strains used in this study. The antibody titers against the GI strains were $10 \times 2^{3.08}$–$10 \times 2^{0.5}$ and those against the GII strains were $10 \times 2^{0.75}$–$10 \times 2^{0.25}$. Preliminary evidence suggested that the antibody titer of the DL39 strain against GI was higher than that against GII. Subsequent cross-neutralization assays with cat serum prepared with the DL39 strain and each strain simultaneously yielded results similar to those described above. *In vivo* challenge tests revealed that the DL39 strain-immunized cats outperformed the positive controls in all measures. The results of several trials demonstrated that strain DL39 can potentially be used as a vaccine strain. The study attempted to combine the genetic diversity and phylogenetic analysis of FCV with the discovery of potential vaccines, which is crucial for developing highly effective FCV vaccines.

KEYWORDS

FCV, VP1, cross-neutralization assay, genotype, challenge tests, broad-spectrum neutralization

1. Introduction

The feline calicivirus (FCV) can cause feline upper respiratory infections, mainly in young cats aged less than 1 year, and the majority of the reported cases of classical FCV are benign (Radford et al., 2007). However, the ultra-high strain of FCV has recently emerged and can cause severe virulent systemic disease (VSD), which is acute and life-threatening in nature. The main VSD symptoms are ulcerative dermatitis, acute arthritis, enteritis, abortion, lameness, and other systemic infections, and VSD has a mortality rate of up to 50%. VSD poses a serious threat to public health and the safety of feline animals (Pedersen et al., 2000). FCV is also highly contagious and sick cats are among the main sources of infection. However, healthy cats infected with the virus (asymptomatic) can continue to detoxify the outside world for months to years as a carrier, which is among the main factors contributing to the high VSD prevalence (Coyne et al., 2006). Although the main hosts of FCV are feline animals and FCV has been identified and isolated from domestic cats and various rare wild animals such as lions, cheetahs, and tigers (Fastier, 1957; Kadoi et al., 1997; Weeks et al., 2001; Gao et al., 2003; Tian et al., 2016), studies have shown that FCV is transmitted across species; the causative agent of the disease was isolated from dogs (Di Martino et al., 2009). FCV is gradually becoming more harmful to feline animals and even other families of animals.

FCV belongs to the Vesivirus family, which includes positive-strand, non-enveloped RNA viruses (Radford et al., 2007). The FCV genome is approximately 7.5-kb long and comprises three open reading frames (ORFs). Nonstructural proteins are encoded by ORF1, whereas major (VP1) and minor (VP2) capsid proteins are encoded by ORF2 and ORF3, respectively (Neill, 1990; Neill et al., 1991; Sosnovtsev and Green, 2000). Of these, ORF2 is the major antigenic protein and consists of approximately 670 amino acids, which can be divided into six regions: A, B, C, D, E, and F (Neill, 1992; Seal et al., 1993). The C and E regions belong to the highly variable regions of FCV and contain amino acids predicted to interact with the feline junctional adhesion molecule-1 (fJAM-1) receptor. In addition, the E region contains many neutralizing B-cell epitopes and is a major region for virus-neutralizing antibodies (Tohya et al., 1997; Geissler et al., 2002).

Because of the many neutralization sites of the VP1 protein and its high denaturation ability, this protein is widely used for the sequence analysis of FCV strains, and thus for genome division. Considering the amino acid differences in the A and E regions of VP1 of the FCV strain, Geissler concluded that FCV has only one genotype (Geissler et al., 1997). Through the sequence analysis of B and F regions, Japanese scholars observed that gene type II could develop gradually. Later, through the preliminary analysis of their domestic strains, China and South Korea also indicated that gene type II might exist in their regions and that the strain may be endemic to East Asia (Sato et al., 2002; Sun et al., 2017; Kim et al., 2021). Undoubtedly, the current genetic evolution and phylogenetic analysis of the VP1 protein (or its highly variant regions) best reflects the genetic evolutionary characteristics of FCV. On the other hand, the high sequence variation of this protein is among the causes of early vaccine immunization failure. In this study, we analyzed the results published in previous literature and conducted the genetic evolutionary and phylogenetic analyses of the full-length sequence of VP1 strains uploaded to the NCBI. Then, cross-neutralization assays were performed on strains of different genotypes to explore the cross-protection between different genotypes by using biological tests. Based on the results, strain DL39 with broad-spectrum neutralization properties was first screened, followed by its preliminary validation and evaluation. Overall, the present study offers new data for FCV vaccine research and an updated theoretical basis for FCV prevention.

2. Materials and methods

2.1. Main materials

Thirteen FCV strains stored in the laboratory (Table 1); 140 specific pathogen-free (SPF) mice; 24 Chinese field cats (age: 2 months); various cell lines (FL: primary feline lung cells; F81: cat kidney cells; CRFK: Crandell–Rees Feline Kidney cells); β-propiolactone; adjuvant (Quick Antibody-Mouse 5 W in Biodragon and Montanide™ GEL in Seppic, two types); goat anti-mouse IgG (H + L) Alexa Fluor® 488; goat anti-mouse IgG (horseradish peroxidase); ImmunoComb® Feline VacciCheck Antibody Test Kit for Feline Calici, Herpes and Panleukopenia Viruses; and phosphate buffer saline (PBS).

2.2. Sequence alignment and phylogenetic analyses of VP1

In total, 105 nucleotide sequences of FCV VP1 were downloaded from the NCBI[1], and their backgrounds (including collection time, collection location, and host) were summarized in detail. At the end, the sample collection time rather than the sequence upload time was used to increase the accuracy of the analysis. The collected sequences were processed, and the codon-based multiple alignment of the sequences was performed using MegAlign software. After the alignment, the VP1 nucleotide sequences were translated into the amino acid sequence by using EditSeq software, which was followed by sequence comparison. Complete nucleotide and amino acid alignments were retained and used for phylogenetic analysis. Using a bootstrap approach with 1,000 replicates, the statistical support of nodes was assessed in the maximum likelihood (ML) phylogeny. Midpoints were used to root trees.

2.3. Estimates of evolutionary divergence over sequence pairs between groups

The number of amino acid substitutions per site from averaging overall sequence pairs between groups was calculated. Analyses were conducted using the Jons-Taylor-Thornton (JTT) matrix-based method (Jones et al., 1992). This analysis involved 105 amino acid sequences, including those from strains isolated from different regions, times, and species. All ambiguous positions were removed for each sequence pair (pairwise deletion option). A total of 676 positions were present in the final dataset. Evolutionary analyses were performed using MEGA-X Software (Kumar et al., 2018).

1 https://www.ncbi.nlm.nih.gov/

TABLE 1 Profiles of some strains used in this study.

FCV Strains	GenBank ID	Acquisition Time	Genotype	Host	Animal Regression Test
F9	M86379	1992 (USA)	GI-3	Cat	Standard Vaccine Strain
FCV-2280	KC835209	2013 (ATCC)	GI-1	Cat	The VSD Strain(Causing the death of the experimental cat)
DL31	MW804427	2020 (CHN)	GI-5	Cat	The body temperature of the test cat increased
DL37	MW804428	2020 (CHN)	GI-5	Cat	Isolated from healthy cats and no regression test was performed
DL38	MW804429	2020 (CHN)	GII	Cat	Isolated from healthy cats and no regression test was performed
DL39	MW804430	2020 (CHN)	GI-5	Cat	The cats had high body temperatures and were depressed
HRB23	MW804431	2020 (CHN)	GI-5	Cat	Isolated from healthy cats and no regression test was performed
HRB21	MW804432	2020 (CHN)	GI-7	Cat	It was isolated from infected cats without regression test and was co-infected with FHV, but it was lost during passage
HRB46	MW804433	2020 (CHN)	GI-1	Cat	Isolated from healthy cats and no regression test was performed
HRB48	MW804434	2020 (CHN)	GI-4	Cat	All the cats showed symptoms such as sneezing, elevated body temperature, cough, mouth ulcer and plantar cracking
HRB-SS	KM016908	2014 (CHN)	GI-1	Cat	Isolated from healthy cats and no regression test was performed
FB-NJ-13	KM111557	2013 (CHN)	GII	Cat	All the cats showed symptoms of sneezing, elevated body temperature, cough, increased secretion of eye and nose, anorexia, tremor of limbs, severe oral ulceration and plantar dehysis
TIG-1	KU373057	2014 (CHN)	GI-4	Tiger	The VSD Strain(Causing the death of the experimental cat)

Including national standard strains and strains that have been subjected to animal regression tests.

2.4. *In vitro* cross-neutralization assay between virus and mouse positive serum

2.4.1. Purification and inactivation of FCV virus

Using the 13 FCV strains (the specific information is presented in Table 1) isolated and preserved in our laboratory, we prepared murine polyclonal antibodies for the preliminary screening of candidate vaccine strains. Then, the 13 FCV strains were plaque-picked and passaged five more times. $TCID_{50}$ measurements were performed using the Reed–Muench method at the indicated times, and the results were used to determine growth curves and to guide virus culture expansion at the optimal time point. Viral particles were purified and concentrated through ultracentrifugation, we used ultracentrifuge centrifugation for 2 h at 4°C, 130000 g; The supernatant was discarded and resuspended in 500 μL of sterile PBS and centrifuged on a sucrose gradient (10, 20, and 30% sucrose) for 2 h at 4°C, 130000 g. The supernatant was discarded and resuspended in 500 μL of sterile PBS. Electron microscopic observation was performed, and a plaque assay was used to quantify the virus (uniform dilution to $2 \times 7 \times 10^6$ PFU/mL). Finally, the FCV antigen was prepared by inactivating the stock virus with β-propiolactone (0.001% final concentration).

2.4.2. Inactivated virus immunization

SPF mice were used as hosts for the initial screening test, and 140 mice were divided into 14 groups (including the negative control group). We first randomly checked mice #8, #9, and #10 in each group, and detected their FCV antibody titers by Elisa. Each mouse was intramuscularly injected with 7×10^5 PFU of virions (50 μL) in the calf, mixed 1:1 with the adjuvant (Quick Antibody-Mouse 5 W, Beijing Biodragon Immunotechnologies Co., Ltd), and the negative control group was immunized with the same dose of the PBS and adjuvant mixture. Immunization was boosted once on day 21 of the experiment, and the sera were collected from each mouse on day 14 after the second immunization. During the experiment, three fixed mice were selected for monitoring.

2.4.3. *In vitro* cross-neutralization assay

IgG levels were monitored dynamically in three mice to confirm the immune response. At the specified immunization time, the serum from each group of mice was collected and verified through the neutralization test of the parental virus in each mouse. The serum of the same FCV strain with a neutralization titer of >24 was screened and mixed. The indirect immunofluorescence assay (IFA) was performed to determine the specificity of the mixed serum and the final titer based on the parental virus. According to the final neutralization titer, mixed serum of each strain was diluted to the same titer, and then, the cross-neutralization assay was performed to ensure more accurate results.

2.5. Validation of ontogenetic animal

2.5.1. Preparation of feline serum of the DL39 strain

Immune sera from native animals were prepared for the initially screened strains with broad-spectrum neutralization. Three 2-month-old Chinese field cats (all antibodies to FCV were negativeand by the ImmunoComb® Feline VacciCheck Antibody Test Kit for Feline Calici, Herpes and Panleukopenia Viruses and born at the same time) were used in the experiment. Each cat was immunized with 7×10^7 PFU of the inactivated vaccine strain through subcutaneous injection into the neck (reference for the preparation of inactivated virus in step 2.4.1), Montanide™ GEL was used as adjuvant, followed by booster immunization at 21 days, which was

performed in the same manner as the first immunization. The vaccinated cats were monitored during immunization, and sera were collected for the cross-neutralization assay on day 14 after the second immunization.

2.5.2. *In vitro* cross-neutralization assay

IgG levels were monitored dynamically to confirm the immune response. At the specified immunization time, the serum from each cat was collected and verified through the neutralization test of the DL39 strain in each cat. Based on the results of the aforementioned neutralization tests, the time of collection of large numbers of sera from the cats was determined, and the cross-neutralization assay with different FCV strains was verified in different cell lines.

2.5.3. Challenge of FCV strains with different genotypes

According to the phylogenetic analysis, the strains of each genotype were selected for the challenge test. The strains DL39 (GI, parental strain), HRB48 (GI), and FB-NJ-13 (GII) were selected. In total, seven groups of 2-month-old cats (each group = 3 cats; all trials were conducted using the cats of the same age and size and all antibodies to FCV were negativeand by the ImmunoComb® Feline VacciCheck Antibody Test Kit for Feline Calici, Herpes and Panleukopenia Viruses) were used in the study design. First, three groups of cats (immunization test groups) were immunized with the DL39 inactivated strain. Each cat was subcutaneously injected with 7×10^7 PFU of the inactivated vaccine strain into the neck (reference for the preparation of inactivated virus in step 2.4.1), followed by booster immunization at 21 days, which was performed in the same manner as the first immunization. We had also maintained three positive control groups and one negative control group. At 14 days after the second immunization in the immunization test group, an attack dose of 1×10^8 $TCID_{50}$ was administered to each cat through nasal drip, except to the negative control group. The negative control group received nasal drops with the same volume of PBS. The test focused on monitoring the clinical manifestations, temperature, body weight, detoxification, viremia, and corresponding antibodies in each group at different times. For the clarity of results, a point assessment system was used to conduct clinical symptom statistics. By referring to the relevant regulations of the European Pharmacopeia along with the clinical symptoms, including oral ulcers, eye and nasal discharges, body temperature, body weight, and mental state, a scoring system was established for animal morbidity. This scoring system can be used for a comparative analysis of clinical symptoms based on the scores (Table 2). Depending on Table 2, the cat with a score of ≤2 points was temporarily deemed unaffected and that with a score of >2 was considered morbid.

3. Results

3.1. Sequence download and partial strain information

The VP1 sequences of FCV strains were downloaded from the NCBI. Biological characteristics of some strains used were described (Table 1) to ensure more clear results.

3.2. Phylogenetic analysis of the FCV VP1 gene

To better understand the evolution of FCV, we used the downloaded FCV VP1 gene to construct the phylogenetic tree of the nucleotide sequence (nt) and amino acid sequence (aa) (Figure 1). Phylogenetic analysis revealed that the FCV evolution was primarily divided into two main genotypes: GI and GII. The GI genotype was categorized into different genetic subtypes according to the branch length of the phylogenetic tree. Although GI genotype strains were still dominant and prevalent all over the world, the nt and aa evolutionary trees demonstrated that all GII genotype strains were isolated from Asia. The Asian lineages gradually formed a new evolutionary tendency. This may also be the reason for the poor prevention and control of the FCV vaccine in China. Later, on analyzing the genetic distance between groups of amino acids (Table 3), we found that the genetic distance between the GII and GI (0.164–0.172) genotypes was significantly greater than that between GI subtypes (0.125–0.154), indicating the possibility of the emergence of new Asian types from a genetic perspective.

3.3. Culture and purification of FCV

According to the $TCID_{50}$ measurement results (Figure 2A) at different time points, the culture time of the 13 virus strains after inoculation was 36 h. During this period, the cultured cells shrunk, shed, and became completely diseased (Figure 2B). A negative strain observed through electron microscopy revealed a significant increase in the amount of virus purified through ultraionization and a decrease in impurity (Figure 2C). The purified virus was then subjected to the plaque assay (Figure 2D). Table 4 presents the statistics of $TCID_{50}$ and PFU of the 13 purified FCV strains.

3.4. Verification of mouse serum results

The serum of three fixed mice in each group was collected every 5 days for IgG determination. The IgG levels of some immunized mice began to increase from the 5th day, accelerated 20 days later, and continued to increase after the end of immunization, whereas serum IgG levels in the control group did not increase significantly (Figure 3A). Then, specificity was verified through IFA, and green fluorescence indicated that each group of mice produced antibodies against the parental virus (Figure 3C). Through the cross-neutralization assay, the mouse serum was verified to produce different neutralization titers against the parental virus. The titers of HRB21, HRB-SS, and FB-NJ-13 strains were on the order of 10×2^6, and those of the other strains were on the order of more than 10×2^7 (Figure 3B).

3.5. Cross-neutralization assay of mouse serum

Serum was diluted to the same order of magnitude titers and cross-neutralized. In Figure 4A, cross-neutralization titers between

TABLE 2 Estimates of evolutionary divergence over sequence pairs between groups.

Genotype	GI-1	GI-2	GI-3	GI-4	GI-5	GI-6	GI-7	GI-8	GII
GI-1	0.000								
GI-2	0.133								
GI-3	0.134	0.132							
GI-4	0.132	0.125	0.129						
GI-5	0.141	0.139	0.141	0.135					
GI-6	0.142	0.144	0.144	0.139	0.140				
GI-7	0.150	0.146	0.151	0.136	0.140	0.138			
GI-8	0.154	0.157	0.149	0.138	0.151	0.149	0.141		
GII	0.172	0.167	0.173	0.164	0.170	0.175	0.167	0.170	0.000

each strain are noted. Blank squares represent titer 0, different values are identified by different colors, and all strains have the highest titers with the parental strain. To more clearly analyze the cross-neutralization effect between strains, the box plot was established for statistical analyses. DL39 exhibited a broad spectrum of cross-neutralizing features ($10\times2^{3.08}$–$10\times2^{0.25}$). It not only generated neutralizing titers against all strains used in the assay but also had the highest indicator midline. This confirmed the broad-spectrum characteristics of the DL39 strain (Figure 4B). Furthermore, data also revealed that the DL39 strain produced higher neutralizing titers against the GII strains ($10\times2^{0.75}$–$10\times2^{0.25}$) than against the other strains (DL37, HRB21, HRB23, etc.), but exhibited higher cross-neutralizing titers against the GI strains ($10\times2^{3.08}$–$10\times2^{0.5}$) (Figure 4C). Results of verification performed using different cell lines demonstrated that the DL39 serum could generate neutralizing titers against all 13 virus strains, which proved that DL39 has broad-spectrum neutralizing properties (Figure 4D).

3.6. Cross-neutralization assay of feline serum

Immunization of the Chinese field cats was followed by the measurement of serum IgG levels and neutralization titers with the parental virus. Serum IgG levels in the three cats continued to increase over the 35 days of immunization (Figure 5A). On day 14 of immunization, neutralization titers were generated in the experimental animals, which increased over time until the titers reached to more than 10×2^4 orders of magnitude (Figure 5B). Neutralization titers for the three cats were similar, which indicated that the immunization experiment was successful. The serum was collected for the cross-neutralization assay with other FCV strains, and the results revealed that the collected serum could neutralize all strains used in this experiment. Neutralizing titers were produced against DL38 and FB-NJ-13 strains belonging to GII genotypes, but were lower than those against strains belonging to GI genotypes. The neutralizing titer against the FCV-2280 strain of VSD was 10×2^2. Furthermore, TIG-1 knockdown in the VSD strain isolated from the tiger also resulted in a neutralizing titer of 10×2^2 orders of magnitude. Similar results were obtained with the FL, F81, and CRFK cells (Figure 5C). The inactivated DL39 strain exhibited a good immune effect in *in vitro* testing.

3.7. Results of the FCV challenge test with different genotypes

3.7.1. Results of an attack challenge assay with DL39 (parental virus)

A summary of the results of the DL39 parental virus challenge assay is presented in Figure 6. In the positive control group, a slight increase in temperature was observed on day 5 with no other symptoms, and the immune and negative control groups did not develop any significant symptoms. Then, the clinical symptoms of each group were counted and scored in detail; however, no significant difference was noted (Figure 6A). Although detoxification and viremia were observed in each trial arm, they were significantly lower in the immune group than in the positive control group. The immune group had slightly higher IgG levels than the positive control group (Figure 6).

3.7.2. Results of an attack challenge assay with HRB48 (genotype I virus)

An attack challenge assay on the HRB48 (GI) strain revealed that the DL39 immune group could prevent HRB48 (GI)-induced harm in cats. According to the analysis of clinical symptoms, all cats in the positive control group of HRB48 exhibited obvious symptoms such as depression, anorexia, runny nose, and oral ulcers. Then, the clinical symptoms of each group were counted and scored in detail (Figure 6A). The positive control HRB48 group had the highest body temperature of 40.3°C, which started to drop and reach normal after 7 days, and the body weight increased slowly. In the immune and negative control groups, none of the aforementioned symptoms were observed (Figures 6B,C). Statistical analysis of the data regarding the amount of detoxification revealed a gradual decrease in the trend for each test group, both for the oral and nasal swabs and for the anal swabs. Overall, swabs from the positive control group had a significantly higher detoxification volume and longer duration of detoxification than those from the immune group (Figures 6D,E). The blood toxicity of each group was also analyzed. The blood virus content was higher in the positive control group than in the immune group, and the duration was longer for the positive control group. In addition, virus content in the positive control group was considerably higher than that in the immune control group when it reached the peak (Figure 6F). IgG and IgM content in each group was determined. IgM content in the

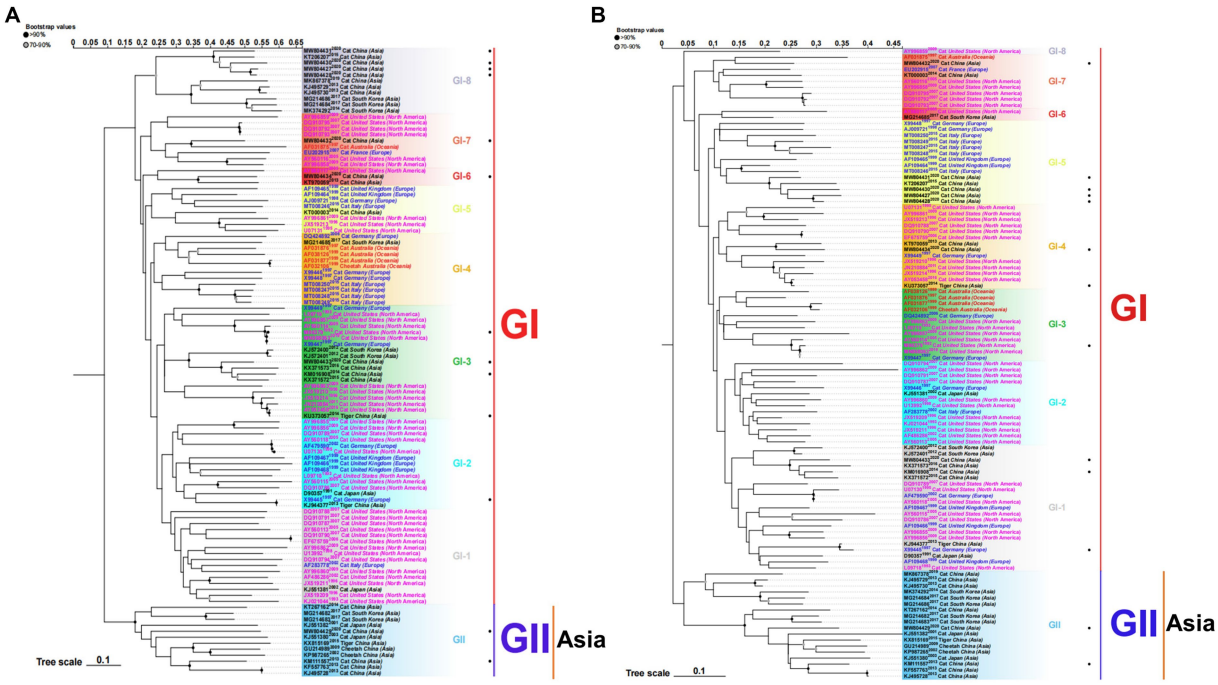

FIGURE 1
ML phylogenetic tree estimated from 105 FCV capsid (VP1) gene nucleotide sequences **(A)** and amino acid sequences **(B)** including the sequences of strains isolated in our laboratory and those downloaded from the NCBI. Model: JTT + G + I; Bootstrap: 1000 replicates. "·" represents the sequence used in this study. Each genotype is shaded by a different color and clearly marked. Strains isolated from different continents are color-coded for easier study. The scale bar indicates the mean number of nucleotide or amino acid substitutions per site. Phylogenetic tree modification: https://www.chiplot.online/.

TABLE 3 Determination of $TCID_{50}$ and PFU of 13 purified FCV strains.

Strains	PFU/ml	Strains	$TCID_{50}$/ml
DL31	5.1×10^7	DL31	2.57×10^8
DL37	3.7×10^8	DL37	3.73×10^9
DL38	3.16×10^9	DL38	1.58×10^{10}
DL39	6.7×10^8	DL39	3.16×10^9
HRB21	4.2×10^9	HRB21	2.15×10^{10}
HRB23	1.3×10^9	HRB23	6.31×10^9
HRB46	1.1×10^8	HRB46	5.88×10^8
HRB48	5.2×10^8	HRB48	2.68×10^9
HRB-SS	6.3×10^8	HRB-SS	3.16×10^9
F9	4.9×10^7	F9	1×10^8
TIG-1	1.2×10^8	TIG-1	6.31×10^8
FCV-2280	3.6×10^8	FCV-2280	3.89×10^9
FB-NJ-13	3×10^{10}	FB-NJ-13	1.58×10^{11}

experimental groups reached the peak at 12–14 days and then began to decline, and the IgM content in the positive control group was higher than that in the immune group (Figure 6G). The IgG content in the immune group remained at a high level, which was significantly greater than that in the positive control group. Measured values did not change significantly in the negative control group (Figure 6H).

3.7.3. Results of an attack challenge assay with FB-NJ-13 (genotype II virus)

An attack challenge assay on the FB-NJ-13 (GII) strain revealed that the DL39 immune group could prevent the FB-NJ-13 (GII)-induced harm in cats. According to the analysis of clinical symptoms, all cats in the positive control group of FB-NJ-13 exhibited obvious symptoms such as depression, anorexia, runny nose, and oral ulcers. Two cats in the FB-NJ-13 challenge positive control group exhibited symptoms of leg ulceration, and three cats had extremely severe oral ulcers. Then, the clinical symptoms of each group were counted and scored in detail (Figure 6A). The body temperature in the FB-NJ-13 positive control group increased to the highest level of 41.2°C, which started to drop and reached the normal levels after 7 days. The weight loss was more severe, which increased by day 9 (Figures 6B,C). Statistical analysis of the data regarding the amount of detoxification, blood toxicity, and antibody titration assays revealed an overall trend similar to the results of the HRB48 assay. The positive control group exhibited a greater amount of detoxification and a longer detoxification time, whereas the immune group had a significantly lower amount of detoxification (Figures 6D,E). Analysis of blood toxicity revealed that the positive control group had a higher blood virus level and a longer duration than the immune group (Figure 6F). IgG and IgM content in each group was measured, and IgM content in the experimental group peaked at 12–14 days and then began to decline (Figure 6G). IgG content in the immune group remained at a higher level and was significantly greater than that in the positive control group (Figure 6H). The measured values did not change significantly in the negative control group.

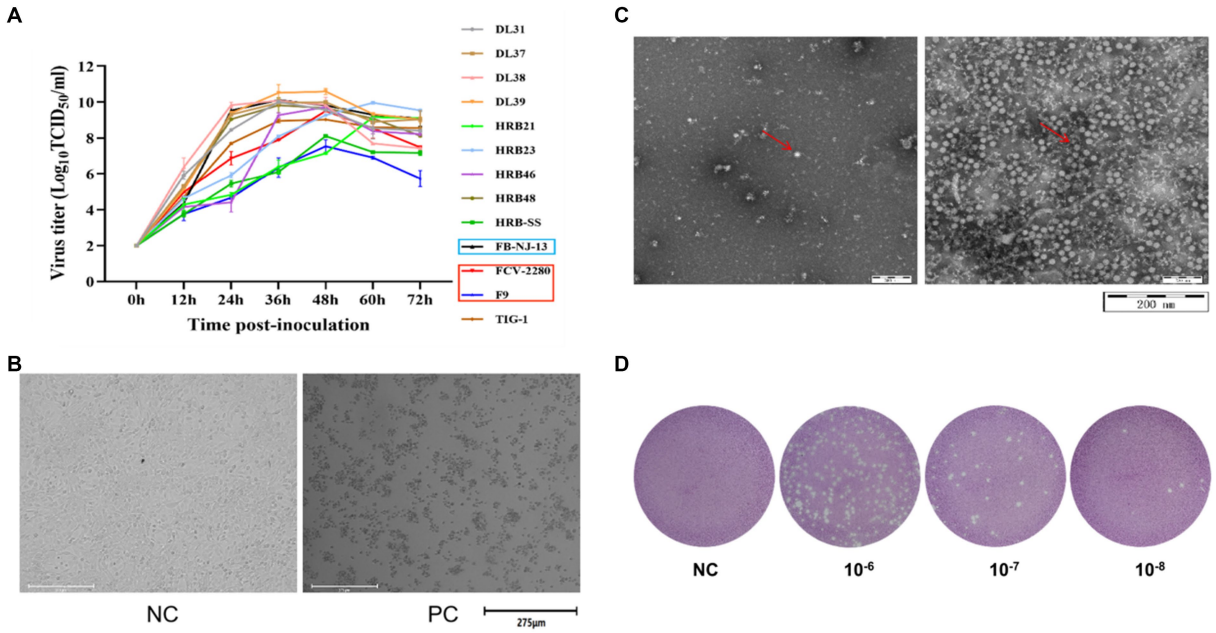

FIGURE 2
Preparation of immune antigens. **(A)** Determination of dynamic growth curves of the 13 FCV strains used in this study. **(B)** CRFK cells were infected with FCV strains. **(C)** FCV was purified, counterstained, and visualized through electron microscopy (left image is the untreated sample, right image is the purified sample). **(D)** Image of plaque test results of FCV strains (The results in above panel **(B-D)** are presented with the FCV-2280 strain as an example).

4. Discussion

FCV is a highly variable virus both genetically and antigenically, which makes its prevention difficult. FCV genotyping is also unclear. However, the VP1 gene is typically used as a locus of analysis for its genetic make-up because the FCV neutralization site is primarily located in the VP1 gene. Scholars have held different opinions on genotyping, possibly due to the different sequences selected. Some scholars believe that there is only one genotype, whereas others believe that FCV can be divided into two genotypes (Geissler et al., 1997; Sato et al., 2002; Sun et al., 2017; Kim et al., 2021). Based on this finding, we here downloaded the sequences of all (as of February 2020) VP1 genes of FCV from the NCBI for analysis and primarily established a phylogenetic tree based on the nucleotide sequence and amino acid sequence of the VP1 gene. The phylogenetic tree was constructed to provide novel insights into FCV prevention from an evolutionary perspective. Phylogenetic analysis of the available data led us to classify the present FCV strains into two major genotypes. Interestingly, all type GII strains were isolated from Asia, which is consistent with the previously reported view that some Asian strains are isolated as a single genotype. Moreover, to test the rationality of splitting the genotypes, we calculated genetic distance between different genotypes. Results have shown that the genetic distance between GI and GII genotypes is greater than that the between GI subtypes. According to the phylogenetic analysis results, the GII genotype is a novel genotype with a territorial origin. These findings may provide a new reference for furthering our understanding of FCV epidemiology and pathogenesis, and help provide novel ideas for our vaccine development.

TABLE 4 Animal morbidity scoring system.

Symptoms of onset	Severity of symptom	Scores
Oral ulcer	Severity	2
	Slight	1
	No	0
Eye and nose discharge	Severity	2
	Slight	1
	No	0
Body temperature	>40°C or < 38°C	2
	38–38.5°C or 39.5–40°C	1
	38.5–39.5°C	0
Body weight	Reduction of 10% and above	2
	Within 10% reduction	1
	Steady increase	0
Mental state	Mental depression and loss of appetite	2
	Mental depression or loss of appetite	1
	Normal	0
Other symptoms	Severity	2
	Slight	1
	No	0

Although all GII strains were isolated from Asia, temporal analysis revealed that a large proportion of the strains isolated from Asia in the past few years were spread across different genotypes,

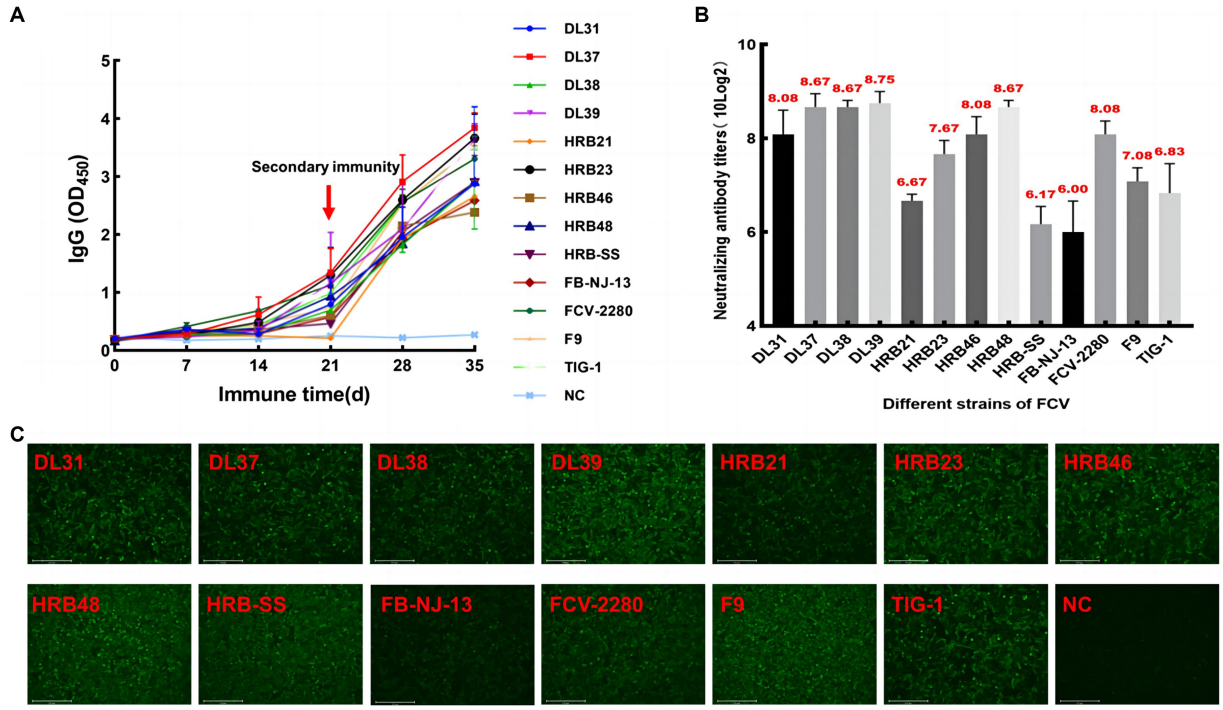

FIGURE 3
Monitoring and identification of mouse serum. **(A)** Dynamic monitoring of IgG antibody in immunized mice. **(B)** Neutralizing titers of pooled mouse serum against the parental virus. **(C)** Indirect immunofluorescent assay results based on each parent virus.

including the G1 genotype. This suggested that the FCV strains prevalent at this stage are not found only in the GII genotype, but in both genotypes. This is possibly the reason for poor FCV vaccine prevention and control in China. We did not identify any amino acid loci with clear typing features, presumably because some loci were not single amino acid mutations, but could result from mutations at multiple loci or from a combination of mutations at some loci. We need to investigate a larger number of strains to more accurately analyze the FCV genetic evolution and thus provide more accurate guidance for FCV prevention. In addition, the emergence of *VS*-FCV has made many researchers investigate the corresponding typing methods in anticipation of microscopic differences; however, no clear differences have been found (Schulz et al., 2011; Guo et al., 2018; Caringella et al., 2019). The present study failed to effectively classify the classical FCV and VSD strains; therefore, an exact conclusion cannot be drawn. Relevant typing studies are warranted in the future. Brunet et al. identified seven different amino acid residues as criteria for FCV typing (the analyzed VSD strains were isolated from France, the United Kingdom, and the United States) (Brunet et al., 2019), but the aforementioned typing method could not be not applied in the subsequent outbreak of VSD strains among cats in Australia (Bordicchia et al., 2021). Whether geographical differences lead to different characteristics of VSD strains in different regions and whether classical strains have geographical limitations are speculated. In addition, more sequences and detailed strain information are required to study FCV in detail and draw a more thorough and accurate conclusion.

Through the study of FCV genetic diversity, and especially the analysis of the VP1 gene, we investigated more effective vaccines for felines. So far, numerous FCV vaccines are commercially available, which are most commonly generated using the FCV F9 strain (Pedersen and Hawkins, 1995; Smith et al., 2020), FCV strain 21 (Rong et al., 2014), and FCV-255 strain (Scott, 1977). Some of them exist as multiplex vaccines; however, several controversies exist regarding the efficacy of available vaccines. For example, the F9 vaccine strain was highly effective in neutralizing 97% of the wild-type virus in six different European countries (Afonso et al., 2017); however, available commercial vaccines have a low neutralization titer for FCV in south west China when analyzed in terms of FCV prevalence in this region (Zhou et al., 2021). The efficacy of FCV vaccines in reducing clinical symptoms associated with classical FCV infections has also been reported in the literature (Johnson, 1992; Radford et al., 2006). Prolonged use of the same vaccine strain may lead to the emergence of wild-type recombinant strains containing the corresponding vaccine strain fragments, which may act as a barrier to disease control. To develop more effective vaccines, we here tried to screen out strains with a potential vaccine value according to the new typing results and thus provide guarantee for vaccine development. In total, 13 lab-preserved FCV strains (including 11 strains of GI and 2 strains of GII) were selected during this process, considering different genotypes and strains with different virulence (including TIG-1, a VSD strain isolated from tigers), as well as F9 and FCV-2280. In the first step of the screening process, SPF mice are used as a substitute for cats. Positive serum is prepared using surrogate animals such as mice and rabbits for neutralization tests to verify the corresponding neutralization titers (Spiri et al., 2021; Zhou et al., 2021). The use of heterologous animals for preparing a positive serum allows for more detailed control of the test, thereby

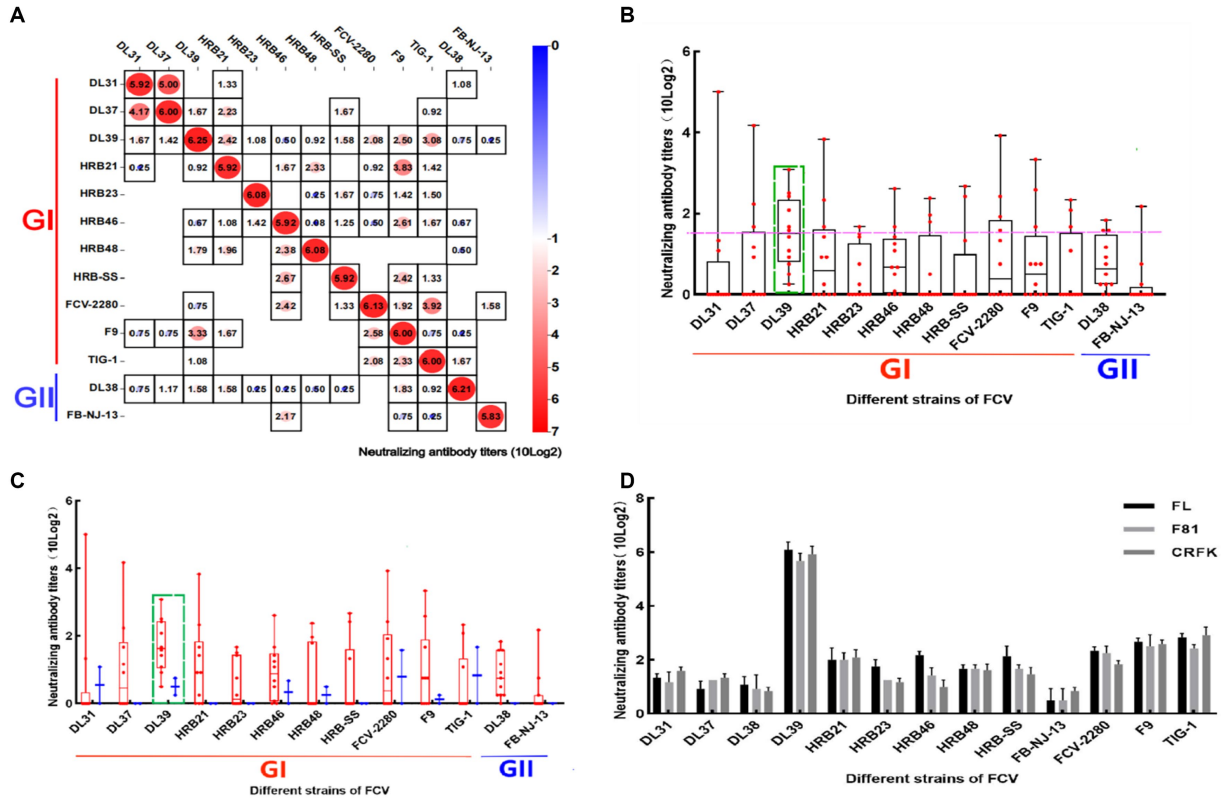

FIGURE 4
Cross neutralization assay of positive serum in mice. **(A)** Results of the cross-neutralization test between FCV strains. Each figure represents the result of a cross -neutralization assay for a serum (the name of the serum is mentioned above the legend, the ordinate is the titer of the virus, 10 (log2) is used to calculate the final value, and the horizontal coordinate is the name of the virus used in the assay). **(B)** Box and violin plots of cross-neutralization titers for each strain. **(C)** Box and violin plots of cross-neutralization titers for each strain of GI and GII genotypes. **(D)** Cross-neutralization test results of the DL39 strain in different cat cell lines.

reducing the impact of errors on the results. Furthermore, 10 SPF mice with a body weight error of ±0.2 g were used in this study, and the inactivated strain was purified using the same immune dose. The positive serum from each strain collected was subjected to neutralization titers. Based on the results, all sera were diluted to the same neutralization titer for the cross-neutralization assay, thus reducing the effect of non-specificity and ensuring the reliability of the results.

Although this study expected to screen multiple strains as potential vaccine candidates for further study, *in vitro* neutralization assays indicated that only DL39 exhibited better cross-neutralization titration for all strains and may be used as a vaccine candidate. The remaining strains exhibited poor cross-neutralization compared with DL39. Results from cross-neutralization assays using the mouse serum also demonstrated that the DL39 strain has better cross-neutralization properties. Although the number of strains belonging to the two genotypes used in the trial were different, with fewer strains of the GII type, the serum of the DL39 strain provided better protection against the GI strain. In addition, DL39 was isolated from respiratory swabs of healthy cats. In subsequent animal regression tests, DL39 caused only a slight increase in body temperature, which indicated that this strain could be used as a vaccine and was associated with reduced risk of infection. Further *in vivo* animal challenges were conducted to verify the potential capability of the screened strain to be a vaccine. To overcome individual differences (each cat is highly variable), three cats were immunized simultaneously. All the three cats were born at the same time and bred to the test phase. They all had nearly the same weight. Each cat was immunized with the same inactivated virus value to reduce error. The cross-neutralization assay performed after serum collection revealed that the DL39 strain produced antibody titers against all strains used in the study and was thus protective against all strains of different genotypes. It also produced high antibody titers against the VSD strain.

Again, the broad neutralization spectrum of DL39 was evident from the results of the *in vitro* cell-mediated neutralization assay, which are in agreement with the results obtained with our replacement animal, the SPF mice. We subsequently conducted a corresponding FCV challenge assay with two GI and GII strains (HRB48 and FB-NJ-13) that could produce significant pathogenicity for a better comparison. During the challenge in the attack phase, the growth status and pathologic features of the cats in each group were recorded in detail, and their oral and nasal swabs, anal swabs, blood viral load, and serum IgG and IgM concentrations were continuously recorded.

On comparing the results, both the buccal and nasal swabs taken indicated the presence of FCV in the cats of the test groups, although the amount of detoxification decreased over time in both groups, the

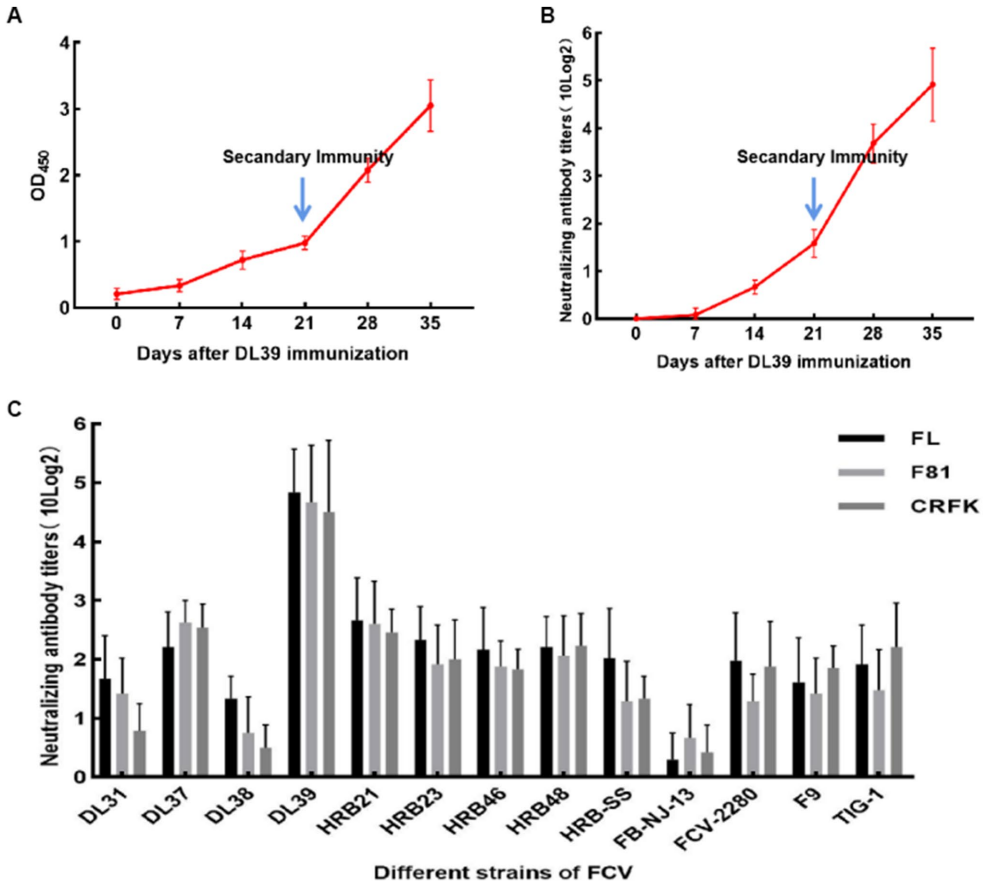

FIGURE 5
Serological test results of cats immunized after inactivation of DL39 strain. **(A)** Determination of serum IgG at different time points. **(B)** The titer of the neutralization test was determined with the parental virus at different time points. **(C)** Neutralization test titers with 13 FCV strains after the completion of immunization in different cat cell lines.

immune challenge group was significantly less detoxified compared with the positive control group. FCV can be classified into respiratory FCV and intestinal FCV (Guo et al., 2022) depending on the location of separation. The former was isolated from nasopharyngeal swabs and the latter from anal swabs, but FCV could be detected throughout the challenge period by using oral and nasal swabs, as well as anal swabs. Moreover, both challenge strains were isolated from the respiratory tract. However, the accuracy of this classification is yet to be verified. Interestingly, FCV was found to be present in the blood but viremia is relatively uncommon for classical FCV strains (Pesavento et al., 2008). Studies of this virus have revealed that its functional fJAM-A receptor is also found on peripheral blood platelets and leukocytes (Pesavento et al., 2011) rather than only on epithelial cells and endothelial tissues, which suggests that FCV is causing viremia in the cat itself.

In both the positive control group and the immune challenge group, blood virus levels declined to the same level as that in the negative control at 2 weeks. Of concern is the potential for the virus present in the blood to increase the route of virus transmission, such as in hematophagous amputees (Mencke et al., 2009), and the study again supports the possibility of this finding. Virus levels and duration in the blood were lower in the immune challenge group than in the respective positive control group, which also suggested that the DL39 strain was protective. Although IgM levels were not significantly different among the groups tested, IgG levels were higher in the immune-challenged group than in the positive control group.

In this study, various methods were used to make the trial as close to perfect as possible. Unsurprisingly, the study had some limitations. The study used a small number of cats and sample sizes for animal testing and would have yielded more accurate results with more animals. Therefore, the trial involved a single dose and vaccination procedure, but the results were convincing in terms of both the dose and inoculation method, because our laboratory has performed many similar animal experiments previously and has sufficient theoretical underpinnings. The simultaneous use of quantitative real-time fluorescence PCR assays for detecting detoxification and viremia does not allow for the efficient uniform quantification of FCV in swabs and does not guarantee if the FCV in the blood is a live virus with pathogenic potential. However, the final data revealed that all the results have some regularity and the infective FCV was also isolated from the serum in subsequent tests, which successfully compensates for the aforementioned shortcomings. Most importantly, a larger number of strains must be isolated for analysis and for performing challenge assays to verify

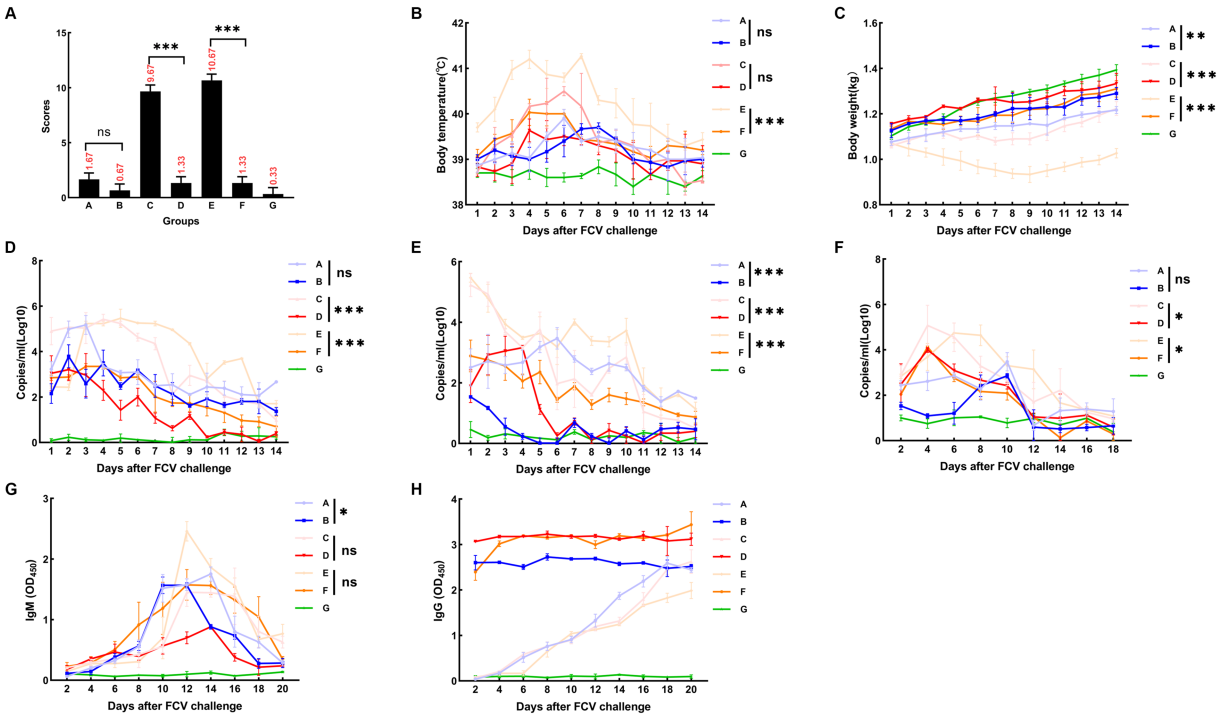

FIGURE 6
FCV challenge assay after immunization with DL39 strain [**(A)** DL39 strain challenge test group. **(B)** The DL39 strain challenged the experimental group after immunization with the DL39 strain. **(C)** HRB48 strain challenge test group. **(D)** The HRB48 strain challenged the experimental group after immunization with the DL39 strain. **(E)** FB-NJ-13 strain challenge test group. **(F)** The FB-NJ-13 strain challenged the experimental group after immunization with the DL39 strain. **(G)** Control group; "ns" no significance, "*"$p<0.05$, "**"$p<0.01$, "***"$p<0.001$. **(A)** Histogram of clinical symptom scores for different groups after the DL39 challenge, with higher scores representing more severe clinical symptoms. **(B)** Body temperature statistics of each group. **(C)** Body weight statistics of each group. **(D)** Detection of viral RNA in oral swabs through RT-qPCR after the DL39 challenge. **(E)** Detection of viral RNA in anal swabs through RT-qPCR after the DL39 challenge. **(F)** Detection of viral RNA in blood through RT-qPCR after the DL39 challenge. **(G)** Determination of IgM in serum. **(H)** Determination of IgG in serum.

the efficacy of the DL39 strain (including the *VS*-FCV strain). HRB48 and FB-NJ-13 were selected for the intertype challenge assay because they belong to different genotypes, have the potential to produce significant lesions, and are representative of strains that have prevailed in China during the recent years. Indisputably, the DL39 vaccine strain has exhibited excellent broad-spectrum performance in *in vitro* neutralization assays and high antibody titers against the *VS*-FCV strain (FCV-2280 and TIG-1). This provides evidence that cats immunized with the DL39 strain have the potential to withstand the challenge with the *VS*-FCV strain. Although the DL39 strain originally screened in this assay is still far from being validated as a vaccine strain, based on the aforementioned results, we confirm that this strain has a great potential to become a vaccine strain with broad-spectrum protection, and future trials are required to validate the DL39 strain in various ways to further evaluate immune protection.

5. Conclusion

In the present study, FCV was categorized into two genotypes: GI and GII. Strains in the GI genotype are still circulating worldwide, but those in the GII genotype are of Asian origin with some degree of territoriality. The *in vitro* neutralization assay of the initially screened DL39 strain revealed that it had good broad-spectrum properties. The *in vivo* attack assay demonstrated protection against GI (DL39 and HRB48) and GII (FB-NJ-13) strains. The DL39 strain initially screened in this study exhibited a good preventive effect against FCV.

Data availability statement

The datasets presented in this study can be found in online repositories. The names of the repository/repositories and accession number(s) can be found in the article/supplementary material.

Ethics statement

The animal studies were approved by The Harbin Veterinary Research Institutional Animal Care Committee. The studies were conducted in accordance with the local legislation and institutional requirements. Written informed consent was obtained from the owners for the participation of their animals in this study.

Author contributions

YY, JL, and LQ: conceptualization and visualization. YY, ZL, MC, KF, RQ, YZ, YW, HK, JL, and LQ: methodology. YY: formal analysis, data curation, writing – original draft preparation, and project administration. YY, ZL, and MC: investigation. YY, ZL, MC, KF, RQ, YZ, YW, HK, QJ, MY, JL, and LQ: writing – review and editing. JL and LQ: supervision and funding acquisition. All authors contributed to the article and approved the submitted version.

Funding

This work was supported by National Key Research and Development Program of China, NKRDPC, 2019YFC1200701.

Conflict of interest

The authors declare that the research was conducted in the absence of any commercial or financial relationships that could be construed as a potential conflict of interest.

Publisher's note

All claims expressed in this article are solely those of the authors and do not necessarily represent those of their affiliated organizations, or those of the publisher, the editors and the reviewers. Any product that may be evaluated in this article, or claim that may be made by its manufacturer, is not guaranteed or endorsed by the publisher.

References

Afonso, M. M., Pinchbeck, G. L., Smith, S. L., Daly, J. M., Gaskell, R. M., Dawson, S., et al. (2017). A multi-national European cross-sectional study of feline calicivirus epidemiology, diversity and vaccine cross-reactivity. *Vaccine* 35, 2753–2760. doi: 10.1016/j.vaccine.2017.03.030

Bordicchia, M., Fumian, T. M., Van Brussel, K., Russo, A. G., Carrai, M., Le, S. J., et al. (2021). Feline Calicivirus virulent systemic disease: clinical epidemiology, analysis of viral isolates and in vitro efficacy of novel antivirals in Australian outbreaks. *Viruses* 13:2040. doi: 10.3390/v13102040

Brunet, S., Sigoillot-Claude, C., Pialot, D., and Poulet, H. (2019). Multiple correspondence analysis on amino acid properties within the variable region of the capsid protein shows differences between classical and virulent systemic feline Calicivirus strains. *Viruses* 11:1090. doi: 10.3390/v11121090

Caringella, F., Elia, G., Decaro, N., Martella, V., Lanave, G., Varello, K., et al. (2019). Feline calicivirus infection in cats with virulent systemic disease, Italy. *Res. Vet. Sci.* 124, 46–51. doi: 10.1016/j.rvsc.2019.02.008

Coyne, K. P., Dawson, S., Radford, A. D., Cripps, P. J., Porter, C. J., McCracken, C. M., et al. (2006). Long-term analysis of feline calicivirus prevalence and viral shedding patterns in naturally infected colonies of domestic cats. *Vet. Microbiol.* 118, 12–25. doi: 10.1016/j.vetmic.2006.06.026

Di Martino, B., Di Rocco, C., Ceci, C., and Marsilio, F. (2009). Characterization of a strain of feline calicivirus isolated from a dog faecal sample. *Vet. Microbiol.* 139, 52–57. doi: 10.1016/j.vetmic.2009.04.033

Fastier, L. B. (1957). A new feline virus isolated in tissue culture. *Am. J. Vet. Res.* 18, 382–389.

Gao, Y. W., Xia, X. Z., Hu, R. L., Huang, G., Xu, C. Z., and Wang, T. D. (2003). Characterization and hypervariable region analysis of two feline calicivirus isolates from cheetah and tiger. *Chin. J. Prev. Vet. Med.* 2003, 19–22.

Geissler, K., Schneider, K., Platzer, G., Truyen, B., Kaaden, O. R., and Truyen, U. (1997). Genetic and antigenic heterogeneity among feline calicivirus isolates from distinct disease manifestations. *Virus Res.* 48, 193–206. doi: 10.1016/S0168-1702(97)01440-8

Geissler, K., Schneider, K., and Truyen, U. (2002). Mapping neutralizing and non-neutralizing epitopes on the capsid protein of feline calicivirus. *J. Vet. Med. B Infect. Dis Vet. Public Health* 49, 55–60. doi: 10.1046/j.1439-0450.2002.00529.x

Guo, J. F., Ding, Y. B., Sun, F. Y., Zhou, H. B., He, P., Chen, J. C., et al. (2022). Co-circulation and evolution of genogroups I and II of respiratory and enteric feline calicivirus isolates in cats. *Transbound. Emerg. Dis.* 69, 2924–2937. doi: 10.1111/tbed.14447

Guo, H., Miao, Q., Zhu, J., Yang, Z., and Liu, G. (2018). Isolation and molecular characterization of a virulent systemic feline calicivirus isolated in China. *Infect. Genet. Evol.* 65, 425–429. doi: 10.1016/j.meegid.2018.08.029

Johnson, R. P. (1992). Antigenic change in feline calicivirus during persistent infection. *Can. J. Vet. Res.* 56, 326–330.

Jones, D. T., Taylor, W. R., and Thornton, J. M. (1992). The rapid generation of mutation data matrices from protein sequences. *Comput. Appl. Biosci.* 8, 275–282. doi: 10.1093/bioinformatics/8.3.275

Kadoi, K., Kiryu, M., Iwabuchi, M., Kamata, H., Yukawa, M., and Inaba, Y. (1997). A strain of calicivirus isolated from lions with vesicular lesions on tongue and snout. *New Microbiol.* 20, 141–148.

Kim, S. J., Kim, C., Chung, H. C., Park, Y. H., and Park, K. T. (2021). Full-length ORF2 sequence-based genetic and phylogenetic characterization of Korean feline caliciviruses. *J. Vet. Sci.* 22:e32. doi: 10.4142/jvs.2021.22.e32

Kumar, S., Stecher, G., Li, M., Knyaz, C., and Tamura, K. (2018). MEGA X: molecular evolutionary genetics analysis across computing platforms. *Mol. Biol. Evol.* 35, 1547–1549. doi: 10.1093/molbev/msy096

Mencke, N., Vobis, M., Mehlhorn, H., Haese, J. D., Rehagen, M., Mangold-Gehring, S., et al. (2009). Transmission of feline calicivirus via the cat flea (Ctenocephalides felis). *Parasitol. Res.* 105, 185–189. doi: 10.1007/s00436-009-1381-5

Neill, J. D. (1990). Nucleotide sequence of a region of the feline calicivirus genome which encodes picornavirus-like RNA-dependent RNA polymerase, cysteine protease and 2C polypeptides. *Virus Res.* 17, 145–160. doi: 10.1016/0168-1702(90)90061-F

Neill, J. D. (1992). Nucleotide sequence of the capsid protein gene of two serotypes of San Miguel Sea lion virus: identification of conserved and non-conserved amino acid sequences among calicivirus capsid proteins. *Virus Res.* 24, 211–222. doi: 10.1016/0168-1702(92)90008-W

Neill, J. D., Reardon, I. M., and Heinrikson, R. L. (1991). Nucleotide sequence and expression of the capsid protein gene of feline calicivirus. *J. Virol.* 65, 5440–5447. doi: 10.1128/jvi.65.10.5440-5447.1991

Pedersen, N. C., Elliott, J. B., Glasgow, A., Poland, A., and Keel, K. (2000). An isolated epizootic of hemorrhagic-like fever in cats caused by a novel and highly virulent strain of feline calicivirus. *Vet. Microbiol.* 73, 281–300. doi: 10.1016/S0378-1135(00)00183-8

Pedersen, N. C., and Hawkins, K. F. (1995). Mechanisms for persistence of acute and chronic feline calicivirus infections in the face of vaccination. *Vet. Microbiol.* 47, 141–156. doi: 10.1016/0378-1135(95)00101-F

Pesavento, P. A., Chang, K. O., and Parker, J. S. (2008). Molecular virology of feline calicivirus. *Vet. Clin. North Am. Small Anim. Pract.* 38, 775–786. doi: 10.1016/j.cvsm.2008.03.002

Pesavento, P. A., Stokol, T., Liu, H., van der List, D. A., Gaffney, P. M., and Parker, J. S. (2011). Distribution of the feline calicivirus receptor junctional adhesion molecule a in feline tissues. *Vet. Pathol.* 48, 361–368. doi: 10.1177/0300985810375245

Radford, A. D., Coyne, K. P., Dawson, S., Porter, C. J., and Gaskell, R. M. (2007). Feline calicivirus. *Vet. Res.* 38, 319–335. doi: 10.1051/vetres:2006056

Radford, A. D., Dawson, S., Coyne, K. P., Porter, C. J., and Gaskell, R. M. (2006). The challenge for the next generation of feline calicivirus vaccines. *Vet. Microbiol.* 117, 14–18. doi: 10.1016/j.vetmic.2006.04.004

Rong, S., Lowery, D., Floyd-Hawkins, K., and King, V. (2014). Characterization of an avirulent FCV strain with a broad serum cross-neutralization profile and protection against challenge of a highly virulent vs feline calicivirus. *Virus Res.* 188, 60–67. doi: 10.1016/j.virusres.2014.03.007

Sato, Y., Ohe, K., Murakami, M., Fukuyama, M., Furuhata, K., Kishikawa, S., et al. (2002). Phylogenetic analysis of field isolates of feline calcivirus (FCV) in Japan by sequencing part of its capsid gene. *Vet. Res. Commun.* 26, 205–219. doi: 10.1023/A:1015253621079

Schulz, B. S., Hartmann, K., Unterer, S., Eichhorn, W., Majzoub, M., Homeier-Bachmann, T., et al. (2011). Two outbreaks of virulent systemic feline calicivirus infection in cats in Germany. *Berl. Munch. Tierarztl. Wochenschr.* 124, 186–193. doi: 10.2376/0005-9366-124-186

Scott, F. W. (1977). Evaluation of a feline viral rhinotracheitis-feline calicivirus disease vaccine. *Am. J. Vet. Res.* 38, 229–234.

Seal, B. S., Ridpath, J. F., and Mengeling, W. L. (1993). Analysis of feline calicivirus capsid protein genes: identification of variable antigenic determinant regions of the protein. *J. Gen. Virol.* 74, 2519–2524. doi: 10.1099/0022-1317-74-11-2519

Smith, S. L., Afonso, M. M., Pinchbeck, G. L., Gaskell, R. M., Dawson, S., and Radford, A. D. (2020). Temporally separated feline calicivirus isolates do not cluster phylogenetically and are similarly neutralised by high-titre vaccine strain FCV-F9 antisera in vitro. *J. Feline Med. Surg.* 22, 602–607. doi: 10.1177/1098612X19866521

Sosnovtsev, S. V., and Green, K. Y. (2000). Identification and genomic mapping of the ORF3 and VPg proteins in feline calicivirus virions. *Virology* 277, 193–203. doi: 10.1006/viro.2000.0579

Spiri, A. M., Riond, B., Stirn, M., Novacco, M., Meli, M. L., Boretti, F. S., et al. (2021). Modified-live feline Calicivirus vaccination reduces viral RNA loads, duration of RNAemia, and the severity of clinical signs after heterologous feline Calicivirus challenge. *Viruses* 13:1505. doi: 10.3390/v13081505

Sun, Y. X., Deng, M. L., Peng, Z., Hu, R. M., Chen, H. C., and Wu, B. (2017). Genetic and phylogenetic analysis of feline calicivirus isolates in China. *Vet. J.* 220, 24–27. doi: 10.1016/j.tvjl.2016.12.014

Tian, J., Liu, D. F., Liu, Y. X., Wu, H. X., Jiang, Y. M., Zu, S. P., et al. (2016). Molecular characterization of a feline calicivirus isolated from tiger and its pathogenesis in cats. *Vet. Microbiol.* 192, 110–117. doi: 10.1016/j.vetmic.2016.07.005

Tohya, Y., Yokoyama, N., Maeda, K., Kawaguchi, Y., and Mikami, T. (1997). Mapping of antigenic sites involved in neutralization on the capsid protein of feline calicivirus. *J. Gen. Virol.* 78, 303–305. doi: 10.1099/0022-1317-78-2-303

Weeks, M. L., Gallagher, A., and Romero, C. H. (2001). Sequence analysis of feline caliciviruses isolated from the oral cavity of clinically normal domestic cats (*Felis catus*) in Florida. *Res. Vet. Sci.* 71, 223–225. doi: 10.1053/rvsc.2001.0491

Zhou, L., Fu, N. S., Ding, L., Li, Y., Huang, J., Sha, X., et al. (2021). Molecular characterization and cross-reactivity of feline Calicivirus circulating in southwestern China. *Viruses* 13:1812. doi: 10.3390/v13091812

frontiers | Frontiers in Microbiology

TYPE Original Research
PUBLISHED 05 October 2023
DOI 10.3389/fmicb.2023.1264172

OPEN ACCESS

EDITED BY
Jingqiang Ren,
Wenzhou University, China

REVIEWED BY
Hang Su,
Albert Einstein College of Medicine, United States
Fangfeng Yuan,
Massachusetts Institute of Technology, United States

*CORRESPONDENCE
Lidia Sánchez-Morales
lidsan05@ucm.es

RECEIVED 20 July 2023
ACCEPTED 22 September 2023
PUBLISHED 05 October 2023

CITATION
Sánchez-Morales L, Sánchez-Vizcaíno JM, Domínguez L and Barroso-Arévalo S (2023) A retrospective study of SARS-CoV-2 seroprevalence in dogs and cats in the Community of Madrid, Spain. *Front. Microbiol.* 14:1264172. doi: 10.3389/fmicb.2023.1264172

A retrospective study of SARS-CoV-2 seroprevalence in dogs and cats in the Community of Madrid, Spain

Lidia Sánchez-Morales [1]*, José M. Sánchez-Vizcaíno[1,2], Lucas Domínguez[1,2] and Sandra Barroso-Arévalo[1,2]

[1]VISAVET Health Surveillance Centre, Complutense University of Madrid, Madrid, Spain, [2]Department of Animal Health, Faculty of Veterinary Science, Complutense University of Madrid, Madrid, Spain

To date, susceptibility to SARS-CoV-2 infection in domestic animals including cats and dogs has been described. However, it is important to carry out passive surveillance of these animals to be aware of any changes in the outcomes of the disease in these species that may occur. In this study, we have performed a retrospective study in which we analyzed sera (*n* = 1,640) from random animals: dogs (*n* = 1,381) and cats (*n* = 259) belonging to both homes (*n* = 1,533) and animal protection centers (*n* = 107) in the Community of Madrid, Spain. Neutralizing antibodies were evaluated between November 2021 and May 2022 using a surrogate ELISA kit to determine the seroprevalence. Based on the results obtained, a few animals (both cats and dogs) presented neutralizing antibodies to SARS-CoV-2 (2.3%), all of them from private owners. However, the seroprevalence in cats (4.6%) resulted to be almost twice as much as in dogs (1.9%) which reinforces that cats' susceptibility to the infection seems higher than in the case of dogs, maybe due to the lower ACE2 expression of the dogs in the respiratory tract. These findings also confirm that the probability of infection is considerably higher in domestic animals in close contact with infected owners, compared to animals living in animal shelters whose contact with humans is markedly lower.

KEYWORDS

seroprevalence, SARS-CoV-2, domestic animals, antibodies, Spain

1. Introduction

Since the beginning of the pandemic (December 2019) caused by the severe acute respiratory syndrome coronavirus 2 (SARS-CoV-2), more than 6 million deaths and over 664 million cases have been reported worldwide (World Health Organization [WHO], 2022). Many vaccine prototypes have been developed for the coronavirus disease 2019 (COVID-19) in a very short time (Hahn and Wiley, 2022) and more than 13,000 million vaccine doses have already been administered (World Health Organization [WHO], 2022). COVID-19 is a disease of potential zoonotic origin whose host affinity is determined by the virus' spike protein (S) (Wan et al., 2020). This protein binds to host cells through the angiotensin-converting enzyme 2 (ACE2) protein receptor which is present in many animal species (Wan et al., 2020). The variety of animal species in which the natural infection with SARS-CoV-2

virus has been detected ranges from domestic to wild animals (Sit et al., 2020; Palmer et al., 2021). In addition, further species have been reported to be susceptible to the virus according to experimental studies such as domestic swine (Pickering et al., 2021) and cattle or goats (Bosco-Lauth et al., 2021). The natural detection of the disease in animals as well as their potential role as intermediate or reservoir hosts led to the need of studying the disease in different experimental animal models (Halfmann et al., 2020; Shi et al., 2020).

Although domestic animals do not seem to suffer from serious consequences in terms of clinical signs from SARS-CoV-2 infection, it is important to carry out active and passive surveillance programs to monitor the presence of the disease as well as the infection trends in the different susceptible animal species. In addition to domestic animals, the virus has been detected in wild species such as white-tailed deer (*Odocoileus virginianus*) (Palmer et al., 2021) and mink (Neovison vison) on mink farms (Larsen et al., 2021; Oude Munnink et al., 2021). In these farms, it was found that the disease had passed from humans to mink and back to humans. Another novel finding is the study of Sila et al. (2022) that hypothesizes the transmission of the disease from an infected cat with SARS-CoV-2 to its veterinarian.

The presence of an active infection in these animals can be evaluated by the detection of viral RNA by a reverse transcription quantitative real-time polymerase chain reaction (RT-qPCR), commonly from samples such as nasopharyngeal or oropharyngeal swabs (Sule and Oluwayelu, 2020). However, viral RNA can only be determined a few days after the infection (Meekins et al., 2021), whereas antibody detection can be performed a long time after the infective period, in order to elucidate whether animals have been exposed to the virus or not. The evidence of infection has already been confirmed by the detection of anti-SARS-CoV-2 antibodies in several field studies conducted on domestic animals in continuous contact with their RT-qPCR-positive owners (Michelitsch et al., 2020, 2021; Patterson et al., 2020; Zhang et al., 2020; Dileepan et al., 2021; Fritz et al., 2021; Stevanovic et al., 2021).

Given all these events related to animals, as well as the continuous appearance of new variants, the importance of sanitary surveillance of the disease in animals is emphasized. To improve the current knowledge on this topic, the present study retrospectively evaluates the seroprevalence of the infection in dogs and cats in the Community of Madrid, a region with a high incidence of disease in humans.

2. Materials and methods

A total of 1,640 serum samples randomly chosen from companion animals (1,381 dogs and 259 cats) were collected from November 2021 to May 2022 in the Community of Madrid and sent to the VISAVET Health Surveillance Center for their analysis. The samples were transported from the laboratory to VISAVET center by a transport company under the regulations stated in UN3373. Upon arrival at the center, samples were taken to the biosafety level 3 (BLS3) facilities and stored at 4°C for processing and further analysis. The information available for each of the samples was: the animal species, the date of sampling and their origin [households or animal protection centers (APCs)] with no data regarding clinical signs or contact with positive owners/caretakers.

A detection of antibodies by SARS-CoV-2 Neutralizing Antibody Detection Kit (GenScript Inc., Piscataway, NJ, United States) was made. The procedure was carried out on all the samples using the GenScript cPass^{TM} SARS-CoV-2 Neutralizing Antibody Detection Kit in which the protein-protein interaction between HRP-RBD (horseradish peroxidase-receptor binding domain) and human angiotensin-converting enzyme II (hACE2) can be blocked by neutralizing antibodies against SARS-CoV-2 RBD, which was already validated (Perera et al., 2021). Samples and controls are diluted with a sample dilution buffer and pre-incubated with the HRP-RBD diluted solution to allow the binding of the circulating neutralization antibodies to HRP-RBD. The mixture is then added to the capture plate which is pre-coated with the hACE2 protein and incubated at. The unbound HRP-RBD as well as any HRP-RBD bound to non-neutralizing antibody will be captured on the plate, while the circulating neutralizing antibodies HRP-RBD complexes remain in the supernatant and get removed during washing. Following a four-wash cycle, solution is added and incubated in dark and then followed by the Stop Solution. The reaction is quenched, and the color turns yellow. The absorbance of the sample is inversely dependents on the titer of the anti-SARS-CoV-2 neutralizing antibodies. Results of each individual samples was calculated using the following formula:

$$\text{Inhibition (\%)} = \left(1 - \left(\frac{\text{OD value of sample}}{\text{OD value of Negative control}}\right) \times 100\right)$$

Samples presenting a cutoff higher or equal to 30% are considered positive results indicating the presence of SARS-CoV-2 neutralizing antibodies and lower than 30% are considered negative results according to the manufacturer's instructions. This negative result indicates the absence or a level of SARS-CoV-2 neutralizing antibodies lower than the limit of detection, but it can also appear in samples taken during an acute infection before antibody seroconversion.

For the statistical analysis, a Chi-square test was performed to assess if there was any difference in the proportion of seropositivity to SARS-CoV-2 between species. All statistical analyses were performed with IBM® SPSS® Statistics v. 23.0.

3. Results

Thirty-eight samples from animals living in houses (26 dogs and 12 cats) out of the total analyzed (n = 1,640) were positive (inhibition percentages between 30 and 94%) for the SARS-CoV-2 Neutralizing Antibody Detection kit, which represented a seroprevalence of 0.023 (38/1,640) of the total (CI 95%: 0.017–0.032). The results depending on species and their origin are represented in **Table 1**.

The number of positive animals sampled over the months as well as accumulative incidence in humans along those months are shown in **Figure 1**.

A significant difference between seropositivity and species (dogs and cats) was found (p-value = 0.007). The seroprevalence in cats reached 0.046 (CI 95%: 0.027–0.079) while in dogs it was 0.019 (CI 95%: 0.013–0.027). All the positive samples, both from cats and dogs proceeded from private owners living in houses.

10.3389/fmicb.2023.1264172

TABLE 1 Positive animals to the presence of neutralizing antibodies out of the total depending on origin.

Species	Seropositive animals/total	Origin	No. of sera	No. of positive samples (%) based on species and origin
Dogs	26/1,381 (1.9%)	APCs	80	0 (0.0%)
		Households	1,301	26 (2%)
Cats	12/259 (4.6%)	APCs	27	0 (0.0%)
		Households	232	12 (5.2%)

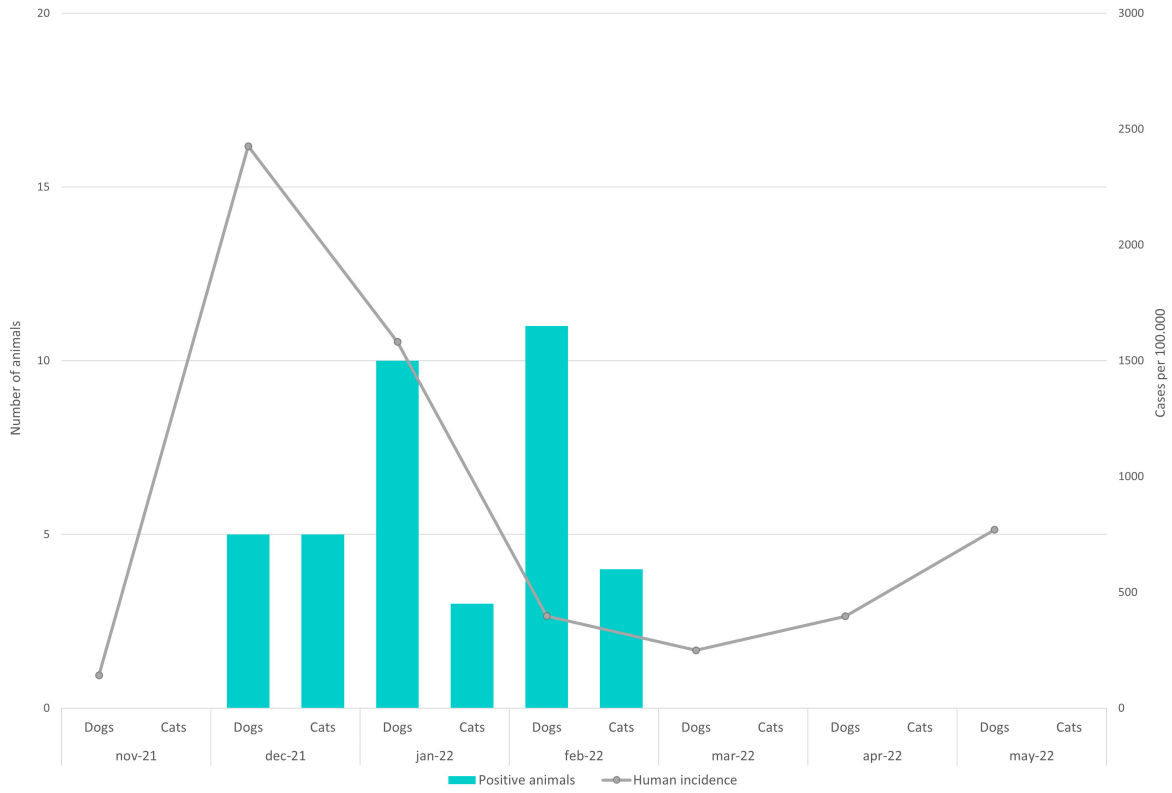

FIGURE 1
Graphical representation showing on a monthly basis the number of dogs and cats presenting neutralizing antibodies against SARS-CoV-2. In addition, the accumulated incidence in humans during the same months in the Community of Madrid is represented.

4. Discussion

Numerous studies have already demonstrated the susceptibility of dogs and cats to SARS-CoV-2 infection (Dileepan et al., 2021; Fritz et al., 2021), so the control and surveillance of the disease in these companion animals is considered of a great importance. In this study, we have evidenced a low seroprevalence in cats and dogs, being all the positive samples from household animals. Sampling of the animals was carried out mainly between November 2021 and February 2022, dates which coincide with the time when the Omicron variant appeared in Spain. Moreover, in mid-December 2021, almost 50% of the sequenced samples in humans belonged to the Omicron variant, while the rest of the sequenced samples belonged to the Delta variant. One month later, the number of cases per 100,000 inhabitants increased exponentially and by mid-January 2022, 95% of the sequenced samples were of the Omicron variant (World Health Organization [WHO], 2022). In the present retrospective randomized study, we have no information on the health status of the animal owners or the degree of contact with the animals. Even though we do not have this information, the appearance of the Omicron variant greatly increased the incidence in people, so this, together with the dates, suggests that in this sampling we could be detecting antibodies to this new variant of concern. However, the Omicron variant was already found to have a lower immunogenicity than previous variants and does not seem to induce a strong antibody response, (Sánchez-Morales et al., 2022; Tyson et al., 2023) which could mean that the antibodies we are detecting are derived from previous variants. However, the emergence of the Omicron variant greatly increased the incidence in people, so this, together with sampling dates, suggests that we may be detecting antibodies to this variant of concern.

The fact that only household animals tested positive for this study is consistent with numerous studies in which a continued exposure of animals to infected people seems to be a determining factor (Dileepan et al., 2021; Bessière et al., 2022). None of the animals from APCs showed neutralizing antibodies, which might

be due to the fact that these animals do not have as continuous and close contact with people as household animals do with their owners. In animal shelters, animals have much more limited contact with their caretakers at specific times. The same negative results were obtained in a study carried out in Italy in stray cats (Stranieri et al., 2022) and similar, with a very low seroprevalence (0.009%) (van der Leij et al., 2021) in animals from APCs in Netherlands.

In addition, we have observed that the prevalence of the presence of neutralizing antibodies in cats (4.6%) was higher than in dogs (1.9%). These results coincide with seroprevalence studies carried out in Minnesota (Dileepan et al., 2021), Italy (Patterson et al., 2020), the UK (Smith et al., 2021), and France (Bessière et al., 2022) with much higher seroprevalence percentages in cats than dogs. In fact, in experimental infection studies, it has been demonstrated that cats are much more susceptible to the infection than dogs (Shi et al., 2020), they can spread SARS-CoV-2 to other cats and sometimes even develop lesions (Bao et al., 2021; Chiba et al., 2021) and have symptoms (Natale et al., 2021). All these results could be related to the lower expression of ACE2 receptors in the respiratory tract of dogs (Zhai et al., 2020). In addition, the ACE2 of dogs, compared to humans, has five mutations while cats only have four (Zhai et al., 2020), which could explain the higher susceptibility to the infection in this species.

The seroprevalence results observed in domestic cats in this study in Madrid (4.6%), were similar to those obtained in Italy in 2020 (5.8%) (Patterson et al., 2020). On the other hand, there were countries in which seroprevalence results were much higher than ours, being the majority of them of domestic cats such as in Minnesota (11–12%) (Dileepan et al., 2021) or France (8.4%) (Bessière et al., 2022). The higher seroprevalence in France may be related to the higher number of SARS-CoV-2 human cases than in Spain, being the cumulative incidence in France in January 2022 of 7.200 cases per 100.000 habitants (World Health Organization [WHO], 2022). There were also studies in which the percentage of seroprevalence was lower than in our study such as Portugal (1.7%) (Oliveira et al., 2022) or Poland (1.79%) (Pomorska-Mól et al., 2021), coinciding with countries in which the number of SARS-CoV-2 cases is lower than in Spain (World Health Organization [WHO], 2022).

The results obtained in this study from a random sampling of dogs and cats in the Autonomous Community of Madrid indicate that the virus is circulating among domestic animals, being cats more susceptible or exposed than dogs and that they are able to develop neutralizing antibodies. These results, together with all the studies that have been carried out to date, both natural and experimental infection in animals, lead us to emphasize the importance of active and passive surveillance of this disease in both wild and domestic animals. In this way, we will be able to learn the behavior of this virus in each of the animal species, as well as the possible changes that may arise.

Data availability statement

The original contributions presented in this study are included in the article/supplementary material, further inquiries can be directed to the corresponding author.

Ethics statement

The animal studies were approved by the Complutense University of Madrid's Ethics Committee for Animal Experiments (Project License 14/2020). The studies were conducted in accordance with the local legislation and institutional requirements. Written informed consent was obtained from the owners for the participation of their animals in this study.

Author contributions

LS-M: Methodology, Writing – original draft. JS-V: Conceptualization, Funding acquisition, Writing – review and editing. LD: Funding acquisition, Writing – review and editing. SB-A: Conceptualization, Writing – review and editing.

Funding

The authors declare financial support was received for the research, authorship, and/or publication of this article. This research was funded by the REACT ANTICIPA-UCM (reference PR38/21) funded by the Community of Madrid and the European Union through the ERDF (European Regional Development Fund) as part of the Union's response to the COVID-19 pandemic and the Institute of Health Carlos III (ISCIII) and Project-Estudio del potencial impacto del COVID-19 en mascotas y linces (reference: COV20/01385).

Acknowledgments

We are very grateful for the cooperation and excellent technical support of Rocío Sánchez and Deborah López, as well as all the members of the COVID SUAT-VISAVET team.

Conflict of interest

The authors declare that the research was conducted in the absence of any commercial or financial relationships that could be construed as a potential conflict of interest.

Publisher's note

References

Bao, L., Song, Z., Xue, J., Gao, H., Liu, J., Wang, J., et al. (2021). Susceptibility and attenuated transmissibility of SARS-CoV-2 in domestic cats. *J. Infect. Dis.* 223, 1313–1321. doi: 10.1093/infdis/jiab104

Bessière, P., Vergne, T., Battini, M., Brun, J., Averso, J., Joly, E., et al. (2022). SARS-CoV-2 infection in companion animals: Prospective serological survey and risk factor analysis in France. *Viruses* 14:1178. doi: 10.3390/v14061178

Bosco-Lauth, A. M., Walker, A., Guilbert, L., Porter, S., Hartwig, A., McVicker, E., et al. (2021). Susceptibility of livestock to SARS-CoV-2 infection. *Emerg. Microbes Infect.* 10, 2199–2201. doi: 10.1080/22221751.2021.2003724

Chiba, S., Halfmann, P. J., Hatta, M., Maemura, T., Fan, S., Armbrust, T., et al. (2021). Protective immunity and persistent lung sequelae in domestic cats after SARS-CoV-2 infection. *Emerg. Infect. Dis.* 27, 660–663. doi: 10.3201/eid2702.203884

Dileepan, M., Di, D., Huang, Q., Ahmed, S., Heinrich, D., Ly, H., et al. (2021). Seroprevalence of SARS-CoV-2 (COVID-19) exposure in pet cats and dogs in Minnesota, USA. *Virulence* 12, 1597–1609. doi: 10.1080/21505594.2021.1936433

Fritz, M., Rosolen, B., Krafft, E., Becquart, P., Elguero, E., Vratskikh, O., et al. (2021). High prevalence of SARS-CoV-2 antibodies in pets from COVID-19+ households. *One Health* 11:100192. doi: 10.1016/j.onehlt.2020.100192

Hahn, W., and Wiley, Z. (2022). COVID-19 vaccines. *Infect. Dis. Clin. N. Am.* 36, 481–494. doi: 10.1016/j.idc.2022.01.008

Halfmann, P. J., Hatta, M., Chiba, S., Maemura, T., Fan, S., Takeda, M., et al. (2020). Transmission of SARS-CoV-2 in domestic cats. *N. Engl. J. Med.* 383, 592–594. doi: 10.1056/NEJMc2013400

Larsen, H. D., Fonager, J., Lomholt, F. K., Dalby, T., Benedetti, G., Kristensen, B., et al. (2021). Preliminary report of an outbreak of SARS-CoV-2 in mink and mink farmers associated with community spread, Denmark, June to November 2020. *Euro Surveill.* 26:2100009. doi: 10.2807/1560-7917.ES.2021.26.5.210009

Meekins, D. A., Gaudreault, N. N., and Richt, J. A. (2021). Natural and experimental SARS-CoV-2 infection in domestic and wild animals. *Viruses* 13:1993. doi: 10.3390/v13101993

Michelitsch, A., Hoffmann, D., Wernike, K., and Beer, M. (2020). Occurrence of antibodies against SARS-CoV-2 in the domestic cat population of Germany. *Vaccines (Basel)* 8:772. doi: 10.3390/vaccines8040772

Michelitsch, A., Schon, J., Hoffmann, D., Beer, M., and Wernike, K. (2021). The second wave of SARS-CoV-2 circulation-antibody detection in the domestic cat population in Germany. *Viruses* 13:1009. doi: 10.3390/v13061009

Natale, A., Mazzotta, E., Mason, N., Ceglie, L., Mion, M., Stefani, A., et al. (2021). SARS-Cov-2 natural infection in a symptomatic cat: Diagnostic, clinical and medical management in a one health vision. *Animals (Basel)* 11:1640. doi: 10.3390/ani11061640

Oliveira, A., Pereira, M. A., Mateus, T. L., Mesquita, J. R., and Vala, H. (2022). Seroprevalence of SARS-CoV-2 in client-owned cats from Portugal. *Vet. Sci.* 9:363. doi: 10.3390/vetsci9070363

Oude Munnink, B. B., Sikkema, R. S., Nieuwenhuijse, D. F., Molenaar, R. J., Munger, E., Molenkamp, R., et al. (2021). Transmission of SARS-CoV-2 on mink farms between humans and mink and back to humans. *Science* 371, 172–177. doi: 10.1126/science.abe5901

Palmer, M. V., Martins, M., Falkenberg, S., Buckley, A., Caserta, L. C., Mitchell, P. K., et al. (2021). Susceptibility of white-tailed deer (*Odocoileus virginianus*) to SARS-CoV-2. *J. Virol.* 95, e83–e21. doi: 10.1128/JVI.00083-21

Patterson, E. I., Elia, G., Grassi, A., Giordano, A., Desario, C., Medardo, M., et al. (2020). Evidence of exposure to SARS-CoV-2 in cats and dogs from households in Italy. *Nat. Commun.* 11:6231. doi: 10.1038/s41467-020-20097-0

Perera, R. A. P. M., Ko, R., Tsang, O. T. Y., Hui, D. S. C., Kwan, M. Y. M., Brackman, C. J., et al. (2021). Evaluation of a SARS-CoV-2 surrogate virus neutralization test for detection of antibody in human, canine, cat, and hamster sera. *J. Clin. Microbiol.* 59, e2504–e2520. doi: 10.1128/JCM.02504-20

Pickering, B. S., Smith, G., Pinette, M. M., Embury-Hyatt, C., Moffat, E., Marszal, P., et al. (2021). Susceptibility of domestic swine to experimental infection with severe acute respiratory syndrome coronavirus 2. *Emerg. Infect. Dis.* 27, 104–112. doi: 10.3201/eid2701.203399

Pomorska-Mól, M., Turlewicz-Podbielska, H., Gogulski, M., Ruszkowski, J. J., Kubiak, M., Kuriga, A., et al. (2021). A cross-sectional retrospective study of SARS-CoV-2 seroprevalence in domestic cats, dogs and rabbits in Poland. *BMC Vet. Res.* 17:322. doi: 10.1186/s12917-021-03033-2

Sánchez-Morales, L., Sánchez-Vizcaíno, J. M., Pérez-Sancho, M., Domínguez, L., and Barroso-Arévalo, S. (2022). The Omicron (B.1.1.529) SARS-CoV-2 variant of concern also affects companion animals. *Front. Veter. Sci.* 9:940710. doi: 10.3389/fvets.2022.940710

Shi, J., Wen, Z., Zhong, G., Yang, H., Wang, C., Huang, B., et al. (2020). Susceptibility of ferrets, cats, dogs, and other domesticated animals to SARS-coronavirus 2. *Science* 368, 1016–1020. doi: 10.1126/science.abb7015

Sila, T., Sunghan, J., Laochareonsuk, W., Surasombatpattana, S., Kongkamol, C., Ingviya, T., et al. (2022). Suspected cat-to-human transmission of SARS-CoV-2, Thailand, July-September 2021. *Emerg. Infect. Dis.* 28, 1485–1488. doi: 10.3201/eid2807.212605

Sit, T. H. C., Brackman, C. J., Ip, S. M., Tam, K. W. S., Law, P. Y. T., To, E. M. W., et al. (2020). Infection of dogs with SARS-CoV-2. *Nature* 586, 776–778. doi: 10.1038/s41586-020-2334-5

Smith, S. L., Anderson, E. R., Cansado-Utrilla, C., Prince, T., Farrell, S., Brant, B., et al. (2021). SARS-CoV-2 neutralising antibodies in dogs and cats in the United Kingdom. *Curr. Res. Virol. Sci.* 2:100011. doi: 10.1016/j.crviro.2021.100011

Stevanovic, V., Vilibic-Cavlek, T., Tabain, I., Benvin, I., Kovac, S., Hruskar, Z., et al. (2021). Seroprevalence of SARS-CoV-2 infection among pet animals in Croatia and potential public health impact. *Transbound. Emerg. Dis.* 68, 1767–1773. doi: 10.1111/tbed.13924

Stranieri, A., Lauzi, S., Giordano, A., Galimberti, L., Ratti, G., Decaro, N., et al. (2022). Absence of SARS-CoV-2 RNA and anti-SARS-CoV-2 antibodies in stray cats. *Transbound. Emerg. Dis.* 69, 2089–2095. doi: 10.1111/tbed.14200

Sule, W. F., and Oluwayelu, D. O. (2020). Real-time RT-PCR for COVID-19 diagnosis: Challenges and prospects. *Pan. Afr. Med. J.* 35(Suppl. 2):121. doi: 10.11604/pamj.supp.2020.35.24258

Tyson, G. B., Jones, S., Montreuil-Spencer, C., Logan, N., Scott, S., Sasvari, H., et al. (2023). Increase in SARS-CoV-2 seroprevalence in UK domestic felids despite weak immunogenicity of post-omicron variants. *Viruses* 15:1661. doi: 10.3390/v15081661

van der Leij, W. J. R., Broens, E. M., Hesselink, J. W., Schuurman, N., Vernooij, J. C. M., and Egberink, H. F. (2021). Serological screening for antibodies against SARS-CoV-2 in dutch shelter cats. *Viruses* 13:1634. doi: 10.3390/v13081634

Wan, Y., Shang, J., Graham, R., Baric, R. S., and Li, F. (2020). Receptor recognition by the novel coronavirus from wuhan: An analysis based on decade-long structural studies of SARS coronavirus. *J. Virol.* 94, e127–e120. doi: 10.1128/JVI.00127-20

World Health Organization [WHO]. (2022). *WHO health emergency dashboard*. Available online at: https://covid19.who.int (accessed October 27, 2022).

Zhai, X., Sun, J., Yan, Z., Zhang, J., Zhao, J., Zhao, Z., et al. (2020). Comparison of severe acute respiratory syndrome coronavirus 2 spike protein binding to ACE2 receptors from human, pets, farm animals, and putative intermediate hosts. *J. Virol.* 94, e831–e820. doi: 10.1128/JVI.00831-20

Zhang, Q., Zhang, H., Gao, J., Huang, K., Yang, Y., Hui, X., et al. (2020). A serological survey of SARS-CoV-2 in cat in Wuhan. *Emerg. Microbes Infect.* 9, 2013–2019. doi: 10.1080/22221751.2020.1817796

frontiers | Frontiers in Microbiology

TYPE Original Research
PUBLISHED 10 October 2023
DOI 10.3389/fmicb.2023.1248573

OPEN ACCESS

EDITED BY
Jianke Wang,
Hebei Agricultural University, China

REVIEWED BY
Jianqiang Ye,
Yangzhou University, China
Orkide O. Koyuncu,
University of California, Irvine, United States

*CORRESPONDENCE
Jichun Wang
✉ jcwang@263.net
Chuanjian Zhang
✉ zcj6717855@126.com

†These authors have contributed equally to this work and share first authorship

RECEIVED 27 June 2023
ACCEPTED 04 September 2023
PUBLISHED 10 October 2023

CITATION
Xu M, Zhu L, Ge A, Liu Y, Chen S, Wei Z, Zheng Y, Tong L, Wang Z, Fei R, Wang J and Zhang C (2023) Construction of pseudorabies virus variant attenuated vaccine: codon deoptimization of *US3* and *UL56* genes based on PRV gE/TK deletion strain. *Front. Microbiol.* 14:1248573. doi: 10.3389/fmicb.2023.1248573

Construction of pseudorabies virus variant attenuated vaccine: codon deoptimization of *US3* and *UL56* genes based on PRV gE/TK deletion strain

Mengwei Xu[1,2,3,4†], Laixu Zhu[1,2,3,4†], Aimin Ge[5], Yamei Liu[1,2,3], Saisai Chen[1,2,3], Ziwen Wei[1,2,3], Yating Zheng[1,2,3], Ling Tong[1,2,3], Zhisheng Wang[1,2,3], Rongmei Fei[4], Jichun Wang[1,2,3*] and Chuanjian Zhang[1,2,3*]

[1]National Research Center of Engineering and Technology for Veterinary Biologicals, Jiangsu Key Laboratory for Food Quality and Safety-State Key Laboratory Cultivation Base of the Ministry of Science and Technology, Institute of Veterinary Immunology and Engineering, Jiangsu Academy of Agricultural Sciences, Nanjing, China, [2]GuoTai (Taizhou) Center of Technology Innovation for Veterinary Biologicals, Taizhou, China, [3]Jiangsu Co-Innovation Center for Prevention and Control of Important Animal Infectious Diseases and Zoonoses, Yangzhou, China, [4]College of Veterinary Medicine, Nanjing Agricultural University, Nanjing, China, [5]Shandong Vocational Animal Science and Veterinary College, Weifang, China

Since 2011, pseudorabies based on the pseudorabies virus (PRV) variant has emerged as a serious health issue in pig farms in China. The PRV gE/TK or gE/gI/TK deletion strains protect against emerging PRV variants. However, these variants may cause lethal infections in newborn piglets without PRV antibodies. Previous studies have shown that codon deoptimization of a virulence gene causes virus attenuation. Accordingly, we deoptimized US3-S (US3 gene encoding a short isoform that represents approximately 95% of the total US3 transcription) and *UL56* genes (first 10 or all codons) of PRV gE/TK deletion strain ($PRV^{\Delta TK\&gE-AH02}$) to generate six recombinant PRVs through bacterial artificial chromosome technology. In swine testicular cells, recombinant PRVs with all codon deoptimization of *US3-S* or *UL56* genes were grown to lower titers than the parental virus. Notably, US3-S or UL56 with all codon deoptimization reduced mRNA and protein expressions. Subsequently, the safety and immunogenicity of recombinant PRVs with codon deoptimization of US3-S or UL56 are evaluated as vaccine candidates in mice and piglets. The mice inoculated with recombinant PRVs with codon deoptimization of US3-S or UL56 showed exceptional survival ability without severe clinical signs. All codons deoptimized (US3-S and UL56) significantly decreased virus load and attenuated pathological changes in the brains of the mice. Moreover, the protection efficiency offered by recombinant PRVs with codon deoptimization of US3-S or UL56 showed similar effects to $PRV^{\Delta TK\&gE-AH02}$. Remarkably, the 1-day-old PRV antibody-negative piglets inoculated with $PRV^{\Delta TK\&gE}$-US3-S^{T-CD} (a recombinant PRV with all codon deoptimization of US3-S) presented no abnormal clinical symptoms, including fever. The piglets inoculated with $PRV^{\Delta TK\&gE}$-US3-S^{T-CD} showed a high serum neutralization index against the PRV variant. In conclusion, these results suggest using codon deoptimization to generate innovative live attenuated PRV vaccine candidates.

KEYWORDS

pseudorabies virus, attenuation, immunogenicity, codon deoptimization, US3-S, UL56

1. Introduction

Swine pseudorabies, an acute disease caused by the pseudorabies virus (PRV), has emerged as the leading cause of fatal encephalitis in newborn piglets, respiratory illness and growth stagnation in the growing pigs, as well as reproductive failure in the sows (Pomeranz et al., 2005). After extensive research, it was increasingly recognized that the utilization of live attenuated PRV Bartha-K61 vaccine combined with gE-ELISA serologic differential diagnosis showed exceptional control in spreading PRV in China from the 1990s to 2010 (Freuling et al., 2017). Nevertheless, pseudorabies outbreaks since 2011 caused by PRV variants have occurred in various Bartha-K61-vaccinated swine herds in China (An et al., 2013; Yu et al., 2014). Previous studies indicated that the Bartha-K61 vaccine could not fully protect against PRV variants, especially in preventing virus shedding (Zhou et al., 2017; Zhang et al., 2019a). To overcome this issue, PRV gE/TK and TK/gE/gI deletion strains based on current PRV variants have been developed, presenting good immunogenicity in pigs against PRV variants (Zhang et al., 2015). Nonetheless, the safety of these PRV deletion vaccines for neonatal piglets is particularly perturbing, hampering their utilization (Wang et al., 2018). In our previous study, we generated a PRV gE/TK deletion strain ($PRV^{\Delta TK\&gE-AH02}$) based on a virulent PRV AH02LA strain. This approach provided 100% clinical protection against the AH02LA strain in weaned pigs. However, the experimental results showed a lethal infection in newborn piglets without PRV antibodies (Wang et al., 2018). Therefore, further attenuation of $PRV^{\Delta TK\&gE-AH02}$ while maintaining immunogenicity is necessary for developing a safe and effective live PRV vaccine.

Most amino acids (except methionine and tryptophan) in organisms are typically coded by synonymous codons (Knight et al., 2001). Notably, these synonymous codons display the same coding potential. However, most species show a codon usage bias in their protein-encoding genes (Kanaya et al., 2001; Knight et al., 2001). Considering the codon usage bias, strategies such as codon optimization or codon deoptimization have been applied to increase or decrease gene expression in different organisms, respectively. To this end, the codon deoptimization strategy is often achieved by replacing original codons with less-preferred usage codons, which do not affect the amino acid sequence of the protein or its function. However, it decreases protein production of recoded genes during transcription and translation at multiple levels (Goncalves-Carneiro and Bieniasz, 2021). Previous studies indicated that codon deoptimization enabled the highly efficient attenuation of RNA viruses (influenza A virus, foot-and-mouth disease virus, and lassa virus) and DNA viruses (vaccinia virus) by reducing the gene expression of a particular viral gene (Nogales et al., 2014; Diaz-San Segundo et al., 2016; Cai et al., 2020; Lorenzo et al., 2022).

The *US3* gene, a virulence gene of PRV, encodes two isoforms of pUS3 (Olsen et al., 2006). The larger US3-L transcript represents approximately 5% of the total US3 transcription, and the smaller US3-S transcript represents about 95% of the total US3 transcription (Sehl et al., 2020). The *UL56* gene, an encoding envelope protein, is an important virulence factor of PRV, enhancing virus spread and pathogenesis (Daniel et al., 2016). In several instances, we demonstrated that the inactivated US3-S or UL56 of PRV (a gene point mutant in the start codon to stop the expression of US3-S or UL56) displayed significantly attenuated virulence in mice (Lv et al., 2020a,b). However, the US3 deletion showed a decrease in PRV immunogenicity in pigs. In a case study, Xu and colleagues demonstrated that the *US3* gene deletion resulted in further attenuation of the PRV TK/gE deletion mutant (Xu et al., 2022). However, the immunogenicity of the PRV PK/TK/gE deletion variant strain was not stable (data not published). Similarly, a previous study showed that the protective efficiency of the PRV PK/gE deletion mutant was lower than that of the PRV gE deletion mutant in pigs (Kimman et al., 1994).

Considering these aspects, this study is aimed to demonstrate the construction of six recombinant PRVs harboring the deoptimized *US3-S* and *UL56* genes (first 10 or all codon deoptimization) based on PRV ΔgE/TK strain using a bacterial artificial chromosome (BAC) technology. Moreover, the experiments are carried out in mice and piglets to determine the pathogenicity and immunogenicity characteristics of recombinant PRVs.

2. Materials and methods

2.1. Condon deoptimization of *US3* and *UL56* genes

The first 10 codons, or all codons of *US3-S* and *UL56* genes, were recoded by rearranging the synonymous codons to minimize the cumulative codon scores based on the pig codon pair bias table. The recoded sequences were synthesized by Beijing Tsingke Biotech Co., Ltd., (Beijing, China) and cloned into the pMD19-T simple vector (Takara Bio Inc., Tokyo, Japan), named US3-S^{F10-CD}-T, US3-S^{T-CD}-T, UL56 $^{F10-CD}$-T, and UL56^{T-CD}-T.

2.2. Viruses, cells, and plasmids

In this study, a PRV variant strain, AH02LA, was isolated from the brain of a dead newborn piglet in Anhui Province by our laboratory (CGMCC No. 10891). In addition, $PRV^{\Delta TK\&gE-AH02}$ with TK/gE deletion based on the AH02LA strain was previously constructed in our lab (Wang et al., 2018). Furthermore, it should be noted that all viruses were transfected and propagated in swine testicular (ST) cells. The ST cells were cultured in Dulbecco's Modified Eagle Medium (DMEM, Gibco, USA) supplemented with 2 or 10% newborn calf serum (Gibco) and 1% penicillin and streptomycin (Sigma-Aldrich, St. Louis, USA) at 37°C under 5% CO_2 atmosphere. On the one hand, the wild-type and recoded US3-S and UL56 were cloned into pmKate2-N plasmid at *Eco*R I restriction sites to construct the pUS3-S-mKate2-N and pUL56-mKate2-N plasmids, respectively. On the other hand, the TK/gE/gI-deleted PRV BAC ($pPRV^{\Delta TK\&gE\&gI}$) in which gI and gE genes were replaced with mini-F was constructed in our lab as reported previously (Wang et al., 2018). Furthermore, a kanamycin resistance gene was respectively inserted in US3-S^{F10-CD}-T, US3-S^{T-CD}-T, UL56 $^{F10-CD}$-T, and UL56^{T-CD}-T, at

the *Xma* I restriction site of US3-S^{F10-CD}-T, *Xba* I restriction site of US3-S^{T-CD}-T, *Nae* I restriction site of UL56^{F10-CD}-T, and *Eco*R V restriction site of UL56^{T-CD}-T to construct *En Passant* recombination.

2.3. Bacterial gene manipulation, polymerase chain reaction, and sequencing

As mentioned in the previous section, US3-S^{F10-CD}-KAN, US3-S^{T-CD}-KAN, UL56 $^{F10-CD}$-KAN, and UL56^{T-CD}-KAN with 40-bp homologous sequences of PRV in both terminals were initially amplified with primers of US3-S^{F10-CD} En pa F/R, US3-S^{T-CD} En pa F/R, UL56 $^{F10-CD}$ En pa F/R, and UL56^{T-CD} En pa F/R (Supplementary Table S1) from US3-S^{F10-CD}-T-KAN, US3-S^{T-CD}-T-KAN, UL56 $^{F10-CD}$-T-KAN, and UL56^{T-CD}-T-KAN. After digestion with *Dpn* I, four PCR products were respectively electroporated into GS1783 with pPRV$^{\Delta TK\&gE\&gI}$ to achieve the primary recombination, and a subsequent secondary red recombination resulted in the removal of the kanamycin resistance gene (Tischer et al., 2010). Four recombinant target clones (pPRV$^{\Delta TK\&gE\&gI}$-US3-S^{F10-CD}-mini-F, pPRV$^{\Delta TK\&gE\&gI}$-US3-S^{T-CD}-mini-F, pPRV$^{\Delta TK\&gE\&gI}$-UL56^{F10-CD}-mini-F, and pPRV$^{\Delta TK\&gE\&gI}$-UL56^{T-CD}-mini-F) were successfully generated. Furthermore, pPRV$^{\Delta TK\&gE\&gI}$-US3-S&UL56^{F10-CD}-mini-F and pPRV$^{\Delta TK\&gE\&gI}$-US3-S&UL56^{T-CD}-mini-F were constructed based on pPRV$^{\Delta TK\&gE\&gI}$-US3-S^{F10-CD}-mini-F and pPRV$^{\Delta TK\&gE\&gI}$-US3-S^{T-CD}-mini-F by *En Passant* recombination. Eventually, these generated six clones were confirmed by restriction fragment length polymorphism (RFLP) with *Bam*H I. The recoded US3-S and UL56 were identified through PCR and sequencing.

2.4. Generation of recombinant viruses

Briefly, the primers of H1-H2-gI-ΔgE F/R (Supplementary Table S1) were designed to amplify H1-H2-gI-ΔgE (the whole gI gene and part of gE gene with homologous arms at both ends) from PRV$^{\Delta TK\&gE-AH02}$. Then, to recover infectious viruses, 1-μg pPRV$^{\Delta TK\&gE\&gI}$-US3-S^{F10-CD}-mini-F, pPRV$^{\Delta TK\&gE\&gI}$-UL56^{F10-CD}-mini-F, pPRV$^{\Delta TK\&gE\&gI}$-US3-S&UL56^{F10-CD}-mini-F, pPRV$^{\Delta TK\&gE\&gI}$-US3-S^{T-CD}-mini-F, pPRV$^{\Delta TK\&gE\&gI}$-UL56^{T-CD}-mini-F, or pPRV$^{\Delta TK\&gE\&gI}$-US3-S&UL56^{T-CD}-mini-F and 1-μg H1-H2-gI-ΔgE were co-transfected into ST cells with Lipofectamine® 3000 reagent (Invitrogen, Waltham, USA) according to the manufacturer's instructions. After 24–48 h of transfection, fluorescent plaques (recombinant PRVs from BAC) and non-fluorescent plaques (gI-ΔgE-recovered PRVs in which the mini-F sequences were replaced with the whole gI gene and part of gE gene) were observed. After three rounds of plaque purification, the resultant non-fluorescent plaques were purified and named PRV$^{\Delta TK\&gE}$-US3-S^{F10-CD} (PRV TK/gE double gene deletion strain with first 10 codon deoptimization of US3-S), PRV$^{\Delta TK\&gE}$-UL56^{F10-CD} (PRV TK/gE double gene deletion strain with first 10 codon deoptimization of UL56), PRV$^{\Delta TK\&gE}$-US3-S&UL56^{F10-CD} (PRV TK/gE double gene deletion strain with first 10 codon deoptimization of US3-S and UL56), PRV$^{\Delta TK\&gE}$-US3-S^{T-CD} (PRV TK/gE double gene deletion strain with all codon deoptimization of US3-S), PRV$^{\Delta TK\&gE}$-UL56^{T-CD} (PRV TK/gE double gene deletion strain with all codon deoptimization of UL56), and PRV$^{\Delta TK\&gE}$-US3-S&UL56^{T-CD} (PRV TK/gE double gene deletion strain with all codon deoptimization of US3-S and UL56). The recombinant viruses were cultured by passaging 20 times on ST cells. Finally, the recoded US3-S and UL56 were confirmed with PCR and sequencing experimentation.

2.5. Multi-step growth kinetics of recombinant viruses

To explore the multi-step growth kinetics of recombinant viruses, ST cells were infected with PRV$^{\Delta TK\&gE-AH02}$ and the before-mentioned six recombinant viruses at a multiplicity of infection (MOI) of 0.01. At 6, 12, 24, 36, 48, 60, and 72 h post-infection, the culture cells were harvested and titrated on monolayers of ST cells. It should be noted that the experiments were performed in triplicate and analyzed using a one-way ANOVA by SPSS 16.0 (SPSS Inc., Chicago, USA).

2.6. RNA and protein expressions of codon-deoptimized *US3-S* and *UL56* genes

Briefly, 1.5 μg of expression plasmids, i.e., pUS3-S-mKate2-N, pUS3-S^{F10-CD}-mKate2-N, pUS3-S^{T-CD}-mKate2, pUL56-mKate2, pUL56^{F10-CD}-mKate2, or pUL56^{T-CD}-mKate2, were initially transfected into ST cells. At 24 h post-infection, the total RNA of the transfected cells was isolated using the TRIzol reagent (Sigma-Aldrich) (Chomczynski and Sacchi, 1987). Furthermore, 1 μg of total RNA was reverse transcribed with a PrimeScript® RT Reagent Kit with gDNA Eraser (Takara Co. Ltd.). Then, the gene-specific primers were used to quantify the transcripts of US3-S and UL56 (Supplementary Table S1). The real-time quantitative PCR (qRT-PCR) was carried out on the Roche Light Cycler® 480 system (Roche Diagnostics, Burgess Hill, UK) using SYBR Premix Ex Taq dye (Takara Co. Ltd.) (Zhang et al., 2019b). Notably, each cDNA was analyzed in triplicate, and sample data were normalized to β-actin expression using the $2^{-\Delta\Delta Ct}$ method.

Furthermore, transcription of the recoded US3-S and UL56 genes in the viral background was assessed as follows: Briefly, ST cells were seeded in a 6-well plate and then infected with PRV$^{\Delta TK\&gE-AH02}$ or six recombinant viruses at an MOI of 1. At 12 and 24 h post-infection, early genes (US3-S, UL40, and UL52), as well as late genes (UL24, UL44, and UL56) mRNA, were quantified by qRT-PCR using the gene-specific primers (Supplementary Table S1). Then, RNA extraction, reverse transcription, and qRT-PCR were performed as described above.

Then, the protein production of recoded US3-S and UL56 was analyzed using the following procedure: ST cells were initially transfected with 1.5 μg of the pmKate2-N, pUS3-S-mKate2-N, pUS3-S^{F10-CD}-mKate2-N, pUS3-S^{T-CD}-mKate2-N, pUL56^{F10-CD}-mKate2-N, pUL56^{T-CD}-mKate2-N, or pUL56-mKate2-N plasmids. At 24 h post-transfection, cells were fixed

with 4% paraformaldehyde for 30 min and dyed with 4′,6-diamidino-2-phenylindole (DAPI; Sigma-Aldrich) for 20 min at room temperature (Weng et al., 2023). An inverted fluorescence microscope was used to examine transfected cells, and the representative cells were photographed.

2.7. Pathogenicity and immunological experiments in mice

Imprinting control region, healthy female mice (age of 6 weeks, $n = 286$) were purchased from Shanghai Laboratory Animal Co. Ltd., (SLAC, Shanghai, China). Initially, the purchased animals were randomly divided into 22 groups ($n = 13$ in each group). Mice were subcutaneously inoculated with $10^{6.5}$ $TCID_{50}$, $10^{5.5}$ $TCID_{50}$, and $10^{4.5}$ $TCID_{50}$ $PRV^{\Delta TK\&gE}$-US3-S^{F10-CD}, $PRV^{\Delta TK\&gE}$-$UL56^{F10-CD}$, $PRV^{\Delta TK\&gE}$-US3-S&$UL56^{F10-CD}$, $PRV^{\Delta TK\&gE}$-US3-S^{T-CD}, $PRV^{\Delta TK\&gE}$-$UL56^{T-CD}$, $PRV^{\Delta TK\&gE}$-US3-S&$UL56^{T-CD}$, or $PRV^{\Delta TK\&gE-AH02}$, and inoculated with DMEM serving as a negative control. The clinical symptoms and mortality of mice were observed daily for 14 days. On day 5 post-inoculation, five mice from each group were sacrificed, and the brain and lung samples were collected. Furthermore, the viral loads in the brain and lung samples of the sacrificed mice were detected using qRT-PCR analysis of the PRV gB in the Roche Light Cycler® 480 system (Roche Diagnostics, Burgess Hill, UK) as described previously (Zhang et al., 2019b). Then, the PRV copy numbers in the brain and lung samples were expressed as log10 copies per gram of tissue sample. To this end, the brain and lung tissues were fixed using 4% paraformaldehyde for 24 h. The fixed tissue samples were embedded in paraffin wax and cut into 3 μm sections. The tissue sections were stained with hematoxylin and eosin and examined by light microscopy. In addition, on day 21 post-inoculation, all surviving mice were confronted with 100 LD_{50} PRV AH02LA strain, and the clinical symptoms and mortality rate of mice were monitored daily for 14 days.

2.8. Pathogenicity and immunological experiments in piglets

To explore the pathogenicity and immunogenicity in pigs, 1-day-old piglets ($n = 15$) free of PRV, porcine reproductive and respiratory syndrome viruses, porcine parvovirus, and porcine

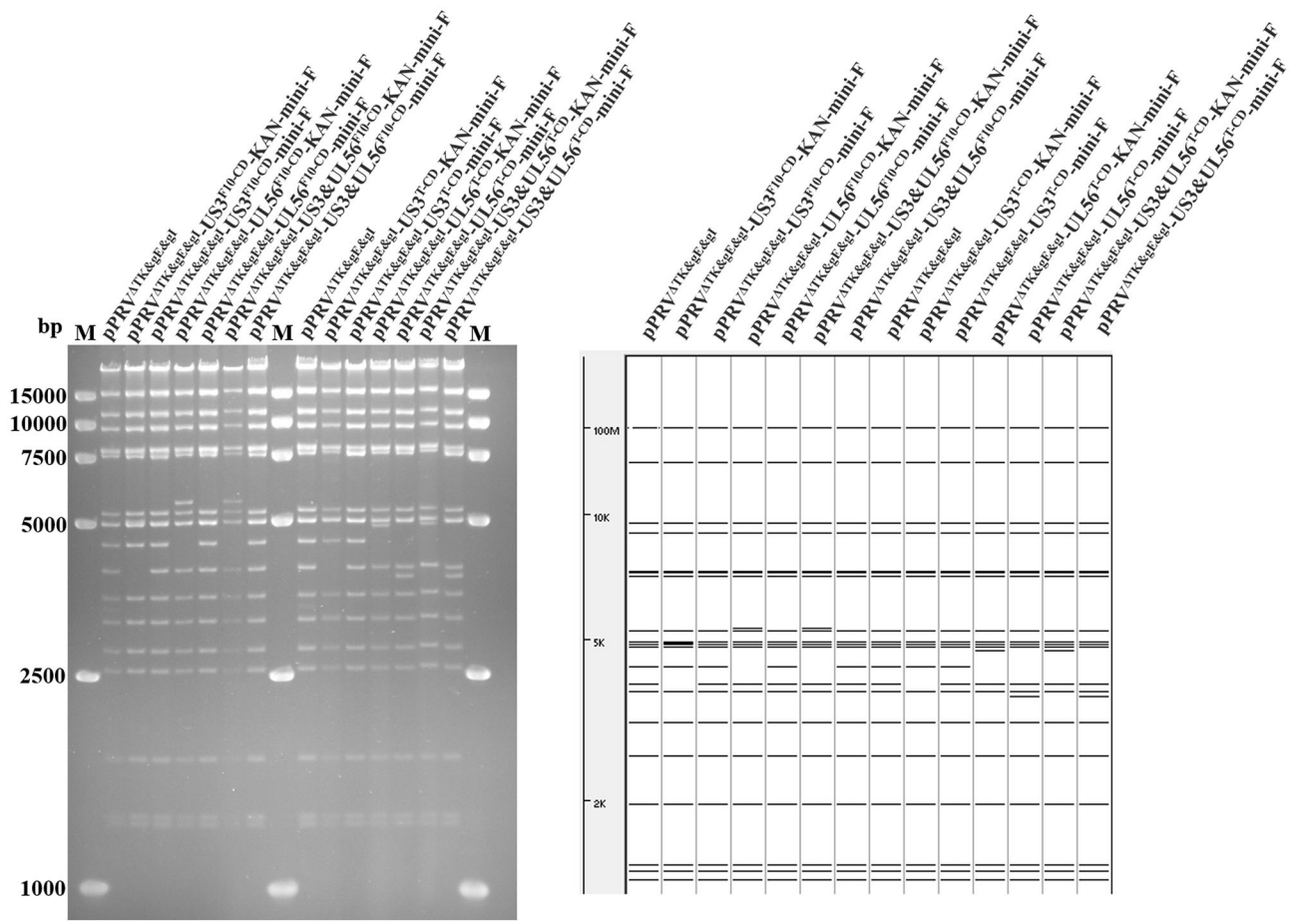

FIGURE 1
RFLP analysis shows the recombinant BACs with codon deoptimization of US3-S and UL56. Predictions of these digestions with *BamH* I using the PRV ZJ01 strain are performed (GenBank: KM061380.1).

10.3389/fmicb.2023.1248573

circovirus 2 were considered. Initially, the randomly distributed piglets were intramuscularly administered with 1 ml PRV$^{\Delta TK\&gE}$-US3-S^{T-CD} ($10^{5.00}$ $TCID_{50}$/ml) and PRV$^{\Delta TK\&gE-AH02}$ ($10^{5.00}$ $TCID_{50}$/ml) and inoculated with DMEM serving as a negative control. Furthermore, the body temperature and clinical signs of all piglets were monitored daily for 14 days. To this end, serum samples were collected on days 7, 14, and 21 post-inoculation to monitor neutralizing antibody index. Then, 100 μl of serum sample (heat inactivated for 30 min at 56°C) was mixed with an equal volume of 10-fold-diluted AH02LA virus. The neutralization indexes were expressed as the $TCID_{50}$ of serum in the test group divided by the $TCID_{50}$ of serum in the control group.

2.9. Statistical analysis

Data were presented as mean ± standard error mean (SEM) and analyzed using a one-way analysis of variance (ANOVA) with a Tukey's *post-hoc* test (SPSS Inc., Chicago, IL, USA), considering the *p*-values of < 0.05 as statistically significant. * indicates $p < 0.05$, ** represents $p < 0.01$, and *** signifies $p < 0.001$.

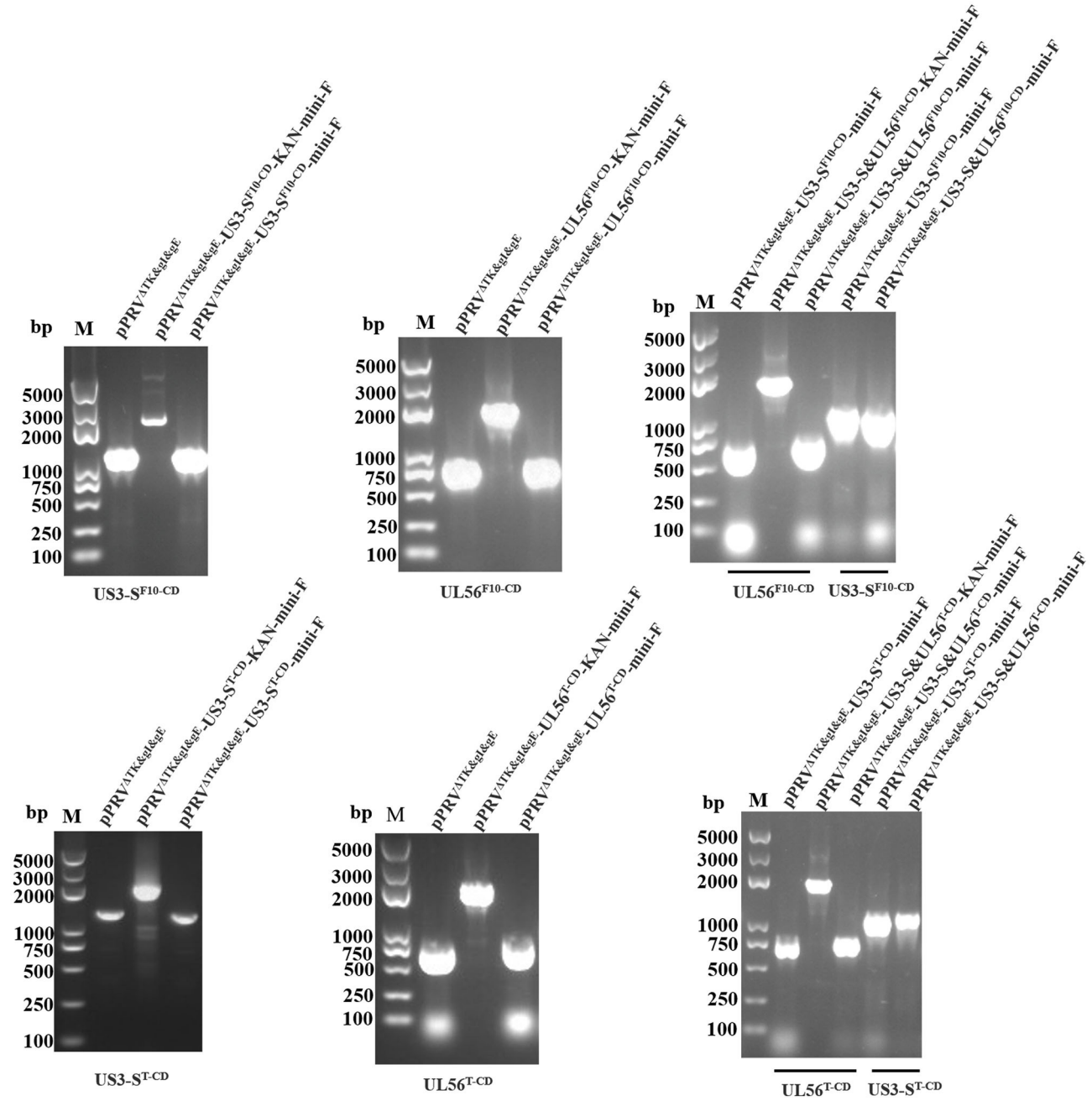

FIGURE 2
PCR identifies the recoded US3-S and UL56, the recoded US3-S with primers (US3-S check F/R), and the recoded UL56 with primers (UL56 check F/R) in the recombinant BACs.

10.3389/fmicb.2023.1248573

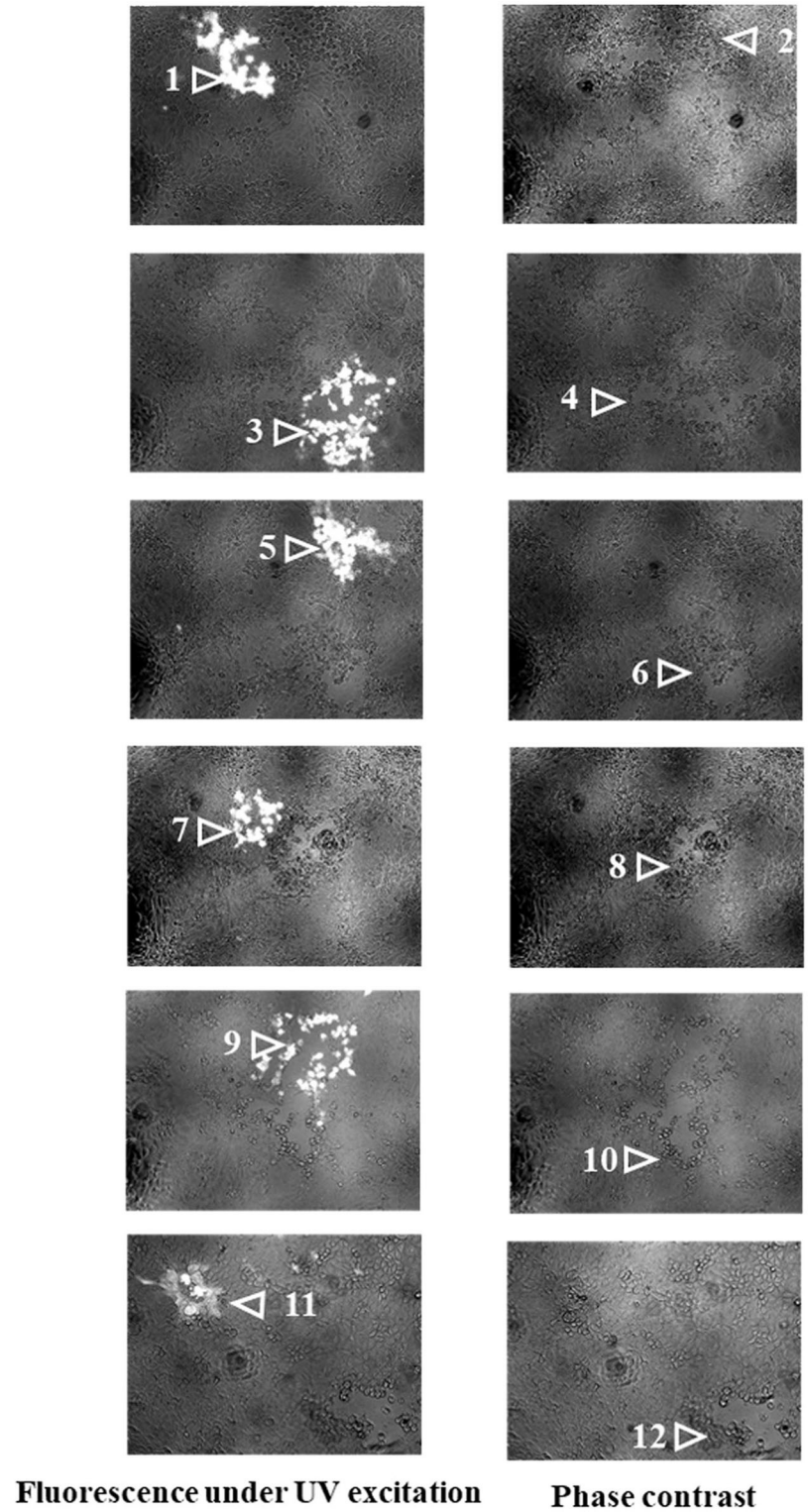

FIGURE 3
The images show recombinant PRVs with the recoded US3-S or UL56 genes under UV excitation and phase contrast. 1-μg pPRV$^{\Delta TK\&gE\&gI}$-US3-S^{F10-CD}-mini-F, pPRV$^{\Delta TK\&gE\&gI}$-UL56^{F10-CD}-mini-F, pPRV$^{\Delta TK\&gE\&gI}$-US3-S&UL56^{F10-CD}-mini-F, pPRV$^{\Delta TK\&gE\&gI}$-US3-S^{T-CD}-mini-F, pPRV$^{\Delta TK\&gE\&gI}$-UL56^{T-CD}-mini-F, or pPRV$^{\Delta TK\&gE\&gI}$-US3-SandUL56^{T-CD}-mini-F and 1-μg H1-H2-gI-ΔgE (the whole gI gene and part of gE gene with homologous arms at both ends) were co-transfected into ST cells. After 24 h of transfection, fluorescent plaques (recombinant PRVs from BAC) and non-fluorescent plaques (gI-ΔgE-recovered PRVs in which the mini-F sequences were replaced with the whole gI gene and part of the gE gene) were observed. Each panel represents a view of 200 × 200 μm in size. 1: PRV$^{\Delta TK\&gE\&gI}$-US3-S^{F10-CD}-mini-F, 2: PRV$^{\Delta TK\&gE}$-US3-S^{F10-CD}, 3: PRV$^{\Delta TK\&gE\&gI}$-UL56^{F10-CD}-mini-F, 4: PRV$^{\Delta TK\&gE}$-UL56^{F10-CD}, 5: PRV$^{\Delta TK\&gE\&gI}$-US3-S&UL56^{F10-CD}-mini-F, 6: PRV$^{\Delta TK\&gE}$-US3-SandUL56^{F10-CD}, 7: PRV$^{\Delta TK\&gE\&gI}$-US3-S^{T-CD}-mini-F, 8: PRV$^{\Delta TK\&gE}$-US3-S^{T-CD}, 9: PRV$^{\Delta TK\&gE\&gI}$-UL56^{T-CD}-mini-F, 10: PRV$^{\Delta TK\&gE}$-UL56^{T-CD}, 11: PRV$^{\Delta TK\&gE\&gI}$-US3-SandUL56^{T-CD}-mini-F, and 12: PRV$^{\Delta TK\&gE}$-US3-SandUL56^{T-CD}.

3. Results

3.1. Codon deoptimization of US3-S and UL56

Initially, the first 10 codons, or all codons of the *US3-S* and *UL56* genes, were deoptimized based on the pig codon pair bias table without any alterations to the amino acid sequences. The nucleotide sequences of US3-S, US3-S^{F10-CD}, US3-S^{T-CD}, UL56, UL56^{F10-CD}, and UL56^{T-CD} are shown in Supplementary material S1. Compared to the wild-type US3-S gene, US3-S^{F10-CD} (accession numbers: OR228539) contained 9 codon changes through 9 nucleotide substitutions, and US3-S^{T-CD} (accession numbers: OR228540) contained 277 codon changes through 279 nucleotide substitutions. Similarly, several substitutions were observed in the UL56 coding region. Compared to the wild-type UL56 gene, UL56^{F10-CD} (accession numbers: OR228541) contained 7 codon changes through 7 nucleotide substitutions, and UL56^{T-CD} (accession numbers: OR228542) contained 155 codon changes through 155 nucleotide substitutions. US3-S^{F10-CD}, US3-S^{T-CD}, UL56^{F10-CD}, and UL56^{T-CD} were synthesized by Beijing Tsingke Biotech Co., Ltd., (Beijing, China).

3.2. Construction of recombinant viruses with US3-S and UL56 codon deoptimization

Based on pPRV$^{\Delta TK\&gE\&gI}$, *US3-S* and *UL56* genes were replaced with the recoded gene by *En Passant* recombination, generating six recombinant clones (pPRV$^{\Delta TK\&gE\&gI}$-US3-S^{F10-CD}-mini-F, pPRV$^{\Delta TK\&gE\&gI}$-US3-S^{T-CD}-mini-F, pPRV$^{\Delta TK\&gE\&gI}$-UL56^{F10-CD}-mini-F, pPRV$^{\Delta TK\&gE\&gI}$-UL56^{T-CD}-mini-F, pPRV$^{\Delta TK\&gE\&gI}$-US3-S&UL56^{F10-CD}-mini-F, and pPRV$^{\Delta TK\&gE\&gI}$-US3-S&UL56^{T-CD}-mini-F). Furthermore, it was observed that the RFLP analysis of six recombinant clones was slightly different from the predicted patterns after digestion with *Bam*H I (Figure 1). To validate these observations, the recoded US3-S and UL56 were confirmed by PCR and sequencing (Figure 2). To substantially generate recombinant PRVs with the recoded *US3-S* and *UL56* genes, the DNA of the six BACs and H1-H2-gI-ΔgE were co-transfected into ST cells. Furthermore, the resultant non-fluorescent plaques were observed under UV light at a wavelength of 488 nm at 24 h post-transfection (Figure 3). It should be noted that a homogeneous population of purified viruses was isolated by picking and plating for three rounds.

PCR and its sequencing analyses validated the correct sequences of recoded US3-S, recoded UL56, and H1-H2-gI-ΔgE (data not shown). The recombinant viruses were passaged 20 times on ST cells to investigate the genetic stability of gI-ΔgE (the whole gI gene and part of gE gene) and the recoded US3-S and UL56. Furthermore, the viral DNAs were extracted, and gI-ΔgE and the recoded US3-S and UL56 were detected by PCR and its sequencing analyses. It was observed from the PCR analysis that there was no change in gI-ΔgE and the recoded US3-S and UL56 (Supplementary Figure S1).

3.3. Multi-step growth kinetics of recombinant viruses with US3-S and UL56 codon deoptimization

The growth kinetics of the PRV$^{\Delta TK\&gE}$-US3-S^{F10-CD}, PRV$^{\Delta TK\&gE}$-UL56^{F10-CD}, PRV$^{\Delta TK\&gE}$-US3-S&UL56^{F10-CD},

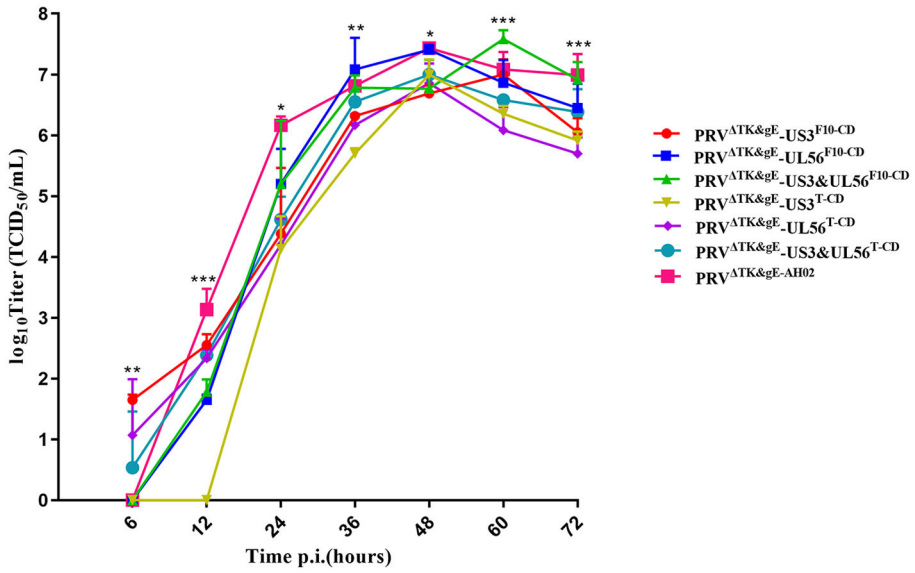

FIGURE 4
The multi-step growth curves indicate recombinant PRVs with the recoded US3-S or UL56 gene. ST cells are infected with PRV$^{\Delta TK\&gE-AH02}$ and its six mutants at an MOI of 0.01. At 6, 12, 24, 36, 48, 60, and 72 h post-infection, the culture cells are harvested and titrated in ST cells. Asterisks indicate statistical significance among seven viruses (* indicates $P < 0.05$, ** represents $P < 0.01$, and *** signifies $P < 0.001$). Data are presented as mean ± SEM and analyzed using a one-way ANOVA with a Tukey's *post-hoc* test (SPSS Inc., Chicago, IL, USA).

10.3389/fmicb.2023.1248573

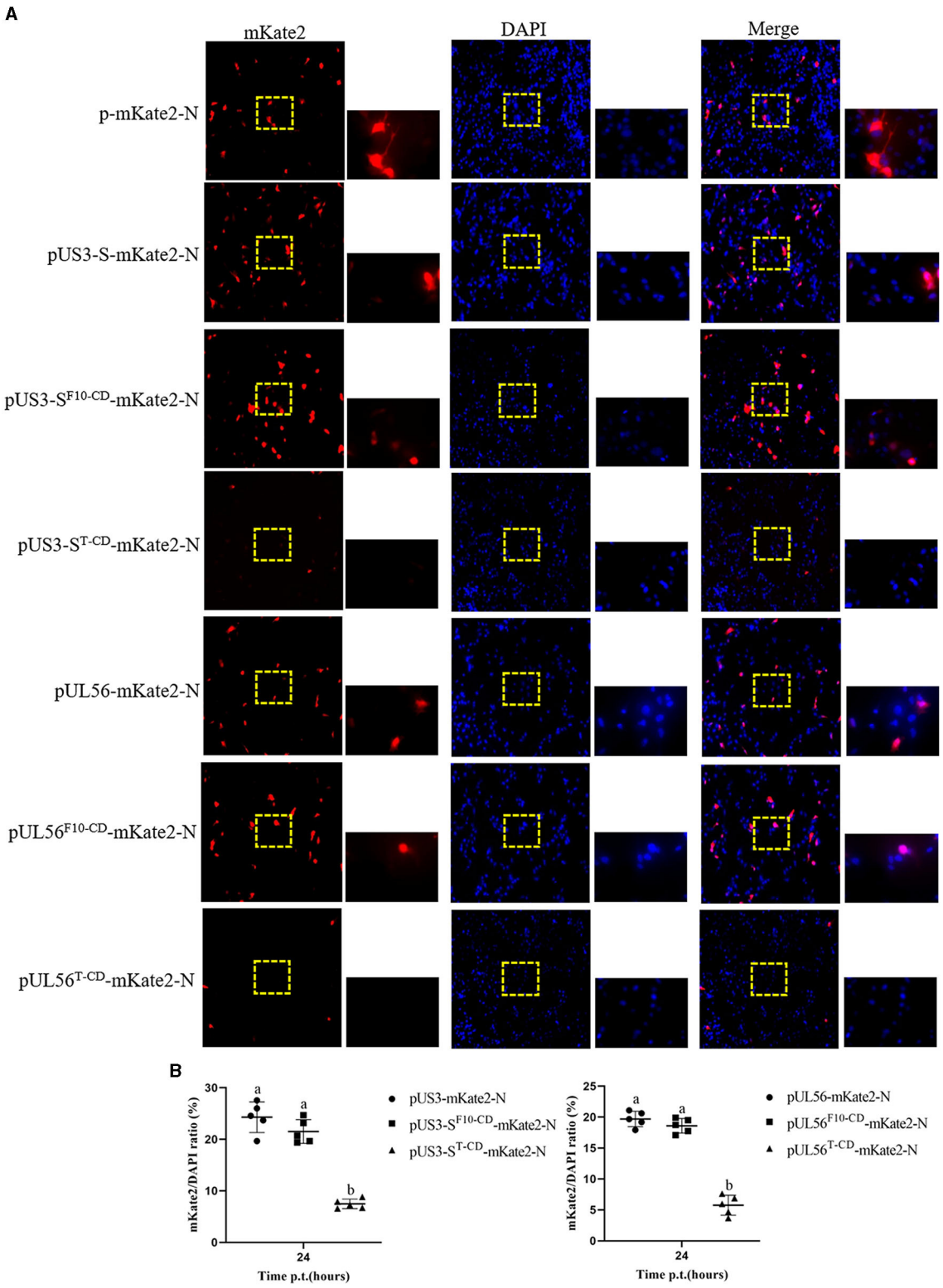

FIGURE 5
Protein expression from the recoded US3-S or UL56. **(A)** The images present ST transfected with recoded US3-S-mKate2 fusion or UL56-mKate2 fusion genes (200× and 800× magnification). **(B)** Quantitative analysis of the mKate2/DAPI ratio. Letters (a, b) above the bars indicate statistical significance ($P < 0.05$) of mKate2/DAPI ratio among the three plasmids.

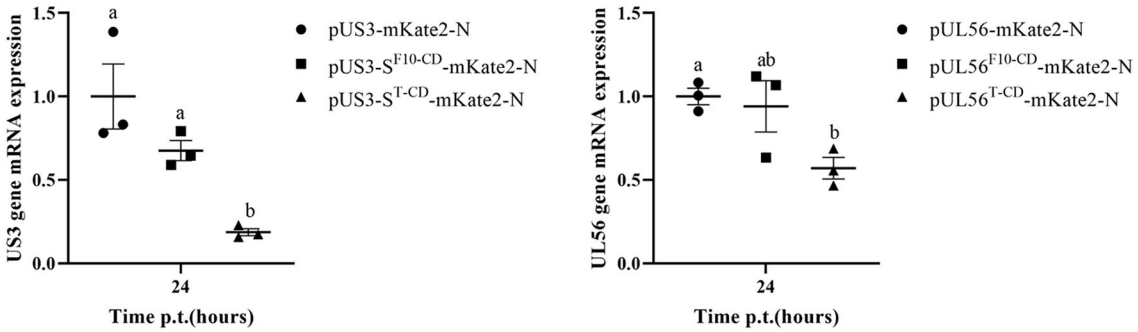

FIGURE 6
The quantification data show the RNA expression from the recoded *US3* gene or *UL56* gene. ST cells are transfected with the recoded US3-mKate2 fusion or UL56-mKate2 fusion genes. RNA expression from the recoded genes is quantified by qRT-PCR at 24 h post-transfection. Letters (a, b) above the bars indicate statistical significance ($P < 0.05$) of RNA expression among the three plasmids.

PRV$^{\Delta TK\&gE}$-US3-S^{T-CD}, PRV$^{\Delta TK\&gE}$-UL56^{T-CD}, PRV$^{\Delta TK\&gE}$-US3-S&UL56^{T-CD}, and PRV$^{\Delta TK\&gE-AH02}$ on ST cells are shown in Figure 4 and Supplementary Table S2. It was observed from the experimental results that PRV$^{\Delta TK\&gE}$-US3-S^{T-CD}, PRV$^{\Delta TK\&gE}$-UL56^{T-CD}, and PRV$^{\Delta TK\&gE}$-US3-S&UL56^{T-CD} grew to lower titers than PRV$^{\Delta TK\&gE-AH02}$, indicating that all codon deoptimization of US3-S or UL56 significantly affected the replication of the parental virus. Moreover, at 36 and 60 h post-infection, the titers of recombinant PRVs with the first 10 codon deoptimization of US3-S ($10^{6.32\pm0.04}$ $TCID_{50}$/ml at 36 h post-infection; $10^{7.00\pm0.14}$ $TCID_{50}$/ml at 60 h post-infection) or UL56 ($10^{7.08\pm0.30}$ $TCID_{50}$/ml at 36 h post-infection; $10^{6.86\pm0.22}$ $TCID_{50}$/ml at 60 h post-infection) were higher than recombinant PRVs with all codon deoptimization of US3-S ($10^{5.70\pm0.05}$ $TCID_{50}$/ml at 36 h post-infection; $10^{6.35\pm0.08}$ $TCID_{50}$/ml at 60 h post-infection) or UL56 ($10^{6.17\pm0.10}$ $TCID_{50}$/ml at 36 h post-infection; $10^{6.08\pm0.22}$ $TCID_{50}$/ml at 60 h post-infection).

3.4. Effect of codon deoptimization on mRNA and protein expression levels of recoded genes

Furthermore, the effect of codon deoptimization on US3-S and UL56 protein production was evaluated. To explore this aspect, we constructed the expression plasmids pUS3-S-mKate2-N and pUL56-mKate2-N, in which US3-S and UL56 expressions were determined by the immediate-early promoter of human cytomegalovirus. In addition, the *US3-S* and *UL56* genes were C-terminally tagged with mKate2. Then, the plasmids containing US3-S, US3-S^{F10-CD}, US3-S^{T-CD}, UL56, UL56^{F10-CD}, or UL56^{T-CD} were transfected into ST cells (Figure 5A). The mKate2/DAPI ratios of pUS3^{T-CD}-mKate2-N and pUL56^{T-CD}-mKate2-N were lower than their parental construct (Figure 5B). qRT-PCR analysis showed that the mRNA level of recoded genes in pUS3-S^{T-CD}-mKate2-N and pUL56^{T-CD}-mKate2-N was lower than their parental construct (Figure 6).

In addition, the RNA expression levels of US3-S, UL40, UL52, UL24, UL44, and UL56 during virus replication were determined (Figure 7). US3-S, UL40, and UL52 possessed the same kinetic gene expression class, representing early genes. UL24, UL44, and UL56 fitted to late genes. The quantification of RNA expression showed that all codon deoptimization negatively affected the mRNA expression of the recoded genes during virus replication.

3.5. Safety and immunogenicity of recombinant viruses with codon deoptimization of US3 or UL56 in mice and piglets

Eventually, the biological safety and significant immunogenicity of the designed recombinant virus were determined using mice and piglets. Mice inoculated with $10^{6.5}$ $TCID_{50}$, $10^{5.5}$ $TCID_{50}$, and $10^{4.5}$ $TCID_{50}$ PRV$^{\Delta TK\&gE}$-US3-S^{F10-CD}, PRV$^{\Delta TK\&gE}$-UL56^{F10-CD}, PRV$^{\Delta TK\&gE}$-US3-S&UL56^{F10-CD}, PRV$^{\Delta TK\&gE}$-US3-S^{T-CD}, PRV$^{\Delta TK\&gE}$-UL56^{T-CD}, PRV$^{\Delta TK\&gE}$-US3-S&UL56^{T-CD}, PRV$^{\Delta TK\&gE-AH02}$, and DMEM were survived without clinical symptoms, indicating no signs of toxicity and presenting excellent biosafety. On day 5 post-inoculation, mice inoculated with $10^{6.5}$ $TCID_{50}$ recombinant PRVs with all codon deoptimization of US3-S and UL56 showed lower virus load in the brain compared with those inoculated with $10^{6.5}$ $TCID_{50}$ PRV$^{\Delta TK\&gE-AH02}$ (Figure 8A). In addition, no virus was detected in the brains and lungs of the mice inoculated with $10^{5.5}$ $TCID_{50}$ and $10^{4.5}$ $TCID_{50}$ PRV$^{\Delta TK\&gE-AH02}$ or recombinant PRVs with codon deoptimization of US3-S or UL56. Furthermore, the histopathological examinations displayed that the mice inoculated with $10^{6.5}$ $TCID_{50}$ PRV$^{\Delta TK\&gE-AH02}$ showed obvious inflammatory cell infiltration in the brain. These abnormal cell infiltration consequences were more severe than those inoculated with $10^{6.5}$ recombinant PRVs with all codon deoptimization of US3-S and UL56 (Figure 8B). All mice inoculated with $10^{6.5}$ $TCID_{50}$ with PRV$^{\Delta TK\&gE-AH02}$ or recombinant PRVs presented slight inflammatory cell infiltration in the lung (Figure 8B). Moreover, it should be noted that no obvious histopathological changes were observed in the brains and lungs of mice inoculated with $10^{5.5}$ $TCID_{50}$ and $10^{4.5}$

10.3389/fmicb.2023.1248573

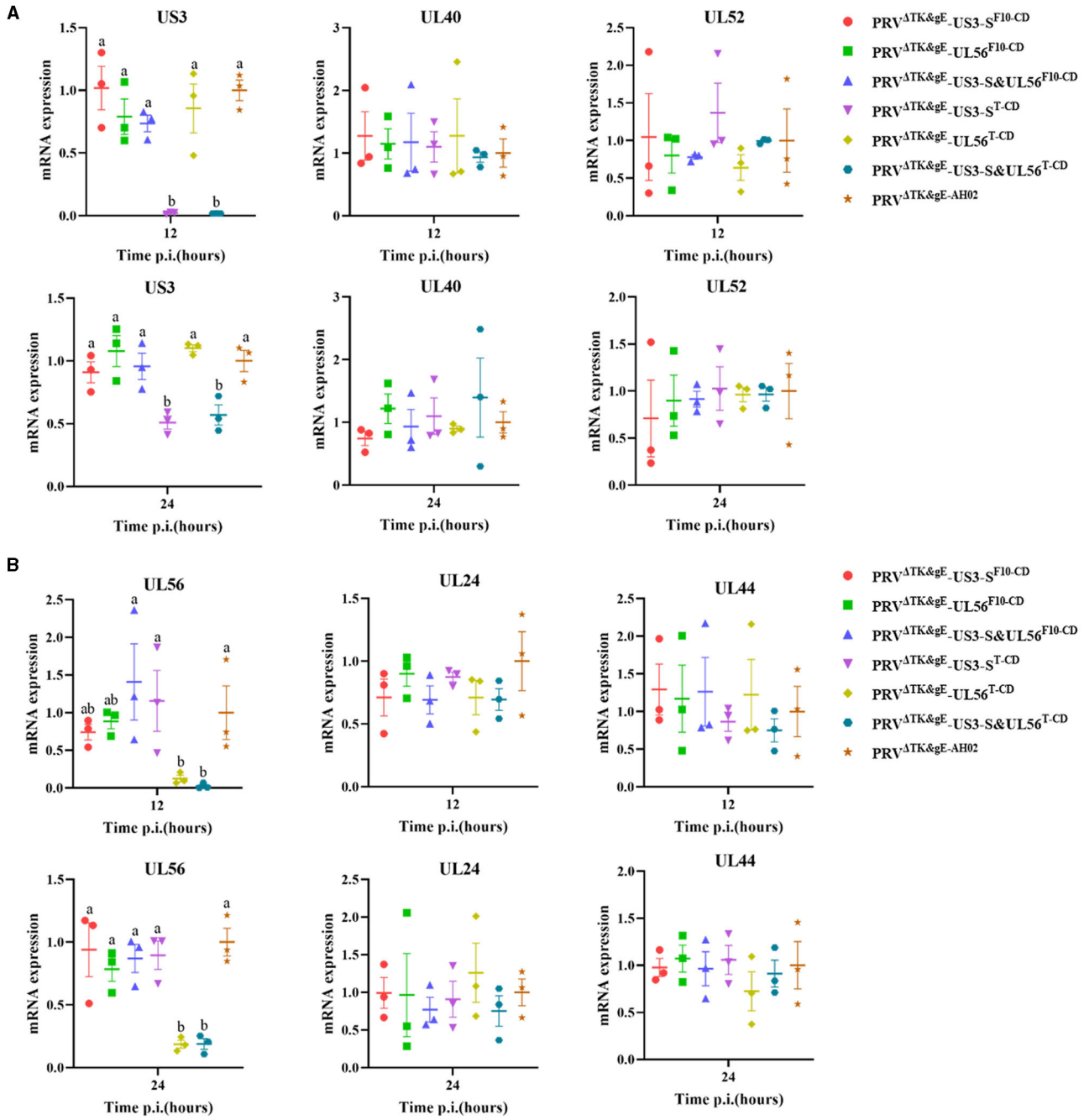

FIGURE 7
The data show the effect of recoding on early genes **(A)** or late genes **(B)** expression from the virus background. ST cells are infected with the parental or mutant virus that carries differently recoded *US3-S* or *UL56* genes. PCR quantifies mRNA expression of early genes (*US3*, *UL40*, and *UL52*) and late genes (*UL24*, *UL44*, and *UL56*) at 12 and 24 h post-infection. Letters (a, b) above the bars indicate statistical significance ($P < 0.05$) of RNA expression among seven viruses.

$TCID_{50}$ with $PRV^{\Delta TK\&gE-AH02}$ or recombinant PRVs. However, $PRV^{\Delta TK\&gE}$-US3-S&$UL56^{T-CD}$ displayed no further reduction in the pathogenicity to mice compared to $PRV^{\Delta TK\&gE}$-$US3\text{-}S^{T-CD}$ and $PRV^{\Delta TK\&gE}$-$UL56^{T-CD}$.

After 3 weeks of immunization, all the surviving mice were challenged with 100 LD_{50} PRV AH02LA strains. Notably, the protection efficiency was substantially provided by $10^{6.5}$ recombinant PRVs with codons deoptimizing US3-S or UL56, similar to $10^{6.5}$ $PRV^{\Delta TK\&gE-AH02}$ (Table 1). Nonetheless, most mice inoculated with $10^{5.5}$ $TCID_{50}$ and $10^{4.5}$ $TCID_{50}$ $PRV^{\Delta TK\&gE-AH02}$ or recombinant PRVs developed clinical signs of disease and died at 72–96 h post-challenge.

Considering the biosafety results in mice, we further performed the safety and immunogenicity checks in 1-day-old piglets. Among the treated piglets, two of five showed typical clinical symptoms of PRV infection from day 3 after the inoculation

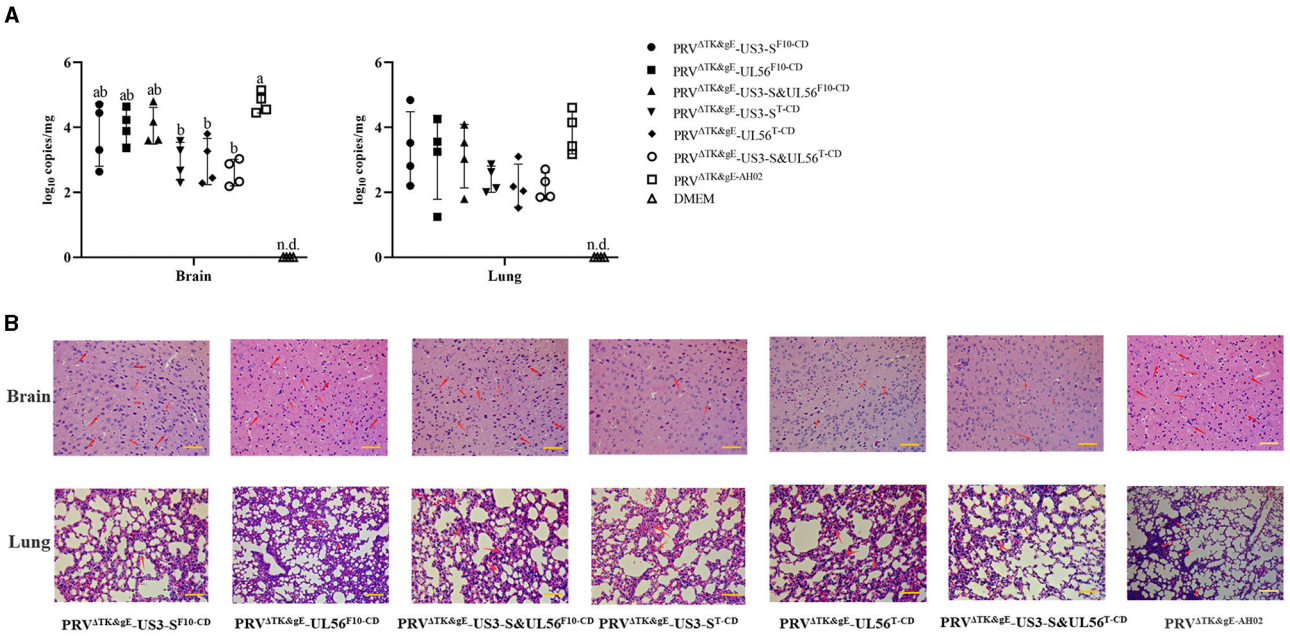

FIGURE 8
The graphs display the viral DNA loads quantification **(A)** and histological analysis **(B)** in the brain and lung of mice inoculated with $10^{6.5}$ $TCID_{50}$ $PRV^{\Delta TK\&gE-AH02}$ or recombinant PRVs with the recoded US3-S or UL56. Letters (a, b) above the bars indicate statistical significance ($P < 0.05$) of DNA loads among the eight groups. Arrows show inflammatory cell infiltration in the brain and lung (hematoxylin and eosin staining, 200× magnification, bar = 10 μm).

with $PRV^{\Delta TK\&gE-AH02}$. In addition, the three piglets inoculated with $PRV^{\Delta TK\&gE-AH02}$ showed higher body temperatures of 40.5°C on days 4 and 5 after inoculation (Figure 9). To this end, no clinical symptoms or body temperatures were observed in all piglets inoculated with $PRV^{\Delta TK\&gE}$-US3-S^{T-CD}. The ability of serum samples to neutralize PRV was detected after 7, 14, and 21 days of inoculation (Figure 10). Piglets vaccinated with $PRV^{\Delta TK\&gE}$-US3-S^{T-CD} showed a high serum neutralization index. After 14 and 21 days of treatment, no significant difference was observed between piglets vaccinated with $PRV^{\Delta TK\&gE}$-US3-S^{T-CD} and piglets vaccinated with $PRV^{\Delta TK\&gE-AH02}$.

4. Discussion

Indeed, pseudorabies, caused by a variant PRV, has emerged as one of the most dreadful infections since 2011 in many Bartha-K61-vaccinated swine herds in China (An et al., 2013; Yu et al., 2014). Furthermore, it was increasingly recognized that the Bartha-K61 vaccine was incompletely protected by highly virulent PRV strains. Considering these challenges, attenuated PRV strains with gE/TK or gE/gI/TK deletions based on PRV variants have been constructed, showing excellent protection against the PRV challenge. Nonetheless, previous reports indicated that the safety of these gene deletion mutants was far from satisfactory (Wang et al., 2018; Xu et al., 2022). To develop a safe and effective live PRV vaccine, in this study, a codon deoptimization strategy was adapted to specifically target virulence genes US3 or UL56 based on the PRV gE/TK deletion strain. All codons deoptimizing US3-S or UL56 resulted in reduced target gene mRNA and protein expressions and decreased virus duplication. In addition, the stability of the recoded gene was confirmed by passaging in ST cells without new mutations. It was observed that all codons deoptimizing US3-S or UL56 based on the PRV gE/TK deletion strain caused attenuation of the recoded virus without affecting immunogenicity in mice and piglets.

Codon deoptimization offers several advantages for the generation of live-attenuated PRV vaccines. First, a live-attenuated vaccine with codon deoptimization contains many mutations that make viral reversion to parental virus extremely unlikely. In our study, we observed no reversion of the recombinant PRVs with codon deoptimization of US3-S or UL56 during serial passage on ST cells. However, serial passage in pigs was required to further evaluate the stability of codon-deoptimized PRV. Second, codon deoptimization shows no effect on the viral protein sequence, retaining the antigenicity of the virus identical to the parental virus. Third, the generation of live-attenuated PRV vaccines with codon deoptimization can be rapidly achieved by combining the synthesis of codon deoptimization genes with BAC technologies. Indeed, the PRV genome is double-stranded DNA that encodes for approximately 70 genes, containing both essential and non-essential genes. Since some non-essential genes often play important roles in PRV pathogenesis and host control, we speculate that their deoptimization may lead to reduced virulence without interfering with immunogenicity.

In the current study, *US3-S* and *UL56* genes were selected to explore the effect of codon deoptimization due to their involvement in viral virulence. Previous studies showed that the degree and position of codon deoptimization are inversely correlated with

10.3389/fmicb.2023.1248573

TABLE 1 Immunogenicity of the recoded viruses with codon deoptimization of US3-S or UL56 in mice.

Virus strain	Doses ($TCID_{50}$)	Numbers	Challenge	
			Survival	Protection ratio
$PRV^{\Delta TK\&gE}$-US3-S^{F10-CD}	$10^{6.5}$	8	5	62.5%
	$10^{5.5}$	8	0	0
	$10^{4.5}$	8	0	0
$PRV^{\Delta TK\&gE}$-$UL56^{F10-CD}$	$10^{6.5}$	8	4	50.0%
	$10^{5.5}$	8	1	12.5%
	$10^{4.5}$	8	0	0
$PRV^{\Delta TK\&gE}$-US3-Sand$UL56^{F10-CD}$	$10^{6.5}$	8	5	62.5%
	$10^{5.5}$	8	1	12.5%
	$10^{4.5}$	8	0	0
$PRV^{\Delta TK\&gE}$-US3-S^{T-CD}	$10^{6.5}$	8	5	62.5%
	$10^{5.5}$	8	0	0
	$10^{4.5}$	8	0	0
$PRV^{\Delta TK\&gE}$-$UL56^{T-CD}$	$10^{6.5}$	8	4	50.0%
	$10^{5.5}$	8	0	0
	$10^{4.5}$	8	0	0
$PRV^{\Delta TK\&gE}$-US3-Sand$UL56^{T-CD}$	$10^{6.5}$	8	6	75.0%
	$10^{5.5}$	8	0	0
	$10^{4.5}$	8	0	0
$PRV^{\Delta TK\&gE-AH02}$	$10^{6.5}$	8	5	62.5%
	$10^{5.5}$	8	0	0
	$10^{4.5}$	8	0	0
DMEM		8		

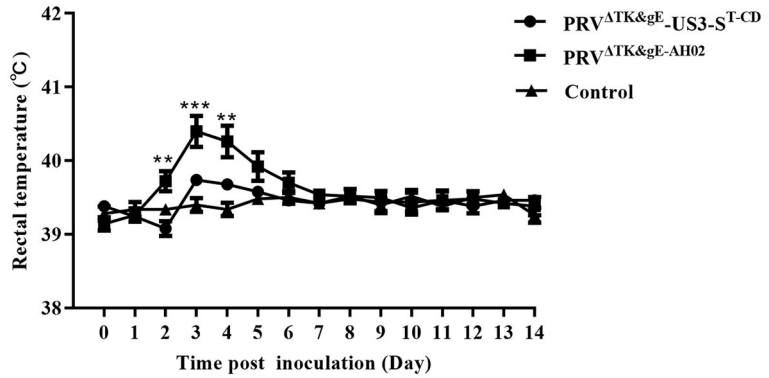

FIGURE 9
The graph shows the daily rectal temperatures of piglets post-inoculation. Data are presented as mean ± SEM. ** represents $P < 0.01$ and *** signifies $P < 0.001$.

the degree of cytopathic effects and plaque size and are crucial to the degree of virus attenuation (Eschke et al., 2018; Lee et al., 2021). In this study, the first 10 codons (a small amount; first segment), or all codons (a large number; whole segment) of *US3-S* and *UL56* genes, were deoptimized to identify the effect of the degree and position of deoptimization on recoded expression and viral virulence. Nonetheless, the first 10 codon deoptimization of US3-S or UL56 showed no effect on the mRNA expression of the recoded gene, suggesting the degree and position of deoptimization could be chosen carefully in vaccine design.

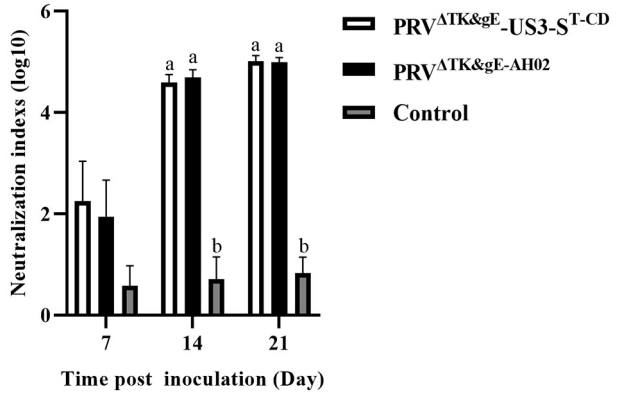

FIGURE 10
The graph presents the serum neutralization indices against PRV AH02LA strain in piglets at days 7, 14, and 21 post-inoculation. Letters (a, b) above the bars indicate statistical significance ($P < 0.05$) of serum neutralization indices among the three groups.

Furthermore, some essential genes are involved in viral egress, cell–cell spread, pathogenicity, and immunogenicity. Further studies involving codon deoptimizing essential genes should be attempted to develop a safe and effective PRV vaccine.

The molecular mechanisms of attenuation by codons deoptimizing US3-S and UL56 remain unknown. Previous studies indicated that codon deoptimization of genes in RNA viruses led to changes in RNA secondary structure, stability gene composition, and protein translation efficiency of the target gene (Kanaya et al., 2001; Knight et al., 2001; Burns et al., 2006; Meng et al., 2014). Moreover, the studies demonstrated that these were usually associated with decreased viral replication and virulence attenuation. In this study, all codon deoptimization negatively affected US3-S or UL56 RNA and protein levels after transient expression and RNA levels during virus replication. Therefore, protein translation efficiency might mediate the attenuation of recombinant PRVs with all codons deoptimizing US3-S and UL56.

Typically, successful live PRV vaccine candidates must show attenuation in the host while retaining immunogenicity. The recombinant PRVs with all codon deoptimization of US3-S or UL56 exhibited significantly reduced replication kinetics *in vitro* compared to the parental virus. Predictably, our *in vivo* data indicated that all codons deoptimizing US3-S or UL56 decreased virus load and attenuated pathological changes in the brains of mice. Surprisingly, PRV$^{\Delta TK\&gE}$-US3-S&UL56^{T-CD} displayed no further reduction in pathogenicity to mice compared with PRV$^{\Delta TK\&gE}$-US3-S^{T-CD} and PRV$^{\Delta TK\&gE}$-UL56^{T-CD}. Nonetheless, the potential mechanism remains unknown and needs further investigation. The protection efficiency provided by recombinant PRVs with codons deoptimizing US3-S or UL56 is similar to that of mice inoculated with their parental virus. Moreover, all codons deoptimizing US3-S caused attenuation of the recoded virus in piglets without loss of immunogenicity. However, future studies involving DNA loads and histological analysis in piglets are necessary to evaluate the pathogenicity of codon-deoptimized PRV in the major host. Furthermore, the safety and protective capacity of the other recoded virus in piglets also need further investigation to identify their potential use as a live vaccine candidate in pigs.

5. Conclusion

The codon deoptimization application in US3-S or UL56 based on PRV gE/TK deletion strain successfully generated six live recoded viruses. Among them, recombinant PRVs with all codon deoptimization of US3-S or UL56 cause virulence attenuation while retaining immunogenicity in mice and piglets. PRV$^{\Delta TK\&gE}$-US3-S^{T-CD} showed good safety and a high serum neutralization index in piglets, which might be a promising vaccine candidate against PRV variants. Finally, our results indicated that codon deoptimization might be useful for attenuating PRV.

Data availability statement

The datasets presented in this study can be found in online repositories. The names of the repository/repositories and accession number(s) can be found below: KM061380, OR228539, OR228540, KM061380, OR228541, and OR228542 (Genbank).

Ethics statement

All animal experiment was approved by the Institutional Animal Care and Ethics Committee at the Jiangsu Academy of Agriculture Sciences [authorization number SYXK (Su) 2015-0019] and performed strictly with the guidelines provided by the Institutional Biosafety Committee. The studies were conducted in accordance with the local legislation and institutional requirements. Written informed consent was obtained from the owners for the participation of their animals in this study.

Author contributions

CZ, RF, and JW conceived and designed the whole trial. CZ and MX wrote the manuscript. YL edited the manuscript. LZ constructed six live recoded viruses. MX, LZ, AG, SC, ZWe, YZ, LT, and ZWa conducted animal experiments and collected samples. All authors read and approved the final manuscript.

Funding

This study was supported by the Jiangsu Agriculture Science and Technology Innovation Fund [CX(21)3130].

Acknowledgments

We thank Professor Nikolaus Osterrieder for kindly providing *E. coli* GS1783.

Conflict of interest

The authors declare that the research was conducted in the absence of any commercial or financial relationships that could be construed as a potential conflict of interest.

Publisher's note

All claims expressed in this article are solely those of the authors and do not necessarily represent those of their affiliated organizations, or those of the publisher, the editors and the reviewers. Any product that may be evaluated in this article, or claim that may be made by its manufacturer, is not guaranteed or endorsed by the publisher.

Supplementary material

The Supplementary Material for this article can be found online at: https://www.frontiersin.org/articles/10.3389/fmicb.2023.1248573/full#supplementary-material

References

An, T. Q., Peng, J. M., Tian, Z. J., Zhao, H. Y., Li, N., Liu, Y. M., et al. (2013). Pseudorabies virus variant in Bartha-K61-vaccinated pigs, China, 2012. *Emerg. Infect. Dis.* 19, 1749–1755. doi: 10.3201/eid1911.130177

Burns, C. C., Shaw, J., Campagnoli, R., Jorba, J., Vincent, A., Quay, J., et al. (2006). Modulation of poliovirus replicative fitness in HeLa cells by deoptimization of synonymous codon usage in the capsid region. *J. Virol.* 80, 3259–3272. doi: 10.1128/JVI.80.7.3259-3272.2006

Cai, Y., Ye, C., Cheng, B., Nogales, A., Iwasaki, M., Yu, S., et al. (2020). A Lassa fever live-attenuated vaccine based on codon deoptimization of the viral glycoprotein gene. *mBio* 11, e00039-20. doi: 10.1128/mBio.00039-20

Chomczynski, P., and Sacchi, N. (1987). Single-step method of RNA isolation by acid guanidinium thiocyanate-phenol-chloroform extraction. *Anal. Biochem.* 162, 156–159. doi: 10.1016/0003-2697(87)90021-2

Daniel, G. R., Sollars, P. J., Pickard, G. E., and Smith, G. A. (2016). The pseudorabies virus protein, pUL56, enhances virus dissemination and virulence but is dispensable for axonal transport. *Virology* 488, 179–186. doi: 10.1016/j.virol.2015.11.014

Diaz-San Segundo, F., Medina, G. N., Ramirez-Medina, E., Velazquez-Salinas, L., Koster, M., Grubman, M. J., et al. (2016). Synonymous deoptimization of foot-and-mouth disease virus causes attenuation in vivo while inducing a strong neutralizing antibody response. *J. Virol.* 90, 1298–1310. doi: 10.1128/JVI.02167-15

Eschke, K., Trimpert, J., Osterrieder, N., and Kunec, D. (2018). Attenuation of a very virulent Marek's disease herpesvirus (MDV) by codon pair bias deoptimization. *PLoS Pathog.* 14, e1006857. doi: 10.1371/journal.ppat.1006857

Freuling, C. M., Muller, T. F., and Mettenleiter, T. C. (2017). Vaccines against pseudorabies virus (PrV). *Vet. Microbiol.* 206, 3–9. doi: 10.1016/j.vetmic.2016.11.019

Goncalves-Carneiro, D., and Bieniasz, P. D. (2021). Mechanisms of attenuation by genetic recoding of viruses. *mBio* 12, e02238–e02220. doi: 10.1128/mBio.02238-20

Kanaya, S., Yamada, Y., Kinouchi, M., Kudo, Y., and Ikemura, T. (2001). Codon usage and tRNA genes in eukaryotes: correlation of codon usage diversity with translation efficiency and with CG-dinucleotide usage as assessed by multivariate analysis. *J. Mol. Evol.* 53, 290–298. doi: 10.1007/s002390010219

Kimman, T. G., De Wind, N., De Bruin, T., de Visser, Y., and Voermans, J. (1994). Inactivation of glycoprotein gE and thymidine kinase or the US3-encoded protein kinase synergistically decreases in vivo replication of pseudorabies virus and the induction of protective immunity. *Virology* 205, 511–518. doi: 10.1006/viro.1994.1672

Knight, R. D., Freeland, S. J., and Landweber, L. F. (2001). A simple model based on mutation and selection explains trends in codon and amino-acid usage and GC composition within and across genomes. *Genome Biol.* 2, RESEARCH0010. doi: 10.1186/gb-2001-2-4-research0010

Lee, M. H. P., Tan, C. W., Tee, H. K., Ong, K. C., Sam, I. C., and Chan, Y. F. (2021). Vaccine candidates generated by codon and codon pair deoptimization of enterovirus A71 protect against lethal challenge in mice. *Vaccine*. 39, 1708–1720. doi: 10.1016/j.vaccine.2021.02.024

Lorenzo, M. M., Nogales, A., Chiem, K., Blasco, R., and Martinez-Sobrido, L. (2022). Vaccinia virus attenuation by codon deoptimization of the a24r gene for vaccine development. *Microbiol. Spectr.* 10, e0027222. doi: 10.1128/spectrum.00272-22

Lv, J., Zhang, C., Hou, J., Fei, R., and Wang, J. (2020a). Construction and biological characterization of pseudorabies virus variant of the inactivated US3 gene. *Anim. Husb. Vet. Med.* 52, 95–100.

Lv, J., Zhang, C., Wang, Z., He, Q., Wang, J., and Fei, R. (2020b). Construction of UL43 and UL56 gene inactivation mutants of pseudorabies virus variant and analysis of their biological characteristics. *Chin. J. Anim. Infect. Dis.* 30, 34–41.

Meng, J., Lee, S., Hotard, A. L., and Moore, M. L. (2014). Refining the balance of attenuation and immunogenicity of respiratory syncytial virus by targeted codon deoptimization of virulence genes. *mBio* 5, e01704–01714. doi: 10.1128/mBio.01704-14

Nogales, A., Baker, S. F., Ortiz-Riano, E., Dewhurst, S., Topham, D. J., and Martinez-Sobrido, L. (2014). Influenza A virus attenuation by codon deoptimization of the NS gene for vaccine development. *J. Virol.* 88, 10525–10540. doi: 10.1128/JVI.01565-14

Olsen, L. M., Ch'ng, T. H., Card, J. P., and Enquist, L. W. (2006). Role of pseudorabies virus Us3 protein kinase during neuronal infection. *J. Virol.* 80, 6387–6398. doi: 10.1128/JVI.00352-06

Pomeranz, L. E., Reynolds, A. E., and Hengartner, C. J. (2005). Molecular biology of pseudorabies virus: impact on neurovirology and veterinary medicine. *Microbiol. Mol. Biol. Rev.* 69, 462–500. doi: 10.1128/MMBR.69.3.462-500.2005

Sehl, J., Portner, S., Klupp, B. G., Granzow, H., Franzke, K., Teifke, J. P., et al. (2020). Roles of the different isoforms of the pseudorabies virus protein kinase pUS3 in nuclear egress. *J. Virol.* 94, e02029–e02019. doi: 10.1128/JVI.02029-19

Tischer, B. K., Smith, G. A., and Osterrieder, N. (2010). En passant mutagenesis: a two step markerless red recombination system. *Methods Mol. Biol.* 634, 421–430. doi: 10.1007/978-1-60761-652-8_30

Wang, J., Song, Z., Ge, A., Guo, R., Qiao, Y., Xu, M., et al. (2018). Safety and immunogenicity of an attenuated Chinese pseudorabies variant by dual deletion of TKandgE genes. *BMC. Vet. Res.* 14, 287. doi: 10.1186/s12917-018-1536-7

Weng, M., Guo, Z., Lu, Q., Jin, Q., Jiang, Y., Wang, F., et al. (2023). Pseudorabies virus regulates the extracellular translocation of annexin A2 to promote its proliferation. *J. Virol.* 97, e0154522. doi: 10.1128/jvi.01545-22

Xu, M., Zhang, C., Liu, Y., Chen, S., Zheng, Y., Wang, Z., et al. (2022). A noval strategy of deletion in PK gene for construction of a vaccine candidate with exellent safety and complete protection efficiency against high virulent Chinese pseudorabies virus variant. *Virus Res.* 313, 198740. doi: 10.1016/j.virusres.2022.198740

Yu, X., Zhou, Z., Hu, D., Zhang, Q., Han, T., Li, X., et al. (2014). Pathogenic pseudorabies virus, China, 2012. *Emerg. Infect. Dis.* 20, 102–104. doi: 10.3201/eid2001.130531

Zhang, C., Guo, L., Jia, X., Wang, T., Wang, J., Sun, Z., et al. (2015). Construction of a triple gene-deleted Chinese Pseudorabies virus variant and its efficacy study as a vaccine candidate on suckling piglets. *Vaccine* 33, 2432–2437. doi: 10.1016/j.vaccine.2015.03.094

Zhang, C., Liu, Y., Chen, S., Qiao, Y., Guo, M., Zheng, Y., et al. (2019a). A gDandgC-substituted pseudorabies virus vaccine strain provides complete clinical protection and is helpful to prevent virus shedding against challenge by a Chinese pseudorabies variant. *BMC. Vet. Res.* 15, 2. doi: 10.1186/s12917-018-1766-8

Zhang, C., Liu, Y., Chen, S., Qiao, Y., Zheng, Y., Xu, M., et al. (2019b). Effects of intranasal pseudorabies virus AH02LA infection on microbial community and immune status in the ileum and colon of piglets. *Viruses* 11, 518. doi: 10.3390/v11060518

Zhou, J., Li, S., Wang, X., Zou, M., and Gao, S. (2017). Bartha-k61 vaccine protects growing pigs against challenge with an emerging variant pseudorabies virus. *Vaccine* 35, 1161–1166. doi: 10.1016/j.vaccine.2017.01.003

frontiers | Frontiers in Microbiology

TYPE Original Research
PUBLISHED 31 October 2023
DOI 10.3389/fmicb.2023.1289065

OPEN ACCESS

EDITED BY
Jianke Wang,
Hebei Agricultural University, China

REVIEWED BY
Limin Li,
Hebei Agricultural University, China
Lauro Velazquez-Salinas,
Agricultural Research Service (USDA), United States

*CORRESPONDENCE
Min Ja Lee
herb12@korea.kr

†These authors have contributed equally to this work and share first authorship

RECEIVED 05 September 2023
ACCEPTED 18 October 2023
PUBLISHED 31 October 2023

CITATION
Shin S, Kim HW, Ko M-K, Park SH, Kim S-M, Park J-H and Lee MJ (2023) Inactivated vaccine with glycyrrhizic acid adjuvant elicits potent innate and adaptive immune responses against foot-and-mouth disease.
Front. Microbiol. 14:1289065.
doi: 10.3389/fmicb.2023.1289065

Inactivated vaccine with glycyrrhizic acid adjuvant elicits potent innate and adaptive immune responses against foot-and-mouth disease

Seokwon Shin†, Hyeong Won Kim†, Mi-Kyeong Ko, So Hui Park, Su-Mi Kim, Jong-Hyeon Park and Min Ja Lee*

Animal and Plant Quarantine Agency, Gimcheon-si, Gyeongsangbuk-do, Republic of Korea

Background: Foot-and-mouth disease (FMD) is an extremely contagious viral disease that is fatal to young animals and is a major threat to the agricultural economy by reducing production and limiting the movement of livestock. The currently commercially-available FMD vaccine is prepared using an inactivated viral antigen in an oil emulsion, with aluminum hydroxide [$Al(OH)_3$] as an adjuvant. However, oil emulsion-based options possess limitations including slow increases in antibody titers (up to levels adequate for defense against viral infection) and risks of local reactions at the vaccination site. Further, $Al(OH)_3$ only induces a T helper 2 (Th2) cell response. Therefore, novel adjuvants that can address these limitations are urgently needed. Glycyrrhizic acid (extracted from licorice roots) is a triterpenoid saponin and has great advantages in terms of price and availability.

Methods: To address the limitations of the currently used commercial FMD vaccine, we added glycyrrhizic acid as an adjuvant (immunostimulant) to the FMD bivalent (O PA2 + A YC) vaccine. We then evaluated its efficacy in promoting both innate and adaptive (cellular and humoral) immune reactions *in vitro* [using murine peritoneal exudate cells (PECs) and porcine peripheral blood mononuclear cells (PBMCs)] and *in vivo* (using mice and pigs).

Results: Glycyrrhizic acid has been revealed to induce an innate immune response and enhance early, mid-, and long-term immunity. The studied bivalent vaccine with glycyrrhizic acid increased the expression of immunoregulatory genes such as pattern-recognition receptors (PRRs), cytokines, transcription factors, and co-stimulatory molecules.

Conclusion: Collectively, glycyrrhizic acid could have utility as a novel vaccine adjuvant that can address the limitations of commercialized FMD vaccines by inducing potent innate and adaptive immune responses.

KEYWORDS

glycyrrhizic acid, adjuvant, foot-and-mouth disease, vaccine, innate and adaptive, immune response

1. Introduction

Foot-and-mouth disease (FMD) is an acute viral disease that spreads rapidly and is highly contagious (Grubman and Baxt, 2004). It is prevalent in over 100 countries globally (Jamal and Belsham, 2013). It affects cloven-hooved livestock such as swine, sheep, cattle, buffalo, and goats, with significant negative impacts on the livestock industry (Grubman

and Baxt, 2004). The FMD virus (FMDV) first enters the oropharynx of swine. Thereafter, it forms a vesicle from the snout toward the breast, nipples, or feet for infection. Animals that have contracted the virus display symptoms such as increased salivation, elevated body temperature, and decreased milk production. Infected animals are at risk of developing secondary infections, experiencing weight loss, and exhibiting reduced productivity over time. This can lead to reduced livestock productivity and high neonatal mortality (Arzt et al., 2011; Stenfeldt et al., 2014; Fukai et al., 2015b; Casey-Bryars et al., 2018). Due to the rapid spread of FMD, regions or countries with endemic FMD should aim to quickly contain any viral spread, the failure of which can lead to national restrictions on animal products and enormous economic losses (Rodriguez and Grubman, 2009; Casey-Bryars et al., 2018).

FMDV is a single-stranded positive-sense RNA virus categorized under the genus *Aphthovirus* within the family *Picornaviridae* (Jamal and Belsham, 2013). Its capsid is made up of 60 copies of structural proteins (SP), namely, VP1, VP2, VP3, and VP4 (Grubman and Baxt, 2004). The VP1 protein is known to be a key target in the prevention of FMD since it has the strongest immunogenicity, many neutralizing sites of the virus, a serotype-determining area, and is closely related to host cell-virus binding (Cheung et al., 1983; Parry et al., 1990; Jackson et al., 2003). FMDV has seven serotypes, namely, O, A, Asia1, South African Territories (SAT)1, SAT2, SAT3, and C. These serotypes do not induce cross-protection toward one other, and each serotype has multiple topotypes (Mason et al., 2003; Grubman and Baxt, 2004). Consequently, to protect against each serotype, appropriate vaccines must be developed and employed accordingly (Lee et al., 2020). Countries with endemic FMD, where many animals are still affected by the disease, need to introduce vaccines to prevent its spread. Vaccines alone are not a fundamental solution and do not completely address the losses related to FMD; nevertheless, vaccination, before FMD occurs, is likely to improve immunity in livestock animals (Rodriguez and Grubman, 2009; Casey-Bryars et al., 2018).

In the early 1930s, formalin was discovered to be capable of killing live FMDV. During the 1960s, the introduction of an FMD vaccine [which used formalin-inactivated FMDV cultured in baby hamster kidney (BHK) cells] resulted in a significant decrease in the prevalence of the disease across various European nations (Leforban and Gerbier, 2002). Currently, Korea supplies vaccines containing antigen-enhanced O, A, and Asia1 to prevent viruses that can simultaneously infect livestock farms vulnerable to FMD, and these vaccines induce high antibody titers. However, FMD remains a problem in numerous countries throughout the Middle East, South America, Africa, and Asia (Barteling, 2002). In addition, currently commercialized FMD vaccines have the following disadvantages; (1) in the case of inactivated virus vaccines, it is difficult to provide substantial disease protection until antibodies are formed post-vaccination; (2) pigs vaccinated with inactivated vaccines develop relatively lower antibody titers than cattle, and there are large inter-individual differences; and (3) side effects such as granulomas and fibrosis at the site of injection can be caused by oil emulsion-based formulations and are emerging as serious problems in pigs (Di Pasquale et al., 2015; Kamel et al., 2019). Numerous attempts to develop improved vaccines have been made. Since FMDV shows the highest antigenicity in its complete form, inactivated vaccines are currently the most efficacious. However, to overcome the existing limitations of inactivated viral vaccines, research on adjuvants capable of improving the immunogenicity of vaccines is currently being conducted.

Adjuvants are agents incorporated into vaccines to regulate and enhance the immune response. Many adjuvants have been isolated from natural products. The first research on adjuvants began in 1925, when tapioca starch was mixed with diphtheria toxoid and effectively increased antigen-specific antibody production (Ramon, 1925, 1926). Aluminum is currently used as a representative adjuvant; in 1926, aluminum-deposited diphtheria toxoid was shown to possess better immunogenicity than the toxoid alone, and aluminum has been in use for over 80 years to date (Hogenesch, 2013). Aluminum hydroxide [$Al(OH)_3$], the most commonly used chemical adjuvant, can induce antibody-mediated T helper 2 (Th2) responses which strongly stimulate IgE production, exerting a potent inflammatory effect at the injection site (Hem and Hogenesch, 2007; Jiang et al., 2018). However, since the cellular immune response mediated by $CD8^+$ and $CD4^+$ T lymphocytes is increasingly recognized to be equally critical for acquired defense in vaccinated animals, many research efforts are now attempting to identify adjuvants that elicit Th1 and Th2 immune responses, as well as innate and adaptive immune responses simultaneously (Guzman et al., 2010; Carr et al., 2013).

Glycyrrhizic acid, a representative component of licorice, is a triterpenoid-based material and comprises approximately 5% of licorice roots. Glycyrrhizic acid is generally recognized as safe and has been approved by the Food and Drug Administration (FDA) as a food additive in the United States since 1985 (Bailly and Vergoten, 2020). In 1925, saponin was found to significantly increase antibody responses to tetanus. Further, saponin can be used as an adjuvant since it has been found to induce a cellular immune response by increasing helper and cytotoxic T-cell responses as well as the antibody response (Ramon, 1925; Egerton et al., 1978). Saponin has been approved as a food and is widely used in medicines and cosmetics due to its various pharmacological effects, including its antioxidant, antiviral, anti-ulcer, and antibacterial activities. Glycyrrhizic acid is a major plant-derived metabolite that is still used in the long-term treatment of human immunodeficiency virus (HIV) infection owing to its low potential for drug resistance and few side effects (De Clercq, 1995; Vlietinck et al., 1998). Recent studies have shown that glycyrrhizic acid is a promising anti-severe acute respiratory syndrome (SARS)-CoV-2 drug candidate, either alone or in conjunction with other therapeutics (Bailly and Vergoten, 2020).

Components isolated from plant-derived natural products have been used as potential chemotherapeutic, chemopreventive, and anti-inflammatory agents over the last 30 years (Surh, 2002). Considering that the ideal adjuvant should be easy to obtain, safe, and easy to store, glycyrrhizic acid holds promise for this application. Although there are many studies on the effects of glycyrrhizic acid, clear results on its use as an adjuvant in the FMD vaccine are yet to be reported. The objective of this research was to explore the impact of glycyrrhizic acid as an adjuvant, overcome the drawbacks of current vaccines, and elicit an enhanced host immune response. Furthermore, we attempted to elucidate the mechanism of glycyrrhizic acid-mediated immune response induction in hosts.

2. Materials and methods

2.1. Glycyrrhizic acid

Glycyrrhizic acid ammonium salt [from glycyrrhiza roots (licorice)] was purchased from Sigma-Aldrich (Sigma-Aldrich, St. Louis, MO, USA).

2.2. Cells, virus, purification of inactivated viral antigens, and preparation of test bivalent vaccine

ZZ-R (fetal goat tongue) cells were grown in DMEM/F12 (Lonza, Basel, Switzerland), and BHK-21 and LF-BK (porcine kidney) cells were grown in DMEM (Lonza, Walkersville, MD, USA) supplemented with 1% antibiotic-antimycotic and 10% fetal bovine serum (FBS) (Gibco, Waltham, MA, USA) at 37°C in 5% CO_2. FMDV O PA2 and A YC antigens were purified according to the method described by Lee et al. (2020). Briefly, when full cytopathic effects (CPE) were noted, viruses (O PA2, A YC; grown in BHK-21 suspension cells) were collected via freezing and thawing. Once the cellular debris was eliminated via centrifugation at 12,000 rotations per minute (rpm) for 20 minutes (min), the viruses were exposed to 0.003 mM of binary ethyleneimine (Sigma-Aldrich) at 26°C for 24 hour (h). The inactivated virus within the transparent clear culture was allowed to precipitate overnight in 7.5% polyethylene glycol (PEG) 6000 and 2.3% NaCl at 4°C (Bahnemann, 1975). The obtained pellets were suspended in Tris-KCl (TK) buffer and further subjected to purification via centrifugation (using a sucrose gradient of 15–45% in TK buffer) at 30,000 rpm for 4 h at 4°C on an SW41Ti rotor (Beckman Coulter, Brea, CA, USA); viral antigen concentrations were assessed by spectrophotometric (Biophotometer, Eppendorf, Hamburg, Germany) analysis at a wavelength of 259 nm. The purified antigens (146S particle) were fixed onto carbon-coated copper grids and observed through a transmission electron microscope (TEM) (Hitachi H7100FA, Tokyo, Japan). The bivalent vaccine formulation for the positive control (PC) group in the mouse experiment included purified antigens isolated from O PA2 (15 μg/dose/mL; 1/40 of the dose for pigs) and A YC (15 μg/dose/mL; 1/40 of the dose for pigs), 10% $Al(OH)_3$, ISA 206 (50% w/w; Seppic, Paris, France), and 15 μg/dose/mouse Quil-A (InvivoGen, San Diego, CA, USA). 100 μg glycyrrhizic acid ammonium salt (Sigma-Aldrich) was also included in the test vaccine for the experimental (Exp.) group. The test bivalent vaccine formulation used in the pig experiment included purified antigens isolated from O PA2 (15 μg/dose/mL) and A YC (15 μg/dose/mL), 10% $Al(OH)_3$, ISA 206 (50% w/w; Seppic), and 150 μg/dose/pig Quil-A (InvivoGen). One mg glycyrrhizic acid ammonium salt (Sigma-Aldrich) was also included in the test vaccine for the Exp. group. All experiments related to FMDV were conducted in the Animal and Plant Quarantine Agency (APQA) under biosafety level 3 (BSL-3) conditions.

2.3. Mice and pigs

Sex- and age-matched wild-type C57BL/6 mice (females, 6–7 weeks old) were obtained from KOSA BIO Inc. (Seongnam-si, Gyeonggi-do, Korea), and FMD-antibody-seronegative pigs (Landrace, 8–9 weeks old) were supplied by BARON BIO Inc. (Uiseong-gun, Gyeongsangbuk-do, Korea). All mice and pigs were allowed at least 1 week to acclimatize to the laboratory environment before being used in experiments. All mice and pigs were accommodated in microisolator enclosures and were allowed unrestricted access to water and food in a dedicated pathogen-free BSL-3 animal (ABSL3) facility at the APQA. The housing facility maintained a relative humidity of approximately 50%, a temperature of 22°C, and a 12 h:12 h light:dark cycle. Investigations were conducted following institutional protocols and regulations and authorized by the Ethics Committee of the APQA (accreditation number: IACUC-2022-670 and IACUC-2023-753).

2.4. Isolation and culture of murine peritoneal exudate cells (PECs) and porcine peripheral blood mononuclear cells (PBMCs)

Naïve mice (6–7 weeks old, $n = 40$) were euthanized via CO_2 inhalation. The peritoneal cavities of the mice were then rinsed with 5 mL Ca^{2+}/Mg^{2+}/free DPBS (Gibco), and the resulting peritoneal lavage fluid was pelleted by centrifugation at 400 × *g* for 10 min at 4°C. The pelleted murine PECs were resuspended and counted using a Bio-Rad TC20 Automated Cell Counter (Bio-Rad, Hercules, CA, USA). All obtained cells were isolated in the fresh state immediately prior to use. None of the experiments involved the use of cryopreserved cells. Subsequently, purified PECs were cultured in a complete medium composed of Roswell Park Memorial Institute (RPMI) 1640 (Gibco) supplemented with 0.05 mM 2-beta-mercaptoethanol (Sigma-Aldrich), 3 mM L-glutamine (Sigma-Aldrich), 10% fetal calf serum (HyClone, Logan, UT, USA), 100 U/mL penicillin/streptomycin (Sigma-Aldrich), and 10 mM HEPES (Sigma-Aldrich) and incubated at 37°C under 5% CO_2. Porcine PBMCs were acquired from pigs (8–9 weeks old, $n = 3$ for the evaluation of IFNγ secretion by ELISpot, $n = 5$–6/group for the validation of gene expression by qRT-PCR) that tested negative for FMD antibodies. They were then purified from whole blood according to the procedure described by Lee et al. (2020) and Jo et al. (2021). Whole blood (20 mL/donor) was collected in BD Vacutainer heparin tubes (BD, Becton, Dickinson and Company, Franklin Lakes, NJ, USA). Porcine PBMCs were isolated through gradient centrifugation using Histopaque solution (Sigma-Aldrich). The remaining red blood cells (RBC) were eliminated with ammonium–chloride–potassium (ACK) lysing buffer (Gibco). Porcine PBMCs were suspended in Ca^{2+}/Mg^{2+}-free DPBS (Gibco). Cell quantification was performed with a Bio-Rad TC20 Automated Cell Counter (Bio-Rad). The separated porcine PBMCs were then suspended in RPMI-1640 (Gibco) medium supplemented with 100 U/mL penicillin/streptomycin (Sigma-Aldrich), 10 mM HEPES (Sigma-Aldrich), 3 mM L-glutamine (Sigma-Aldrich), and 10% FBS (Gibco). All purified cells were cultured in a moist environment at 37°C with 5% CO_2.

2.5. Glycyrrhizic acid-mediated cell viability assay and IFNγ ELISpot assay in PECs and porcine PBMCs *in vitro*

BHK-21, LF-BK, and ZZ-R cell lines, murine PECs, and porcine PBMCs were used in the cell viability assay. BHK-21, LF-BK, and

ZZ-R cells (2×10^4 cells/well) were cultured in a 96-well microplate and incubated for 48 h in 5% CO_2 at 37°C. Isolated murine PECs and porcine PBMCs (1×10^5 cells/well) were seeded in a 96-well microplate and stabilized for 1 h in 5% CO_2 at 37°C. After incubation, the media was changed and BHK-21, LF-BK, and ZZ-R cells, murine PECs, and porcine PBMCs were treated with glycyrrhizic acid (0, 0.625, 1.25, 2.5, or 5 μg/mL) for 4 h. Cell viability was determined using an MTS (inner salt)-based colorimetric assay. Investigations were performed by introducing a small quantity of CellTiter® 96 AQueous One Solution Reagent (Promega, Madison, WI, USA) directly to the culture wells, incubating the plates for 4 h in 5% CO_2 at 37°C, and subsequently measuring the absorbance at 490 nm with a Hidex 300SL spectrophotometer (Hidex, Turku, Finland). Commercial ELISpot assay kits (R&D Systems, Minneapolis, MN, USA) were used to analyze glycyrrhizic acid-induced IFNγ secretion, with or without inactivated O PA2 and A YC antigens, according to the manufacturer's instructions. In brief, isolated murine PECs (5×10^5 cells/well) or porcine PBMCs (5×10^5 cells/well) were incubated in a 96-well PVDF microplate which was backed with a monoclonal capture antibody that targets either mouse or porcine IFNγ, which had been pre-coated onto the plate. Subsequently, the cells were exposed to inactivated FMDV (O PA2 and A YC) antigens at a concentration of 2 μg/mL (final concentration), either with or without 0.625, 1.25, 2.5, or 5 μg/mL glycyrrhizic acid in a humidified incubator for 18 h in 5% CO_2 at 37°C. PBS and 2 μg/mL inactivated FMDV (O PA2 or A YC) antigen were used for the negative control (NC) and PC, respectively. The plates were rinsed with wash buffer and then incubated overnight at 4°C with biotinylated anti-mouse IFNγ (1:119) or anti-porcine IFNγ (1:119) antibodies. Thereafter, they were treated with AP-conjugated streptavidin (1:119) for 2 h at room temperature (RT, approximately 25°C). The plates were rinsed, developed with 5-bromo-4-chloro-3′ indolyl phosphate p-toluidine salt (BCIP)/nitro blue tetrazolium chloride (NBT), and quantified using an ImmunoSpot ELISpot reader (AID iSpot Reader System; Autoimmune Diagnostika GmbH, Strassberg, Germany). Data were reported as the number of spot-forming cells (SFC).

2.6. Effects of glycyrrhizic acid alone on inducing host defenses against FMDV infection in mice

Prior to evaluating the adjuvant efficacy of glycyrrhizic acid, we investigated the host defense induced by glycyrrhizic acid alone (without FMDV antigen) against FMDV infection in mice. The following challenge viruses were used; FMDV type O [O/VET/2013 (ME-SA topotype, GenBank Accession No. MF947143.1)] and FMDV type A [(A/Malay/97, SEA topotype, GenBank Accession No. KJ933864)]. Since there were two types of viruses used in the challenge, C57BL/6 mice (females, 6–7 weeks old, $n = 5$/group) were divided into two sets and then into two groups; NC, Exp. I on 3 days-post injection (dpi) challenged group; NC, Exp. II on 7 dpi challenged group for each virus. After intramuscular (I.M.) injection, all mice were challenged with 100 LD_{50} of O/VET/2013 or A/Malay/97 viruses via intraperitoneal (I.P.) injection on 3 or 7 dpi, and the survival rate and body weights were observed for 7 days post-challenge (dpc). The Exp. I and Exp. II groups received an injection of 100 μg glycyrrhizic acid/100 μL PBS, and the NC groups were given an equivalent volume of PBS via the same route.

2.7. Efficacy of FMD vaccine containing glycyrrhizic acid in inducing adjuvant-mediated host defense in mice

To evaluate the potential of glycyrrhizic acid as a vaccine adjuvant and the initial protective effect of the vaccine containing glycyrrhizic acid against viral infection, we performed challenge experiments in mice. C57BL/6 mice (females, 6–7 weeks old, $n = 5$/group) were divided into two sets for each virus and then into three groups (NC, PC, and Exp.). After I.M. vaccination, all mice were challenged with 100 LD_{50} of FMDV O/VET/2013 or A/Malay/97 virus via I.P. injection at 7 days post-vaccination (dpv), and observed for 7 dpc. The PC group was given the test bivalent vaccine, the Exp. group was given the test bivalent vaccine with glycyrrhizic acid, and the NC group was given an equivalent volume of PBS via the same route.

2.8. Efficacy of FMD vaccine containing glycyrrhizic acid in inducing adjuvant-mediated early, mid-term, and long-term immune responses in mice

To assess the efficacy of glycyrrhizic acid in eliciting innate and adaptive (cellular and humoral) immune responses as an FMD vaccine adjuvant, we performed mice experiments as follows. C57BL/6 mice (females, 6–7 weeks old, $n = 5$/group) were divided into three groups (NC, PC, Exp.). Following I.M. injection of the test bivalent vaccine, blood samples were collected at 0, 7 (early), 28 (mid-term), 56, and 84 (long-term) dpv to monitor antibody titers and virus neutralization (VN) titers using structural protein (SP) ELISA and VN tests, respectively. The serum samples were preserved at −80°C until further use.

2.9. Efficacy of FMD vaccine containing glycyrrhizic acid in inducing adjuvant-mediated early, mid-term, and long-term immune responses in pigs

FMD-antibody-seronegative pigs (8–9 weeks old, $n = 5$–6/group) were used for the experiments. Animals were randomly divided into three groups (NC, PC, Exp.). After the initial I.M. injection for primary vaccination, booster doses were given via the same route on 28 dpv. Blood samples were collected at 0, 7, 14 (early), 28, 42 (mid-term), 56, and 84 (long-term) dpv to measure the antibody titers and VN titers via SP ELISA and VN tests, respectively. The serum samples were preserved at −80°C until further use.

2.10. Serological assay

2.10.1. Structural protein (SP) ELISA

To identify serum antibodies against structural proteins, we utilized PrioCheck™ FMDV type A (Prionics AG, Switzerland)

kits and VDPro® FMDV type O (Median Diagnostics, Chuncheon-si, Gangwon, Korea) kits. Optical density readings from the ELISA plates were transformed into a percentage inhibition (PI) value. When the PI value ≥50% for the PrioCheck™ FMDV kit or ≥40% for the VDPro® FMDV kit, the animals were classified as antibody-positive.

2.10.2. VN tests

VN tests were carried out following guidelines from the World Organization for Animal Health (WOAH). Serum from the vaccinated animals was inactivated via heating at 56°C for 30 min in a water bath. The cell density was adjusted to achieve a 70% monolayer, and the serum samples were serially diluted by 2-fold (ranging from 1:8 to 1:1024). These diluted serum samples were then exposed to a homologous virus (O PA2 or A YC) at a concentration of [100 × the tissue culture infectious dose $(TCID)_{50}$]/0.5 mL and incubated for 1 h at 37°C. After 1 h, an LF-BK cell suspension was introduced to all wells. CPE was noted after 2–3 days in order to determine the titers, which were presented as the $\log_{10}$ of the reciprocal antibody dilution necessary to neutralize 100 × $TCID_{50}$ of the virus (Fowler et al., 2010; Fukai et al., 2015a).

2.10.3. Immunoglobulin subtype (IgG, IgA, and IgM) ELISA

To detect specific Ig isotype antibodies, we carried out ELISA targeting porcine IgG, IgA, and IgM (Bethyl Laboratories. Inc., Montgomery, Texas, USA) within the serum samples according to the manufacturer's instructions. In brief, diluted serum and standards were introduced to their respective wells, each with a volume of 100 µL/well, and incubated for 1 h at RT. Afterward, the plates were rinsed and allowed to air-dry. Following this, 100 µL of the 1× biotinylated detection antibodies were treated into all wells, and the plates were subjected to incubation at RT for 1 h. Following rinsing and drying of the wells, 100 µL of 1× streptavidin-horseradish peroxidase conjugate was introduced into each well. Subsequently, the plates underwent a 30 min incubation at RT. Following this, the plates underwent an additional cycle of rinsing and drying. Peroxidase activity was visualized by adding 100 µL/well of 1× TMB solution and allowing the plates to incubate at RT for 30 min. The reaction was terminated with 100 µL of 2 N H_2PO_4, and the absorbances at 450 nm were detected using a Hidex 300SL spectrophotometer (Hidex).

2.11. RNA isolation, cDNA synthesis, and quantitative real-time PCR (qRT-PCR)

Isolated porcine PBMCs were employed for RNA extraction via a RNeasy Mini Kit (QIAGEN, Valencia, CA, USA) and TRIzol® reagent (Invitrogen; Thermo Fisher Scientific, Inc., Carlsbad, CA, USA). Subsequently, reverse transcription into cDNA was accomplished using a GoScript Reverse Transcription System (Promega) according to the manufacturer's guidelines. The reverse-transcribed cDNA were then subjected to qRT-PCR using a Bio-Rad CFX96™ Touch Real-time PCR system. Quantitative gene expression levels were normalized to that of HPRT (endogenous housekeeping gene) and presented relative to the control values. The list of primers used in this study is presented in Supplementary Table S1.

2.12. Statistical analysis

All quantitative data are expressed as the mean ± standard error (SEM) unless otherwise specified. Variations between groups were evaluated utilizing two-way ANOVA with Tukey's *post hoc* test or one-way ANOVA followed by Tukey's *post hoc* test or Dunnett's *post hoc* test, as appropriate. Statistical significance is indicated as follows: $^{*}p < 0.05$, $^{**}p < 0.01$, $^{***}p < 0.001$, and $^{****}p < 0.0001$. Parametric examinations were employed to compare diverse groups. Survival curves were generated using the Kaplan–Meier method, and variations were analyzed using log-rank sum tests. GraphPad Prism 10.0.2 (GraphPad, San Diego, CA, USA) was used for all statistical analyses.

3. Results

3.1. Glycyrrhizic acid can stimulate an innate immune response

Prior to performing the subsequent experiments using glycyrrhizic acid, we assessed glycyrrhizic acid-mediated cytotoxicity via an MTS assay. Glycyrrhizic acid at various concentration did not exhibit cytotoxicity on any of the cell lines used in the study, including BHK-21, LF-BK, and ZZ-R cells, murine PECs, and porcine PBMCs (Supplementary Figure S1).

To demonstrate the innate and cellular immune response-inducing potential of glycyrrhizic acid, we conducted IFNγ ELISpot analysis by including glycyrrhizic acid at varying concentrations with or without inactivated FMDV (O PA2 or A YC) antigens. This assay used murine PECs and porcine PBMCs. When murine PECs were treated with 0.625 µg/mL glycyrrhizic acid along with FMDV (O PA2 or A YC) antigens, a significant increase in IFNγ secretion was observed compared to when antigen alone was administered (Figures 1A,B). Furthermore, in porcine PBMCs, it was observed that, apart from glycyrrhizic acid at 5 µg/mL, all concentrations led to a significant increase in IFNγ secretion when compared to antigen only (Figures 1C,D). Thus, glycyrrhizic acid is able to stimulate innate and cellular immune responses.

3.2. Glycyrrhizic acid as an adjuvant induces a strong host defense against FMDV infection in mice

Prior to evaluating the FMD vaccine containing glycyrrhizic acid-mediated host defense, we investigated the efficacy of glycyrrhizic acid alone in inducing host defense responses against FMDV O/VET/2013 and A/Malay/97 infection in mice. In previous experiments, glycyrrhizic acid significantly increased IFNγ secretion via induction of an innate immune response. However, our results showed that glycyrrhizic acid alone (without inactivated FMDV antigen) did not induce a host defense response against viral infection (Supplementary Figures S2B–E).

In order to evaluate the protective effect of the test vaccine (containing glycyrrhizic acid as an adjuvant) against FMDV infection, the experiment was performed according to the protocol shown in Figure 2A. A 100% survival rate was seen in the group

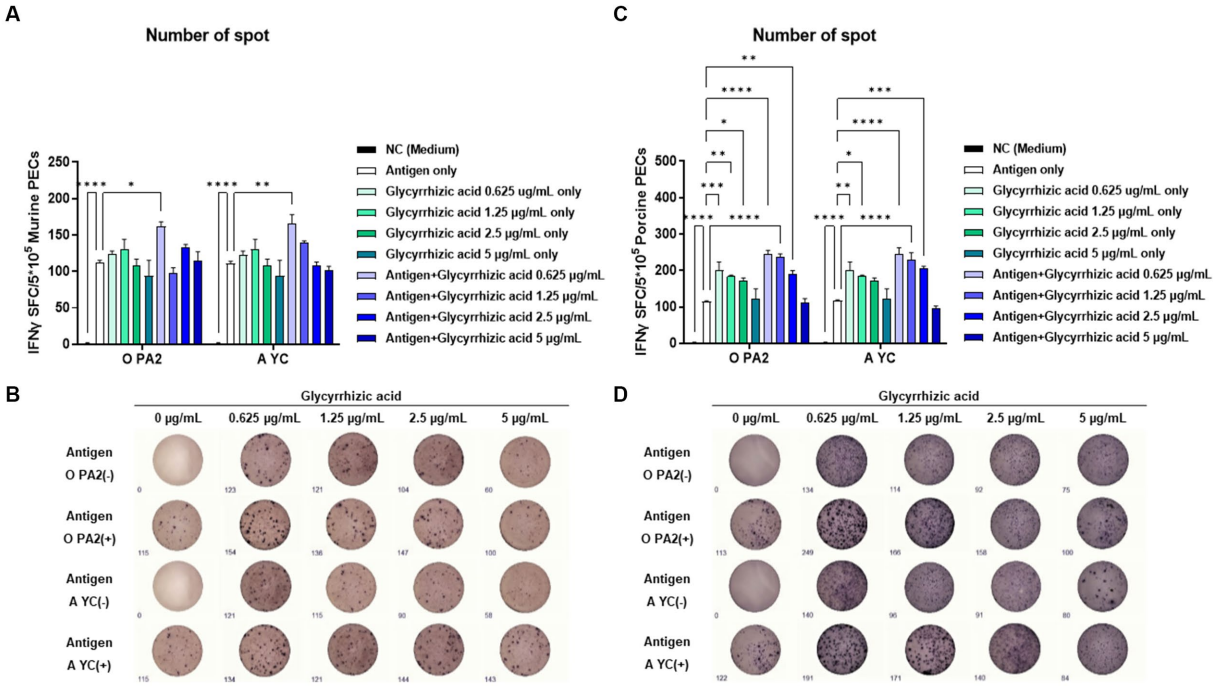

FIGURE 1
Inactivated FMDV type O (O PA2) or A (A YC) antigen-mediated innate immune response (in the presence or absence of glycyrrhizic acid) via secretion of interferon (IFN)γ in murine peritoneal exudate cells (PECs) and porcine peripheral blood mononuclear cells (PBMCs). To evaluate the innate immune response to inactivated FMDV type O (O PA2) or A (A YC) antigen (in the presence or absence of glycyrrhizic acid), IFNγ secretion was determined using an ELISpot assay. **(A–D)** IFNγ-secreting cell spots in murine PECs **(A)**; Images of IFNγ secretion in murine PECs **(B)**; IFNγ-secreting cell spots in porcine PBMCs **(C)**; Images of IFNγ secretion in porcine PBMCs **(D)**. Data are represented as the means ± SEM of spot-forming cells (SFCs) from triplicate measurements ($n = 3$/group). Statistical analyses were conducted using one-way ANOVA followed by Tukey's *post-hoc* test. *$p < 0.05$, **$p < 0.01$, ***$p < 0.001$, and ****$p < 0.0001$.

which was vaccinated with the glycyrrhizic acid adjuvant (Exp. Group) post infection with FMDV type O (O/VET/2013) compared to that in both the PBS-injected (NC) group (0% survival rate) and the test vaccine without glycyrrhizic acid-vaccinated (PC) group (40% survival rate) (Figure 2B). When experiments were conducted using FMDV type A (A/Malay/97), the survival rate was 100% in the Exp. group (Figure 2D). The NC and PC groups lost weight while the Exp. group showed an increasing trend in weight (Figures 2C,E).

3.3. Efficacy of vaccines containing glycyrrhizic acid in inducing early, mid-term, and long-term immunity in mice

In order to confirm that the test vaccine (with glycyrrhizic acid as an adjuvant) elicits an immune-enhancing effect as well as innate and adaptive (cellular and humoral) immune responses, we evaluated early, mid-, and long-term immunity in mice (Figure 3A). Mice were divided into three groups (NC, PC, and Exp.) and samples of blood were collected for serological analyses, which included SP O ELISA, SP A ELISA, and VN tests (Figures 3B–E).

After vaccination, antibody titers initially increased in both the PC and Exp. groups; however, the PC group's antibody titers gradually decreased over time, while the Exp. group's increased (measured by SP O ELISA and SP A ELISA) (Figures 3B,C). In terms of VN titers against O PA2 and A YC, the Exp. group demonstrated higher levels than the PC group, and this difference increased significantly with time (Figures 3D,E).

Therefore, the test vaccine, which includes glycyrrhizic acid as an adjuvant, demonstrated exceptional immunity-inducing effects in mice, including early (7 dpv), mid- (28 dpv), and long-term (56 and 84 dpv) immune responses.

3.4. Efficacy of vaccines containing glycyrrhizic acid in inducing early, mid-term, and long-term immunity in pigs

Next, we conducted animal experiments on target animals to confirm whether glycyrrhizic acid as an adjuvant has synergistic effects in inducing innate and adaptive (cellular and humoral) immunity. FMD antibody-seronegative pigs were vaccinated with test vaccines (containing glycyrrhizic acid as an adjuvant), and cellular and humoral immune responses were evaluated along with early, mid-, and long-term immunity. A booster vaccine was administered at 28 dpv. Blood samples were collected at 0, 7, 14, 28, 42, 56, and 84 dpv, and serological tests were performed (Figure 4A).

Results showed that after the initial vaccination period, the Exp. group had significantly higher antibody titers (measured via SP O ELISA and SP A ELISA) than the PC group, and at 84 dpv, antibody titers in the PC group had decreased, whereas those in the Exp. group remained consistent or increased (Figures 4B,C). Similarly, VN titers for O PA2 and A YC showed comparable results based on SP O ELISA and SP A ELISA

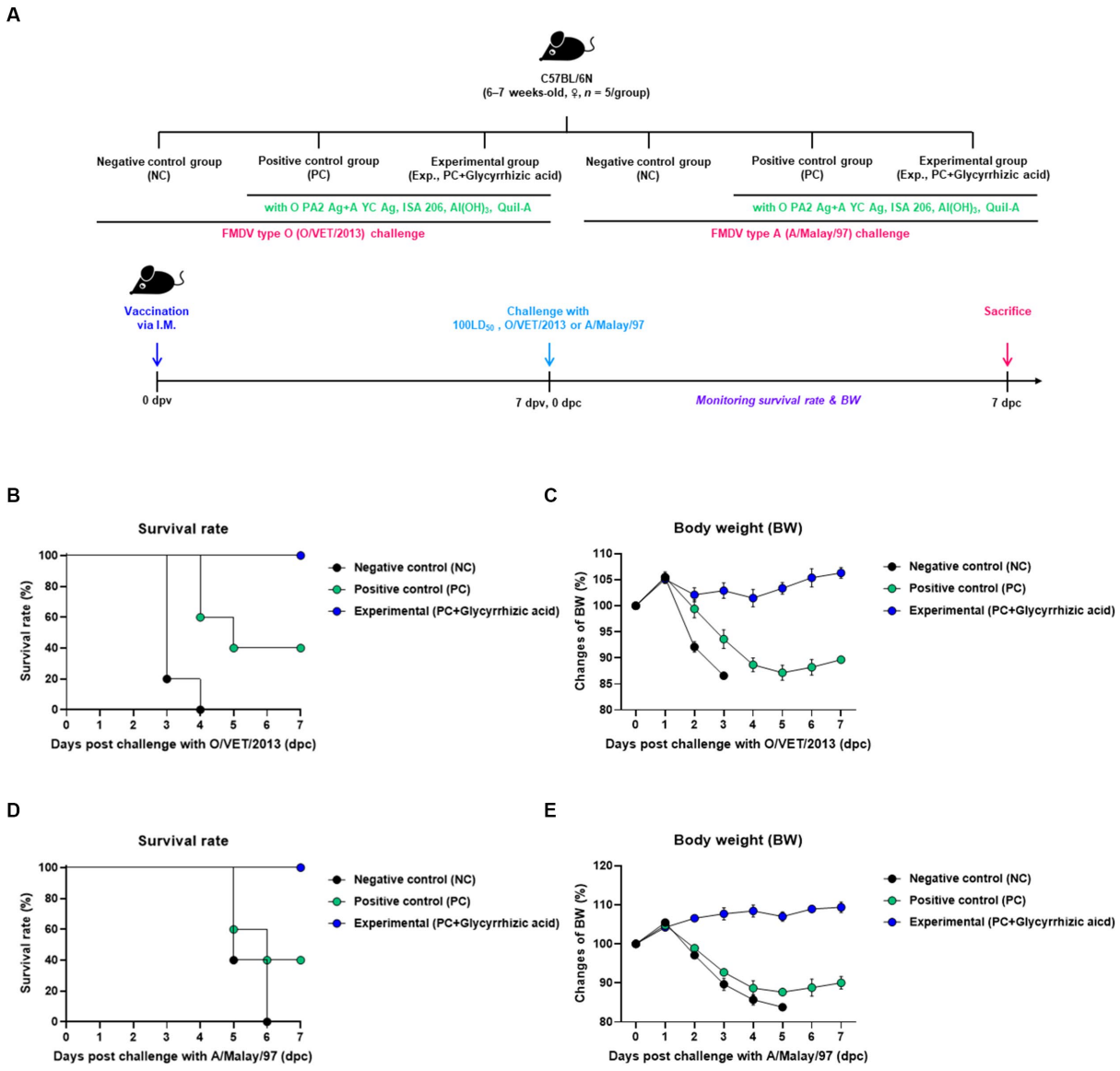

FIGURE 2
Efficacy and protective effects of FMD vaccine (containing glycyrrhizic acid) in the early stage of vaccination against viral infection in mice. C57BL/6 mice (females, 6–7 weeks old, $n = 5$/group) were divided into six groups, namely, a negative control (NC) group for FMDV type O (O/VET/2013) challenge ($n = 5$/group), a positive control (PC) group for FMDV type O (O/VET/2013) challenge ($n = 5$/group), an experimental (Exp.) group for FMDV type O (O/VET/2013) challenge ($n = 5$/group), an NC group for FMDV type A (A/Malay/97) challenge ($n = 5$/group), a PC group for FMDV type A (A/Malay/97) challenge ($n = 5$/group), and an Exp. group for FMDV type A (A/Malay/97) challenge ($n = 5$/group). The Exp. group was administered test vaccines containing 0.375 μg of O PA2 + 0.375 μg of A YC antigen (1/40 dose for cattle and pig use) with ISA 206 (oil-based emulsion, 50%, w/w), 10% $Al(OH)_3$, 15 μg Quil-A, and 100 μg glycyrrhizic acid. The PC group was administered all the above except glycyrrhizic acid. The NC group was injected with an equivalent amount of PBS. Vaccination was performed once with 100 μL vaccine (1/10 the normal dose for cattle and pigs) injected intramuscularly into the thigh, and the mice were challenged with FMDV type O (100 LD_{50} O/VET/2013) and FMDV type A (100 LD_{50} A/Malay/97) at 7 days post-vaccination (dpv). Survival rates and body weights were monitored for 7 days post-challenge (dpc). **(A–E)** Experimental strategy **(A)**; Survival rates post-challenge with O/VET/2013 **(B)**; Changes in body weight post-challenge with O/VET/2013 **(C)**; Survival rates post-challenge with A/Malay/97 **(D)**; Changes in body weight post-challenge with A/Malay/97 **(E)**. Data are represented as the means ± SEM of triplicate measurements ($n = 5$/group).

(Figures 4D,E). Furthermore, an immunoassay was performed using sera from vaccinated pigs to assess the impact of vaccination (with a glycyrrhizic acid as an adjuvant) on immunoglobulin levels (Figures 5A–C). At 56 dpv, the concentrations of both IgG and IgA were significantly higher in the Exp. group than in the PC group (Figures 5A,B). In terms of IgM levels, inter-individual differences were observed but the overall level of IgM was elevated in the Exp. group when compared with the PC group at 56 dpv (Figure 5C).

Overall, the test vaccine containing glycyrrhizic acid showed superior immune-enhancing effects in pigs when compared to the vaccine without glycyrrhizic acid in terms of early- (7 and 14 dpv), mid- (28 and 42 dpv), and long-term (56 and 84 dpv) immunity.

10.3389/fmicb.2023.1289065

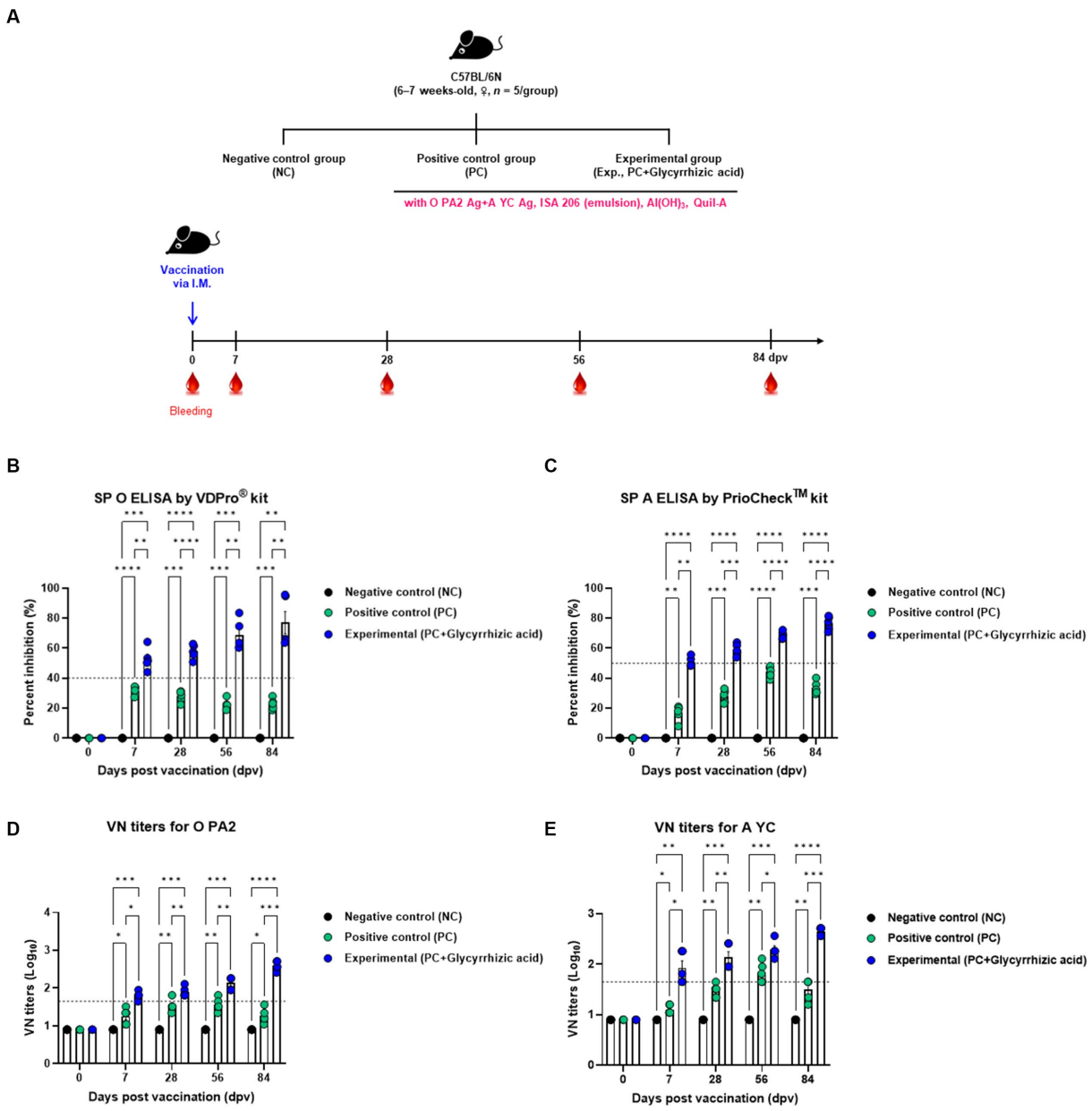

FIGURE 3
FMD vaccine containing glycyrrhizic acid mediates early, and mid- and long-term immune responses in mice. C57BL/6 mice (females, 6–7 weeks old, $n = 5$/group) were divided into three groups, namely, a negative control (NC) group ($n = 5$/group), a positive control (PC) group ($n = 5$/group), and an experimental (Exp.) group ($n = 5$/group). The Exp. group was administered test vaccines containing 0.375 μg of O PA2 + 0.375 μg of A YC antigen (1/40 dose for cattle and pig use) with ISA 206 (oil-based emulsion, 50%, w/w), 10% $Al(OH)_3$, 15 μg Quil-A, and 100 μg glycyrrhizic acid in a total volume of 100 μL. The PC group was administered all the above except glycyrrhizic acid. The NC group was injected with an equivalent amount of PBS. Vaccination was performed once with 100 μL of vaccine (1/10 of the normal dose for cattle and pigs) injected intramuscularly into the thigh. Blood samples were collected at 0, 7, 28, 56, and 84 days post-vaccination (dpv) for serological assays. **(A–E)** Experimental strategy **(A)**; SP O antibody titers (VDPro® kit) **(B)**; SP A antibody titers (PrioCheck™ kit) **(C)**; VN titers for O PA2 **(D)**; VN titers for A YC **(E)**. Data are represented as the means ± SEM of triplicate measurements ($n = 5$/group). Statistical analyses were conducted using two-way ANOVA followed by Tukey's test. *$p < 0.05$; **$p < 0.01$; ***$p < 0.001$; and ****$p < 0.0001$.

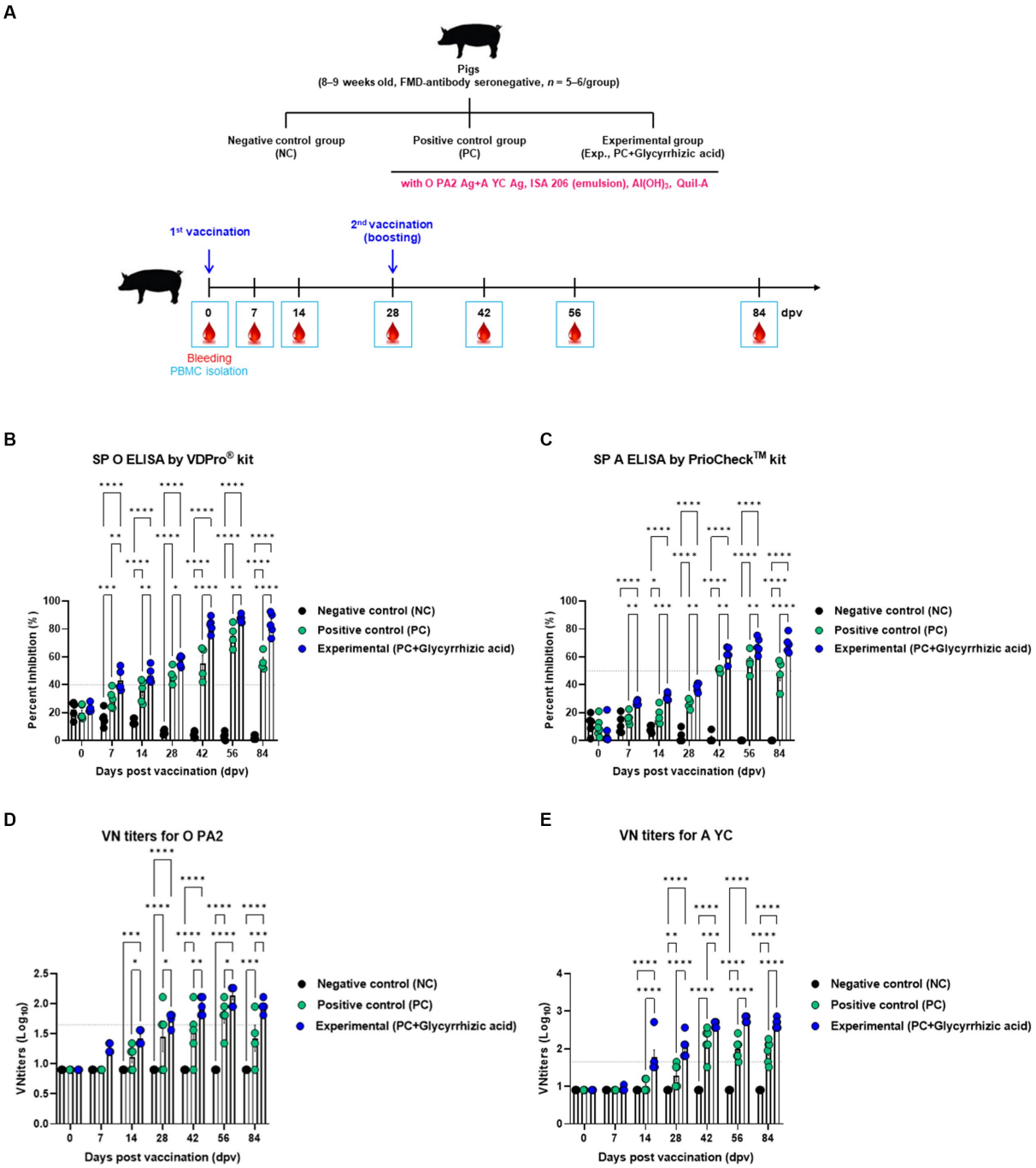

FIGURE 4
FMD vaccine containing glycyrrhizic acid mediates early, and mid- and long-term immune responses in pigs. Pigs (8–9 weeks old, FMD antibody-seronegative, $n = 5–6$) were divided into three groups, namely, a negative control (NC) group ($n = 5–6$/group), a positive control (PC) group ($n = 5–6$/group), and an experimental (Exp.) group ($n = 5–6$/group). The Exp. group was administered test vaccines containing 15 μg O PA2 + 15 μg A YC antigen (1 dose for cattle and pig use) with ISA 206 (oil-based emulsion, 50%, w/w), 10% $Al(OH)_3$, 150 μg Quil-A, and 1 mg glycyrrhizic acid. The PC group was administered all the above except glycyrrhizic acid. Vaccination was performed twice at 28-day intervals, with 1 mL vaccine (1 dose for cattle and pigs) injected intramuscularly in the neck. Blood samples were collected from the pigs at 0, 7, 14, 28, 42, 56, and 84 days post-vaccination for serological assays. **(A–E)** Experimental strategy **(A)**; SP O antibody titers (VDPro® kit) **(B)**; SP A antibody titers (PrioCheck™ kit) **(C)**; O PA2 VN titers **(D)**; A YC VN titers **(E)**. Data are represented as the means ± SEM of triplicate measurements ($n = 5–6$/group). Statistical analyses were conducted using two-way ANOVA followed by Tukey's test. *$p < 0.05$; **$p < 0.01$; ***$p < 0.001$; and ****$p < 0.0001$.

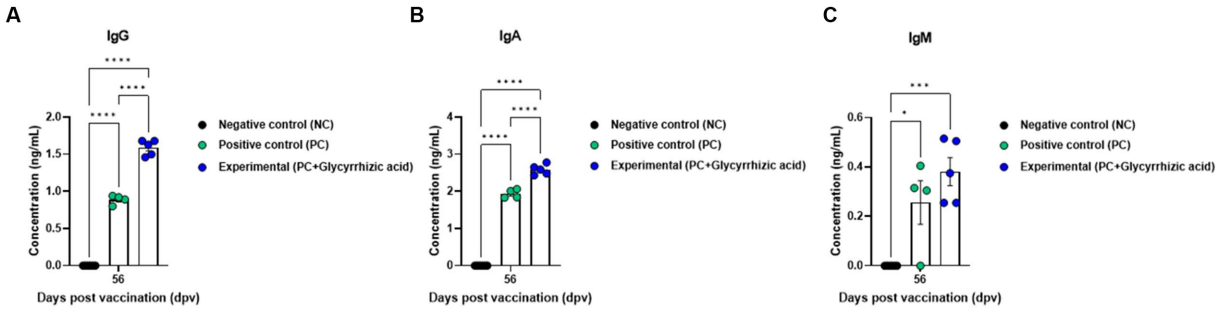

FIGURE 5
FMD vaccine containing glycyrrhizic acid mediates increases in immunoglobulin levels, including IgG, IgM, and IgA, in pigs. Pigs (8–9 weeks old, FMD antibody-seronegative, $n = 5–6$) were divided into three groups, namely, a negative control (NC) group ($n = 5–6$/group), a positive control (PC) group ($n = 5–6$/group), and an experimental (Exp.) group ($n = 5–6$/group). The Exp. group was administered test vaccines containing 15 μg O PA2 + 15 μg A YC antigen (1 dose for cattle and pig use) with ISA 206 (oil-based emulsion, 50%, w/w), 10% $Al(OH)_3$, 150 μg Quil-A, and 1 mg glycyrrhizic acid. The PC group was administered all the above except glycyrrhizic acid. Vaccination was performed twice at 28-day intervals, with 1 mL vaccine (1 dose for cattle and pigs) injected intramuscularly in the neck. Blood samples from pigs were collected at 0, 7, 14, 28, 42, 56, and 84 days post-vaccination for serological assays. **(A–C)** IgG concentration **(A)**; IgA concentration **(B)**; IgM concentration **(C)**. Data are represented as the means ± SEM of triplicate measurements ($n = 5–6$/group). Statistical analyses were conducted using two-way ANOVA followed by Tukey's test. *$p < 0.05$; **$p < 0.01$; ***$p < 0.001$; and ****$p < 0.0001$.

3.5. FMD vaccine with glycyrrhizic acid adjuvant induces strong cellular and adaptive immune responses by inducing pattern-recognition receptor (PRR), transcription factor, cytokine, and co-stimulatory molecule expression in PBMCs

To determine the effectiveness and mechanisms of vaccines containing glycyrrhizic acid, we performed qRT-PCR using porcine PBMCs isolated from whole blood samples from pigs vaccinated with the test vaccine containing glycyrrhizic acid (Figures 6A–X). In the Exp. group, retinoic acid-inducible gene (RIG)-I expression had increased significantly at 14 dpv and decreased slightly at 56 dpv. However, these differences were also observed in the PC group (Figure 6A). In addition, Sirtuin (SIRT)1 expression significantly increased at 56 dpv (Figure 6B). Myeloid differentiation primary response (MyD)88 expression significantly increased over time (Figure 6C). Tumor necrosis factor (TNF) receptor associated factor (TRAF)6 increased significantly higher in the Exp. group than in the PC group at 14 dpv; however, levels in both groups decreased at 56 dpv, although they remained higher in the Exp. group (Figure 6D). Nuclear factor kappa-light-chain-enhancer of activated B cells (NF-κB) was also found to increase at both 14 dpv and 56 dpv (Figure 6E). Although signal transducer and activator of transcription (STAT)1 level had increased in the Exp. group compared to that in the PC group at 14 dpv, there was no difference at 56 dpv (Figure 6F). STAT4 expression increased significantly in the Exp. group compared to that in the PC group at 14 dpv and decreased slightly at 56 dpv, although it remained significantly higher in the PC group (Figure 6G).

Cluster of differentiation (CD)80, CD86, and CD28 levels were all significantly increased in the Exp. group compared to those in the PC group at both 14 and 56 dpv (Figures 6H–J). CD81 expression was significantly higher than that of PC group at 14 dpv; however, level in Exp. group decreased at 56 dpv, although they remained higher in the Exp. group (Figure 6K). Regarding CD19, CD21, and C3d levels, the Exp. group showed increases at 14 dpv and slightly higher levels at 56 dpv (Figures 6L–N). This indicated that glycyrrhizic acid is involved in the activation and proliferation of T and B cells by acting as a co-stimulating signal.

TNFα levels were significantly elevated in the Exp. group when compared with the PC group at 14 dpv (Figure 6O). IFNα, IFNβ, and IFNγ levels were significantly increased at 14 dpv; at 56 dpv, they were still higher than in the PC group, although they decreased thereafter (Figures 6P–R). Based on these results, glycyrrhizic acid appears to induce a balanced innate immune response.

Interleukin (IL)-1β and IL-6 levels significantly increased at 14 dpv and decreased at 56 dpv, but remained significantly higher in the Exp. group than in the PC group (Figures 6S,T). IL-12p40 levels increased over time and were significantly higher in the Exp. group (Figure 6U). IL-23p19 and IL-23R levels were also higher in the Exp. group when compared to the NC and PC groups at 56 dpv (Figures 6V,W).

No significant difference was observed in IL-17A levels between the PC and Exp. groups at 14 dpv; however, the level in the Exp. group was remarkably higher at 56 dpv (Figure 6X).

Collectively, these findings suggest that glycyrrhizic acid could stimulate RIG-I to induce inflammation, activate NF-κB through the MyD88 and TRAF6 signaling pathways despite SIRT1 differentiation, mediate responses to IL-12p40 via STAT4, and regulate the differentiation of T helper cells.

4. Discussion

FMD is a disease that affects hooved livestock and has been prevalent throughout history (Grubman and Baxt, 2004; Jamal and Belsham, 2013). In some European countries, emergency vaccination is mandatory once a FMD outbreak occurs, even if the country was considered FMD-free previously (Arzt et al., 2011; Stenfeldt et al., 2014).

Since its discovery, there have been many studies on vaccines for FMDV. Recombinant protein vaccines such as virus-like particle (VLP) vaccines (Xiao et al., 2016), peptide vaccines (Cao et al., 2013),

10.3389/fmicb.2023.1289065

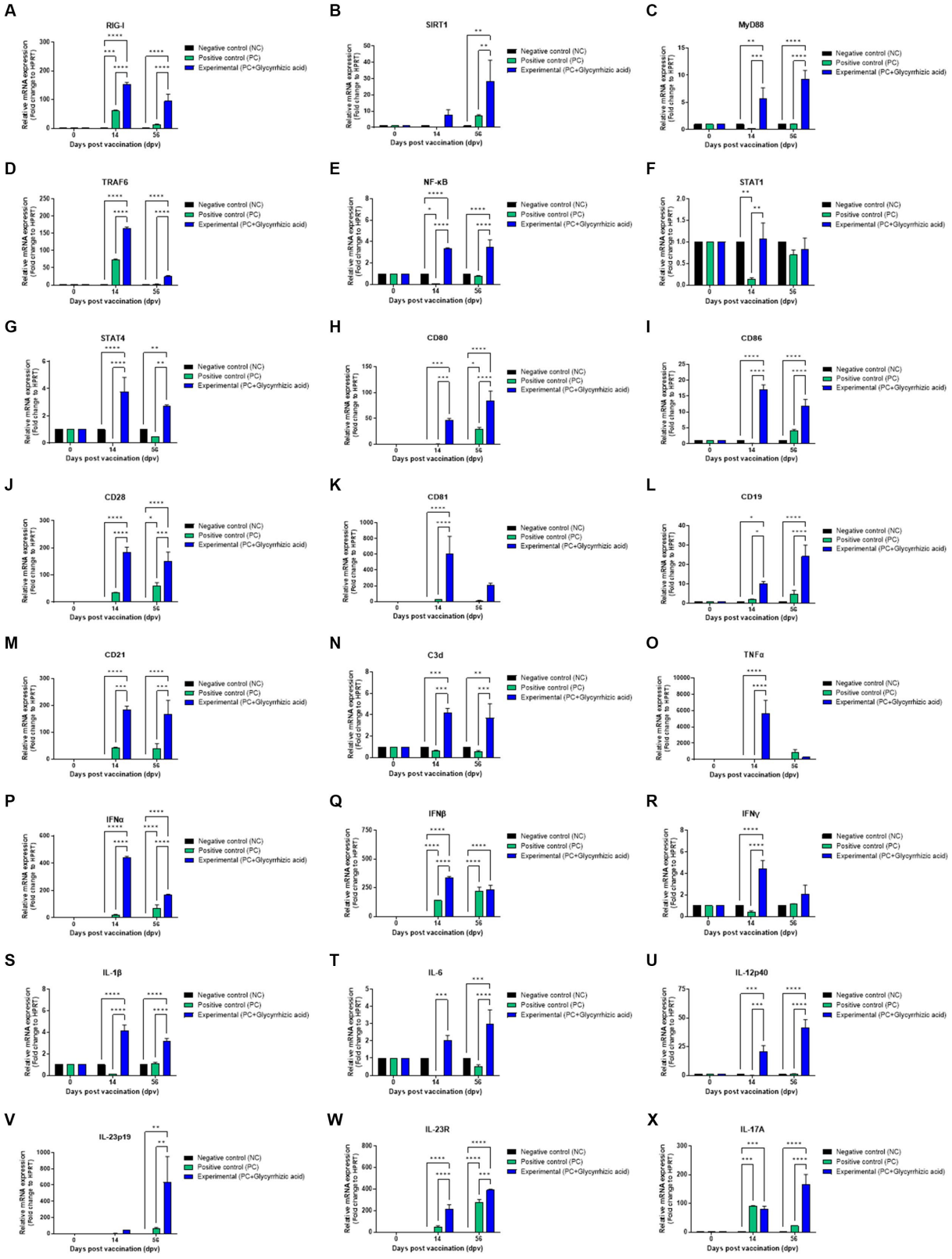

FIGURE 6
FMD vaccine containing glycyrrhizic acid mediates immunoregulatory gene expression in porcine peripheral blood mononuclear cells isolated from vaccinated pigs. Porcine peripheral blood mononuclear cells (PBMCs) isolated from the whole blood of vaccinated pigs [*n*=5–6/group; as described in Figure 4 **(A)**] were used for qRT-PCR assays. Gene expression levels were normalized to HPRT levels and presented as a relative ratio to the control. **(A–X)** Gene expression levels of RIG-I **(A)**; SIRT1 **(B)**; MyD88 **(C)**; TRAF6 **(D)**; NF-κB **(E)**; STAT1 **(F)**; STAT4 **(G)**; CD80 **(H)**; CD86 **(I)**; CD28 **(J)**; CD81 **(K)**; CD19 **(L)**; CD21 **(M)**; C3d **(N)**; TNFα **(O)**; IFNα **(P)**; IFNβ **(Q)**; IFNγ **(R)**; IL-1β **(S)**, IL-6 **(T)**; IL-12p40 **(U)**; IL-23p19 **(V)**; IL-23R **(W)**; and IL-17A **(X)**. Data are represented as the means ± SEM of triplicate measurements (*n*=5–6/group). Statistical analyses were conducted using two-way ANOVA followed by Tukey's test. **p*<0.05; ***p*<0.01; ****p*<0.001; and *****p*<0.0001.

and DNA (Kotla et al., 2016) and RNA (Borrego et al., 2017) vaccines have become a research hotspot. Alternatively, inactivated vaccines have the highest immunogenicity; however, shielding facilities (such as BSL3 facilities) are required to make inactivated vaccines and there is always a risk of live virus leakage due to incomplete inactivation. Therefore, currently commercially available vaccines are prepared in the form of double oil emulsions, where the oil-soluble adjuvant is mixed with the inactivated whole virus (Nagendrakumar et al., 2011).

Typically, an adjuvant is a substance that is administered with a vaccine and can enhance its efficacy by triggering a host immune response. Currently commercially available inactivated vaccines contain oil-based adjuvants. However, these vaccines have disadvantages including the long period required for antibody titers to rise to defensive levels post-vaccination, limiting their ability to induce an initial host response post-vaccination. Moreover, significant side effects (such as local adverse reactions at the vaccination site) can be caused by oil-based adjuvants.

Aluminum has been used as a safe adjuvant in many vaccines since 1926 (Ramon, 1925; Hogenesch, 2013), and is still widely used. However, $Al(OH)_3$, the most commonly used adjuvant, has the limitation of only stimulating Th2-mediated immune responses (Hem and Hogenesch, 2007; Jiang et al., 2018).

If these limitations are overcome through the addition of novel immunostimulants, the immune response after vaccination can be expected to increase significantly. This may improve the efficacy of the vaccine in inducing immunity at all stages, including early, mid-term, and long-term immunity.

Therefore, we aimed to identify an immunostimulant without the side effects of oil-based adjuvants with broad immunogenic properties [as opposed to $Al(OH)_3$, which only induces a Th2 immune response]. In this study, we developed an FMD vaccine which has potential to overcome the limitations of commercially available FMD vaccines.

An ideal adjuvant must be easy to obtain and handle, safe, and stable, and should be able to maximize vaccine effectiveness by enhancing host immunity. Plant extracts have been actively studied over the past 30 years as vaccine adjuvants, as they contain natural substances with medicinal properties and are easy to obtain (Surh, 2002). In addition, natural compounds from plant extracts have the advantages of being stable and safe in terms of molecular structure, making them suitable as adjuvants, and are hence widely used in the pharmaceutical fields.

Saponins have various effects including antioxidant, antiviral, ulcer prevention, and antibacterial effects; some are currently approved as food products and are used in medicines and cosmetics (Bailly and Vergoten, 2020). Quil-A extracted from the bark of *Quillaja saponaria* is currently used as a vaccine adjuvant (i.e., in HIV vaccines) and belongs to the triterpenoid family of saponins. However, Quil-A has serious drawbacks; it is highly toxic, unstable in liquid conditions, and demonstrates hemolytic effects. For these reasons, many studies have recently been conducted on the use of different natural saponins as immunostimulants (Marciani et al., 2003; Sun et al., 2009). Glycyrrhizic acid is a triterpenoid saponin extracted from licorice roots, a medicinal plant that has been used for approximately 4,000 years in both the East and the West. There are 22.2 to 32.3 g of glycyrrhizic acid per 100 g of dried licorice root. Glycyrrhizic acid is a potent immunoreactive anti-inflammatory agent that functions at the cellular and membrane levels. At the membrane level, it induces cholesterol-dependent degradation of lipid rafts which are important for coronavirus entry into cells. It traps high mobility group box 1 protein (HMGB1) at both intracellular and circulatory sites and inhibits the alarmin function of HMGB1. It also shows simultaneous antiviral and antitumor activity in clinical studies, and is known for its immunomodulatory function in dendritic cells via the expression of CD40, CD86, and major histocompatibility complex (MHC)-II markers (Bailly and Vergoten, 2020; Kenubih, 2021). Glycyrrhizic acid is suitable for use as a vaccine adjuvant based on its immunomodulatory properties, and licorice, the raw material, is readily available. However, the effectiveness of glycyrrhizic acid on inducing immune responses as an FMD vaccine adjuvant has not been studied previously.

A prior cell viability assay was conducted to explore whether various concentrations of glycyrrhizic acid are cytotoxic. No cytotoxicity was observed at the concentrations of glycyrrhizic acid used in our experiments (Supplementary Figure S1). We used ELISpot to investigate whether glycyrrhizic acid could promote innate immune cell-derived IFNγ expression and lead to innate immune and Th1 responses, with the aim of addressing the shortcomings of $Al(OH)_3$, a currently used vaccine adjuvant (Figure 1).

Innate immune cells, including natural killer (NK) cells, identify and eliminate infected cells (which exhibit decreased MHC class I molecule expression) while also triggering the production of cytokines like IFNγ, IL-12, and IL-18. The secreted IFNγ further enhances the immune response by binding to NK cells, while cytokines such as IL-12 and IL-18 promote the differentiation of naïve $CD4^+$ T cells into Th1 cells (Annunziato et al., 2015). When glycyrrhizic acid was administered at a concentration of 0.625 μg/mL alongside the studied viral antigens (O PA2 and A YC), IFNγ expression in murine PECs and porcine PBMCs was maximized (Figure 1). The results suggest that glycyrrhizic acid can sufficiently stimulate the innate immune system to promote IFNγ expression and induce Th1 responses even at low concentrations, thereby overcoming the shortcomings of $Al(OH)_3$ adjuvants which only induce a Th2 response.

Since the peritoneal cavity contains many naive macrophages, it is a preferred site for the collection of naive tissue-resident macrophages. We have described PECs and discussed the reasons for using them in experiments in previous studies (Jo et al., 2021; Kim et al., 2023). PECs include innate immune cells such as antigen-presenting cells (APCs), which include dendritic cells, macrophages, monocytes, and unconventional T cells. Therefore, PECs are especially suitable for studying cellular and systemic immune responses.

Bailly and Vergoten (2020) reported the antiviral effects of glycyrrhizic acid against various human viruses including hepatitis A/B/C virus, Epstein Barr virus (EBV), Dengue virus (DENV), Chikungunya virus (CHIKV), Semliki Forest virus (SFV), parainfluenza virus, Varicella-zoster virus (VZV), and influenza virus. In particular, glycyrrhizic acid is known to have potent anti-HIV1 and anti-SARS-CoV-2 activities. Glycyrrhizic acid also has antiviral activity against several animal viruses, such as duck hepatitis virus (DHV), avian infectious bronchitis virus (IBV), porcine reproductive and respiratory syndrome virus (PRRSV), and porcine epidemic diarrhea virus (PEDV).

Therefore, before evaluating the adjuvanticity of glycyrrhizic acid, we first performed mice experiments to determine whether glycyrrhizic acid alone exerts a protective effect in the host against FMDV infection. However, our results showed that

glycyrrhizic acid alone did not protect the host against viral infection (Supplementary Figure S2).

Next, animal experiments were performed using experimental (mice) and target (pigs) animals to evaluate the adjuvanticity (immunostimulatory effect) of glycyrrhizic acid. A vaccine containing O PA2 and A YC antigens, ISA 206, $Al(OH)_3$, and Quil-A was administered to the PC group. Glycyrrhizic acid was added to the vaccine administered to the Exp. group. To verify that the vaccine containing glycyrrhizic acid was effective in inducing an early defense response, animal experiments were conducted using mice to assess their survival rate and body weight; the Exp. group exhibited a higher survival rate and increased body weight when compared to the PC group (Figure 2). These results suggest that glycyrrhizic acid has sufficient effects on early defense responses when used as an adjuvant.

Subsequently, animal experiments using mice and pigs were conducted to evaluate whether vaccines containing glycyrrhizic acid have a positive effect on early-, mid-, and long-term immunity. In mice, antibody titers increased at 7 dpv in the PC group while they increased steadily until 84 dpv in the Exp. group (Figure 3). In the target animal experiment, antibody titers were confirmed to increase faster in the Exp. group than in the PC group after boosters were administered (Figure 4).

In the case of the Exp. group, the inter-individual difference was smaller than that of the PC group. A critical issue in pigs is that that complete host defense is difficult due to the large inter-individual differences in antibody and VN titers after vaccination. Thus, glycyrrhizic acid may improve resistance against FMDV by inducing more consistent immunity across individuals.

In addition, VN titers for O PA2 and A YC were measured to confirm the virus neutralization effects of the vaccine. In the mice experiment, only one individual in the PC group had a VN titer greater than 1.65 Log_{10} at 28 dpv, and titers in all individuals had dropped by 84 dpv. In contrast, most of the individuals in the Exp. group had titers of 1.65 Log_{10} or higher at 7 dpv, and the titers had increased further by 84 dpv (Figure 3). When assessing VN titers in the target animals, individuals in the Exp. group had superior titers over those in the PC group (Figure 4). Regarding A YC, the Exp. group demonstrated VN titers of 1.65 Log_{10} or greater at 14 dpv, and maintained this increase at 84 dpv. When considering O PA2, although both the Exp. and PC groups demonstrated a reduction in VN titers at 84 dpv, the Exp. group consistently demonstrated levels of 1.65 Log_{10} or higher.

Previous studies have suggested that FMD vaccine-induced serum titers higher than 1.74 Log_{10} in pigs can be used as an alternative to challenge experiments with oil emulsion vaccines (Black et al., 1984). As per the evaluation standards for FMD vaccines in Korea (Jo et al., 2021), a VN titer of 1.65 Log_{10} or higher post-vaccination indicates that the host is capable of defending against viral challenge. According to the WOAH guidelines, it is recommended to challenge pigs 4 weeks (28 days) post-vaccination to evaluate host defenses against viral infection. In this study, the FMD vaccine containing glycyrrhizic acid as an adjuvant-induced VN titer higher than 1.65 Log_{10} for both FMDV types O and A at 28 dpv, whereas the PC group (FMD vaccine without glycyrrhizic acid) showed VN titers lower than 1.65 Log_{10}. Based on these results, although we did not conduct FMDV challenge experiments in this study, we speculated that an FMD vaccine containing glycyrrhizic acid would exhibit effective host protection against viral infection in pigs.

Vaccines containing glycyrrhizic acid had superior efficacy in inducing early-, mid-, and long-term immune responses, as represented by increased levels of IgG, IgA, and IgM. IgM is the first immunoglobulin to be generated during infection, and its levels increase in the blood to counter external intrusion. Following that, IgG levels rise, and IgM and IgG activate complement to induce an immune response against the invading pathogen. IgA is mainly secreted from the mucous membranes to defend the mucosa. IgG and IgA levels were higher in the Exp. group than in the PC group; IgM levels were also higher in the Exp. group (on an average), although this difference was not statistically significant. Based on these results, vaccines with glycyrrhizic acid as an adjuvant can efficiently elicit active immunity by inducing cellular immune responses shortly after vaccination, stimulating humoral immune responses, and maintaining these responses long-term (Figure 5).

We performed qRT-PCR to elucidate the mechanisms of how the test bivalent vaccine (containing glycyrrhizic acid as an adjuvant) elicited innate and adaptive (cellular and humoral) immune responses (Figure 6).

The expression of RIG-I, a member of the RIG-I-like receptor (RLR) family, was significantly increased in the Exp. group when compared with the PC group. RIG-I plays a crucial role in initiating the immune response by detecting and identifying viral RNA, leading to the activation of the type I interferon (IFNα and IFNβ) response. Furthermore, at 14 dpv, there was a significant increase in the levels of type I interferons and TRAF6. At 56 dpv, we observed that IFNβ expression had decreased in the Exp. group when compared to 14 dpv but remained higher than that of the PC group. Additionally, both IFNα and TRAF6 levels remained significantly elevated when compared to the PC group. In summary, glycyrrhizic acid has been confirmed to exert a positive influence on cellular immune responses when used as an adjuvant.

IL-12 plays a pivotal role in promoting the differentiation of naïve T cells toward Th1 cells (Hsieh et al., 1993). This is instrumental in inducing IFNγ and TNFα production, forming a critical bridge between innate and adaptive immunity. IL-12Rβ1 and IL-12Rβ2, via phosphorylation of STAT4, help stimulate the expression of IFNγ. IL-23 is a heterodimeric cytokine that comprises the IL-12p40 and IL-23p19 subunits and belongs to the IL-12 family (Schön and Erpenbeck, 2018). IL-23 is vital in amplifying and sustaining Th17 cells and unconventional T cells. When it binds to IL-1β, it triggers the expression of IL-17. Notably, IL-17A recruit neutrophils to the site of pathogenic infection, where it forms neutrophil extracellular traps (NETs). This process is essential in early-stage host defenses against infections (Papayannopoulos, 2018; Giusti et al., 2019). IL-1β, IL-12p40, IL-23p19, IL-23R, and IL-17A levels were confirmed to gradually increase over a long period post-vaccination (56 dpv) in the Exp. group. Further, STAT4 levels slightly decreased at 56 dpv, but remained significantly higher than that in the PC group. These results suggest that glycyrrhizic acid affects early host defense and can simultaneously induce innate and adaptive immune responses by enhancing IFNγ expression and Th1 cell stimulation.

The Exp. group showed a significant increase in type II IFN (IFNγ) expression in the mid-term post-vaccination (14 dpv), and retained higher IFNγ expression than the PC group in the long-term (56 dpv). IFNγ is an important autocrine signal for APCs and can cause T cell-mediated cellular immune responses. In addition, STAT1 levels increased significantly at 14 dpv when compared to that in the PC

group. STAT1 responds to IFNγ stimulation by forming a heterodimer with STAT2 which binds to the Interferon-Stimulated Response Element (ISRE) promoter, thereby affecting immune regulation. Collectively, glycyrrhizic acid was confirmed to increase the expression of both type I and type II IFNs, thereby increasing the immune response.

MyD88 is an immunoregulatory gene that plays an important role in innate immunity. It mediates the triggering of inflammatory cytokines through NF-κB via TRAF6 (Sugiyama et al., 2016) and affects immune-related membrane proteins such as CD28, CD80, and CD86. The detached NF-κB translocates to the nucleus, where it attaches to a distinct DNA sequence and promotes cytokine release. MyD88 levels were found to decrease over time in the PC group, whereas they increased significantly over time in the Exp. group. NF-κB levels increased significantly from 14 dpv in the Exp. group, and this increase was maintained at 56 dpv. This increase could be attributed to SIRT1. SIRT1 is known to suppress NF-κB by inactivating p53 (Gonfloni et al., 2014). SIRT1 levels had increased significantly in the Exp. group at 56 dpv. These results suggest that glycyrrhizic acid, by regulating the expression of NF-κB, can consistently provide immune stimulation without triggering a cytokine storm, and its use as an adjuvant may enhance the safety of vaccines.

Collectively, we propose a putative mechanism of how the FMD vaccine (containing glycyrrhizic acid) induces an immune response in pigs as follows; first, after vaccination with the test vaccine containing glycyrrhizic acid, glycyrrhizic acid-antigen complexes become bound to porcine PBMCs and are endocytosed. RIG-I is stimulated after recognition of the glycyrrhizic acid-antigen complexes, inducing NF-κB activation through TRAF6 expression. SIRT1 suppresses excessive NF-κB activity, thereby suppressing the inflammatory response and maintaining homeostasis in the host. NF-κB promotes the secretion of proinflammatory cytokines (such as IL-1β, IFNα, IFNβ, IFNγ, TNFα, IL-12p40, and IL-23p19) via activation of inflammasomes, and the secreted cytokines enter cells through their respective receptors (such as IL-1β, IL-12R, and IL-23R). These receptors are present on the surface of APCs, conventional T cells, and unconventional T cells, and these interactions induce a reversible response. The induced responses lead to cytokine (i.e., NF-κB and IFNγ) release from APCs, conventional T cells, and unconventional T cells via MyD88, STAT1, and STAT4. Specifically, IL-17A (secreted from unconventional T cells) forms NETs to clear the virus in the early stages of viral infection, thereby protecting the host. In the mid-term immune response, CD80/86 (expressed on APCs) reacts with CD28 on the surface of $CD4^+$ T cells to induce a cellular immune response, and IFNγ (secreted from conventional and unconventional T cells) stimulates naïve B cells to promote their differentiation into mature B cells. In the long-term immune response, glycyrrhizic acid promotes the expression of CD19-CD21-CD81 (a core receptor for B cells) and C3d (which acts as an adjuvant when binding an antigen), which also promotes the differentiation of memory B cells and induces a long-lasting immune response.

In summary, it has been proven that the test vaccine containing glycyrrhizic acid as an adjuvant induces an innate immune response, strengthens the initial defense mechanism, and induces improved antibody titers, VN titers, and immune-related gene expression in the long term. Consequently, glycyrrhizic acid has been shown to positively affect host defenses by contributing to cellular and humoral immune responses and inducing long-lasting immunity. Glycyrrhizic acid is a valuable adjuvant candidate as it is both soluble and economical, and also has potential as a practical novel immunomodulator because it specifically targets immune cell-mediated responses.

Nevertheless, the absence of challenge experiment to evaluate the host protective effect of FMD vaccines containing glycyrrhizic acid against viral infection is a critical limitation of this study. Demonstrating the effectiveness of host defense through viral challenge experiments is undoubtedly the most important factor in evaluating the efficacy of vaccines and adjuvants. FMDV challenge experiments in experimental (mice) and target (pigs) animals can only be conducted within ABSL3 facilities. Our institute is affiliated with the Korean government and is the only facility in Korea capable of conducting large scale of animal testing within an ABSL3. Due to the high demand for challenge experiment against veterinary viral disease including FMD and African swine fever (ASF) experiments and limited space, ABSL3 animal experiments are strictly managed on an annual plan. For this reason, we were unable to perform the challenge experiment in this study in pigs. Further studies are planned to evaluate the efficacy of the FMD vaccine, including assessments of the glycyrrhizic acid-mediated host defense response (based on clinical indicators, viral titers in sera and oral swab samples, etc.) in pigs.

Although this study demonstrated the effectiveness of glycyrrhizic acid as an adjuvant for FMD vaccine, further studies are needed for other diseases such as ASF virus (ASFV) and PRRSV.

The current study evaluated the immunomodulatory effects of glycyrrhizic acid when administered via the intramuscular route. Previous studies have shown that glycyrrhizic acid can be detected in human plasma after oral ingestion, and may have the potential to induce mucosal and systemic immune responses when administered orally (Suzuki et al., 2017). Oral administration offers advantages over direct intramuscular vaccination because it can simultaneously stimulate mucosal and systemic immunity, is convenient, and allows for the delivery of large doses (Brownlie, 1985; Wang et al., 2015).

Based on the current results, we are planning a future study to evaluate the feasibility and efficacy of glycyrrhizic acid in inducing immune responses when orally administered as a feed or drinking water additive. In addition, we aim to examine the potential utility of glycyrrhizic acid as a bait vaccine, especially for animal diseases that are difficult-to-prevent and control.

Data availability statement

The original contributions presented in the study are included in the article/Supplementary material, further inquiries can be directed to the corresponding author.

Ethics statement

The animal study was approved by the Ethics Committee of the APQA (accreditation number: IACUC-2022-670 and IACUC-2023-753). The study was conducted in accordance with the local legislation and institutional requirements.

Author contributions

SS: Investigation, Validation, Writing – original draft. HWK: Formal analysis, Investigation, Visualization, Writing – original draft, Writing – review & editing. M-KK: Investigation, Writing – original

draft. SHP: Investigation, Writing – original draft. S-MK: Resources, Writing – review & editing. J-HP: Resources, Writing – review & editing. MJL: Conceptualization, Data curation, Formal analysis, Funding acquisition, Investigation, Methodology, Project administration, Resources, Software, Supervision, Validation, Visualization, Writing – original draft, Writing – review & editing.

Funding

The author(s) declare financial support was received for the research, authorship, and/or publication of this article. This work was supported by grants from the Animal and Plant Quarantine Agency (APQA) (B-1543386-2021-24).

Acknowledgments

We would like to thank the staff and researchers of the Center for Foot-and-Mouth Disease Vaccine Research in the APQA for helping us with this study.

Conflict of interest

The authors declare that the research was conducted in the absence of any commercial or financial relationships that could be construed as a potential conflict of interest.

Publisher's note

Supplementary material

The Supplementary material for this article can be found online at: https://www.frontiersin.org/articles/10.3389/fmicb.2023.1289065/full#supplementary-material

References

Annunziato, F., Romagnani, C., and Romagnani, S. (2015). The 3 major types of innate and adaptive cell-mediated effector immunity. *J. Allergy Clin. Immunol.* 135, 626–635. doi: 10.1016/j.jaci.2014.11.001

Arzt, J., Baxt, B., Grubman, M. J., Jackson, T., Juleff, N., Rhyan, J., et al. (2011). The pathogenesis of foot-and-mouth disease II: viral pathways in swine, small ruminants, and wildlife; myotropism, chronic syndromes, and molecular virus–host interactions. *Transbound. Emerg. Dis.* 58, 305–326. doi: 10.1111/j.1865-1682.2011.01236.x

Bahnemann, H. G. (1975). Binary ethylenimine as an inactivant for foot-and-mouth disease virus and its application for vaccine production. *Arch. Virol.* 47, 47–56. doi: 10.1007/BF01315592

Bailly, C., and Vergoten, G. (2020). Glycyrrhizin: an alternative drug for the treatment of COVID-19 infection and the associated respiratory syndrome? *Pharmacol. Ther.* 214:107618. doi: 10.1016/j.pharmthera.2020.107618

Barteling, S. J. (2002). Development and performance of inactivated vaccines against foot and mouth disease. *Rev. Sci. Tech.* 21, 577–588. doi: 10.20506/rst.21.3.1361

Black, L., Francis, M. J., Rweyemamu, M. M., Umebara, O., and Boge, A. (1984). The relationship between serum antibody titres and protection from foot and mouth disease in pigs after oil emulsion vaccination. *J. Biol. Stand.* 12, 379–389. doi: 10.1016/s0092-1157(84)80062-1

Borrego, B., Blanco, E., Rodríguez Pulido, M. R., Mateos, F., Lorenzo, G., Cardillo, S., et al. (2017). Combined administration of synthetic RNA and a conventional vaccine improves immune responses and protection against foot-and-mouth disease virus in swine. *Antivir. Res.* 142, 30–36. doi: 10.1016/j.antiviral.2017.03.009

Brownlie, J. (1985). Clinical aspects of the bovine virus diarrhoea/mucosal disease complex in cattle. *In Pract.* 7, 195–202. doi: 10.1136/inpract.7.6.195

Cao, Y., Lu, Z., Li, Y., Sun, P., Li, D., Li, P., et al. (2013). Poly (I: C) combined with multi-epitope protein vaccine completely protects against virulent foot-and-mouth disease virus challenge in pigs. *Antivir. Res.* 97, 145–153. doi: 10.1016/j.antiviral.2012.11.009

Carr, B. V., Lefevre, E. A., Windsor, M. A., Inghese, C., Gubbins, S., Prentice, H., et al. (2013). CD4+ T-cell responses to foot-and-mouth disease virus in vaccinated cattle. *J. Gen. Virol.* 94, 97–107. doi: 10.1099/vir.0.045732-0

Casey-Bryars, M., Reeve, R., Bastola, U., Knowles, N. J., Auty, H., Bachanek-Bankowska, K., et al. (2018). Waves of endemic foot-and-mouth disease in eastern Africa suggest feasibility of proactive vaccination approaches. *Nat. Ecol. Evol.* 2, 1449–1457. doi: 10.1038/s41559-018-0636-x

Cheung, A., Delamarter, J., Weiss, S., and Küpper, H. (1983). Comparison of the major antigenic determinants of different serotypes of foot-and-mouth disease virus. *J. Virol.* 48, 451–459. doi: 10.1128/JVI.48.2.451-459.1983

De Clercq, E. (1995). Toward improved anti-HIV chemotherapy: therapeutic strategies for intervention with HIV infections. *J. Med. Chem.* 38, 2491–2517. doi: 10.1021/jm00014a001

Di Pasquale, A., Preiss, S., Tavares Da Silva, F., and Garçon, N. (2015). Vaccine adjuvants: from 1920 to 2015 and beyond. *Vaccine* 3, 320–343. doi: 10.3390/vaccines3020320

Egerton, J. R., Laing, E. A., and Thorley, C. M. (1978). Effect of Quil a, a saponin derivative, on the response of sheep to alum precipitated *Bacteroides nodosus* vaccines. *Vet. Res. Commun.* 2, 247–252. doi: 10.1007/BF02291455

Fowler, V. L., Knowles, N. J., Paton, D. J., and Barnett, P. V. (2010). Marker vaccine potential of a foot-and-mouth disease virus with a partial VP1 G-H loop deletion. *Vaccine* 28, 3428–3434. doi: 10.1016/j.vaccine.2010.02.074

Fukai, K., Morioka, K., Yamada, M., Nishi, T., Yoshida, K., Kitano, R., et al. (2015a). Comparative performance of fetal goat tongue cell line ZZ-R 127 and fetal porcine kidney cell line LFBK-αvβ6 for foot-and-mouth disease virus isolation. *J. Vet. Diagn. Investig.* 27, 516–521. doi: 10.1177/1040638715584156

Fukai, K., Yamada, M., Morioka, K., Ohashi, S., Yoshida, K., Kitano, R., et al. (2015b). Dose-dependent responses of pigs infected with foot-and-mouth disease virus O/JPN/2010 by the intranasal and intraoral routes. *Arch. Virol.* 160, 129–139. doi: 10.1007/s00705-014-2239-4

Gonfloni, S., Iannizzotto, V., Maiani, E., Bellusci, G., Ciccone, S., and Diederich, M. (2014). P53 and Sirt1: routes of metabolism and genome stability. *Biochem. Pharmacol.* 92, 149–156.

Giusti, D., Bini, E., Terryn, C., Didier, K., Le Jan, S., Gatouillat, G., et al. (2019). NET formation in bullous pemphigoid patients with relapse is modulated by IL-17 and IL-23 interplay. *Front. Immunol.* 10:701. doi: 10.3389/fimmu.2019.00701

Grubman, M. J., and Baxt, B. (2004). Foot-and-mouth disease. *Clin. Microbiol. Rev.* 17, 465–493. doi: 10.1128/CMR.17.2.465-493.2004

Guzman, E., Taylor, G., Charleston, B., and Ellis, S. A. (2010). Induction of a cross-reactive CD8(+) T cell response following foot-and-mouth disease virus vaccination. *J. Virol.* 84, 12375–12384. doi: 10.1128/JVI.01545-10

Hem, S. L., and Hogenesch, H. (2007). Relationship between physical and chemical properties of aluminum-containing adjuvants and immunopotentiation. *Expert Rev. Vaccines* 6, 685–698. doi: 10.1586/14760584.6.5.685

Hogenesch, H. (2013). Mechanism of immunopotentiation and safety of aluminum adjuvants. *Front. Immunol.* 3:406. doi: 10.3389/fimmu.2012.00406

Hsieh, C. S., Macatonia, S. E., Tripp, C. S., Wolf, S. F., O'Garra, A., and Murphy, K. M. (1993). Development of TH1 CD4+ T cells through IL-12 produced by Listeria-induced macrophages. *Science* 260, 547–549. doi: 10.1126/science.8097338

Jackson, T., King, A. M., Stuart, D. I., and Fry, E. (2003). Structure and receptor binding. *Virus Res.* 91, 33–46. doi: 10.1016/s0168-1702(02)00258-7

Jamal, S. M., and Belsham, G. J. (2013). Foot-and-mouth disease: past, present and future. *Vet. Res.* 44:116. doi: 10.1186/1297-9716-44-116

Jiang, H., Wang, Q., Li, L., Zeng, Q., Li, H., Gong, T., et al. (2018). Turning the old adjuvant from gel to nanoparticles to amplify CD8+ T cell responses. *Adv. Sci.* 5:1700426. doi: 10.1002/advs.201700426

Jo, H., Kim, B. Y., Park, S. H., Kim, H. M., Shin, S. H., Hwang, S. Y., et al. (2021). The HSP70-fused foot-and-mouth disease epitope elicits cellular and humoral immunity and drives broad-spectrum protective efficacy. *NPJ Vaccines* 6:42. doi: 10.1038/s41541-021-00304-9

Kamel, M., El-Sayed, A., and Castañeda Vazquez, H. (2019). Foot-and-mouth disease vaccines: recent updates and future perspectives. *Arch. Virol.* 164, 1501–1513. doi: 10.1007/s00705-019-04216-x

Kenubih, A. (2021). Foot and mouth disease vaccine development and challenges in inducing long-lasting immunity: trends and current perspectives. *Vet. Med.* 12, 205–215. doi: 10.2147/VMRR.S319761

Kim, H. W., Ko, M. K., Park, S. H., Hwang, S. Y., Kim, D. H., Park, S. Y., et al. (2023). Dectin-1 signaling coordinates innate and adaptive immunity for potent host defense against viral infection. *Front. Immunol.* 14:1194502. doi: 10.3389/fimmu.2023.1194502

Kotla, S., Sanghratna Vishanath, B., H, J. D., K, G., V, V. S. S., and Reddy, G. R. (2016). DNA vaccine (P1-2A-3C-pCDNA) co-administered with bovine IL-18 gives protective immune response against foot and mouth disease in cattle. *Vet. Microbiol.* 193, 106–115. doi: 10.1016/j.vetmic.2016.07.007

Lee, M. J., Jo, H., Park, S. H., Ko, M. K., Kim, S. M., Kim, B., et al. (2020). Advanced foot-and-mouth disease vaccine platform for stimulation of simultaneous cellular and humoral immune responses. *Vaccine* 8:254. doi: 10.3390/vaccines8020254

Leforban, Y., and Gerbier, G. (2002). Review of the status of foot and mouth disease and approach to control/eradication in Europe and Central Asia. *Rev. Sci. Tech.* 21, 477–492. doi: 10.20506/rst.21.3.1345

Marciani, D. J., Reynolds, R. C., Pathak, A. K., Finley-Woodman, K., and May, R. D. (2003). Fractionation, structural studies, and immunological characterization of the semi-synthetic Quillaja saponins derivative GPI-0100. *Vaccine* 21, 3961–3971. doi: 10.1016/s0264-410x(03)00298-6

Mason, P. W., Grubman, M. J., and Baxt, B. (2003). Molecular basis of pathogenesis of FMDV. *Virus Res.* 91, 9–32. doi: 10.1016/s0168-1702(02)00257-5

Nagendrakumar, S. B., Srinivasan, V. A., Madhanmohan, M., Yuvaraj, S., Parida, S., Di Nardo, A., et al. (2011). Evaluation of cross-protection between O1 Manisa and O1 Campos in cattle vaccinated with foot-and-mouth disease virus vaccine incorporating different payloads of inactivated O1 Manisa antigen. *Vaccine* 29, 1906–1912. doi: 10.1016/j.vaccine.2010.12.127

Papayannopoulos, V. (2018). Neutrophil extracellular traps in immunity and disease. *Nat. Rev. Immunol.* 18, 134–147. doi: 10.1038/nri.2017.105

Parry, N., Fox, G., Rowlands, D., Brown, F., Fry, E., Acharya, R., et al. (1990). Structural and serological evidence for a novel mechanism of antigenic variation in foot-and-mouth disease virus. *Nature* 347, 569–572. doi: 10.1038/347569a0

Ramon, G. (1925). Sur l'augmentation anormale de l'antitoxine chez les chevaux producteurs de serum antidiphterique. *Bull. Soc Centr Vet.* 101, 227–234.

Ramon, G. (1926). Proceeds pour acroitre la production des antitoxins. *Ann. Inst. Pasteur* 40, 1–10.

Rodriguez, L. L., and Grubman, M. J. (2009). Foot and mouth disease virus vaccines. *Vaccine* 27, D90–D94. doi: 10.1016/j.vaccine.2009.08.039

Schön, M. P., and Erpenbeck, L. (2018). The interleukin-23/interleukin-17 axis links adaptive and innate immunity in psoriasis. *Front. Immunol.* 9:1323. doi: 10.3389/fimmu.2018.01323

Stenfeldt, C., Pacheco, J. M., Rodriguez, L. L., and Arzt, J. (2014). Early events in the pathogenesis of foot-and-mouth disease in pigs; identification of oropharyngeal tonsils as sites of primary and sustained viral replication. *PLoS One* 9:e106859. doi: 10.1371/journal.pone.0106859

Sugiyama, K.-I., Muroi, M., Kinoshita, M., Hamada, O., Minai, Y., Sugita-Konishi, Y., et al. (2016). NF-κB activation via MyD88-dependent toll-like receptor signaling is inhibited by trichothecene mycotoxin deoxynivalenol. *J. Toxicol. Sci.* 41, 273–279. doi: 10.2131/jts.41.273

Sun, H. X., Xie, Y., and Ye, Y. P. (2009). Advances in saponin-based adjuvants. *Vaccine* 27, 1787–1796. doi: 10.1016/j.vaccine.2009.01.091

Surh, Y. J. (2002). Anti-tumor promoting potential of selected spice ingredients with antioxidative and anti-inflammatory activities: a short review. *Food Chem. Toxicol.* 40, 1091–1097. doi: 10.1016/s0278-6915(02)00037-6

Suzuki, T., Tsukahara, M., Akasaka, Y., and Inoue, H. (2017). A highly sensitive LC–MS/MS method for simultaneous determination of glycyrrhizin and its active metabolite glycyrrhetinic acid: application to a human pharmacokinetic study after oral administration. *Biomed. Chromatogr.* 31:e4032. doi: 10.1002/bmc.4032

Vlietinck, A. J., De Bruyne, T., Apers, S., and Pieters, L. A. (1998). Plant-derived leading compounds for chemotherapy of human immunodeficiency virus (HIV) infection. *Planta Med.* 64, 97–109. doi: 10.1055/s-2006-957384

Wang, S., Liu, H., Zhang, X., and Qian, F. (2015). Intranasal and oral vaccination with protein-based antigens: advantages, challenges and formulation strategies. *Protein Cell* 6, 480–503. doi: 10.1007/s13238-015-0164-2

Xiao, Y., Chen, H.-Y., Wang, Y., Yin, B., Lv, C., Mo, X., et al. (2016). Large-scale production of foot-and-mouth disease virus (serotype Asia1) VLP vaccine in *Escherichia coli* and protection potency evaluation in cattle. *BMC Biotechnol.* 16:56. doi: 10.1186/s12896-016-0285-6

frontiers | Frontiers in Microbiology

TYPE Original Research
PUBLISHED 06 November 2023
DOI 10.3389/fmicb.2023.1288458

OPEN ACCESS

EDITED BY
Jianke Wang,
Hebei Agricultural University, China

REVIEWED BY
Yan-Dong Tang,
Chinese Academy of Agricultural Sciences, China
Yuan Sun,
Harbin Veterinary Research Institute (CAAS), China
Liu Sidang,
Shandong Agricultural University, China

*CORRESPONDENCE
Zi-Guo Yuan
✉ ziguoyuan@scau.edu.cn
Xiaohu Wang
✉ wangxiaohu2020@163.com

†These authors have contributed equally to this work

RECEIVED 04 September 2023
ACCEPTED 24 October 2023
PUBLISHED 06 November 2023

CITATION
Zhao M, Chen J, Luo S, Yan R, Zhang P, Ren Z, Chen X, Wang G, Xiang H, Cai R, Huang Y, Li N, Li H, Yuan Z-G and Wang X (2023) Pseudorabies gD protein protects mice and piglets against lethal doses of pseudorabies virus.
Front. Microbiol. 14:1288458.
doi: 10.3389/fmicb.2023.1288458

Pseudorabies gD protein protects mice and piglets against lethal doses of pseudorabies virus

Mengpo Zhao[1,2†], Jing Chen[1†], Shengjun Luo[1†], Renhe Yan[3†], Pian Zhang[1], Zhaowen Ren[1,2], Xiaofan Chen[1,2], Gang Wang[1], Hua Xiang[1], Rujian Cai[1], Yuan Huang[1], Na Li[1,2], Hongwei Li[4], Zi-Guo Yuan[2*] and Xiaohu Wang[1*]

[1]Key Laboratory of Livestock Disease Prevention of Guangdong Province, Scientific Observation and Key Laboratory for Prevention and Control of Avian Influenza and Other Major Poultry Diseases, Ministry of Agriculture and Rural Affairs, Institute of Animal Health, Guangdong Academy of Agricultural Sciences, Guangzhou, China, [2]College of Veterinary Medicine, South China Agricultural University, Guangzhou, China, [3]Department of Research and Development, Guangzhou Bioneeds Biotechnology Co., LTD, Guangzhou, China, [4]School of Laboratory and Biotechnology, Southern Medical University, Guangzhou, China

Introduction: Pseudorabies (PR) is a highly contagious viral disease caused by the pseudorabies virus (PRV), which can cause disease in a wide range of domestic and wild animals. Studies have shown that new mutant strains have emerged in pig farms in many regions and that commercial inactivated and live attenuated vaccines are becoming less effective at protecting pigs.

Methods: Porcine pseudorabies glycoprotein D (gD) gene (GenBank: QEY95774.1) with hexa-His tag to the C terminus for further purification processes was cloned into the lentiviral expression plasmid pLV-CMV-eGFP by restriction enzyme, the resulting plasmid was designated as pLV-CMV-gD. HEK-293T cells with robust and stable expression of recombinant gD protein was established by infection with recombinant lentivirus vector pLV-CMV-gD. We expressed porcine pseudorabies virus gD protein using HEK-293T cells.

Results: We describe in this study that individual gD proteins produced by a mammalian cell expression system are well immunogenic and stimulate high levels of PRV-specific and neutralizing antibodies in mice and piglets. All mice and piglets survived lethal doses of PRV, significantly reducing the amount of PRV virus in piglets' lymph nodes, lungs, spleen, and other tissues. It also significantly reduced the time cycle and amount of viral excretion from piglets to the environment through the nasal and anal cavities.

Discussion: The results suggest that PRV gD protein is expected to be a potential candidate for the preparation of genetically engineered PR vaccines for the prevention of PRV infection and the control of PR epidemics.

KEYWORDS

pseudorabies virus, 293T cells, recombinant gD protein, subunit vaccine, immune protection

1. Introduction

Pseudorabies (PR) is caused by pseudorabies virus (PRV),which can infect both domestic animals (such as pigs, cattle, sheep, etc.) and wildlife (such as lynx, foxes, wild boars, etc.), Recent studies suggest that humans may also be potential hosts for this pathogen (Kong et al., 2013; Masot et al., 2017; Minamiguchi et al., 2019; Cheng et al., 2020). PRV, also known as suid herpesvirus (SuHV-1) or Aujeszky's disease virus (ADV), belongs to the herpesvirus subfamily of the herpesvirus family (Nauwynck et al., 2007; Ai et al., 2018; Liu et al., 2021). Pigs are the only known natural hosts of PRV, which has a diverse host spectrum. PRV can be transmitted through the respiratory tract, digestive tract, and seminal placenta, and clinical manifestations of infection in pigs are diarrhea, vomiting, and neurological disorders (Mettenleiter, 1996; Marcaccini et al., 2008). It will disrupt the reproduction of maternal pigs, slow the growth of fertile pigs, and increase the incidence of piglets, making PR removal more difficult and causing huge losses to the world pig industry (Sun et al., 2016; Verpoest et al., 2017; Jiang et al., 2020).

PRV is a double-stranded DNA virus with a viral genome of about 145 kb that encodes 70–100 proteins, the majority of which are capsid proteins, envelope proteins, epidermal proteins, and enzymes (Mettenleiter, 2000). Eleven glycoproteins (gB, gC, gD, gE, gG, gH, gI, gK, gL, gM, and gN) and four transmembrane proteins (UL20, UL43, US9, and UL24) were identified on the virion envelope (Granzow et al., 2001). In the course of infection, gC, gB, gD, gH, and gL participate in the invasion of the virus and are the main antigens, which stimulate the host's innate immune response (Kramer et al., 2011; Ye et al., 2015). Additionally, gD identifies and binds to molecules that resemble immunoglobulin (Ig), including connexin-1, connexin-2, and acetyl heparan sulfate (HS), which have a similar affinity to nectin-1 in humans and pigs (Li et al., 2017). Notably, PRV gD is the typical viral ligand for α herpesvirus entry into the host cell, Viral invasion of cells depends on the binding of gD to cell surface receptors (Krummenacher et al., 2005; Petrina et al., 2021). Moreover, gD is the main glycoprotein of PRV, which can stimulate the body to produce neutralizing antibodies against PRV infection (Fusco et al., 2005; He et al., 2019). PRV gB is essential for virus entry and transmission across cells, and gD is required for receptor engagement, stabilization of viral particle-cell interactions, and further activation of gB to become required for fusion competence (Hochrein et al., 2004; Oku et al., 2021). Growing evidence suggests that gD is a crucial protein for activating both humoral and cellular immune responses, making it a promising target for the development of new vaccines (Freuling et al., 2017; Aschner and Herold, 2021).

Due to the continuous evolution of PRV strains, currently available attenuated and inactivated vaccines do not provide adequate protection for pigs. Therefore, researchers are exploring subunit vaccines as a potential avenue for novel vaccines. Evidence from previous research indicates that subunit vaccines producing PRV gC and gD proteins in *Bacillus subtilis* may successfully induce a mucosal immune response, and the vaccine initiates the immune system more effectively than conventional vaccines in the presence of maternal immunity (Wang et al., 2019). PRV-gD mRNA triggered specific neutralizing antibodies, significantly higher cytokine IFN-γ/IL-2 levels than controls, and a considerable rise in the percentage of $CD4^+$/$CD8^+$ cells in peripheral lymphocytes, therefore protecting mice against PRV (Jiang et al., 2020). Expression of gB, gC, and gD through the baculovirus system can provide better protection for piglets. At 7 days post-immunization, piglets in the gD and gB + gD groups produced the highest NAs. After challenge with the PRV-HNLH mutant strain, none of the piglets showed clinical signs, such as elevated body temperature, and viral load and pathological damage were significantly reduced. In addition, the duration of gD vaccine-induced NAs was maintained for 4 months after a single vaccination (Zhang et al., 2020). By constructing chimeric viruses, it was found that injecting gC or gD may create excellent immunological effects and protect piglets against PRV-HB1201 challenge (Ren et al., 2020). Cao Z used baculovirus and *Escherichia coli* expression systems to express gB, gD, and GM-CSF, respectively. The inoculated rabbits had normal body temperatures, less pathological tissue damage, and a significantly lower viral load in tissues (Cao et al., 2022).

As science and technology have advanced, more and more viral proteins with favorable immunogenicity have been thoroughly investigated by scientists. The recombinant porcine circovirus type 2 VP2 protein and swine fever virus E2 protein have been shown to provide effective protection for piglets. Compared with prokaryotic expression, mammalian cells can correctly process both self-expressed and exogenous proteins and are the expression system of choice for obtaining highly active proteins *in vitro*. To develop a more effective vaccine against PRV variants, we generated gD protein using the HEK-293T expression system, and the immunization effect of gD protein in mice and piglets was evaluated.

2. Materials and methods

2.1. Viruses, cells, and antibodies

HEK-293T cells were grown in Dulbecco's Modified Eagle Medium (DMEM; Gibco) with 10% fetal bovine serum (FBS; Gibco). It was maintained at 37°C and 5% carbon dioxide (CO_2) incubator. PRV-HY was isolated from a pig farm in Guangdong, China, where a PR outbreak occurred. We purchased Mouse monoclonal antibody from Shenzhen Kejie Industrial Development that was tailored to the PRV gE.

2.2. Construction of the expression plasmids

Porcine pseudorabies glycoprotein D (gD) gene (GenBank: QEY95774.1) with a hexa-His tag to the C terminus for further purification processes was cloned into the lentiviral expression plasmid pLV-CMV-eGFP by restriction enzyme, the resulting plasmid was designated as pLV-CMV-gD. HEK-293T cells with robust and stable expression of recombinant gD protein was established by infection with recombinant lentivirus vector pLV-CMV-gD as previously described (Chen et al., 2021). A total of 4×10^4 HEK 293T cells /well were prepared in a 24-wells plate. On the following day, cells in each well were infected with packaged recombinant lentivirus pLV-CMV-gD at a MOI of 10 in DMEM medium containing 10% FBS with 6 ~ 8 μg/ml hexadimethrine bromide (Polybrene, Sigma, Germany) 0.24 h after infection, cell culture media was replaced with fresh DMEM with 10% FBS and for 3 ~ 5 days at 37°C and 5% CO_2, the optimal cell clone was selective and named HEK 293T-gD. Recombinant gD protein in the

supernatant of cell cultures was collected and purified with Ni NTA resin affinity chromatography (GE Healthcare, US). In a nutshell, using a GE AKTA Pure system, 100 ml of culture supernatants were filtered through a 0.22 μm filter and put onto a 5 ml Ni-NTA column (GE) that had been equilibrated in 20 mM Tris [pH 8.0]. Unbound proteins were cleaned off the column by washing it with washing buffer (50 mM NaH_2PO_4, 300 mM NaCl, 20 mM imidazole). The hexa-His-tagged recombinant protein was eluted using elution buffer containing 50 mM NaH_2PO_4, 300 mM NaCl, and 250 mM imidazole. SDS-PAGE was used to verify the pure protein, and the BCA Protein Assay Kit (Thermo, USA) was used to quantify it according to the manufacturer's instructions. For animal immunization, the purified protein was diluted to 100 μg/ml in PBS and mixed with an equal amount of Montanide (TM) ISA 201 VG oil adjuvant (Seppic; 1 ml + 1 ml).

2.3. Immunization scheme

The purified gD protein was diluted to 50 μg/ml and then used in immunization tests in mice and piglets. Mice were immunized with subcutaneous multipoint injection on 0 and 14 days. Blood was collected from mice at 7, 14, 21, and 28 days after the first immunization, and the levels of PRV-specific and neutralizing antibodies were measured. At the end of the experiment, the surviving mice were euthanized (Figure 1A). Piglets were immunized by intramuscular injection at 0 and 14 days. Blood was collected from piglets at 7, 14, 21, and 28 days after the first immunization, and serum levels of PRV gD antibodies and neutralizing antibodies were measured and challenged against PRV-HY at 14 and 28 days. After the challenge, the rectal temperatures of piglets were measured daily, and nasal and anal swabs of piglets were collected every other day to determine the PRV gE gene copy number. At the end of the experiment, surviving piglets were euthanized and tissue samples were collected for HE and IHC experiments (Figure 1B).

2.4. Animal experiments

Four-week-old mice ($n = 40$) were divided into three groups. After acclimation, immunized mice with equal amounts of gD protein, commercial porcine inactivated vaccine (PCIV; Keqian Biological Company, Wuhan, China), DMEM, and PBS, the groups and doses are shown in Table 1. The gD group was immunized with 10 μg gD protein and subsequently immunized for the second time at 14 days, in addition to the PBS group, all mice were challenged with 10^3 $TCID_{50}$ PRV-HY at 28 days post-immunization. Every other week, the tails of the mice are amputated for blood collection and serum isolation. Mice were infected with PRV-HY at 28 days after the first inoculation and monitored for 14 days to determine survival. Each dead mouse was euthanized by intraperitoneal injection of pentobarbital sodium (200 μg/g).

Twenty healthy piglets at 4 weeks of age were randomly assigned to four groups: gD group, commercial vaccine group, DMEM group, and PBS group; the groups and doses are shown in Table 2. Antigens and antibodies of PRRSV, CSFV, PRV, and PCV2 in the serum of all piglets were negative. Each group was given 2 ml of gD protein, or commercial vaccine, DMEM culture media, and PBS through the muscle. Following the initial vaccination, piglets' eating habits and rectal temperature were regularly monitored. Sera was isolated from piglets' anterior vena cava blood to assess PRV-specific and neutralizing antibody levels. In addition to the PBS group, all piglets were infected with 10^7 $TCID_{50}$ PRV-HY through the nasal cavity at 28 days post-immunization. Piglet rectal temperatures should be taken once daily; clinical signs such as piglet feeding should be observed; and nasal and fecal swabs should be taken at 1, 3, 5, 7, 9,11,18, and 25 days post-challenge. Use qPCR to determine viral load. At 25 days post-challenge, the surviving piglets were euthanized by intravenous injection of pentobarbital sodium (100 mg/kg), Illness samples were collected, either fixed in 4% formalin zinc fixative (Sigma Aldrich) for histopathology and immunohistochemistry detection or frozen at −80°C for eventual viral gene copies assessment.

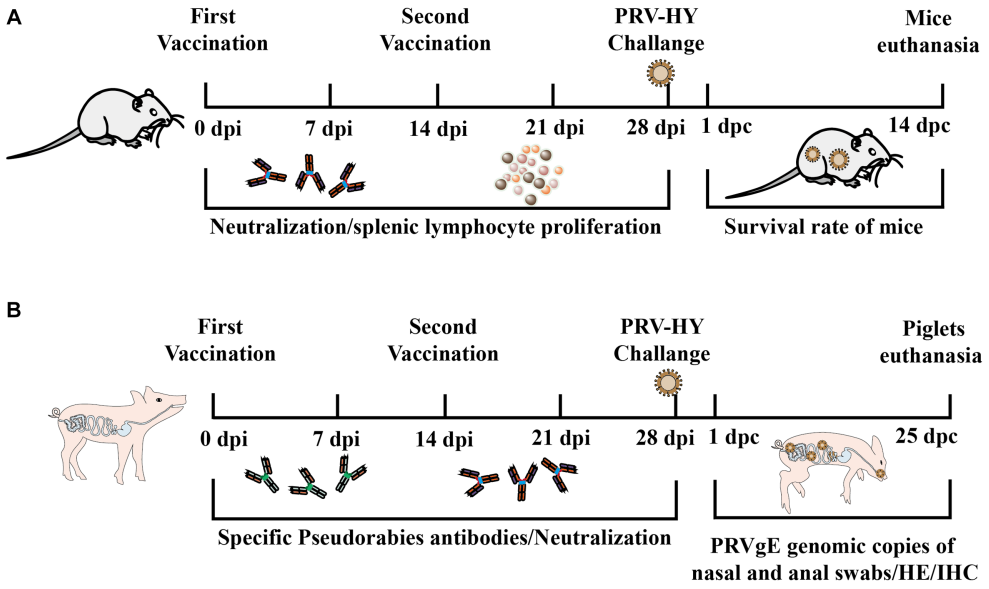

FIGURE 1
Experimental procedure for immune protection in mice and piglets. **(A)** Schematic diagram of antigen inoculation, challenge, and sample collection in mice. **(B)** Schematic diagram of piglet inoculation antigen, challenge, and experimental sample collection.

TABLE 1 Immunization strategy in mice.

Group	Formulation	Immunization time points (DAI)	Immunization pathway	Vaccine dose
1	gD	0.14	Subcutaneous immunization	200 μl
2	commercial vaccine	0.14	Subcutaneous immunization	200 μl
3	DMEM	0.14	Subcutaneous immunization	200 μl
4	(PBS) negative control	0.14	Subcutaneous immunization	200 μl

TABLE 2 Immunization strategy in piglets.

Group	Formulation	Immunization time points (DAI)	Immunization pathway	Vaccine dose
1	gD	0.14	Intramuscular injection	2 ml
2	Commercial vaccine	0.14	Intramuscular injection	2 ml
3	DMEM	0.14	Intramuscular injection	2 ml
4	(PBS) Negative control	0.14	Intramuscular injection	2 ml

2.5. Neutralizing antibody test

Sera was tested for neutralizing PRV-HY antibodies using Vero cells. Serum samples from mice and piglets were heat-inactivated at 60°C for 30 min and then diluted with DMEM. A similar amount of PRV-HY (200 $TCID_{50}$) was mixed thoroughly with 50 μl of the diluted, inactivated serum. The mixture was then added to a 96-well plate with monolayer Vero cells. Positive serum and blank cells were set up as controls and cultured in DMEM containing 2% fetal bovine serum for observation. The plates were incubated for 5 days at 37°C in a 5% carbon dioxide environment to check for cytopathic effect (CPE). Neutralizing antibodies were calculated using the Reed-Muench method.

2.6. Lymphocyte isolation and stimulation

Lymphocytes were extracted from the spleen of mice 14 and 28 days after the first immunization. Check for cell division using the CCK-8 assay. Separate mouse spleen lymphocytes, then add 10^5 cells per well to a 96-well plate with the ConA. After 48 h of incubation at 37°C, 10 μl of CCK-8 was added to each well, followed by an additional 2 h of incubation at 37°C. At a wavelength of 450 nm, absorption was determined for each well. The stimulation index (SI) indicates the proliferation level of mouse spleen cells.

2.7. Quantification of viral loads

Using a viral DNA/RNA kit, extract viral DNA from the sample and set up the reaction apparatus according to ChamQTM SYBR qPCR Master Mix instructions. Using qPCR, determine copies of the PRV gE gene in the liver, lungs, and other piglet organs. The primer sequences used for amplification were: upstream: 5′-GTCT GTGAAGCGGTTCGTGAT-3′ and downstream: 5′-ACAAGTC AAGGCGCATCTAC-3′. A standard curve was generated using a series of 7 dilutions containing the gE gene at copy numbers of 10^2 to 10^8 copies/μl as a template. The qPCR settings were 50°C for 2 min, 95°C for 2 min, 95°C for 15 s, 60°C for 15 s, and 72°C for 45 s for 40 cycles.

2.8. Histopathology and immunohistochemistry

After euthanasia, all animals were assessed for gross tissue damage to the lungs, lymph nodes, kidneys, tonsils, and brain during autopsy examinations. Three piglet organ samples were treated with 4% formaldehyde, prepared in paraffin, and subsequently frozen. To stain the slices with HE (Solarbio, China), they were dewaxed and washed. Then, for 20 min at 37°C, soak in 3% H_2O_2, followed by an hour of blocking in 37% horse serum. Slices were washed three times in PBS, then incubated with PRV gE monoclonal antibody (1:200) at 37°C for 30 min, and then at 4°C overnight. The slices are washed in PBS to get rid of any lingering antibodies, then incubated with HRP-labeled goat anti-mouse IgG (1,500) for an hour at 37°C. To detect antibody binding, use the HRPDAB chromogenic reagent kit purchased from Tiangen Biotechnology in Beijing, China. Use the Leica DMI3000B microscope (manufactured by Leica in Wetzlar, Germany) to take photographs.

2.9. Statistical analysis

One-way analysis of variance (ANOVA) was performed on the data between groups by using GraphPad Prism 9 (San Diego, CA, USA). Significance is presented as $^*p < 0.05$, $^{**}p < 0.01$, $^{***}p < 0.001$.

3. Results

3.1. Identification of gD protein expression in HEK-293T cells

We obtained recombinant lentivirus using a lentiviral packaging system based on four plasmids (pPACKH1-GAG, pVSV-G, pPACKH1-REV, and pLV-CMV-eGFP). Secretory expression was achieved in mammalian HEK-293T cells by lentiviral mediation, and the recombinant gD protein was obtained by collecting cell cultures. The expression of gD protein in transfected cell supernatant was detected by Western blot using both anti-his antibody (Figure 2A) and anti-PRV hyperimmune serum (Figure 2B). The results showed that

gD protein with the expected molecular weight (50 kDa) was efficiently expressed in HEK 293T-gD cells. Approximately 100 ml culture supernatants collected from HEK 293T-gD cells were purified by the BioLogic LP protein purification system using nickel affinity columns. The purified proteins were analyzed by experimental SDS-PAGE (Figure 2C), and the purified recombinant gD concentration was detected by the BCA Protein Assay Kit. The results showed that after the cell culture supernatant was purified by Ni NTA resin Affinity chromatography, the purity of gD was significantly improved, and the amount of gD protein reached 1.14 mg/ml.

3.2. Immunoprotective effect of PRV-gD in mice

To determine whether gD protein paired with ISA 201VG adjuvant protects mice from prevalent strains. At 7, 14, 21, and 28 days after mice were immunized with the vaccine, we measured PRV-specific antibody levels in mouse serum using the PRV-Ab antibody quantification kit and found that both the gD protein group and the commercial vaccine group reached higher levels after the initial immunization. At 28 days after immunization, PRV-Ab was significantly higher in the gD protein group than in the commercial vaccine group (Figure 3A). At 7 days after the first immunization, the neutralizing antibody reached a higher level; at 28 days after the booster immunization, the serum NAs potency of mice in the gD protein group reached 28, which was significantly higher than that of the commercial vaccine group (Figure 3B). The results indicated that the gD protein group could induce a higher level of humoral immune response within a shorter time after immunization. Mice were stimulated with ConA 14 and 28 days after immunization with the vaccine, and then their proliferation levels were detected by CCK-8. It was found that the stimulation index was significantly higher in both the gD protein group and the commercial vaccine group, and the stimulation index of the gD protein group was significantly higher than that of the commercial vaccine group (Figure 3D). The results indicated that the gD protein group was able to induce a higher level of cellular immune response within a shorter time after immunization. Mice were infected by intraperitoneal injection using a dose of 10^3 $TCID_{50}$ of PRV-HY at 28 days after vaccination. After the challenge with PRV-HY, typical clinical signs such as pruritus, neurological signs, and death were observed in the DMEM group of mice at 2–6 days post-challenge; on day 6 post-challenge, all mice in the DMEM group died (100%), while none of the other groups showed typical clinical signs and death (Figure 3C). Overall, gD protein stimulated mice to produce higher levels of PRV-Ab, NAs, and lymphocytes, and could completely protect mice from lethal doses of PRV infection.

3.3. Immunoprotective effect of PRV-gD in piglets

To further evaluate the protective effect of gD protein on piglets, 100 μg of gD protein was injected intramuscularly. At 7, 14, 21, and 28 days after piglets were vaccinated, we measured PRV gD antibodies in piglets' sera using an indirect ELISA quantification kit, and the results were expressed as S/P values at 40-fold serum dilution. Twenty one days after immunization, both the gD protein group and the commercial vaccine group had reached high levels, and the gD protein group had significantly higher antibody levels than the commercial vaccine group (Figure 4A). Seven days after the initial immunization, both the gD protein group and the commercial vaccine group reached higher levels of neutralizing antibodies; 28 days after immunization, the potency of NAs titer in the serum of piglets in the gD protein group reached 2^7, which was significantly higher than that of the commercial vaccine group (Figure 4B). The results showed that the gD protein group was able to induce a higher level of humoral immune response within a shorter time after immunization. Piglets were infected with the PRV-HY through the nasal cavity using a dose of 10^7 $TCID_{50}$ 28 days after vaccination. After the challenge, rectal temperature, clinical symptoms, and piglet mortality were measured daily. The results showed that the rectal temperature of piglets in the DMEM group continued to increase for 4 days, and the rectal temperature of piglets in the DMEM group exceeded 40.5°C. The rectal temperature of piglets in the gD protein, commercial vaccine,

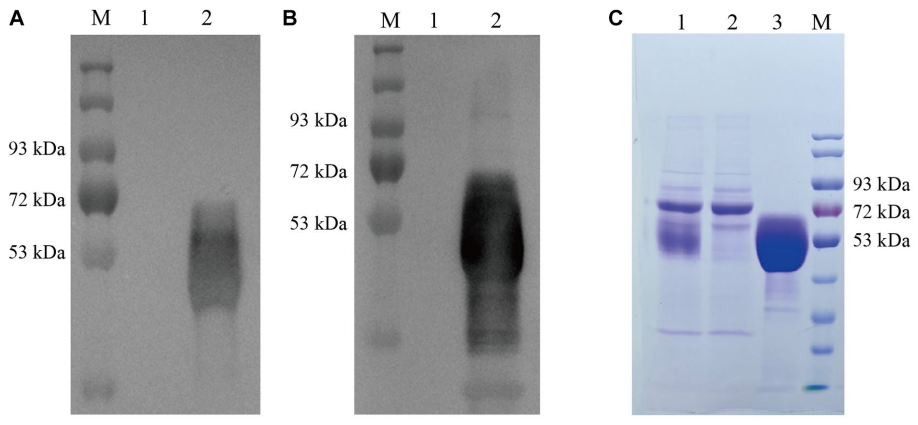

FIGURE 2
Identification and quantification of gD protein expression. Western blot detection of gD protein expression in HEK 293T-gD cell supernatant using anti his labeled antibody **(A)** and PRV high immune serum **(B)**. M: marker, lane 1: pLV-CMV-eGFP control, lane 2: pLV-CMV-gD. **(C)** SDS-PAGE was used to analyze the purified gD protein. Lane 1: crude culture supernatant; Lane 2: filtrate; Lane 3: eluate (500 mM imidazole); M: protein marker.

10.3389/fmicb.2023.1288458

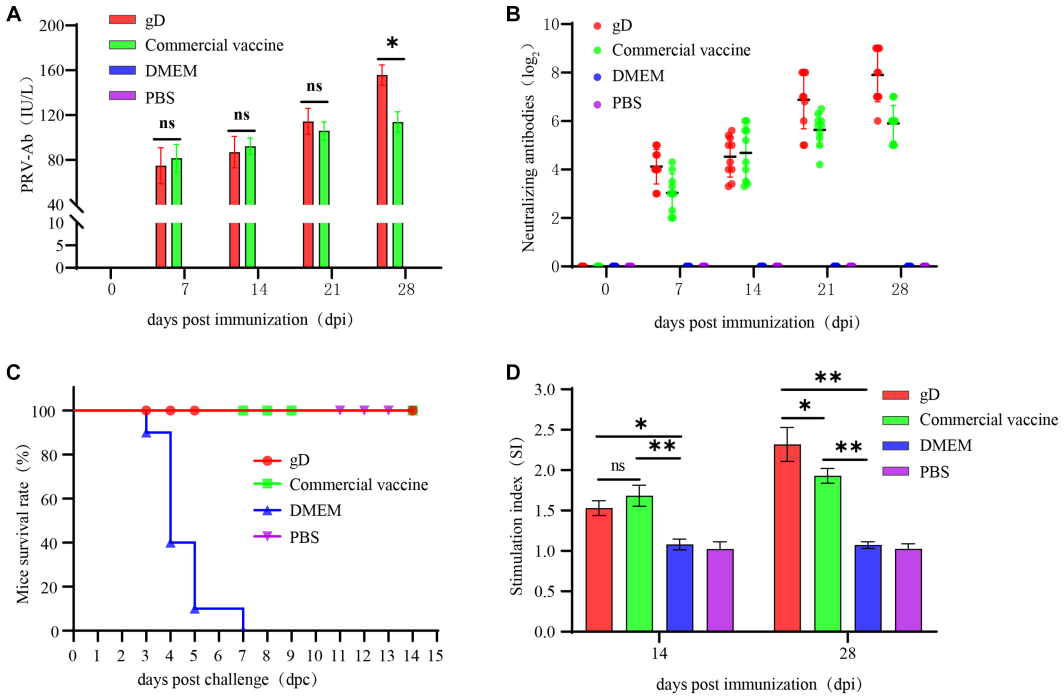

FIGURE 3
Protection against challenge with virulent PRV-HY strain in mice. Mice were inoculated with gD protein, commercial vaccine, DMEM, and PBS. All mice were immunized twice at 1 and 14 days and then challenged at 28 days with PRV-HY (10^3 $TCID_{50}$). Blood samples were collected weekly, and PRV-Ab antibodies **(A)** to gD and neutralizing antibodies **(B)** in mice sera were determined. **(C)** The survival rate of mice. **(D)** Lymphocyte proliferation level in mice. The data are representative of three independent experiments. Data were analyzed by One-Way ANOVA using GraphPad Prism 9. Significance is presented as $*p < 0.05$, $**p < 0.01$, $***p < 0.001$.

and PBS groups did not increase significantly (Figure 4C). We also observed that piglets in the DMEM group showed typical clinical signs such as severe respiratory problems, decreased appetite, convulsions, diarrhea, and recumbency, while the other groups showed no significant clinical signs. In addition, three piglets in the DMEM group died at 7, 9, and 10 days after the PRV-HY challenge (Figure 5D). In contrast, piglets in the gD protein group, the commercial vaccine group, and the PBS group survived without any significant CNS signs. Overall, the gD protein stimulates piglets to produce higher levels of PRV-gD antibodies and NAs, which could completely protect piglets against lethal doses of PRV-HY challenge.

3.4. Virus loads in nasal swabs, anal swabs, and tissues of the piglets

At 28 days after immunization, piglets were challenged with high doses of potent PRV-HY via the nasal route, and nasal swabs, anal swabs, and piglet tissues were collected to detect the PRV gE gene copy number by fluorescent quantitative nucleic acid amplification. The results showed that nasal and anal swabs from all groups of piglets were negative for the PRV gE gene at 1 day post-challenge. At 3–9 days after the challenge, the PRV gE gene was detected in piglet samples from all groups except the PBS negative control group, and the PRV gE gene copy number in the gD protein and commercial vaccine groups was significantly lower than in the DMEM group. On days 7 and 9, the nasal swab viral load was significantly lower in the gD protein group than in the commercial vaccine group (Figure 5A). In addition, the PRV gE gene could not be detected in nasal and anal swabs of the gD protein group on day 9 after the challenge. However, the PRV gE gene could still be detected in the nasal swabs of the commercial vaccine group on day 18 after the challenge, and the PRV gE gene could also be detected in anal swabs of the commercial vaccine group littermates on days 11 after the challenge (Figure 5B). At the end of the experiment, all piglets were euthanized and then pathologically dissected and tissue samples were collected to copies of the PRV gE gene in lymph nodes, brain, lung, spleen, liver, and kidney tissues. The results showed that the PRV gE gene was detected in piglet tissues from the commercial vaccine and DMEM groups, but only a small amount of the PRV gE gene was detected in the lymph nodes, brain, and lung tissues of piglets in the gD protein group, and the spleen and kidney were negative. In addition, the PRV gE gene copy number in all piglet tissues from the gD protein and commercial vaccine groups was significantly lower than in the DMEM group (Figure 5C). In summary, after the challenge, piglets in the gD protein group had lower viral shedding loads and shorter viral shedding times through the nasal and anal, which may be related to the fact that gD protein can stimulate the host to produce high levels of neutralizing antibodies.

3.5. Pathological examination of piglet tissues

Twenty-five days after the challenge, the surviving piglets were euthanized by intravenous sodium pentobarbital (100 mg/kg),

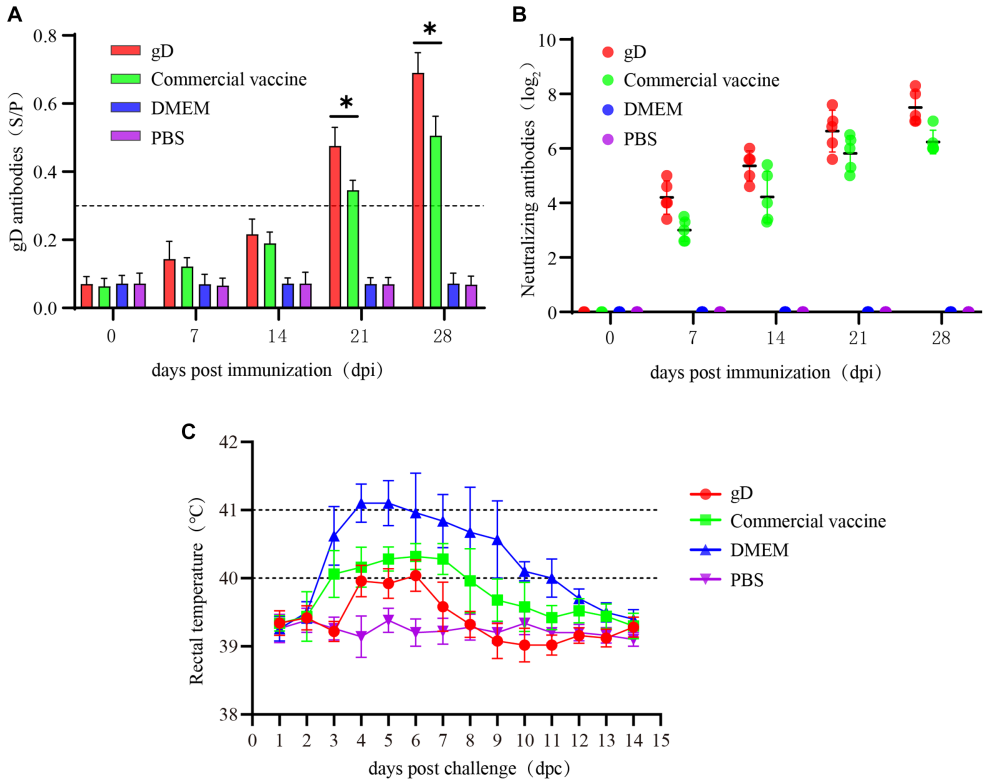

FIGURE 4
Blood samples were collected weekly after immunization in Piglets. Serum levels of gD and gB antibodies were measured at different time points. **(A)** gD antibodies were determined for piglet serum. **(B)** NAs titers in piglets at different times after immunization with the vaccine. **(C)** Rectal temperature of each group of immunized piglets after lethal dose challenge of PRV-HY. Data were analyzed by one-way ANOVA using GraphPad Prism 9. Significance is expressed as $*p < 0.05$, $**p < 0.01$, $***p < 0.001$.

followed by necropsy and histopathological examination. Lymph nodes, tonsils, lungs, spleen, liver, and kidneys were essentially normal in PBS, gD protein, and commercial vaccine groups. Lungs of piglets in the DMEM group exhibited severe pulmonary bruising, pulmonary edema, and solid lung lesions; lymph nodes were bruised and enlarged; tonsils were severely present and edematous; spleen was hemorrhagic infarcted; liver had striated gray-white necrotic foci on the surface; and renal medulla and renal cortex were severely hemorrhagic (Figure 6A). Sections were stained with hematoxylin–eosin (HE) to observe histopathological changes. The results showed that compared with the PBS group, the gD protein group, and the commercial vaccine group, the piglets in the DMEM group had reduced lymphocytes in the submandibular lymph nodes and hemorrhage in the medulla; inflammatory cell infiltration and bruising in the brain capillaries; extensive alveolar epithelial cell hyperplasia with massive inflammatory cell infiltration in the lungs, significant widening of the alveolar diaphragm, and a small number of inflammatory cells visible in the lumen of the fine bronchi; necrotic tissue in the spleen, focal lymphocytes in the red medulla necrosis and excessive congestion in the spleen; cell proliferation in the liver was quite obvious; some glomeruli had inflammatory cell infiltration, capillary hyperplasia, and massive neutrophil infiltration, and some renal cystic lumens disappeared. The results showed that the gD protein prepared in this study significantly attenuated the lesions in lymph nodes, tonsils, lungs, spleen, liver, and kidneys caused by PRV-HY infection (Figure 6B).

3.6. Immunohistochemistry of piglet tissues

Immunohistochemistry (IHC) experiments on piglet tissues using PRV gE monoclonal antibody showed that a large number of PRV-infected tan cells were present in lymph nodes, brain, lung, and spleen tissues in the DMEM group, while the gD protein and commercial vaccine groups had a smaller number of PRV-infected cells and lighter staining (Figure 7A). In addition, we analyzed the IHC results using ImageJ to calculate the ratio of positive cells for each tissue and score them. The results showed that the gD protein group and the commercial vaccine group scored significantly lower than the DMEM group (Figure 7B). These findings suggest that the gD protein prepared in this study may reduce replication in PRV lymph nodes, brain, lung, and spleen tissues, thus protecting piglets from lethal doses of PRV-HY infection.

4. Discussion

PR is an acute infectious disease caused by PRV infection. Under the current situation in China, PRV-infected pigs occur from time to time, which has seriously jeopardized the development of the Chinese pig industry and caused significant economic losses to the Chinese pig industry (Freuling et al., 2017; Tan et al., 2021). Since late 2011, genetic recombination has occurred between vaccine and wild strains of

10.3389/fmicb.2023.1288458

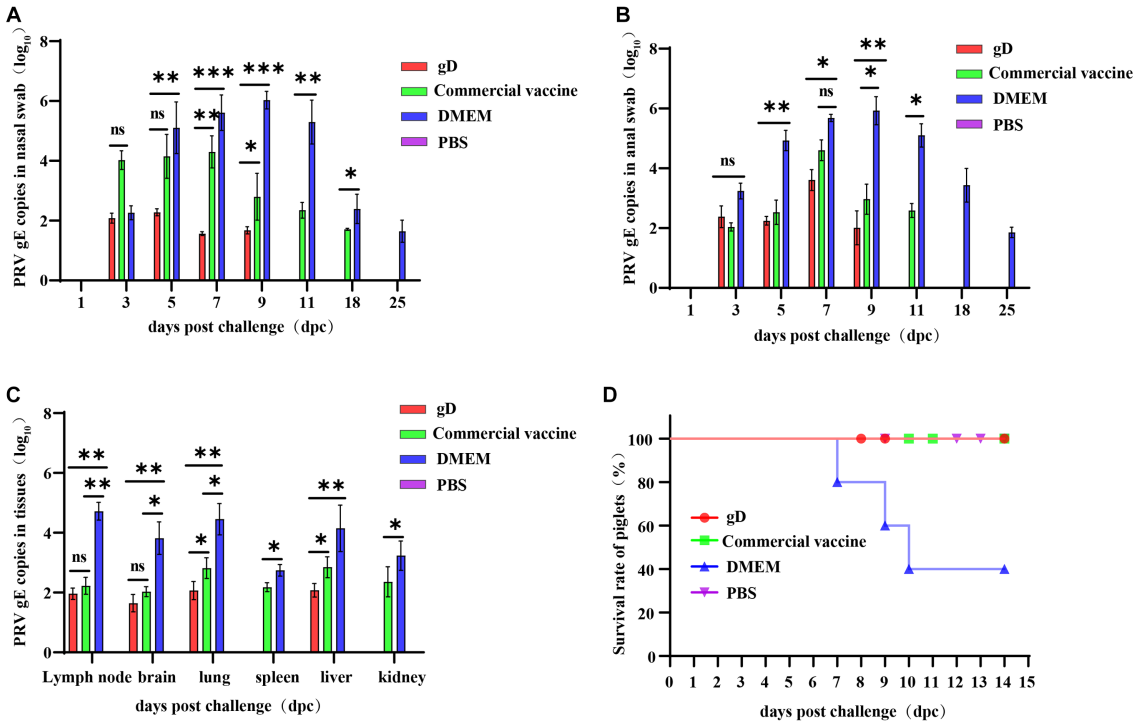

FIGURE 5
Protection against challenge with virulent PRV-HY strain in piglets. Absolute fluorescence quantification of PRV gE gene on oral swabs, anal swabs, and tissues from three groups of piglets. Nasal swabs **(A)** and anal swabs **(B)** were collected from piglets after the challenge, and qPCR amplification was performed to detect PRV gE genomic copies (Log_{10} copies/g). **(C)** Tissues of piglets from each group were collected and qPCR was amplified to detect PRV gE gene copies (Log_{10} copies/g). **(D)** Survival of immunized piglets in each group after challenge with a lethal dose of PRV-HY. Data were analyzed by one-way ANOVA using GraphPad Prism 9. Asterisks indicate significant differences (*$p < 0.05$, **$p < 0.01$, ***$p < 0.001$).

porcine pseudorabies virus, resulting in a significant increase in virulence of newly emerged recombinant PRV strains, and new porcine pseudorabies virus strains can evade the protection of traditional inactivated and live vaccines, resulting in increased morbidity and mortality in pigs, posing new challenges for porcine pseudorabies disease prevention, control, and decontamination in China (Hu D. et al., 2015; Ye et al., 2016). Therefore, the development of safe and effective novel genetically engineered vaccines is essential for the prevention, control, and prevalence of porcine pseudorabies, and subunit vaccines have become a potential option due to their stability and safety.

The selection of proteins with good immunogenicity is essential for the development of genetically engineered vaccines. Numerous studies have shown that porcine pseudorabies gD protein facilitates viral adhesion to the host cell surface. gD is a key recognition receptor involved in pathogen binding that stimulates the host to produce high titers of neutralizing antibodies and exhibits good immunogenicity, and this molecular recognition pattern of gD protein is essential for PRV infection (Takahashi et al., 1993; Fan et al., 2014; Zhang et al., 2021). In addition, gD proteins can recognize and attach to immunoglobulin-like cell adhesion molecules, such as connexin-1, connexin-2, and acetyl heparan sulfate. In humans and pigs, Nectin-1 is the only receptor reported for PRV cell entry. gD may have a similar affinity to connexin-1, and gD-specific mAbs (10B6) exhibit potent inhibition of PRV cell attachment and prevent virus transmission between cells (Hammond et al., 2001; Krummenacher et al., 2005). One study replaced the gD gene of the PRV Bartha-K61 strain with the gD gene of the HB1201 strain, and the recombinant Bartha-K61 strain gave pigs strong humoral and cellular immunity and protected them from the lethal challenge of HB1201, suggesting that gD may induce cellular immunity in cross-protection (Ren et al., 2020). In addition, immunization of piglets with recombinant adenovirus-expressing porcine pseudorabies virus gD protein stimulated the host to produce high levels of neutralizing antibodies, and no viremia was detected in piglets after the PRV challenge (Brisse et al., 2020). These studies suggest that expression of porcine pseudorabies virus individual gD protein may well induce re-emergence to produce humoral and cellular immunity and reduce the PRV mutant strain against piglets. The gD protein, which is essential for porcine pseudorabies virus infection in host cells, can encode a protein closer to the natural protein structure using the full-length gD gene. Taking into account the conditions available in a fairly pre-laboratory setting, a human embryonic kidney cell line (HEK 293T-gD) that can stably express the gD protein was constructed by a lentiviral packaging system in this study. The results showed that the HEK 293T-gD cell line could secretly express porcine pseudorabies virus gD protein. In subsequent experimental animal studies, the gD protein was found to be sufficient to induce higher levels of humoral and cellular immunity in mice, protecting them from lethal doses of PRV-HY.

Compared to viral and whole virus vaccines, recombinant protein-based subunit vaccines are relatively stable and easy to produce using recombinant protein technology, making them an attractive vaccine platform (Manoj et al., 2004). In addition, the lack of an active viral component minimizes the disease risk of subunit

10.3389/fmicb.2023.1288458

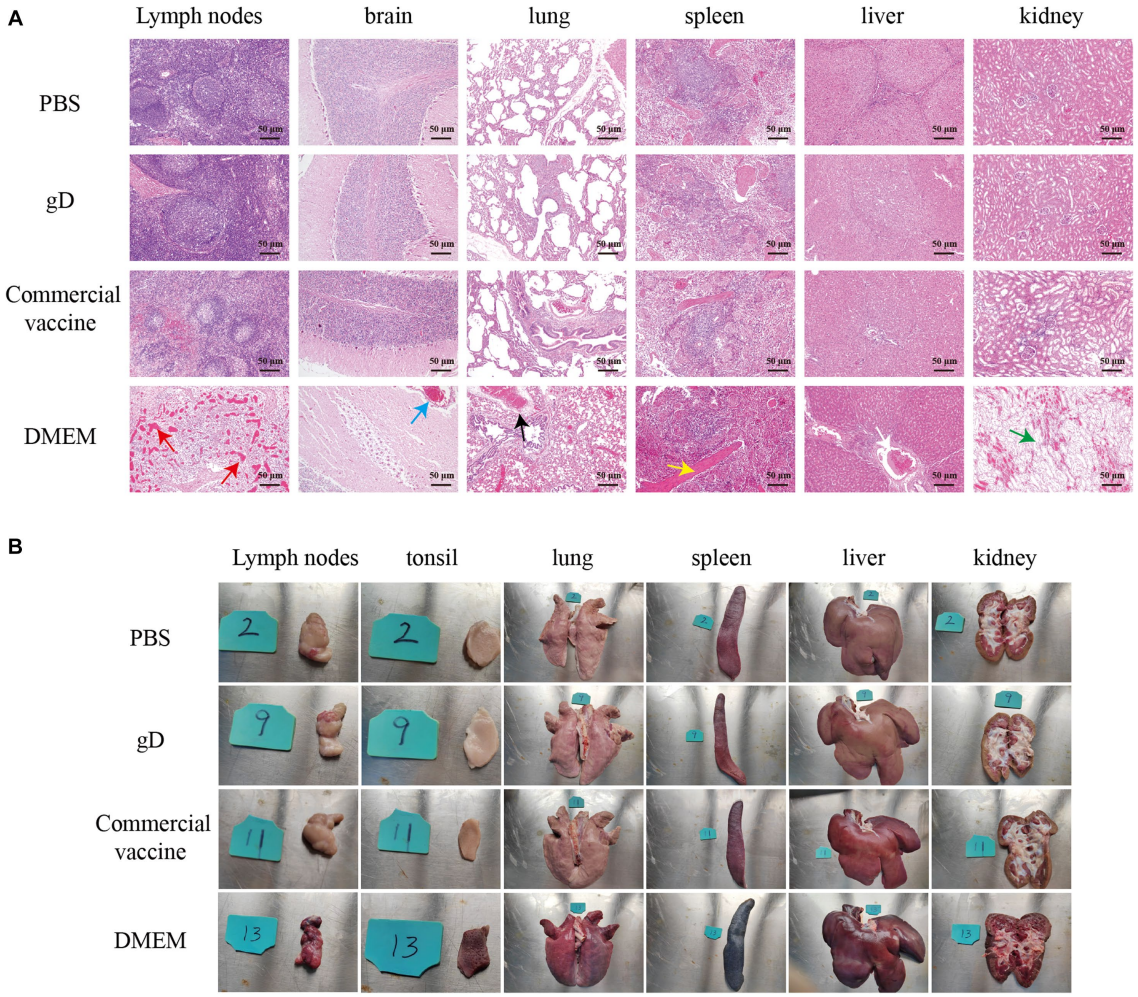

FIGURE 6
Overall changes in organ damage after challenging immunized pigs with PRV-HY. **(A)** Different piglet tissues (lymph nodes, tonsils, lungs, spleen, liver, and kidneys) were collected and euthanized on the 25th day after the challenge and dissected for pathological examination, here showing representative lesions in different organs. **(B)** Histopathological lesions rendering pigs immune after challenge with PRV-HY strain. The various tissues shown were fixed, segmented, and stained with hematoxylin and eosin (HE).

vaccination, demonstrating an extraordinary safety profile. The HEK 293T mammalian cell expression system with high-efficiency promoter (CMV) control allows high expression of recombinant proteins, post-translational modification of proteins and correct protein folding complexation, and expression products with good immunogenicity and safety, which can compensate for the prokaryotic expression system expressed proteins with low purity, immunogenicity, and CHO expression system expressed proteins (Luckow et al., 1993). In this study, the nucleotide sequence of recombinant gD protein was optimized, His tag was introduced at the C-terminus of the target protein, and HEK 293T cells that could be secreted for protein expression were selected, and the final amount of purified PRV gD protein expression reached 1.14 mg/ml, and Western blot results showed that the resulting gD protein had good antigenicity. High levels of NAs could be detected in the serum of piglets immunized with gD protein 28 days after immunization, and some piglet serum-neutralizing antibodies have a titer of 2^8.

To further evaluate the protective effect of gD protein on piglets against challenge, piglets were challenged by nasal drops 28 days after immunization. The results showed that all piglets in the gD protein group survived, indicating that gD protein induced immunity in piglets sufficient to resist lethal challenge by 10^7 $TCID_{50}$ PRV at a dose that was 10 to 100 times higher than the normal dose used. It is important to note that in contrast to previous studies, Hu found that piglets inoculated with the rSMXgI/gE1TK attenuated drug line (at a dose of 10^6 $TCID_{50}$) had a fever lasting 4 days and rectal temperatures at 40 and 42°C after challenge with the PRV variant SMX strain at 10^7 $TCID_{50}$ (Hu R.-M. et al., 2015). In this study, after the challenge, piglets in the gD protein group showed no typical clinical signs and all piglets did not develop fever, while some piglets in the commercial vaccine group epidemic had rectal temperatures above 40.5°C. The results of the study by Ren, J showed that two piglets in the Bartha-K61 group that died after the challenge exhibited severe hemorrhage in the lungs, lymph nodes, and kidneys, pulmonary coagulation, and cerebral edema. Piglets immunized with Bartha-gCHB1201 and Bartha-gDHB1201 showed moderate or mild hemorrhagic and coagulopathic lesions in the lungs and only mild lymph node enlargement (Ren et al., 2020), and these results were consistent with

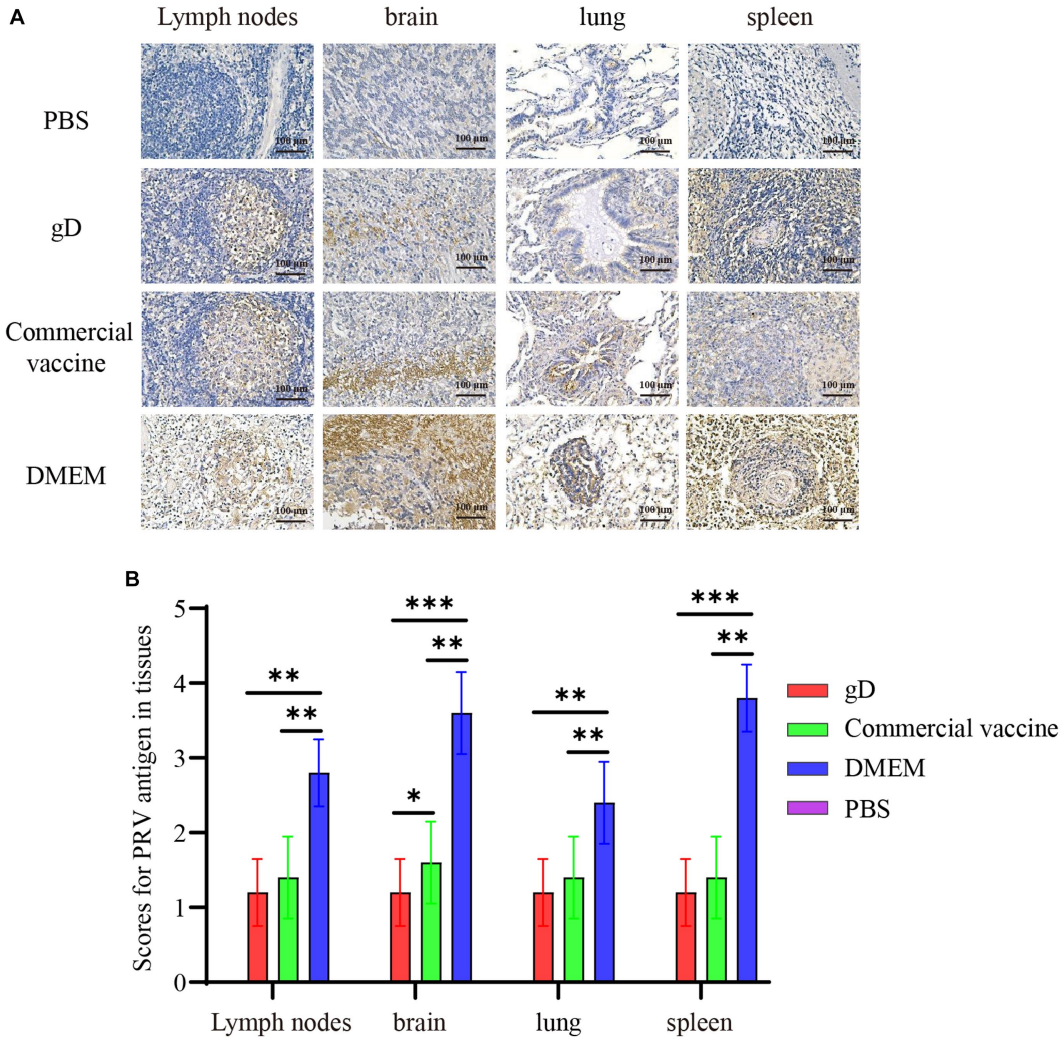

FIGURE 7
Immunohistochemical examination and scoring of piglet tissues. **(A)** Piglet lymph nodes, brain, lung, and spleen tissues were fixed, divided, and stained with PRV monoclonal antibody (1:400). Yellowish-brown color indicates a PRV-positive signal. **(B)** The percentage of positive cells was scored by ImageJ calculation. Asterisk indicates a significant difference: $*p < 0.05$, $**p < 0.01$, $***p < 0.001$.

our results (Figure 6A). In addition, the number of viral gene copies in nasal swabs and anal swabs of piglets in the gD group significantly resisted the commercial vaccine group and had a shorter detoxification cycle to the environment. Compared to the commercial vaccine group, piglets in the gD group showed fewer pathological changes in lymph nodes, lungs, spleen, liver, and kidneys, and fewer positive cells in tissues were infected with PRV. We speculate that this may be due to the ability of the gD protein to rapidly induce higher levels of neutralizing antibodies in the host and that PRV-neutralizing antibodies can neutralize most of the virus when it enters the peripheral blood. On the other hand, the ISA 201 adjuvant effectively stimulates the host to produce strong mucosal immunity in concert with the gD protein, and these speculations need to be investigated in our subsequent studies. Based on this, the genetically engineered PR vaccine prepared from the HEK 293T expression system is a potential vaccine candidate for the prevention of PRV infection and the control of PR epidemics. Although the preliminary results of this study demonstrated that PRV gD protein could induce high titers of neutralizing antibodies in mice and piglets, there was no in-depth discussion on the organism's level of cellular immunity, whether it could protect against different PRV strains, and the mechanism of the immune effect exerted by the gD protein, which is the direction of our future work.

5. Conclusion

In conclusion, we describe in this study that individual gD proteins produced by a mammalian cell expression system are well immunogenic and stimulate high levels of PRV-specific and neutralizing antibodies in mice and piglets. All mice and piglets survived lethal doses of PRV, significantly reducing the amount of PRV virus in piglets' lymph nodes, lungs, spleen, and other tissues. It also significantly reduced the time cycle and amount of viral excretion from piglets to the environment through nasal and anal cavities. The results suggest that the PRV gD protein is expected to be a potential candidate for the preparation of genetically engineered PR vaccines for the prevention of PRV infection and the control of PR epidemics.

Data availability statement

The original contributions presented in the study are included in the article/supplementary material, further inquiries can be directed to the corresponding authors.

Ethics statement

The animal study was approved by Experimental Animal Ethics Committee of Institute of the Animal Health, Guangdong Academy of Agricultural Science. The study was conducted in accordance with the local legislation and institutional requirements.

Author contributions

MZ: Data curation, Visualization, Writing – original draft. JC: Writing – review & editing, Data curation. SL: Writing – review & editing. RY: Methodology, Writing – review & editing. PZ: Validation, Writing – review & editing. ZR: Software, Writing – review & editing. XC: Writing – review & editing. GW: Funding acquisition, Writing – review & editing. HX: Writing – review & editing. RC: Writing – review & editing. YH: Writing – review & editing. NL: Writing – review & editing. HL: Writing – review & editing. Z-GY: Resources, Supervision, Writing – review & editing. XW: Funding acquisition, Writing – review & editing.

Funding

The author(s) declare financial support was received for the research, authorship, and/or publication of this article. We gratefully acknowledge support from the Planning Funds for Science and Technology of Guangdong Province (grant number 2021B1212050021), "The 14th Five-Year Plan" National Key Research and Development program (grant number 2021YFD1801400), the Scientific and Technological Plan Projects of Guangzhou (grant number 2023E04J1256), and the Guangdong Modern Agroindustry Technology Research System (grant number 2022KJ114).

Conflict of interest

HL and RY was employed by Guangzhou Bioneeds Biotechnology Co., LTD.

The remaining authors declare that the research was conducted in the absence of any commercial or financial relationships that could be construed as a potential conflict of interest.

Publisher's note

References

Ai, J.-W., Weng, S.-S., Cheng, Q., Cui, P., Li, Y.-J., Wu, H.-L., et al. (2018). Human Endophthalmitis caused by pseudorabies virus infection, China, 2017. *Emerg. Infect. Dis.* 24, 1087–1090. doi: 10.3201/eid2406.171612

Aschner, C. B., and Herold, B. C. (2021). Alphaherpesvirus Vaccines. *Curr. Issues Mol. Biol.* 41, 469–508. doi: 10.21775/cimb.041.469

Brisse, M., Vrba, S. M., Kirk, N., Liang, Y., and Ly, H. (2020). Emerging concepts and Technologies in Vaccine Development. *Front. Immunol.* 11:583077. doi: 10.3389/fimmu.2020.583077

Cao, Z., Zhang, K., Zhang, H., Zhang, H., Yu, Y., Yin, D., et al. (2022). Efficacy of a gB + gD-based subunit vaccine and the adjuvant granulocyte-macrophage colony stimulating factor for pseudorabies virus in rabbits. *Front. Microbiol.* 13:965997. doi: 10.3389/fmicb.2022.965997

Chen, H., Chen, Z., Bai, N., Yan, R., Xu, M., Wu, W., et al. (2021). Construction of a eukaryotic expression system with stable and secretory expression of *Mycobacterium tuberculosis* 38 kDa protein. *World J. Microbiol. Biotechnol.* 37:175. doi: 10.1007/s11274-021-03143-x

Cheng, Z., Kong, Z., Liu, P., Fu, Z., Zhang, J., Liu, M., et al. (2020). Natural infection of a variant pseudorabies virus leads to bovine death in China. *Transbound. Emerg. Dis.* 67, 518–522. doi: 10.1111/tbed.13427

Fan, Q., Longnecker, R., and Connolly, S. A. (2014). Substitution of herpes simplex virus 1 entry glycoproteins with those of Saimiriine herpesvirus 1 reveals a gD-gH/gL functional interaction and a region within the gD profusion domain that is critical for fusion. *J. Virol.* 88, 6470–6482. doi: 10.1128/JVI.00465-14

Freuling, C. M., Müller, T. F., and Mettenleiter, T. C. (2017). Vaccines against pseudorabies virus (PrV). *Vet. Microbiol.* 206, 3–9. doi: 10.1016/j.vetmic.2016.11.019

Fusco, D., Forghieri, C., and Campadelli-Fiume, G. (2005). The pro-fusion domain of herpes simplex virus glycoprotein D (gD) interacts with the gD N terminus and is displaced by soluble forms of viral receptors. *Proc. Natl. Acad. Sci. U. S. A.* 102, 9323–9328. doi: 10.1073/pnas.0503907102

Granzow, H., Klupp, B. G., Fuchs, W., Veits, J., Osterrieder, N., and Mettenleiter, T. C. (2001). Egress of Alphaherpesviruses: comparative ultrastructural study. *J. Virol.* 75, 3675–3684. doi: 10.1128/JVI.75.8.3675-3684.2001

Hammond, J. M., Jansen, E. S., Morrissy, C. J., Van Der Heide, B., Goff, W. V., Williamson, M. M., et al. (2001). Vaccination of pigs with a recombinant porcine adenovirus expressing the gD gene from pseudorabies virus. *Vaccine* 19, 3752–3758. doi: 10.1016/S0264-410X (01)00084-6

He, W., Auclert, L. Z., Zhai, X., Wong, G., Zhang, C., Zhu, H., et al. (2019). Interspecies transmission, genetic diversity, and evolutionary dynamics of pseudorabies virus. *J. Infect. Dis.* 219, 1705–1715. doi: 10.1093/infdis/jiy731

Hochrein, H., Schlatter, B., O'Keeffe, M., Wagner, C., Schmitz, F., Schiemann, M., et al. (2004). Herpes simplex virus type-1 induces IFN-α production via Toll-like receptor 9-dependent and -independent pathways. *Proc. Natl. Acad. Sci. U. S. A.* 101, 11416–11421. doi: 10.1073/pnas.0403555101

Hu, D., Zhang, Z., Lv, L., Xiao, Y., Qu, Y., Ma, H., et al. (2015). Outbreak of variant pseudorabies virus in Bartha-K61–vaccinated piglets in Central Shandong Province, China. *J. Vet. Diagn. Investig.* 27, 600–605. doi: 10.1177/1040638715593599

Hu, R.-M., Zhou, Q., Song, W.-B., Sun, E.-C., Zhang, M.-M., He, Q.-G., et al. (2015). Novel pseudorabies virus variant with defects in TK, gE and gI protects growing pigs against lethal challenge. *Vaccine* 33, 5733–5740. doi: 10.1016/j.vaccine.2015.09.066

Jiang, Z., Zhu, L., Cai, Y., Yan, J., Fan, Y., Lv, W., et al. (2020). Immunogenicity and protective efficacy induced by an mRNA vaccine encoding gD antigen against pseudorabies virus infection. *Vet. Microbiol.* 251:108886. doi: 10.1016/j.vetmic.2020.108886

Kong, H., Zhang, K., Liu, Y., Shang, Y., Wu, B., and Liu, X. (2013). Attenuated live vaccine (Bartha-K16) caused pseudorabies (Aujeszky's disease) in sheep. *Vet. Res. Commun.* 37, 329–332. doi: 10.1007/s11259-013-9568-8

Kramer, T., Greco, T. M., Enquist, L. W., and Cristea, I. M. (2011). Proteomic characterization of pseudorabies virus extracellular Virions. *J. Virol.* 85, 6427–6441. doi: 10.1128/JVI.02253-10

Krummenacher, C., Supekar, V. M., Whitbeck, J. C., Lazear, E., Connolly, S. A., Eisenberg, R. J., et al. (2005). Structure of unliganded HSV gD reveals a mechanism for receptor-mediated activation of virus entry: structure of unliganded HSV gD. *EMBO J.* 24, 4144–4153. doi: 10.1038/sj.emboj.7600875

Li, A., Lu, G., Qi, J., Wu, L., Tian, K., Luo, T., et al. (2017). Structural basis of nectin-1 recognition by pseudorabies virus glycoprotein D. *PLoS Pathog.* 13:e1006314. doi: 10.1371/journal.ppat.1006314

Liu, Q., Wang, X., Xie, C., Ding, S., Yang, H., Guo, S., et al. (2021). A novel human acute encephalitis caused by pseudorabies virus variant strain. *Clin. Infect. Dis.* 73, e3690–e3700. doi: 10.1093/cid/ciaa987

Luckow, V. A., Lee, S. C., Barry, G. F., and Olins, P. O. (1993). Efficient generation of infectious recombinant baculoviruses by site-specific transposon-mediated insertion of foreign genes into a baculovirus genome propagated in *Escherichia coli*. *J. Virol.* 67, 4566–4579. doi: 10.1128/jvi.67.8.4566-4579.1993

Manoj, S., Griebel, P. J., Babiuk, L. A., and Van Drunen Littel-Van Den Hurk, S. (2004). Modulation of immune responses to bovine herpesvirus-1 in cattle by immunization with a DNA vaccine encoding glycoprotein D as a fusion protein with bovine CD154. *Immunology* 112, 328–338. doi: 10.1111/j.1365-2567.2004.01877.x

Marcaccini, A., López Peña, M., Quiroga, M. I., Bermúdez, R., Nieto, J. M., and Alemañ, N. (2008). Pseudorabies virus infection in mink: a host-specific pathogenesis. *Vet. Immunol. Immunopathol.* 124, 264–273. doi: 10.1016/j.vetimm.2008.03.013

Masot, A. J., Gil, M., Risco, D., Jiménez, O. M., Núñez, J. I., and Redondo, E. (2017). Pseudorabies virus infection (Aujeszky's disease) in an Iberian lynx (*Lynx pardinus*) in Spain: a case report. *BMC Vet. Res.* 13:6. doi: 10.1186/s12917-016-0938-7

Mettenleiter, T. C. (1996). Immunobiology of pseudorabies (Aujeszky's disease). *Vet. Immunol. Immunopathol.* 54, 221–229. doi: 10.1016/S0165-2427(96)05695-4

Mettenleiter, T. C. (2000). Aujeszky's disease (pseudorabies) virus: the virus and molecular pathogenesis - state of the art, June 1999. *Vet. Res.* 31, 99–115. doi: 10.1051/vetres:2000110

Minamiguchi, K., Kojima, S., Sakumoto, K., and Kirisawa, R. (2019). Isolation and molecular characterization of a variant of Chinese gC-genotype II pseudorabies virus from a hunting dog infected by biting a wild boar in Japan and its pathogenicity in a mouse model. *Virus Genes* 55, 322–331. doi: 10.1007/s11262-019-01659-x

Nauwynck, H., Glorieux, S., Favoreel, H., and Pensaert, M. (2007). Cell biological and molecular characteristics of pseudorabies virus infections in cell cultures and in pigs with emphasis on the respiratory tract. *Vet. Res.* 38, 229–241. doi: 10.1051/vetres:200661

Oku, M., Ishino, R., Uchida, S., Imataki, O., Sugimoto, N., Todo, T., et al. (2021). Oncolytic herpes simplex virus type 1 (HSV-1) in combination with lenalidomide for plasma cell neoplasms. *Br. J. Haematol.* 192, 343–353. doi: 10.1111/bjh.17173

Petrina, M., Martin, J., and Basta, S. (2021). Granulocyte macrophage colony-stimulating factor has come of age: from a vaccine adjuvant to antiviral immunotherapy. *Cytokine Growth Factor Rev.* 59, 101–110. doi: 10.1016/j.cytogfr.2021.01.001

Ren, J., Wang, H., Zhou, L., Ge, X., Guo, X., Han, J., et al. (2020). Glycoproteins C and D of PRV strain HB1201 contribute individually to the escape from Bartha-K61 vaccine-induced immunity. *Front. Microbiol.* 11:323. doi: 10.3389/fmicb.2020.00323

Sun, Y., Luo, Y., Wang, C.-H., Yuan, J., Li, N., Song, K., et al. (2016). Control of swine pseudorabies in China: opportunities and limitations. *Vet. Microbiol.* 183, 119–124. doi: 10.1016/j.vetmic.2015.12.008

Takahashi, H., Yoshikawa, Y., Kai, C., and Yamanouchi, K. (1993). Mechanism of pruritus and Peracute death in mice induced by pseudorabies virus (PRV) infection. *J. Vet. Med. Sci.* 55, 913–920. doi: 10.1292/jvms.55.913

Tan, L., Yao, J., Yang, Y., Luo, W., Yuan, X., Yang, L., et al. (2021). Current status and challenge of pseudorabies virus infection in China. *Virol. Sin.* 36, 588–607. doi: 10.1007/s12250-020-00340-0

Verpoest, S., Cay, B., Favoreel, H., and De Regge, N. (2017). Age-dependent differences in pseudorabies virus neuropathogenesis and associated cytokine expression. *J. Virol.* 91, e02058–e02016. doi: 10.1128/JVI.02058-16

Wang, J., Wang, Y., Zhang, E., Zhou, M., Lin, J., and Yang, Q. (2019). Intranasal administration with recombinant *Bacillus subtilis* induces strong mucosal immune responses against pseudorabies. *Microb. Cell Factories* 18:103. doi: 10.1186/s12934-019-1151-8

Ye, C., Guo, J.-C., Gao, J.-C., Wang, T.-Y., Zhao, K., Chang, X.-B., et al. (2016). Genomic analyses reveal that partial sequence of an earlier pseudorabies virus in China is originated from a Bartha-vaccine-like strain. *Virology* 491, 56–63. doi: 10.1016/j.virol.2016.01.016

Ye, C., Zhang, Q.-Z., Tian, Z.-J., Zheng, H., Zhao, K., Liu, F., et al. (2015). Genomic characterization of emergent pseudorabies virus in China reveals marked sequence divergence: evidence for the existence of two major genotypes. *Virology* 483, 32–43. doi: 10.1016/j.virol.2015.04.013

Zhang, T., Liu, Y., Chen, Y., Wang, J., Feng, H., Wei, Q., et al. (2021). A monoclonal antibody neutralizes pesudorabies virus by blocking gD binding to the receptor nectin-1. *Int. J. Biol. Macromol.* 188, 359–368. doi: 10.1016/j.ijbiomac.2021.07.170

Zhang, T., Liu, Y., Chen, Y., Wang, A., Feng, H., Wei, Q., et al. (2020). A single dose glycoprotein D-based subunit vaccine against pseudorabies virus infection. *Vaccine* 38, 6153–6161. doi: 10.1016/j.vaccine.2020.07.025

frontiers | Frontiers in Microbiology

TYPE Methods
PUBLISHED 16 November 2023
DOI 10.3389/fmicb.2023.1285268

OPEN ACCESS

EDITED BY
Jingqiang Ren,
Wenzhou University, China

REVIEWED BY
Tuofan Li,
College of Veterinary Medicine,
Yangzhou University, China
Hualei Wang,
College of Veterinary Medicine,
Jilin University, China

*CORRESPONDENCE
Xiaofeng Shan
✉ 7949534@qq.com
Yuening Cheng
✉ 89331641@qq.com
Erkai Feng
✉ tcsfek@126.com

RECEIVED 29 August 2023
ACCEPTED 03 November 2023
PUBLISHED 16 November 2023

CITATION
Yan M, Shang J, Zhang X, Wu S, Wang C, Wang Z, Luo G, Yi L, Shan X, Cheng Y and Feng E (2023) The establishment and application of a dual Nano-PCR detection method for feline calicivirus and feline herpesvirus type I.
Front. Microbiol. 14:1285268.
doi: 10.3389/fmicb.2023.1285268

The establishment and application of a dual Nano-PCR detection method for feline calicivirus and feline herpesvirus type I

Manping Yan[1,2], Jinyuan Shang[1], Xiaohao Zhang[3], Shun Wu[1], Chunxia Wang[1], Zhenjun Wang[1], Guoliang Luo[1], Li Yi[1], Xiaofeng Shan[2]*, Yuening Cheng[1]* and Erkai Feng[1]*

[1]Key Laboratory of Economic Animal Diseases, Ministry of Agriculture, Institute of Special Animal and Plant Sciences, Chinese Academy of Agricultural Sciences, Changchun, China, [2]College of Animal Science and Technology, Jilin Agricultural University, Changchun, China, [3]Department of Cardiology, The Second Hospital of Jilin University, Changchun, China

Feline calicivirus (FCV) and Feline herpesvirus type I (FHV-I) are the main pathogens causing upper respiratory tract infections in cats, and some wild animals. These two viruses always coinfection and cause serious harm to pet industry and wild animals protection. Established a rapid and accurate differential diagnosis method is crucial for prevention and control of disease, however, the current main detection method for these two viruses, either is low sensitivity (immunochromatographic strip), or is time-consuming and cannot differential diagnosis (conventional single PCR). Nanoparticle-assisted polymerase chain reaction (Nano-PCR) is a recently developed technique for rapid detection method of virus and bacteria. In this study, we described a dual Nano-PCR assay through combining the nanotechnology and PCR technology, which for the clinical simultaneous detection of FCV and FHV-I and differential diagnosis of upper respiratory tract infections in cats or other animals. Under optimized conditions, the optimal annealing temperature for dual Nano-PCR was 51.5°C, and specificity test results showed it had no cross reactivity to related virus, such as feline panleukopenia virus (FPV), feline Infectious peritonitis virus (FIPV) and rabies virus (RABV). Furthermore, the detection limit of dual Nano-PCR for FCV and FHV-I both were 1×10^{-8} ng/μL, convert to number of copies of virus DNA was 6.22×10^{3}copies/μL (FCV) and 2.81×10^{3}copies/μL (FHV-I), respectively. The dual Nano-PCR detected result of 52 cat clinical samples, including ocular, nasal and faecal swabs, and (3 FCV-positive samples), was consistent with ordinary PCR and the clinical detection results. The dual Nano-PCR method established in this study with strong specificity and high sensitivity can be used for virus nucleic acid (FCV and FHV-I) detection of clinical samples of feline upper respiratory tract infections feline calicivirus and feline herpesvirus while providing support for the early diagnosis of cats that infected by FCV and FHV-I.

KEYWORDS

feline calicivirus, feline herpesvirus type I, Nano-PCR, detection diagnostic technology, infectious disease

1. Introduction

As the main pathogen causing upper respiratory tract infections in cats and some wild animals such as lions, tigers, and leopards, the clinical characterization of FHV-I and FCV is almost identical, include respiratory inflammation, ocular inflammation, hair loss around the eyes, and thick secretions from the eyes and nose. Therefore, it is nearly impossible to distinguish the viruses based on clinical symptoms. Most of the time, laboratory nucleic acid detection methods are needed. In these methods, specific PCR amplification technology plays an important role in differential diagnosis (Bo et al., 2023; Jindong et al., 2023; Ying et al., 2023).

FCV, belongs to the order of *Picornavirales* and the family of *Caliciviridae*, is a nonenveloped single-stranded positive-sense RNA virus with a genome length of approximately 7,700 bp and three open reading frames (ORFs) (Kai et al., 2017). The ORF1 encodes 7 non-structural proteins, and ORF2 and ORF3 encode the major structural protein VP1 and the minor structural protein VP2, respectively. VP1 is encoded by the conserved region of the gene sequence, and the presence of the virus is often determined by identifying the VP1 fragment. FCV is highly contagious and can cause mild to severe respiratory and oral disease in cats. Most strains are nonlethal, but a few are lethal. FCV is easily mutated, so FCV vaccines do not completely protect against the mutated strains (Zhanding et al., 2019; Chengyun et al., 2023; Weijie et al., 2023).

FHV-I, also known as viral rhinobronchitis, is a member of the Var*icellovirus* genus of the herpesvirus subfamily *Alphaherpesvirina*. It is an enveloped, double-stranded DNA virus with a genome length of approximately 126–135 kb with 78 open reading frames that can encode 74 kinds of proteins. Currently, only one serotype of the virus has been identified. FHV-I replicates and proliferates on the conjunctiva, respiratory epithelial cells, and neuronal cells. The virus mainly infects domestic cats and cats such as lions, tigers and leopards and has a mortality rate of up to 50%. FHV-I is different from FCV in that its survivability is relatively low, and it is sensitive to organic solvents such as acid, ether, and chloroform. It can be killed by common disinfectants, and it does not survive at high temperatures (Meihui et al., 2023; Weijie et al., 2023; Xinyan et al., 2023).

Currently, the detection method of FCV and FHV-I is based on the initial judgment of clinical symptoms, or using test strips but the sensitivity is very low, and the early stage of the disease cannot be detected. There is also a method of virus isolation, but the efficiency is low and time-consuming.

Nanoparticle-assisted polymerase chain reaction (Nano-PCR) is a recently developed technique for rapid detection method of virus and bacteria (Jianke et al., 2015). Gold nanoparticles can promote the combination of primers and templates by increasing the thermal conductivity of the PCR, which can improve the specificity and sensitivity of the detection method (Lin et al., 2017). In 2019, Qin T, et al. established nanoparticle-assisted PCR (Nano-PCR) assay for the detection of canine parvovirus (CPV), and in 2022, Jingfei et al. published the Nano-PCR detection method of feline panleukopenia virus (FPV) (Tong et al., 2019; Jingfei et al., 2022). All of these just detect one pathogen, and not-simultaneous detection of FCV and FHV-I and differential diagnosis of upper respiratory tract infections in cats or other animals.

Therefore, in this study, we described a dual Nano-PCR method, which can specifically detect FHV-I and FCV at the same time and it will provide important technical support for the prevention of animal diseases in the pet industry. Meanwhile, this study also provides more sensitive and efficient detection methods for the timely diagnosis and prevention of other wild protected animal diseases susceptible to FCV and FHV-I.

2. Materials and methods

2.1. Sources of experimental materials

FCV, FHV-I, FPV, Rabies virus (RABV) cDNA and FIPV were isolated and preserved by the Institution of Special Animals and Plant Sciences, Chinese Academy of Agricultural Sciences (CAAS). Gold nanoparticles were purchased from Shiao Biotechnology Co., Ltd. (Changchun, Jilin). EasyPure® Viral DNA/RNA Kit was purchased from TransGen Biotech (Beijing, China). RevertAid Master Mix was purchased from ThermoFisher Scientific. Plasmid Mini Kit I and Gel Extraction Kit were purchased from Omega. pMD™ 19-T Vector Cloning Kit was purchased from Takara (Beijing). 2 × M5 HiPer plus Taq HiFi PCR mix (with blue dye) was purchased from Beijing Jumei Biotechnology Co., Ltd.

2.2. Experimental instruments

A high-speed centrifuge was purchased from Thermo Fisher Scientific (China) Co., Ltd.; a nanophotometer was purchased from Implen GmbH; a Multi-Temp Platform was purchased from Monad Biotech Co. Ltd.; a gene amplification instrument was purchased from Beijing Dinghaoyuan Technology Co., Ltd.

2.3. Design primers

According to the gene sequences of FCV strains and FHV-I strains in GenBank, primers were designed using Oligo7.0 and Primer5.0, and the primers were synthesized by Jilin Province Kumei Biotechnology Co., Ltd. Refering to Table 1 for details.

2.4. Viral nucleic acid extraction

The FCV and FHV-I viruses frozen at −80°C were thawed, and the RNA of FCV and the DNA of FHV-I were extracted using the EasyPure ® Viral DNA/RNA Kit purchased from TransGen Biotech. The DNA was stored at −20°C, and the RNA was obtained from

TABLE 1 Primers for the dual Nano-PCR method.

Primer	Primer sequences (5′-3′)	Segment length (bp)	Target gene
FCV-F	TAGATATGGGTTTAGAAGGG	242	VP1
FCV-R	TTAGATTGGAAGCGGATG		
FHV-I-F	AGATTTGCCGCACCATACCTTC	518	TK
FHV-I-R	CCGGGCTTTGAAAACACTGAAT		

Thermo Scientific RevertAid Master Mix and reverse transcribed into cDNA. The remaining RNA was stored at −80°C, and the obtained cDNA was stored at −20°C.

2.5. Construction of FCV- and FHV-I-positive plasmids

Using the extracted FCV cDNA and FHV-I DNA as templates, the primer sequences designed in 2.3 were used to amplify the target fragments, gel recovery and purification of the target fragments were then performed, and they were connected to the pMD™ 19-T vector. Technology Co., Ltd. provided sequencing services and finally FCV-positive plasmids and FHV-I-positive plasmids were obtained.

2.6. Establishment of a common dual PCR method for FCV and FHV-I

The FCV- and FHV-I-positive plasmids obtained in 2.5 were used as templates for PCR amplification. Reaction system (20 μL): 10 μL 2 × M5 HiPer plus Taq HiFi PCR mix (with blue dye); 0.5 μL FCV-F, 0.5 μL FCV-R, 0.5 μL FHV-I-F, 0.5 μL FHV-I-R; 0.25 μL template; volume to 20 μL. The reaction conditions were as follows: predenaturation at 95°C for 3 min; denaturation at 94°C for 25 s, annealing at 53°C for 25 s, and extension at 72°C for 10s for a total of 35 cycles; and extension at 72°C for 5 min. PCR amplification products were detected by agarose gel electrophoresis.

2.7. Establishment of a dual Nano-PCR detection method for FCV and FHV-I

2.7.1. Optimization of nanoparticle size and dosage

Gold Nanoparticles of different sizes (30, 50, 70, 100 nm) were used sequentially. There was a total of four groups; each group used different amounts of Nanoparticles (0.5, 1.0, 1.5, 2.0 μL). PCR system (20 μL): 10 μL 2 × M5 HiPer plus Taq HiFi PCR mix (with blue dye); 0.5 μL FCV-F, 0.5 μL FCV-R, 0.5 μL FHV-I-F, 0.5 μL FHV-I-R, respectively; different amounts (0.5, 1.0, 1.5, 2.0 μL) of Nano gold particles (30, 50, 70, 100 nm) were added, and 0.25 μL of the template was added, respectively. The mix was volumed up to 20 μL with water. The reaction conditions were predenaturation at 95°C for 3 min; denaturation at 94°C for 25 s, annealing at 53°C for 25 s, 72°C for 10s, for a total of 35 cycles; and 72°C for 5 min. PCR amplification products were detected by agarose gel electrophoresis.

2.7.2. Optimization of annealing temperature

The FCV- and FHV-I-positive plasmids obtained in 2.5 were used as templates, the annealing temperature gradient was set at 50.0–60.0°C, and the other reaction conditions were the same. Nano-PCR system (20 μL): 10 μL 2 × M5 HiPer plus Taq HiFi PCR mix (with blue dye); 0.5 μL FCV-F, 0.5 μL FCV-R, 0.5 μL FHV-I-F, 0.5 μL FHV-I-R; 0.25 μL template; volume up to 20 μL with water. The reaction conditions were as follows: predenaturation at 95°C for 3 min; denaturation at 94°C for 25 s, annealing at 50.0–60.0°C (12 annealing temperatures in total) for 25 s, and extension at 72°C for 10s for a total of 35 cycles; and extension at 72°C for 5 min. PCR amplification products were detected by agarose gel electrophoresis.

2.7.3. Specificity test

The optimized dual Nano-PCR detection method for FCV and FHV-I was used to detect the DNA or cDNA of FCV and FHV-I, FCV, FHV-I, FPV, FIP, and RABV to verify the specificity of the method.

2.7.4. Sensitivity test

The concentrations of FCV- and FHV-I-positive plasmids determined by the Nanophotometer were 165.20 ng/μL and 159.45 ng/μL, respectively, and the converted copy numbers were 6.22×10^{11}copies/μL and 2.81×10^{11}copies/μL, respectively. ddH_2O was used to dilute the two groups of positive plasmids according to a 10-fold ratio, and the plasmids of each dilution were used as templates to perform dual Nano-PCRs and common dual-PCRs. The products were subjected to agarose gel electrophoresis, and the electrophoresis bands were compared.

2.8. Clinical sample testing

Fifty-two cat eye, nose and faecal swabs were collected from different regions in Changchun City virual DNA and RNA were extracted by using Takara Mini BEST Viral RNA/DNA Extraction Kit Ver.5.0 (Takara, Beijing China) extracting. The RNA was reverse transcribed into cDNA. The DNA and cDNA of samples were detected by the established common Nano-PCR and dual Nano-PCR.

3. Results

3.1. Establishment of a common dual PCR method for FCV and FHV-I

Through PCR amplification of the target fragments of FCV- and FHV-I-positive plasmids, after detection by agarose gel electrophoresis, the expected target fragments of 242 bp and 518 bp were obtained, and the ordinary dual PCR detection experiment was successfully established, as shown in Figure 1.

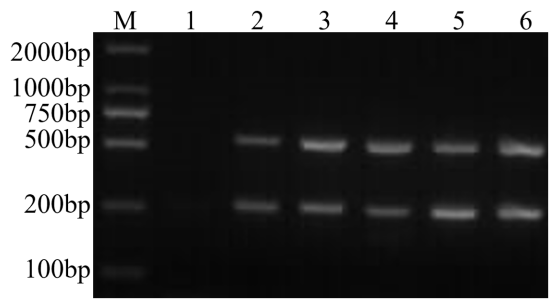

FIGURE 1
Establishment of a common dual PCR method. M: DNA molecular quality standard; 1: negative control; 2: positive control; 3–6: FCV- and FHV-I common dual PCR.

3.2. Establishment of the FCV and FHV-I dual Nano-PCR method

Using the dual Nano-PCR system, the target fragments of FCV- and FHV-I-positive plasmids were amplified, and after agarose gel electrophoresis, target fragments with expected sizes of 242 bp and 518 bp were obtained, as shown in Figure 2.

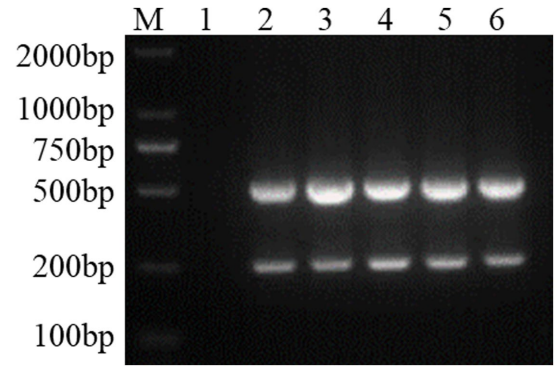

FIGURE 2
Establishment of a dual Nano-PCR method. M: DNA molecular quality standard; 1: negative control; 2: positive control; 3–6: FCV- and FHV-I dual Nano-PCR.

3.2.1. Optimization of nanoparticle size and dosage

By simultaneously controlling the nanometre size as an independent variable and the amounts of nanoparticles as an independent variable, and keeping other conditions unchanged, the results of PCR products detected by agarose gel electrophoresis are shown in Figure 3. It can be seen from the figure that the target fragment is the brightest when the nanoparticle size is 50 nm and the amount added is 2 μL, so this condition is the final result of optimizing the nanoparticle size and dosage.

3.2.2. Optimization of annealing temperature

Figure 4 shows the results of agarose gel electrophoresis after the FCV- and FHV-I-positive plasmids underwent an annealing temperature gradient (50.0–60.0°C) PCR. It can be seen from the figure that the target band is the clearest when the annealing temperature is 51.0°C and 52.0°C, so the final optimal annealing temperature was 51.5°C.

3.2.3. Specificity test

Bands of 242 bp and 518 bp appeared in the amplification results of FCV and FHV-I viruses using the established dual Nano-PCR

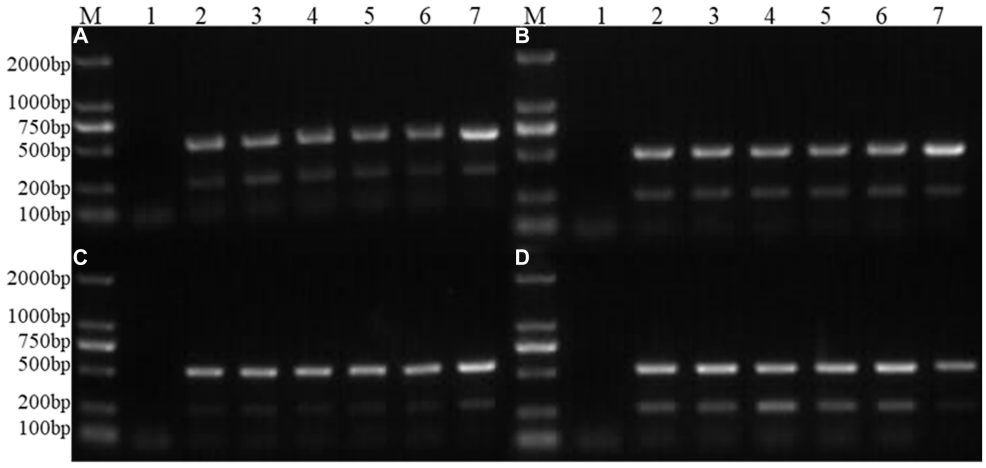

FIGURE 3
Optimization of nanoparticle size and dosage. M: DNA molecular quality standard; 1: Negative control; 2; 25 nm; 3: 30 nm; 4: 50 nm; 5: 70 nm; 6: 100 nm; 7: Positive control; 1 μL; **(A)**: 0.5 μL of nanoparticle; **(B)**: 1.0 μL of nanoparticle; **(C)**: 1.5 μL of nanoparticle; **(D)**: 2.0 μL of nanoparticle.

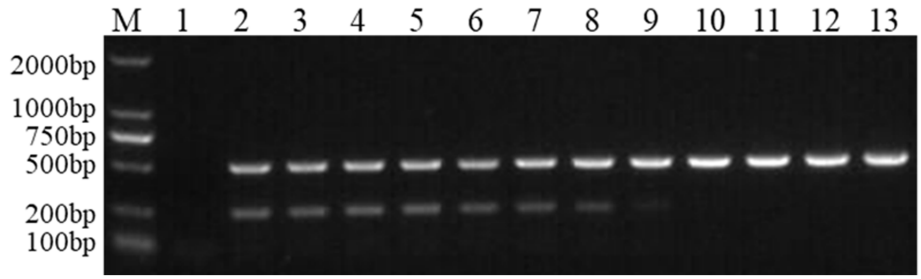

FIGURE 4
Optimization of annealing temperature. M: DNA molecular quality standard; 1: negative control; 2: 50.0°C; 3: 50.4°C; 4: 51.0°C; 5: 52.0°C; 6: 53.2°C; 7: 54.0°C; 10: 57.0°C; 11: 58.0°C; 12: 59.5°C; 13: 60.0°C.

method; only 242 bp bands appeared in the detection results of FCV virus; and only 518 bp bands appeared in the detection results of FHV-I virus. There were no bands in the detection of other pathogens, and the results are shown in Figure 5. It can be seen that the established dual Nano-PCR method has good specificity.

3.2.4. Sensitivity experiment

FCV- and FHV-I-positive plasmids were diluted 10 times to 10^{-1}, 10^{-2}, 10^{-3}, 10^{-4}, 10^{-5}, 10^{-6}, 10^{-7}, 10^{-8}, and 10^{-9}. Each dilution was used as a template, and dual Nano-PCR and ordinary PCR experiments were carried out at the same time. It can be seen from Figure 6 that the dual Nano-PCR still had bands at 1×10^{-8} ng/μL, which was two orders of magnitude higher than the sensitivity of ordinary PCR.

3.3. Clinical sample testing

Using the dual Nano-PCR method established in this study to detect viruses in a total of 52 cat eye, nose and faecal swabs obtained from different regions in Changchun City, three bands were detected at 242 bp, the positive rate of FCV was 5.8%, and there were no cases of FHV-I. This result was consistent with the ordinary PCR detection established in 2.6.

4. Discussion

FCV was first isolated from the gastrointestinal tract of cats in New Zealand in 1957 and FCV vaccines have been used for more than 40 years, but outbreaks still occur, which due to the strong mutation ability of FCV. Sometimes, feline calicivirus virulent systemic disease (FCV-VSD), with higher mobility was always record in many contries (Caringella et al., 2019), FHV-I is a double-stranded DNA virus with stable structure. FHV-I rarely mutates, and it can detoxify intermittently and easy to lose activity. Therefore, it is not easy to cause large-scale outbreaks and the detection rate is low, but 80% of cats will carry it for life after infection (Yuzhen et al., 2023). Therefore, in this study, only 3 FCV strains were detected in 52 clinical samples, and no FHV-I strains were detected.

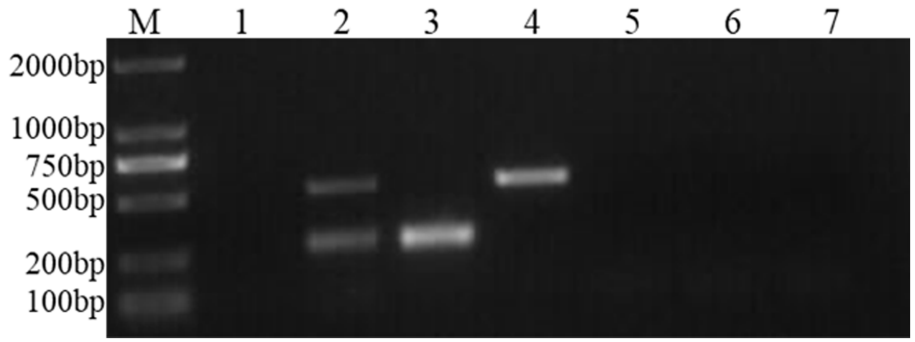

FIGURE 5
Specificity experiment of the dual Nano-PCR method. M: DNA molecular quality standard; 1: negative control; 2: FCV and FHV-I; 3: FCV; 4: FHV-I; 5: FPV; 6: FIPV; 7: RABV.

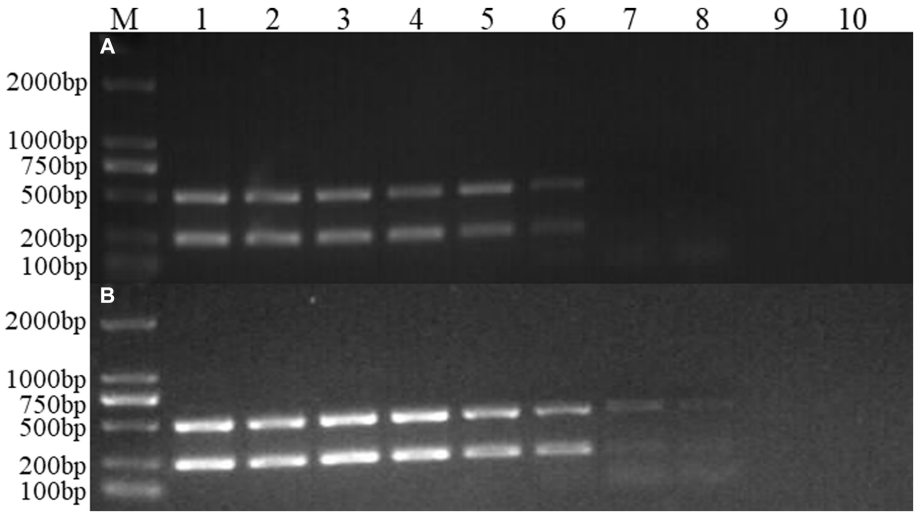

FIGURE 6
Sensitivity experiment of the dual Nano-PCR method. M: DNA molecular quality standard; 1–9: Plasmid dilutions are 10^{-1}, 10^{-2}, 10^{-3}, 10^{-4}, 10^{-5}, 10^{-6}, 10^{-7}, 10^{-8}, 10^{-9}; 10: negative control; **(A)**: double ordinary PCR; **(B)**: dual Nano-PCR.

Among various detection technologies for viral pathogens such as FCV and FHV-I, quantitative real-time PCR (qPCR) can achieve relative quantification, with high sensitivity. However, it takes longer, costs more, and experimental operation is strict. It can only detect one pathogen at a time. In recent years, FCV and FHV-I have shown a trend of clustering in domestic cats or Feline animals, which has seriously threatened to the health of felines and the prevalence of families with pets (Huahua, 2021; Kingyan et al., 2022). The dual Nano-PCR detection method of FCV and FHV-I established in this study is convenient and fast, and the optimized annealing temperature is approximately 4°C lower than that of common Nano-PCR (Jun and Chunhai, 2007). This method has the advantages of thermostabilising the surface of DNA polymerase, adjusting the stability of DNA polymerization and reaction, reducing the Tm value, improving the amplification efficiency and having higher sensitivity and specificity than traditional PCR methods. According to the brightness of the strips under different nanometre diameters, it can be inferred that the brightness and diameter have a normal distribution trend, the optimum size is reached at approximately 50 nm, and the amplification efficiency is the highest at this time. Nanocarriers have advantages for basic research in the field of traumatic brain injury. This is worthy of indepth research (Jain et al., 2021; Sajinia and Roger, 2021; Xingshuang et al., 2023).

In this study, the dual Nano-PCR established also has some limitations. Although this method can simultaneously detect two pathogens causing upper respiratory tract infections, its sensitivity may be lower than that of a single detection (Sailike et al., 2021). Although we have bound nanoparticles, there may still be efficiency issues in primer substrate binding under both single and simultaneous reaction conditions, making it difficult to achieve a lower detection limit. We hope to further enhance reaction sensitivity by combining other chemical or biological materials that can promote the reaction in the future.

In conclusion, the dual Nano-PCR method of FCV and FHV-I established in this study has good specificity, and high sensitivity, and the minimum detection amount can reach 10^{-8} ng/μL. Early diagnosis of FCV and FHV-I, which present similar clinical characteristics, high infection rates, and easy spread provides important diagnostic support. This method provides important testing methods for the prevention and treatment of upper respiratory tract diseases in cats, as well as early differential diagnosis and timely next step treatment in wild protected animals susceptible to infection with the virus. This study further applies the combination of chemical materials and animal disease detection reactions, and also confirms the widespread application value of nanotechnology.

Data availability statement

The original contributions presented in the study are included in the article/supplementary material, further inquiries can be directed to the corresponding authors.

Ethics statement

The animal study was approved by this study was approved by the Animal Ethics Committee of Institute of Special Animal and Plant Sciences, Chinese Academy of Agricultural Sciences. The study was conducted in accordance with the local legislation and institutional requirements.

Author contributions

MY: Data curation, Methodology, Writing – original draft, Writing – review & editing. JS: Software, Writing – review & editing. XZ: Formal analysis, Writing – review & editing. SW: Investigation, Writing – review & editing. CW: Supervision, Writing – review & editing. ZW: Formal analysis, Writing – review & editing. GL: Data curation, Writing – review & editing. LY: Project administration, Writing – review & editing. XS: Data curation, Project administration, Writing – review & editing. YC: Funding acquisition, Project administration, Writing – review & editing. EF: Data curation, Formal Analysis, Writing – review & editing.

Funding

The author(s) declare financial support was received for the research, authorship, and/or publication of this article. This work was supported by the Science and Technology Development Plan of Jilin Province (No. 20210202099NC), Innovation Project of the Chinese Academy of Agricultural Sciences (CAAS-ASTIP-2021-ISAPS) and Basic Construction Funds within the budget of Jilin Province (No. 2022C042-9).

Acknowledgments

The authors would like to thank the reviewers and editors for their detailed comments and feedback that assisted in the revising of our original manuscript. We also wish to acknowledge Zhijie Li for his guidance and assistance in the analysis of experimental data in this study.

Conflict of interest

The authors declare that the research was conducted in the absence of any commercial or financial relationships that could be construed as a potential conflict of interest.

The reviewer HW declared a shared parent affiliation with the author XZ to the handling editor at the time of review.

Publisher's note

References

Bo, C., Haoyang, Z., Hanhong, W., Shoujun, L., and Pei, Z. (2023). Development and application of a dual ERA method for the detection of feline Calicivirus and feline herpesvirus type I. *Virol. J.* 20:62. doi: 10.1186/S12985-023-02020-3

Caringella, F., Elia, G., Decaro, N., Martella, V., Lanave, G., Varello, K., et al. (2019). Feline calicivirus infection in cats with virulent systemic disease, Italy. *Res. Vet. Sci.* 124, 46–51. doi: 10.1016/j.rvsc.2019.02.008

Chengyun, L., Xuejiao, L., Ranran, S., Weijie, T., Yongle, Y., Haiyan, Y., et al. (2023). Genetic and pathogenicity analysis for the two FCV strains isolated from eastern China. *Vet. Res. Commun.* doi: 10.1007/S11259-023-10167-1 [Epub ahead of print].

Huahua, X. (2021) *Epidemiological investigation and therapeutic effect estimation odfeline herpesvirus and calicivirus infection cases in Shanghai*. [master's thesis] Ningxia: Ningxia university.

Jain, V., Khusnud, A., Tiwari, J., Mishra, M., and Mishra, P. K. (2021). Biogenic proceedings and characterization of copper-gold nanoalloy: evaluation of their innate antimicrobial and catalytic activities. *Inorg. Nano-Metal Chem.* 51, 230–238. doi: 10.1080/24701556.2020.1783313

Jianke, W., Yuening, C., Miao, Z., Hang, Z., Peng, L., Li, Y., et al. (2015). Development of a nanoparticle-assisted PCR (nanoPCR) assay for detection of mink enteritis virus (MEV) and genetic characterization of the NS1 gene in four Chinese MEV strains. *BMC Vet. Res.* 11:1. doi: 10.1186/s12917-014-0312-6

Jindong, G., Yan, L., Qiyun, X., Mayasar, I. A., Fatimah, A. A., Ali, A. S., et al. (2023). Epidemiological investigation of feline upper respiratory tract infection encourages a geographically specific FCV vaccine. *Vet. Sci.* 10:46. doi: 10.3390/VETSCI10010046

Jingfei, Y., Feiyan, S., Yu, W., Erkai, F., Zixian, W., Yuening, C., et al. (2022). Establishment and preliminary application of a Nano-PCR method for detection of feline panleukopenia virus. *Chin. Vet. Sci.* 50, 946–951. doi: 10.16656/j.issn.1673-4696.2022.0123

Jun, H., and Chunhai, F. (2007). Mechanism of the interaction between au nano-particles and polymerase in nanoparticle PCR. *Sci. Bullet.* 17, 43–47.

Kai, W., Zhihua, P., and Guixue, H. (2017). First report of feline Calicivirus (FCV) infection in stray cats in Northeast China. *Pol. J. Vet. Sci.* 20, 595–598. doi: 10.1515/pjvs-2017-0072

Kingyan, S., Shuping, H., Lin, G., Xiang, L., Xian, W., Yuxin, L., et al. (2022). Nested PCR detection and gD gene sequence analysis of FHV-I-1 from the captive panthera tigirs altaica in Harbin. *Chin. J. Wildlife.* 3, 810–815. doi: 10.12375/ysdwxb.20220328

Lin, L., Chunhua, P., Yakun, L., Ling, Z., Jing, W., Chang, L., et al. (2017). Establishment and rudimentary Application of the nano-dPCR for detection of PCV2 and PCV3. *China Animal Husbandry and Veterinary Medicine.* 12, 3440–3445. doi: 10.16431/j.cnki.1671-7236.2017.12.007

Meihui, L., Cuicui, J., Xianping, C., Mengtao, Y., Hailun, Z., Haili, Z., et al. (2023). Establishment and evaluation of visual nucleic acid detection method for deline herpesvirus type I. *Chin. J. Vet. Sci.* 5, 915–923. doi: 10.16303/j.cnki.1005-4545.2023.05.10

Sailike, B., Cun, L., Yanhan, L., Ruiying, L., Tong, Q., Lin, L., et al. (2021). Establishment of Nano-PCR assay for detection of feline calicivirus. *Chin. Vet. Sci.* 51, 684–688. doi: 10.16656/j.issn.1673-4696.2021.0117

Sajinia, H., and Roger, L. (2021). Dual targeting nano-approaches for Alzheimer's disease etiology. *Neural Regen. Res.* 16, 119–120. doi: 10.4103/1673-5374.286965

Tong, Q., Ling, Z., Xinyue, Y., Lin, L., Lijun, S., Jianwei, Z., et al. (2019). Establishment and application of Nano PCR assay for detection of the canine parvovirus. *Acta Veterinaria et Zootechnica Sinica.* 50, 1268–1274. doi: 10.11843/j.issn.0366-6964.2019.06.017

Weijie, T., Xuejiao, L., Xiaoli, S., Baoyun, C., Yongle, Y., Hu, S., et al. (2023). Isolation, identification and biological characteristics of feline herpesvirus I. *Chin. J. Virol.* 4, 1053–1061. doi: 10.13242/j.cnki.bingduxuebao.004347

Xingshuang, S., Yizhi, Z., Ziyan, T., and Lina, D. (2023). Advantages of nanocarriers for basic research in the field of traumatic brain injury. *Neural Regen. Res.* 19, 237–245. doi: 10.4103/1673-5374.379041

Xinyan, X., Yating, Z., Di, L., Bo, M., Jiasen, L., and Liandong, Q. (2023). Isolation and identification of feline herpesvirus-I strain. *Acta Veterinaria et Zootechnica Sinica.* 4, 1713–1720. doi: 10.11843/j.issn.0366-6964.20023.04.03

Ying, W., Ruibin, Q., Saisai, C., Yupeng, Y., Kexin, F., Jiasen, L., et al. (2023). Establishment and application of RAA detection method of feline herpesvirus-I. *Chin. Vet. Sci.* 1, 29–33. doi: 10.16656/j.issn.1673-4696.2023.0006

Yuzhen, T., Yanfei, L., and Jiande, Y. (2023). Epidemiological investigation of feline herpesvirus and calicivirus in a pet hospital of Zhengzhou. *J. Tianjin Agricul. Univ.* 30. doi: 10.19640/j.cnki.jtau.2023.03.011

Zhanding, C., Dengliang, L., Shushuai, Y., Yanbing, G., Guoying, D., Jiangting, N., et al. (2019). Equine immunoglobulin F (ab') 2 fragments protect cats against feline calicivirus infection. *Int. Immunopharmacol.* 75:105714. doi: 10.1016/j.intimp.2019.105714

frontiers | Frontiers in Microbiology

TYPE Original Research
PUBLISHED 21 November 2023
DOI 10.3389/fmicb.2023.1295678

OPEN ACCESS

EDITED BY
Rajesh Kumar Pathak,
Chung-Ang University, Republic of Korea

REVIEWED BY
Kalpana Singh,
Guru Angad Dev Veterinary and Animal Sciences University, India
Nadeem Shabir,
Sher-e-Kashmir University of Agricultural Sciences and Technology, India
Muguntan Susithra Priyadarshni,
Thiruvalluvar University, India

*CORRESPONDENCE
Haidong Wang
✉ wanghaidong@sxau.edu.cn

RECEIVED 18 September 2023
ACCEPTED 07 November 2023
PUBLISHED 21 November 2023

CITATION
Hou W, Wu H, Wang W, Wang R, Han W, Wang S, Wang B and Wang H (2023) Developing a multi-epitope vaccine candidate to combat porcine epidemic diarrhea virus and porcine deltacoronavirus co-infection by employing an immunoinformatics approach. *Front. Microbiol.* 14:1295678. doi: 10.3389/fmicb.2023.1295678

Developing a multi-epitope vaccine candidate to combat porcine epidemic diarrhea virus and porcine deltacoronavirus co-infection by employing an immunoinformatics approach

Wei Hou[1], Heqiong Wu[1], Wenting Wang[1], Ruolan Wang[1], Wang Han[1], Sibei Wang[1], Bin Wang[1,2] and Haidong Wang[1]*

[1]College of Veterinary Medicine, Shanxi Agricultural University, Jinzhong, China, [2]Single Molecule Nanometry Laboratory (Sinmolab), Nanjing Agricultural University, Nanjing, China

Coinfection of porcine epidemic diarrhea virus (PEDV) and porcine deltacoronavirus (PDCoV) is common in pig farms, but there is currently no effective vaccine to prevent this co-infection. In this study, we used immunoinformatics tools to design a multi-epitope vaccine against PEDV and PDCoV co-infection. The epitopes were screened through a filtering pipeline comprised of antigenic, immunogenic, toxic, and allergenic properties. A new multi-epitope vaccine named *rPPMEV*, comprising cytotoxic T lymphocyte-, helper T lymphocyte-, and B cell epitopes, was constructed. To enhance immunogenicity, the TLR2 agonist Pam2Cys and the TLR4 agonist RS09 were added to *rPPMEV*. Molecular docking and dynamics simulation were performed to reveal the stable interactions between *rPPMEV* and TLR2 as well as TLR4. Additionally, the immune stimulation prediction indicated that *rPPMEV* could stimulate T and B lymphocytes to induce a robust immune response. Finally, to ensure the expression of the vaccine protein, the sequence of *rPPMEV* was optimized and further performed *in silico* cloning. These studies suggest that *rPPMEV* has the potential to be a vaccine candidate against PEDV and PDCoV co-infection as well as a new strategy for interrupting the spread of both viruses.

KEYWORDS

PEDV, PDCoV, vaccine, multi-epitope, immunoinformatics

1 Introduction

Currently, the alphacoronavirus porcine epidemic diarrhea virus (PEDV) and deltacoronavirus porcine delta coronavirus (PDCoV) are two main swine enteric coronaviruses (Koonpaew et al., 2019; Hou et al., 2023): the former can infect swine of all ages and cause watery diarrhea, vomiting, and dehydration, and the latter causes acute diarrhea, vomiting, and dehydration in neonatal piglets (Tang et al., 2021; Hou et al., 2023). Especially, the co-infection of the two viruses, which both continue to emerge and reemerge worldwide, causing more severe mortality and economic losses.

To rapidly and efficiently prevent and control PEDV and PDCoV co-infection, the vaccine is a valuable means (Trovato et al., 2020). As a vaccine development route, the traditional methods are time-consuming and labor-intensive (Nabel, 2002), and such vaccines often contain large proteins or the entire organism, resulting in an unnecessary antigenic load and increasing the likelihood of eliciting an allergic reaction (Chauhan et al., 2019). These problems can be solved by using peptide-based vaccines, which are made up of brief immunogenic peptide fragments that can elicit highly targeted immune responses, thereby reducing the likelihood of an allergic reaction. In peptide-based vaccine development, effective screening and immunogen design are major challenges since short peptides typically have weak immunogenic effects due to their small molecular weights (Sun et al., 2022). According to reported works, the coronavirus S protein plays an important role in viral entry and virus-host interaction, and it is the primary target for stimulating the host cell immune response and inducing neutralizing antibodies (Sun et al., 2008; Li et al., 2021). Furthermore, it was also reported that the S proteins of PEDV and PDCoV have good immunity and the potential for vaccine development (Wang et al., 2016; Zhai et al., 2023). Therefore, the S protein is the preferred region for immunogen screening and the design of the PEDV and PDCoV vaccine. For immunogen screening, the typical epitope screening is to insert a peptide with the target epitope into the plasmid and verify the immune effect of the epitope through large experiments (De Groot et al., 2001). Immunoinformatics approaches, which can eliminate the need for time-consuming and expensive manipulation as well as complex procedures, have emerged as a crucial tool for epitope localization and are playing an increasingly important role in epitope discovery as well as in successful vaccine design (Khan et al., 2018; Dong et al., 2020). Khan et al. (2021) used immunoinformatics methods to design a universal multi-epitope vaccine against SARS-CoV-2. Rowaiye et al. (2023) developed a multiepitope vaccine candidate to curb the outbreaks of African swine fever virus using the immunoinformatics. Therefore, these immunoinformatics approaches can be employed for vaccine design for the PEDV and PDCoV co-infection.

In this study, we employed immunoinformatic approaches to predict and design a safe and effective multi-epitope candidate vaccine derived from the S protein for prevalent PEDV and PDCoV variants. The designed vaccine named *rPPMEV* comprises a range of predicted epitopes, can interact with TLRs, and has the potential to stimulate T and B lymphocytes to induce a strong immunological response. The findings of this study provide a new vaccine candidate for the prevention of PEDV and PDCoV co-infection.

2 Materials and methods

To predict and design a safe and effective multi-epitope candidate vaccine for PEDV and PDCoV co-infection, procedures listed in Figure 1 were implemented. In this section, these procedures are briefly mentioned below.

2.1 Identification of target antigens

PEDV strains CH/HLJJS/2022, CH/HBXT/2018, and SXSL were selected since they have been highly pathogenic in recent years (Zhang et al., 2019; Liu et al., 2022; Yao et al., 2023). The spike (S) glycoproteins UUT43943.1, AZL49329.1, and UWU45211.1 of these three PEDV strains were selected as candidate antigens for epitope prediction due to their significant usefulness in PEDV vaccines (Zhang et al., 2019, Liu et al., 2022, Yao et al., 2023). In addition, PDCoV strains CH-HLJ-20, HNZK-02, Swine/CHN/SC/2018/1, CHN/Sichuan/2019-MK993519.1, and CHN-TS1-2019-MT663769.1 were selected for vaccine development as these have been prevalent in recent years (Kong et al., 2022). The S glycoproteins QZA57171.1, AXP32216.1, QCO76963.1, QGZ00525.1, and QZX45753.1 of these five PDCoV strains were selected as preparatory antigens because the S protein has good immunity for PDCoV vaccine design (Zhai et al., 2023). The sequences of all S proteins were obtained from the National Center for Biotechnology Information (NCBI) database.[1]

2.2 Prediction of signal peptide

To determine whether the signal peptide is present in the candidate antigen proteins, the signal peptide of the S protein was predicted using SignalP-5.0 server[2] (Almagro Armenteros et al., 2019). The following T and B cell epitope predictions all need to remove the signal peptides.

2.3 Prediction of cytotoxic T lymphocyte epitopes

The Immune Epitope Database (IEDB) server[3] was used to predict cytotoxic T lymphocyte epitopes (CTLs) (Fleri et al., 2017). The epitope length of 9 residues was used to predict the epitope through 45 common swine leukocyte antigen (SLA) class I molecules by running the "IEDB-recommended" method. Then, the epitopes were screened using a TAP score >1.0, an IC50 <500 nM, and a proteasome score >1.0. The dominant epitopes, which simultaneously appeared in at least three SLA-I alleles in each viral strain and had high antigenicity (> 0.9 for PEDV, > 0.8 for PDCoV), were further predicted by using VaxiJen v2.0.[4] Finally, the common dominant epitopes of the PEDV and PDCoV strains were used to construct the final vaccine.

2.4 Prediction of helper T lymphocyte epitopes

The online server NetMHCIIpan 4.0[5] was used to predict helper T lymphocyte epitopes (HTLs). A length of 15 amino acid residues was used for epitope prediction through 27 high-frequency human MHC II (HLA-II) alleles (Ros-Lucas et al., 2020). The threshold for strongly binding peptides was set to its default value. The dominant epitopes, which simultaneously appeared in at least three HLA-II alleles in each viral strain and had high antigenicity (> 0.9 for PEDV, > 0.5 for PDCoV), were further predicted by using VaxiJen v2.0.

1 https://www.ncbi.nlm.nih.gov/gene/
2 http://www.cbs.dtu.dk/services/SignalP/
3 https://www.iedb.org
4 http://www.ddg-pharmfac.net/vaxijen/VaxiJen/VaxiJen.html
5 https://services.healthtech.dtu.dk/service.php?NetMHCIIpan-4.0

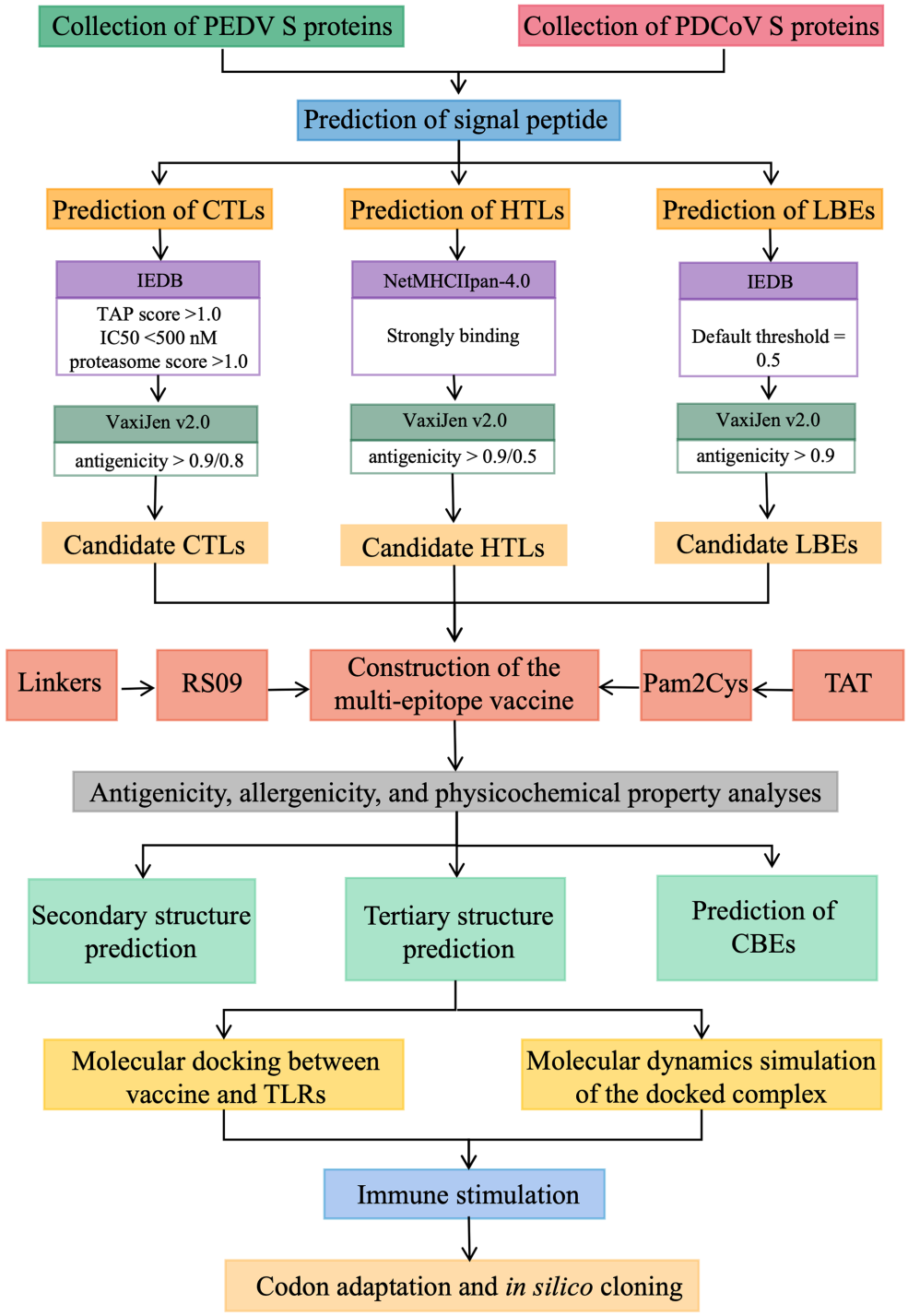

FIGURE 1
The prediction procedures of the multi-epitope candidate vaccine for PEDV and PDCoV co-infection.

Finally, the common dominant epitopes of the PEDV and PDCoV strains were used to construct the final vaccine.

2.5 Prediction of linear B cell epitopes

For the prediction of linear B cell epitopes (LBEs), the IEDB server with the method of Bepipred Linear Epitope Prediction 2.0 at the default threshold of 0.5 was used. Then, the predicted epitopes were screened using VaxiJen v2.0. Finally, the common epitopes with high antigenicity (>0.9) of the PEDV or PDCoV strains were used for vaccine construction.

2.6 Construction of the multi-epitope vaccine

The final subunit vaccine was constructed by sequentially combining the generated peptide sequences with appropriate linkers.

To improve the antigenicity and immunogenicity of the vaccine, the toll-like receptor 4 (TLR4) agonist RS09 and the TLR2 agonist dipalmitoyl-S-*glycero*-cysteine (Pam2Cys) were added to the N-terminal and C-terminal via the EAAAK linker, respectively (Jackson et al., 2004; Meza et al., 2017; Albutti, 2021). The CTLs, HTLs, and B cell epitopes were joined by AAY, GPGPG, and KK, respectively. In addition, the TAT sequence (11 aa) was added to its carboxyl terminus to enhance the intracellular delivery of the vaccine (Frankel and Pabo, 1988).

2.7 Antigenicity, allergenicity, and physicochemical property analyses of the multi-epitope vaccine

The antigenicity and allergenicity of the multi-epitope vaccine were analyzed using the online software VaxiJen v2.0 and AllerTop v. 2.0,[6] respectively. The physicochemical characteristics of the multi-epitope vaccine, such as its molecular weight, atomic composition, theoretical isoelectric point (PI), half-life, stability, hydropathicity, and other properties, were predicted using the online program Protparam.[7]

2.8 Prediction of the secondary and tertiary structures of the multi-epitope vaccine

The secondary structure of the multi-epitope vaccine was predicted using SOPMA online analysis software[8] (Deléage, 2017). The initial tertiary structure was predicted by Robetta server[9] (Baek et al., 2021). After primary 3D modeling, the initial tertiary structure was further optimized by GalaxyRefine server[10] (Yu et al., 2022). Later, the refined structure was validated using two online tools: SWISS-MODEL workspace[11] and ProSA-web.[12] The SWISS-MODEL workspace was used to evaluate the quality of protein by analyzing the Ramachandran plot (Waterhouse et al., 2018). The ProSA-web was used for protein validation by generating a *z*-score (Wiederstein and Sippl, 2007).

2.9 Prediction of conformational B cell epitopes

The conformational B cell epitopes (CBEs) of the multi-epitope vaccine were predicted using the online software IEDB ElliPro tool[13] with the default parameters of a minimum score of 0.5 and a maximum distance of 6 angstrom (Ponomarenko et al., 2008), and visualized with PyMol.

2.10 Molecular docking between the multi-epitope vaccine and TLRs

The molecular docking between the vaccine construct and the TLRs was performed using ClusPro server[14] (Kozakov et al., 2017). The receptors were TLR2 (PDB ID: 6NIG) and TLR4 (PDB ID: 4G8A), and the ligand was the multi-epitope vaccine. The PDB file of the docking results was loaded into Ligplot and PyMol to analyze the interaction interface residues.

2.11 Molecular dynamics simulation of the docked complex

To understand any state changes in a given biological environment, the molecular dynamics (MD) simulation was applied to the TLR2-Vaccine and TLR4-Vaccine complexes using GROMACS (GROningen MAchine for Chemical Simulations) (He et al., 2021). First, in all MD simulations, the protein-ligand complex architecture was generated using the AMBER99 force field. The protein was then solvated in a cubic box of TIP3P waters (Grifoni et al., 2020), with a minimum distance of 1.0 nm (TLR2-Vaccine, TLR4-Vaccine) between the protein and box edge (Ismail et al., 2020). The charged protein complex was neutralized by the addition of ions using a genion tool (Shukla et al., 2018). Additionally, the solvated electroneutral system was relaxed through energy minimization in order to avoid steric conflicts and inappropriate geometry. Then, 100 ps of NVT [substance (N), volume (V), and temperature (T)] equilibration and 100 ps of NPT [substance (N), pressure (P), and temperature (T)] equilibration were used to acclimate the system without restrictions. After proper minimizations and equilibrations, a productive MD run of 20 ns was performed for all the complex systems, and the parameters, root mean square deviation (RMSD) and root mean square fluctuation (RMSF), which define the stability of the docked complex on simulation, were computed.

2.12 Immune stimulation

To detect the immune response of the multi-epitope vaccine to the host, the C-ImmSim server[15] was used for the immune simulation (Rapin et al., 2010). The time steps were set at 1, 84, and 168 (one time step corresponds to 8 h). The number of simulation steps was set at 1,050 (Bhatnager et al., 2021). The other parameters were used as the default simulation parameters.

2.13 Codon adaptation and *in silico* cloning

To achieve superior expression of recombinant protein, the codon adaptation of the multi-epitope vaccine was performed by the online tool Java Codon Adaptation Tool (JCat)[16] (Grote et al., 2005). *Escherichia coli* (Strain K12) was chosen to express the vaccine protein.

6 http://www.ddg-pharmfac.net/AllerTOP
7 https://web.expasy.org/protparam/
8 https://npsa-prabi.ibcp.fr/cgi-bin/npsa_automat.pl?page=npsa_sopma.html
9 https://robetta.bakerlab.org
10 http://galaxy.seoklab.org/
11 http://swissmodel/expasy.org/assess
12 https://prosa.services.came.sbg.ac.at/prosa.php
13 http://tools.iedb.org/ellipro/
14 https://cluspro.bu.edu/login.php?redir/queue.php
15 http://kraken.iac.rm.cnr.it/C-IMMSIM/
16 https://www.jcat.de/

The indicators, codon adaptation index (CAI) the ideal value is (1) and percentage GC content (the ideal range is 30%–70%), were analyzed (Puigbo et al., 2007). For *in silico* cloning of the vaccine construct, pET28a (+) was selected as the vector. The codon-optimized sequence of the vaccine was cloned into the vector through the *XhoI* and *BamHI* restriction sites by SnapGene tool.[17]

3 Results and discussion

3.1 The acquisition of vaccine-candidate antigens

Nowadays, the co-infection of PEDV and PDCoV, which both continue to emerge and reemerge worldwide, causes massive economic losses to the swine industry globally (Jiao et al., 2021). To rapidly and efficiently prevent and control virus infection, the development of vaccines has become imperative. In this study, we used immunoinformatics to discover and design a multivalent epitope vaccine to combat PEDV and PDCoV. The schematic procedure of the multi-epitope selection and the final vaccine construction is shown in Figure 2. The development of a new vaccine derived from a highly virulent virus provides cross-protection against low-virulence virus infection (Yao et al., 2023), and a vaccine developed from the strains responsible for the current outbreak will be successful in preventing viral infection (Rock, 2017; Borca et al., 2020; Moise et al., 2020). Thus, the three highly pathogenic PEDV strains and five prevalent PDCoV strains were selected for vaccine development. Furthermore, because the S proteins of PEDV and PDCoV strains have strong immunogenicity and the potential to generate vaccines (Wang et al., 2016; Zhai et al., 2023), the S proteins were selected as the preparatory antigens for immunogen screening and the design of a new PEDV and PDCoV vaccine. The GeneBank accession numbers of the three PEDV strains and five PDCoV strains, as well as the antigenicity of all S proteins, are shown in Supplementary Table S1, and the amino acid sequence of all S proteins is shown in Supplementary Data.

To prepare an epitope vaccine, obtaining the epitopes of the relative antigen is the key point (Li et al., 2013). Firstly, to determine whether these S proteins contain signal peptide regions, the signal peptide was examined before the epitope prediction. The findings reveal that the signal peptide sequence of PEDV is 1–18 (MKSLTYFWLLLPVLSTLS), while the signal peptide region of PDCoV is 1–19 (MQRALLIMTLLCLVRAKFA) (Supplementary Table S1). Then, to avoid specifying or inhibiting protein localization, the signal peptide sequences were removed from the epitope prediction of all S proteins (Mahmud et al., 2021). Secondly, it was reported that cytotoxic T cells are important for specific antigen recognition and the helper T cells are an essential component of adaptive immunity, which function in activating B cells, macrophages, and even cytotoxic T cells (Dimitrov et al., 2013; Gupta et al., 2013), the two types of epitopes, CTLs and HTLs, of T cell epitopes were predicted in this study. Furthermore, the B cell epitope was also screened for the vaccine construct since it could trigger the production of antigen-specific immunoglobulins, which are crucial components of adaptive immunity (Sarkar et al., 2022). After epitope prediction, the inclusion criteria for immunodominant epitopes are as follows: (1) the common dominant CTLs simultaneous appearance in at least three SLA-I alleles of each PEDV strain or PDCoV strain and with a high antigenicity score; (2) the common dominant HTLs simultaneous appearance in at least three HLA-II alleles in each PEDV strain or PDCoV strain and with a high antigenicity score; (3) the common dominant LBEs simultaneous appearance in each PEDV or PDCoV strain and with high antigenicity. Finally, 10 CTLs, 8 HTLs, and 9 LBEs were chosen for constructing the new multi-epitope vaccine *rPPMEV* (Supplementary Table S2). Then, according to the reports, TLRs are constitutively expressed in innate immune cells and play a vital role in viral recognition, leading to antiviral signaling cascades. Specifically, cell membrane receptors TLR2 and TLR4 play an important role in recognizing envelope glycoproteins (Kurt-Jones et al., 2000; Boehme and Compton, 2004; Takeda and Akira, 2004; Barton, 2007; Temeeyasen et al., 2018). To significantly improve the immunogenicity and antigenicity of *rPPMEV*, the TLR2 agonist Pam2Cys (FNNFTVSFWLRVPKVSASHLE) and TLR4 agonist RS-09 (APPHALS), which can trigger activation of TLR2 and TLR4 signaling, respectively (Jiang et al., 2023), were incorporated into the vaccine design. Additionally, to conjugate and enhance expression function and prevent the production of neo-epitopes, linker selection is a significant concern in the development of multi-epitope vaccines (Chen et al., 2013). The EAAAK linker, which can effectively separate and decrease interaction between vaccines as well as increase the thermal stability of the chimeric protein (Saadi et al., 2017), was used to join the adjuvants RS-09 and Pam2Cys. The AAY, GPGPG, and KK linkers were utilized to join the CTLs, HTLs, and B cell epitopes, respectively. The TAT sequence was attached to the C-terminal of the vaccine construct to enhance vaccine intercellular delivery. Finally, the new multivalent vaccine, *rPPMEV*, which was designed using immunoinformatics techniques, has a length of 439 amino acids, as illustrated in Figure 3.

3.2 Allergenicity, antigenicity, and physicochemical property analyses of *rPPMEV*

To evaluate the safety of *rPPMEV*, an allergenicity analysis was carried out using the AllerTop v. 2.0 server. The results show that *rPPMEV* and its closest protein (UniProtKB accession number O14514) are non-allergic. Moreover, the antigenicity analysis of VaxiJen v2.0 reveals that *rPPMEV* exhibits strong antigenicity with a score of 0.7241, which is above the threshold of 0.4. These results demonstrate that *rPPMEV* is safe for administration to swine. Additionally, the physicochemical properties of *rPPMEV* were also analyzed, as the physical properties of proteins significantly affect their immune function (Ikai, 1980). The finding shows that *rPPMEV* has 439 amino acids, 6,617 total atoms, the formula $C_{2154}H_{3274}N_{554}O_{627}S_8$, and a molecular weight of 47 KD, which can be easily purified since the molecular weight of the protein is less than 110 KD (Barh et al., 2013). The theoretical pI of *rPPMEV* is 9.39, and it includes 28 negatively charged residues and 46 positively charged residues. The instability index of *rPPMEV* was calculated to be 33.81 (a value below the threshold value of 40 means that the protein is stable), indicating that *rPPMEV* should be stable upon

17 http://www.snapgene.com/

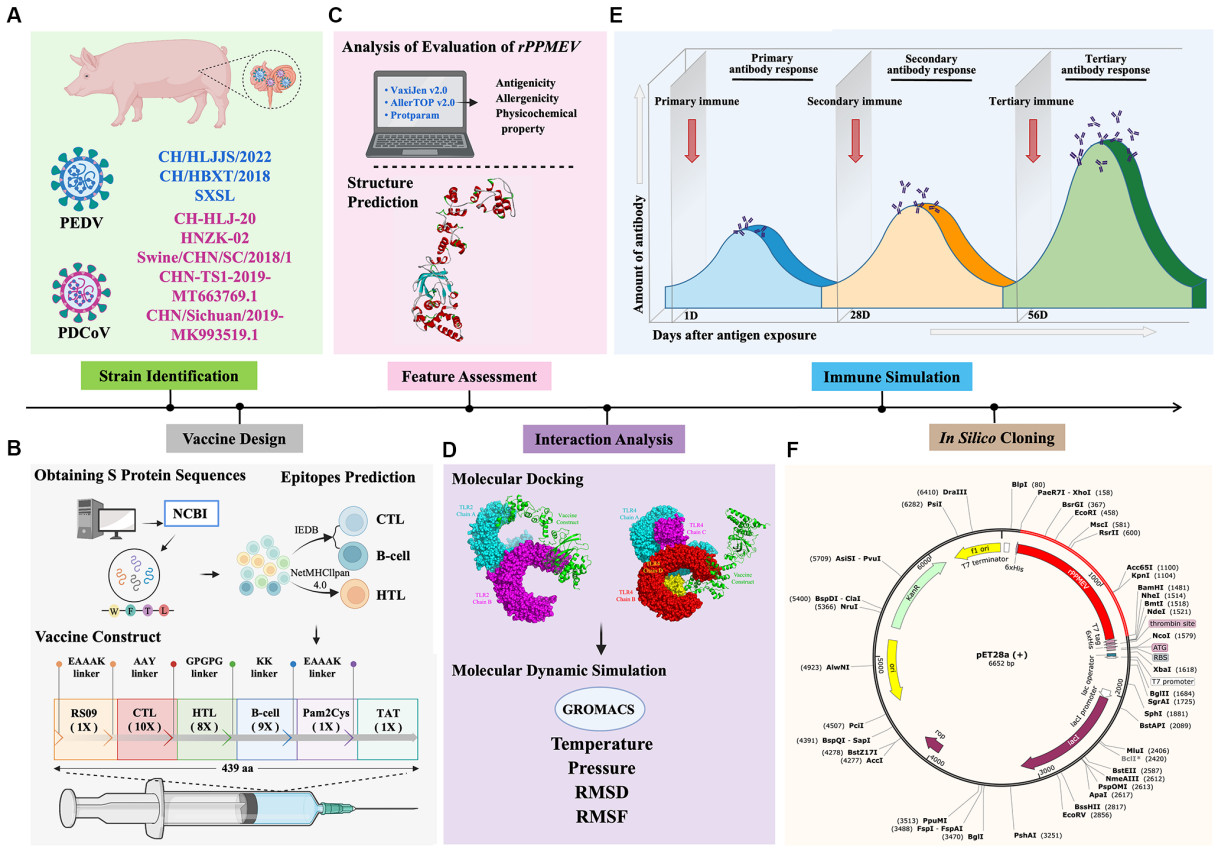

FIGURE 2
Flow chart of the multi-epitope selection and the final rPPMEV construction. The rPPMEV was designed in six steps with different colors, including PEDV and PDCoV strain identification **(A)**, vaccine design **(B)**, *rPPMEV* feature assessment **(C)**, the interaction analysis of *rPPMEV* with TLR2 and TLR4 immune receptors **(D)**, *rPPMEV* immunological characteristics analysis **(E)**, and *in silico* cloning **(F)**.

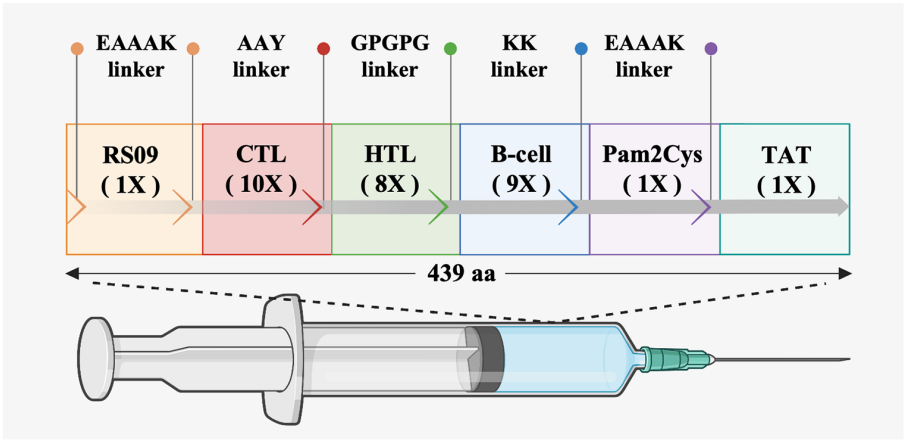

FIGURE 3
The design and construction of *rPPMEV*. The *rPPMEV* contains 439 amino acids, and the components needed in *rPPMEV* construction are represented in different colors.

expression in host systems. Furthermore, the aliphatic index of *rPPMEV* is 68.54, and the Grand average of hydropathicity (GRAVY) of *rPPMEV* is-0.249 (the range of GRAVY is −2 to 2, a negative value means that protein is hydrophilic) (Sha et al., 2020), showing that *rPPMEV* is hydrophilic.

3.3 The prediction of *rPPMEV* secondary and tertiary structure

An ideal peptide-based vaccination designed using immunoinformatics techniques should trigger a strong immunological

response without having any negative side effects (Tahir ul Qamar et al., 2020; Shantier et al., 2022). The secondary structure determines the stability of protein structure, which is essential for antigen proteolysis, presentation, and activation of T and B cells (Scheiblhofer et al., 2017), and the tertiary structure determines the molecular recognition by the TCR (Greenbaum et al., 2007). As a result of secondary prediction, there is 31.89% alpha helix, 25.06% extended strand, 7.52% beta turn, and 35.54% random coil in *rPPMEV*, as shown in Figure 4A. Among these regions, the naturally unfolding protein regions and alpha-helical coiled coils, as basic types of "structural antigens," can induce antibody recognition after infection (Corradin et al., 2007). Subsequently, the tertiary structure of the vaccine was predicted using the Robetta server. There are five models outputted in the result. The *z*-score was calculated on all models through ProSA-web. The *z*-scores of models 1–5 are −7.43, −7.64, −6.92, −6.19, and −6.59, respectively, as shown in Supplementary Figure S1. Model 2 was selected as the initial model of *rPPMEV* (Figure 4B) since it has the highest quality with the lowest *z*-score (Figure 4C). The Ramachandran plot shows that Model 2 has 91.53% favored region, 1.60% outlier region, and 0.00% rotamer region (Figure 4D). To improve the structure quality and protein stability, the initial model was refined by the GalaxyRefine server. As a result, five optimized 3D models are presented. The *z*-scores of these optimized models 1–5 are −7.84, −7.69, −7.62, −7.93, and −7.66, respectively (Supplementary Figure S2). Similar to the initial model selection, the optimized Model 4 was adopted as the final tertiary structure of *rPPMEV* (Figure 4E), which has the lowest *z*-score (Figure 4F) and performs at 93.59%, 1.14%, and 1.16% in the favored, outlier, and rotamer regions, respectively (Figure 4G).

3.4 Prediction of conformational B cell epitopes

To predict CBEs, the *rPPMEV* was analyzed through the ElliPro server. The results show that there are 238 residues, with values ranging from 0.676 to 0.842, distributed across the eight B cell epitopes in *rPPMEV*. The epitopes range from 11 to 77 amino acid residues, as shown in Figure 5 and Supplementary Table S3.

3.5 Molecular docking between *rPPMEV* and TLRs

To prevent and control viruses, the ability of vaccines to induce a brisk and consistent immune response is critical. To achieve the objective of the proposed work, it is necessary to design a vaccine that can interact with the target immune cell receptors (Choudhury et al., 2022). The TLRs are a class of essential protein molecules involved in innate immunity as well as a link between nonspecific and specific immunity (Takeda and Akira, 2004). TLR2 and TLR4 can recognize viral structural glycoproteins, resulting in the production of inflammatory cytokines (Choudhury et al., 2022). To evaluate the interaction and binding consistency between *rPPMEV* and TLRs, molecular docking was performed with the *rPPMEV* ligand and TLR2 as well as TLR4 receptors, respectively. The results show that there are 30 docking results of *rPPMEV*-TLR2 (Supplementary Table S4) and *rPPMEV*-TLR4 (Supplementary Table S5), respectively. The conformation of the docked *rPPMEV*-TLR2 with the lowest interaction energy (−1119.4 kcal/mol) is shown in Figure 6A. The interaction interface residues of this *rPPMEV*-TLR2 complex were analyzed by PyMol in 3D and Ligplot in 2D, respectively. The findings reveal that the complex subunits interact through one ionic bond and 11 hydrogen bonds, as illustrated in Figures 6B,C. Similar to the *rPPMEV*-TLR2, the *rPPMEV*-TLR4 model was selected according to its lowest energy weighted score (−1032.7 kcal/mol), as shown in Figures 7A,D. The interaction interface residue analysis in 3D and 2D formats reveal that there are 2 ionic bonds and 25 hydrogen bonds at the docking interface of *rPPMEV* and the TLR4 Chain B, as shown in Figures 7B,C, one hydrogen bond at the docking interface of *rPPMEV* and the TLR4 Chain C, as shown in Figures 7E,F, and 4 hydrogen bonds at the docking interface of *rPPMEV* and the TLR4 Chain D, as shown in Figures 7G,H. These results indicate that *rPPMEV* has excellent performance in tightly binding to TLR2 and TLR4 to trigger a strong immune response.

3.6 Molecular dynamics simulations between *rPPMEV* and TLRs

To evaluate the structural stability of the *rPPMEV*-TLR2 and *rPPMEV*-TLR4 complexes, the MD simulation was conducted using GROMACS. The results of MD simulations of the *rPPMEV*-TLR2 and *rPPMEV*-TLR4 complexes are presented in Figure 8. With 100 ps of the time interval, the temperatures of the two simulation systems (*rPPMEV*-TLR2, *rPPMEV*-TLR4) are both around 300 K (Figures 8A,B), and the pressure of the two systems is around 1.4 atmosphere (Figure 8C) and 0.75 atmospheres (Figure 8D), respectively. These results indicate that the system is stable, and the MD operation is successful. In addition, during a 20 ns MD simulation, the RMSD value of the *rPPMEV*-TLR2 complex rises sharply to 0.4 nm in 2 ns and then remains at 0.43 nm (Figure 8E), while the RMSD value of the *rPPMEV*-TLR4 complex reveals a large fluctuation between 0 and 2 ns before being constant around 0.5 nm (Figure 8F). It was reported that the RMSD of the ligand is considered to be fixed within 1 nm, stable below 2 nm, and unstable above 2 nm during molecular docking (Eweas et al., 2021). The RMSD results of *rPPMEV*-TLR2 and *rPPMEV*-TLR4 are both less than 1 nm within 20 ns, indicating that the interaction of the two complexes at the docking interface is fixed. Furthermore, RMSF values demonstrate that the RMSF profiles of most amino acid residues of the *rPPMEV*-TLR2 complex (Figure 8G) and the *rPPMEV*-TLR4 complex (Figure 8H) are below 0.45 nm, and only a few residues have significant changes. These results prove that the two complexes have stability and stiffness.

3.7 Immune simulation

As an intracellular pathogen, cellular and humoral immunity induced by vaccines is essential for killing and eliminating viruses. To evaluate the immunological efficacy of *rPPMEV*, the immune stimulation of *rPPMEV* was performed by the C-ImmSim Server. The results show that the *rPPMEV* can induce three peaks in antibody levels after three vaccine doses, as shown in Figure 9A. The antibodies IgM + IgG, IgM, and IgG2

10.3389/fmicb.2023.1295678

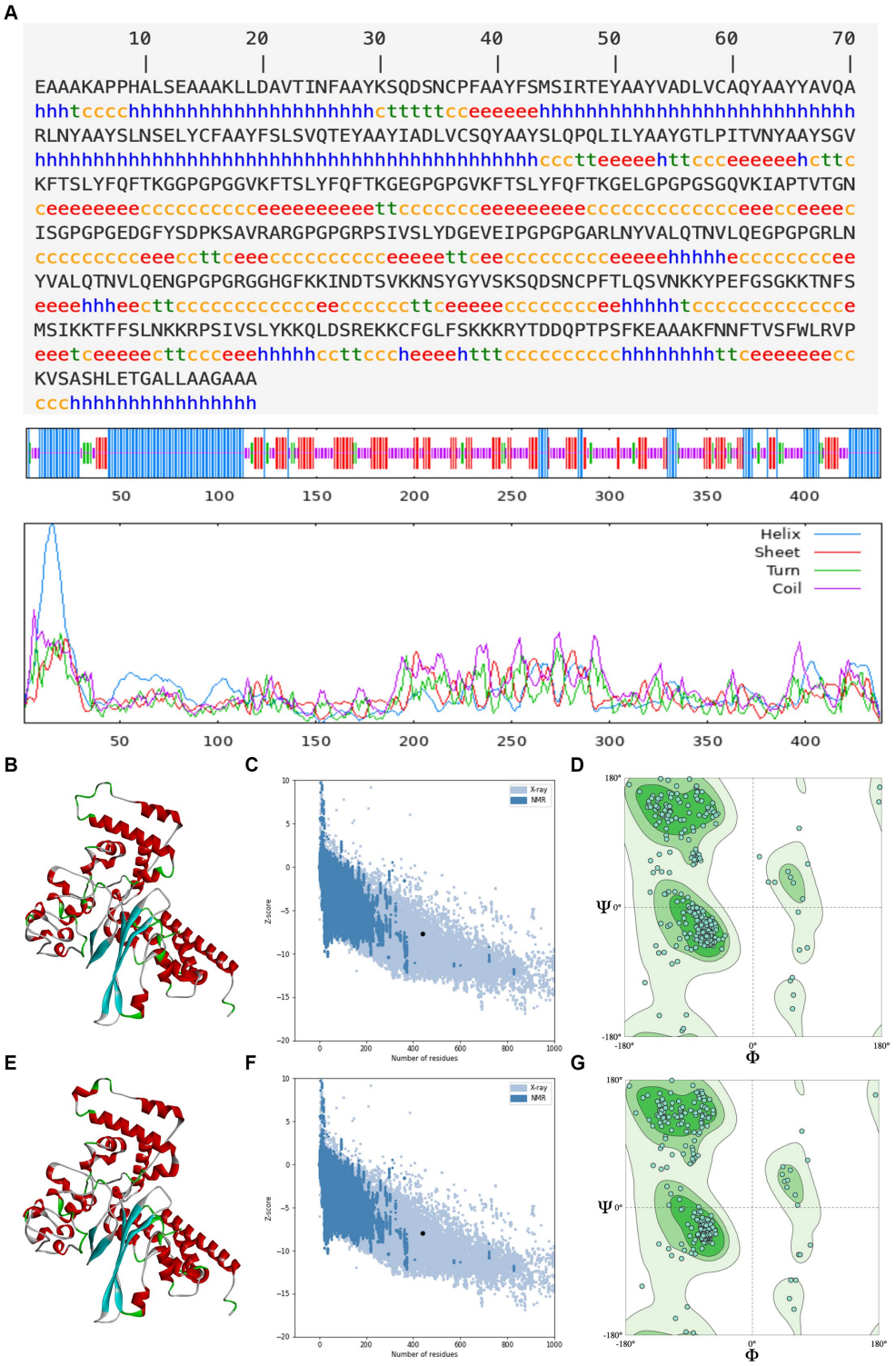

FIGURE 4
The prediction of *rPPMEV* secondary and tertiary structure. **(A)** The prediction of *rPPMEV* secondary structure. The blue "h" represents the alpha helix, the red "e" represents the extended strand, the green "t" represents the beta turn, and the yellow "c" represents the random coil. **(B)** The prediction of *rPPMEV* initial tertiary structure. The alpha helix, extended strand, beta turn, and random coil are marked in the 3D model with the colors of red, cyan, green, and gray, respectively. **(C)** The *z*-score of the *rPPMEV* initial tertiary structure. **(D)** The Ramachandran plots of the *rPPMEV* initial tertiary structure. **(E)** The prediction of the *rPPMEV* final tertiary structure. In the 3D model, the "red," "cyan," "green," and "gray" parts represent alpha helix, extended strand, beta turn, and random coil, respectively. **(F)** The *z*-score of the *rPPMEV* final tertiary structure. **(G)** The Ramachandran plots of the *rPPMEV* final tertiary structure.

are found in the primary immunization. Further, as immune responses enhance, the levels of total IgM + IgG, IgM, and IgG1 + IgG2 antibodies elevate, indicating that antibody titers increase after the second and third injections. These increasing levels of antibodies in the immune response are mainly attributed to the increase in the total count of B-lymphocytes and T-lymphocytes. As shown in Figure 9B, the B cell population is highly

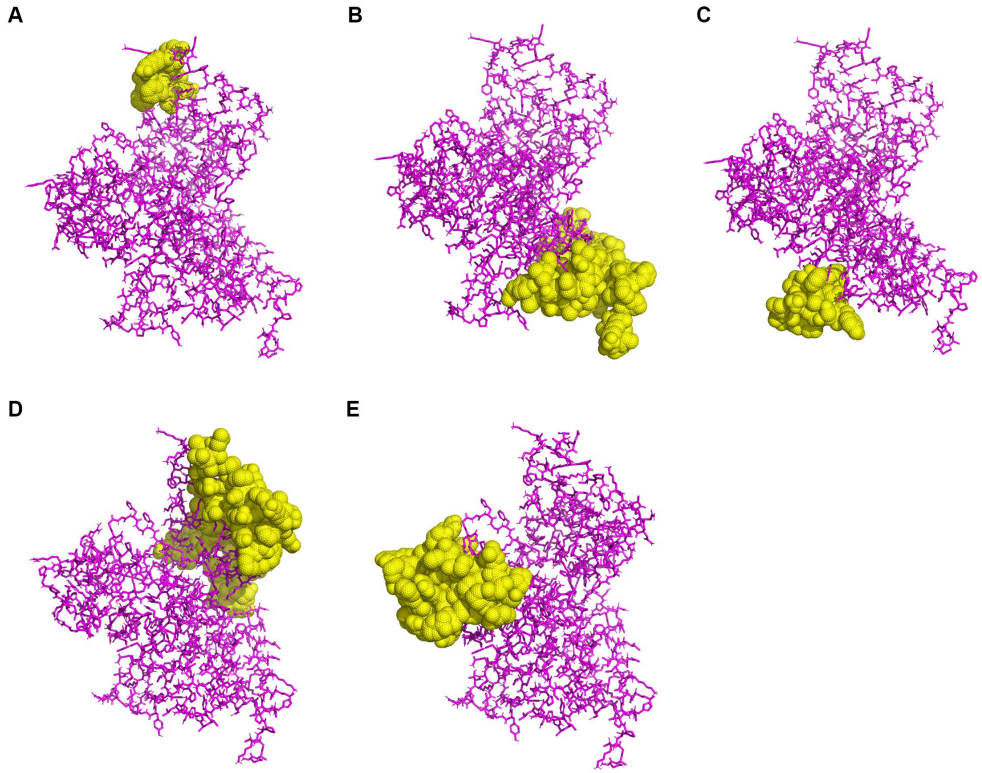

FIGURE 5
The prediction of conformational B cell epitopes. **(A)** to **(E)** display the five CBEs of *rPPMEV*. The "yellow" regions are the predicted conformational B cell epitopes of *rPPMEV*.

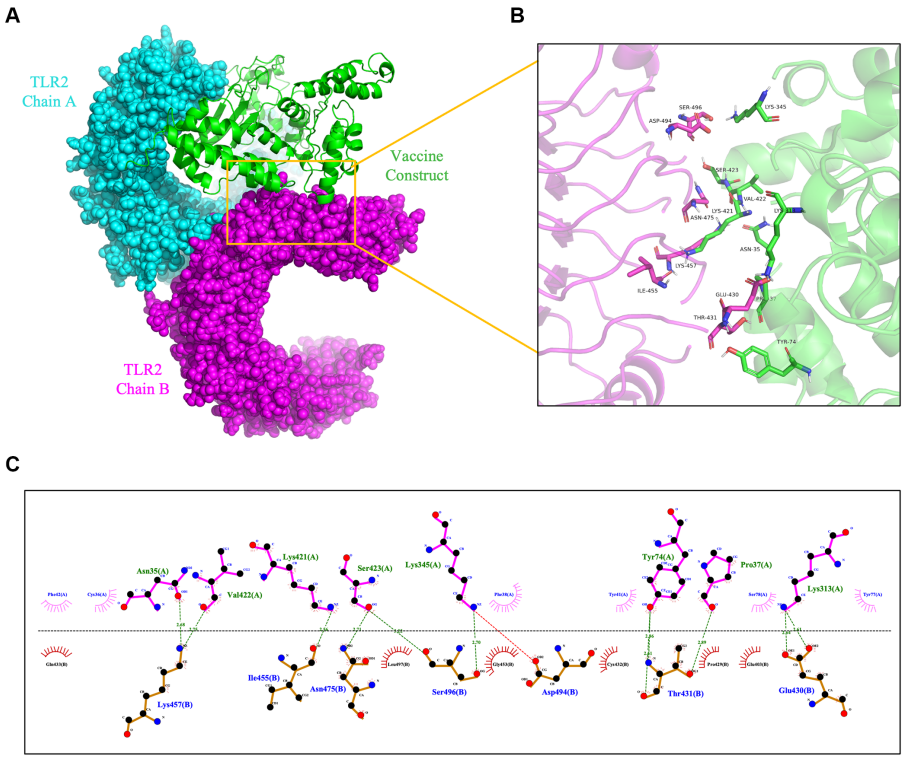

FIGURE 6
The molecular docking of *rPPMEV* and TLR2. **(A)** The docked complexes of *rPPMEV* and TLR2 with the lowest interaction energy. **(B)** The interaction interface residues of *rPPMEV* and TLR2 predicted by PyMol in 3D. **(C)** The interaction interface residues of *rPPMEV* and TLR2 predicted by Ligplot in 2D. The green dotted line represents the hydrogen bond, and the red dotted line represents the ionic bond.

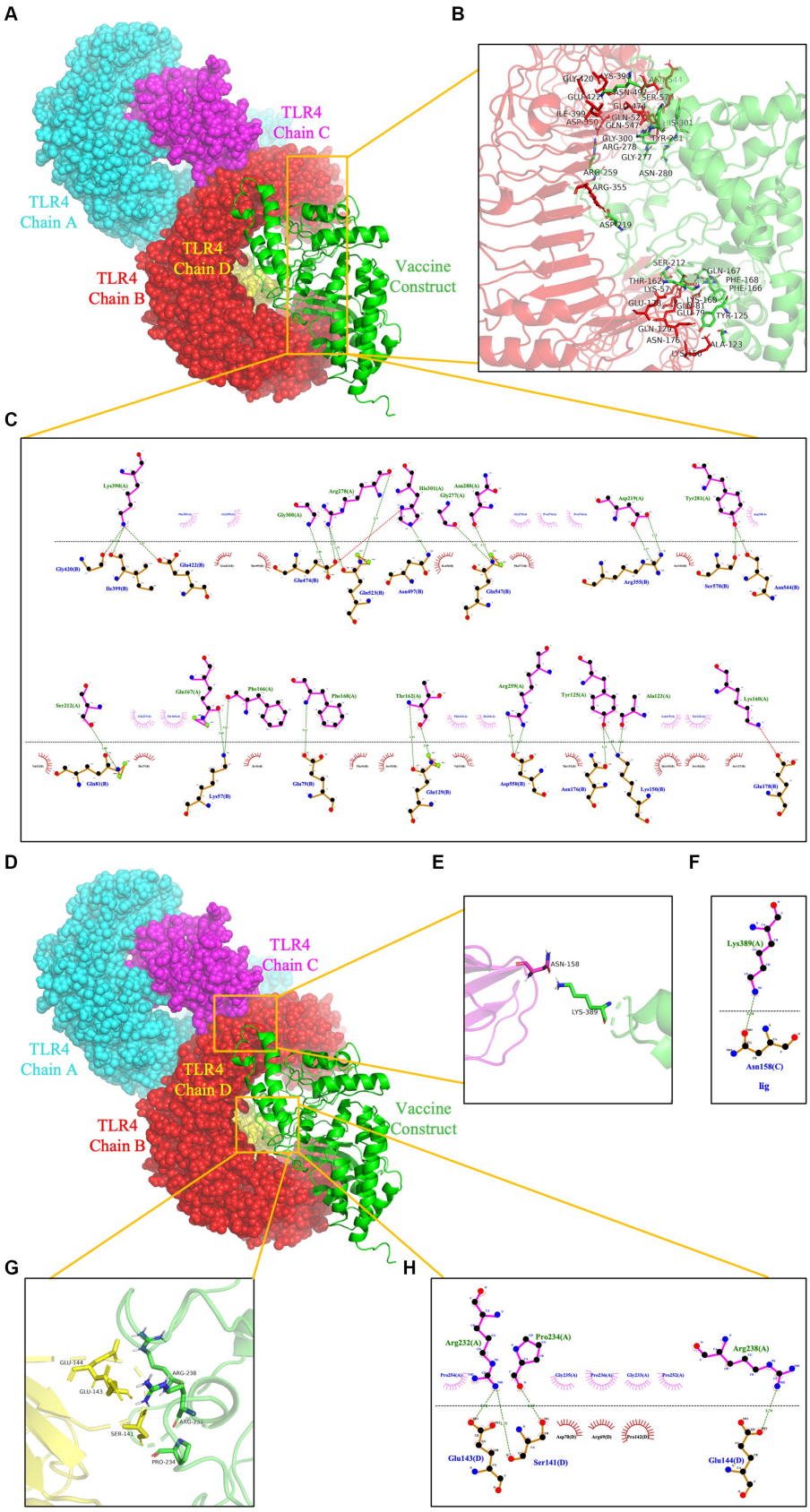

FIGURE 7
The molecular docking of *rPPMEV* and TLR4. The docked complexes of *rPPMEV* and TLR4 with the lowest interaction energy **(A,D)**. The interaction interface residues predicted by PyMol in 3D of *rPPMEV* with TLR4 Chain B **(B)**, TLR4 Chain C **(E)**, and TLR4 Chain D **(G)**. The interaction interface residues predicted by Ligplot in 2D of *rPPMEV* with TLR4 Chain B **(C)**, TLR4 Chain C **(F)**, and TLR4 Chain D **(H)**. The green dotted line represents the hydrogen bond, and the red dotted line represents the ionic bond.

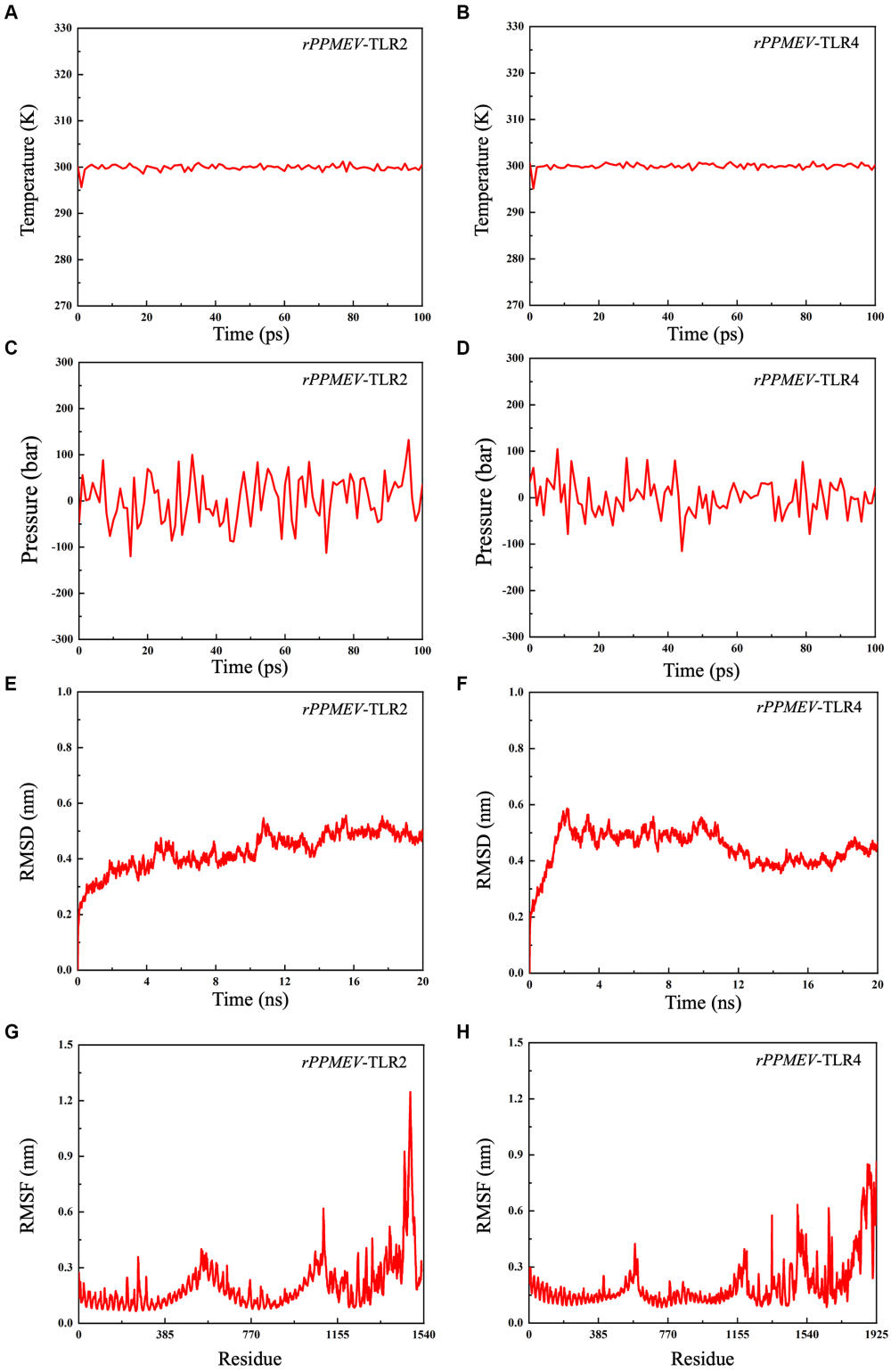

FIGURE 8
Molecular dynamics simulations between *rPPMEV* and TLRs. The temperature plots of the *rPPMEV*-TLR2 complex **(A)** and the *rPPMEV*-TLR4 complex **(B)**. The pressure plots of the *rPPMEV*-TLR2 complex **(C)** and the *rPPMEV*-TLR4 complex **(D)**. The RMSD analysis of the *rPPMEV*-TLR2 complex **(E)** and the *rPPMEV*-TLR4 complex **(F)**. The RMSF analysis of the *rPPMEV*-TLR2 complex **(G)** and the *rPPMEV*-TLR4 complex **(H)**.

stimulated upon immunization. Apart from B-lymphocytes, *rPPMEV* also induces the formation of three gradually rising peaks in the T helper (TH) (Figure 9C) cell and active TH cell (Figure 9D) populations after three injections, respectively. Moreover, the active cytotoxic T lymphocyte (TC cell) count sustains growth after each immunization (Figure 9E). In the end, as shown in Figure 9F, the concentrations of IFN-γ and IL-2 are

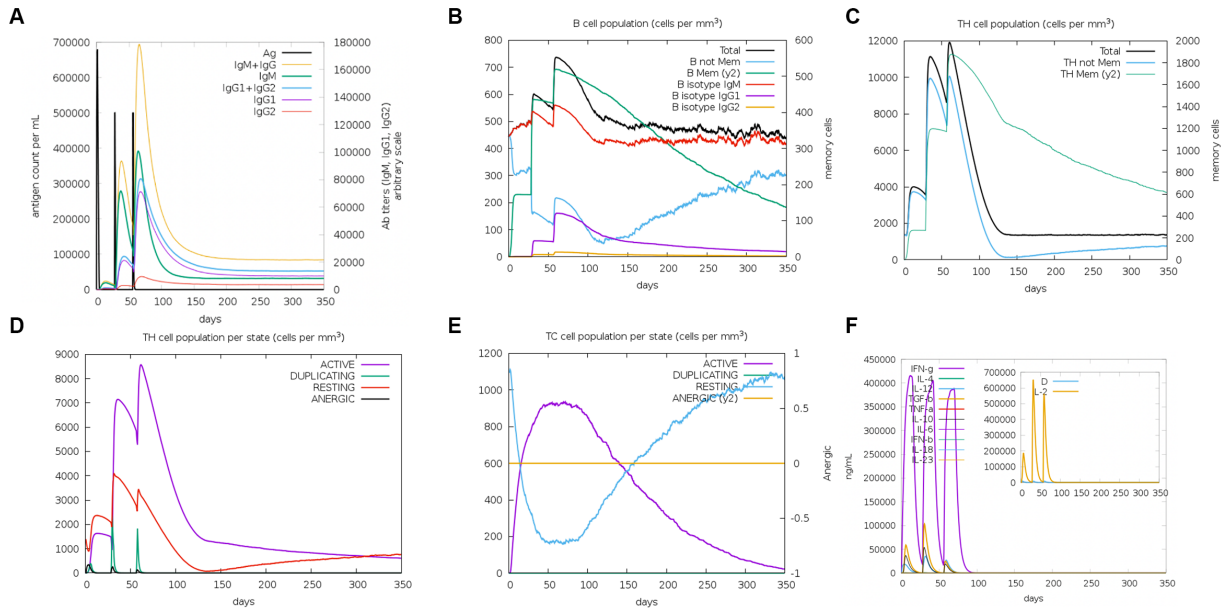

FIGURE 9
The immune simulated response spectrum of *rPPMEV* in the C-ImmSim server. **(A)** The production of various types of antibodies after vaccination. **(B)** The population of B cells after vaccination. **(C)** The population of helper T cells after vaccination. **(D)** The population of helper T cells in various states. **(E)** The population of cytotoxic T cells in various states. **(F)** Secretion levels of cytokines after vaccination.

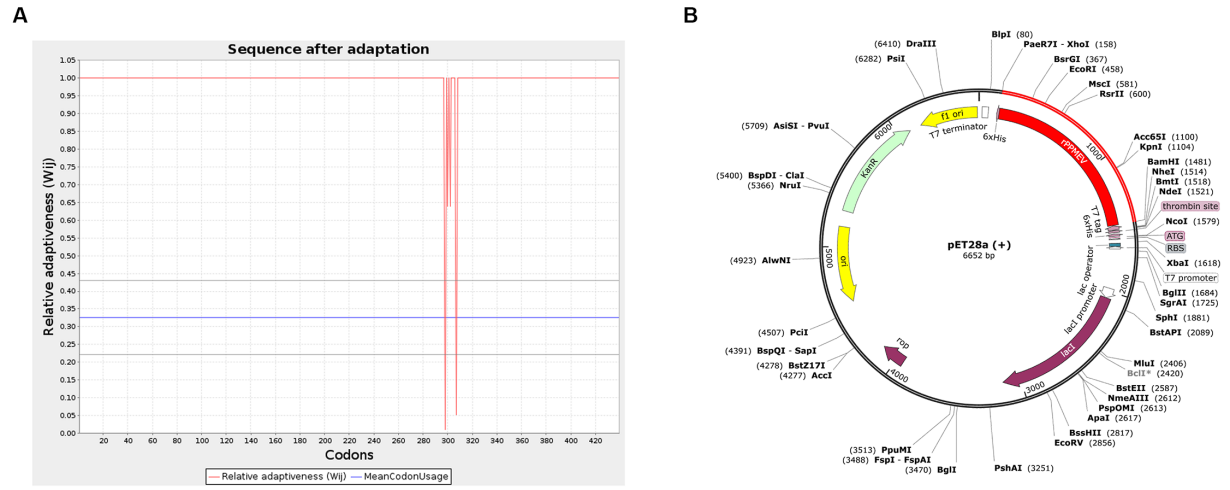

FIGURE 10
Codon optimization and *in silico* cloning. **(A)** The codon optimization of *rPPMEV*. **(B)** *In silico* cloning of *rPPMEV* in the pET28a (+) vector. The red areas represent the *rPPMEV*, while the black areas represent the pET28a (+) expression vector.

both at high levels during each injection, indicating that *rPPMEV* may have the ability to induce a sufficient immune response (Kar et al., 2020).

3.8 Codon optimization and *in silico* cloning

To generate an appropriate plasmid construct harboring the vaccine construct sequence, codon optimization was embarked upon, as shown in Figure 10A. The results show that the improved sequence has a codon adaptation index (CAI) value of 0.98 and a GC content of 50.87, indicating that the protein of the vaccine has a high potential to be well expressed in *E. coli* (Ali et al., 2017). Subsequently, the improved sequence of 1,317 bases was cloned into the pET28a (+) vector between the *XhoI* and *BamHI* restriction sites using Snap-Gene software, as shown in Figure 10B.

4 Conclusion

In summary, our study highlights a promising vaccine for PEDV and PDCoV prevention. The vaccine has several advantages. (1) The

peptides of the vaccine, derived from the S proteins with the good immune activity of the current common PEDV and PDCoV strains, have a more promising protective effect for the host in either the case of the current epidemic PEDV or PDCoV infection alone or in the case of co-infection than the original peptide molecules for the prevention of PEDV or PDCoV alone. (2) The vaccine, which contains multiple MHC epitopes, the TLR2 agonist Pam2Cys, and The TLR4 agonist RS-09, could target antigen-presenting cells to initiate innate immune responses and provide high levels of either antibody production or cytotoxic cellular response. (3) The vaccine has strong immunogenicity, antigenicity, non-toxicity, and non-sensitization properties. The physicochemical and immunological properties of the vaccine are based on bioinformatics analysis. Although it was reported that the vaccines designed by this method have been proven to produce protective effects *in vivo* and some of them have entered the clinical trial stage (Mahmud et al., 2021), the efficacy evaluation of the vaccine *rPPMEV* still needs to be evaluated by *in vivo* and *in vitro* tests to finally prove the efficacy of this vaccine.

Data availability statement

The original contributions presented in the study are included in the article/Supplementary material, further inquiries can be directed to the corresponding author.

Author contributions

WeiH: Conceptualization, Funding acquisition, Investigation, Methodology, Writing – original draft, Writing – review & editing. HeW: Investigation, Writing – review & editing. WW: Investigation, Writing – review & editing. RW: Investigation, Writing – review & editing. WH: Investigation, Writing – review & editing. SW: Investigation, Writing – review & editing. BW: Investigation, Writing – review & editing. HaiW: Conceptualization, Funding acquisition, Investigation, Writing – review & editing.

Funding

The author(s) declare financial support was received for the research, authorship, and/or publication of this article. This study was supported by Fundamental Research Program of Shanxi Province (No. 202103021223168), the Shanxi Province Excellent Doctoral Work Award-Scientific Research Project (No. SXBYKY2022053), the Start-up Fund for Doctoral Research, Shanxi Agricultural University (No. 2021BQ71), Shanxi Provincial Key Research and Development Program (No. 202102140601020), the "Six New" Project of Agriculture and Rural Department of Shanxi Province, the Fund for Shanxi "1331 Project" Key Innovative Research Team (No. 20211331-16), the Fund for Shanxi "1331 Project" (No. 20211331-12).

Conflict of interest

The authors declare that the research was conducted in the absence of any commercial or financial relationships that could be construed as a potential conflict of interest.

Publisher's note

Supplementary material

The Supplementary material for this article can be found online at: https://www.frontiersin.org/articles/10.3389/fmicb.2023.1295678/full#supplementary-material

References

Albutti, A. (2021). An integrated computational framework to design a multi-epitopes vaccine against *Mycobacterium tuberculosis*. *Sci. Rep.* 11:21929. doi: 10.1038/s41598-021-01283-6

Ali, M., Pandey, R. K., Khatoon, N., Narula, A., Mishra, A., and Prajapati, V. K. (2017). Exploring dengue genome to construct a multi-epitope based subunit vaccine by utilizing immunoinformatics approach to battle against dengue infection. *Sci. Rep.* 7:9232. doi: 10.1038/s41598-017-09199-w

Almagro Armenteros, J. J., Tsirigos, K. D., Sønderby, C. K., Petersen, T. N., Winther, O., Brunak, S., et al. (2019). SignalP 5.0 improves signal peptide predictions using deep neural networks. *Nat. Biotechnol.* 37, 420–423. doi: 10.1038/s41587-019-0036-z

Baek, M., Dimaio, F., Anishchenko, I., Dauparas, J., Ovchinnikov, S., Lee, G. R., et al. (2021). Accurate prediction of protein structures and interactions using a three-track neural network. *Science* 373, 871–876. doi: 10.1126/science.abj8754

Barh, D., Barve, N., Gupta, K., Chandra, S., Jain, N., Tiwari, S., et al. (2013). Exoproteome and secretome derived broad spectrum novel drug and vaccine candidates in *Vibrio cholerae* targeted by *Piper betel* derived compounds. *PLoS One* 8:e52773. doi: 10.1371/journal.pone.0052773

Barton, G. M. (2007). Viral recognition by toll-like receptors. *Semin. Immunol.* 19, 33–40. doi: 10.1016/j.smim.2007.01.003

Bhatnager, R., Bhasin, M., Arora, J., and Dang, A. S. (2021). Epitope based peptide vaccine against SARS-COV2: an immune-informatics approach. *J. Biomol. Struct. Dyn.* 39, 5690–5705. doi: 10.1080/07391102.2020.1787227

Boehme, K. W., and Compton, T. (2004). Innate sensing of viruses by toll-like receptors. *J. Virol.* 78, 7867–7873. doi: 10.1128/JVI.78.15.7867-7873.2004

Borca, M. V., Ramirez-Medina, E., Silva, E., Vuono, E., Rai, A., Pruitt, S., et al. (2020). Development of a highly effective African swine fever virus vaccine by deletion of the I177L gene results in sterile immunity against the current epidemic Eurasia strain. *J. Virol.* 94, e02017–e02019. doi: 10.1128/JVI.02017-19

Chauhan, V., Rungta, T., Goyal, K., and Singh, M. P. (2019). Designing a multi-epitope based vaccine to combat Kaposi sarcoma utilizing immunoinformatics approach. *Sci. Rep.* 9:2517. doi: 10.1038/s41598-019-39299-8

Chen, X., Zaro, J. L., and Shen, W.-C. (2013). Fusion protein linkers: property, design and functionality. *Adv. Drug Deliv. Rev.* 65, 1357–1369. doi: 10.1016/j.addr.2012.09.039

Choudhury, A., Gupta, P. S. S., Panda, S. K., Rana, M. K., and Mukherjee, S. (2022). Designing AbhiSCoVac-A single potential vaccine for all "corona culprits": Immunoinformatics and immune simulation approaches. *J. Mol. Liq.* 351:118633. doi: 10.1016/j.molliq.2022.118633

Corradin, G., Villard, V., and Kajava, A. V. (2007). Protein structure based strategies for antigen discovery and vaccine development against malaria and other pathogens. *Endocr. Metab. Immune. Disord. Drug. Targets* 7, 259–265. doi: 10.2174/187153007782794371

De Groot, A. S., Bosma, A., Chinai, N., Frost, J., Jesdale, B. M., Gonzalez, M. A., et al. (2001). From genome to vaccine: in silico predictions, *ex vivo* verification. *Vaccine* 19, 4385–4395. doi: 10.1016/s0264-410x(01)00145-1

Deléage, G. (2017). Alignsec: viewing protein secondary structure predictions within large multiple sequence alignments. *Bioinformatics* 33, 3991–3992. doi: 10.1093/bioinformatics/btx521

Dimitrov, I., Flower, D. R., and Doytchinova, I. (2013). AllerTOP-a server for in silico prediction of allergens. *BMC Bioinformatics*:S4. doi: 10.1186/1471-2105-14-S6-S4

Dong, R., Chu, Z., Yu, F., and Zha, Y. (2020). Contriving multi-epitope subunit of vaccine for COVID-19: immunoinformatics approaches. *Front. Immunol.* 11:1784. doi: 10.3389/fimmu.2020.01784

Eweas, A. F., Alhossary, A. A., and Abdel-Moneim, A. S. (2021). Molecular docking reveals ivermectin and remdesivir as potential repurposed drugs against SARS-CoV-2. *Front. Microbiol.* 11:592908. doi: 10.3389/fmicb.2020.592908

Fleri, W., Paul, S., Dhanda, S. K., Mahajan, S., Xu, X., Peters, B., et al. (2017). The immune epitope database and analysis resource in epitope discovery and synthetic vaccine design. *Front. Immunol.* 8:278. doi: 10.3389/fimmu.2017.00278

Frankel, A. D., and Pabo, C. O. (1988). Cellular uptake of the tat protein from human immunodeficiency virus. *Cells* 55, 1189–1193. doi: 10.1016/0092-8674(88)90263-2

Greenbaum, J. A., Andersen, P. H., Blythe, M., Bui, H. H., Cachau, R. E., Crowe, J., et al. (2007). Towards a consensus on datasets and evaluation metrics for developing B-cell epitope prediction tools. *J. Mol. Recognit.* 20, 75–82. doi: 10.1002/jmr.815

Grifoni, A., Sidney, J., Zhang, Y., Scheuermann, R. H., Peters, B., and Sette, A. (2020). A sequence homology and bioinformatic approach can predict candidate targets for immune responses to SARS-CoV-2. *Cell Host Microbe* 27, 671–680.e2. doi: 10.1016/j.chom.2020.03.002

Grote, A., Hiller, K., Scheer, M., Münch, R., Nörtemann, B., Hempel, D. C., et al. (2005). JCat: a novel tool to adapt codon usage of a target gene to its potential expression host. *Nucleic Acids Res.* 33, W526–W531. doi: 10.1093/nar/gki376

Gupta, S., Kapoor, P., Chaudhary, K., Gautam, A., Kumar, R., Consortium, O. S. D. D., et al. (2013). *In silico* approach for predicting toxicity of peptides and proteins. *PLoS One* 8:e73957. doi: 10.1371/journal.pone.0073957

He, J., Huang, F., Zhang, J., Chen, Q., Zheng, Z., Zhou, Q., et al. (2021). Vaccine design based on 16 epitopes of SARS-CoV-2 spike protein. *J. Med. Virol.* 93, 2115–2131. doi: 10.1002/jmv.26596

Hou, W., Wu, H., Wang, S., Wang, W., Wang, B., and Wang, H. (2023). Designing a multi-epitope vaccine to control porcine epidemic diarrhea virus infection using immunoinformatics approaches. *Front. Microbiol.* 14:1264612. doi: 10.3389/fmicb.2023.1264612

Ikai, A. (1980). Thermostability and aliphatic index of globular proteins. *J. Biochem.* 88, 1895–1898.

Ismail, S., Ahmad, S., and Azam, S. S. (2020). Immunoinformatics characterization of SARS-CoV-2 spike glycoprotein for prioritization of epitope based multivalent peptide vaccine. *J. Mol. Liq.* 314:113612. doi: 10.1016/j.molliq.2020.113612

Jackson, D. C., Lau, Y. F., Le, T., Suhrbier, A., Deliyannis, G., Cheers, C., et al. (2004). A totally synthetic vaccine of generic structure that targets toll-like receptor 2 on dendritic cells and promotes antibody or cytotoxic T cell responses. *Proc. Natl. Acad. Sci. U. S. A.* 101, 15440–15445. doi: 10.1073/pnas.0406740101

Jiang, F., Liu, Y., Xue, Y., Cheng, P., Wang, J., Lian, J., et al. (2023). Developing a multiepitope vaccine for the prevention of SARS-CoV-2 and monkeypox virus co-infection: a reverse vaccinology analysis. *Int. Immunopharmacol.* 115:109728. doi: 10.1016/j.intimp.2023.109728

Jiao, Z., Liang, J., Yang, Y., Li, Y., Yan, Z., Hu, G., et al. (2021). Coinfection of porcine deltacoronavirus and porcine epidemic diarrhea virus altered viral tropism in gastrointestinal tract in a piglet model. *Virology* 558, 119–125. doi: 10.1016/j.virol.2021.03.006

Kar, T., Narsaria, U., Basak, S., Deb, D., Castiglione, F., Mueller, D. M., et al. (2020). A candidate multi-epitope vaccine against SARS-CoV-2. *Sci. Rep.* 10:10895. doi: 10.1038/s41598-020-67749-1

Khan, M. T., Islam, M. J., Parihar, A., Islam, R., Jerin, T. J., Dhote, R., et al. (2021). Immunoinformatics and molecular modeling approach to design universal multi-epitope vaccine for SARS-CoV-2. *Inform. Med. Unlocked* 24:100578. doi: 10.1016/j.imu.2021.100578

Khan, A., Junaid, M., Kaushik, A. C., Ali, A., Ali, S. S., Mehmood, A., et al. (2018). Computational identification, characterization and validation of potential antigenic peptide vaccines from hrHPVs E6 proteins using immunoinformatics and computational systems biology approaches. *PLoS One* 13:e0196484. doi: 10.1371/journal.pone.0196484

Kong, F., Wang, Q., Kenney, S. P., Jung, K., Vlasova, A. N., and Saif, L. J. (2022). Porcine deltacoronaviruses: origin, evolution, cross-species transmission and zoonotic potential. *Pathogens* 11:79. doi: 10.3390/pathogens11010079

Koonpaew, S., Teeravechyan, S., Frantz, P. N., Chailangkarn, T., and Jongkaewwattana, A. (2019). PEDV and PDCoV pathogenesis: the interplay between host innate immune responses and porcine enteric coronaviruses. *Front. Vet. Sci.* 6:34. doi: 10.3389/fvets.2019.00034

Kozakov, D., Hall, D. R., Xia, B., Porter, K. A., Padhorny, D., Yueh, C., et al. (2017). The ClusPro web server for protein–protein docking. *Nat. Protoc.* 12, 255–278. doi: 10.1038/nprot.2016.169

Kurt-Jones, E. A., Popova, L., Kwinn, L., Haynes, L. M., Jones, L. P., Tripp, R. A., et al. (2000). Pattern recognition receptors TLR4 and CD14 mediate response to respiratory syncytial virus. *Nat. Immunol.* 1, 398–401. doi: 10.1038/80833

Li, Y., Liu, X., Zhu, Y., Zhou, X., Cao, C., Hu, X., et al. (2013). Bioinformatic prediction of epitopes in the Emy162 antigen of Echinococcus multilocularis. *Exp. Ther. Med.* 6, 335–340. doi: 10.3892/etm.2013.1142

Li, Y., Wang, J., Hou, W., Shan, Y., Wang, S., and Liu, F. (2021). Dynamic dissection of the endocytosis of porcine epidemic diarrhea coronavirus cooperatively mediated by clathrin and caveolae as visualized by single-virus tracking. *mBio* 12, e00256–e00221. doi: 10.1128/mBio.00256-21

Liu, H. A.-O., Yin, X., Tian, H., Qiu, Y., Wang, Z., Chen, J., et al. (2022). The S protein of a novel recombinant PEDV strain promotes the infectivity and pathogenicity of PEDV in mid-West China. *Transbound. Emerg. Dis.* 69, 3704–3723. doi: 10.1111/tbed.14740

Mahmud, S., Rafi, M. O., Paul, G. K., Promi, M. M., Shimu, M., Sultana, S., et al. (2021). Designing a multi-epitope vaccine candidate to combat MERS-CoV by employing an immunoinformatics approach. *Sci. Rep.* 11:15431. doi: 10.1038/s41598-021-92176-1

Meza, B., Ascencio, F., Sierra-Beltrán, A. P., Torres, J., and Angulo, C. (2017). A novel design of a multi-antigenic, multistage and multi-epitope vaccine against *Helicobacter pylori*: an *in silico* approach. *Infect. Genet. Evol.* 49, 309–317. doi: 10.1016/j.meegid.2017.02.007

Moise, L., Gutiérrez, A. H., Khan, S., Tan, S., Ardito, M., Martin, W. D., et al. (2020). New immunoinformatics tools for swine: designing epitope-driven vaccines, predicting vaccine efficacy, and making vaccines on demand. *Front. Immunol.* 11:563362. doi: 10.3389/fimmu.2020.563362

Nabel, G. J. (2002). HIV vaccine strategies. *Vaccine* 20, 1945–1947. doi: 10.1016/s0264-410x(02)00074-9

Ponomarenko, J., Bui, H.-H., Li, W., Fusseder, N., Bourne, P. E., Sette, A., et al. (2008). ElliPro: a new structure-based tool for the prediction of antibody epitopes. *BMC Bioinformatics* 9:514. doi: 10.1186/1471-2105-9-514

Puigbo, P., Romeu, A., and Garcia-Vallve, S. (2007). HEG-DB: a database of predicted highly expressed genes in prokaryotic complete genomes under translational selection. *Nucleic Acids Res.* 36, D524–D527. doi: 10.1093/nar/gkm831

Rapin, N., Lund, O., Bernaschi, M., and Castiglione, F. (2010). Computational immunology meets bioinformatics: the use of prediction tools for molecular binding in the simulation of the immune system. *PLoS One* 5:e9862. doi: 10.1371/journal.pone.0009862

Rock, D. (2017). Challenges for African swine fever vaccine development—… perhaps the end of the beginning. *Vet. Microbiol.* 206, 52–58. doi: 10.1016/j.vetmic.2016.10.003

Ros-Lucas, A., Correa-Fiz, F., Bosch-Camós, L., Rodriguez, F., and Alonso-Padilla, J. (2020). Computational analysis of African swine fever virus protein space for the design of an epitope-based vaccine ensemble. *Pathogens* 9:1078. doi: 10.3390/pathogens9121078

Rowaiye, A. B., Oli, A. N., Asala, M. T., Nwonu, E. J., Njoku, M. O., Asala, O. O., et al. (2023). Design of multiepitope vaccine candidate from a major capsid protein of the African swine fever virus. *Vet. Vaccine* 2:100013. doi: 10.1016/j.vetvac.2023.100013

Saadi, M., Karkhah, A., and Nouri, H. R. (2017). Development of a multi-epitope peptide vaccine inducing robust T cell responses against brucellosis using immunoinformatics based approaches. *Infect. Genet. Evol.* 51, 227–234. doi: 10.1016/j.meegid.2017.04.009

Sarkar, B., Ullah, M. A., Araf, Y., Islam, N. N., and Zohora, U. S. (2022). Immunoinformatics-guided designing and *in silico* analysis of epitope-based polyvalent vaccines against multiple strains of human coronavirus (HCoV). *Expert Rev. Vaccines* 21, 1851–1871. doi: 10.1080/14760584.2021.1874925

Scheiblhofer, S., Laimer, J., Machado, Y., Weiss, R., and Thalhamer, J. (2017). Influence of protein fold stability on immunogenicity and its implications for vaccine design. *Expert Rev. Vaccines* 16, 479–489. doi: 10.1080/14760584.2017.1306441

Sha, T., Li, Z., Zhang, C., Zhao, X., Chen, Z., Zhang, F., et al. (2020). Bioinformatics analysis of candidate proteins Omp2b, P39 and BLS for *Brucella* multivalent epitope vaccines. *Microb. Pathog.* 147:104318. doi: 10.1016/j.micpath.2020.104318

Shantier, S. W., Mustafa, M. I., Abdelmoneim, A. H., Fadl, H. A., Elbager, S. G., and Makhawi, A. M. (2022). Novel multi epitope-based vaccine against monkeypox virus: vaccinomic approach. *Sci. Rep.* 12:15983. doi: 10.1038/s41598-022-20397-z

Shukla, R., Shukla, H., Sonkar, A., Pandey, T., and Tripathi, T. (2018). Structure-based screening and molecular dynamics simulations offer novel natural compounds as potential inhibitors of *Mycobacterium tuberculosis* isocitrate lyase. *J. Biomol. Struct. Dyn.* 36, 2045–2057. doi: 10.1080/07391102.2017.1341337

Sun, D., Feng, L., Shi, H., Chen, J., Cui, X., Chen, H., et al. (2008). Identification of two novel B cell epitopes on porcine epidemic diarrhea virus spike protein. *Vet. Microbiol.* 131, 73–81. doi: 10.1016/j.vetmic.2008.02.022

Sun, Q., Huang, Z., Yang, S., Li, Y., Ma, Y., Yang, F., et al. (2022). Bioinformatics-based SARS-CoV-2 epitopes design and the impact of spike protein mutants on epitope humoral immunities. *Immunobiology* 227:152287. doi: 10.1016/j.imbio.2022.152287

Tahir ul Qamar, M., Shokat, M., Muneer I, Z., Ashfaq, U. A., Javed, H., Bari, A. F., et al. (2020). Multiepitope-based subunit vaccine design and evaluation against respiratory syncytial virus using reverse vaccinology approach. *Vaccines* 8:288. doi: 10.3390/vaccines8020288

Takeda, K., and Akira, S. (2004). TLR signaling pathways. *Semin. Immunol.* 16, 3–9. doi: 10.1016/j.smim.2003.10.003

Tang, P., Cui, E., Song, Y., Yan, R., and Wang, J. (2021). Porcine deltacoronavirus and its prevalence in China: a review of epidemiology, evolution, and vaccine development. *Arch. Virol.* 166, 2975–2988. doi: 10.1007/s00705-021-05226-4

Temeeyasen, G., Sinha, A., Gimenez-Lirola, L., Zhang, J., and Piñeyro, P. (2018). Differential gene modulation of pattern-recognition receptor TLR and RIG-I-like and downstream mediators on intestinal mucosa of pigs infected with PEDV non S-INDEL and PEDV S-INDEL strains. *Virology* 517, 188–198. doi: 10.1016/j.virol.2017.11.024

Trovato, M., Sartorius, R., D'Apice, L., Manco, R., and De Berardinis, P. (2020). Viral emerging diseases: challenges in developing vaccination strategies. *Front. Immunol.* 11:2130. doi: 10.3389/fimmu.2020.02130

Wang, D., Fang, L., and Xiao, S. (2016). Porcine epidemic diarrhea in China. *Virus Res.* 226, 7–13. doi: 10.1016/j.virusres.2016.05.026

Waterhouse, A., Bertoni, M., Bienert, S., Studer, G., Tauriello, G., Gumienny, R., et al. (2018). Swiss-model: homology modelling of protein structures and complexes. *Nucleic Acids Res.* 46, W296–W303. doi: 10.1093/nar/gky427

Wiederstein, M., and Sippl, M. J. (2007). ProSA-web: interactive web service for the recognition of errors in three-dimensional structures of proteins. *Nucleic Acids Res.* 35, W407–W410. doi: 10.1093/nar/gkm290

Yao, X., Qiao, W.-T., Zhang, Y.-Q., Lu, W.-H., Wang, Z.-W., Li, H.-X., et al. (2023). A new PEDV strain CH/HLJJS/2022 can challenge current detection methods and vaccines. *Virol. J.* 20:13. doi: 10.1186/s12985-023-01961-z

Yu, M., Zhu, Y., Li, Y., Chen, Z., Li, Z., Wang, J., et al. (2022). Design of a recombinant multivalent epitope vaccine based on SARS-CoV-2 and its variants in immunoinformatics approaches. *Front. Immunol.* 13:884433. doi: 10.3389/fimmu.2022.884433

Zhai, K., Zhang, Z., Liu, X., Lv, J., Zhang, L., Li, J., et al. (2023). Mucosal immune responses induced by oral administration of recombinant *Lactococcus lactis* expressing the S1 protein of PDCoV. *Virology* 578, 180–189. doi: 10.1016/j.virol.2022.12.010

Zhang, L., Liu, X., Zhang, Q., Zhou, P., Fang, Y., Dong, Z., et al. (2019). Biological characterization and pathogenicity of a newly isolated Chinese highly virulent genotype GIIa porcine epidemic diarrhea virus strain. *Arch. Virol.* 164, 1287–1295. doi: 10.1007/s00705-019-04167-3

frontiers | Frontiers in Microbiology

TYPE Original Research
PUBLISHED 07 December 2023
DOI 10.3389/fmicb.2023.1254060

OPEN ACCESS

EDITED BY
Hongliang Chai,
Northeast Forestry University, China

REVIEWED BY
Ganesh Kumar Maurya,
Banaras Hindu University, India
Hosny El-Adawy,
Friedrich Loeffler Institut, Germany
Serageldeen Sultan,
South Valley University, Egypt

*CORRESPONDENCE
Asmaa Magouz
✉ asmaa.magoz@vet.kfs.edu.eg
Ehab Kotb Elmahallawy
✉ eehaa@unileon.es

RECEIVED 06 July 2023
ACCEPTED 16 November 2023
PUBLISHED 07 December 2023

CITATION
Magouz A, El-Kon I, Raya-Álvarez E, Khaled E, Alkhalefa N, Alhegaili AS, El-khadragy MF, Agil A and Elmahallawy EK (2023) Molecular typing of canine parvovirus type 2 by VP2 gene sequencing and restriction fragment length polymorphism in affected dogs from Egypt. *Front. Microbiol.* 14:1254060. doi: 10.3389/fmicb.2023.1254060

Molecular typing of canine parvovirus type 2 by VP2 gene sequencing and restriction fragment length polymorphism in affected dogs from Egypt

Asmaa Magouz[1]*, Ismail El-Kon[2], Enrique Raya-Álvarez[3], Enas Khaled[1], Noura Alkhalefa[1], Alaa S. Alhegaili[4], Manal F. El-khadragy[5], Ahmad Agil[6] and Ehab Kotb Elmahallawy[7,8]*

[1]Department of Virology, Faculty of Veterinary Medicine, Kafrelsheikh University, Kafrelsheikh, Egypt, [2]Department of Gynaecology, Obstetrics and Artificial Insemination, Faculty of Veterinary Medicine, Kafrelsheikh University, Kafrelsheikh, Egypt, [3]Rheumatology Department, Hospital Universitario San Cecilio, Granada, Spain, [4]Department of Medical Laboratory, College of Applied Medical Sciences, Prince Sattam bin Abdulaziz University, Alkharj, Saudi Arabia, [5]Department of Biology, College of Science, Princess Nourah bint Abdulrahman University, Riyadh, Saudi Arabia, [6]Department of Pharmacology, Biohealth Institute Granada (IBs Granada) and Neuroscience Institute, School of Medicine, University of Granada, Granada, Spain, [7]Departamento de Sanidad Animal, Grupo de Investigación en Sanidad Animal y Zoonosis (GISAZ), Facultad de Veterinaria, Universidad de Córdoba, Córdoba, Spain, [8]Department of Zoonoses, Faculty of Veterinary Medicine, Sohag University, Sohag, Egypt

Introduction: Canine parvovirus-2 (CPV-2) is one of the most common infectious diseases in dogs characterized by severe gastroenteritis, vomiting, and bloody diarrhea. Little information is available about this topic in Egypt, particularly in the Delta region. This study reports the prevalence and molecular analysis of CPV-2 variants collected from El-Gharbia and Kafrelsheikh governorates in the Delta of Egypt.

Methods: In this study, 320 rectal swabs were collected from infected domestic dogs from two districts in delta Egypt. The samples were investigated by rapid immunochromatographic test and polymerase chain reaction for detection the prevalence of CPV-2 variants. The genetic characterization was performed using restriction fragment length polymorphism (RFLP) analysis and partial VP2 gene sequence.

Results and discussion: The viral antigen was detected in (264/320, 82.5%) of samples by IC test, while PCR was found more sensitive by detecting (272/320, 85%) positive samples. The RFLP technique using *Mbo*II restriction enzyme was successfully used for the differentiation of CPV-2c antigenic variants from CPV-2a/2b strains. Interestingly, the molecular and phylogenetic analysis revealed that both CPV-2a and CPV-2c are circulating in the study area. Deduced amino acid sequence analysis showed changes at residue (N426E) and residue (T440A).: Our results indicated that CPV-2 is prevalent among dogs in Egypt, and therefore further molecular and epidemiological studies of CPV-2 are warranted.

KEYWORDS

canine parvovirus, PCR, RFLP, VP2 gene, Egypt

1 Introduction

Canine parvovirus (CPV) is a highly infectious and fatal viral disease of canines since the late 1970s. Despite intensive vaccination, the virus is still a leading cause of acute gastroenteritis and canine mortality, especially among non-immunized young puppies (Liu et al., 2017). Dogs of all ages can get parvovirus, but puppies are more sensitive to the infection showing clinical signs within 3–8 days, in the form of fever, hemorrhagic gastroenteritis, vomiting, and bloody or watery diarrhea (Kim et al., 2017). Canine parvovirus is classified in the family of *Parvoviridae*, *Parvovirinae* subfamily, and *Protoparvovirus* genus (Timurkan et al., 2019). It is a naked DNA virus containing a linear, negative single-stranded genome of approximately 5.2 kb in length. The viral DNA is featured by two major open reading frames (ORFs). The first ORF includes/encodes two non-structural proteins (namely NS1 and NS2) that involve in virus multiplication, while the second one encodes the capsid proteins (VP1 and VP2) (Saei et al., 2017).

It seems that the virus was a host mutant from the feline panleukopenia virus in 1978 in the United States after point mutations in few nucleotide in the VP2 gene, and consequently, the virus spreads worldwide (Timurkan et al., 2019). It was first reported as CPV type-2 (CPV-2) to be differentiated from canine parvovirus type 1 (CPV-1) which is non-pathogenic to canine species (Yip et al., 2020). A few years after the emergence of the original strain, two antigenic variants of CPV-2 emerged and were classified as CPV-2a and CPV-2b and within few months they had become the predominant types worldwide (Buonavoglia et al., 2001). The VP2 is the main capsid protein expressing the main antigenic determinants, and amino acid mutations in this protein have important biological effects such as changes in the antigenic properties, host range and viral pathogenicity (Zhou et al., 2017). Typing CPV-2 variants is mainly based on changes in amino acids in VP2 protein residue 426 (Asn in CPV-2a and CPV-2b besides Glu in CPV-2c), though other specific amino acid alterations in VP2 residues have also been observed (Buonavoglia et al., 2001).

The CPV2a and CPV2b variants are both circulating throughout the world and can infect both dogs and cats, however, they exhibit a low virulence in cats. In 1990, the novel variants with one amino acid alteration (CPV2a297A) and (CPV2b297A) in the VP2 gene replaced CPV2a and CPV2b (Charoenkul et al., 2019). The amino acid substitution (Asp-426 Glu) in VP2 gene generated a new variant, known as CPV-2c, that infects several canine breeds (Lambe et al., 2016). This new variant initially emerged in Italy in 2000 but recently has spread to other countries (Timurkan et al., 2019). This amino acid change (D426E) of CPV-2c strain is caused by the change of (T → A) in the third codon position at nt 4,062 ± 4,066, creating a M*bo*II restriction site (GAAGA) which is unique to CPV-2c (Liu et al., 2017). Therefore, these mutants (types 2c) can be distinguished from the other antigenic types (2a and 2b) by enzyme digestion using M*bo*II enzyme (Timurkan et al., 2019). However, restriction fragment length polymorphism (RFLP) analysis is not capable of differentiating CPV-2b from CPV-2a, because both types are not digested by *Mbo*II (Buonavoglia et al., 2001). Diagnosis of CPV-2 based on clinical signs is misleading since many other pathogens can cause similar symptoms in dogs. Therefore, a clinical diagnosis should always be confirmed with laboratory tests (Sun et al., 2019). A number of molecular assays (gene amplification- based) have been applied for CPV-2 diagnosis, such as PCR, real-time PCR, loop-mediated isothermal amplification, multiplex PCR, and RFLP (AL-Hosary, 2018). In Egypt, the virus was initially recorded in 1982, in military police dogs (AL-Hosary, 2018). Since then, it has been circulating among dog population in Egypt. In 2012, the presence of CPV2b in Egypt was confirmed by sequence analysis and in 2014, serotypes 2b and 2c were detected among dog population (Amthal, 2014). Genetic characterization was used in 2018 to identify genotypes 2a and 2b, with special emphasis on numerous mutations in genotype 2b (Zaher et al., 2020). Another Egyptian study revealed the predominance of CPV-2c strains among the collected dog samples (Ndiana et al., 2022). At present, all variants (CPV-2a, CPV-2b and CPV-2c) are reported in Egypt (AL-Hosary, 2018; Soliman et al., 2018; El-Neshwy et al., 2019). Although several research studies regarding the molecular characterization of CPV variants in Egypt are present (AL-Hosary, 2018), for the best of our knowledge no previous reports were conducted on El-Gharbeya and Kafrelsheikh governorates in the Delta of Egypt Clearly, further studies are needed to highlight the different CPV-2 variants circulating in Egypt in Nile Delta region. The present study was designed to perform molecular characterization of CPV-2 variants from clinically infected dogs in the El-Gharbia and Kafrelsheikh governorates, using PCR and RFLP followed by VP2 sequencing.

2 Materials and methods

2.1 Ethical considerations

The study was performed according to the regulating rules of Institutional Review Board of Faculty of Veterinary Medicine, Kafrelsheikh University, Egypt (IRB number KFS-2019/09).

2.2 Study area and sampling

A total of 320 rectal swabs were collected from private veterinary clinics in El-Gharbia, and Kafrelsheikh governorates (Delta of Egypt) during the period from September 2019 to January 2021 from clinically infected domestic dogs showing fever, bloody diarrhea, dehydration and vomiting with history of previous vaccination in some dogs. The studied area, El-Gharbia and Kafrelsheikh governorates are based in the middle of the Delta of Egypt. The data of each puppy regarding age, breed, sex and clinical signs are recorded in Table 1. Samples were collected by licensed veterinarians following obtaining informed consent from the animals' owners.

Rectal swabs were immersed in labeled tubes containing sterile phosphate-buffer saline (PBS) with 10% of antibiotic solution and centrifuged at 12.000 rpm (10 min). The supernatant fluids were then collected and kept at −80°C until processing.

2.3 Rapid Immunochromatic test for CPV antigen detection

All rectal swabs were tested by CPV rapid Ag detection kits (APETCARE) (China) as per manufacturer's instructions. Briefly, fecal samples were collected from dogs using rectal swabs. The swabs were then introduced into the specimen tube containing 1 mL of assay

10.3389/fmicb.2023.1254060

TABLE 1 Details of examined puppies (breed, age, sex, clinical signs and vaccination status).

Number of samples	Bread	Age (months)	Sex	Vomit/ diarrhea	Vaccination status	PCR(–) samples
10	Griffon	3	Male	Severe	Not vaccinated	+
4	Husky	3.5	Female	Severe	Not vaccinated	–
8	Pit bull	3	Female	Moderate	Vaccinated	+
12	Pit bull	2	Male	Severe	Unknown	–
2	G. Shepherd*	3	Female	Mild	Vaccinated	+
6	Golden	6	Female	Moderate	Vaccinated	+
4	Pit bull	4	Male	Moderate	Vaccinated	+
6	G. Shepherd	4	Male	Mild	Vaccinated	+
8	G. Shepherd	2	Male	Severe	Unknown	+
4	Pit Bull	4	Male	Mild	Vaccinated	+
10	G. Shepherd	2.5	Female	Moderate	Not vaccinated	–
10	G. Shepherd	2.5	Male	Severe	Not vaccinated	+
12	G. Shepherd	2.5	Female	Severe	Vaccinated	–
10	Griffon	12	Female	Mild	Vaccinated	+
12	G. Shepherd	3	Female	Moderate	Not vaccinated	+
4	Pit Bull	6	Male	Moderate	Vaccinated	–
10	Golden	3.5	Male	Mild	Vaccinated	+
10	Pikinwa	12	Male	Mild	Vaccinated	+
8	Boxer	2	Male	Severe	Not vaccinated	–
10	Pit bull	3	Male	Moderate	Unknown	–
4	Pit Bull	2	Male	Severe	Vaccinated	+
6	Golden	2	Female	Severe	Vaccinated	+
8	Pit Bull	3	Female	Severe	Vaccinated	+
4	Pit Bull	2	Male	Moderate	Not vaccinated	+
2	G. Shepherd	2.5	Male	Severe	Vaccinated	–
10	G. Shepherd	2.5	Female	Severe	Vaccinated	+
14	G. Shepherd	3	Male	Severe	Vaccinated	+
4	Pit Bull	2.5	Male	Severe	Not vaccinated	+
6	Pikinwa	3	Male	Severe	Vaccinated	–
4	Pit Bull	3	Female	Severe	Not vaccinated	+
8	Pit Bull	6	Male	Moderate	Vaccinated	+
2	G. Shepherd	4	Male	Severe	Unknown	+
8	G. Shepherd	3	Female	Severe	Not vaccinated	–
10	Golden	12	Male	Moderate	Vaccinated	+
10	Golden	4	Male	Mild	Vaccinated	–
14	Boxer	3.5	Female	Severe	Unknown	+
8	Boxer	2	Male	Moderate	Not vaccinated	+
14	G. Shepherd	6	Male	Moderate	Not vaccinated	+
6	G. Shepherd	8	Female	Severe	Not vaccinated	+
16	Golden	6	Male	Severe	Unknown	–

G. Shepherd* = German shepherd.

TABLE 2 Oligonucleotide primers used for amplification of VP2 gene of suspected CPV infected field cases.

Primer	Oligonucleotide sequence	Gene	Length of amplified fragment	Reference
Forward	5′ CAGGAAGATATCCAGAAGGA 3′	VP2 gene	583 bp	Buonavoglia et al. (2001)
Reverse	5'GGTGCTAGTTGATATGTAATAAACA 3			

diluent. The samples were mixed with the diluent and applied into the sample hole of the device of the test strip. Positive results are indicated by a visible T band in the corresponding testing window.

2.4 DNA extraction

The Viral genomic DNA was extracted from 300 µL of rectal swab suspensions using Gene Jet Viral DNA/RNA Extraction Kit (ThermoFisher Scientific, United States) as per the manufacturer's protocol then the purified DNA was preserved at −20°C till used.

2.5 PCR amplification of VP2 gene

The PCR was conducted in 25 µL volumes, consisting of 12.5 µL of 2X PCR Master Mix (ThermoFisher Scientific, USA), 1 µL of forward and reverse primers, 5 µL of DNA, and 5.5 µL of PCR grade water. PCR was conducted in an Applied biosystem 2,720 thermal cycler using 2 sets of primers which amplify a 583 bp of the VP2 gene. DNA was amplified using primers described elsewhere (Buonavoglia et al., 2001) (Table 2). The PCR cycle condition comprised an initial denaturation step at 94°C for 5 min, followed by denaturation at 95°C for 30 s, annealing at 55°C /2 min and extension at 70°C/2 min (35 cycles), and a cycle of final extension at 72°C for 5 min. Regarding the positive control samples, DNA was extracted from a lyophilized Vanguard Plus CPV vaccine (Pfizer), while the negative control tube included only primers and nuclease free water to reach the final volume. Visualization of the resulting amplified PCR products was performed using 1.5% agarose gel electrophoresis and amplicons' size was estimated using the 100 bp DNA marker (ThermoFisher Scientific, US). PCR -positive products were purified with purification kit (Thermo Fisher, United States) as per the manufacturer's protocol."

2.6 Restriction fragment length polymorphism analysis

This step was carried out by digestion of purified amplicons with 5 units of the M*bo* II restriction enzyme (Fast Digest, ThermoFisher Scientific, USA) following the manufacturer's instructions. Briefly, 10 µL of DNA, 1 µL of restriction Enzyme, 2 µL of green buffer and 17 µL of nuclease free water were mixed and incubated at 37°C in a heat block (5 min). Then, the enzyme was inactivated by heating at 65°C for 5 min. The cleavage manner of the amplicons was detected on 2% agarose gel.

2.7 DNA sequencing and phylogenetic analysis

QIAquick PCR product extraction kit (Qiagen, Valencia) was used to purify amplicons of the CPV-2 VP2 gene of four selected isolates based on different geographical areas. Using the same PCR primers, isolates were sequenced by BigDye Terminator V3.1 cycle sequencing kit using an Applied Biosystems 3,130 genetic analyzer (ABI, USA). The resulting sequence data were then submitted and deposited in the GenBank databases under the following accession numbers MW544032 (CPV/Egy1/2021), MW544033 (CPV/Egy2/2021), MW544034 (CPV/Egy3/2021), and MW544031 (CPV/Egy4/2021). The VP2 gene's identity to GenBank accessions was established using blast analyses (BLASTn).[1] By using the CLUSTAL W Multiple Sequence Alignment tool of the MEGA X software, the nucleotide sequences were then aligned and compared with other CPV reference strains accessible in the GenBank database, and then translated into amino acid sequences. MEGA X software was used for phylogenetic analyses using the neighbor-joining method and 1,000 bootstrap repetitions.

2.8 Sequence retrieval and alignment

In this study, sequence retrieval and alignment of canine parvovirus VP2 sequences were performed using the CLC Genomics Software. The primary objective was to align these sequences with the wild-type reference sequence (NP_955539.1). The alignment process facilitated the identification of conserved regions and potential mutations, shedding light on the genetic diversity and possible implications for virulence and vaccine development (Figure 1).

2.9 Molecular modelling

To determine the functional importance of the mutated residues in the retrieved sequences, requests for building 3D molecular models were submitted to the SWISSMODEL server (Waterhouse et al., 2018). The model building and quality were assessed by GMQE and QMEANDisCo Global score (Studer et al., 2020). To evaluate the influence of mutations on the collective binding potency amid interactions among VP2 protein monomers, computations were carried out to gauge both the binding efficacy and the dissociation constant (Kd). The analysis was performed at "Predicting the change in proteins binding affinity" tool (PANDA) (Abbasi et al., 2021).

1 http://www.ncbi.nlm.nih.gov/

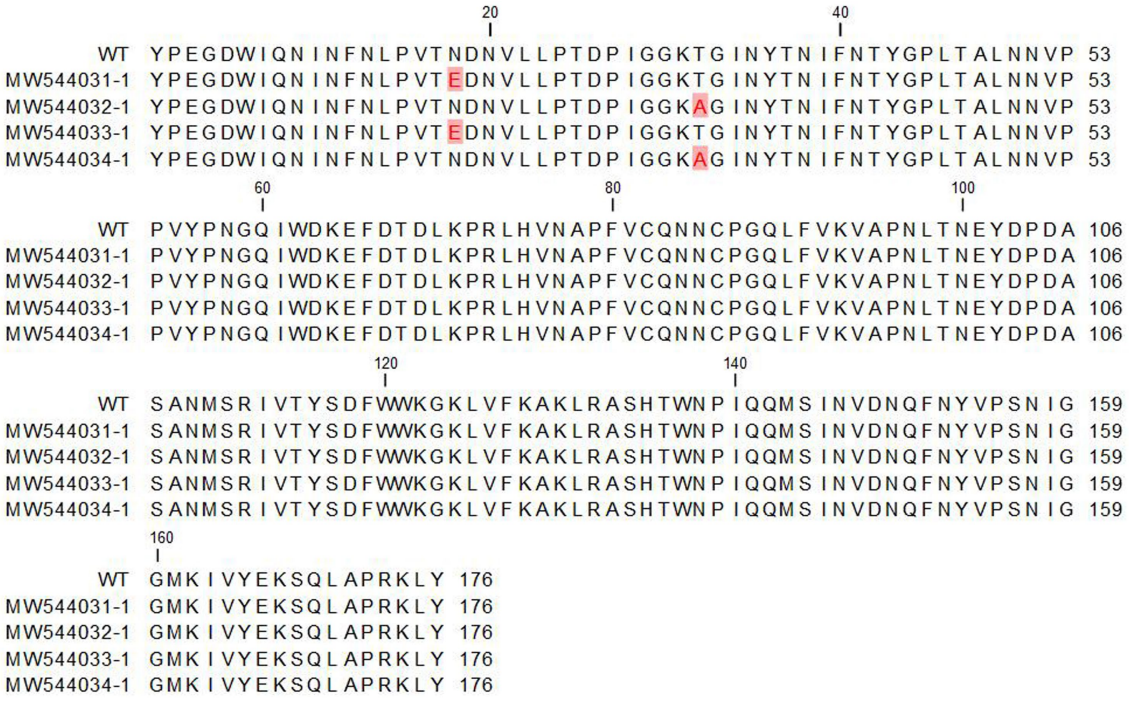

FIGURE 1
Multiple sequence alignment of the retrieved canine parvovirus VP2 proteins with the reference sequence (NP_955539.1). The alignment was performed by CLC genomic software.

2.10 Prediction of changes in canine capsid VP2 protein antigenicity

Molecular modeling investigations indicated that the predicted mutations are situated on the outer aspects of the capsid VP2 viral protein and are accessible to the surrounding liquid. This could potentially alter the immune recognition properties or antigenicity of the canine VP2 protein. Inquiries to assess the antigenicity of both the original and altered versions of the VP2 protein were submitted to the VaxiJen server (Doytchinova and Flower, 2007).

3 Results

3.1 Clinical manifestations and CPV antigen detection

In the present study, 320 clinically suspected CPV-2 infected puppies were clinically investigated in private veterinary clinics for pet animals in El-Gharbia and Kafrelsheikh provinces. The animals showed clinical signs ranging from mild to severe (Table 1). Out of 320 examined rectal swabs, 264/320 were found positive for CPV antigen by rapid IC test. The infection rate was higher in dogs aged less than 6 months (224/272) (82.3%) while dogs in the aged group of 6–12 months exhibit a lower infection rate (48/272) (17.6%). The German shepherd breed was found to be the most predisposed breed in this study (112/272) followed by Pit bull (72/272), Golden (40/272), Pikinwa (16/272) Boxer (24/272), Griffon (8/272).

3.2 PCR amplification of CPV-2 VP2 gene

Using conventional PCR, 85% (272/320) of samples were identified as positive by successful amplification a 583 bp of VP2 gene.

3.3 RFLP characterization for CPV strains

Restriction Fragment Length Polymorphism was performed successfully on 272 PCR-positive samples. The RFLP analysis of 272 samples classified 69 samples as CPV-2c strains by digestion of the purified DNA fragments into 500 bp and 83 bp fragments while the other 203 samples remained undigested indicating that they belong to CPV -2a/b strains.

3.4 Sequence alignment and phylogenetic analysis

Pairwise statistical analysis of the sequences indicated that there were from 0 to 2 substitutions of amino acids, suggesting a sequence identity ranging from 99.43 to 100% (Figure 2). Analysis of the nucleotide and deduced amino acid sequences showed changes at position 1,278–1,280 resulting in (Asn → Glu) amino acid change at residue 426 (N426E) of the VP2 in strains CPV/Egy2/2021 and CPV/Egy4/2021 which is CPV-2c specific. Another amino acid substitution at residue 440 (Thr → Ala) (T440A) was observed in strains CPV/Egy1/2021 and CPV/Egy3/2021 compared to the reference strain (accession number AAB02800.1) (Figure 3). The Phylogenetic analysis showed that the resulting CPV VP2 partial sequences belonged to two

		1	2	3	4	5
WT	1		1	1	1	1
MW544031-1	2	99.4318		2	0	2
MW544032-1	3	99.4318	98.8636		2	0
MW544033-1	4	99.4318	100.0000	98.8636		2
MW544034-1	5	99.4318	98.8636	100.0000	98.8636	

FIGURE 2
Pairwise comparison of the retrieved canine parvovirus VP2 proteins with the reference sequence (NP_955539.1). The upper right diagonal panel is the number of amino acid differences. The lower left diagonal panel is the identity%.

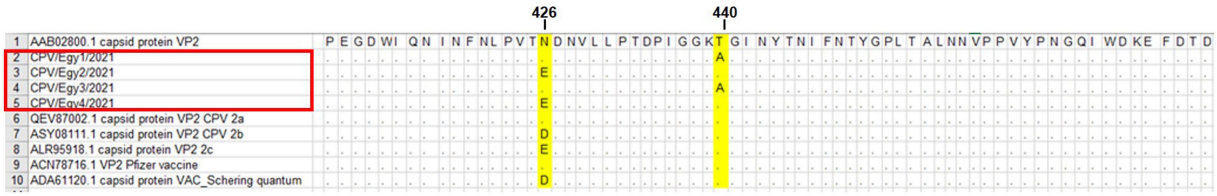

FIGURE 3
Deduced amino acid sequence alignment of CPV/Egy1/2021, CPV/Egy2/2021, CPV/Egy3/2021 and CPV/Egy4/2021 showing amino acid substitution at residue 426 and 440 in partial VP2 gene. Dots indicate identical letters.

different clades CPV-2a and CPV-2c. The strains CPV/Egy1/2021 and CPV/Egy3/2021 were clustered in the CPV-2a clade with 99.4–100% identity to other Egyptian and non-Egyptian (China, Korea, Thailand) strains. Whereas, strains CPV/Egy2/2021 and CPV/Egy4/2021 were clustered in CPV-2c clade with 99.6–100% identity to other Egyptian and non -Egyptian (Taiwan/Vietnam/China/Nigeria) strains. In addition, a comparison of the current 4 Egyptian CPV sequences to the commercially used vaccine strains CPV Pfizer (FJ197847.1) and VAC Schering quantum (GU212792.1) proved that the vaccinal strains were from a different branch (Figure 4).

3.5 Molecular modeling studies

The VP2 protein structures of the sequenced hits were generated using the SWISSMODEL website (Figures 5A, B). All the sequences exhibited the closest resemblance to the canine parvovirus capsid VP2 protein structure with the PDB ID 1P5Y, determined at a resolution of 3.20 Å. The percentage of similarity in sequence between the reference and obtained sequences was 98.86%, with a complete coverage of 100%. The structural analysis demonstrated that neither of the mutants, N426E and T440A, have binding sites at the interface of capsid proteins; instead, they are both oriented toward the solvent (Figure 5A). For deeper understanding of the impact of mutations on the overall binding strength among VP2 protein monomer interactions, calculations were performed to assess the binding energy and the dissociation constant (Kd). Results showed that both mutations induced a decrease in the binding energy of $\Delta\Delta G = -2.026$ kcal/mol and in Kd by 0.033. This indicates stronger binding of VP2 monomers in the mutant forms. This might contribute to more stabilized capsid in the mutant forms of the virus.

3.6 Predicted changes in antigenicity

Table 3 provides a summary of changes in the antigenicity of the canine parvovirus capsid VP2 protein across different variants. Antigenic probability values have been calculated, along with corresponding antigenic scores, for each protein. The antigenic probability values range from 0.5390 to 0.5513, indicating the likelihood of these variants to be recognized by the immune system. The antigenic scores mirror these probabilities and suggest a consistent antigenic nature among the listed variants. The "Antigenic probability" column seems to indicate the likelihood of a protein to trigger an immune response. The values for all variants fall within a relatively close range, suggesting that these proteins share similar potential for antigenicity. However, the mutants has a little bit lower antigenicity score, which might indicate that the mutants might escape the immune reaction and hold possible immune resistance.

4 Discussion

Canine parvovirus is a serious infectious viral disease, which attacks puppies during the first few months of their lives. Clinical diagnosis of CPV infection seems very difficult since vomiting and diarrhea are similar to other enteric diseases (Parthiban et al., 2012). In the current study, the identification and molecular characterization of CPV-2 from rectal swabs collected from diseased dogs were done using IC, PCR and RFLP followed by VP2 sequencing and phylogenetic analysis. The infection rate was higher in dogs aged less than 6 months which is in accordance with the hypothesis that maternal antibodies are transmitted via colostrum, protecting the young puppies against infectious diseases (Sharma et al., 2018). In

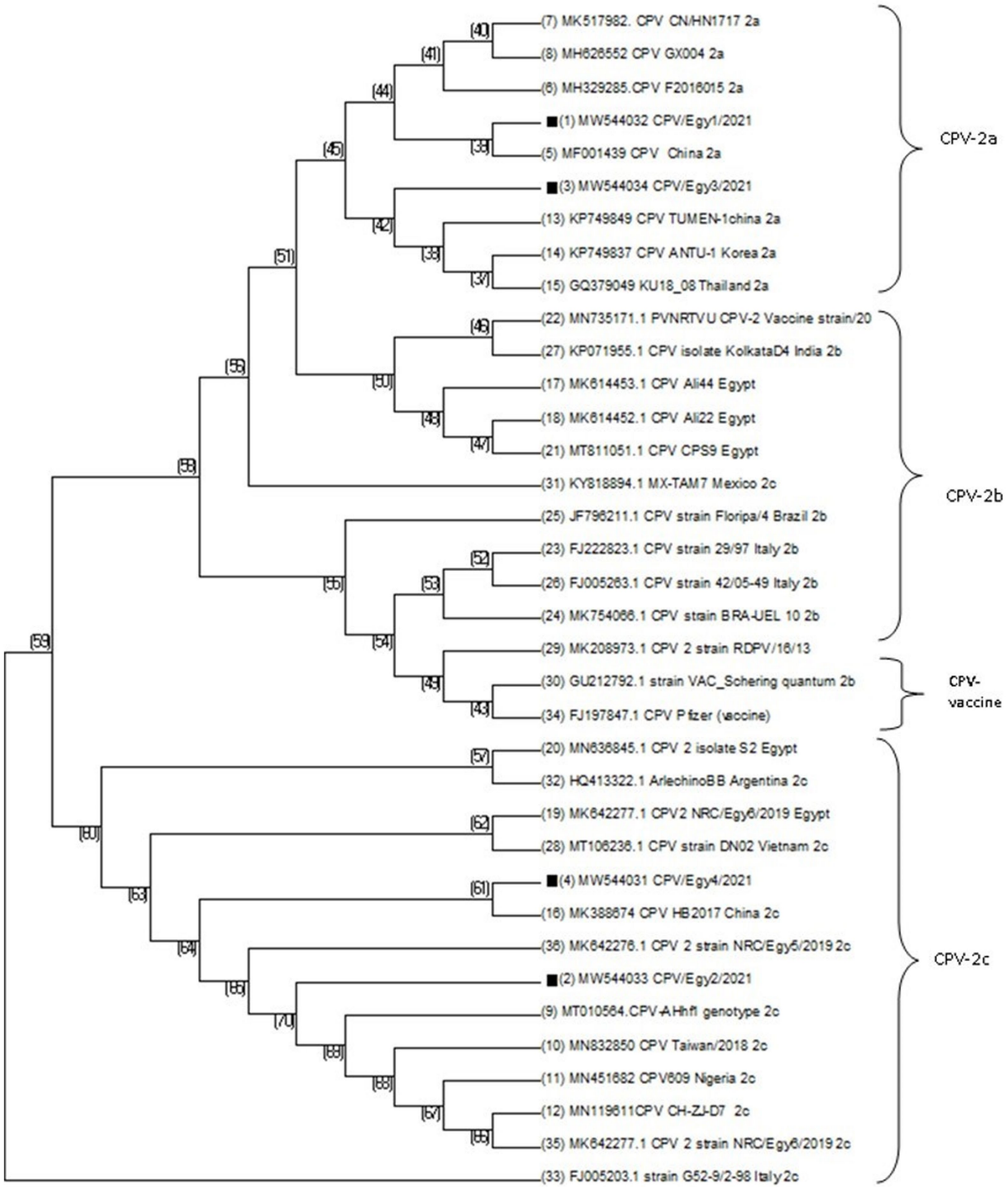

FIGURE 4
Phylogenetic analysis of CPV-2 samples based on VP2 nucleotide sequences of previously published sequences in Genbank database. Phylogenetic tree was constructed and prepared via multiple alignments of nucleotide sequences and analyzed using Neighbor-Joining method with bootstrapping (1000).

contrast, a previous work (Phukan et al., 2010) recorded the highest infection rate among dogs aging 6–12 months suggesting that it may be due to vaccination failure. Regarding breed disposition, the German shepherd breed was found to be the most predisposed breed in this study followed by Pit bull, Golden Pikinwa, Boxer and Griffon. This came in agreement with previous studies which reported that Pit bull and German shepherd are more susceptible to be infected with CPV-2 than other dog breeds (AL-Hosary, 2018; Elbaz et al., 2021). The immunochromatographic assay is a simple, inexpensive, and rapid CPV diagnostic method available in veterinary clinic practice. It was able to detect (264/272) (82.5%) of infected cases. Meanwhile, PCR technology seems more sensitive than IC for the detection of

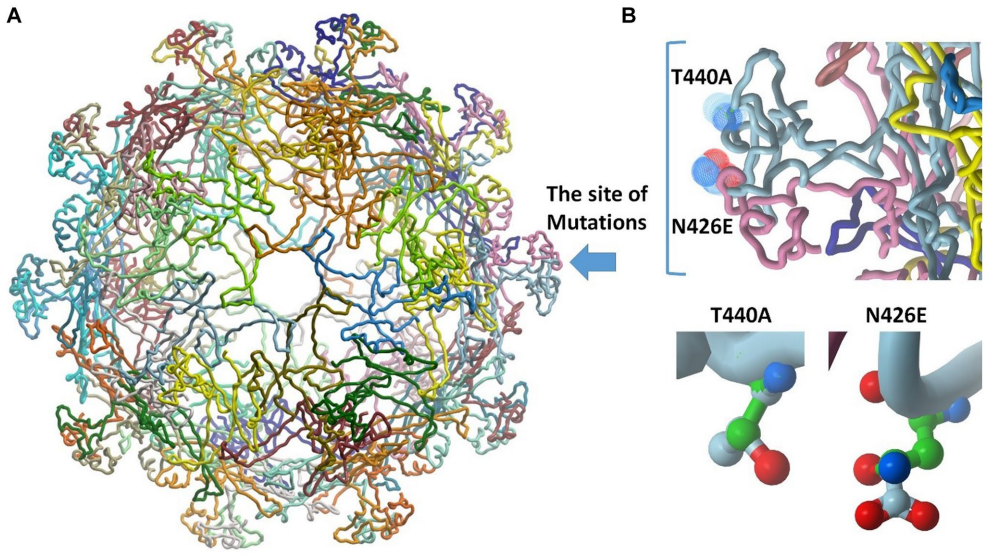

FIGURE 5
Molecular modeling studies and 3D model generation. **(A)** The obtained structure model of the retrieved sequences shows the site of mutations (blue arrow). The structure comprises 60 replicates of VP2 protein. **(B)** Insight into the site of mutation showing the N426E and T440A mutants. The backbone of alanine and asparagine are displayed in green. The structure of glutamate and threonine is colored by atoms.

TABLE 3 The changes in canine parvovirus capsid VP2 protein antigenicity.

Protein	Antigenic probability	Antigenic score
Wild type	Antigenic	0.5513
MW544031	Antigenic	0.5390
MW544032	Antigenic	0.5390
MW544033	Antigenic	0.5441
MW544034	Antigenic	0.5441

CPV-2, as it was able to detect 272/320 (85%) of infected cases based on the amplification of a highly conserved region of the VP2 gene, which is similar to previous research at the national level (Elbaz et al., 2021). Previous study revealed that negative IC test results do not exclude CPV-2 infection, but positive IC test result always indicates CPV-2 infection (Kantere et al., 2015). The high rate of PCR-positive samples (85%) suggests that CPV2 plays a significant role in producing diarrhea in puppies in Egypt, as previously documented (Zaghawa and Abualkhier, 2019; Sayed-Ahmed et al., 2020). In the present study, many animals were unvaccinated which enforces the need to increase vaccination efforts to decrease CPV-2 prevalence. However, CPV-2 negative results suggested that other contributing factors may be associated with severe diarrhea, which needs more investigation (Castillo et al., 2020). Mutation of the VP2 is critical in CPV evolution playing a significant role in the differentiation of CPV-2 variants. Molecular and sequence analysis of the VP2 gene of CPV-2 is the gold standard for identifying CPV-2 strains and provides crucial information on the circulating viruses in the study area and their relationship with other worldwide circulating strains (Hoang et al., 2019).

The RFLP approach with the MboII restriction enzyme was utilized successfully to differentiate CPV-2 variants (Moon et al., 2020). The nucleotide variation of strains CPV/Egy2/2021 and CPV/Egy4/2021 created an *Mbo*II restriction site (GAAGA) unique to CPV-2c, and so it was possible to distinguish these genotypes from the CPV-2a/2b by simple digestion of the 583 bp amplicon that yielded two fragments of about 500 and 80 bp in size. This is similar to a previous work (Buonavoglia et al., 2001) that found that the PCR-RFLP assay with enzyme *Mbo*II can only detect CPV-2c genotypes. Other studies revealed that the PCR-RFLP test had a 100% typeability, while that of the southern blot test was only (75%) (Smith et al., 2002). On the other hand, this work is inconsistent with previous research (Castro et al., 2011) which reported that CPV-2a can display the same RFLP results as CPV 2c, suggesting that *Mbo*II-based RFLP analysis is a defective technique. On the other hand, a previous study (Timurkan et al., 2019) showed that CPV 2a/2b are not digested with M*bo*II enzyme and consequently are indistinguishable, suggesting the importance of sequence analysis to definitively characterize these strains by indicating the amino acid residues (Timurkan et al., 2019). Therefore, to obtain precise results in the molecular typing of CPV-2 variants, future research must involve both sequencing and RFLP analysis (Castro et al., 2011).

Reviewing the previous studies, there are molecular characterization studies of CPV341 2 in Egypt. A lower prevalence of parvovirus (43% using PCR) (35% using IC test) was detected in an Egyptian study included three provinces (Cairo, Sohag and Assiut) (Abdel-Baky et al., 2023). Others (Zaher et al., 2020) also reported a lower prevalence of CPV-2 (40%) by rapid Ag Test Kit. In a study among 3,864 diseased dogs in Egypt, parvovirus infection was the major cause of diarrhea and vomiting (Rakha et al., 2015) The presence of CPV-2b has been reported by (Awad et al., 2019), while other study (AL-Hosary, 2018) revealed the close antigenic relationship of CPV-2a with Chinese serotypes suggested that this serotype may be introduced from China to Egypt. While (Awad et al., 2018) reported Parvovirus isolates which were 100% related to Portugalian isolates. Serotypes CPV-2b/2c were reported by Elbaz et al. (2021) and CPV- 2a and

CPV- 2b were also reported in previous Egyptian studies (AL-Hosary, 2018; Soliman et al., 2018; El-Neshwy et al., 2019). At present (Zaghawa and Abualkhier, 2019) recorded that the three variants are circulating in dog population in Egypt. In this study, nucleotide sequencing of four selected samples showed that they belong to CPV-2 type 2a and 2c.

The exposed region that comprises amino acids 267–498 of the VP2 protein is identified as the large GH loop which shows the greatest variability among CPV variants exhibiting the main antigenic site which manages tissue tropism, host range and antigenicity of virions by interlinkage with cell transferrin receptors (TfR). Numerous studies reported that TfR have a significant role in the host cell susceptibility to CPV 2 infection. Replacement of amino acids of the 3 fold residues may also interfere with the neutralization of virus by monoclonal antibodies (Fagbohun and Omobowale, 2018). Since the appearance of the new viral strains, research about mutations of their amino acid has been ongoing (Hao et al., 2020). By continuous tracking of these point mutations, the emergence of new sublineages can be expected before significant changes in amino acids take place (Jantafong et al., 2022). These mutations aid in capsid stability, enhanced receptor-binding capability, resulting in wide host range, and increased the pathogenicity of the new viruses (Ndiana et al., 2022). Here, amino acid substitutions in the VP2 were detected at residue 426 in samples CPV/Egy2/2021 and CPV/Egy4/2021 (N426E) confirming the CPV-2c genotype. This amino acid substitution tendency of (N426E) (CPV-2c carrying a Glu) on residue 426 of VP2 was first detected in 2000 in Italy (Jantafong et al., 2022). This mutation has been also emphasized by Elbaz et al. (2021) who confirmed that the main residue to distinguish between the three strains was residue 426. Changing an asparagine (N) to glutamine (E) in a protein can have significant ramifications for its arrangement, operation, and interactions. Asparagine is an uncharged, polar amino acid featuring an amide side chain, while glutamine, also polar, and bears a negative charge because of its carboxylic acid side chain (illustrated in Figure 5B). The shift from a neutral side chain (Asn) to a negatively charged one (Glu) could introduce repulsions or attractions with adjacent residues due to electrostatic forces. This alteration might induce modifications in local structural components like α-helices and β-sheets. The difference in size between the two side chains might cause clashes or create novel chances for interactions within the protein's three-dimensional structure. The negative charge of glutamine could establish fresh interactions or disrupt existing ones, potentially influencing the protein's operation. Another amino acid mutation at residue 440 (T440A) in CPV-2a strains (CPV/Egy1/2021 and CPV/Egy3/2021) were also detected in this study. This residue which represents at the top of the threefold spike was also recorded as the major viral antigenic site and that high rates of this substitution are associated with the emerging of new CPV 2 variants (Capozza et al., 2023). This was similar to previous research (Timurkan et al., 2019) reported that (T440A) mutations have emerged probably as a result of antigenic drift of the viral genome leading to positive selection to improve escaping from the immune system suggesting that these modifications could lower vaccine efficacy and/or expand the pathogenicity of CPV-2 variants. This amino acid T440A mutation in CPV-2a strains has also observed in Italy (Dei Giudici et al., 2017), Taiwan (Chiang et al., 2016), and Korea (Yoon et al., 2009). While a previous study (Dei Giudici et al., 2017) has reported this mutation also in CPV-2b and CPV-2c strains. The mutation of threonine to alanine (depicted in Figure 5B) can yield varied outcomes based on the protein, its particular function, and the nearby conditions. Threonine (T), a polar amino acid, has a hydroxyl (-OH) group in its side chain. It is comparatively larger and bulkier than alanine (A), a nonpolar amino acid with a simple methyl group in its side chain. The hydroxyl group in threonine often engages in hydrogen bonding interactions. In contrast, alanine lacks a hydroxyl group and usually avoids hydrogen bonding interactions. It is commonly known for promoting helix formation due to its compact side chain. Substituting threonine (polar) with alanine (nonpolar) could lead to shifts in the local hydrophobic properties of the protein segment where the alteration happens. If threonine participated in hydrogen bonding interactions, the mutation could disturb those connections, potentially impacting the protein's stability and folding. On the other hand, deduced amino acid alignment showed some unique mutations (S542L, H543Q, Q549H, and N557T) in the CPV-2 c serotype which were not detected in the present study.

5 Conclusion

A molecular survey of CPV-2 in domestic dogs was carried out in two governorates at the Delta region of Egypt. Results revealed that both CPV-2a and CPV-2c are obviously circulating in the study area. Deduced amino acid sequence analysis showed changes at residue (N426E) and residue (T440A). Continuous and periodical monitoring and molecular detection of CPV-2 variants should be further explored on a large scale investigations to determine the dynamics of the prevalent variants in contributing pathogenicity, host range, vaccine failure, and even the sensitivity of diagnostic tests. These data will facilitate early and proper diagnosis of the disease and aid in the development of different strategies for future vaccination.

Data availability statement

The original contributions presented in the study are included in the article/supplementary material, further inquiries can be directed to the corresponding authors.

Ethics statement

The study meets the guidelines of the Declaration of Helsinki and obtained the approval (approval number KFS-2019/09) from the Institutional Review Board of the Faculty of Veterinary Medicine, Kafrelsheikh University, Egypt. The studies were conducted in accordance with the local legislation and institutional requirements. Written informed consent was obtained from the owners for the participation of their animals in this study.

Author contributions

AM: Conceptualization, Data curation, Formal analysis, Investigation, Supervision, Validation, Visualization, Writing – original draft, Writing – review & editing, Methodology, Project administration, Software. IE-K: Conceptualization, Data curation, Investigation, Supervision, Visualization, Writing – original draft, Project administration. ER-Á: Data curation, Formal analysis, Validation, Visualization, Writing – original draft, Writing – review & editing,

Funding acquisition, Resources. EK: Conceptualization, Data curation, Investigation, Project administration, Supervision, Visualization, Writing – original draft, Formal analysis, Methodology, Software, Validation, Writing – review & editing. NA: Data curation, Formal analysis, Validation, Writing – original draft, Writing – review & editing, Conceptualization, Investigation, Methodology, Project administration, Software, Supervision. AlA: Formal analysis, Project administration, Validation, Visualization, Writing – original draft, Funding acquisition, Resources. ME-k: ___. AhA: Funding acquisition, Investigation, Resources, Validation, Writing – original draft, Writing – review & editing. EE: Conceptualization, Data curation, Formal analysis, Funding acquisition, Investigation, Resources, Supervision, Validation, Visualization, Writing – original draft, Writing – review & editing.

Funding

The author(s) declare financial support was received for the research, authorship, and/or publication of this article. This study was supported by Princess Nourah bint Abdulrahman University Researchers Supporting Project number (PNURSP2023R23), Princess Nourah bint Abdulrahman University, Riyadh, Saudi Arabia.

Conflict of interest

The authors declare that the research was conducted in the absence of any commercial or financial relationships that could be construed as a potential conflict of interest.

Publisher's note

All claims expressed in this article are solely those of the authors and do not necessarily represent those of their affiliated organizations, or those of the publisher, the editors and the reviewers. Any product that may be evaluated in this article, or claim that may be made by its manufacturer, is not guaranteed or endorsed by the publisher.

References

Abbasi, W. A., Abbas, S. A., and Andleeb, S. (2021). PANDA: predicting the change in proteins binding affinity upon mutations by finding a signal in primary structures. *J. Bioinforma. Comput. Biol.* 19:2150015. doi: 10.1142/S0219720021500153

Abdel-Baky, M. M., El-Khabaz, K. A., Abdelbaset, A. E., et al. (2023). Clinico-epidemiological survey of feline parvovirus circulating in three Egyptian provinces from 2020 to 2021. *Arch. Virol.* 168:126. doi: 10.1007/s00705-023-05751-4

AL-Hosary, A. A. (2018). Detection and molecular characterization of parvovirus serotypes in Egypt. *J. Adv. Vet. Res.* 8, 79–83.

Amthal, AF. Molecular characterization of canine Parvovirus-2 in Egypt. Master Thesis, Cairo University, Egypt (2014).

Awad, R., Attallah, A., and Khalil, W. (2019). Prevalence of canine parvovirus infection in Egypt: reliability of some molecular methods used for its diagnosis in dogs. *J. Biol. Sci.* 19, 192–200. doi: 10.3923/jbs.2019.192.200

Awad, R., Khalil, W., and Attallah, A. (2018). Epidemiology and diagnosis of feline panleukopenia virus in Egypt: clinical and molecular diagnosis in cats. *Vet. World* 11, 578–584. doi: 10.14202/vetworld.2018.578-584

Buonavoglia, C., Martella, V., Pratelli, A., Tempesta, M., Cavalli, A., Buonavoglia, D., et al. (2001). Evidence for evolution of canine parvovirus type 2 in Italy. *J. Gen. Virol.* 82, 3021–3025. doi: 10.1099/0022-1317-82-12-3021

Capozza, P., Buonavoglia, A., Pratelli, A., Martella, V., and Decaro, N. (2023). Old and novel enteric parvoviruses of dogs. *Pathogens* 12:722. doi: 10.3390/pathogens12050722

Castillo, C., Neira, V., Aniñir, P., Grecco, S., Pérez, R., Panzera, Y., et al. (2020). First molecular identification of canine parvovirus type 2 (CPV2) in Chile reveals high occurrence of CPV2c antigenic variant. *Front. Vet. Sci.* 7:194. doi: 10.3389/fvets.2020.00194

Castro, T., Costa, E., Leite, J., Labarthe, N., and Garcia, R. C. (2011). Monitoring of canine parvovirus (CPV) strains detected in vaccinated puppies in Brazil. *Res. Vet. Sci.* 90, 336–340. doi: 10.1016/j.rvsc.2010.06.005

Charoenkul, K., Tangwangvivat, R., Janetanakit, T., Boonyapisitsopa, S., Bunpapong, N., Chaiyawong, S., et al. (2019). Emergence of canine parvovirus type 2c in domestic dogs and cats from Thailand. *Transbound. Emerg. Dis.* 66, 1518–1528. doi: 10.1111/tbed.13177

Chiang, S.-Y., Wu, H.-Y., Chiou, M.-T., Chang, M.-C., and Lin, C.-N. (2016). Identification of a novel canine parvovirus type 2c in Taiwan. *Virol. J.* 13, 1–7.

Dei Giudici, S., Cubeddu, T., Giagu, A., Sanna, G., Rocca, S., and Oggiano, A. (2017). First molecular characterization of canine parvovirus strains in Sardinia Italy. *Arch. Virol.* 162, 3481–3486. doi: 10.1007/s00705-017-3457-3

Doytchinova, I. A., and Flower, D. R. (2007). VaxiJen: a server for prediction of protective antigens, tumour antigens and subunit vaccines. *BMC Bioinform.* 8, 1–7.

Elbaz, E., El-Tholoth, M., Elfadl, E. A. A., and Mosad, S. M. (2021). Molecular investigation on the presence of canine parvovirus in Egypt. *Comp. Immunol. Microbiol. Infect. Dis.* 74:101576. doi: 10.1016/j.cimid.2020.101576

El-Neshwy, W., El-Zahar, H., Morsi, A., and Shety, T. (2019). Molecular and phylogenetic analysis of canine parvovirus variants (2a-2b-2c) in Egypt. *Res J Vet Pract.* 7, 74–82.

Fagbohun, O., and Omobowale, T. (2018). Sequence and phylogenetic analysis of canine parvovirus-2 isolates in dogs revealed circulation of three subtypes in Nigeria. *Virus* 29, 411–415. doi: 10.1007/s13337-018-0475-z

Hao, X., He, Y., Wang, C., Xiao, W., Liu, R., Xiao, X., et al. (2020). The increasing prevalence of CPV-2c in domestic dogs in China. *PeerJ.* 8:e9869. doi: 10.7717/peerj.9869

Hoang, M., Wu, H. Y., Lien, Y. X., Chiou, M. T., and Lin, C. N. (2019). A SimpleProbe® real-time PCR assay for differentiating the canine parvovirus type 2 genotype. *J. Clin. Lab. Anal.* 33:e22654. doi: 10.1002/jcla.22654

Jantafong, T., Ruenphet, S., Garner, H. R., and Ritthipichai, K. (2022). Tracing the genetic evolution of canine parvovirus type 2 (CPV-2) in Thailand. *Pathogens* 11:1460. doi: 10.3390/pathogens11121460

Kantere, M. C., Athanasiou, L. V., Spyrou, V., Kyriakis, C. S., Kontos, V., Chatzopoulos, D. C., et al. (2015). Diagnostic performance of a rapid in-clinic test for the detection of canine parvovirus under different storage conditions and vaccination status. *J. Virol. Methods* 215-216, 52–55. doi: 10.1016/j.jviromet.2015.02.012

Kim, S.-G., Kang, M.-H., and Park, H.-M. (2017). Comparative study of two point-of-care enzyme-linked immunosorbent assays for the detection of antibodies against canine parvovirus and canine distemper virus. *Pak. Vet. J.* 37, 405–410.

Lambe, U., Guray, M., Bansal, N., Kumar, P., Joshi, V. G., Khatri, R., et al. (2016). Canine parvovirus-an insight into diagnostic aspect. *J. Exp. Biol.* 4, 279–290. doi: 10.18006/2016.4(3S).279.290

Liu, J., Wu, Q., and Qiu, H. (2017). Effect of Kuqin compound Total polysaccharides on CD4+, CD8+ T cells and cytokines of blood in dogs infected by canine parvovirus. *Pak. Vet. J.* 37, 305–310.

Moon, B. Y., Jang, J., Kim, S. H., Kim, Y. H., Hk, L., So, B., et al. (2020). Genetic characterization of canine parvovirus type 2c from domestic dogs in Korea. *Transbound. Emerg. Dis.* 67, 1645–1653. doi: 10.1111/tbed.13501

Ndiana, L. A., Lanave, G., Zarea, A. A. K., Desario, C., Odigie, E. A., Ehab, F. A., et al. (2022). Molecular characterization of carnivore protoparvovirus 1 circulating in domestic carnivores in Egypt. *Front. Vet. Sci.* 9:932247. doi: 10.3389/fvets.2022.932247

Parthiban, M., Divya, K. C., Kumanan, K., and Bargavi, D. (2012). A rapid and highly reliable field-based LAMP assay of canine parvovirus. *Acta Virol.* 56, 71–74. doi: 10.4149/av_2012_01_71

Phukan, A., Baishya, B., Deka, D., and Boro, P. (2010). Prevalence of canine parvovirus infection in Assam. *Indian Vet. J.* 87, 972–974.

Rakha, G. M., Abdl-Haleem, M. M., Farghali, H. A., and Abdel-Saeed, H. (2015). Prevalence of common canine digestive problems compared with other health problems in teaching veterinary hospital, Faculty of Veterinary Medicine, Cairo University. *Egypt. Vet. World* 8, 403–411. doi: 10.14202/vetworld.2015.403-411

Saei, H. D., Javadi, S., Akbari, S., Hadian, N., and Zarza, E. (2017). Molecular characterization of canine parvovirus (CPV) antigenic variants from healthy and diarrheic dogs in Urmia region, Iran. Iranian. *J. Vet. Med.* 11, 9–19.

Sayed-Ahmed, M. Z., Elbaz, E., Younis, E., and Khodier, M. (2020). Canine parvovirus infection in dogs: prevalence and associated risk factors in Egypt. *World Vet. J.* 10, 571–577. doi: 10.54203/scil.2020.wvj68

Sharma, K. K., Kalyani, I. H., Pandya, S. M., and Vala, J. A. (2018). Diagnosis and characterization of canine parvovirus-2 affecting canines of South Gujarat India. *Acta Vet. Brno.* 87, 247–254. doi: 10.2754/avb201887030247

Smith, S., Cantet, F., Angelini, F., Marais, A., Mégraud, F., Bayerdöffer, E., et al. (2002). Discriminatory power of RAPD,PCR-RFLP and southern blot analyses of ureCD or ureA gene probes on *Helicobacter pylori* isolates. *Zeitschrift für Naturforschung C.* 57, 516–521.

Soliman, R., Baker, N., Nasr, M., and Khodeir, M. (2018). Clinical, virological and molecular characterization of canine parvovirus in dogs. *Euro. J. Pharm. Med. Res.* 5, 525–535.

Studer, G., Rempfer, C., Waterhouse, A. M., Gumienny, R., Haas, J., and Schwede, T. (2020). QMEANDisCo—distance constraints applied on model quality estimation. *Bioinformatics* 36, 1765–1771. doi: 10.1093/bioinformatics/btz828

Sun, Y., Cheng, Y., Lin, P., Zhang, H., Yi, L., Tong, M., et al. (2019). Simultaneous detection and differentiation of canine parvovirus and feline parvovirus by high resolution melting analysis. *BMC Vet. Res.* 15, 1–8. doi: 10.1186/s12917-019-1898-5

Timurkan, M. O., Polat, P. F., Şahan, A., Dinçer, E., and Aksoy, G. (2019). Molecular and restriction fragment length polymorphism analysis of canine parvovirus 2 (CPV-2) in dogs in Southeast Anatolia Turkey. *Onderstep. J. Vet. Res.* 86, 1–8.

Waterhouse, A., Bertoni, M., Bienert, S., Studer, G., Tauriello, G., Gumienny, R., et al. (2018). SWISS-MODEL: homology modelling of protein structures and complexes. *Nucleic Acids Res.* 46, W296–W303. doi: 10.1093/nar/gky427

Yip, H. Y. E., Peaston, A., Woolford, L., Khuu, S. J., Wallace, G., Kumar, R. S., et al. (2020). Diagnostic challenges in canine parvovirus 2c in vaccine failure cases. *Viruses* 12:980. doi: 10.3390/v12090980

Yoon, S. H., Jeong, W., Kim, H.-J., and An, D.-J. (2009). Molecular insights into the phylogeny of canine parvovirus 2 (CPV-2) with emphasis on Korean isolates: a Bayesian approach. *Arch. Virol.* 154, 1353–1360. doi: 10.1007/s00705-009-0444-3

Zaghawa, A., and Abualkhier, M. (2019). Genetic and molecular typing of canine parvovirus strains circulating in symptomatic dogs in Egypt. *J. Curr. Vet. Res.* 1, 75–85. doi: 10.21608/jcvr.2019.36556

Zaher, K. S., El-Dabae, W. H., El-Sebelgy, M. M., Aly, N. I., and Salama, Z. T. (2020). Genotyping and phylogenetic analysis of canine parvovirus circulating in Egypt. *Vet. World* 13, 326–333. doi: 10.14202/vetworld.2020.326-333

Zhou, P., Zeng, W., Zhang, X., and Li, S. (2017). The genetic evolution of canine parvovirus–a new perspective. *PLoS One* 12:e0175035. doi: 10.1371/journal.pone.0175035

frontiers | Frontiers in Microbiology

TYPE Original Research
PUBLISHED 10 January 2024
DOI 10.3389/fmicb.2023.1290302

OPEN ACCESS

EDITED BY
Jingqiang Ren,
Wenzhou University, China

REVIEWED BY
Lauro Velazquez-Salinas,
Agricultural Research Service (USDA), United States
Yu Liu,
Heilongjiang Bayi Agricultural University, China

*CORRESPONDENCE
Xinglong Wang
✉ wxlong@nwsuaf.edu.cn
Xiaowen Li
✉ lxw8272@163.com

†These authors have contributed equally to this work and share first authorship

RECEIVED 07 September 2023
ACCEPTED 18 December 2023
PUBLISHED 10 January 2024

CITATION
Li Y, Wang Z, Qing J, Hu D, Vo HT, Thi KT, Wang X and Li X (2024) Application of propidium monoazide quantitative PCR to discriminate of infectious African swine fever viruses.
Front. Microbiol. 14:1290302.
doi: 10.3389/fmicb.2023.1290302

Application of propidium monoazide quantitative PCR to discriminate of infectious African swine fever viruses

Yang Li[1†], Zewei Wang[1†], Jie Qing[1], Dajun Hu[2], Hong Trang Vo[2], Kim Thanh Thi[2], Xinglong Wang[3*] and Xiaowen Li[1,2,3*]

[1]Xiajin New Hope Liuhe Agriculture and Animal Husbandry Co., Ltd., (Shandong Engineering Laboratory of Pig and Poultry Healthy Breeding and Disease Diagnosis Technology), Dezhou, China, [2]New Hope Binh Phuoc livestock Co., Ltd., Huyen Hon Quan, Vietnam, [3]College of Veterinary Medicine, Northwest A&F University, Xianyang, Yangling, China

Introduction: The detection of African swine fever virus (ASFV) is commonly performed using quantitative real-time PCR (qPCR), a widely used virological method known for its high sensitivity and specificity. However, qPCR has a limitation in distinguishing between infectious and inactivated virus, which can lead to an overestimation of viral targets.

Methods: To provide insights into ASFV infectivity, we evaluated the suitability of PMAxx, an improved version of propidium monoazide (PMA), as a means to differentiate between infectious and non-infectious ASFV. Pre-treatment with 50 μM PMAxx for 15 min significantly reduced the qPCR signal of ASFV in the live vaccine. Additionally, thermal treatment at 85°C for 5 min effectively inactivated the live ASFV in the vaccine. Based on a standard curve, the sensitivity of the PMAxx-qPCR assay was estimated to be approximately 10 copies/μL. Furthermore, we observed a strong agreement between the results obtained from PMAxx-qPCR and pig challenge experiments. Moreover, we utilized the PMAxx-qPCR assay to investigate the persistence of ASFV, revealing a close relationship between viral persistence and factors such as temperature and type of piggery materials.

Conclusion: The findings of this study suggest that pre-treating viruses with PMAxx prior to qPCR is a reliable method for distinguishing between infectious and non-infectious ASFV. Thus, integrating of PMAxx-qPCR into routine diagnostic protocols holds potential for improving the interpretation of positive ASFV results obtained through qPCR.

KEYWORDS

African swine fever virus, propidium monoazide, quantitative PCR, viability, persistence

Introduction

African swine fever (ASF) is a devastating disease that affects domestic pigs and wild boars. ASF outbreaks are currently occurring in Africa, Eastern Europe and Asia, causing significant economic losses globally (Costard et al., 2009; Norbert Mwiine et al., 2019). The African swine fever virus (ASFV), the pathogen responsible for ASF, is the sole member

of the *Asfarviridae* family. It has a double-stranded DNA genome of approximately 180–190 kb and encodes over 150 open reading frames (ORFs) (Dixon et al., 2013). ASFV can survive in the environment for extended periods and can be transmitted through infected tick bites, direct contact with infected pigs, and contaminated materials (Gaudreault et al., 2020; Pereira De Oliveira et al., 2020). Due to the lack of commercial vaccines in the past few decades, preventing severe ASF outbreaks heavily relies on restricting animal movements and culling infected herds (Zhang et al., 2020; Borca et al., 2021). Recently, a promising recombinant vaccine candidate, ASFV-G-1I177L, has been developed by deleting the I177L gene from the genome of the highly virulent ASFV Georgia strain (Borca et al., 2020, 2021; Tran et al., 2021, 2022). This attenuated vaccine has been authorized as the first commercial gene-modified live vaccine in Vietnam and has shown no residual toxicity in long-term clinical studies (Borca et al., 2023). However, the vaccine can be only given to pigs aged between 8 and 10 weeks according to the directions. The residual infectious particles in the environment poses significant challenges to ASF risk management in the clearance of ASFV.

Quantitative real-time polymerase chain reaction (qPCR) is highly sensitive and specific for detecting the presence of viral genomes (Choi and Jiang, 2005; Hamza et al., 2011). However, qPCR cannot differentiate between infectious and inactivated viruses to directly indicate infectivity (Fittipaldi et al., 2010). Methods that can rapidly provide information about viral infectivity are of interest, given that only active viruses pose a public health threat (Knight et al., 2013). Various methods have been employed to detect infectious viruses, including cytopathic effect, fluorescent microscopy, flow cytometry, and detection of genome or envelope integrity (Zeng et al., 2022). Detection methods involving cell culture are considered the gold standard for quantifying certain viral infectivity. However, ASFV cultivation requires costly primary porcine alveolar macrophages and is constrained to biosafety level 3 laboratories (Blackmer et al., 2000; Rodríguez et al., 2009; Hamza et al., 2011). Additionally, the proposal to analyze the integrity of viral genomes through PCR amplification of long target regions may be related to viral infectivity (Li et al., 2002; Simonet and Gantzer, 2006). Nevertheless, viral inactivation can occur without damaging the viral genome, limiting the general applicability of long target region PCR as a surrogate marker for viral infectivity (Hamza et al., 2011).

Cellular or envelope integrity is one of the characteristics used to distinguish between live and inactivated cells or enveloped viruses. One promising strategy to overcome the limitations of qPCR is pre-treating samples with photosensitizing dyes such as ethidium monoazide (EMA) and propidium monoazide (PMA) before qPCR (Parshionikar et al., 2010). This approach has been successfully used to differentiate infectious and non-infectious bacteria, protozoa, nematode eggs, fungi and viruses (Brescia et al., 2009; Fittipaldi et al., 2010; Graiver et al., 2010; Kim et al., 2011; Dreo et al., 2014). Theoretically, the dyes are membrane-impermeant and bind irreversibly to nucleic acids by photoactivation, leaving the DNA in viable cells intact (Nocker et al., 2006). Modified nucleic acid structures interfere with PCR amplification, resulting in reduced signal intensity in subsequent qPCR (Rudi et al., 2005; Nocker and Camper, 2009). Moreover, light exposure leads to the reaction of unbound excess dye with water molecules, preventing the purified DNA from being further modified in cells with intact cell membranes (Nocker and Camper, 2009). Some studies have shown significant DNA loss in the genomic DNA of live bacteria induced by EMA (Flekna et al., 2007), while PMA has been demonstrated to be more selective, only penetrating dead bacterial cells and not cells with intact membranes (Nocker et al., 2006). PMAxx, an improved version of PMA with a higher molecular charge, inhibits PCR amplification of modified DNA templates through a combination of removal of modified DNA during purification and inhibition of template amplification by DNA polymerases (**Figure 1**). In experimental bacterial strains, PMAxx increased the difference between live and dead bacteria by an additional 3 to 7 CT values compared to PMA (Nocker et al., 2006). Recently, Liu et al. conducted a study to investigate the addition of Triton X-100 for enhancing the penetration of PMAxx into inactivated ASFV virions, which may be helpful to interpret the results, though the infectivity of samples was still distinguishable by PMAxx-qPCR without the assistance of Triton X-100 (Liu et al., 2022). Moreover, these experiments were carried out solely under laboratory conditions and the validity of the results was not confirmed through animal inoculation.

The objective of this study was to evaluate the applicability of pure PMAxx pre-treatment for differentiating infectious and non-infectious ASFV and the correlation between PMAxx-qPCR detection results and animal challenges. We also used PMAxx-qPCR to assess the persistence of ASFV on commonly encountered materials in pig farms. Our data demonstrate that PMAxx-qPCR detection can improve the interpretation of ASFV qPCR-positive results and provide better risk management strategies.

Materials and methods

Preparation of ASFV samples

NAVET-ASFVAC vaccine containing live-attenuated ASFV-G-ΔI177L strain was purchased from Navetco National Veterinary Joint Stock Company (NAVETCO). The vaccine was diluted with saline at a twofold dilution ratio (ranging from 1:10 to 1:2560), aliquoted and stored at −80°C until use. The experiments of animal inoculation and viral persistence using NAVET-ASFVAC vaccine were performed in a fattening pig farm in Binh Phuoc province, Vietnam.

PMAxx treatment

Each sample was divided into three portions: one portion was heat-inactivated at 85°C for 10 min, while the other two portions were kept at room temperature. PMAxx (Biotium, Inc., Hayward, CA, USA) was dissolved in deionized water to obtain a stock solution of 1 mM. Then, 10 μL of the PMAxx solution was added to 190 μL aliquots of both the non-heated and heat-treated samples, resulting in a final concentration of 50 μM. Additionally, 10 μL of deionized water was added to an untreated aliquot as a control template for standard qPCR. These three aliquots were incubated in the dark at 37°C for 15 min with occasional mixing to allow reagent penetration. Subsequently, the samples were irradiated with a PMA-Lite^{TM} LED photoactivator (E90002, Biotium) at room

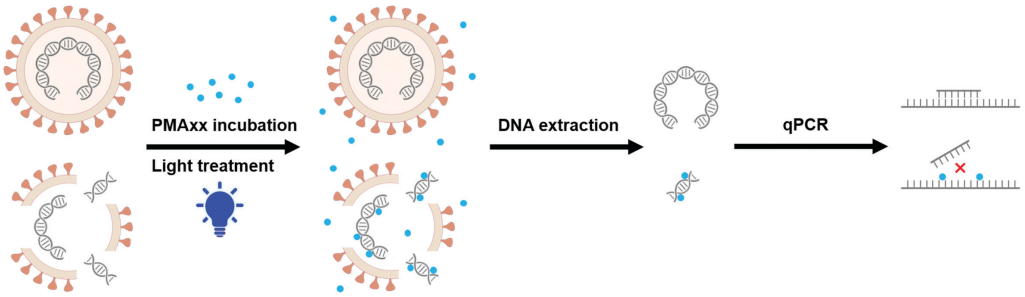

FIGURE 1
Proposed mechanism of PMAxx modification of dead viruses. The envelope impermeant PMAxx dye (purple dot) selectively penetrates dead viruses with compromised membranes. Upon exposure to light, PMAxx covalently modifies dissociated DNA. Genomic DNA was extracted from these samples, while some of the PMAxx-modified DNA became insoluble and was lost during DNA extraction. Subsequent qPCR amplification of modified DNA templates is inhibited, allowing selective quantification of DNA from viable viruses.

temperature for 15 min. The experiment was repeated in triplicate, and DNA extraction of the samples was performed. Only when the CT values of the heat-treated-PMAxx treated aliquots were significantly higher than those of the PMAxx treated aliquots, the presence of ASFV viral particles was considered to be existed.

Nucleic acid extraction

Samples were vortexed and centrifuged at 8,000 × *g* for 2 min. Genomic DNA from the samples (200 μL) was extracted using the Virus DNA Extraction Kit II (Geneaid, Taiwan) according to the instructions provided. The extracted nucleic acid was eluted in 50 μL elution buffer and stored at 4°C for subsequent qPCR analysis.

Quantitative PCR (qPCR)

African swine fever virus-specific primers (forward: 5′-AAAATGATACGCAGCGAAC-3′, reverse: 5′-TTGTTTACCT GCTGTTTGGAT-3′) and a probe (5′-FAM-TTCACAGCATT TTCCCGAGAACT-BHQ1-3′) targeting the B646L gene were used for qPCR detection. A qPCR reaction mixture of 20 μL was prepared, containing 10 μL PerfectStart R II Probe qPCR SuperMix (TransGen Biotech, China), 0.5 μM primers and probe, 5 μL DNA template, and PCR-grade water. The reaction consisted of an initial denaturation step at 95°C for 10 min, followed by 40 cycles of denaturation at 95°C for 15 s, annealing at 60°C for 15 s, and extension at 72°C for 30 s. qPCR results were recorded using the Step One Plus^{TM} Real-Time PCR System (ABI, 4376600).

Standard curve

A standard plasmid containing the ASFV B646L gene was constructed as described previously (Li et al., 2022). Briefly, partial sequences of the B646L gene were amplified by PCR. The products and pMD18-T plasmids (D101A, Takara, Japan) were digested with the same restriction enzymes. The fragment was gel-purified and ligated to the vector using DNA ligase (C301-01, Vazyme) following standard procedures. Positive clones were screened and identified by sequencing. The standard curve was constructed using logarithmic 10-fold dilutions ranging from 2.5×10^7 to 2.5 genome copies. The ASFV genome copy numbers corresponding to the copy numbers of the standard plasmid were calculated using the following formula:

$$Copy\ number = \frac{m \times 6.022 \times 10^{23}}{1,840,105.22 \times 1 \times 10^{9}}$$

where m (/g) is the amount of plasmids measured using a BioSpec-nano Micro-volume UV-Vis Spectrophotometer (Shimadzu, Kyoto, Japan), 6.022×10^{23} is the Avogadro number, 1,840,105.22 (Da) is the molecular weight of standard plasmids calculated using the Sequence Manipulation Suite (Stothard, 2000), and 1×10^9 is used to convert the molecular weight of the plasmids to nanograms. A fresh dilution set was prepared to construct the standard curve for each qPCR run, which could convert CT values obtained from qPCR analysis to ASFV genome equivalents.

Animal inoculation

The NAVET-ASFVAC vaccine was diluted with saline (1:2560) and divided into four portions, with three portions (Groups B, C, and D) subjected to water bath heating at 85°C for 0.5, 1, and 10 min, respectively. The infectiousness of ASFV particles in the samples was quantified using PMA-qPCR. Then, each sample was injected into the muscles of three ASFV-negative fattening pigs. Throat swab samples were collected from each fattening pig 7 days later as previously described (Li et al., 2022) and ASFV DNA was measured using qPCR.

Detection of ASFV persistence on the piggery materials

The vaccine was diluted with saline to a CT value of 25. Latex gloves and packaging bags from the pig farm were cut into squares with sides measuring 2 cm and soaked in the vaccine. Dry feed particles of approximately 1 cm in length were selected, and 50 μL of vaccine was added to each particle. The foam

plastic heads of fertilization tubes were dipped into the vaccine. These materials were then thoroughly air-dried and placed in an incubator at temperatures of 4, 15, or 25°C for several days. The samples' ASFV infectivity was measured by PMAxx-qPCR in three separate experiments after dissolution in 2 mL of saline. The experiments were performed in a fattening pig farm in Binh Phuoc province, Vietnam.

Statistical analysis

The significance of differences between CT values was evaluated by unpaired Student's *t*-test using GraphPad Prism v8.3.0. In all cases, a value of $P < 0.05$ was considered significant.

Results

Optimization of the experimental conditions

To determine the appropriate working concentration, various doses of PMAxx were added to ASFV-positive vaccine samples and exposed to light for 15 min. Subsequently, genomic DNA was extracted and subjected to qPCR using ASFV-specific primers and probes. The results displayed in **Figure 2A** demonstrated that increasing concentrations of PMAxx led to higher CT values, indicating greater inhibition of qPCR amplification. Concentrations ranging from 25 to 50 μM led to substantial inhibition, whereas higher concentrations did not entirely eliminate qPCR signals in samples with high ASFV content.

To optimize the efficacy of PMAxx-DNA cross-linking, ASFV nucleic acids were incubated with 50 μM PMAxx at 37°C for varying durations. As depicted in **Figure 2B**, inhibition increased with longer incubation times. Pre-treatment with PMAxx for 15 min yielded similar results as a 30-min pre-treatment, suggesting that a 15-min period achieved complete cross-linking of PMAxx with ASFV DNA.

For the preparation of an inactive ASFV control, genomic DNA solutions were subjected to thermal inactivation using water baths set at 85°C for different durations. Subsequently, PMAxx was added at a final concentration of 50 μM and incubated at 37°C for 15 min with periodic mixing. **Figure 2C** indicated that heat treatment of infectious ASFV for up to 30 min did not affect the qPCR CT values. However, the signal from PMAxx-treated DNA was reduced compared to untreated DNA at all-time points. Based on the degree of inhibition, a thermal inactivation period of 5–30 min efficiently inactivated ASFV and released DNA for subsequent reaction with PMAxx at 85°C.

To guarantee efficient cross-linking, a PMAxx concentration of 50 μM, an incubation time of 15 min, and the thermal inactivation at 85°C for 10 min were selected for subsequent experiments.

Sensitivity of the PMAxx-qPCR assay

To assess the sensitivity of the PMAxx-qPCR assay, a standard curve was generated using a 10-fold serial dilution of standard plasmids containing ASFV B646L partial sequences. The CT values were plotted against the logarithm of the standard plasmid copies to perform linear regression analysis (**Figure 3A**). The experimental points aligned in a straight line with a high correlation coefficient ($R^2 = 0.9983$), indicating accurate prediction. The limit of quantification for the PMAxx-qPCR assay was determined by testing serially diluted vaccine samples containing ASFV-G-ΔI177L. As shown in **Figure 3B**, samples with a mean CT value of 34.38 were identified as having infectious ASFV by PMAxx-qPCR, corresponding to approximately 10.57 copies of total ASFV according to the linear relationship in **Figure 3A**. Therefore, the detection limit of this assay was approximately 10 copies/μL when testing for infectious ASFV in this vaccine.

Concordance between PMAxx-qPCR assay and pig challenge results

To validate the reliability of the PMAxx-qPCR assay, the diluted vaccine containing viable ASFV was subjected to different durations of heat treatment at 85°C. The PMAxx-qPCR assay was then performed to detect the ASFV activity in all samples. **Figure 4A** demonstrated that heat treatment for 0.5 min (B) and 1 min (C) did not completely inactivate ASFV, while samples heated for 10 min (D) showed no infectious ASFV. Each sample was intramuscularly injected into three ASFV-negative fattening pigs, and their throat swab samples was collected after 7 days. ASFV genomic DNA was quantified using specific primers and probes targeting the B646L gene. **Figure 4B** revealed that pigs challenged with sample A (positive control), B, or C were successfully infected with ASFV, while pigs injected with sample D remained ASFV-negative throughout the experiment. These results demonstrated a strong agreement between the PMAxx-qPCR assay and pig challenge results.

Application of PMAxx-qPCR to determine ASFV survival time on piggery materials

African swine fever virus can be transmitted to pigs through close contact with contaminated piggery supplies (Gaudreault et al., 2020). In this study, the persistence of ASFV particles on the surface of piggery materials at different temperatures was estimated.

Different materials, including dry feed, the head of fertilization tubes, latex gloves, and packaging bags were soaked in ASFV vaccine, air-dried, and stored at different temperatures for several days. ASFV on the materials was eluted with saline, and viral infectivity was measured using PMAxx-qPCR (**Table 1**). Overall, the survival time of infectious ASFV on the four different matrices decreased with increasing temperature (from 20–45 days at 4°C to 7–15 days at 25°C). The fertilization tubes showed the greatest delay in ASFV survival time from 25 to 4°C (30 days), while latex gloves exhibited the shortest change of survival time (13 days) when the temperature decreased. Infectious ASFV persisted for 20 days on latex gloves at 4°C, whereas the survival time on fertilization tubes was 45 days at the same temperature. Significant differences in ASFV survival time were observed between latex gloves and fertilization tubes at 25°C and 15°C, but no significant

10.3389/fmicb.2023.1290302

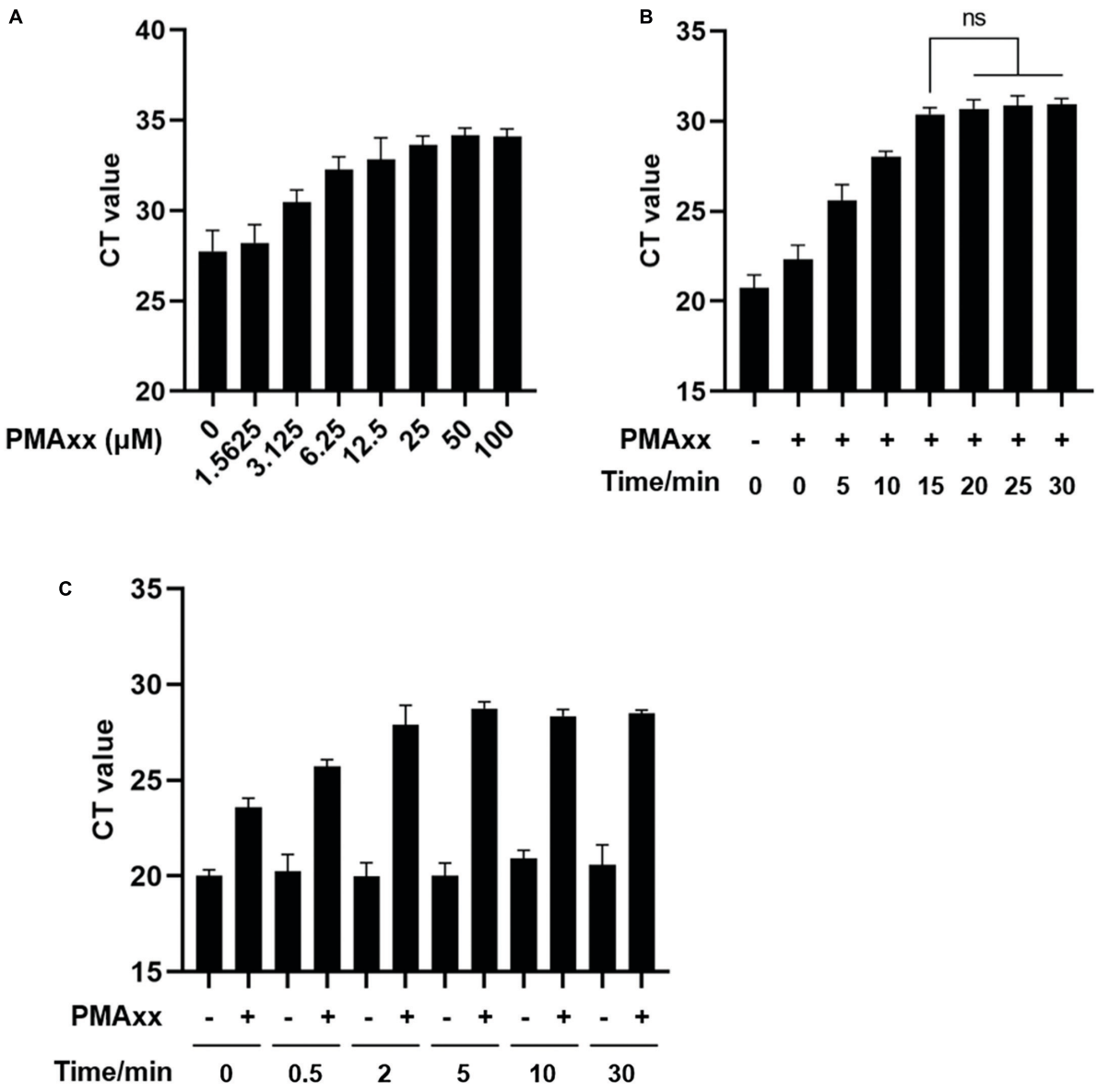

FIGURE 2
Optimization of PMAxx-qPCR assay conditions. **(A)** Vaccine samples containing ASFV-G-ΔI177L were treated with different concentrations of PMAxx-qPCR at 37°C for 15 min. Genomic DNA content was detected by qPCR using ASFV B646L gene-specific primers and probe. **(B)** Vaccine samples containing ASFV-G-ΔI177L were incubated with 50 μM PMAxx at 37°C for different times. ASFV DNA was detected by qPCR. **(C)** Vaccine samples containing ASFV-G-ΔI177L were heat-killed at 85°C for various times and then incubated with 50 μM PMAxx at 37°C for 15 min. ASFV DNA was detected by qPCR. All assays were performed in triplicate.

difference was found between dry feeds and packaging bags at all temperatures. These findings indicate that the persistence of ASFV infectivity varied depending on the type of piggery material and temperature.

Discussion

Quantitative PCR-based methods are commonly used for risk assessment in pig production. However, samples from farms often contain a mixture of infectious and non-infectious causative agents, limiting the significance of qPCR without information on residual infectivity. Furthermore, incomplete or excessive disinfection is a prevalent issue due to the lack of information on disinfection efficiency, resulting in residual live virus and failed reproduction, or wasted resources and environmental pollution. A technically easy, highly sensitive, widely applicable, and cost-effective method is required to determine virus infectivity. To address this, alternative methods have been proposed, such as using photoactivatable dyes to eliminate signal interference from inactivated viruses during PCR amplification. This technique has demonstrated success in detecting infectivity in many viruses (Parshionikar et al., 2010; Hamza et al., 2011; Sanchez et al., 2012; Leifels et al., 2015; Prevost et al., 2016; Randazzo et al., 2016).

One photoactivatable dye that has garnered significant attention, particularly for its potential use in assessing ASFV

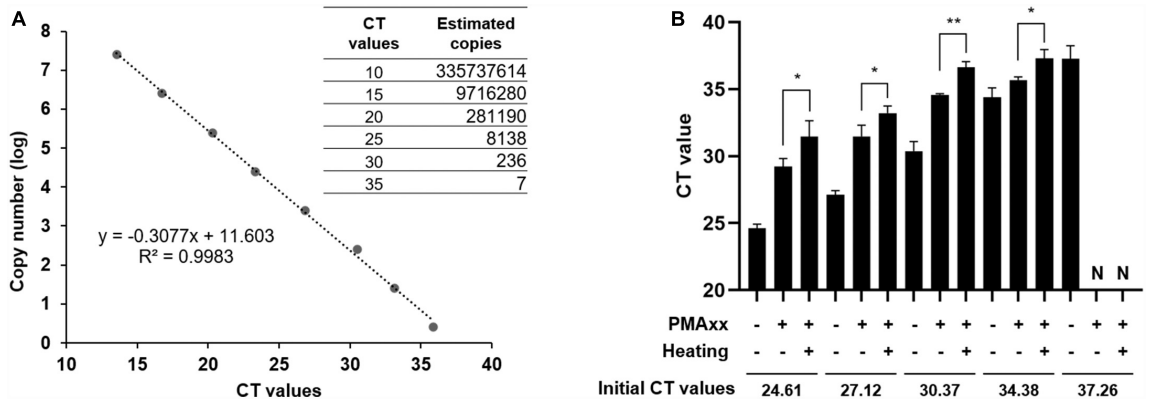

FIGURE 3
PMAxx-qPCR sensitivity estimated from the standard curve. **(A)** Correlation between ASFV copy numbers and CT values was established using ASFV B646L gene standard plasmids. **(B)** Vaccine samples containing ASFV-G-ΔI177L were subjected to PMAxx-qPCR assay. All assays were performed in triplicate. N, negative. *$P < 0.05$, **$P < 0.01$.

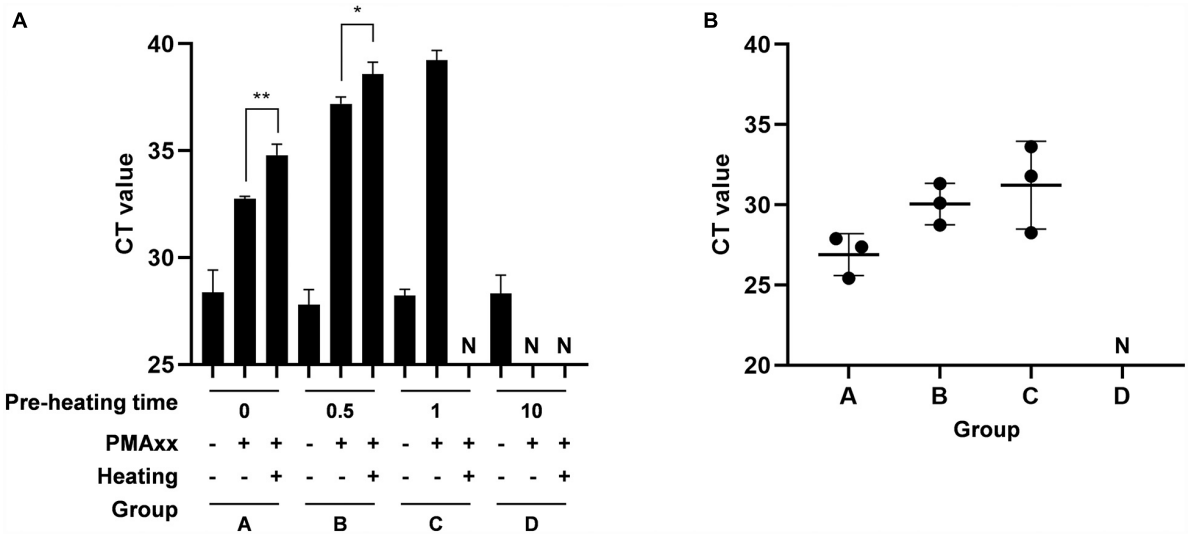

FIGURE 4
Comparison of agreement between PMAxx-qPCR and inoculation of animals. The vaccine containing ASFV-G-ΔI177L was heated at 85°C for different times. **(A)** The infectivity of samples was quantified by PMAxx-qPCR. **(B)** Each sample was intramuscularly injected into the neck of three ASFV-negative fatting pigs. Throat swab samples were collected from all pigs after 7 days and ASFV DNA levels were determined by qPCR. N, negative. *$P < 0.05$, **$P < 0.01$.

infectivity, is PMAxx. A recent review highlighted the promising application prospects of a rapid infectious ASFV detection technology based on PMA pre-treatment, which could greatly enhance various aspects of ASF prevention and control, including epidemic surveillance, disinfection treatment, and drug development (Zeng et al., 2022). In our study, we aimed to demonstrate the potential of PMAxx pre-treatment in distinguishing between infectious and non-infectious ASFV strains in vaccine. We successfully detected as few as 10 copies/μL of infectious ASFV using PMAxx-qPCR. Furthermore, there was a strong correlation between the results of PMAxx-qPCR and animal inoculation (**Figure 4**). Hence, the PMAxx-qPCR assay may serve as a rapid and cost-effective analytical tool for assessing the efficacy of virus-inactivating disinfectants by monitoring capsid damage. By employing PMAxx-qPCR, the appropriate working concentration of disinfectants could be determined, ensuring effective and economical usage. It should be noted we utilized a vaccine containing ASFV-G-ΔI177L as the sole material to develop the method. This choice was made in accordance with biosafety management requirements. However, for potential clinical application, it is crucial to assess the applicability of the developed method to clinical samples such as blood, saliva, and environmental samples in future studies. What's more, PMA is not suitable for monitoring UV irradiation of bacteria and viruses. This is because viability dyes rely on membrane integrity as a viability criterion, whereas UV light primarily damages viral nucleic acids (Nocker et al., 2006; Leifels et al., 2015). Similarly, PMAxx-qPCR is not applicable to non-enveloped viruses.

In the case of thermally inactivated ASFV, theoretically, the addition of PMAxx should completely eliminate the qPCR signal.

TABLE 1 Detection of ASFV survival time on the piggery materials by PMAxx-qPCR.

Temperature	Materials	1	2	3	5	7	10	15	20	25	30	35	40	45	50	55	60
25°C	Dry feed	+	+	+	+	+	+	−	−	−							
	Fertilization tubes	+	+	+	+	+	+	+	−	−	−						
	Latex gloves	+	+	+	+	+	−	−	−								
	Packaging bags	+	+	+	+	+	+	−	−	−							
15°C	Dry feed	+	+	+	+	+	+	+	−	−	−						
	Fertilization tubes	+	+	+	+	+	+	+	+	−	−	−					
	Latex gloves	+	+	+	+	+	+	+	−	−	−						
	Packaging bags	+	+	+	+	+	+	+	−	−	−						
4°C	Dry feed	+	+	+	+	+	+	+	+	+	+	−	−	−			
	Fertilization tubes	+	+	+	+	+	+	+	+	+	+	+	+	+	−	−	−
	Latex gloves	+	+	+	+	+	+	+	+	−	−	−					
	Packaging bags	+	+	+	+	+	+	+	+	+	+	−	−	−			

Piggery materials, including latex gloves, dry feed, packing bags and the head of fertilization tubes were soaked using vaccine of ASFV-G-ΔI177L. The materials were then laid out to dry thoroughly and stored at 25, 15, or 4°C for several days. ASFV infectivity was measured by PMAxx-qPCR until no infectious ASFV was detected in three continuous sampling. All experiments were performed in duplicate under same conditions and representative results are shown. +: infectious ASFV positive; −: infectious ASFV negative.

10.3389/fmicb.2023.1290302

However, even with relatively high levels of PMAxx, CT values could still be detected in the presence of high viral genome concentrations (**Figure 2**). These findings align with observations in viability qPCR, where complete prevention of PCR amplification of thermally inactivated viruses is challenging (Leifels et al., 2015; Moreno et al., 2015; Randazzo et al., 2016). The incomplete inhibition could be attributed to several factors. Firstly, it may stem from the limited concentration of PMAxx, which aims to effectively eliminate non-infectious ASFV genomic DNA while avoiding potential DNA loss due to overconcentration. Moreover, the background levels could be influenced by the target sequence, amplicon size, incubation temperature, and secondary structure of the viral genome (Contreras et al., 2011; Soejima et al., 2011; Schnetzinger et al., 2013; Leifels et al., 2015; Prevost et al., 2016). Therefore, further studies should focus on optimizing the working conditions of PMAxx to maximize the differentiation between signals from infectious and inactivated viruses. This includes determining the optimal concentration, incubation time, and considering the addition of Triton, PMA enhancer, and protease K (Randazzo et al., 2016).

The estimated survival time of infectious ASFV is affected by several environmental factors, including pH, temperature, type of fomite, light exposure, and the presence of viral aggregates (Arzumanyan et al., 2021; Nuanualsuwan et al., 2022). Previous studies have evaluated the persistence of infectious ASFV on different materials under ambient temperatures. At 20°C, infectious ASFV was detected in complete feed until 1 dpi, in soybean meal until at least 21 dpi and in corncob particles until 1 dpi (Niederwerder et al., 2022). ASFV survived longer in pork (18–83 days) than in tissues (9–17 days) and plasma (14 days) at room temperature (Petrini et al., 2019; Mazur-Panasiuk and Wozniakowski, 2020; Fischer et al., 2021). Additionally, porous materials, such as rubber and cellulose paper, supported ASFV viability for longer periods (14–22 days) than non-porous materials, like glass and metal (11–17 days) at 25°C (Nuanualsuwan et al., 2022). Infectious ASFV has also been detected in sterile sand for at least 3 weeks, beach sand for up to 2 weeks, yard soil for 1 week, and swamp soil for 3 days (Carlson et al., 2020). However, farmers are particularly concerned about the survival time of live ASFV on daily input materials accessible to pigs. In our study, we estimated that ASFV remained infectious on the surface of piggery materials for 7–15 days at 25°C (**Table 1**), which aligns with previous research on other materials. Furthermore, we observed variations in the persistence of ASFV on four matrices. The causes of these differences remain unclear, but it is likely linked to differences in their physicochemical properties, such as the micropore size in the head of fertilization tubes and the watertightness of latex gloves. Nonetheless, it is essential to disinfect piggery materials thoroughly as they are significant carriers of ASFV between domestic pigs. For those materials that cannot be conventionally disinfected, sufficient static storage before transport to pig farms is a viable option. The duration of static storage should increase as the ambient temperature decreases.

Conclusion

This study aimed to develop and optimize the PMAxx-qPCR assay for effective discrimination of infectious ASFV. The authenticity of the PMAxx-qPCR assay was verified by animal inoculation experiments. Furthermore, the persistence of ASFV was assessed on various surfaces, including latex gloves, dry feed, packaging bags, and fertilization tubes. The results revealed that the longevity of infectious ASFV decreased with rising temperatures on the four different matrices tested. Notably, the porous head of the fertilization tube exhibited higher stability than the waterproof latex gloves. Based on these findings, it can be concluded that the PMAxx-qPCR assay holds promise as an alternative method for assessing ASFV infectivity. Its integration into routine diagnostics can significantly enhance the interpretation of positive ASFV results, leading to improved accuracy in identifying infected cases.

Data availability statement

The original contributions presented in this study are included in the article/supplementary material, further inquiries can be directed to the corresponding authors.

Ethics statement

The animal study was approved by the Ethics Committee at Northwest A&F University. The study was conducted in accordance with the local legislation and institutional requirements.

Author contributions

YL: Writing – original draft, Project administration, Methodology, Visualization. ZW: Methodology, Visualization, Writing – review and editing. JQ: Methodology, Visualization, Writing – review and editing. DH: Resources, Supervision, Validation, Writing – review and editing. HV: Data curation, Writing – review and editing. KT: Data curation, Writing – review and editing. XW: Supervision, Writing – review and editing. XL: Conceptualization, Funding acquisition, Writing – review and editing.

Funding

The author(s) declare financial support was received for the research, authorship, and/or publication of this article. This work was supported by the Taishan Industry Leadership Talent Project of Shandong Province in China.

Conflict of interest

YL, ZW, JQ, and XL are employed by Xiajin New Hope Liuhe Agriculture and Animal Husbandry Co., Ltd. DH, HV, KT, and XL are employed by New Hope Binh Phuoc livestock Co., Ltd.

The remaining author declares that the research was conducted in the absence of any commercial or financial relationships that could be construed as a potential conflict of interest.

Publisher's note

References

Arzumanyan, H., Hakobyan, S., Avagyan, H., Izmailyan, R., Nersisyan, N., and Karalyan, Z. (2021). Possibility of long-term survival of African swine fever virus in natural conditions. *Vet. World* 14, 854–859. doi: 10.14202/vetworld.2021.854-859

Blackmer, F., Reynolds, K. A., Gerba, C. P., and Pepper, I. L. (2000). Use of integrated cell culture-PCR to evaluate the effectiveness of poliovirus inactivation by chlorine. *Appl. Environ. Microbiol.* 66, 2267–2268. doi: 10.1128/aem.66.5.2267-2268.2000

Borca, M. V., Ramirez-Medina, E., Silva, E., Rai, A., Espinoza, N., Velazquez-Salinas, L., et al. (2023). ASF vaccine candidate ASFV-G-ΔI177L does not exhibit residual virulence in long-term clinical studies. *Pathogens* 12:805. doi: 10.3390/pathogens12060805

Borca, M. V., Ramirez-Medina, E., Silva, E., Vuono, E., Rai, A., Pruitt, S., et al. (2021). ASFV-G-ΔI177L as an effective oral nasal vaccine against the Eurasia strain of Africa swine fever. *Viruses* 13:765. doi: 10.3390/v13050765

Borca, M. V., Ramirez-Medina, E., Silva, E., Vuono, E., Rai, A., Pruitt, S., et al. (2020). Development of a highly effective African swine fever virus vaccine by deletion of the I177L gene results in sterile immunity against the current epidemic Eurasia strain. *J. Virol.* 94:e02017-19. doi: 10.1128/jvi.02017-19

Brescia, C. C., Griffin, S. M., Ware, M. W., Varughese, E. A., Egorov, A. I., and Villegas, E. N. (2009). *Cryptosporidium* propidium monoazide-PCR, a molecular biology-based technique for genotyping of viable *Cryptosporidium* oocysts. *Appl. Environ. Microbiol.* 75, 6856–6863. doi: 10.1128/aem.00540-09

Carlson, J., Fischer, M., Zani, L., Eschbaumer, M., Fuchs, W., Mettenleiter, T., et al. (2020). Stability of African swine fever virus in soil and options to mitigate the potential transmission risk. *Pathogens* 9:977. doi: 10.3390/pathogens9110977

Choi, S., and Jiang, S. C. (2005). Real-time PCR quantification of human adenoviruses in urban rivers indicates genome prevalence but low infectivity. *Appl. Environ. Microbiol.* 71, 7426–7433. doi: 10.1128/aem.71.11.7426-7433.2005

Contreras, P. J., Urrutia, H., Sossa, K., and Nocker, A. (2011). Effect of PCR amplicon length on suppressing signals from membrane-compromised cells by propidium monoazide treatment. *J. Microbiol. Methods* 87, 89–95. doi: 10.1016/j.mimet.2011.07.016

Costard, S., Wieland, B., de Glanville, W., Jori, F., Rowlands, R., Vosloo, W., et al. (2009). African swine fever: how can global spread be prevented? *Philos. Trans. R. Soc. Lond. B Biol. Sci.* 364, 2683–2696. doi: 10.1098/rstb.2009.0098

Dixon, L. K., Chapman, D. A., Netherton, C. L., and Upton, C. (2013). African swine fever virus replication and genomics. *Virus Res.* 173, 3–14. doi: 10.1016/j.virusres.2012.10.020

Dreo, T., Pirc, M., Ramšak, Ž, Pavšič, J., Milavec, M., Zel, J., et al. (2014). Optimising droplet digital PCR analysis approaches for detection and quantification of bacteria: a case study of fire blight and potato brown rot. *Anal. Bioanal. Chem.* 406, 6513–6528. doi: 10.1007/s00216-014-8084-1

Fischer, M., Pikalo, J., Beer, M., and Blome, S. (2021). Stability of African swine fever virus on spiked spray-dried porcine plasma. *Transbound. Emerg. Dis.* 68, 2806–2811. doi: 10.1111/tbed.14192

Fittipaldi, M., Rodriguez, N. J., Codony, F., Adrados, B., Peñuela, G. A., and Morató, J. (2010). Discrimination of infectious bacteriophage T4 virus by propidium monoazide real-time PCR. *J. Virol. Methods* 168, 228–232. doi: 10.1016/j.jviromet.2010.06.011

Flekna, G., Stefanic, P., Wagner, M., Smulders, F. J., Mozina, S. S., and Hein, I. (2007). Insufficient differentiation of live and dead *Campylobacter jejuni* and *Listeria monocytogenes* cells by ethidium monoazide (EMA) compromises EMA/real-time PCR. *Res. Microbiol.* 158, 405–412. doi: 10.1016/j.resmic.2007.02.008

Gaudreault, N. N., Madden, D. W., Wilson, W. C., Trujillo, J. D., and Richt, J. A. (2020). African swine fever virus: an emerging DNA arbovirus. *Front. Vet. Sci.* 7:215. doi: 10.3389/fvets.2020.00215

Graiver, D. A., Saunders, S. E., Topliff, C. L., Kelling, C. L., and Bartelt-Hunt, S. L. (2010). Ethidium monoazide does not inhibit RT-PCR amplification of nonviable avian influenza RNA. *J. Virol. Methods* 164, 51–54. doi: 10.1016/j.jviromet.2009.11.024

Hamza, I. A., Jurzik, L., Überla, K., and Wilhelm, M. (2011). Methods to detect infectious human enteric viruses in environmental water samples. *Int. J. Hyg. Environ. Health* 214, 424–436. doi: 10.1016/j.ijheh.2011.07.014

Kim, K., Katayama, H., Kitajima, M., Tohya, Y., and Ohgaki, S. (2011). Development of a real-time RT-PCR assay combined with ethidium monoazide treatment for RNA viruses and its application to detect viral RNA after heat exposure. *Water Sci. Technol.* 63, 502–507. doi: 10.2166/wst.2011.249

Knight, A., Li, D., Uyttendaele, M., and Jaykus, L. A. (2013). A critical review of methods for detecting human noroviruses and predicting their infectivity. *Crit. Rev. Microbiol.* 39, 295–309. doi: 10.3109/1040841x.2012.709820

Leifels, M., Jurzik, L., Wilhelm, M., and Hamza, I. A. (2015). Use of ethidium monoazide and propidium monoazide to determine viral infectivity upon inactivation by heat, UV- exposure and chlorine. *Int. J. Hyg. Environ. Health* 218, 686–693. doi: 10.1016/j.ijheh.2015.02.003

Li, J. W., Xin, Z. T., Wang, X. W., Zheng, J. L., and Chao, F. H. (2002). Mechanisms of inactivation of hepatitis a virus by chlorine. *Appl. Environ. Microbiol.* 68, 4951–4955. doi: 10.1128/aem.68.10.4951-4955.2002

Li, X., Li, Y., Fan, M., Fan, S., Gao, W., Ren, J., et al. (2022). Inguinal lymph node sample collected by minimally invasive sampler helps to accurately diagnose ASF in dead pigs without necropsy. *Front. Vet. Sci.* 9:1000969. doi: 10.3389/fvets.2022.1000969

Liu, H., Meng, F., Nyaruaba, R., He, P., Hong, W., Jiang, M., et al. (2022). A triton X-100 assisted PMAxx-qPCR assay for rapid assessment of infectious African swine fever virus. *Front. Microbiol.* 13:1062544. doi: 10.3389/fmicb.2022.1062544

Mazur-Panasiuk, N., and Wozniakowski, G. (2020). Natural inactivation of African swine fever virus in tissues: influence of temperature and environmental conditions on virus survival. *Vet. Microbiol.* 242:108609. doi: 10.1016/j.vetmic.2020.108609

Moreno, L., Aznar, R., and Sánchez, G. (2015). Application of viability PCR to discriminate the infectivity of hepatitis A virus in food samples. *Int. J. Food Microbiol.* 201, 1–6. doi: 10.1016/j.ijfoodmicro.2015.02.012

Niederwerder, M. C., Khanal, P., Foland, T., Constance, L. A., Stoian, A. M. M., Deavours, A., et al. (2022). Stability of African swine fever virus in feed during environmental storage. *Transbound. Emerg. Dis.* 69, 3216–3224. doi: 10.1111/tbed.14666

Nocker, A., and Camper, A. K. (2009). Novel approaches toward preferential detection of viable cells using nucleic acid amplification techniques. *FEMS Microbiol. Lett.* 291, 137–142. doi: 10.1111/j.1574-6968.2008.01429.x

Nocker, A., Cheung, C. Y., and Camper, A. K. (2006). Comparison of propidium monoazide with ethidium monoazide for differentiation of live vs. dead bacteria by selective removal of DNA from dead cells. *J. Microbiol. Methods* 67, 310–320. doi: 10.1016/j.mimet.2006.04.015

Norbert Mwiine, F., Nkamwesiga, J., Ndekezi, C., and Ochwo, S. (2019). Molecular characterization of African swine fever viruses from outbreaks in Peri-Urban Kampala, Uganda. *Adv. Virol.* 2019:1463245. doi: 10.1155/2019/1463245

Nuanualsuwan, S., Songkasupa, T., Boonpornprasert, P., Suwankitwat, N., Lohlamoh, W., and Nuengjamnong, C. (2022). Persistence of African swine fever virus on porous and non-porous fomites at environmental temperatures. *Porcine Health Manag.* 8:34. doi: 10.1186/s40813-022-00277-8

Parshionikar, S., Laseke, I., and Fout, G. S. (2010). Use of propidium monoazide in reverse transcriptase PCR to distinguish between infectious and noninfectious enteric viruses in water samples. *Appl. Environ. Microbiol.* 76, 4318–4326.

Pereira De Oliveira, R., Hutet, E., Lancelot, R., Paboeuf, F., Duhayon, M., Boinas, F., et al. (2020). Differential vector competence of Ornithodoros soft ticks for African swine fever virus: what if it involves more than just crossing organic barriers in ticks? *Parasit. Vectors* 13:618. doi: 10.1186/s13071-020-04497-1

Petrini, S., Feliziani, F., Casciari, C., Giammarioli, M., Torresi, C., and De Mia, G. M. (2019). Survival of African swine fever virus (ASFV) in various traditional Italian dry-cured meat products. *Prev. Vet. Med.* 162, 126–130.

Prevost, B., Goulet, M., Lucas, F. S., Joyeux, M., Moulin, L., and Wurtzer, S. (2016). Viral persistence in surface and drinking water: suitability of PCR pre-treatment with intercalating dyes. *Water Res.* 91, 68–76. doi: 10.1016/j.watres.2015.12.049

Randazzo, W., López-Gálvez, F., Allende, A., Aznar, R., and Sánchez, G. (2016). Evaluation of viability PCR performance for assessing norovirus infectivity in fresh-cut vegetables and irrigation water. *Int. J. Food Microbiol.* 229, 1–6. doi: 10.1016/j.ijfoodmicro.2016.04.010

Rodríguez, R. A., Pepper, I. L., and Gerba, C. P. (2009). Application of PCR-based methods to assess the infectivity of enteric viruses in environmental samples. *Appl. Environ. Microbiol.* 75, 297–307. doi: 10.1128/aem.01150-08

Rudi, K., Moen, B., Drømtorp, S. M., and Holck, A. L. (2005). Use of ethidium monoazide and PCR in combination for quantification of viable and dead cells in complex samples. *Appl. Environ. Microbiol.* 71, 1018–1024. doi: 10.1128/aem.71.2.1018-1024.2005

Sanchez, G., Elizaquivel, P., and Aznar, R. (2012). Discrimination of infectious hepatitis A viruses by propidium monoazide real-time RT-PCR. *Food Environ. Virol.* 4, 21–25. doi: 10.1007/s12560-011-9074-5

Schnetzinger, F., Pan, Y., and Nocker, A. (2013). Use of propidium monoazide and increased amplicon length reduce false-positive signals in quantitative PCR for bioburden analysis. *Appl. Microbiol. Biotechnol.* 97, 2153–2162. doi: 10.1007/s00253-013-4711-6

Simonet, J., and Gantzer, C. (2006). Degradation of the Poliovirus 1 genome by chlorine dioxide. *J. Appl. Microbiol.* 100, 862–870. doi: 10.1111/j.1365-2672.2005.02850.x

Soejima, T., Schlitt-Dittrich, F., and Yoshida, S. (2011). Polymerase chain reaction amplification length-dependent ethidium monoazide suppression power for heat-killed cells of *Enterobacteriaceae*. *Anal. Biochem.* 418, 37–43. doi: 10.1016/j.ab.2011.06.027

Stothard, P. (2000). The sequence manipulation suite: JavaScript programs for analyzing and formatting protein and DNA sequences. *Biotechniques* 28, 1102, 1104. doi: 10.2144/00286ir01

Tran, X. H., Le, T. T. P., Nguyen, Q. H., Do, T. T., Nguyen, V. D., Gay, C. G., et al. (2021). African swine fever virus vaccine candidate ASFV-G-ΔI177L efficiently protects European and native pig breeds against circulating Vietnamese field strain. *Transbound. Emerg. Dis.* 69, e497–e504. doi: 10.1111/tbed.14329

Tran, X. H., Phuong, L. T. T., Huy, N. Q., Thuy, D. T., Nguyen, V. D., Quang, P. H., et al. (2022). Evaluation of the safety profile of the ASFV vaccine candidate ASFV-G-ΔI177L. *Viruses* 14:896. doi: 10.3390/v14050896

Zeng, D., Qian, B., Li, Y., Zong, K., Peng, W., Liao, K., et al. (2022). Prospects for the application of infectious virus detection technology based on propidium monoazide in African swine fever management. *Front. Microbiol.* 13:1025758. doi: 10.3389/fmicb.2022.1025758

Zhang, S., Sun, A., Wan, B., Du, Y., Wu, Y., Zhang, A., et al. (2020). Development of a directly visualized recombinase polymerase amplification-SYBR Green I method for the rapid detection of African swine fever virus. *Front. Microbiol.* 11:602709. doi: 10.3389/fmicb.2020.602709

frontiers | Frontiers in Microbiology

TYPE Original Research
PUBLISHED 24 January 2024
DOI 10.3389/fmicb.2024.1345236

OPEN ACCESS

EDITED BY
Lihua Wang,
Kansas State University, United States

REVIEWED BY
Fernando Costa Ferreira,
University of Lisbon, Portugal
Mir Mubashir Khalid,
Gladstone Institutes, United States

*CORRESPONDENCE
Teng Chen
ctcx1991@163.com
Rongliang Hu
ronglianghu@hotmail.com

†These authors have contributed equally to this work

RECEIVED 27 November 2023
ACCEPTED 08 January 2024
PUBLISHED 24 January 2024

CITATION
Fan J, Zhang J, Wang F, Miao F, Zhang H, Jiang Y, Qi Y, Zhang Y, Hui L, Zhang D, Yue H, Zhou X, Li Q, Wang Y, Chen T and Hu R (2024) Identification of *L11L* and *L7L* as virulence-related genes in the African swine fever virus genome.
Front. Microbiol. 15:1345236.
doi: 10.3389/fmicb.2024.1345236

Identification of *L11L* and *L7L* as virulence-related genes in the African swine fever virus genome

Jiaqi Fan[1,2,3†], Jingyuan Zhang[4†], Fengjie Wang[1,2,3], Faming Miao[2,3], Han Zhang[2,3], Yiqian Jiang[2,3], Yu Qi[2,3], Yanyan Zhang[2,3], Lili Hui[2,3], Dan Zhang[2,3], Huixian Yue[2,3], Xintao Zhou[1,2,3], Qixuan Li[2,3], Yu Wang[2,3], Teng Chen[2,3*] and Rongliang Hu[1,2,3*]

[1]College of Life Sciences, Ningxia University, Yinchuan, Ningxia, China, [2]Key Laboratory of Prevention and Control for African Swine Fever and Other Major Pig Diseases, Ministry of Agriculture and Rural Affairs, Changchun, Jilin, China, [3]Chinese Academy of Agricultural Sciences Changchun Veterinary Research Institute, Changchun, Jilin, China, [4]Institute of Rare Diseases, West China Hospital of Sichuan University, Chengdu, Sichuan, China

Introduction: African swine fever (ASF) is an infectious disease that causes considerable economic losses in pig farming. The agent of this disease, African swine fever virus (ASFV), is a double-stranded DNA virus with a capsid membrane and a genome that is 170-194 kb in length encoding over 150 proteins. In recent years, several live attenuated strains of ASFV have been studied as vaccine candidates, including the SY18ΔL7-11. This strain features deletion of *L7L*, *L8L*, *L9R*, *L10L* and *L11L* genes and was found to exhibit significantly reduced pathogenicity in pigs, suggesting that these five genes play key roles in virulence.

Methods: Here, we constructed and evaluated the virulence of ASFV mutations with SY18ΔL7, SY18ΔL8, SY18ΔL9, SY18ΔL10, and SY18ΔL11L.

Results: Our findings did not reveal any significant differences in replication efficiency between the single-gene deletion strains and the parental strains. Pigs inoculated with SY18ΔL8L, SY18ΔL9R and SY18ΔL10L exhibited clinical signs similar to those inoculated with the parental strains. Survival rate of pigs inoculated with $10^{3.0}TCID_{50}$ of SY18ΔL7L was 25%, while all pigs inoculated with $10^{3.0}TCID_{50}$ of SY18ΔL11L survived, and 50% inoculated with $10^{6.0}TCID_{50}$ SY18ΔL11L survived.

Discussion: The results indicate that *L8L*, *L9R* and *L10L* do not affect ASFV SY18 virulence, while the *L7L* and *L11L* are associated with virulence.

KEYWORDS

African swine fever virus, *L7L*, *L11L*, virulence, recombinant virus

1 Introduction

African swine fever virus (ASFV) is the sole member of the *Asfarviridae* family and *Asfivirus* genus (Iyer et al., 2006). ASFV is a double-stranded DNA virus that replicates in the cytoplasm, and has a genome approximately 170–194 kb in length, containing 150–167 open reading frames (ORFs), and encoding over 150 proteins (Chapman et al., 2011). Various genes in ASFV genome cause clinical differences, resulting in chronic, subacute, acute, and hyperacute forms of infection in pigs, with domestic pigs typically exhibiting pronounced clinical signs (Gómez-Villamandos et al., 2013). Pigs with acute ASF infection generally succumb within about 10 days, displaying symptoms like high fever, anorexia, prostration, and

cyanosis. In contrast, pigs with hyperacute ASF infection show no symptoms, and die within a week (Bosch-Camós et al., 2020). The mortality rate for subacute and chronic ASF is less than 100%. Subacute and chronic forms of the disease are mainly characterized by less virulent strains with a longer course of disease and Chronic disease signs (include intermittent fever, arthritis, weight loss, and skin ulcers; Sun et al., 2021a).

ASF was first identified in Kenya in 1921 (Wardley et al., 1983). Genotype I ASFV, initially transmitted from Africa in 1957, has been eradicated from all countries and regions except Sardinia, Italy, and Africa, through aggressive prevention and control measures (Mur et al., 2016; Dixon et al., 2019). Since its introduction from Africa to the Republic of Georgia in 2007, genotype II ASFV has continued to spread to neighboring countries (Rowlands et al., 2008). In 2018, ASFV emerged in China and several other Asian countries, and posed a significant threat to the global pig industry (Zhou et al., 2018; Ankhanbaatar et al., 2021; Mai et al., 2021). Endemic in China for nearly 5 years, ASFV was later detected in surveillance studies, which have identified naturally mutated low-virulence genotype II strains in swine farms (Sun et al., 2021b). Additionally, genotype I ASFV has been isolated from farms in China's Shandong and Henan provinces (Sun et al., 2021a). The emergence of low-virulence and genotype I ASFV presents new challenges in the diagnosis, treatment, prevention, and control of ASF in China (Urbano and Ferreira, 2022).

Researchers worldwide have strived to develop effective vaccines to prevent and control ASFV infections (Borca et al., 2020; Zhang Y. et al., 2021). In these endeavors, live attenuated vaccines (LAVs) have become a significant focus. LAVs are created by deleting one or more specific genes in ASFV through homologous recombination, leading to attenuated virulence and resistance to highly virulent parental strains. Examples include ASFV-G-ΔI177L (Borca et al., 2020), SY18ΔI226R (Zhang Y. et al., 2021), ASFV-GZΔI73R (Liu et al., 2023a), ASFV-G-ΔA137R (Gladue et al., 2021), ASFV-ΔQP509L/QP383R (Li et al., 2022), ASFV-G-ΔMGF (Deutschmann et al., 2022), ASFV-G-ΔI177L/ΔLVR (Borca et al., 2021), ASFV SY18ΔL7-11 (Zhang J. et al., 2021). ASFV SY18ΔL7–11 is an attenuated strain obtained by deleting the ORFs of the *L7L* (alternative name *I7L*), *L8L* (*I8L*), *L9R* (*I9R*), *L10L* (*I10L*), and *L11L* genes in the highly virulent strain ASFV SY18. The deletion of *L7L-L11L* from ASFV SY18 genome was not found to alter the ability of the virus to replicate *in vitro*. After intramuscular injection of animals with SY18ΔL7–11 at $10^{3.0}$TCID$_{50}$ and $10^{6.0}$TCID$_{50}$, all pigs, except for one in the $10^{3.0}$TCID$_{50}$-inoculated group, died during a 21-day observation period. Thus, L7L-L11L genes were not associated with replication, but instead virulence. Therefore, *L7L*, *L8L*, *L9R*, *L10L* and *L11L* were separately deleted from ASFV SY18 genome here to identify which of these genes were related to virulence. Our results showed that pigs inoculated with the virus at $10^{3.0}$TCID$_{50}$ had overall survival rates of 25 and 100% upon deletion of *L7L* and *L11L*, respectively. The overall survival rate was 0% in the remaining three groups. Thus, deletion of the *L7L* and *L11L* genes reduced the virulence of the virus.

2 Materials and methods

2.1 Cells and viruses

Porcine primary alveolar macrophages (PAMs) were prepared as described previously (Zhang Y. et al., 2021). The viral titer assay was performed according to the method described by Reed and Muench. The strain ASFV SY18 (GenBank number: MH766894) used is a porcine-derived isolate from the Changchun Institute of Veterinary Medicine, Chinese Academy of Agricultural Sciences (Zhou et al., 2018).

2.2 Multiple sequence alignment of L7L-L11 gene sequences

Twelve ASFV strains of seven genotypes were selected to perform a multiple sequence alignment of *L7L*, *L8L*, *L9R*, *L10L*, and *L11L* fragments. For this purpose, the MAFFT website was used, and the Jalview was used to visualize alignment results.

2.3 Construction of ASFV mutants

The recombinant transfer vector (p72EGFPΔL7L) contained a fragment of about 1,200 bp of the gene flanking the L7L gene, and the p72 promoter EGFP gene cassette. p72EGFPΔL8L, p72EGFPΔL9R, p72EGFPΔL10L, and p72EGFPΔL11L were obtained identically. PAM cells (2×10^6) PAM cells were spread into a 6-well plate, the recombinant transfer vector was added to the cells using Jet-Macrophage (Polyplus) transfection reagent, 1 MOI of ASFV SY18 was added after 4 h, and fluorescence was observed after 24 h. The fluorescence intensity was screened, and the purified virus was obtained using the limited dilution method. Polymerase chain reaction was used to identify the ASFV mutants, and specific sequences are shown in Table 1. Recombinant viral DNA was extracted and sent to Novogene (Tianjin, China) for next-generation sequencing.

2.4 Viral growth curves

A total of 2 × 106 PAM cells were spread into 6-well plates, and infected with ASFV SY18, SY18ΔL7L, SY18ΔL8L, SY18ΔL9R, SY18ΔL10L, SY18ΔL11L at an amount of 0.1 MOI. The samples were collected at 2, 12, 24, 48, 72, and 96 h after infection. The samples were then freeze-thawed three times, and the TCID50 of each sample was determined.

2.5 Animal experiments

Experiments were conducted according to standard procedures approved by the Animal Welfare and Ethics Committee of the Changchun Veterinary Research Institute and the Animal Biosafety Level 3 (ABSL-3) Laboratory.

2.5.1 Experiment 1

The virulences of SY18ΔL7L, SY18ΔL8L, SY18ΔL9R, SY18ΔL10L, SY18ΔL11L with respect to ASFV SY18 were assessed using commercial pigs weighing around 15 kg. Each group of pigs ($n = 4$) was inoculated intramuscularly (i.m.) with $10^{3.0}$TCID$_{50}$ of the virus. Clinical symptoms and temperature changes were recorded daily throughout the experiment, and blood was collected on days 0, 3, 7, 10, 14, and 21 for nucleic acid and antibody detection. The experimental observation period was 21 days, and surviving animals

TABLE 1 Primer information.

Virus	Forward Primer (5′-3′)	Reverse Primer (5′-3′)
SY18△L7L, SY18△L8L	TGGTAGTATTGTCCAAACCG	TAGGGACTTATGTAGTTTCGTC
SY18△L9R, SY18△L10L	TCTTATGGATGGACGACCTC	GGATTTGGACGACTTGGTC
SY18△L11L	ACATATGATGTCTAGGAATA	AACTTATAACAATTGCACTC

were euthanized. Viral loads in the tissues and organs of each test animal were determined.

2.5.2 Experiment 2

Using commercial pigs around 15 kg, each group of pigs (n = 4) was injected intramuscularly with $10^{3.0}$TCID$_{50}$ SY18ΔL11L, $10^{6.0}$TCID$_{50}$ SY18ΔL11L and an equal amount of saline as a negative control. After 28 days after inoculation, each group of animals was inoculated intramuscularly with $10^{3.0}$TCID$_{50}$ ASFV SY18. Clinical performance and temperature changes were detected daily during the test period, and blood was collected every 7 days for nucleic acid and antibody detection. At the end of the test, the surviving animals were euthanized and the viral load in the tissues and organs of the test animals was detected.

2.6 Anti-African swine fever p54 antibody assay

Indirect ELISA was used to detect anti-p54 antibodies. Anti-p54 antibodies were detected in each serum sample as previously described, and sample optical density (OD) values were measured at 450 nm. Samples were considered antibody positive when the sample OD450 nm/positive control OD450 nm (S/P) was greater than 0.25.

3 Results

3.1 Genetic diversity of L7L-L11L of ASFV strains

A total of 309 bp in *L7L* encodes 102-amino-acids, 312 bp in *L8L* encodes 103, 291 bp in *L9R* encodes 96, 531 bp in *L10L* encodes 170, and 282 bp in *L11L* encodes 93 (Figure 1). They were located between nucleotide positions 180,724 and 181,032 of the reverse strand, 181,246 and 181,557 of the antisense strand, 181,752 and 182,042 of the plus strand, 182,118 and 182,630 of the antisense strand, and 182,869 and 183,150 of the antisense strand of the ASFV SY18 genome (Figure 2). Degree of conservation of *L7L, L8L, L9R, L10L*, and *L11L* in ASFV isolates of multiple genotypes. A comparison of the amino acid sequences of the isolate ASFV SY18 with those of genotype II strains isolated from Heilongjiang, China (Pig/HLJ/2018), Georgia (Georgia/2007/1), and Estonia (Estonia/2014) revealed that the amino acid sequences of *L7L-L11L* were completely identical. The amino acid sequence of *L8L* was identical in genotype I and II isolates. The amino acid sequences of *L7L, L8L, L9R, L10L*, and *L11L* were identical in the same genotype, and a large gap was observed between the different genotypes. The *L7L* sequence in the Pretoriuskop/96/4 strain (genotype X) was significantly different than those in other strains. The ASFV genotype II is prevalent globally. Positions 1, 17, 21, 24, and 67 of *L11L* in genotype II ASFV SY18, Pig/HLJ/2018, Georgia/2007/1, and Estonia/2014 included a methionine. However, *L11L* of OURT88/3, NHV, Benin97/1 (genotype I) had 77 amino acids, *L11L* of Malawi Lil/20/1 (genotype VIII) has 78, *L11L* of R8 (genotype IX) had 78, *L11L* of Pretoriuskop/96/4 (genotype XX) had 78 amino acids. These strains did not include the first 16 amino acids found in *L11L* of ASFV SY18, with the 17th amino acid in the L11L of ASFV SY18 being the most common initial amino acid (the second occurrence of methionine in the *L11L* of genotype II). The *L11L* of Tengani/62 (genotype V) contained 93 amino acids. The *L11L* of warm baths (genotype III) had the same sequence of amino acids between positions 3 and16 compared to *L11L* of ASFV SY18, except that the first amino acid was not methionine. Therefore, the first 16 amino acids of *L11L* in warm baths were also non-functional.

3.2 Creation of ASFV mutants

In order to identify the specific virulence genes among *L7L-L11L*, we designed and constructed single-gene deletion strains (SY18ΔL7L, SY18ΔL8L, SY18ΔL9R, SY18ΔL10L, and SY18ΔL11L). The construction method is shown in Figure 2. Target genes were replaced with a green fluorescent gene cassette containing the p72 promoter using a recombinant method. The recombinant viruses were purified using fluorescence activity. The PCR assay determined that the target bands of the gene were not detected, whereas the ASFV SY18 control showed the target bands, confirming that single-gene deletion viruses missing each target gene were successfully obtained (Figure 3). Comparison of the whole-genome sequences of the ASFV mutant and parental ASFV SY18 using second-generation sequencing revealed that, apart from design changes, no unwanted mutations were detected in the genomes of the constructed mutants.

3.3 Replication of ASFV mutants in porcine macrophages

Macrophages were infected with each deletion strain at an MOI of 0.1, and the parental ASFV SY18 was used as a control. Samples were collected at 2, 12, 24, 48, 72, and 96 h post-infection (hpi). The results shown in Figure 4 revealed no significant differences between the growth curves of single-gene deletion viruses in target cells than those of the parental strains *in vitro*. There was also no difference in the replication pattern between the single-gene deletion strains, all of which reached the highest titer at 72 hpi. These findings demonstrate that the deletion of *L7L*, *L8L*, *L9R*, *L10L*, and *L11L* did not affect the proliferative ability of ASFV in macrophages *in vitro*.

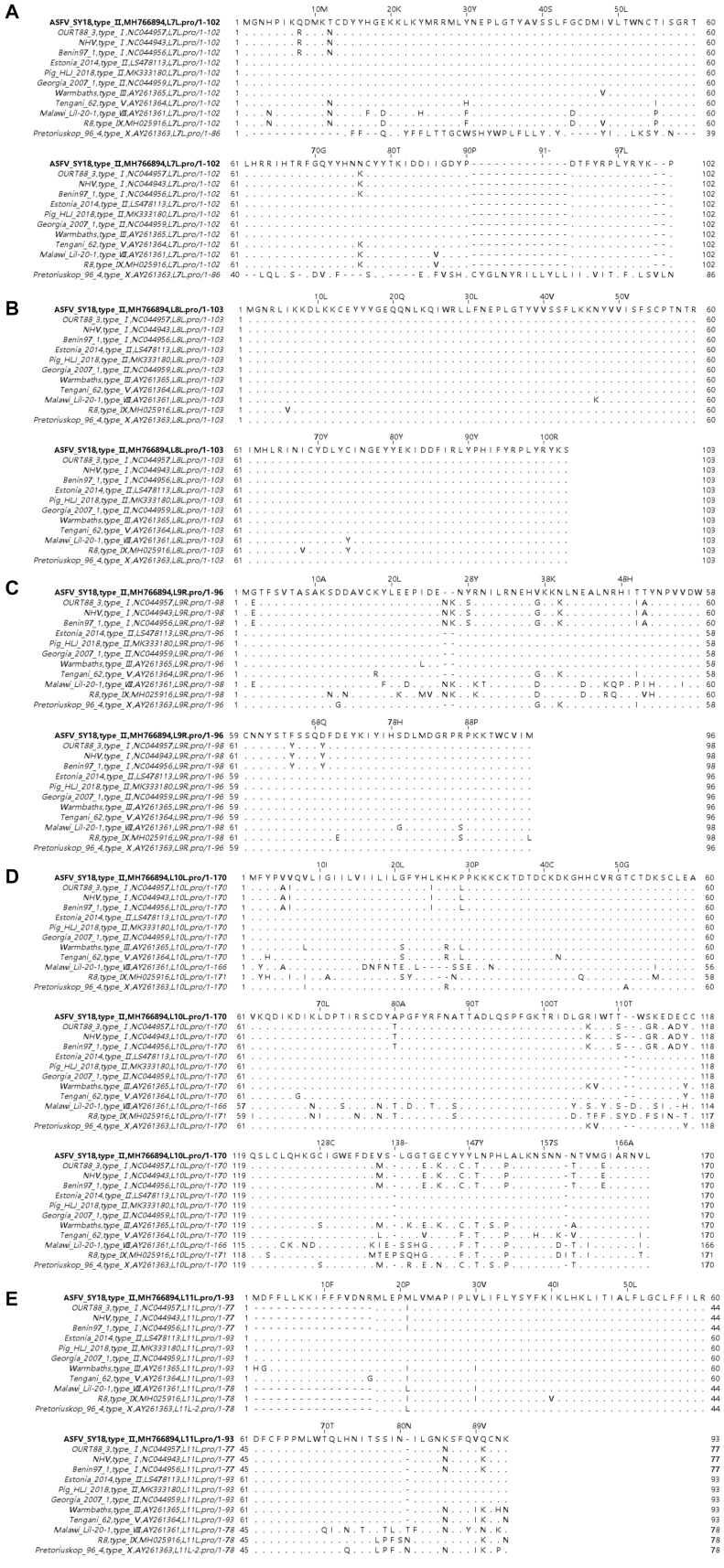

FIGURE 1
Multiple sequence alignment of amino acid sequences of *L7L-L11L*. Panels **(A–E)** show sequences of *L7L, L8L, L9R, L10L*, and *L11L*, respectively. The sequence of ASFV SY18 is placed on the top row for reference. Amino acids are indicated by their respective single letter codes. Matches are indicated with ". ", and gaps are denoted with "-." Sequences were aligned using the MAFFT algorithm and Jalview software (Accessed 5 October 2023).

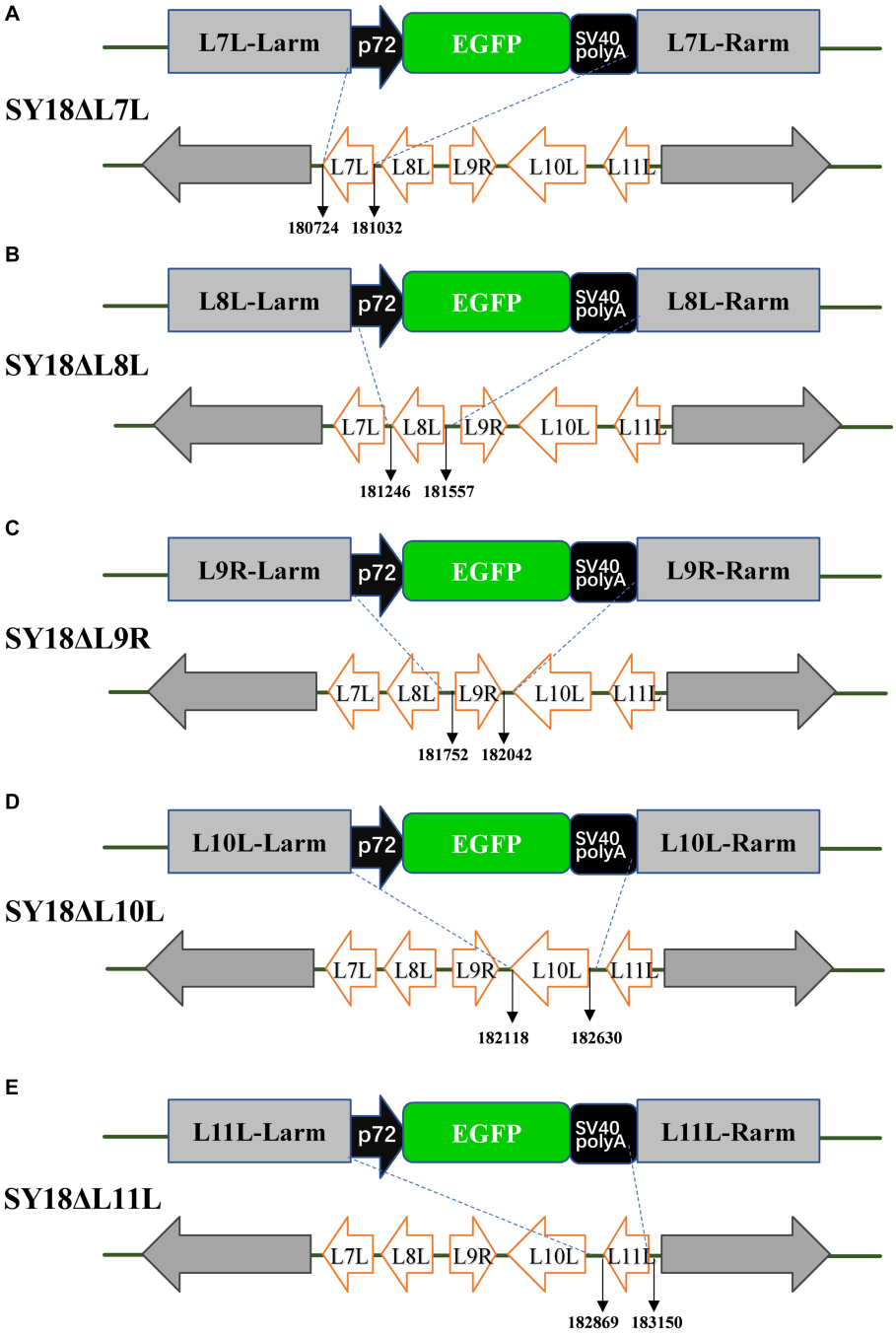

FIGURE 2
Schematic diagrams of recombinant viral constructs. **(A)** A schematic diagram of the SY18ΔL7L construct ASFV SY18 in which the *L7L* was replaced by a green fluorescent protein expression cassette. Panels **(B–E)** indicate the schematic diagrams of the constructs of SY18ΔL8L, SY18ΔL9R, SY18ΔL10L, and SY18ΔL11L, respectively, where the target genes were replaced by an EGFP expression cassette.

3.4 Evaluation of the virulence of ASFV mutants

To assess the virulence of SY18ΔL7L, SY18ΔL8L, SY18ΔL9R, SY18ΔL10L, SY18ΔL11L, and ASFV SY18 (positive control group) for pigs, each group was injected intramuscularly with $10^{3.0}$ $TCID_{50}$ of virus. The survival and body temperature results are shown in Figures 5A,B and Table 2. Pigs in the ASFV SY18 group became febrile on day 4 after infection, and showed typical symptoms of ASF, and died on day 8 post infection. Pigs in the SY18ΔL7L group showed persistent fever between days 1 and 5. Three of these pigs died on the 9th, 12th, and 13th dpi, and one pig (S7-1) survived during the observation period. Pigs in the SY18ΔL8L group died on days 7 and 8 post-infection, which was consistent with the timing of death in the control group. However, only one animal in the SY18ΔL8L group showed elevated body temperature, whereas the remaining three animals had normal body temperatures. Pigs in the SY18ΔL9R group died 10 to 16 days and pigs in the SY18ΔL10L group died 10 to 13 days

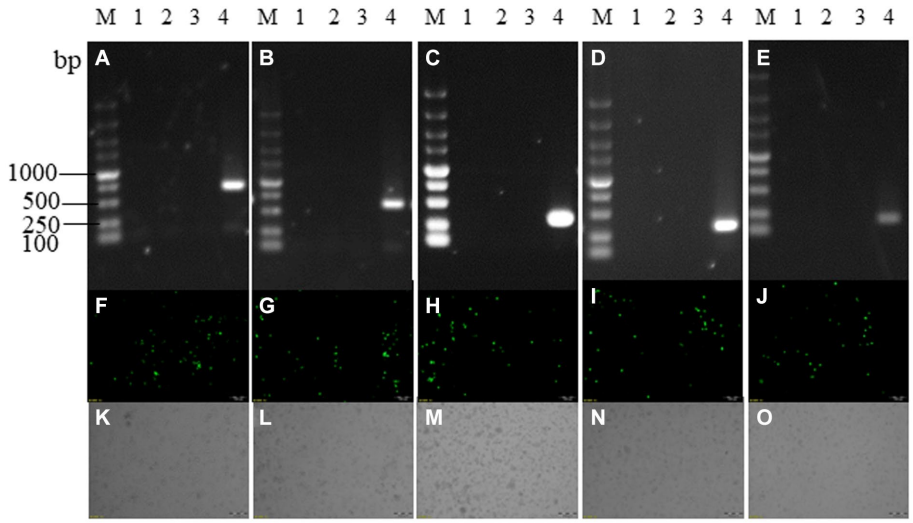

FIGURE 3
Recombinant virus identification. Panels **(A–E)** are PCR identification and purification results of SY18ΔL7L, SY18ΔL8L, SY18ΔL9R, SY18ΔL10L, SY18ΔL11L, panels **(F–J)** are the fluorescence maps of each single-gene deletion viruses, and panels **(K–O)** are the bright field of each single-gene deletion viruses. M: DL5000 marker; a1~a3, b1~b3, c1~c3, d1~d3, e1~e3: each single-gene deletion virus detection samples; 4: ASFV SY18 control. SY18ΔL7L and SY18ΔL8L amplified a 643 bp fragment in the presence of ASFV SY18; SY18ΔL9R amplified a 280 bp fragment in the presence of ASFV SY18; SY18ΔL10L, and SY18ΔL11L amplified a 200 bp fragment in the presence of ASFV SY18.

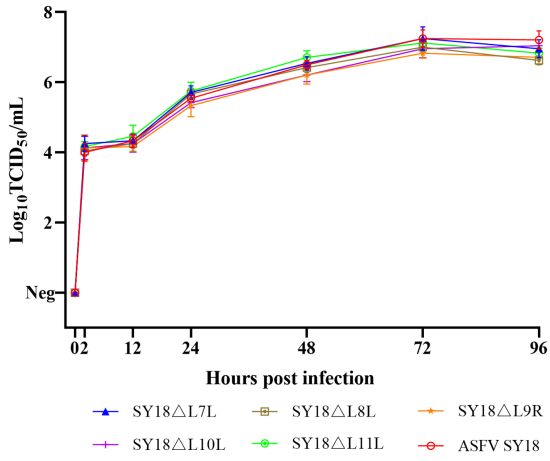

FIGURE 4
In vitro growth characteristics of recombinant viruses. PAM was infected with ASFV SY18, SY18ΔL7L, SY18ΔL8L, SY18ΔL9R, SY18ΔL10L, SY18ΔL11L at 0.1 MOI, and the viral titers of three independent experimental samples were determined at different times of infection. y-axis represents the viral titer expressed as log10 $TCID_{50}$/mL, and the x-axis represents the time after infection (hours).

post infection, respectively. Deaths in both groups delayed backwards compared with the control. All pigs in the SY18ΔL11L group survived the 21 days of observation, with three pigs experiencing a transient increase in body temperature and one returning to normal temperature after 6 days of fever.

The viral loads in the blood of the experimental animals are shown in Figure 5C. Viral nucleic acids were detected in the blood of all animals on day 3 after infection, except for one pig in the SY18ΔL7L group. On the 3rd day of infection, all pigs in the ASFV SY18 group showed high viral loads in their blood ($10^{6.19}$–$10^{6.86}$ copies/mL), and pigs in the SY18ΔL8L and SY18ΔL9R groups similarly showed high viremia ($10^{6.72}$–$10^{7.72}$ copies/mL and $10^{6.16}$–$10^{7.13}$ copies/mL). On the 3rd day of infection, pigs in the SY18ΔL7L, SY18ΔL10L, and SY18ΔL11L groups had lower viral loads in their blood compared to the control group (0–$10^{5.08}$ copies/mL, $10^{3.58}$–$10^{7.12}$ copies/mL, and $10^{3.37}$–$10^{5.42}$ copies/mL, respectively). The highest viral levels in the blood of all animals were reached on the 7th dpi. Subsequently, the viral load in the blood of surviving animals tended to decrease. The presence of virus was not detected in the blood of 1 pig without fever (S7-1) in the SY18ΔL7L group on the 3rd day, and the presence of the virus was detected on the 7th day, after which and the virus level was consistently low ($10^{3.56}$–$10^{4.44}$ copies/mL).

3.5 Viral load of pig tissues after infection with ASFV mutants

The pigs used in Experiment 1 were dissected, and organs including the heart, liver, spleen, lungs, kidneys, inguinal lymph nodes, thymus, submandibular lymph nodes, colon, bone marrow, muscles, and joint fluids were collected and tested for the presence of the virus. Figure 5D indicates that most animals had the virus in their organs, with the spleen, liver, and bone marrow showing the highest detection rates. In the SY18ΔL11L group, both the detection rate and viral load in the organs were lower compared to other groups. In the SY18ΔL7L group of non-febrile pigs (S7-1), post-dissection testing of tissues showed no viral nucleic acid except in the muscle tissue ($10^{2.68}$ copies/mL).

Specific antibody responses in pigs infected with ASFV mutants. To assess the specific immune response, we determined the levels of anti-p54 antibodies in the serum. As shown in Figure 5E, the sera of each animal were negative for anti-p54 antibodies on day 7 of

10.3389/fmicb.2024.1345236

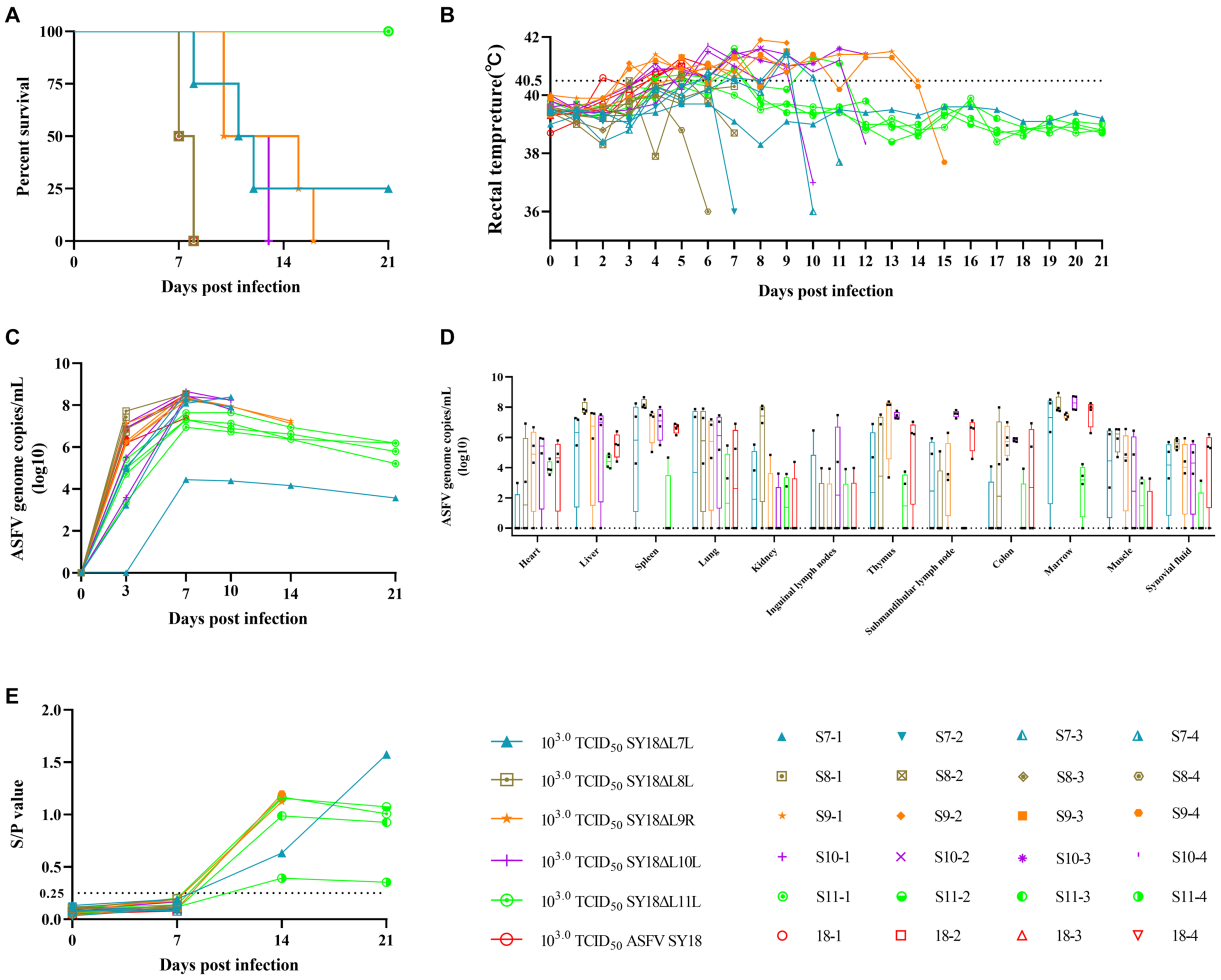

FIGURE 5
Survival, rectal temperature, viraemia, viral load in tissues and anti-p54 antibody levels in pigs inoculated with $10^{3.0}$ $TCID_{50}$ ASFV recombinant virus. **(A)** Survival of animals in each group. **(B)** Each line represents temperature data for individual animals. The dashed line indicates the fever threshold of 40.5°C. **(C)** Detection of ASFV genomic DNA in porcine blood. **(D)** Detection of ASFV genomic DNA in porcine tissues. **(E)** Anti-p54 antibody level in pig serum. y-axis represents the S/P ratio (sample OD_{450nm}/positive control OD_{450nm}), x-axis represents the number of days of immunization, and the dotted line represents the critical value of 0.25.

immunization, and those that survived until day 14 (all pigs in the S9-1, S9-4, S7-1 and SY18ΔL11L groups) were positive for anti-p54 antibodies. Pigs S9-1 and S9-4 produced higher levels of anti-p54 antibodies (S/*p* values of 1.123 and 1.197, respectively), yet died on days 15th and 16th days. The S11-4 pigs in the SY18ΔL11L group expressed lower anti-p54 antibodies than S9-1, S9-4, but the S11-4 pigs survived the observation period. This finding demonstrates that the expression of ASF-specific antibodies is not a marker for animal survival.

3.6 Assessment of protective capacity of SY18ΔL11L mutant

To assess the degree of attenuation of SY18ΔL11L, a low dose ($10^{3.0}TCID_{50}$) and a high dose ($10^{6.0}TCID_{50}$) of SY18ΔL11L were inoculated intramuscularly. Another group of pigs was injected with an equal amount of saline as control (Figures 6A,B; Table 3). All pigs in the low-dose SY18ΔL11L-infected group survived, with two pigs experiencing a transient increase in body temperature and two pigs having persistent fever for 4–5 days. All animals in the high-dose SY18ΔL11L-infected group showed elevated body temperatures (>40.5°C), with symptoms of ASF in H-2 and H-3, which were euthanized on days 11th and 15th days post-inoculated due to the severity of the disease in both animals. Pigs in the control group showed no adverse reactions. To determine the response of the surviving pigs when challenged with the parental virus, a virus provocation test was performed on all pigs that survived the inoculation observation period (Figures 6C,D; Table 4). Each pig was intramuscularly injected with $10^{3.0}TCID_{50}$ of SY18 cells, and observed for 28 days. During the viral challenge, all pigs in the control group had elevated temperatures, developed an ASF clinical reaction, and were euthanized by the 9th day post-challenge (dpc). Pigs inoculated with SY18ΔL11L all survived during the challenge.

Animals inoculated with SY18ΔL11L strain developed viremia on day 7 after immunization (Figure 7A), with the viral load in blood reaching its maximum on day 7 or 14 post-infection, followed by a slow decrease. After ASFV SY18 challenge, control animals exhibited

10.3389/fmicb.2024.1345236

high viral loads in their blood. SY18ΔL11L-infected animals challenged with the parental virus exhibited a steady decline in blood viral load after an increased on day 7. Then, no virus in blood of all but 1 pig on the 28th dpc was be detected (Figure 7B). The ASFV load in the tissues and organs of the animals was measured at the end of the observation period. The results showed that pigs in the control group had higher viral detection in tissues and higher viral loads (Figure 7C). Pigs that died during the immunization period (H2 and H3) had relatively higher virus detection in tissues compared to other pigs immunized with SY18ΔL11L.

The host antibody responses in animals inoculated with SY18ΔL11L are shown in Figure 7D. Animals inoculated with

TABLE 2 Clinical manifestations and survival after immunization with ASFV mutants.

Groups	No. of survivors/ total	No. of fever/ total	Mean value for fever parameter (SD) Fever (≥40.5°C)		
			Day of onset (days ± SD)	Duration no. of days (days ± SD)	Highest rectal temp (°C ± SD)
$10^{3.0}$ $TCID_{50}$ SY18ΔL7L	1/4	3/4	6.67 ± 0.47	2.00 ± 1.58	40.80 ± 0.72
$10^{3.0}$ $TCID_{50}$ SY18ΔL8L	0/4	1/4	5[a]	2[a]	40.25 ± 0.28
$10^{3.0}$ $TCID_{50}$ SY18ΔL9R	0/4	4/4	4.45 ± 0.83	7.75 ± 3.11	41.56 ± 0.19
$10^{3.0}$ $TCID_{50}$ SY18ΔL10L	0/4	4/4	4.50 ± 0.50	6.50 ± 1.11	41.60 ± 0.07
$10^{3.0}$ $TCID_{50}$ SY18ΔL11L	4/4	4/4	5.75 ± 1.30	2.25 ± 2.16	40.85 ± 0.22
$10^{3.0}$ $TCID_{50}$ ASFV SY18	0/4	4/4	4.00 ± 0.00	2.50 ± 0.50	41.03 ± 0.04

[a]Only 1 pig in this group had fever and the rest of the pigs did not die directly after the fever was detected.

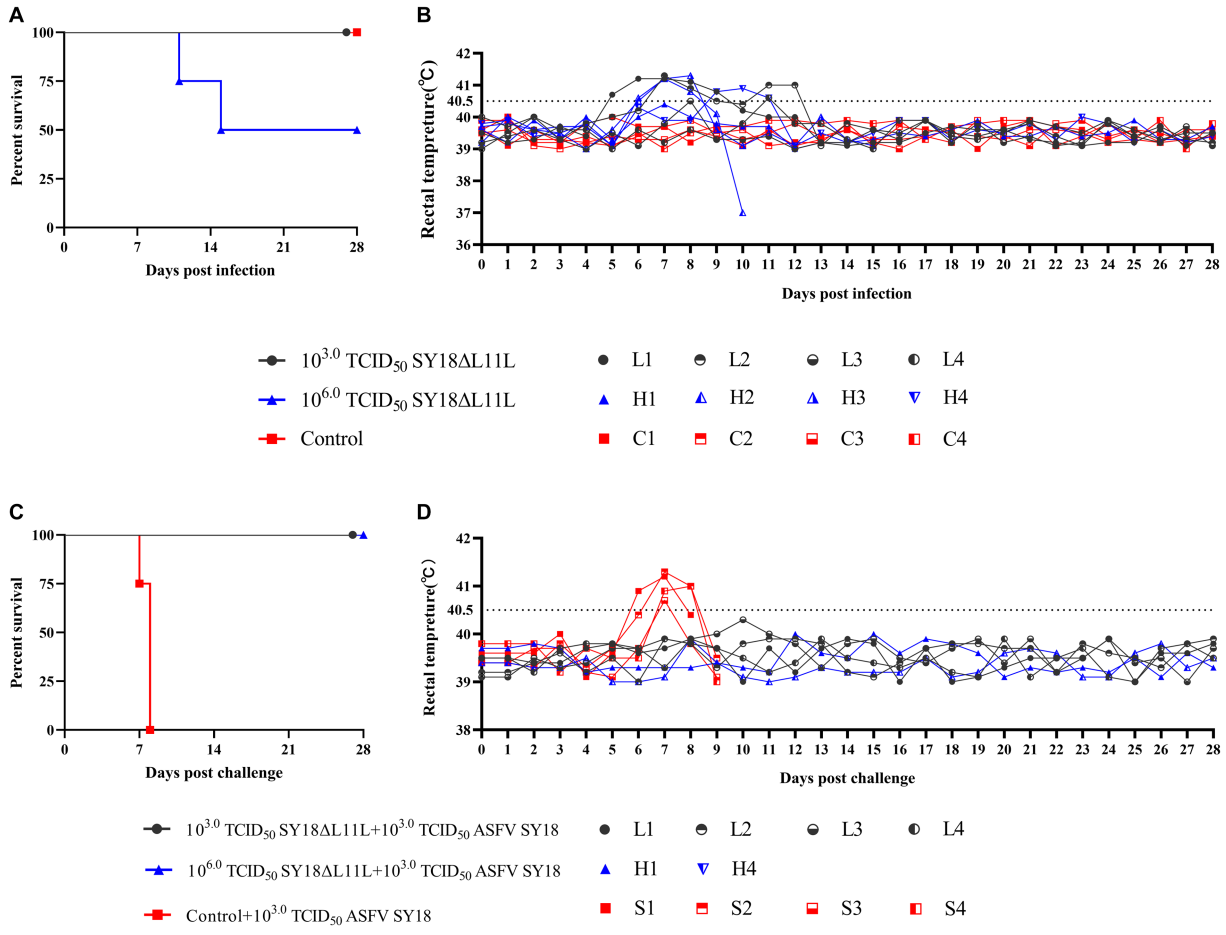

FIGURE 6
Survival and body temperature of pigs after immunization and attack challenge. Survival **(A)** and rectal temperature **(B)** of pigs immunized with $10^{3.0}$ $TCID_{50}$ SY18ΔL11L, $10^{6.0}$ $TCID_{50}$ SY18ΔL11L and control saline. Survival **(C)** and rectal temperature **(D)** of pigs challenged with $10^{3.0}$ $TCID_{50}$ ASFV SY18 tapping. Each line in the graph represents body temperature data for a single animal.

SY18ΔL11L were weakly positive for anti-p54 antibodies in sera of L3 and H4 on day 7 of immunization, and positive for antibodies on day 14, followed by high levels of antibodies in sera thereafter. H3 pigs in the high-dose SY18ΔL11L group died on day 15 even though they were positive for antibodies in serum on day 14 of immunization. After the takedown challenge, pigs in the control group remained negative, and antibodies in pigs inoculated with SY18ΔL11L remained at high levels.

4 Discussion

African swine fever continues to adversely impact the global pig farming industry, and is expanding into new endemic areas. Vaccination remains one of the most effective methods to prevent the spread of this virus. However, the effectiveness of inactivated vaccines has been unsatisfactory (Blome et al., 2014; Cadenas-Fernández et al., 2021). Subunit vaccines have seen limited research due insufficient knowledge on viral proteins (Liu et al., 2023). Effective subunit vaccines are still being investigated (Goatley et al., 2020). Live attenuated virus vaccines, which are produced by passaging tissues or cell cultures to generate ASFV and genetically-engineered and attenuated ASFV, induce strong immunity against ASFV-related strains. After years of ASF epidemics in some areas, a decrease in pig mortality has been observed, leading to isolation of naturally attenuated ASFV that cause subacute, chronic, or subclinical forms of the disease (Arias et al., 2017). However, these have very poor safety profiles, and are prone to causing persistent viremia in pigs, along with symptoms of chronic ASF infection (Gallardo et al., 2018). When ASFV grows in maladapted cells, significant portions of the virus can be lost or mutated, resulting in cell-adapted attenuated ASFV (Koltsova et al., 2021). The number of passages of cell-adapted attenuated ASFV is unpredictable, and immunogenicity decreases when the number of passages is excessive (Krug et al., 2015). Currently, genetically engineered live ASFV with reduced virulence is the most promising ASF vaccine; however, it may not completely clear the virus from pigs, and there is a risk of virulence reversal. Therefore, the construction of ASFV mutants by genetic engineering and the selection of rational virulence-related genes are essential for the development of future ASF vaccines.

ASFV has a genome 170–194 kb in size, containing more than 150 open reading frames (ORFs). Functions of only a small fraction of these ORFs have been characterized. The *L7L-L11L* ORF is located in the right variable region of the ASFV genome, where *L10L* is homologous to *KP177R* (encoding the p22 protein), and *L7L* and L8L genes are thought to be members of MGF110 (Vydelingum et al., 1993; Zhang J. et al., 2021; Cackett et al., 2022). We found that the replication efficiency of the 5 ASFV-mutants was similar to that of the parental strains during *in vitro* experiments. Therefore, *L7L-L11L* are not replication-associated genes. Current research on live attenuated ASFV vaccines has focused on the rational attenuation of virulent viruses through deletion of immunosuppressive genes (Liu et al., 2023b). In a previous study, deletion of the *L7L-L11L* ORF in the ASFV SY18 strain (genotype II) was found to significantly attenuate virulence (Zhang J. et al., 2021). Therefore, virulence-related genes are found in the ORF of *L7L-L11L*. Here, we found that inoculation of pigs with deletion strains of the *L8L*, *L9R*, and *L10L* led to deaths of all the pigs in each group. However, compared with the parental strains, the death time of pigs infected with the deletion strains of the *L9R* and *L10L* genes was delayed to a certain extent, one pig survived after being infected by the deletion strain of the *L7L* gene, and all pigs infected with the deletion strain of the L11L gene survived during the observation period, despite showing fever. We reason that the reduced

TABLE 3 Clinical performance and survival of pigs immunized with SY18△L11L.

Groups	No. of survivors/ total	No. of fever/ total	Mean value for fever parameter (SD) Fever (≥40.5°C)		
			Day of onset (days ± SD)	Duration no. of days (days ± SD)	Highest rectal temp (°C ± SD)
$10^{3.0}$ $TCID_{50}$ SY18ΔL11L	4/4	4/4	7.75 ± 2.17	3 ± 2	40.9 ± 0.35
$10^{6.0}$ $TCID_{50}$ SY18ΔL11L	2/4	4/4	7 ± 1.22	2.75 ± 1.09	40.9 ± 0.31
Mock	4/4	0/4	a	a	a

[a]The pigs did not have a fever.

TABLE 4 Clinical performance and survival rate after challenge.

Groups	No. of survivors/ total	No. of fever/ total	Mean value for fever parameter (SD) Fever (≥40.5°C)		
			Day of onset (days ± SD)	Duration no. of days (days ± SD)	Highest rectal temp (°C ± SD)
$10^{3.0}$ $TCID_{50}$ SY18ΔL11L + $10^{3.0}$ $TCID_{50}$ ASFV SY18	4/4	0/4	a	a	a
$10^{6.0}$ $TCID_{50}$ SY18ΔL11L + $10^{3.0}$ $TCID_{50}$ ASFV SY18	2/2	0/2	a	a	a
$10^{3.0}$ $TCID_{50}$ ASFV SY18	0/4	3/4	5.57 ± 0.47	2.33 ± 0.47	41.17 ± 0.12

[a]The pigs did not have a fever.

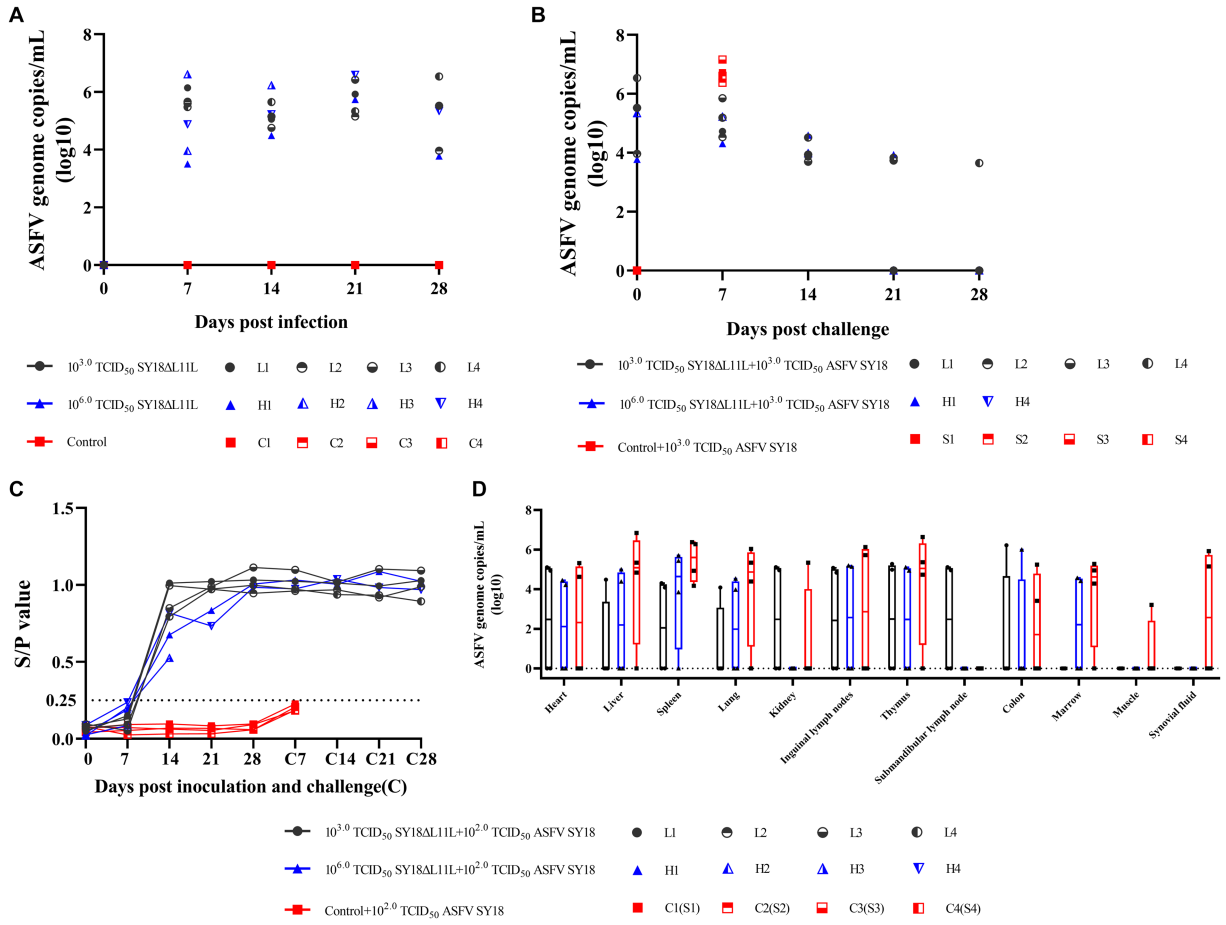

FIGURE 7
Viraemia, changes in antibody levels and tissue viral content in pigs after immunization and attack attacks. Detection of ASFV genomic DNA in the blood of pigs after immunization **(A)** and attack challenge **(B)**. y values denote log10 copies/mL and x values denote time of inoculation and challenge. **(C)** Viral loads in tissues of immunized pigs after takedown challenge. Each symbol represents each pig. Values represent log10 copies/mL. H2 and H3 died during immunization and were not challenged with the parental virus; H2 and H3 only represent viral loads in tissues of immunized pigs. **(D)** Anti-p54 antibodies in pig sera after immunization and challenge. y-axis represents the S/P (sample OD_{450nm}/positive control OD_{450nm}) ratio and x-axis represents the number of days of immunization. The threshold of 0.25 is indicated by the dashed line.

pathogenicity of SY18ΔL7–11 is the result of the combined deletion of the *L7L* and *L11L* genes.

The virulence of ASFV SY18 was not significantly altered by deletion of *L8L*, and deletion of the *L11L* significantly reduced the pathogenicity of ASFV SY18. Vuono et al. performed a deletion of the *I8L* (L8L) alone in the Georgia2010 strain (genotype II), and reported no effects on viral replication or virulence, which is in agreement with our findings (Vuono et al., 2021). Kleiboeker et al. deleted *L11L* from Malawi Lil-20/1 strain, which resulted in the death of all three pigs inoculated with $10^{2.0}HAD_{50}$, and the *L11L* deletion did not reduce the virulence of Malawi Lil-20/1 (Kleiboeker et al., 1998). Malawi Lil-20/1 is a highly virulent strain isolated in Malawi, Africa, whose p72 type belongs to genotype VIII, whereas the epidemic strain in China is genotype II. The deletion of the same gene in different ASFVs may thus result in different virulence-reducing effects. The *CD2v* gene affects the virulence of BA71, ASFV-Kenya-IX-1033, and ASFV HLJ/18, yet has no effect on the virulence of Lil-20/1 in Malawi (Borca et al., 1998; Hemmink et al., 2022). Deletion of the *DP148R* reduced the virulence of Benin 97/1 but had no effect on the virulence of ASFV Georgia 2007/1 and ASFV HLJ18 (Reis et al., 2017; Chen et al., 2020; Rathakrishnan et al., 2021). This phenomenon also suggests that studies on ASFV genes should take the background of the strains and the differences between them into consideration. Because of space constraints we conducted trials using young strains (weaner pigs or grower pigs). The resistance and immunity of young pigs is lower compared to that finisher pigs. ASF causes abortions in sows in late pregnancy (Lohse et al., 2022). We demonstrated the virulence of five ASFV-mutants only in young pigs. However, the specific effects of these ASFV mutants on finishing pigs or gestating sows are uncertain and will require further experimental studies.

5 Conclusion

Previous studies have shown that deletion of *L7L-L11L* genes in ASFV SY18 significantly reduces viral virulence, and that virulence-related genes exist among *L7L-L11L*. In this study, we constructed five recombinant viruses with single-gene deletions using homologous recombination technology, $10^{3.0}TCID_{50}$ doses of the recombinant viruses were used to immunize pigs. All pigs in the SY18ΔL8L,

SY18ΔL9R, and SY18ΔL10L immunization groups died during the observation period, while one pig survived in the SY18ΔL7L group, and all pigs in the SY18ΔL11L group survived. The results demonstrated that *L8L*, *L9R*, and *L10L* are not ASFV SY18 virulence genes, whereas *L7L* and *L11L* are related virulence. Pigs were immunized with $10^{3.0}$TCID$_{50}$ or $10^{6.0}$TCID$_{50}$ doses of recombinant virus SY18ΔL11L, and virus challenge protection experiments were performed. The results showed that SY18ΔL11L could not be completely detoxified by pigs after immunization, and large doses of immunization could still lead to death. However, surviving pigs could resist attack by the parental strain. Here, we found that SY18ΔL11L is an attenuated strain that protects against the parental strain, but not suitable as a vaccine candidate. *L11L* is an ASFV SY18 virulence gene, whereas *L7L* has a slight effect on virus virulence. An in-depth analysis of the functions of this gene may identify new targets for the development of effective vaccines in the future.

Data availability statement

The datasets presented in this study can be found in online repositories. The names of the repository/repositories and accession number(s) can be found at: (Genbank: OR944087), SY18ΔL8L (Genbank: OR944088), SY18ΔL9R (Genbank: OR944089), SY18ΔL10L (Genbank: OR944090), and SY18ΔL11L (Genbank: OR944091).

Ethics statement

The animal study was approved by Animal Welfare and Ethics Committee of the Changchun Veterinary Research Institute. The study was conducted in accordance with the local legislation and institutional requirements.

Author contributions

JF: Methodology, Validation, Writing – original draft. JZ: Validation, Writing – review & editing. FW: Validation, Writing – review & editing. FM: Validation, Writing – review & editing. HZ: Validation, Writing – review & editing. YJ: Validation, Writing – review & editing. YQ: Validation, Writing – review & editing. YZ: Validation, Writing – review & editing. LH: Validation, Writing – review & editing. DZ: Validation, Writing – review & editing. HY: Validation, Writing – review & editing. XZ: Validation, Writing – review & editing. QL: Validation, Writing – review & editing. YW: Validation, Writing – review & editing. TC: Funding acquisition, Writing – review & editing. RH: Funding acquisition, Writing – review & editing.

Funding

The author(s) declare financial support was received for the research, authorship, and/or publication of this article. This work was funded by the National Natural Science Foundation of China (no. 32102656) and National Key Research and Development Program of China (grant nos. 2021YFD1800100 and 2021YFD1801204).

Acknowledgments

The authors thank all the teachers of the Animal Biosafety Level 3 (ABSL-3) Laboratory of the Changchun Veterinary Research Institute for their help, and we are grateful to Editage for their help in revising the article.

Conflict of interest

The authors declare that the research was conducted in the absence of any commercial or financial relationships that could be construed as a potential conflict of interest.

Publisher's note

References

Ankhanbaatar, U., Sainnokhoi, T., Khanui, B., Ulziibat, G., Jargalsaikhan, T., Purevtseren, D., et al. (2021). African swine fever virus genotype II in Mongolia, 2019. *Transbound. Emerg. Dis.* 68, 2787–2794. doi: 10.1111/tbed.14095

Arias, M., Torre, A., Dixon, L., Gallardo, C., Jori, F., Laddomada, A., et al. (2017). Approaches and perspectives for development of African swine fever virus vaccines. *Vaccines* 5:35. doi: 10.3390/vaccines5040035

Blome, S., Gabriel, C., and Beer, M. (2014). Modern adjuvants do not enhance the efficacy of an inactivated African swine fever virus vaccine preparation. *Vaccine* 32, 3879–2882. doi: 10.1016/j.vaccine.2014.05.051

Borca, M., Carrillo, C., Zsak, L., Laegreid, W., Kutish, G., Neilan, J., et al. (1998). Deletion of a CD2-like gene, 8-DR, from African swine fever virus affects viral infection in domestic swine. *J. Virol.* 72, 2881–2889. doi: 10.1128/JVI.72.4.2881-2889.1998

Borca, M., Rai, A., Ramirez-Medina, E., Silva, E., Velazquez-Salinas, L., Vuono, E., et al. (2021). A cell culture-adapted vaccine virus against the current African swine fever virus pandemic strain. *J. Virol.* 95:e0012321. doi: 10.1128/JVI.00123-21

Borca, M., Ramirez-Medina, E., Silva, E., Vuono, E., Rai, A., Pruitt, S., et al. (2020). Development of a highly effective African swine fever virus vaccine by deletion of the I177L gene results in sterile immunity against the current epidemic Eurasia strain. *J. Virol.* 94, e02017–e02019. doi: 10.1128/JVI.02017-19

Bosch-Camós, L., López, E., and Rodriguez, F. (2020). African swine fever vaccines: a promising work still in progress. *Porcine Health Manag.* 6:17. doi: 10.1186/s40813-020-00154-2

Cackett, G., Portugal, R., Matelska, D., Dixon, L., and Werner, F. (2022). African swine fever virus and host response: transcriptome profiling of the Georgia 2007/1 strain and porcine macrophages. *J. Virol.* 96:e0193921. doi: 10.1128/jvi.01939-21

Cadenas-Fernández, E., Sánchez-Vizcaíno, J., Born, E., Kosowska, A., Kilsdonk, E., Fernández-Pacheco, P., et al. (2021). High doses of inactivated African swine fever virus are safe, but do not confer protection against a virulent challenge. *Vaccines* 9:242. doi: 10.3390/vaccines9030242

Chapman, D. A. G., Darby, A. C., Silva, M. D., Upton, C., Radford, A. D., and Dixon, L. D. (2011). Genomic analysis of highly virulent Georgia 2007/1 isolate of African swine fever virus. *Emerg. Infect. Dis.* 17, 599–605. doi: 10.3201/eid1704.101283

Chen, W., Zhao, D., He, X., Liu, R., Wang, Z., Zhang, X., et al. (2020). A seven-gene-deleted African swine fever virus is safe and effective as a live attenuated vaccine in pigs. *Sci. China Life Sci.* 63, 623–634. doi: 10.1007/s11427-020-1657-9

Deutschmann, P., Carrau, T., Sehl-Ewert, J., Forth, J., Viaplana, E., Mancera, J., et al. (2022). Taking a promising vaccine candidate further: efficacy of ASFV-G-ΔMGF after intramuscular vaccination of domestic pigs and Oral vaccination of wild boar. *Pathogens.* 11:996. doi: 10.3390/pathogens11090996

Dixon, L., Sun, H., and Roberts, H. (2019). African swine fever. *Antiviral Res.* 165, 34–41. doi: 10.1016/j.antiviral.2019.02.018

Gallardo, C., Sánchez, E., Pérez-Núñez, D., Nogal, M., León, P., Carrascosa, Á., et al. (2018). African swine fever virus (ASFV) protection mediated by NH/P68 and NH/P68 recombinant live-attenuated viruses. *Vaccine* 36, 2694–2704. doi: 10.1016/j.vaccine.2018.03.040

Gladue, D., Ramirez-Medina, E., Vuono, E., Silva, E., Rai, A., Pruitt, S., et al. (2021). Deletion of the A137R gene from the pandemic strain of African swine fever virus attenuates the strain and offers protection against the virulent pandemic virus. *J. Virol.* 95:e0113921. doi: 10.1128/JVI.01139-21

Goatley, L., Reis, A., Portugal, R., Goldswain, H., Shimmon, G., Hargreaves, Z., et al. (2020). A Pool of eight virally vectored African swine fever antigens protect pigs against fatal disease. *Vaccines* 8:234. doi: 10.3390/vaccines8020234

Gómez-Villamandos, J. C., Bautista, M. J., Sánchez-Cordón, P. J., and Carrasco, L. (2013). Pathology of African swine fever: the role of monocyte-macrophage. *Virus Res.* 173, 140–149. doi: 10.1016/j.virusres.2013.01.017

Hemmink, J., Khazalwa, E., Abkallo, H., Oduor, B., Khayumbi, J., Svitek, N., et al. (2022). Deletion of the CD2v gene from the genome of ASFV-Kenya-IX-1033 partially reduces virulence and induces protection in pigs. *Viruses* 14:1917. doi: 10.3390/v14091917

Iyer, L. M., Balaji, S., Koonin, E. V., and Aravind, L. (2006). Evolutionary genomics of nucleo-cytoplasmic large DNA viruses. *Virus Res.* 117, 156–184. doi: 10.1016/j.virusres.2006.01.009

Kleiboeker, S., Kutish, G., Neilan, J., Lu, Z., Zsak, L., and Rock, D. (1998). A conserved African swine fever virus right variable region gene, l11L, is non-essential for growth in vitro and virulence in domestic swine. *J. Gen. Virol.* 79, 1189–1195. doi: 10.1099/0022-1317-79-5-1189

Koltsova, G., Koltsov, A., Krutko, S., Kholod, N., Tulman, E., and Kolbasov, D. (2021). Growth kinetics and protective efficacy of attenuated ASFV strain Congo with deletion of the EP402 gene. *Viruses* 13:1259. doi: 10.3390/v13071259

Krug, P., Holinka, L., O'Donnell, V., Reese, B., Sanford, B., Fernandez-Sainz, I., et al. (2015). The progressive adaptation of a georgian isolate of African swine fever virus to vero cells leads to a gradual attenuation of virulence in swine corresponding to major modifications of the viral genome. *J. Virol.* 89, 2324–2332. doi: 10.1128/JVI.03250-14

Li, D., Wu, P., Liu, H., Feng, T., Yang, W., Ru, Y., et al. (2022). A QP509L/QP383R-deleted African swine fever virus is highly attenuated in swine but does not confer protection against parental virus challenge. *J. Virol.* 96:e0150021. doi: 10.1128/jvi.01210-22

Liu, W., Li, H., Liu, B., Lv, T., Yang, C., Chen, S., et al. (2023). A new vaccination regimen using adenovirus-vectored vaccine confers effective protection against African swine fever virus in swine. *Emerg Microbes Infect* 12:2233643. doi: 10.1080/22221751.2023.2233643

Liu, Y., Shen, Z., Xie, Z., Song, Y., Li, Y., Liang, R., et al. (2023a). African swine fever virus I73R is a critical virulence-related gene: a potential target for attenuation. *Proc. Natl. Acad. Sci. U. S. A.* 120:e2210808120. doi: 10.1073/pnas.2302161120

Liu, Y., Xie, Z., Li, Y., Song, Y., di, D., Liu, J., et al. (2023b). Evaluation of an I177L gene-based five-gene-deleted African swine fever virus as a live attenuated vaccine in pigs. *Emerg Microbes Infect.* 12:2148560. doi: 10.1080/22221751.2022.2148560

Lohse, L., Nielsen, J., Uttenthal, Å., Olesen, A. S., Strandbygaard, B., Rasmussen, T. B., et al. (2022). Experimental infections of pigs with African swine fever virus (genotype II); studies in young animals and pregnant sows. *Viruses* 14:1387. doi: 10.3390/v14071387

Mai, N., Vu, X., Nguyen, T., Nguyen, V., Trinh, T., Kim, Y., et al. (2021). Molecular profile of African swine fever virus (ASFV) circulating in Vietnam during 2019-2020 outbreaks. *Arch. Virol.* 166, 885–890. doi: 10.1007/s00705-020-04936-5

Mur, L., Atzeni, M., Martínez-López, B., Feliziani, F., Rolesu, S., and Sanchez-Vizcaino, J. M. (2016). Thirty-five-year presence of African swine fever in Sardinia: history, evolution and risk factors for disease maintenance. *Transbound. Emerg. Dis.* 63, e165–e177. doi: 10.1111/tbed.12264

Rathakrishnan, A., Reis, A., Goatley, L., Moffat, K., and Dixon, L. (2021). Deletion of the K145R and DP148R genes from the virulent ASFV Georgia 2007/1 isolate delays the onset, but does not reduce severity, of clinical signs in infected pigs. *Viruses* 13:1473. doi: 10.3390/v13081473

Reis, A., Goatley, L., Jabbar, T., Sanchez-Cordon, P., Netherton, C., Chapman, D., et al. (2017). Deletion of the African swine fever virus gene DP148R does not reduce virus replication in culture but reduces virus virulence in pigs and induces high levels of protection against challenge. *J. Virol.* 91, e01428–e01417. doi: 10.1128/JVI.01428-17

Rowlands, R., Michaud, V., Heath, L., Hutchings, G., Oura, C., Vosloo, W., et al. (2008). African swine fever virus isolate, Georgia, 2007. *Emerg. Infect. Dis.* 14, 1870–1874. doi: 10.3201/eid1412.080591

Sun, E., Huang, L., Zhang, X., Zhang, J., Shen, D., Zhang, Z., et al. (2021a). Genotype I African swine fever viruses emerged in domestic pigs in China and caused chronic infection. *Emerg Microbes Infect.* 10, 2183–2193. doi: 10.1080/22221751.2021.1999779

Sun, E., Zhang, Z., Wang, Z., He, X., Zhang, X., Wang, L., et al. (2021b). Emergence and prevalence of naturally occurring lower virulent African swine fever viruses in domestic pigs in China in 2020. *Sci. China Life Sci.* 64, 752–765. doi: 10.1007/s11427-021-1904-4

Urbano, A. C., and Ferreira, F. (2022). African swine fever control and prevention: an update on vaccine development. *Emerg Microbes Infect.* 11, 2021–2033. doi: 10.1080/22221751.2022.2108342

Vuono, E., Ramirez-Medina, E., Pruitt, S., Rai, A., Silva, E., Espinoza, N., et al. (2021). Evaluation in swine of a recombinant Georgia 2010 African swine fever virus lacking the I8L gene. *Viruses* 13:39. doi: 10.3390/v13010039

Vydelingum, S., Baylis, S., Bristow, C., Smith, G., and Dixon, L. (1993). Duplicated genes within the variable right end of the genome of a pathogenic isolate of African swine fever virus. *J. Gen. Virol.* 74, 2125–2130. doi: 10.1099/0022-1317-74-10-2125

Wardley, R., Andrade, C. M., Black, D. N., Portugal, F. L. C., Enjuanes, L., Hess, W. R., et al. (1983). African swine fever virus. Brief review. *Arch. Virol.* 76, 73–90.

Zhang, Y., Ke, J., Zhang, J., Yang, J., Yue, H., Zhou, X., et al. (2021). African swine fever virus bearing an I226R gene deletion elicits robust immunity in pigs to African swine fever. *J. Virol.* 95:e0119921. doi: 10.1128/JVI.01199-21

Zhang, J., Zhang, Y., Chen, T., Yang, J., Yue, H., Wang, L., et al. (2021). Deletion of the L7L-L11L genes attenuates ASFV and induces protection against homologous challenge. *Viruses* 13:225. doi: 10.3390/v13020255

Zhou, X., Li, N., Luo, Y., Liu, Y., Miao, F., Chen, T., et al. (2018). Emergence of African swine fever in China, 2018. *Transbound. Emerg. Dis.* 65, 1482–1484. doi: 10.1111/tbed.12989

frontiers | Frontiers in Microbiology

TYPE Original Research
PUBLISHED 31 January 2024
DOI 10.3389/fmicb.2024.1328987

OPEN ACCESS

EDITED BY
Jingqiang Ren,
Wenzhou University, China

REVIEWED BY
Weihong Qi,
ETH Zürich, Switzerland
Xingyu Yan,
Jiangsu Academy of Agricultural Sciences (JAAS), China
Rahul Sharma,
Advanta Genetics, United States

*CORRESPONDENCE
David L. Suarez
✉ david.suarez@usda.gov

RECEIVED 27 October 2023
ACCEPTED 09 January 2024
PUBLISHED 31 January 2024

CITATION
Goraichuk IV, Harden M, Spackman E and Suarez DL (2024) The 28S rRNA RT-qPCR assay for host depletion evaluation to enhance avian virus detection in Illumina and Nanopore sequencing.
Front. Microbiol. 15:1328987.
doi: 10.3389/fmicb.2024.1328987

The 28S rRNA RT-qPCR assay for host depletion evaluation to enhance avian virus detection in Illumina and Nanopore sequencing

Iryna V. Goraichuk[1], Mark Harden[2], Erica Spackman[1] and David L. Suarez[1]*

[1]Southeast Poultry Research Laboratory, U.S. National Poultry Research Center, Agriculture Research Service, U.S. Department of Agriculture, Athens, GA, United States, [2]College of Veterinary Medicine, Tuskegee University, Tuskegee, AL, United States

Abundant host and bacterial sequences can obscure the detection of less prevalent viruses in untargeted next-generation sequencing (NGS). Efficient removal of these non-targeted sequences is vital for accurate viral detection. This study presents a novel 28S ribosomal RNA (rRNA) RT-qPCR assay designed to assess the efficiency of avian rRNA depletion before conducting costly NGS for the detection of avian RNA viruses. The comprehensive evaluation of this 28S-test focuses on substituting DNase I with alternative DNases in our established depletion protocols and finetuning essential parameters for reliable host rRNA depletion. To validate the effectiveness of the 28S-test, we compared its performance with NGS results obtained from both Illumina and Nanopore sequencing platforms. This evaluation utilized swab samples from chickens infected with highly pathogenic avian influenza virus, subjected to established and modified depletion protocols. Both methods significantly reduced host rRNA levels, but using the alternative DNase had superior performance. Additionally, utilizing the 28S-test, we explored cost- and time-effective strategies, such as reduced probe concentrations and other alternative DNase usage, assessed the impact of filtration pre-treatment, and evaluated various experimental parameters to further optimize the depletion protocol. Our findings underscore the value of the 28S-test in optimizing depletion methods for advancing improvements in avian disease research through NGS.

KEYWORDS

next-generation sequencing (NGS), Illumina, Nanopore, MinION, 28S, RNA virus, depletion

1 Introduction

In recent years, untargeted next-generation sequencing (NGS) technology has been increasingly employed for the detection and characterization of RNA viruses, particularly in the context of avian diseases (Chen et al., 2013; Tang et al., 2015; Goraichuk et al., 2016, 2017, 2019, 2021a,b; Croville et al., 2018; Ferreri et al., 2019; Tal et al., 2019; Patzina-Mehling et al., 2020; Crossley et al., 2021; Chrzastek et al., 2022; Damir et al., 2023; Ip et al., 2023; Kariithi et al., 2023; Techera et al., 2023). Avian viruses, including highly pathogenic avian influenza

virus (AIV) and Newcastle disease virus (NDV), pose significant threats to poultry populations and public health (Alexander, 1998; Suarez, 2017; Swayne et al., 2020). One of the biggest risks to the global poultry industry is the loss of animals and reduced egg production associated with infection by these RNA viruses. Whole-genome sequencing has become an important tool for the characterization of transmission and epidemiology of infectious diseases (Eyre, 2022). For example, the sequencing of AIV was instrumental in defining the multiple introductions of highly pathogenic AIV into North America in 2021–2022 (Alkie et al., 2022; Bevins et al., 2022; Caliendo et al., 2022; Engelsma et al., 2022; Günther et al., 2022) and tracking outbreaks (Rasmussen et al., 2023; Williams et al., 2023), farm-to-farm spread (Nagy et al., 2023; Youk et al., 2023), and spillovers to mammals (Agüero et al., 2023; Elsmo et al., 2023; Leguia et al., 2023; Nguyen et al., 2023; Puryear et al., 2023; Vreman et al., 2023). The diversity of poultry viruses is large, and concurrent infection with other infectious agents can complicate disease diagnosis. Therefore, the accurate and timely detection and characterization of avian viruses is crucial for effective disease control, surveillance, and management.

The typical NGS run is both cost and labor-intensive. Thus, a common aim of all NGS experiments is to maximize the yield of sequence reads of interest. The successful application of NGS for virus detection in samples faces a critical challenge—the presence of abundant host and bacterial sequences. These non-target sequences commonly include ribosomal RNA (rRNA), which can comprise up to 95% of total reads depending on the sample type (Morlan et al., 2012; Fauver et al., 2019). These sequences can overshadow the viral genetic material, making it difficult to detect and characterize the less prevalent viruses of interest (Morlan et al., 2012; Shi et al., 2022). The removal of the most abundant host-specific rRNA (18S, 28S, mitochondrial) and bacterial rRNA (16S, 23S) is a fundamental step in addressing this issue, as it can substantially improve the sensitivity and accuracy of viral detection in NGS data.

Currently, depletion methods often involve enzymatic treatment (Allander et al., 2001; Kapoor et al., 2008; Victoria et al., 2008; Bal et al., 2018; Marotz et al., 2018; Oechslin et al., 2018; Oristo et al., 2018; Nelson et al., 2019; Shi et al., 2019; Amar et al., 2021; Bruggeling et al., 2021; Gan et al., 2021), probe hybridization-based methods (Metsky et al., 2017; Stark et al., 2019; Zeng et al., 2020; Gu et al., 2021; Parris et al., 2022), DNA-intercalating dyes (Nocker et al., 2009; Fittipaldi et al., 2012), cell lysis (Hasan et al., 2016; Charalampous et al., 2019; Yeoh, 2021), size selection (Ng et al., 2009; Hall et al., 2014; Kohl et al., 2015; Liang and Bushman, 2021; Wang et al., 2021), and targeted enrichment (Lee et al., 2017; Imai et al., 2018; Freed et al., 2020; Galli et al., 2022; Singh, 2022). While these methods are effective to some extent, their efficiency can vary, and the choice of enzymes, filter size, etc., can significantly impact NGS outcomes and add to the cost of testing each sample. Thus, there is a need for a systematic evaluation and optimization of depletion methodologies to enhance the detection of avian viruses via NGS. In our prior studies, we developed a targeted RNase H-based depletion approach (Parris et al., 2022; Bakre et al., 2023) to reduce the abundance of host and bacterial reads using DNA probes designed to target chicken 18S and 28S rRNA, specific chicken mitochondrial RNA, and select 16S and 23S bacterial rRNA (O'Flaherty et al., 2018; Wille et al., 2018). Nonetheless, we consistently engage in an optimization process to ensure that our protocols are tuned for improved viral detection capabilities through increased sequencing depth and genome breadth of coverage for various avian viral pathogens of interest. Therefore, a reliable cost-effective quantitative polymerase chain reaction (qPCR) assay was sought as an alternative to the cost-intensive NGS in the further optimization of the depletion methods for effective reduction of host rRNA abundance in the analyzed samples, ultimately heightening sequencing depth and breadth of coverage of the target viral pathogens in these specimens.

The objective of this work was to develop a superior method to deplete host rRNA before NGS library preparation and we also introduce a novel 28S rRNA reverse transcription qPCR (RT-qPCR) assay. This assay was designed to assess the efficiency of depletion methods before conducting costly NGS for avian virus detection. This comprehensive evaluation focuses on evaluating different DNAses in our established RNase H-based depletion protocol (Parris et al., 2022; Bakre et al., 2023), fine-tuning essential parameters for reliable host rRNA depletion, and exploring other cost- and time-effective strategies. The significance of this work lies in the 28S-test potential to facilitate the further optimization of different depletion protocols to improve the accuracy and sensitivity of avian virus detection via NGS, ultimately contributing to better disease management and our understanding of avian virus abundance.

2 Materials and methods

2.1 Samples

To validate the performance of the 28S rRNA RT-qPCR assay, we compared its results to Nanopore and Illumina NGS data. Five oropharyngeal (OP) and cloacal (CL) swabs were collected from 5 six-week-old specific-pathogen-free (SPF) white leghorn chickens (*Gallus domesticus*; obtained from the Southeast Poultry Research Laboratory in-house flocks, Athens, GA, United States) after they succumbed to infection with a high dose of 6 $\log_{10}EID_{50}$ per bird in 0.1 mL of highly pathogenic H5N1 AIV A/turkey/Indiana/22-003707-003/2022 in the animal BSL-3E facilities. Chickens had *ad libitum* access to food and water throughout the experiment. The swabs were immediately deposited into sterile cryovials containing 2 mL of brain heart infusion (BHI) transport media and were stored at 4°C. Additionally, OP and CL swabs obtained from four euthanized SPF chickens (n = 8) were spiked with low pathogenic LaSota Newcastle Disease Virus (NDV) and were used to mimic field samples for the optimization of 28S rRNA RT-qPCR.

2.2 Depletion methods

Aliquots of RNA extracts from the samples described above were treated with different depletion methods designed to remove abundant non-target host and bacterial sequences (Figure 1). These treatments included filtration pre-treatment before nucleic acid extraction (0.45 µm Nylon, 0.45 µm Nalgene surfactant-free cellulose acetate (SFCA), and 0.22 µm Nalgene SFCA Syringe Filters, Thermo Scientific, United States) and RNase H probe hybridization followed by different DNase digestions. Our main focus was to refine our established rRNA depletion method to enhance its capability to selectively remove specific rRNA (18S, 28S, mitochondrial) and bacterial rRNA (16S, 23S). This method was compared to modified

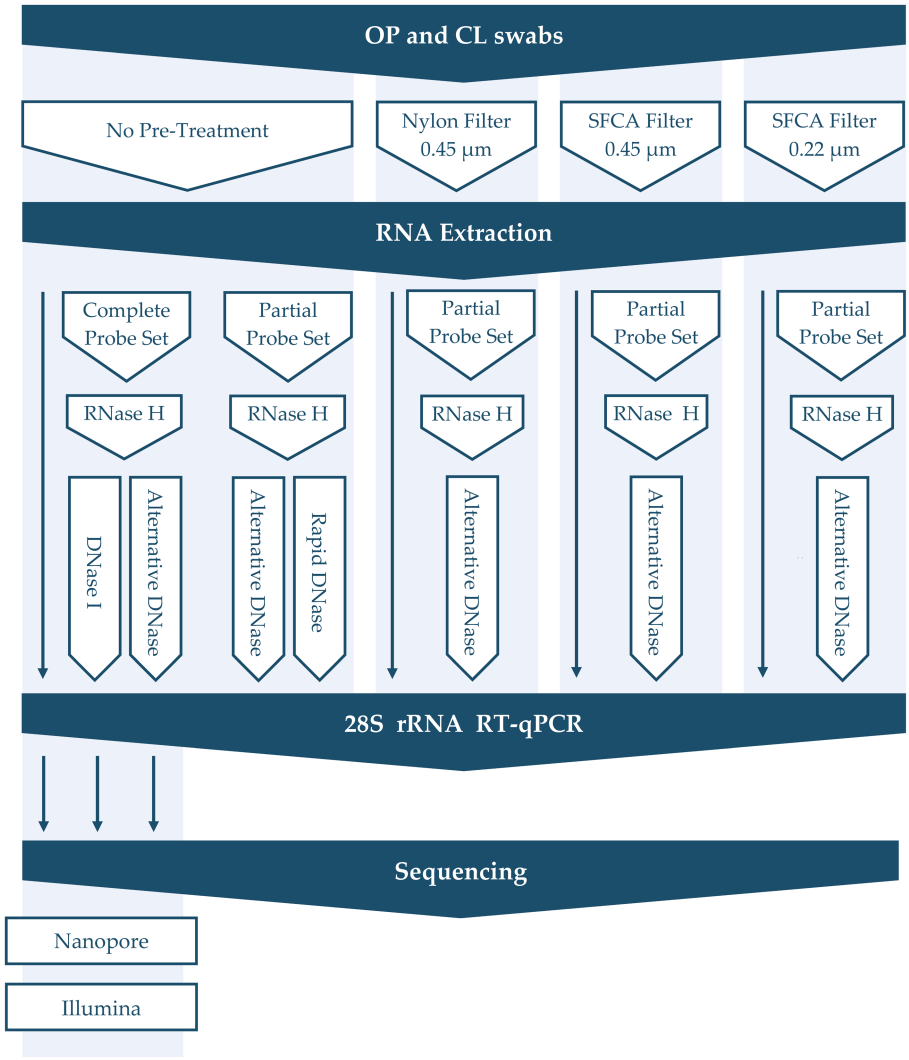

FIGURE 1
Overview of depletion methods applied in this study.

protocols in which DNase I (NEB, United States) was substituted with the alternative DNase (TURBO DNA-free kit; Invitrogen, United States) or rapid DNase (ezDNase, Invitrogen, United States), which were all done in parallel. Additionally, a partial probe set (CK28s rRNA4 and CK28s rRNA5) of varying concentrations was tested in conjunction with the alternative DNase digestion to selectively deplete chicken 28S rRNA (Parris et al., 2022; Bakre et al., 2023). Briefly, 12-µL aliquots of RNA (with and without filtration pre-treatment) were hybridized with DNA probes by incubating at 95°C for 5 min, cooling gradually (0.1°C/s) to 22°C, and incubating for an additional 5 min at 22°C. RNA–DNA hybrids were then degraded by incubating with RNase H at 37°C for 30 min, and either DNase I, alternative DNase, or rapid DNase were used for further digestion (30, 30, or 2 min, correspondently) to remove excess DNA probes. The alternative DNase digestion was stopped by adding 0.2 volumes of DNase Inactivation Reagent as per the manufacturer's recommendations. DNase digestion time (30, 45, 60 min), repeated RNase H degradation, as well as concentration of probes were also tested. Finally, RNA was purified with the AMPure RNAClean XP beads (Beckman Coulter, United States) at 2.2 volume. Untreated controls were included for each sample to provide a baseline reference.

2.3 Primer and probe design

We designed the 28S rRNA RT-qPCR assay for the performance evaluation of different depletion methods before NGS sequencing. After testing different sets of primers and probes targeting host 28S rRNA, the final set of forward primer 28S+3894 (5′-GTCGGCTCTTCCTATCATTGTG-3′), reverse primer 28S-4026 (5′-CGCAACAACACATCATCAGTAGG-3′) and probe 28S+3198 (5′-GCAGAATTCACCAAGCGTTGGATTGTTCACC-3′ FAM reporter dye with Zen/Black Hole Quencher 1; Integrated DNA Technologies, Iowa City, IA) was selected. We then optimized the annealing temperature RT-qPCR and evaluated the primer/probe concentration and ratio to attain optimal conditions.

The RT-qPCR 28S-test was performed using the AgPath-ID One-Step RT-PCR kit (Applied Biosystems, United States) in 25-µL

reaction volumes comprised of 2 μL of total RNA, 12.5 μL of 2 × RT-PCR buffer, 0.5 μL of the forward and reverse primers (20 pmol/μL), 0.5 μL of the probe (6 pmol/μL), 1 μL of AgPath Enzyme Mix (Ambion, United States), and sterile nuclease-free water. The test included an initial RT step (10 min at 45°C and 10 min at 95°C) and PCR steps of 40 cycles (10 s at 94°C, 30 s at 57°C, and 10 s at 72°C). All RT-qPCR tests were performed on a QuantStudio 5 real-time PCR system (Applied Biosystems, United States).

Additionally, viral RNA preservation after different depletion methods was evaluated by the NVSL AIV matrix gene (M-test) RT-qPCR with the forward primer M+25 (5′-AGATGAGT CTTCTAACCGAGGTCG-3′), two reverse primers M-124 2002 (5′-TGCAAAAACATCTTCAAGTCTCTG-3′), M-124p 2009 (5′-TG CAAAGACACTTTCCAGTCTCTG-3′) and probe M+64 (5′-TCA GGCCCCCTCAAAGCCGA-3′) and the USDA-validated NDV M-test RT-qPCR with the forward primer M+4100 (5′-AGTG ATGTGCTCGGACCTTC-3′), reverse primer M-4220 (5′-CCTGAG GAGAGGCATTTGCTA-3′) and probe M+4169 (5′-TTCTCTAGCA GTGGGACAGCCTGC-3′), as previously described (Spackman et al., 2002; Wise et al., 2004).

2.4 Library preparation and sequencing

To assess the effectiveness of our RT-qPCR 28S-test, we compared its performance to the results of long-read Nanopore and short-read Illumina sequencing. For this, 5 untreated RNA extracts from swab samples collected from AIV-infected birds were compared to the same extracts but treated with our custom depletion protocol using DNase I and the alternative DNase. Treated and untreated RNA extracts from each sample were amplified via sequence-independent, single-primer amplification (SISPA) as described previously (Chrzastek et al., 2017). Briefly, first-strand cDNA was synthesized using 100 pmol of K-8 N primer (5′-GACCATCTAGCGACCTCCACNNNNNNNN-3′) with the SuperScript IV First-Strand System (Invitrogen, United States) following the manufacturer's instructions. Second-strand synthesis was performed using the DNA Polymerase I, Large (Klenow) Fragment (NEB Inc., United States) with 10 pmol of K-8 N primer and 10 μM dNTPs and resulting dsDNA was bead purified using the AMPure XP beads (Beckman Coulter, United States). Amplification of cDNA was performed using the Phusion High-Fidelity PCR Kit (NEB Inc., United States) with the 10 μM of K primer (5′-GACCATCTAGCGACCTCCAC-3′) under the following conditions: 98°C for 30 s, followed by 35 cycles of 98°C for 10 s, 55°C for 30 s, and 72°C for 1 min, with a final extension at 72°C for 10 min. After the SISPA amplification step, amplicons were bead-purified in a 1:1.8 sample volume to bead volume ratio and quantified using the Qubit 1X dsDNA High Sensitivity Assay Kit (Invitrogen, United States), followed by sample library preparation for Nanopore and Illumina sequencing libraries.

The Nanopore sequencing libraries were prepared using the Native Barcoding Kit 24 V14 (SQK-NBD114.24, Oxford Nanopore Technologies, England) following the manufacturer's instructions. The final library was quantified using a High Sensitivity D5000 Screen Tape on a 4150 TapeStation (Agilent Technologies, United States). We then sequenced 20 fmol of the prepared library on a single R10.4.1 flow cell (FLO-MIN114, Oxford Nanopore Technologies, England) using a MinION Mk1C instrument with the MinKNOW 23.04.8 software. Sequencing was run until all pores of the flow cell were exhausted (~48 h).

The Illumina libraries were prepared using the Illumina DNA Prep (Illumina, United States) according to the manufacturer's recommendations. After quantification using the Qubit 1X dsDNA High Sensitivity Assay Kit (Invitrogen, United States) and High Sensitivity D5000 Screen Tape (Agilent Technologies, United States), the libraries were pooled (4 nM, 10 μL each), spiked with a control library (5% PhiX library v3), diluted to 12 pM final concentration and sequenced (paired-end; 2 × 300 bp) using the 600-cycle MiSeq Reagent Kit v3 (Illumina, United States) on an Illumina MiSeq instrument.

2.5 Data analysis

After the sequencing run, Nanopore raw Pod5 files were basecalled (high-accuracy, 400kbs) to generate FastQ files, that were further demultiplexed and trimmed using Guppy 6.5.7 within the MinKNOW 23.04.8 software on a MinION Mk1C instrument. Reads with a minimum quality of 9 were considered for further analysis.

The Illumina raw sequencing data was pre-processed within the Galaxy platform, as described previously (Dimitrov et al., 2017). Raw sequence reads were quality assessed using FastQC v0.63 (Andrews, 2010) residual adaptor sequence and low-quality bases were trimmed using Cutadapt v1.16.6 (Martin, 2011). After control library reads were removed using the Burrows-Wheeler alignment tool (BWA-MEM; Li and Durbin, 2009), forward and reverse reads were merged using PEAR v.0.9.6.1 (Zhang et al., 2014).

The host (*Gallus gallus*) reads were removed from the pre-processed Nanopore and Illumina reads using a BWA-MEM tool. The remaining unmapped reads were further used for taxonomical classification by Kraken2 v2.0.8 using the PlusPF database (Wood and Salzberg, 2014; Wood et al., 2019) and AIV genome consensus assembly by BWA-MEM mapping with reference genome A/Turkey/Indiana/22–003707-003/2022 (H5N1; GenBank accession numbers OQ965225 to OQ965232) within the Galaxy platform. The Kraken2 classified reads were further processed with Bracken v2.5 (Lu et al., 2017) to estimate relative abundance at the family level. Individual Bracken taxonomy tables for each treatment were merged with the "combine_bracken_outputs.py" python script. The merged Bracken data was processed with the R application "bracken_plot" (Vill, 2023) to determine and visualize the top 10 taxa with the greatest median relative abundances.

2.6 Statistical analysis

GraphPad Prism 9.3.1 was used for data representation and statistical analysis. The One-way ANOVA followed by Tukey's multiple comparisons test was utilized to compare the relative difference of cycle threshold (Ct) values among different depletion methods with untreated control samples. For statistical purposes, all swab samples with negative RT-qPCR results were assigned a Ct value of 40. The value of $p < 0.05$ was considered statistically significant.

3 Results

3.1 RT-qPCR 28S-test design and optimization

In our efforts to optimize the RT-qPCR 28S-test conditions, we focused on refining the primer annealing temperature, primer/probe concentration, and selecting the most suitable primer pair set. To achieve this, we designed four pairs of sequence-specific primers targeting host 28S rRNA based on sequences available in the NCBI database. These primers were carefully designed to meet specific criteria. They were relatively short, ranging from 20 to 25 base pairs in length. We avoided the presence of three or more consecutive nucleotides of the same type (e.g., AAA or GGG) in any of the primers. Additionally, we ensured that each primer had a C or G at the last nucleotide position at either or both ends, and their GC content ranged from 45 to 50%.

Serial dilutions (1:10 dilution) of total RNA extracted from OP and CL swabs collected from SPF birds were used to test the performance of different primer/probe sets and their concentration. To identify the optimal annealing temperature for each primer pair, we conducted gradient RT-qPCR. After a series of tests, we determined that the best-performing primer/probe set was 28S+3894, 28S-4026, and 28S+3918. We further refined the assay by selecting the optimal primer/probe concentration and annealing temperature (data not shown). after testing different concentrations, 10 pmol of each primer and 3 pmol of probe per reaction were chosen as optimal, at an annealing temperature of 57°C.

3.2 Next-generation sequencing

First, we evaluated the performance of the RT-qPCR 28S-test comparing our established RNase H-based rRNA depletion assay (Parris et al., 2022; Bakre et al., 2023) and a modified protocol in which evaluating alternative DNases. This assessment was performed on five swabs collected from SPF chickens experimentally infected with the highly pathogenic H5N1 AIV. These samples were subjected to the established and modified depletion methods utilizing our complete set of custom probes, which selectively depletes host-specific rRNA (18S, 28S, mitochondrial) and bacterial rRNA (16S, 23S). Next, we prepared Nanopore and Illumina sequencing libraries for three sets of samples: untreated, samples after depletion with DNase I, and samples after depletion with the alternative DNase. Both depletion treatments substantially ($p < 0.0001$) increased the average Ct values in the RT-qPCR 28S-test when compared to untreated control samples (Figure 2A; Supplementary Table 1). However, significantly higher Ct values ($p < 0.001$) were observed in samples treated with the alternative DNase compared to samples treated with DNase I, indicating a more effective reduction in host-specific rRNA. Notably, these results corresponded to the NGS outcome on both Nanopore and Illumina platforms (Figure 2B). In swabs with higher Ct values a reduced number of host-specific reads per 100 k obtained was observed on both sequencing platforms. The trend between depletion methods in the elevation of the average Ct values had an inverse correlation with the decrease in the average percentage of host reads on both sequencing platforms (Figure 2C; Supplementary Table 1). Although both depletion treatments led to a decrease in the average percentage of host-specific reads, a statistically significant reduction ($p < 0.05$) was only evident in samples treated with the alternative DNase.

Regardless of the depletion assay used, both DNase treatments led to a reduction not only in host-specific but also bacterial reads (Supplementary Figure 1), consequently enabling a notable increase in the number of sequenced viral reads (Supplementary Table 1). The changes in bacterial abundance correlated with the bacterial rRNA (16S, 23S) that were targeted by hybridization probes during depletion. Thus, we observed the reduction of reads belonging to families that were targeted during depletion (*Lactobacillaceae*, *Oscillospiraceae*, *Yersiniaceae, except Enterobacteriaceae*) and a consequent rise of untargeted reads (*Orthomyxoviridae*, *Hominidae*, *Enterococcaceae*, *Staphylococcaceae*, *Streptomycetaceae*, *Prevotellaceae*) compared to untreated samples (Supplementary Figure 2). Notably, while DNase I and alternative DNase depletion treatments both slightly reduced viral RNA ($p < 0.01$ and $p < 0.05$, correspondently), represented by elevated Ct values in the AIV M-test (Figure 3A), they provided increase in the relative abundances of sequenced reads belonging to family *Orthomyxoviridae* (Supplementary Figure 2). The alternative DNase outperformed DNase I, resulting in higher Ct values in the 28S-test, lower Ct values in the AIV M-test, and a higher increase of sequenced viral reads. Specifically, in samples treated with the alternative DNase, viral reads constituted 7.7% and 3.1% of the total reads, whereas only 0.4% and 0.6% of viral reads were presented in untreated samples when sequenced on Nanopore and Illumina platforms, respectively. Moreover, a substantial 7-fold and 5-fold increase in the average number of viral reads per 100 k sequences was observed in samples treated with the alternative DNase compared to those treated with DNase I and subsequently sequenced on Nanopore and Illumina platforms, correspondently (Figure 3B). This elevation in sequenced viral reads subsequently contributed to the improved breadth of the AIV genome after consensus assembly (Figure 3C; Supplementary Table 1). It is noteworthy that, although there was an increase in the average percentage of AIV genome breadth in samples subject to both depletion assays, only the use of the alternative DNase resulted in a statistically significant ($p < 0.05$) enhancement in viral genome breadth (Figure 3C). In fact, both Nanopore and Illumina platforms yielded an average AIV genome breadth exceeding 90% after the alternative DNase treatment. Furthermore, regardless of the type of DNase used, the depletion of host-specific and bacterial rRNA correlated with the enhanced breadth of viral genome coverage obtained on both sequencing platforms (Figure 3D). Therefore, the results of the developed RT-qPCR 28S-test were confirmed by positive correlation with the sequencing outcome, demonstrating its potential to facilitate further optimizations of host rRNA depletion for improved detection of avian pathogens.

3.3 Depletion treatments

3.3.1 DNase digestion

After confirming RT-qPCR 28S-test results with the NGS results using swabs collected from birds infected with highly pathogenic H5N1 AIV, we repeated the comparison of substituting DNase I with the alternative DNase in our depletion protocol using swab samples collected from SPF chickens and spiked with the low pathogenic LaSota NDV. The RT-qPCR NDV M-test was conducted to assess the preservation of viral RNA after the depletion

10.3389/fmicb.2024.1328987

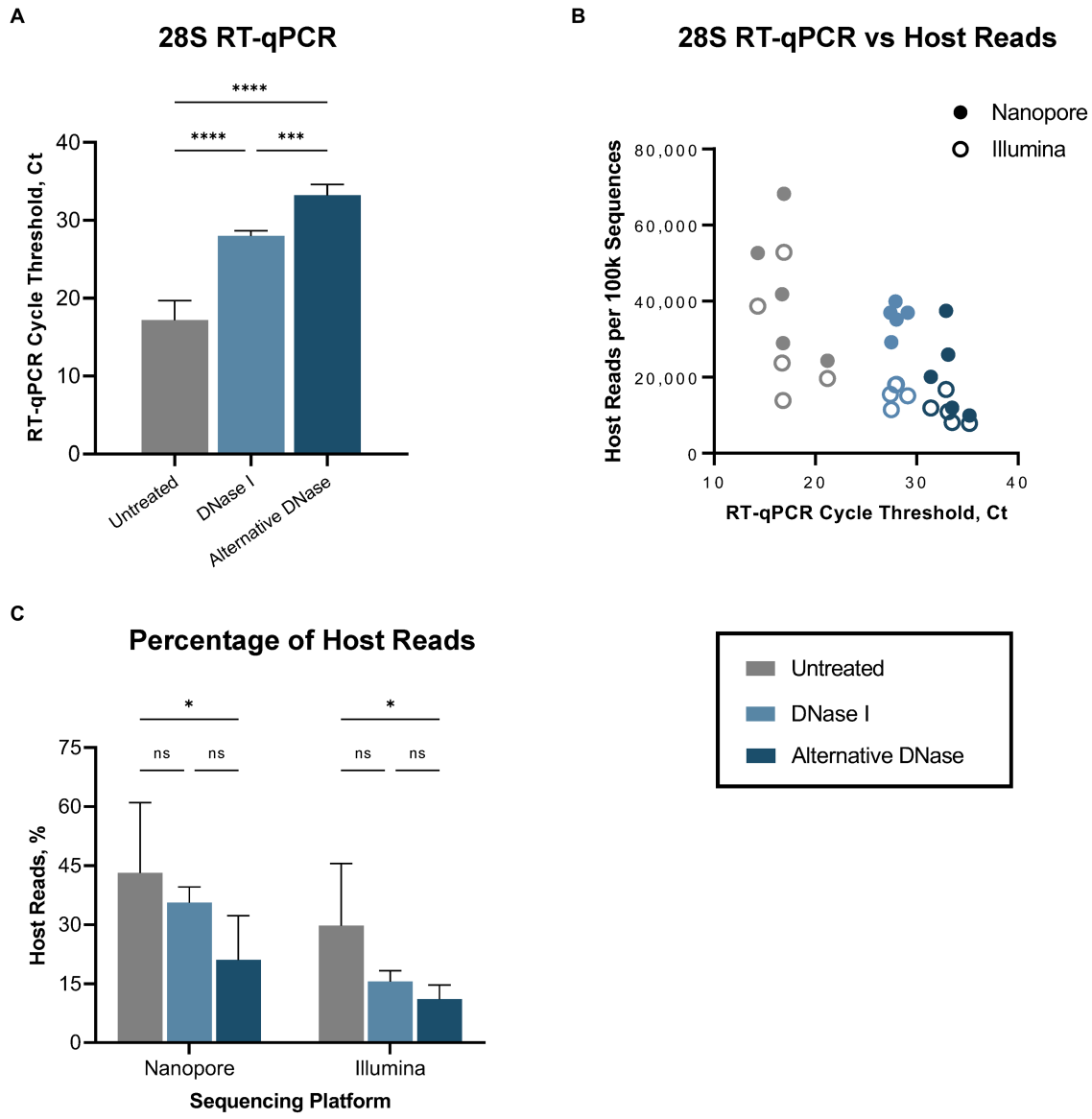

FIGURE 2
Host (*Gallus gallus*) reads depletion outcome. **(A)** Average cycle threshold (Ct) values of 28S rRNA RT-qPCR assay in different depletion methods. **(B)** Relationship between 28S rRNA RT-qPCR Ct values and number of sequenced host-specific reads. **(C)** The average percentage of reads mapping to the host genome in different depletion treatments obtained on Nanopore and Illumina sequencing platforms. One-way ANOVA with Tukey's multiple comparison analysis was used to evaluate the significance between different depletion methods. A value of $p<0.05$ was considered to be significant. *$p < 0.05$; **$p < 0.01$; ***$p < 0.001$; ****$p < 0.0001$.

treatments. Consistent with our prior observations, the results indicated that both DNase I and alternative DNase treatments significantly ($p < 0.0001$) reduced host rRNA levels compared to untreated controls (Figure 4A), as evidenced by the elevated Ct values in RT-qPCR 28S-test. Depletion treatment with the alternative DNase resulted in a more substantial increase in RT-qPCR threshold values (ranging from 33.5 to 40 Ct), with an average increase of 15.7 Ct compared to untreated control samples (17.8–23.6 Ct). In contrast, depletion with the use of DNase I increased threshold values only by an average of 10.5 Ct (ranging from 28.5 to 34.2 Ct). Importantly, the threshold values in the NDV M-test exhibited only a modest increase with the alternative DNase treatment resulting in a 1.4 Ct increase ($p < 0.05$), while DNase I resulted in a more substantial increase of a 2.6 Ct ($p < 0.0001$) compared to untreated samples (Figure 4B). These findings suggest that both depletion methods effectively reduce host rRNA levels, with the alternative DNase showing a more pronounced effect.

For further evaluation of depletion methods and performance of RT-qPCR 28S-test, we selected the alternative DNase based on its superior performance in reducing host rRNA levels. Additionally, to reduce the price per reaction during testing, we compared our RNase H-based depletion protocol using a complete set of probes with a partial set of probes (chicken 28S rRNA4 and rRNA5). To facilitate this, the amplification region of the 28S-test was within the targeted region for depletion with the reduced set of probes. As anticipated, depletion with the partial set of probes performed

10.3389/fmicb.2024.1328987

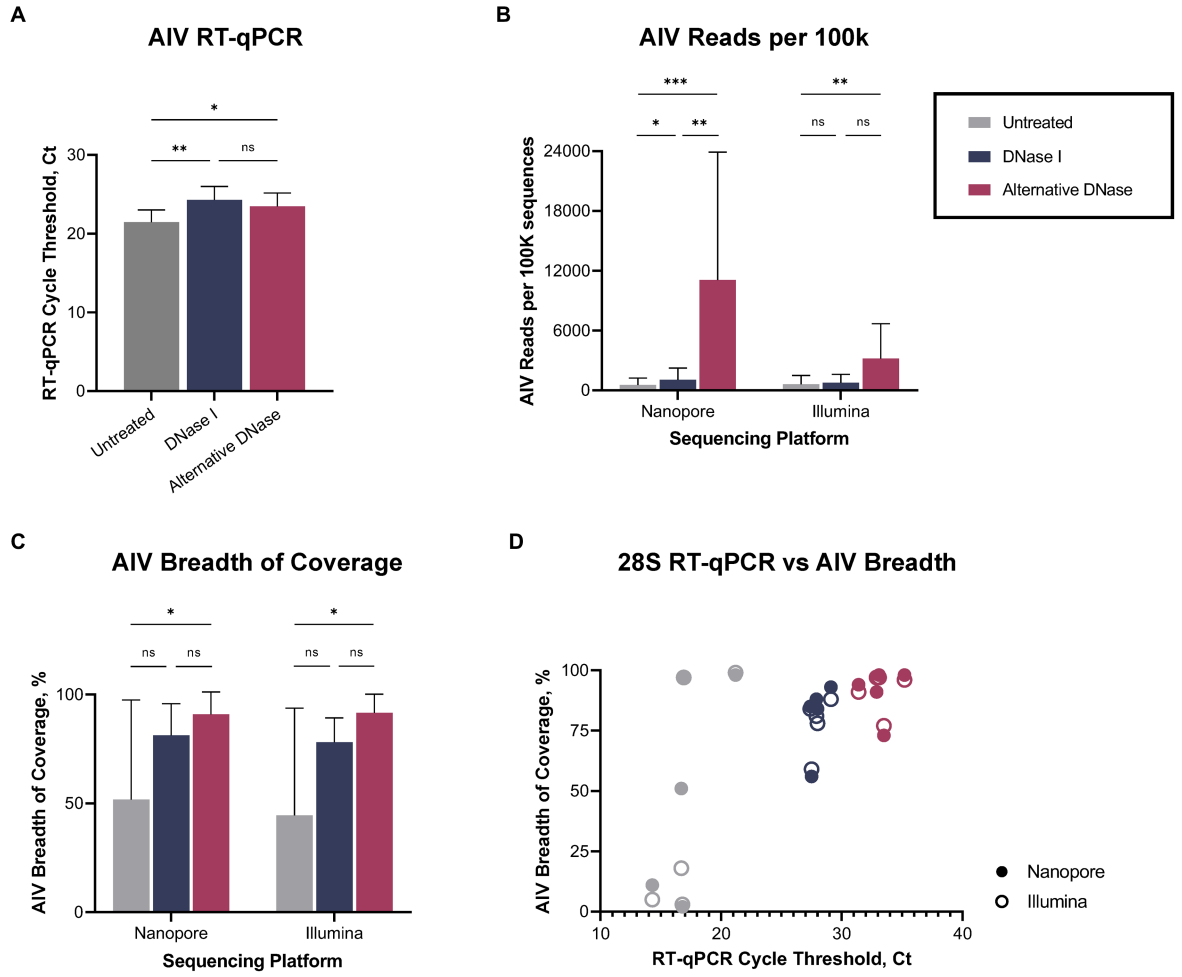

FIGURE 3
Viral reads recovery after DNase I and alternative DNase treatments. **(A)** Average cycle threshold (Ct) values of avian influenza virus (AIV) M gene RT-qPCR assay in different depletion methods. **(B)** Average number of AIV reads per 100 k sequences. **(C)** Average percentage of the breadth of AIV genome coverage. **(D)** Relationship between 28S rRNA RT-qPCR Ct value and percentage of the breadth of AIV genome coverage in different depletion treatments obtained on Nanopore and Illumina sequencing platforms. One-way ANOVA with Tukey's multiple comparison analysis was used to evaluate the significance between different depletion methods. A value of $p<0.05$ was considered to be significant. *$p<0.05$; **$p<0.01$; ***$p<0.001$; ****$p<0.0001$.

comparably to depletion with the complete set, and there were no significant differences between these two sets in the RT-qPCR 28S-test (Figures 4A,B). The average cycle threshold values were elevated by 15.7 Ct (ranging from 35.4 to 37.4 Ct) compared to untreated control samples (Figure 4A). Similarly, in the NDV M-test, there was only a minor increase of 0.7 Ct compared to untreated controls (Figure 4B).

Furthermore, we evaluated the feasibility of substituting DNase I and the alternative DNase with rapid DNase to reduce preparation time. DNase I and the alternative DNase digestion typically require 30-min incubation at 37°C, whereas rapid DNase requires only 2 min. It is important to note that despite the elevation of average Ct values compared to untreated samples, depletion with rapid DNase resulted in a significantly lower reduction ($p<0.0001$) of host rRNA compared to the alternative DNase (Figure 4A). The average Ct values in samples after rapid DNAse treatment were 11.6 Ct lower (ranging from 24.3 to 26.1 Ct) than those in samples treated with the alternative DNase.

3.3.2 Extraction pre-treatment

We evaluated the impact of filtration pre-treatment using different types of syringe filters (0.45 µm Nylon, 0.45 µm Nalgene SFCA, and 0.22 µm Nalgene SFCA) prior to nucleic acid extraction. We assessed the effects of filtration methods independently and in combination with our depletion protocol using the alternative DNase. When evaluating the three different filters compared to each other, we observed no significant differences in the reduction of 28S chicken rRNA, regardless of whether post-extraction depletion treatment was applied or not (Figure 5A). However, when compared to untreated samples, only the filtration with cellulose acetate filters significantly reduced host rRNA levels, when no subsequent deletion was applied. Specifically, the 0.45 µm Nalgene SFCA filter led to a reduction with $p<0.001$, and the 0.22 µm Nalgene SFCA filter resulted in a reduction with $p<0.05$ (Figure 5A). Still, these reductions were observed to be lower than the reductions achieved when the filters were used in combination with the alternative DNase treatment. All filtration pre-treatments combined with the depletion treatment significantly

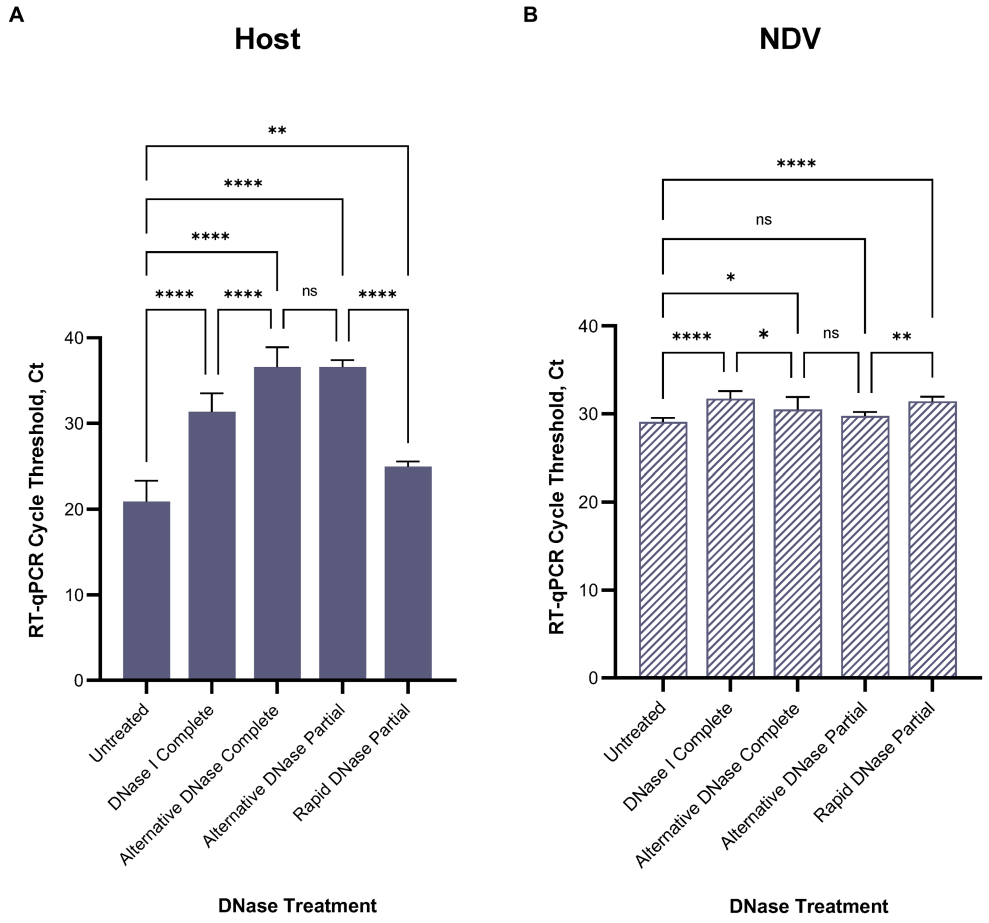

FIGURE 4
Average **(A)** chicken 28S rRNA and **(B)** Newcastle disease virus (NDV) M gene RT-qPCR cycle threshold (Ct) values in each depletion treatment. All treatments significantly reduced host rRNA, which was represented by elevated Ct values compared to untreated control samples. One-way ANOVA with Tukey's multiple comparison analysis was used to evaluate the significance between Ct values in different depletion methods. A value of $p<0.05$ was considered to be significant. *$p < 0.05$; **$p < 0.01$; ***$p < 0.001$; ****$p < 0.0001$.

reduced ($p < 0.0001$) host rRNA. Though, these pre-treatments provided no significant difference with the alternative DNase alone.

Adversely, viral RNA was significantly reduced ($p < 0.0001$) by filtration, regardless of filter type used and whether depletion treatment was applied or not (Figure 5B) when compared to untreated samples and samples after the alternative DNase treatment. This suggests that filtration pre-treatment had a detrimental effect on viral RNA, leading to a substantial reduction in its quantity. In contrast, the depletion using the alternative DNase without any extraction pre-treatment not only significantly ($p < 0.0001$) reduced 28S host rRNA, as intended, but at the same time did not significantly reduce the amount of viral RNA.

3.3.3 Optimization of depletion protocol

In our study, we evaluated the impact of various experimental parameters on the reduction of host rRNA and preservation of viral RNA. Specifically, we examined the effect of extending the alternative DNase digestion time to 45 and 60 min, explored different concentrations of the partial probe set, and conducted repeated RNase H treatments. Extending the alternative DNase digestion time beyond the recommended 30 min did not significantly impact the reduction of 28S rRNA or viral RNA levels (Supplementary Figure 3A). Comparison of different partial probe set concentrations revealed a common trend of reduced Ct values or RT-qPCR targeting 28S rRNA when probe concentrations decreased (Supplementary Figure 3B). Furthermore, our RNase H-based depletion with a partial probe set yielded a significant reduction in host rRNA levels ($p < 0.0001$) across all concentrations tested, without affecting viral Ct values. When comparing repeated RNase H treatments to improve degradation of probe-bound rRNAs, one and three rounds of RNase H treatment resulted in a significant reduction in host rRNA levels compared to untreated samples ($p < 0.0001$ and $p < 0.05$, respectively). In contrast, depletion without RNase H treatment or with two RNase H treatments did not yield any statistically significant difference (Supplementary Figure 3C).

4 Discussion

In this study, we conducted a comprehensive evaluation of the newly developed 28S rRNA RT-qPCR as a tool to facilitate the optimization of host depletion methods to enhance avian virus detection via next-generation sequencing. Our approach involved a systematic assessment of this 28S-test in conjunction with various depletion protocols, with a particular focus on substituting DNase

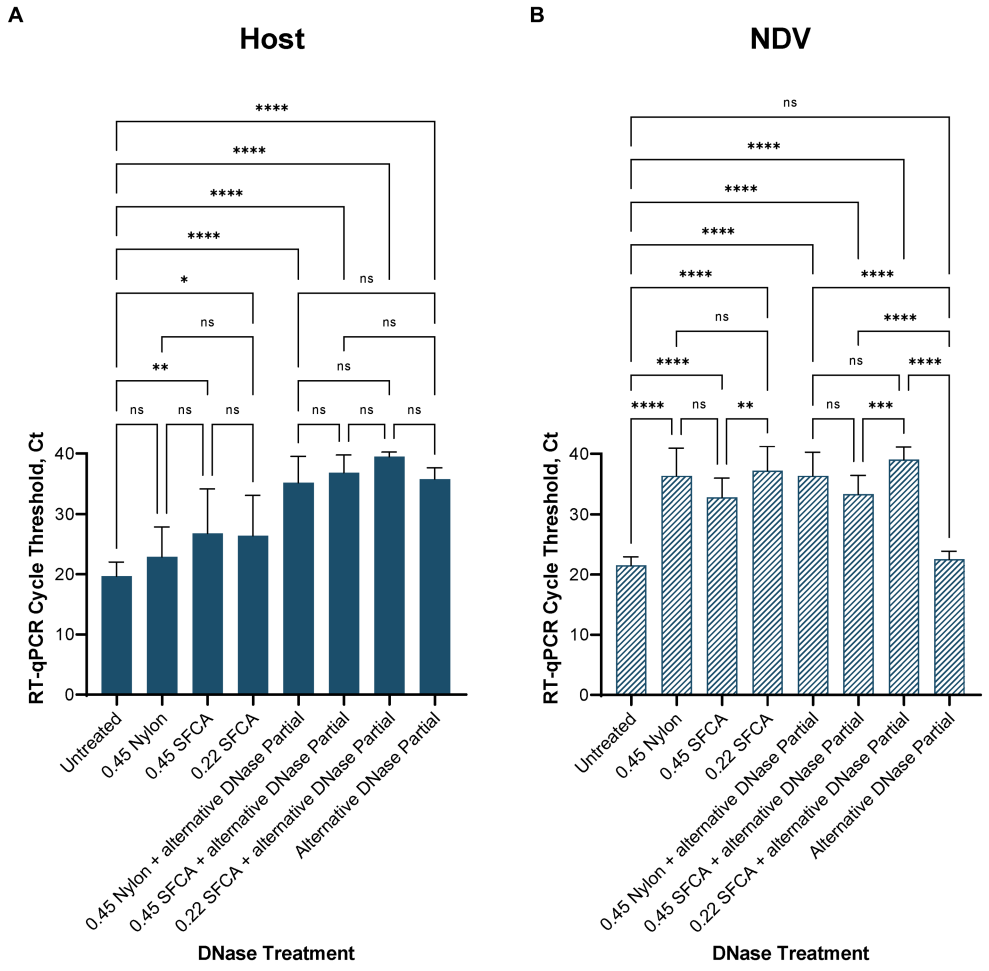

FIGURE 5
Average **(A)** chicken rRNA 28S and **(B)** Newcastle disease virus (NDV) M gene RT-qPCR cycle threshold (Ct) values in the alternative DNase depletion with and without filtration pre-treatment. Without subsequent alternative DNase treatment, only filtration with cellulose acetate syringe filters (SFCA) before extraction significantly reduced host rRNA. Filtration together with the alternative DNase depletion reduced host rRNA significantly better than filtration alone. However, regardless of whether post-extraction depletion treatment was applied or not, all filters significantly reduced viral RNA. One-way ANOVA with Tukey's multiple comparison analysis was used to evaluate the significance between Ct values in different depletion methods. A value of $p<0.05$ was considered to be significant. *$p < 0.05$; **$p < 0.01$; ***$p < 0.001$; ****$p < 0.0001$.

I with the alternative DNase in our established RNase H-based rRNA depletion protocol (Parris et al., 2022; Bakre et al., 2023). To ensure reliable detection of avian 28S rRNA, we fine-tuned primer annealing temperatures, optimized primer/probe concentrations, and selected the most suitable primer pair set. Our primer design adhered to specific criteria, including short lengths, nucleotide diversity, and a balanced GC content. Through rigorous testing, we identified the optimal primer/probe set as 28S+3894/-4026/+3918 and determined their ideal concentrations and annealing temperature.

It is known that commonly used conventional DNase I, which was first characterized more than a half-century ago, is salt-sensitive, has a poor affinity for DNA, and inefficiently cleaves DNA of low concentration (Kunitz, 1950; ThermoFisher, 2012). In addition, DNase I is purified from bovine pancreas, one of the richest natural sources of RNase A, which can be crucial when working with RNA viruses. The alternative DNase is an engineered version of wild-type DNase I with 350% greater catalytic efficiency and a markedly higher affinity for DNA, making it more effective in removing trace quantities of DNA contamination. The alternative DNase is also capable of maintaining up to 50-fold greater activity than DNase I in solutions at physiological salt concentrations and is RNase-free by nature (ThermoFisher, 2018). Therefore, our initial RT-qPCR 28S-test evaluation was performed using the Nanopore and Illumina sequencing instruments with results comparing untreated samples with the samples that underwent our custom depletion assay with DNase I, and a modified protocol using the alternative DNase. For this evaluation, we employed clinical swabs from SPF chickens infected with a highly pathogenic avian influenza virus A/turkey/Indiana/22–003707-003/2022 (H5N1). Both depletion methods significantly increased the average Ct values in the RT-qPCR 28S-test, indicating substantial host-specific rRNA reduction. Notably, substituting DNase I with the alternative DNase yielded significantly improved results, as evidenced by even a further elevation of Ct values in the 28S-test, signifying a more pronounced reduction in host-specific rRNA, and a lower Ct value elevation in the AIV M-test, indicating the preservation of viral RNA integrity. These improvements were consistent with NGS outcomes on both Nanopore and Illumina platforms. It is important to highlight that while both depletion

methods decreased the average percentage of host-specific reads according to the data obtained on both sequencing platforms, a statistically significant reduction was observed only in samples treated with the alternative DNase. Metataxonomic analysis of the abundant reads confirmed a reduction of most targeted bacterial reads during depletion and a consequent rise of untargeted bacterial, viral, and human reads. The increase of targeted reads belonging to family *Enterobacteriaceae* in treated samples may be attributed to potential contamination from polymerases and other enzymes, which are known source of *Escherichia coli* contamination (Koponen et al., 2002; Silkie et al., 2008; Stinson et al., 2019). This reduction in abundant host and bacterial rRNAs was instrumental in facilitating a notable increase in the number of sequenced influenza viral reads, contributing to enhanced breadth of viral genome coverage after consensus assembly. Similarly, to the host rRNA reduction results, the improvement in the breadth of viral genome was also statistically significant only in samples treated with the alternative DNase. The observed correlation between the reduction of host rRNA levels and the subsequent improvement in viral genome breadth highlights the potential utility of the RT-qPCR 28S-test in guiding further refinements of host rRNA depletion methods for enhanced detection of avian pathogens.

Furthermore, we conducted a thorough evaluation of the developed RT-qPCR 28S-test to monitor the effectiveness of different host depletion methods. In swab samples spiked with low pathogenic NDV, the comparison between DNase I and alternative DNase demonstrated the superior performance of the alternative DNase as well. Both methods significantly reduced host rRNA levels, as evidenced by elevated Ct values in the 28S-test. However, the alternative DNase outperformed DNase I, resulting in higher Ct values in the 28S-test, indicating more effective host rRNA reduction, and lower Ct values in the NDV M-test, signifying the preservation of viral RNA integrity. Thus, the alternative DNase was selected for further optimization of the depletion protocol due to its superior performance. Additionally, we explored cost-effective measures by utilizing a reduced set of probes (chicken 28S rRNA4 and rRNA5) instead of a complete probe set, which performed comparably to the complete set in the 28S-test. Also, we examined the potential use of rapid DNase to reduce preparation time. While rapid DNase offered a quicker incubation period (2 min) compared to DNase I (30 min) and the alternative DNase (30 min), it exhibited lower efficacy in host rRNA reduction compared to DNase I and the alternative DNase. This emphasizes the importance of balancing efficiency and effectiveness in depletion protocols.

We also investigated filtration pre-treatment using different syringe filters (0.45 µm Nylon, 0.45 µm Nalgene SFCA, and 0.22 µm Nalgene SFCA) before nucleic acid extraction. Comparing the three different filters among themselves, we observed no significant differences in the reduction of 28S chicken rRNA, regardless of whether post-extraction alternative DNase depletion treatment was applied or not. However, when compared to untreated samples, only the filtration with cellulose acetate filters led to a significant reduction in host rRNA levels when used for pre-extraction treatment without subsequent alternative DNase depletion. However, when combined with the depletion treatment, all extraction pre-treatments significantly reduced host rRNA compared to untreated samples. Nevertheless, these reductions were more pronounced than those achieved when the filters were used without following alternative DNase treatment. Though filtration combined with the alternative DNase effectively reduced host rRNA, it significantly decreased viral RNA as well. In contrast, the alternative DNase without filtration pre-treatment maintained host rRNA reduction while preserving viral RNA. The primary rationale behind using filtration was to selectively remove host and bacterial cells, with the expectation that virus particles, being significantly smaller, would pass through the filter and be present in higher concentrations and allow a higher percentage of viral sequencing reads. However, our unexpected outcome suggests two plausible explanations for the observed significant reduction of the viral RNA. The most likely explanation is that the virus particles are attached to host cells through receptor mediated interaction, and these virus/host cells were then removed by the filters. Second, variations in viral sizes may have played a role. For instance, orthomyxo- and paramyxoviruses are known to be pleomorphic and capable of producing virions of different shapes (Donald and Isaacs, 1954; Badham and Rossman, 2016). Generally, NDV virions are rounded and 100–500 nm in diameter, although filamentous forms of about 100 nm across and of variable length are often seen (Alexander and Senne, 2008; Goff et al., 2012; Miller and Koch, 2013; Burrell et al., 2017). Clinical isolates of influenza A virus have been shown to produce elongated filamentous particles up to 30 µm, whereas laboratory-adapted strains are predominantly spherical ranging from 80 to 120 nm (Cox et al., 1980; Roberts et al., 1998; Vijayakrishnan et al., 2013; Dadonaite et al., 2016; Leyson et al., 2021). Therefore, while filtration is a widely used technique for separating viruses from bacterial and host cells, our findings align with a prior observation (Conceição-Neto et al., 2015; Burke et al., 2019) and emphasize the importance of carefully considering filter pore size and material. Because of the large reduction in viral RNA as measured by RT-qPCR, we did not evaluate the filtered samples by sequence analysis, and additional investigation is needed to evaluate if there is a positive effect from filtering in increasing viral RNA reads.

Finally, our study explored various experimental parameters to optimize the depletion protocol's performance. These investigations included extending the alternative DNase digestion time, testing different concentrations of the partial probe set, and conducting repeated RNase H treatments. Extending the alternative DNase digestion time beyond the recommended 30 min did not significantly impact the reduction of host rRNA or viral RNA levels. Similarly, varying the concentrations of the partial probe set did not yield significant differences in the 28S-test when probe concentrations were increased. When assessing repeated RNase H treatments to enhance the degradation of probe-bound rRNAs, one and three rounds of RNase H treatment resulted in a significant reduction in host rRNA levels compared to untreated samples. However, no statistically significant difference was observed when depletion was performed without RNase H treatment or with two rounds of RNase H treatment.

In summary, our comprehensive assessment of different depletion treatments with a specific emphasis on the performance evaluation of the 28S rRNA RT-qPCR, provides valuable insights to enhance avian virus detection through NGS. Careful selection of depletion methods, probe sets, and filtration pre-treatment steps is crucial for optimizing NGS outcomes. Therefore, this systematic optimization process ensures that our custom RNase H-based depletion protocol is fine-tuned for effective reduction of the most abundant host and bacterial rRNA, ultimately improving the detection, number of sequenced reads, and genome coverage for various avian viruses. The results presented in this study offer significant findings for further refining

depletion methods and their influence on NGS performance in avian disease research.

5 Conclusion

In conclusion, our study highlights the effectiveness of the developed 28S rRNA RT-qPCR in evaluating host depletion methods for NGS detection of avian viruses. This assay facilitated the optimization of our established depletion protocol and the evaluation of other depletion methods. Substituting DNase I with the alternative DNase in our established depletion protocol resulted in improved outcomes, as validated by NGS data. Ultimately, our refined protocol, utilizing the alternative DNase, proved to be the overall optimal depletion method when compared to other DNases or filtration pre-treatments. The 28S-test provides a valuable foundation for the development and further refinement of host depletion strategies, ultimately enhancing the sensitivity and accuracy of avian virus detection in clinical samples. Additional investigations into optimizing depletion methods and their application in avian virology are warranted to advance our understanding of avian diseases and improve surveillance and control measures.

Data availability statement

The original contributions presented in the study are publicly available. This data can be found at: NCBI Sequencing Read Archive (SRA) under BioProject Number PRJNA1021187.

Ethics statement

The animal study protocol was approved by the Institutional Laboratory Animal Care and Use Committee of the United States National Poultry Research Center, ARS, USDA.

Author contributions

IG: Conceptualization, Data curation, Formal analysis, Investigation, Methodology, Software, Validation, Visualization, Writing – original draft. MH: Formal analysis, Investigation, Methodology, Software, Validation, Writing – review & editing. ES: Funding acquisition, Methodology, Resources, Supervision, Writing – review & editing. DS: Conceptualization, Data curation, Formal analysis, Funding acquisition, Methodology, Project administration, Supervision, Writing – review & editing.

Funding

The author(s) declare financial support was received for the research, authorship, and/or publication of this article. This study was funded by the U.S. Department of Agriculture through NBAF Agreement and by NIFA grant AP22VSD&B000C010. The mention of trade names or commercial products in this publication is solely for providing specific information and does not imply recommendation or endorsement by the USDA-ARS.

Acknowledgments

The authors thank Ricky Zoller, Suzanne Deblois, Scott Lee, Emily Newton, Melinda Vonkungthong, and Jesse Gallagher for technical assistance with this work.

Conflict of interest

The authors declare that the research was conducted in the absence of any commercial or financial relationships that could be construed as a potential conflict of interest.

Publisher's note

Supplementary material

The Supplementary material for this article can be found online at: https://www.frontiersin.org/articles/10.3389/fmicb.2024.1328987/full#supplementary-material

References

Agüero, M., Monne, I., Sánchez, A., Zecchin, B., Fusaro, A., Ruano, M. J., et al. (2023). Highly pathogenic avian influenza a(H5N1) virus infection in farmed minks, Spain, October 2022. *Euro Surveill.* 28:2300001. doi: 10.2807/1560-7917.ES.2023.28.3.2300001

Alexander, D. J. (1998). "Newcastle disease virus and other avian paramyxoviruses" in *A laboratory manual for the isolation and identification of avian pathogens*. eds. G. J. S. DE, M. W. Jackwood, J. E. Pearson and W. M. Reed (Kennett Square, PA: The American Association of Avian Pathologists)

Alexander, D. J., and Senne, D. A. (2008). "Newcastle disease and other avian paramyxoviruses" in *A laboratory manual for the isolation, identification and characterization of avian pathogens*. eds. L. Dufour-Zavala, J. R. Glisson, M. W. Jackwood, J. E. Pearson, W. M. Reed and P. R. Woolcock (Athens, GA: American Association of Avian Pathologists)

Alkie, T. N., Lopes, S., Hisanaga, T., Xu, W., Suderman, M., Koziuk, J., et al. (2022). Berhane: a threat from both sides: multiple introductions of genetically distinct H5 HPAI viruses into Canada via both East Asia-Australasia/Pacific and Atlantic flyways. *Virus Evol* 8:veac077. doi: 10.1093/ve/veac077

Allander, T., Emerson, S. U., Engle, R. E., Purcell, R. H., and Bukh, J. (2001). A virus discovery method incorporating DNase treatment and its application to the identification of two bovine parvovirus species. *Proc. Natl. Acad. Sci. USA.* 98, 11609–11614. doi: 10.1073/pnas.211424698

Amar, Y., Lagkouvardos, I., Silva, R. L., Ishola, O. A., Foesel, B. U., Kublik, S., et al. (2021). Pre-digest of unprotected DNA by Benzonase improves the representation of living skin bacteria and efficiently depletes host DNA. *Microbiome* 9:123. doi: 10.1186/s40168-021-01067-0

Andrews, S. (2010) *FastQC a quality control tool for high throughput sequence data*. Available at: http://www.bioinformatics.babraham.ac.uk/projects/fastqc/

Badham, M. D., and Rossman, J. S. (2016). Filamentous Influenza Viruses. *Curr Clin Microbiol Rep* 3, 155–161. doi: 10.1007/s40588-016-0041-7

Bakre, A., Kariithi, H. M., and Suarez, D. L. (2023). Alternative probe hybridization buffers for target RNA depletion and viral sequence recovery in NGS for poultry samples. *J. Virol. Methods* 321:114793. doi: 10.1016/j.jviromet.2023.114793

Bal, A., Pichon, M., Picard, C., Casalegno, J. S., Valette, M., Schuffenecker, I., et al. (2018). Quality control implementation for universal characterization of DNA and RNA viruses in clinical respiratory samples using single metagenomic next-generation sequencing workflow. *BMC Infect. Dis.* 18:537. doi: 10.1186/s12879-018-3446-5

Bevins, S. N., Shriner, S. A., Cumbee, J. C., Dilione, K. E., Douglass, K. E., Ellis, J. W., et al. (2022). Intercontinental movement of highly pathogenic avian influenza a(H5N1) clade 2.3.4.4 virus to the United States, 2021. *Emerg. Infect. Dis.* 28, 1006–1011. doi: 10.3201/eid2805.220318

Bruggeling, C. E., Garza, D. R., Achouiti, S., Mes, W., Dutilh, B. E., and Boleij, A. (2021). Optimized bacterial DNA isolation method for microbiome analysis of human tissues. *Microbiology* 10:e1191. doi: 10.1002/mbo3.1191

Burke, A., Hirst, J., and Hutchinson, E. (2019). Altering the size distribution of influenza virion populations. *Access. Microbiology* 1:122. doi: 10.1099/acmi.ac2019.po0122

Burrell, C. J., Howard, C. R., and Murphy, F. A. (2017). "Paramyxoviruses" in *Fenner and White's medical virology*. eds. C. R. H. C. J. Burrell and F. A. Murphy (London, UK: Academic Press)

Caliendo, V., Lewis, N. S., Pohlmann, A., Baillie, S. R., Banyard, A. C., Beer, M., et al. (2022). Transatlantic spread of highly pathogenic avian influenza H5N1 by wild birds from Europe to North America in 2021. *Sci. Rep.* 12:11729. doi: 10.1038/s41598-022-13447-z

Charalampous, T., Kay, G. L., Richardson, H., Aydin, A., Baldan, R., Jeanes, C., et al. (2019). Nanopore metagenomics enables rapid clinical diagnosis of bacterial lower respiratory infection. *Nat. Biotechnol.* 37, 783–792. doi: 10.1038/s41587-019-0156-5

Chen, G. Q., Zhuang, Q. Y., Wang, K. C., Liu, S., Shao, J. Z., Jiang, W. M., et al. (2013). Identification and survey of a novel avian coronavirus in ducks. *PloS One* 8:e72918. doi: 10.1371/journal.pone.0072918

Chrzastek, K., Lee, D. H., Smith, D., Sharma, P., Suarez, D. L., Pantin-Jackwood, M., et al. (2017). Use of sequence-independent, single-primer-amplification (SISPA) for rapid detection, identification, and characterization of avian RNA viruses. *Virology* 509, 159–166. doi: 10.1016/j.virol.2017.06.019

Chrzastek, K., Sellers, H. S., and Kapczynski, D. R. (2022). A universal, single-primer amplification protocol to perform whole-genome sequencing of segmented dsRNA avian Orthoreoviruses. *Avian Dis.* 66, 479–485. doi: 10.1637/aviandiseases-D-22-99999

Conceição-Neto, N., Zeller, M., Lefrère, H., De Bruyn, P., Beller, L., Deboutte, W., et al. (2015). Modular approach to customise sample preparation procedures for viral metagenomics: a reproducible protocol for virome analysis. *Sci. Rep.* 5:16532. doi: 10.1038/srep16532

Cox, J. C., Hampson, A. W., and Hamilton, R. C. (1980). An immunofluorescence study of influenza virus filament formation. *Arch. Virol.* 63, 275–284. doi: 10.1007/BF01315033

Crossley, B. M., Rejmanek, D., Baroch, J., Stanton, J. B., Young, K. T., Killian, M. L., et al. (2021). Nanopore sequencing as a rapid tool for identification and pathotyping of avian influenza a viruses. *J. Vet. Diagn. Invest.* 33, 253–260. doi: 10.1177/1040638720984114

Croville, G., Le Loc'h, G., Zanchetta, C., Manno, M., Camus-Bouclainville, C., Klopp, C., et al. (2018). Rapid whole-genome based typing and surveillance of avipoxviruses using nanopore sequencing. *J. Virol. Methods* 261, 34–39. doi: 10.1016/j.jviromet.2018.08.003

Dadonaite, B., Vijayakrishnan, S., Fodor, E., Bhella, D., and Hutchinson, E. C. (2016). Filamentous influenza viruses. *J. Gen. Virol.* 97, 1755–1764. doi: 10.1099/jgv.0.000535

Damir, H. A., Ahmad, W., Panicker, N. G., Mohamed, L. I., Omer, E. A., Kinne, J., et al. (2023). Investigation of a herpesvirus outbreak in mixed breeds of adult domestic ducks using next generation sequencing. *PloS One* 18:e0280923. doi: 10.1371/journal.pone.0280923

Dimitrov, K. M., Sharma, P., Volkening, J. D., Goraichuk, I. V., Wajid, A., Rehmani, S. F., et al. (2017). A robust and cost-effective approach to sequence and analyze complete genomes of small RNA viruses. *Virol. J.* 14:72. doi: 10.1186/s12985-017-0741-5

Donald, H. B., and Isaacs, A. (1954). Some properties of influenza virus filaments shown by electron microscopic particle counts. *J. Gen. Microbiol.* 11, 325–331. doi: 10.1099/00221287-11-2-325

Elsmo, E., Wünschmann, A., Beckmen, K., Broughton-Neiswanger, L., Buckles, E., Ellis, J., et al. Pathology of natural infection with highly pathogenic avian influenza virus (H5N1) clade 2.3.4.4b in wild terrestrial mammals in the United States in 2022. *bioRxiv* [Preprint], (2023)

Engelsma, M., Heutink, R., Harders, F., Germeraad, E. A., and Beerens, N. (2022). Multiple introductions of Reassorted highly pathogenic avian influenza H5Nx viruses clade 2.3.4.4b causing outbreaks in wild birds and poultry in the Netherlands, 2020-2021. *Microbiol Spectr* 10:e0249921. doi: 10.1128/spectrum.02499-21

Eyre, D. W. (2022). Infection prevention and control insights from a decade of pathogen whole-genome sequencing. *J. Hosp. Infect.* 122, 180–186. doi: 10.1016/j.jhin.2022.01.024

Fauver, J. R., Akter, S., Morales, A. I. O., Black, W. C., Rodriguez, A. D., Stenglein, M. D., et al. (2019). A reverse-transcription/RNase H based protocol for depletion of mosquito ribosomal RNA facilitates viral intrahost evolution analysis, transcriptomics and pathogen discovery. *Virology* 528, 181–197. doi: 10.1016/j.virol.2018.12.020

Ferreri, L. M., Ortiz, L., Geiger, G., Barriga, G. P., Poulson, R., Gonzalez-Reiche, A. S., et al. (2019). Improved detection of influenza a virus from blue-winged teals by sequencing directly from swab material. *Ecol. Evol.* 9, 6534–6546. doi: 10.1002/ece3.5232

Fittipaldi, M., Nocker, A., and Codony, F. (2012). Progress in understanding preferential detection of live cells using viability dyes in combination with DNA amplification. *J. Microbiol. Methods* 91, 276–289. doi: 10.1016/j.mimet.2012.08.007

Freed, N. E., Vlková, M., Faisal, M. B., and Silander, O. K. (2020). Silander: rapid and inexpensive whole-genome sequencing of SARS-CoV-2 using 1200 bp tiled amplicons and Oxford Nanopore rapid barcoding. *Biol Methods Protoc* 5:bpaa014. doi: 10.1093/biomethods/bpaa014

Galli, C., Ebranati, E., Pellegrinelli, L., Airoldi, M., Veo, C., Della Ventura, C., et al. (2022). From clinical specimen to whole genome sequencing of a(H3N2) influenza viruses: a fast and reliable high-throughput protocol. *Vaccines* 10:1359. doi: 10.3390/vaccines10081359

Gan, M., Wu, B., Yan, G., Li, G., Sun, L., Lu, G., et al. (2021). Combined nanopore adaptive sequencing and enzyme-based host depletion efficiently enriched microbial sequences and identified missing respiratory pathogens. *BMC Genomics* 22:732. doi: 10.1186/s12864-021-08023-0

Goff, P. H., Gao, Q., and Palese, P. (2012). A majority of infectious Newcastle disease virus particles contain a single genome, while a minority contain multiple genomes. *J. Virol.* 86, 10852–10856. doi: 10.1128/JVI.01298-12

Goraichuk, I. V., Davis, J. F., Kulkarni, A. B., Afonso, C. L., and Suarez, D. L. (2021a). Suarez: a 24-year-old sample contributes the complete genome sequence of fowl Aviadenovirus D from the United States. *Microbiol Resour Announc* 10:20. doi: 10.1128/MRA.01211-20

Goraichuk, I. V., Davis, J. F., Parris, D. J., Kariithi, H. M., Afonso, C. L., and Suarez, D. L. (2021b). Near-complete genome sequences of five Siciniviruses from North America. *Microbiol Resour Announc* 10:21. doi: 10.1128/MRA.00364-21

Goraichuk, I. V., Dimitrov, K. M., Sharma, P., Miller, P. J., Swayne, D. E., Suarez, D. L., et al. (2017). Afonso: complete genome sequences of four avian paramyxoviruses of serotype 10 isolated from Rockhopper penguins on the Falkland Islands. *Genome Announc.* 5:17. doi: 10.1128/genomeA.00472-17

Goraichuk, I. V., Kulkarni, A. B., Williams-Coplin, D., Suarez, D. L., and Afonso, C. L. (2019). First complete genome sequence of currently circulating infectious bronchitis virus strain DMV/1639 of the GI-17 lineage. *Microbiol Resour Announc* 8, e00840–e00819. doi: 10.1128/MRA.00840-19

Goraichuk, I., Sharma, P., Stegniy, B., Muzyka, D., Pantin-Jackwood, M. J., Gerilovych, A., et al. (2016). Complete genome sequence of an avian paramyxovirus representative of putative new serotype 13. *Genome Announc.* 4:16. doi: 10.1128/genomeA.00729-16

Gu, H., Sun, Y. H., and Li, X. Z. (2021). Novel rRNA-depletion methods for total RNA sequencing and ribosome profiling developed for avian species. *Poult. Sci.* 100:101321. doi: 10.1016/j.psj.2021.101321

Günther, A., Krone, O., Svansson, V., Pohlmann, A., King, J., Hallgrimsson, G. T., et al. (2022). Iceland as stepping Stone for spread of highly pathogenic avian influenza virus between Europe and North America. *Emerg. Infect. Dis.* 28, 2383–2388. doi: 10.3201/eid2812.221086

Hall, R. J., Wang, J., Todd, A. K., Bissielo, A. B., Yen, S., Strydom, H., et al. (2014). Evaluation of rapid and simple techniques for the enrichment of viruses prior to metagenomic virus discovery. *J. Virol. Methods* 195, 194–204. doi: 10.1016/j.jviromet.2013.08.035

Hasan, M. R., Rawat, A., Tang, P., Jithesh, P. V., Thomas, E., Tan, R., et al. (2016). Depletion of human DNA in spiked clinical specimens for improvement of sensitivity of pathogen detection by next-generation sequencing. *J. Clin. Microbiol.* 54, 919–927. doi: 10.1128/JCM.03050-15

Imai, K., Tamura, K., Tanigaki, T., Takizawa, M., Nakayama, E., Taniguchi, T., et al. (2018). Whole genome sequencing of influenza a and B viruses with the MinION sequencer in the clinical setting: a pilot study. *Front. Microbiol.* 9:2748. doi: 10.3389/fmicb.2018.02748

Ip, H. S., Uhm, S., Killian, M. L., and Torchetti, M. K. (2023). Torchetti: an evaluation of avian influenza virus whole-genome sequencing approaches using Nanopore technology. *Microorganisms* 11:529. doi: 10.3390/microorganisms11020529

Kapoor, A., Victoria, J., Simmonds, P., Wang, C., Shafer, R. W., Nims, R., et al. (2008). A highly divergent picornavirus in a marine mammal. *J. Virol.* 82, 311–320. doi: 10.1128/JVI.01240-07

Kariithi, H. M., Volkening, J. D., Chiwanga, G. H., Pantin-Jackwood, M. J., Msoffe, P. L. M., and Suarez, D. L. (2023). Genome sequences and characterization of chicken Astrovirus and avian nephritis virus from Tanzanian live bird markets. *Viruses* 15:1247. doi: 10.3390/v15061247

Kohl, C., Brinkmann, A., Dabrowski, P. W., Radonić, A., Nitsche, A., and Kurth, A. (2015). Protocol for metagenomic virus detection in clinical specimens. *Emerg. Infect. Dis.* 21, 48–57. doi: 10.3201/eid2101.140766

Koponen, J. K., Turunen, A. M., and Ylä-Herttuala, S. (2002). *Escherichia coli* DNA contamination in AmpliTaq gold polymerase interferes with TaqMan analysis of lacZ. *Mol. Ther.* 5, 220–222. doi: 10.1006/mthe.2002.0548

Kunitz, M. (1950). Crystalline desoxyribonuclease; isolation and general properties; spectrophotometric method for the measurement of desoxyribonuclease activity. *J. Gen. Physiol.* 33, 349–362. doi: 10.1085/jgp.33.4.349

Lee, J. S., Mackie, R. S., Harrison, T., Shariat, B., Kind, T., Kehl, T., et al. (2017). Targeted enrichment for pathogen detection and characterization in three felid species. *J. Clin. Microbiol.* 55, 1658–1670. doi: 10.1128/JCM.01463-16

Leguia, M., Garcia-Glaessner, A., Muñoz-Saavedra, B., Juarez, D., Barrera, P., Calvo-Mac, C., et al. (2023). Highly pathogenic avian influenza a (H5N1) in marine mammals and seabirds in Peru. *Nat. Commun.* 14:5489. doi: 10.1038/s41467-023-41182-0

Leyson, C. M., Youk, S., Ferreira, H. L., Suarez, D. L., and Pantin-Jackwood, M. (2021). Multiple gene segments are associated with enhanced virulence of clade 2.3.4.4 H5N8 highly pathogenic avian influenza virus in mallards. *J. Virol.* 95:e0095521. doi: 10.1128/JVI.00955-21

Li, H., and Durbin, R. (2009). Fast and accurate short read alignment with burrows-wheeler transform. *Bioinformatics* 25, 1754–1760. doi: 10.1093/bioinformatics/btp324

Liang, G., and Bushman, F. D. (2021). The human virome: assembly, composition and host interactions. *Nat. Rev. Microbiol.* 19, 514–527. doi: 10.1038/s41579-021-00536-5

Lu, J., Breitwieser, F., Thielen, P., and Salzberg, S. (2017). Bracken: estimating species abundance in metagenomics data. *PeerJ Comput Sci* 3:e104. doi: 10.7717/peerj-cs.104

Marotz, C. A., Sanders, J. G., Zuniga, C., Zaramela, L. S., Knight, R., and Zengler, K. (2018). Improving saliva shotgun metagenomics by chemical host DNA depletion. *Microbiome* 6:42. doi: 10.1186/s40168-018-0426-3

Martin, M. (2011). Cutadapt removes adapter sequences from high-throughput sequencing reads. *EMBnet J* 17, 10–12. doi: 10.14806/ej.17.1.200

Metsky, H. C., Matranga, C. B., Wohl, S., Schaffner, S. F., Freije, C. A., Winnicki, S. M., et al. (2017). Zika virus evolution and spread in the Americas. *Nature* 546, 411–415. doi: 10.1038/nature22402

Miller, P. J., and Koch, G. (2013) Newcastle disease. In: *Diseases of poultry*. Ed D. E. Swayne, J. R. Glisson and L. R. McDougald, Nolan, L. K., Suarez, D. L., and Nair, V. L. Wiley-Blackwell in partnership with the American Association of Avian Pathologists, Ames, IA.

Morlan, J. D., Qu, K., and Sinicropi, D. V. (2012). Selective depletion of rRNA enables whole transcriptome profiling of archival fixed tissue. *PloS One* 7:e42882. doi: 10.1371/journal.pone.0042882

Nagy, A., Stará, M., Černíková, L., Hofmannová, L., and Sedlák, K. (2023). Genotype diversity, wild bird-to-poultry transmissions, and farm-to-farm carryover during the spread of the highly pathogenic avian influenza H5N1 in the Czech Republic in 2021/2022. *Viruses* 15:293. doi: 10.3390/v15020293

Nelson, M. T., Pope, C. E., Marsh, R. L., Wolter, D. J., Weiss, E. J., Hager, K. R., et al. (2019). Human and extracellular DNA depletion for metagenomic analysis of complex clinical infection samples yields optimized viable microbiome profiles. *Cell Rep.* 26, 2227–2240.e5. doi: 10.1016/j.celrep.2019.01.091

Ng, T. F., Manire, C., Borrowman, K., Langer, T., Ehrhart, L., and Breitbart, M. (2009). Discovery of a novel single-stranded DNA virus from a sea turtle fibropapilloma by using viral metagenomics. *J. Virol.* 83, 2500–2509. doi: 10.1128/JVI.01946-08

Nguyen, H. T., Chesnokov, A., De La Cruz, J., Pascua, P. N. Q., Mishin, V. P., Jang, Y., et al. (2023). Antiviral susceptibility of clade 2.3.4.4b highly pathogenic avian influenza a(H5N1) viruses isolated from birds and mammals in the United States, 2022. *Antiviral Res.* 217:105679. doi: 10.1016/j.antiviral.2023.105679

Nocker, A., Mazza, A., Masson, L., Camper, A. K., and Brousseau, R. (2009). Selective detection of live bacteria combining propidium monoazide sample treatment with microarray technology. *J. Microbiol. Methods* 76, 253–261. doi: 10.1016/j.mimet.2008.11.004

Oechslin, C. P., Lenz, N., Liechti, N., Ryter, S., Agyeman, P., Bruggmann, R., et al. (2018). Limited correlation of shotgun metagenomics following host depletion and routine diagnostics for viruses and Bacteria in low concentrated surrogate and clinical samples. *Front. Cell. Infect. Microbiol.* 8:375. doi: 10.3389/fcimb.2018.00375

O'Flaherty, B. M., Li, Y., Tao, Y., Paden, C. R., Queen, K., Zhang, J., et al. (2018). Comprehensive viral enrichment enables sensitive respiratory virus genomic identification and analysis by next generation sequencing. *Genome Res.* 28, 869–877. doi: 10.1101/gr.226316.117

Oristo, S., Lee, H. J., and Maunula, L. (2018). Performance of pre-RT-qPCR treatments to discriminate infectious human rotaviruses and noroviruses from heat-inactivated viruses: applications of PMA/PMAxx, benzonase and RNase. *J. Appl. Microbiol.* 124, 1008–1016. doi: 10.1111/jam.13737

Parris, D. J., Kariithi, H., and Suarez, D. L. (2022). Non-target RNA depletion strategy to improve sensitivity of next-generation sequencing for the detection of RNA viruses in poultry. *J. Vet. Diagn. Invest.* 34, 638–645. doi: 10.1177/10406387221102430

Patzina-Mehling, C., Falkenhagen, A., Gadicherla, A. K., Grützke, J., Tausch, S. H., and Johne, R. (2020). Whole genome sequence analysis of cell culture-adapted rotavirus a strains from chicken. *Infect. Genet. Evol.* 81:104275. doi: 10.1016/j.meegid.2020.104275

Puryear, W., Sawatzki, K., Hill, N., Foss, A., Stone, J. J., Doughty, L., et al. (2023). Highly pathogenic avian influenza a(H5N1) virus outbreak in New England seals, United States. *Emerg. Infect. Dis.* 29, 786–791. doi: 10.3201/eid2904.221538

Rasmussen, E. A., Czaja, A., Cuthbert, F. J., Tan, G. S., Lemey, P., Nelson, M. I., et al. (2023). Influenza a viruses in gulls in landfills and freshwater habitats in Minnesota, United States. *Front. Genet.* 14:1172048. doi: 10.3389/fgene.2023.1172048

Roberts, P. C., Lamb, R. A., and Compans, R. W. (1998). The M1 and M2 proteins of influenza a virus are important determinants in filamentous particle formation. *Virology* 240, 127–137. doi: 10.1006/viro.1997.8916

Shi, X., Shao, C., Luo, C., Chu, Y., Wang, J., Meng, Q., et al. (2019). Microfluidics-based enrichment and whole-genome amplification enable strain-level resolution for airway metagenomics. *mSystems* 4:19. doi: 10.1128/mSystems.00198-19

Shi, Y., Wang, G., Lau, H. C., and Yu, J. (2022). Metagenomic sequencing for microbial DNA in human samples: emerging technological advances. *Int. J. Mol. Sci.* 23:2181. doi: 10.3390/ijms23042181

Silkie, S. S., Tolcher, M. P., and Nelson, K. L. (2008). Reagent decontamination to eliminate false-positives in *Escherichia coli* qPCR. *J. Microbiol. Methods* 72, 275–282. doi: 10.1016/j.mimet.2007.12.011

Singh, R. R. (2022). Target enrichment approaches for next-generation sequencing applications in oncology. *Diagnostics* 12:1539. doi: 10.3390/diagnostics12071539

Spackman, E., Senne, D. A., Myers, T. J., Bulaga, L. L., Garber, L. P., Perdue, M. L., et al. (2002). Development of a real-time reverse transcriptase PCR assay for type a influenza virus and the avian H5 and H7 hemagglutinin subtypes. *J. Clin. Microbiol.* 40, 3256–3260. doi: 10.1128/JCM.40.9.3256-3260.2002

Stark, R., Grzelak, M., and Hadfield, J. (2019). RNA sequencing: the teenage years. *Nat. Rev. Genet.* 20, 631–656. doi: 10.1038/s41576-019-0150-2

Stinson, L. F., Keelan, J. A., and Payne, M. S. (2019). Identification and removal of contaminating microbial DNA from PCR reagents: impact on low-biomass microbiome analyses. *Lett. Appl. Microbiol.* 68, 2–8. doi: 10.1111/lam.13091

Suarez, D. L. (2017). "Influenza A virus" in *Animal Influenza*. ed. D. E. Swayne (Ames, IA, USA: Wiley-Blackwell)

Swayne, D., Suarez, D., and Sims, L. (2020). Influenza. In: *Diseases of poultry*. Ed M. B. DE Swayne and C. M. Logue, MD, L. R., V. Nair and D. L. Suarez et al. John Wiley & Sons, Inc., Hoboken, NJ. doi: 10.1002/9781119371199.ch6

Tal, S., Ben Izhak, M., Wachtel, C., Wiseman, A., Braun, T., Yechezkel, E., et al. (2019). Evaluating methods for avian avulavirus-1 whole genome sequencing. *Gene X* 721:100004. doi: 10.1016/j.gene.2019.100004

Tang, Y., Lu, H., Sebastian, A., Yeh, Y. T., Praul, C. A., Albert, I. U., et al. (2015). Genomic characterization of a Turkey reovirus field strain by next-generation sequencing. *Infect. Genet. Evol.* 32, 313–321. doi: 10.1016/j.meegid.2015.03.029

Techera, C., Tomás, G., Grecco, S., Williman, J., Hernández, M., Olivera, V., et al. (2023). A rapid and affordable amplicon-based method for next-generation genome sequencing of the infectious bursal disease virus. *J. Virol. Methods* 322:114807. doi: 10.1016/j.jviromet.2023.114807

ThermoFisher. (2012) TURBO™ DNase. In: Molecular biology education. ThermoFisher. Available at: https://www.thermofisher.com/order/catalog/product/AM2238

ThermoFisher (2018) The World's best DNase. Available at: https://www.thermofisher.com/us/en/home/references/ambion-tech-support/nuclease-enzymes/tech-notes/the-world-s-best-dnase.html

Victoria, J. G., Kapoor, A., Dupuis, K., Schnurr, D. P., and Delwart, E. L. (2008). Rapid identification of known and new RNA viruses from animal tissues. *PLoS Pathog.* 4:e1000163. doi: 10.1371/journal.ppat.1000163

Vijayakrishnan, S., Loney, C., Jackson, D., Suphamungmee, W., Rixon, F. J., and Bhella, D. (2013). Cryotomography of budding influenza a virus reveals filaments with diverse morphologies that mostly do not bear a genome at their distal end. *PLoS Pathog.* 9:e1003413. doi: 10.1371/journal.ppat.1003413

Vill, A. C. (2023). *Bracken_plot: A shiny app for taxonomic abundance visualization*. Available at: https://github.com/acvill/bracken_plot/tree/main

Vreman, S., Kik, M., Germeraad, E., Heutink, R., Harders, F., Spierenburg, M., et al. (2023). Zoonotic mutation of highly pathogenic avian influenza H5N1 virus identified in the brain of multiple wild carnivore species. *Pathogens* 12:168. doi: 10.3390/pathogens12020168

Wang, X., Zhao, L., Wu, X., Luo, H., Wu, D., Zhang, M., et al. (2021). Development of a simplified and inexpensive RNA depletion method for plasmid DNA purification using

size selection magnetic beads (SSMBs). *Genes Dis* 8, 298–306. doi: 10.1016/j.gendis.2020.04.013

Wille, M., Eden, J. S., Shi, M., Klaassen, M., Hurt, A. C., and Holmes, E. C. (2018). Virus-virus interactions and host ecology are associated with RNA virome structure in wild birds. *Mol. Ecol.* 27, 5263–5278. doi: 10.1111/mec.14918

Williams, T. G. S., Snell, L. B., Alder, C., Charalampous, T., Alcolea-Medina, A., Sehmi, J. K., et al. (2023). Feasibility and clinical utility of local rapid Nanopore influenza a virus whole genome sequencing for integrated outbreak management, genotypic resistance detection and timely surveillance. *Microb Genom* 9:1083. doi: 10.1099/mgen.0.001083

Wise, M. G., Suarez, D. L., Seal, B. S., Pedersen, J. C., Senne, D. A., King, D. J., et al. (2004). Development of a real-time reverse-transcription PCR for detection of Newcastle disease virus RNA in clinical samples. *J. Clin. Microbiol.* 42, 329–338. doi: 10.1128/jcm.42.1.329-338.2004

Wood, D. E., Lu, J., and Langmead, B. (2019). Improved metagenomic analysis with kraken 2. *Genome Biol.* 20:257. doi: 10.1186/s13059-019-1891-0

Wood, D. E., and Salzberg, S. L. (2014). Kraken: ultrafast metagenomic sequence classification using exact alignments. *Genome Biol.* 15:R46. doi: 10.1186/gb-2014-15-3-r46

Yeoh, Y. K. (2021). Removing host-derived DNA sequences from microbial metagenomes via mapping to reference genomes. *Methods Mol. Biol.* 2232, 147–153. doi: 10.1007/978-1-0716-1040-4_13

Youk, S., Torchetti, M. K., Lantz, K., Lenoch, J. B., Killian, M. L., Leyson, C., et al. (2023). H5N1 highly pathogenic avian influenza clade 2.3.4.4b in wild and domestic birds: introductions into the United States and reassortments, December 2021-April 2022. *Virology* 587:109860. doi: 10.1016/j.virol.2023.109860

Zeng, Z., Huang, B., Wang, X., Fan, J., Zhang, B., Yang, L., et al. (2020). A reverse transcriptase-mediated ribosomal RNA depletion (RTR2D) strategy for the cost-effective construction of RNA sequencing libraries. *J. Adv. Res.* 24, 239–250. doi: 10.1016/j.jare.2019.12.005

Zhang, J., Kobert, K., Flouri, T., and Stamatakis, A. (2014). PEAR: a fast and accurate Illumina paired-end reAd mergeR. *Bioinformatics* 30, 614–620. doi: 10.1093/bioinformatics/btt593

frontiers | Frontiers in Microbiology

TYPE Original Research
PUBLISHED 16 April 2024
DOI 10.3389/fmicb.2024.1380849

OPEN ACCESS

EDITED BY
Jingqiang Ren,
Wenzhou University, China

REVIEWED BY
Xing Liu,
Nanjing Agricultural University, China
Venkatramana D. Krishna,
University of Minnesota Twin Cities, United States

*CORRESPONDENCE
Xiaowen Li
✉ lxw8272@163.com

RECEIVED 02 February 2024
ACCEPTED 01 April 2024
PUBLISHED 16 April 2024

CITATION
Ren J, Zu C, Li Y, Li M, Gu J, Chen F and Li X (2024) Establishment and application of a TaqMan-based multiplex real-time PCR for simultaneous detection of three porcine diarrhea viruses. *Front. Microbiol.* 15:1380849. doi: 10.3389/fmicb.2024.1380849

Establishment and application of a TaqMan-based multiplex real-time PCR for simultaneous detection of three porcine diarrhea viruses

Jing Ren[1,2], Congcong Zu[3], Yang Li[3], Meng Li[1,2], Jinyuan Gu[1,2], Fengling Chen[1,2] and Xiaowen Li[1,3]*

[1]Shandong Engineering Research Center of Swine Health Data and Intelligent Monitoring, Dezhou University, Dezhou, China, [2]Shandong Key Laboratory of Biophysics, Institute of Biophysics, Dezhou University, Dezhou, China, [3]Shandong New Hope Liuhe Agriculture and Animal Husbandry Technology Co., Ltd. (NHLH Academy of Swine Research), Dezhou, China

Introduction: Porcine viral diarrhea is a common clinical disease, which results in high mortality and economic losses in the pig industry. Porcine epidemic diarrhea virus (PEDV), porcine rotavirus (PoRV), and porcine deltacoronavirus (PDCoV) are important diarrhea viruses in pig herds. The similarities of their clinical symptoms and pathological changes make it difficult to distinguish these three viruses clinically. Therefore, there is a need for a highly sensitive and specific method to simultaneously detect and differentiate these viruses.

Methods: A multiplex real-time PCR assay using TaqMan probes was developed to simultaneously detect PEDV, PoRV, and PDCoV. To assess the efficacy of the established assay, 30 clinical samples with diarrhea symptoms were used to compare the results obtained from the multiplex real-time PCR assay with those obtained from commercial singleplex real-time PCR kit. Importantly, a total of 4,800 diarrhea samples were tested and analyzed to validate the utility of the assay.

Results: This multiplex real-time PCR assay showed high sensitivity, specificity, and excellent repeatability with a detection limit of 1×10^2 copies/μL. Comparing the results of the commercial singleplex real-time PCR kit and the multiplex real-time PCR method for detecting PEDV, PoRV, and PDCoV, there was complete agreement between the two approaches. Clinical data revealed single infection rates of 6.56% for PEDV, 21.69% for PoRV, and 6.65% for PDCoV. The co-infection rates were 11.83% for PEDV + PoRV, 0.29% for PEDV + PDCoV, 5.71% for PoRV + PDCoV, and 1.29% for PEDV + PDCoV + PoRV, respectively.

Discussion: The multiplex real-time PCR method established in this study is a valuable diagnostic tool for simultaneously differentiating PEDV, PoRV, and PDCoV. This method is expected to significantly contribute to prevent and control the spread of infectious diseases, as well as aid in conducting epidemiological investigations.

KEYWORDS

multiplex real-time PCR, PEDV, PoRV, PDCoV, porcine viral diarrhea

1 Introduction

Viral diarrheal disease poses a serious threat to the swine industry, causing substantial global economic losses (Wu et al., 2022; Hou et al., 2023). Numerous diarrhea viruses have been identified in swine, including transmissible gastroenteritis virus (TGEV), porcine epidemic diarrhea virus (PEDV), porcine delta coronavirus (PDCoV), porcine enteric alpha coronavirus (PEAV), porcine rotavirus (PoRV), porcine sapvirus (PSaV), porcine norovirus (PNoV), porcine teschenvirus (PTV), porcine kobuvirus (PKV), seneca valley virus (SVV), porcine reovirus (ReoV), porcine bocavirus (PBoV), porcine astrovirus (PAstV), and so on (Huang et al., 2019). Among these swine diarrhea viruses, PEDV, PoRV, and PDCoV are the most destructive pathogens causing anorexia, vomiting, diarrhea, and dehydration (Hou et al., 2023). With the rapid development of intensive aquaculture, co-infection or secondary infection with these viruses is prevalent, resulting in significant morbidity and mortality (Huang et al., 2019; Hou et al., 2023).

PEDV is an enveloped, single-stranded RNA virus that belongs to the *Alphacoronavirus* genus in the *Coronaviridae* family (Huang et al., 2013; Hu et al., 2021). The spherical PEDV particles vary in size, with an average diameter of ∼130 nm (Hu et al., 2021). The PEDV genome is ∼28 kb (Huang et al., 2013; Hu et al., 2021). While PEDV can infect pigs of any age, it is especially severe in piglets, often resulting in 100% morbidity and mortality (Shibata et al., 2000; Huang et al., 2013). The first reported cases of porcine epidemic diarrhea (PED) occurred in England in 1971, followed by a subsequent outbreak in Belgium in 1977 (Si et al., 2020; Hou et al., 2023). It was later identified in China in the 1980's (Wang et al., 2016). In December 2010, a new strain of PEDV with high virulence emerged in China, resulting in the death of over 1 million piglets and a 100% mortality rate among suckling piglets (Wang et al., 2016; Wu et al., 2022). Since then, the emerging and highly virulent strains of PEDV have gradually spread throughout the global swine industry, causing significant economic losses and becoming a leading cause of diarrhea in pigs (Wang et al., 2016; Hou et al., 2023).

PDCoV is a new swine enteric coronavirus that belongs to the newly identified genus *Deltacoronavirus* in the *Coronaviridae* family (Ma et al., 2015). It is an enveloped, single-stranded positive-stranded RNA virus with a genome size of ∼25.4 kb. PDCoV was first detected in Hong Kong, China in 2012, and then in the United States in 2014 (Woo et al., 2012; Wang et al., 2014). The first outbreak of PDCoV occurred in the United States in 2014 and quickly spread to at least 20 states, resulting in significant economic losses in the global pig industry (Ma et al., 2015; He et al., 2020). PoRV is a non-enveloped, double-stranded RNA virus from the genus *Rotavirus* in *Reoviridae* family. Its genome is ∼18,500 bp long, consisting of 11 segments of dsRNA (Chepngeno et al., 2020). PoRV is a major cause of diarrhea in piglets, particularly those aged 1–8 weeks (Chepngeno et al., 2020; Tao et al., 2023). It can also spread between pigs and humans, posing a significant threat to public health and safety in China (Li et al., 2018).

Pigs infected with PEDV, PoRV, and PDCoV exhibit similar clinical symptoms and pathological changes, making it hard to differentiate them. Moreover, the prevalence of co-infection and secondary infection among PEDV, PoRV, and PDCoV poses significant challenges in clinical diagnostics (Shu et al., 2022; Hou et al., 2023). It is therefore urgent to develop an efficient molecular method for distinguishing these viruses in the clinic. Real-time PCR utilizes fluorescence signals to monitor the PCR process in real-time, offering advantages in terms of speed, sensitivity, and reproducibility when compared to conventional PCR method. Hence, it is commonly used in clinical detection. However, singleplex real-time PCR is not convenient for the simultaneous detection of co-infection of multiple pathogens, and repeated detection of various pathogens wastes time and makes operations cumbersome (Ben Salem et al., 2010; Liu et al., 2019). Multiplex real-time PCR is a method that can detect multiple pathogens in a single reaction system (Huang et al., 2019; Li et al., 2022). In this study, we developed a multiple real-time PCR based on TaqMan probe to simultaneously and accurately detect PEDV, PoRV, and PDCoV. This assay exhibited high sensitivity and specificity for the target genes. Additionally, we used this method to detect and analyze 4,800 clinical samples collected from pig farms in multiple provinces of China, providing valuable data to help formulate prevention and control strategies in this particular region.

2 Materials and methods

2.1 Viruses, primers, and probes

The nucleic acid of various viruses and bacteria, including respiratory syndrome virus (PRRSV), pseudorabies virus (PrV), porcine circovirus (PCV1), PCV2, classical swine fever virus (CSFV), African swine fever virus (ASFV), *Streptococcus suis* (SS), *Salmonella enteritidis* (SE), PEDV, PoRV, and PDCoV were stored at −80°C in our laboratory until needed. At least 30 genome sequences of PEDV, PoRV, and PDCoV were downloaded from NCBI for analysis. After comparison, the M gene of PEDV and PDCoV, and the NSP3 gene of PoRV were found to be the most conserved gene sequences. Primers and probes were designed using Primer Premier 5 software (Premier, Canada) based on the most conserved region. TaqMan probes for PEDV, PoRV, and PDCoV were labeled with FAM, VIC, and Cy5 at the 5′ end, respectively, with all quenchers at the 3′ end being BHQ. The sequences of the primers and probes designed in this study are presented in Table 1. Primers and probes were synthesized by Sangon Biotech (Shanghai) Co., Ltd.

2.2 Construction of plasmid standards

The target fragments of PEDV, PoRV, and PDCoV were amplified separately using the HiScript II One Step RT-PCR Kit (Dye Plus; Nanjing Vazyme Biotech Co., Ltd.). The PCR fragments were purified and cloned into the pMD18-T vector (Takara Biomedical Technology (Beijing) Co., Ltd.). The transformed clones were then introduced into the E.coli DH5α strain. Positive clones were cultured and plasmid extraction was performed using the TaKaRa MiniBEST Universal Genomic DNA Extraction Kit [Takara Biomedical Technology (Beijing) Co., Ltd.]. The constructed plasmid was confirmed by DNA sequencing and used as the standard positive control. The copy number of

TABLE 1 Primers and probes designed for the multiplex real-time PCR.

Virus	Primer/probe	Sequence (5′-3′)	Size (bp)	Target gene
PEDV	Forward	CATCTGATTCTGGACAGTTG	226	M
	Reverse	CTATACACCAACACAGGCTC		
	Probe	(FAM)TTTCAGAGCAGGCTGCATAT(BHQ1)		
PoRV	Forward	ACCATCTACACATGACCCTCTATGAG	83	NSP3
	Reverse	ACATAACGCCCCTATAGCCATTTAG		
	Probe	(VIC)ACAATAGTTAAAAGCTAACACTG(BHQ1)		
PDCoV	Forward	ATCGACCACATGGCTCCAA	72	M
	Reverse	CAGCTCTTGCCCATGTAGCTT		
	Probe	(Cy5)CACACCAGTCGTTAAGCATGGCAAGCT(BHQ3)		

recombination plasmids was calculated using the following formula (Li et al., 2022):

$$Plasmid\ copies/\mu L = \frac{\left(6.02 \times 10^{23}\right) \times \left(\mathrm{X\ ng}/\mu L \times 10^{-9}\right)}{plasmid\ length\ (bp) \times 660}$$

A 10-fold series dilution was conducted for each plasmid, ranging from 1.0×10^8 to 1.0×10^1 copies/μL. Singleplex real-time PCR was performed for each virus using the 10-fold diluted plasmids to generate standard curve. For multiplex standard curves, each plasmid was diluted to 3.0×10^9 copies/μL and pooled in equal volume to make a concentration of 1.0×10^9 copies/μL for each plasmid. The pooled plasmid was then diluted in a 10-fold series, ranging from 1.0×10^8 to 1.0×10^3 copies/μL, to establish multiplex standard curves.

2.3 Reaction conditions of the singleplex real-time PCR

All real-time PCR reaction systems were set to a volume of 20 μL. For singleplex real-time PCR of PDCoV, RV, and PEDV, the reaction system included 10 μL 2×PerfectStart Probe One-Step qPCR SuperMix, 0.4 μL TransScript Probe One-Step RT Enzyme Mix (Transgen, Beijing), 0.4 μL each of forward/reverse primer (10 μM), 0.4 μL TaqMan probe (10 μM), 5.5 μL RNA template, and 2.9 μL nuclease-free water.

Amplification was performed on a Bio-Rad CFX96™ Real-time System (Bio-Rad, Hercules, CA, USA) using the following program: 45°C for 5 min, 94°C for 30 s, 40 cycles of 94°C for 5 s, and 52°C for 30 s. Fluorescence signal was automatically collected at the end of each cycle. All qPCR results were analyzed using CFX Manager™ software.

2.4 Optimization of multiplex real-time PCR assay

The concentrations of primers and probes were optimized as previously described (Pan et al., 2020). After repeated tests, the optimal reaction conditions for multiplex real-time PCR were determined as follows: 10 μL 2×PerfectStart Probe One-Step qPCR SuperMix, 0.4 μL TransScript Probe One-Step RT Enzyme Mix (Transgen, Beijing), 0.4 μL each of forward/reverse primer and probe (10 μM) for PoRV and PDCoV, 0.2 μL each of forward/reverse primer and probe (10 μM) for PEDV, 5.5 μL RNA template, 1.1 μL nuclease-free water, with a total reaction volume of 20 μL. The same instrument and real-time PCR program were used as described above.

2.5 Sensitivity, specificity, and repeatability test of the multiplex real-time PCR assay

To determine the limit of detection (LOD) for the multiplex real-time PCR method, the aforementioned pooled standard plasmids were diluted in a 10-fold serial manner, ranging from 1.0×10^3 to 1.0×10^0 copies/μL in nuclease-free water. These diluted standard plasmids were then used as templates for multiplex real-time PCR amplification. The reliable LOD was the lowest concentration that achieved a 95% positive detection rate.

To avoid false positives caused by other viruses or bacteria that may be present in the samples, two RNA viruses (PRRSV and CSFV), three DNA viruses (PCV1, PCV2, and ASFV), and two bacterias (*S. suis* and *S. enteritidis*) were used for specificity test of multiplex real-time PCR assay. Nucleic acids were extracted using the VAMNE Virus DNA/RNA Extraction Kit (Nanjing Vazyme Biotech Co., Ltd.). For RNA viruses, the cDNA was generated with the TransScript Probe One-Step qRT-PCR SuperMix (Beijing Transgen Biotech Co., Ltd.). These DNA and cDNA samples were first detected using commercial kits, and positive samples with CT values <25 were selected as template for specificity test of the multiplex real-time PCR assay. The standard plasmids of PEDV, PoRV, and PDCoV were used as positive controls, while nuclease-free water served as the negative control.

To assess its repeatability of the multiplex real-time PCR, a 10-fold serially diluted standard template was used, ranging from 1.0×10^8 to 1.0×10^3 copies/μL. Each reaction was performed with three replicates. Intra-assay repeatability was determined by conducting three simultaneous detections of each

10.3389/fmicb.2024.1380849

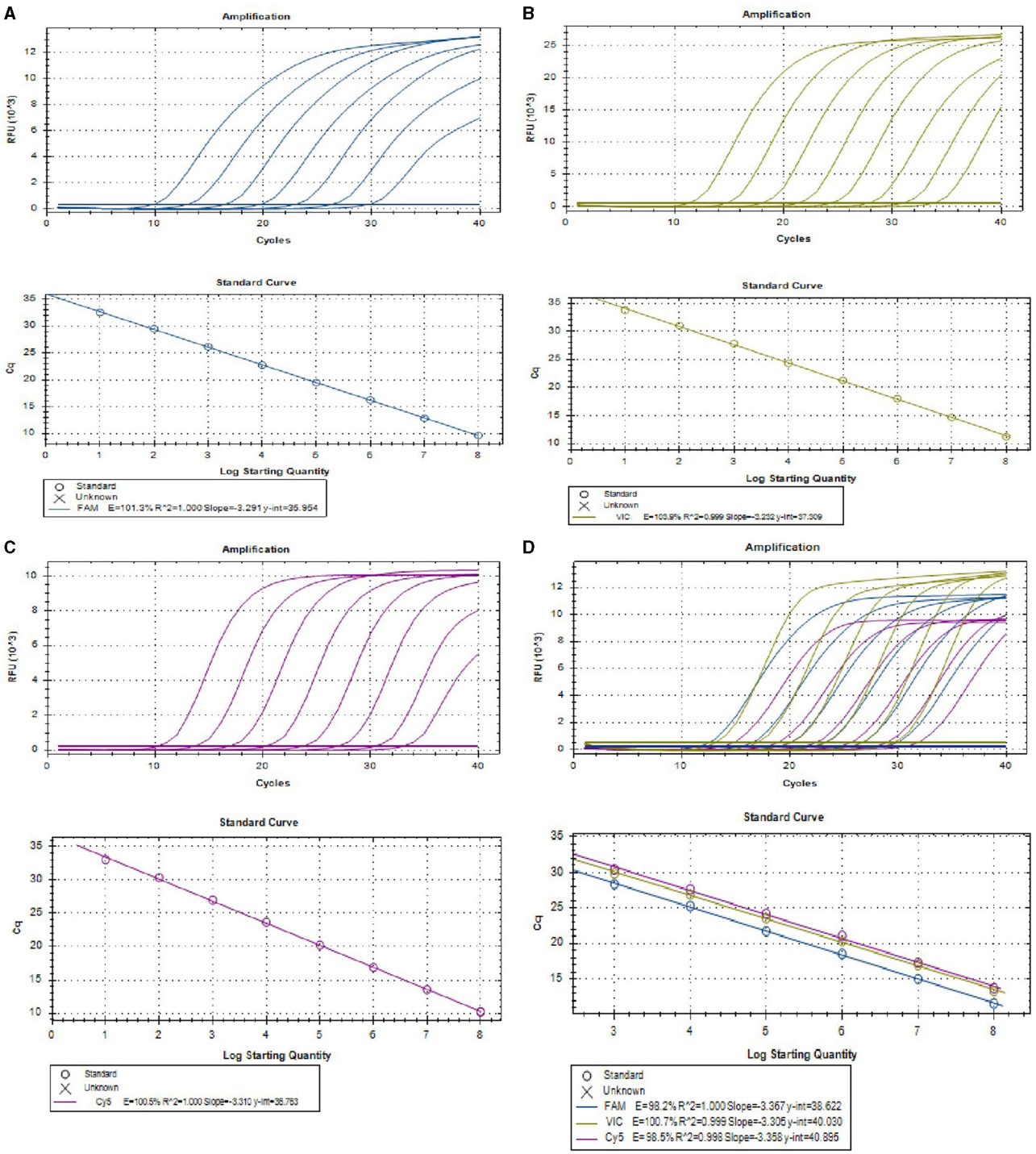

FIGURE 1
The amplification curves **(top)** and the standard curve **(bottom)** of the single and multiplex real-time PCR assay. **(A–C)** The amplification curves **(top)** and the standard curve **(bottom)** of single real-time PCR assay for detection of PEDV **(A)**, PoRV **(B)**, and PDCoV **(C)**, respectively, with concentrations of each plasmid standard ranging from 1.0×10^8 to 1.0×10^1 copies/μL. **(D)** Amplification curves **(top)** and standard curves **(bottom)** of optimized multiplex real-time PCR for simultaneous detection of PEDV, PoRV, and PDCoV. The concentrations of each plasmid standard are from 1.0×10^8 to 1.0×10^3 copies/μL.

plasmid under identical conditions. Inter-assay repeatability was evaluated by repeating the assays three times individually at different time points. The coefficient of variation (CV) of the Cq values from the three experiments was calculated to estimate the level of repeatability. Data analysis was conducted using Microsoft Excel.

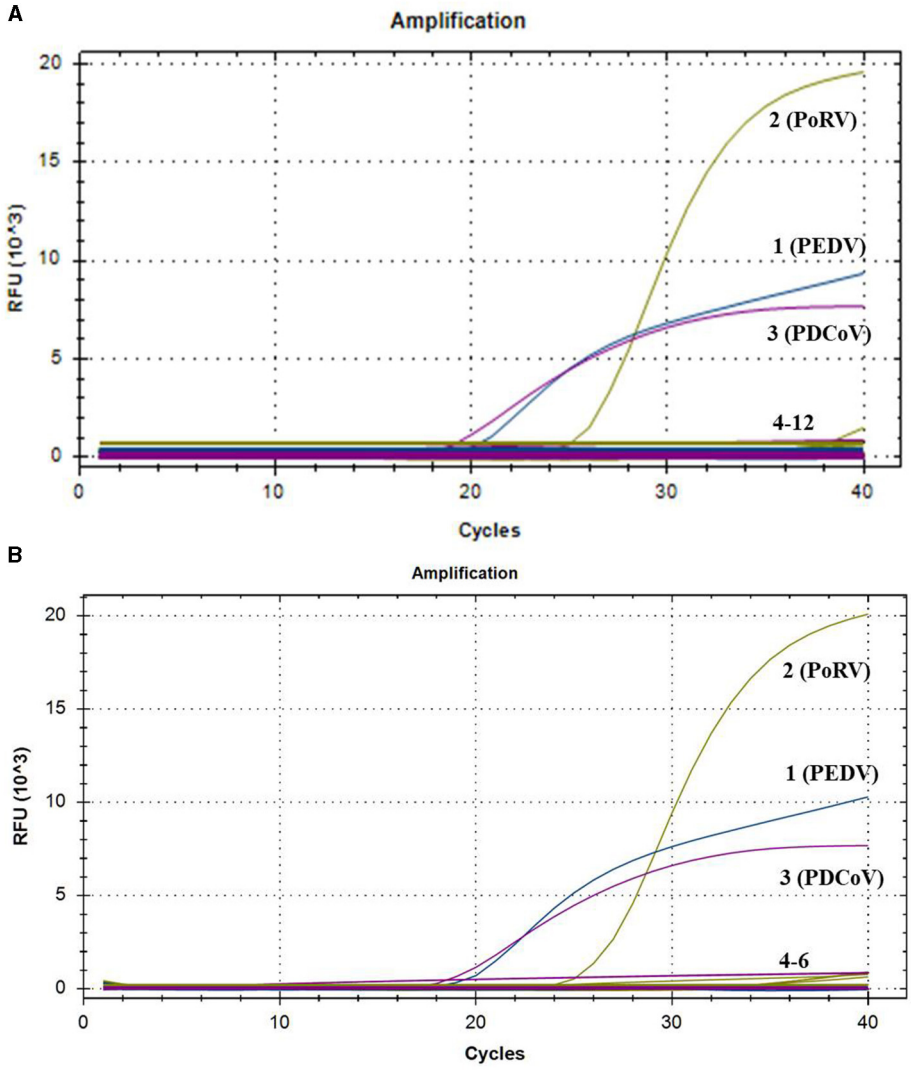

FIGURE 2
The amplification curves of specificity tests of multiplex real-time PCR. Only PEDV, PoRV, and PDCoV showed positive fluorescence signals, while other swine pathogens and clinical samples from healthy pigs exhibited no fluorescence signals. **(A)** 1–3: positive templates of PEDV, PoRV, and PDCoV. 4–12: negative control and positive templates of PRRSV, PRV, PCV1, PCV2, CSFV, ASFV, SS, and SE. **(B)** 1–3: positive templates of PEDV, PoRV, and PDCoV. 4–6: templates of clinical samples from healthy pigs.

2.6 Verification of the multiplex real-time PCR assay

Our multiplex real-time PCR method and a commercial singleplex real-time PCR Kit were used to simultaneously detect 30 clinical samples with diarrhea symptoms. The detection results obtained from our established methods were then compared with those obtained from singleplex real-time PCR.

2.7 Clinical application of the multiplex real-time PCR assay

A total of 4,800 samples including fecal samples (n = 2,341), rectal swabs (n = 1,874), oral fluid (n = 145), and oropharyngeal swabs (n = 440), were used to investigate the prevalence of PEDV, PoRV, and PDCoV using the multiplex real-time PCR assay. These samples were collected from pig farms located in numerous provinces of China, including Gansu, Shanxi, Shaanxi, Shandong, Henan, Hubei, Anhui, Zhejiang, Jiangsu, Guangdong, Guangxi, Guizhou, Sichuan, Hunan, Chongqing, and Jiangxi, during the period from November 2021 to July 2022.

Clinical samples were treated with phosphate buffer saline (PBS), and the supernatant was collected after vortexing and centrifugation. Nucleic acids were extracted using the VAMNE Virus DNA/RNA Extraction Kit (Nanjing Vazyme Biotech Co., Ltd.). Reverse transcription was done with the TransScript Probe One-Step qRT-PCR SuperMix (Beijing Transgen Biotech Co., Ltd.). The constructed plasmid and nuclease-free were employed as positive and negative controls, respectively. All samples were tested with the multiplex real-time PCR assay to determine virus positivity. Infection rates were analyzed after obtaining assay results for all clinical samples.

3 Results

3.1 Single real-time PCR assay for individual virus

To develop a multiplex real-time PCR, we first established singleplex real-time PCR for each virus using different fluorescence-labeled target probes. Standard curve for each virus was created using 10-fold serial dilutions of plasmids ranging from 1.0×10^8 to 1.0×10^1 copies/μL. All the standard curves showed excellent correlation coefficients and amplification efficacy, with PEDV ($R^2 = 1.000$; E = 101.3%), PoRV ($R^2 = 0.999$; E = 103.9%), PDCoV ($R^2 = 1.000$; E = 100.5%), respectively. This indicates that our plasmid standards were qualified, and the designed primers and probes were efficient (Figures 1A–C).

3.2 Establishment of multiplex real-time PCR assay

Serial dilutions of mixed viral standard plasmids were tested with the using the optimized multiplex assay. The results demonstrated that the multiplex real-time PCR successfully detected all target genes of these three viruses (Figure 1D). The standard curves exhibited excellent correlation coefficients and amplification efficacy for each virus, for details, PEDV ($R^2 = 1.000$; E = 98.2%), PoRV ($R^2 = 0.999$; E = 100.7%), and PDCoV ($R^2 = 0.998$; E = 98.5%; Figure 1D), indicating the validity and reliability of the multiplex real-time PCR.

3.3 The specificity of the multiplex real-time PCR assay

To evaluate the specificity of the multiplex real-time PCR, the positive samples of PRRSV, PRV, PCV1, PCV2, CSFV, ASFV, SS, and SE were used as templates for amplification with this multiplex system. The standard plasmids of PEDV, PoRV, and PDCoV were tested as the positive controls, while nuclease-free water was tested as negative control. As shown Figure 2A, all the target pathogens were successfully detected, while no positive signal was observed from other eight viruses and negative control. Additionally, three clinical samples from healthy pigs were further tested to confirm the specificity. Amplification curves also demonstrated that only target genes from the standard plasmids were detected, with no positive signal detected in the clinical samples from healthy pigs (Figure 2B). These findings indicated that the multiplex real-time PCR assay was highly specific.

3.4 The sensitivity of the multiplex real-time PCR assay

To access the sensitivity of this multiplex real-time PCR assay, we tested pooled standard plasmids with concentrations ranging from 1.0×10^3 to 1.0×10^0 copies/μL under optimized reaction conditions. The method was able to detect positive samples with concentrations as low as 1.0×10^1 copies/μL (Table 2). However, further experiments showed the detection rate for samples at 1.0×10^1 copies/μL was <95% of replicates (Table 2). Therefore, the reliable limit of detection for this method is 1×10^2 copies/μL.

3.5 Repeatability of the multiplex real-time PCR assay

The multiplex real-time PCR assay was confirmed to be repeatable by detecting standard plasmids at concentrations ranging from 1.0×10^8 to 1.0×10^3 copies/μL. As shown in Table 3, the variation coefficients (CVs) of Cq values in the intra-group and inter-group reproducibility tests were between 0.11 and 0.87% and between 0.11 and 1.63%, respectively. These results indicated that the multiplex real-time PCR assay established in this study had satisfactory repeatability.

3.6 Verification of the multiplex real-time PCR assay by commercial singleplex real-time PCR kit

Thirty clinical samples were used to compare the results of the multiplex real-time PCR with commercial singleplex real-time PCR kit. As shown in Supplementary Table 1, the results of the multiplex real-time PCR were consistent with the commercial singleplex real-time PCR, suggesting that it can effectively replace the commercial singleplex real-time PCR for simultaneous detection of PEDV, PoRV, and PDCoV.

3.7 Clinical application of the multiplex real-time PCR

A total of 4,800 clinical samples were detected using the multiplex real-time PCR assay established in this study. As shown in Figure 3A, the single infection rates for PEDV, PoRV, and PDCoV were 6.56% (315/4,800), 21.69% (1,041/4,800), and 6.65% (319/4,800), respectively. The co-infection rates for PEDV + PoRV, PEDV + PDCoV, and PoRV + PDCoV were 11.83% (568/4,800), 0.29% (14/4,800), and 5.71% (274/4,800), respectively. The mixed infection rate for PEDV + PDCoV + PoRV was 1.29% (62/4,800).

These 4,800 clinical samples were collected from 16 provinces which were divided into three regions based on the geographical distribution: Northern China (Gansu, Shanxi, and Shaanxi), Mideastern China (Shandong, Henan, Hubei, Anhui, Zhejiang, and Jiangsu), and Southern China (Guangdong, Guangxi, Guizhou, Sichuan, Hunan, Chongqing, and Jiangxi). In the Northern China, PEDV, PoRV, and PDCoV had infection rates of 10.33% (224/2,169), 14.71% (319/2,169), and 11.66% (253/2,169), respectively (Figure 3B). Co-infection rates were 18.63% (404/2,169) for PEDV + PoRV, 0.60% (13/2,169) for PEDV + PDCoV, 10.28% (223/2,169) for PoRV + PDCoV, 0.55% (12/2,169) for PEDV + PDCoV + PoRV, respectively (Figure 3B). In the Mideastern China, PEDV, PoRV, and PDCoV had infection rates of 2.44% (40/1,642), 26.79% (440/1,642), and

TABLE 2 The sensitivity tests of multiplex real-time PCR.

Templates	Concentrations (copies/μL)	The number of tested samples	Positive number	Positive rate (%)	95% confidence region
PEDV	1×10^3	30	30	100	√
	1×10^2	30	30	100	√
	1×10^1	30	28	93.3	×
	1×10^0	30	0	0	×
	Negative control	30	0	0	×
PoRV	1×10^3	30	30	100	√
	1×10^2	30	30	100	√
	1×10^1	30	27	90.0	×
	1×10^0	30	0	0	×
	Negative control	30	0	0	×
PDCoV	1×10^3	30	30	100	√
	1×10^2	30	30	100	√
	1×10^1	30	28	93.3	×
	1×10^0	30	0	0	×
	Negative control	30	0	0	×

3.59% (59/1,642), respectively (Figure 3B). Co-infection rates were 5.66% (93/1,642) for PEDV + PoRV, 0.06% (1/1,642) for PEDV + PDCoV, 2.68% (44/1,642) for PoRV + PDCoV, 1.22% (20/1,642) for PEDV + PDCoV + PoRV, respectively (Figure 3B). In the Southern China, PEDV, PoRV, and PDCoV had infection rates of were 5.16% (51/989), 28.51% (282/989), and 0.71% (7/989), respectively (Figure 3B). Co-infection rates were 7.18% (71/989) for PEDV + PoRV, 0 (0/989) for PEDV + PDCoV, 0.71% (7/989) for PoRV + PDCoV, 3.03% (30/989) for PEDV + PDCoV + PoRV, respectively (Figure 3B).

4 Discussion

Porcine viral diarrhea is a prevalent occurrence observed in clinical setting, resulting in substantial economic losses within the pig industry. Notably, PEDV, PoRV, and PDCoV are recognized as crucial pathogens causing this disease (Hou et al., 2023). With the development of large-scale and intensive swine production, mixed infections of these three pathogens are increasingly becoming common in swine farms (Huang et al., 2015). Detecting and identifying the pathogens quickly and accurately is crucial for preventing and controlling the spread of infectious diseases. Given the similarities in symptoms and pathology, as well as the frequent co-infection of these three viruses, it is challenging to differentiate them through clinical diagnosis alone (Vlasova et al., 2017; Shu et al., 2022). Hence, there is a need for a rapid and accurate method to simultaneously distinguish PEDV, PoRV, and PDCoV.

In this study, specific primers and probes were designed for the conserved regions of the PEDV M gene, PoRV NSP3 gene, and PDCoV M gene. After optimizing multiple times, a successful multiplex real-time PCR method was developed to simultaneously detect PEDV, PoRV, and PDCoV in a single amplification reaction. The method established in this study is highly sensitive, with a detection limit of 100 copies/μL. The multiplex real-time PCR also showed good repeatability, with coefficient of variation ranging from 0.11 to 0.87% for intra-assay and 0.11–1.63% for inter-assay. Thirty clinical samples with diarrhea symptoms were used to compare the results of the commercial singleplex real-time PCR kit and our multiplex real-time PCR method for detecting PEDV, PoRV, and PDCoV. The two methods showed complete agreement, indicating that the multiplex real-time PCR assay developed in this study could effectively replace the commercial singleplex real-time PCR kit for simultaneously differentiating PEDV, PoRV, and PDCoV.

Due to its rapid, highly sensitive, and specific characteristics, the multiplex real-time PCR assay established in this study has been widely used in early detection of pathogens in clinical samples. A total of 4,800 diarrhea samples from 18 provinces of china were used to investigate the prevalence of PEDV, PoRV, and PDCoV. Out of these samples, 2,207 were negative and 2,593 were positive for single or co-infections of these viruses. Among the positive samples, PoRV had the highest infection rate at 75% (1,945/2,593), followed by PEDV at 36.98% (959/2,593) and PDCoV at 25.8% (669/2,593), confirming PoRV as the primary cause of porcine diarrhea. These findings align with previous research showing a steady increase in PoRV infection rates, with some countries reporting 100% seropositivity in adult pigs (Pettersson et al., 2019).

Previous reports have shown that co-infection of these three viruses can lead to severe symptoms (Vlasova et al., 2017; Saeng-Chuto et al., 2021). Our study found that co-infections account for 35.4% (918/2,593) of positive samples, indicating that multiple pathogen co-infections are becoming more common with the development of large-scale and intensive swine production (Figure 3A). Specifically, co-infections of PoRV and PEDV accounted for 21.9% (568/2,593) of positive samples, followed

TABLE 3 The repeatability tests of multiplex real-time PCR.

Templates	Concentrations (copies/μL)	Intra-assay		Inter-assay	
		Cq values (mean ± SD)	CV%	Cq values (mean ± SD)	CV%
PEDV	1×10^8	11.53 ± 0.05	0.40	11.41 ± 0.16	1.38
	1×10^7	15.45 ± 0.09	0.55	15.30 ± 0.15	0.98
	1×10^6	19.00 ± 0.13	0.68	18.84 ± 0.18	0.96
	1×10^5	22.19 ± 0.05	0.21	21.93 ± 0.17	0.78
	1×10^4	25.75 ± 0.11	0.43	25.31 ± 0.14	0.56
	1×10^3	29.02 ± 0.15	0.50	28.61 ± 0.11	0.38
	Negative control	ND	ND	ND	ND
PoRV	1×10^8	12.96 ± 0.11	0.85	12.89 ± 0.21	1.63
	1×10^7	16.77 ± 0.15	0.87	16.93 ± 0.23	1.33
	1×10^6	20.03 ± 0.06	0.29	20.16 ± 0.18	0.88
	1×10^5	23.18 ± 0.03	0.15	23.23 ± 0.16	0.68
	1×10^4	26.66 ± 0.08	0.11	26.59 ± 0.35	1.33
	1×10^3	29.53 ± 0.11	0.39	29.58 ± 0.16	0.52
	Negative control	ND	ND	ND	ND
PDCoV	1×10^8	13.36 ± 0.11	0.83	13.73 ± 0.02	0.11
	1×10^7	17.39 ± 0.14	0.80	17.47 ± 0.04	0.22
	1×10^6	21.03 ± 0.03	0.14	21.10 ± 0.03	0.14
	1×10^5	24.15 ± 0.10	0.42	24.20 ± 0.06	0.25
	1×10^4	27.72 ± 0.16	0.56	27.61 ± 0.06	0.23
	1×10^3	30.37 ± 0.04	0.12	30.58 ± 0.23	0.76
	Negative control	ND	ND	ND	ND

ND means no data.

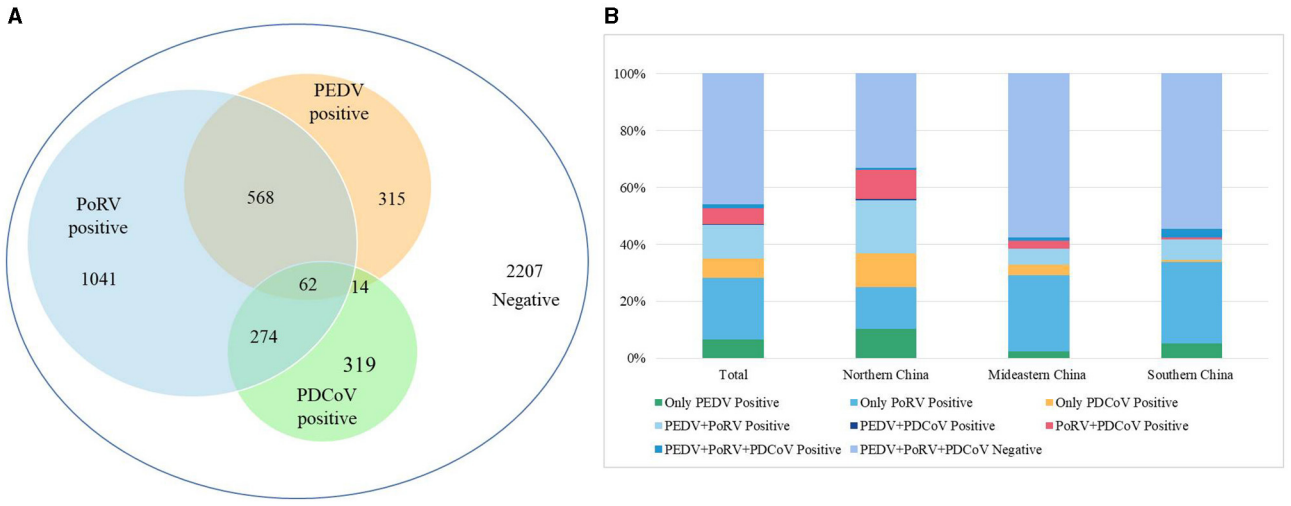

FIGURE 3
The detection results of clinical diarrhea samples using the multiplex real-time PCR assay established in this study. **(A)** The detection results of 4,800 clinical diarrhea samples. **(B)** A comparison of positive rates from different regions of China. These 4,800 clinical diarrhea samples were collected from 16 provinces of China, which were divided into three regions: Northern China (Gansu, Shanxi, and Shaanxi), Mideastern China (Shandong, Henan, Hubei, Anhui, Zhejiang, and Jiangsu), and Southern China (Guangdong, Guangxi, Guizhou, Sichuan, Hunan, Chongqing, and Jiangxi).

by co-infections of PoRV and PDCoV at 10.57% (274/2,593; Figure 3A). Co-infections of PEDV and PDCoV were very rare, at only 0.54% (14/2,593; Figure 3A). Notably, 2.39% (62/2,593) of positive samples were co-infected with PEDV, PoRV, and PDCoV (Figure 3A). The findings align with previous studies indicating that the co-infection of PEDV and PoRV is the primary cause of porcine diarrhea in certain Chinese provinces (Zhang et al., 2019; Shu et al., 2022; Hou et al., 2023).

There were significant differences in positivity rate for these three viruses among the three regions: Northern China, Mideastern China), and Southern China. Northern China had the highest positivity rate for the three viruses at 66.76%, followed by Mideastern China at 42.40% and Southern China at 45.5% (Figure 3B). Northern China also had a higher incidence of co-infection at 45.03% compared to Mideastern China at 22.69% and Southern China at 24% (Figure 3B). However, Mideastern and Southern China had a higher positive rate of single PoRV than Northern China (Figure 3B). These results suggest that viral diarrhea disease in China pig farms is complex, possibly due to climate differences between the north and south and rapid pig population renewal in northern China. In summary, we have successfully developed a reliable multiplex real-time PCR assay for distinguishing PEDV, PoRV, and PDCoV. This assay has demonstrated excellent specificity, sensitivity, and repeatability. It has also been effectively used to detect clinical samples, making it a valuable tool for quickly identifying these viruses. Rapid and precise diagnostics, followed by prompt quarantine and treatment, could be helpful to prevent and control the spread of infectious diseases.

Data availability statement

The original contributions presented in the study are included in the article/Supplementary material, further inquiries can be directed to the corresponding author.

Author contributions

JR: Conceptualization, Funding acquisition, Writing—review & editing, Formal analysis, Methodology, Project administration, Writing—original draft. CZ: Writing—original draft, Data curation, Software. YL: Software, Writing—original draft, Resources. ML: Data curation, Writing—review & editing. JG: Data curation, Investigation, Writing—review & editing. FC: Data curation, Formal analysis, Writing—review & editing. XL: Conceptualization, Data curation, Funding acquisition, Resources, Writing—review & editing.

Funding

The author(s) declare financial support was received for the research, authorship, and/or publication of this article. This work was funded by the Natural Science Foundation of Shandong Province (Grant Nos. ZR2022MC158 and ZR2020QC177), Taishan Industry Leadership Talent Project of Shandong Province in China (Grant No. tscx202306093), and Talent Introduction Project of Dezhou University of China (2022xjrc413).

Conflict of interest

CZ, YL, and XL were employed by Shandong New Hope Liuhe Agriculture and Animal Husbandry Technology Co., Ltd. (NHLH Academy of Swine Research).

The remaining authors declare that the research was conducted in the absence of any commercial or financial relationships that could be construed as a potential conflict of interest.

Publisher's note

All claims expressed in this article are solely those of the authors and do not necessarily represent those of their affiliated organizations, or those of the publisher, the editors and the reviewers. Any product that may be evaluated in this article, or claim that may be made by its manufacturer, is not guaranteed or endorsed by the publisher.

Supplementary material

The Supplementary Material for this article can be found online at: https://www.frontiersin.org/articles/10.3389/fmicb.2024.1380849/full#supplementary-material

References

Ben Salem, A. N., Chupin Sergei, A., Bjadovskaya Olga, P., Andreeva Olga, G., Mahjoub, A., and Prokhvatilova Larissa, B. (2010). Multiplex nested RT-PCR for the detection of porcine enteric viruses. *J. Virol. Methods* 165, 283–293. doi: 10.1016/j.jviromet.2010.02.010

Chepngeno, J., Takanashi, S., Diaz, A., Michael, H., Paim, F. C., Rahe, M. C., et al. (2020). Comparative sequence analysis of historic and current porcine rotavirus c strains and their pathogenesis in 3-day-old and 3-week-old piglets. *Front. Microbiol.* 11:780. doi: 10.3389/fmicb.2020.00780

He, W. T., Ji, X., He, W., Dellicour, S., Wang, S., Li, G., et al. (2020). Genomic epidemiology, evolution, and transmission dynamics of porcine deltacoronavirus. *Mol. Biol. Evol.* 37, 2641–2654. doi: 10.1093/molbev/msaa117

Hou, W., Fan, M., Zhu, Z., and Li, X. (2023). Establishment and application of a triplex Real-Time RT-PCR assay for differentiation of PEDV, PoRV, and PDCoV. *Viruses* 15:1238. doi: 10.3390/v15061238

Hu, Y., Xie, X., Yang, L., and Wang, A. (2021). A comprehensive view on the host factors and viral proteins associated with porcine epidemic diarrhea virus infection. *Front. Microbiol.* 12:762358. doi: 10.3389/fmicb.2021.762358

Huang, X., Chen, J., Yao, G., Guo, Q., Wang, J., and Liu, G. (2019). A TaqMan-probe-based multiplex real-time RT-qPCR for simultaneous detection of porcine enteric coronaviruses. *Appl. Microbiol. Biot.* 103, 4943–4952. doi: 10.1007/s00253-019-09835-7

Huang, Y., Xing, N., Wang, Z., Zhang, X., Zhao, X., Du, Q., et al. (2015). Ultrasensitive detection of RNA and DNA viruses simultaneously using duplex undp-pcr assay. *PLoS ONE* 10:e0141545. doi: 10.1371/journal.pone.0141545

Huang, Y. W., Dickerman, A. W., Piñeyro, P., Li, L., Fang, L., Kiehne, R., et al. (2013). Origin, evolution, and genotyping of emergent porcine epidemic diarrhea virus strains in the United States. *mBio* 4, e00737–e00713. doi: 10.1128/mBio.00737-13

Li, W., Hulswit, R. J. G., Kenney, S. P., Widjaja, I., Jung, K., Alhamo, M. A., et al. (2018). Broad receptor engagement of an emerging global coronavirus may potentiate its diverse cross-species transmissibility. *Proc. Natl. Acad. Sci. U. S. A.* 115, E5135–E5143. doi: 10.1073/pnas.1802879115

Li, X., Hu, Y., Liu, P., Zhu, Z., Liu, P., Chen, C., et al. (2022). Development and application of a duplex real-time PCR assay for differentiation of genotypes I and II African swine fever viruses. *Transbound Emerg. Dis.* 69, 2971–2979. doi: 10.1111/tbed.14459

Liu, G., Jiang, Y., Opriessnig, T., Gu, K., Zhang, H., and Yang, Z. (2019). Detection and differentiation of five diarrhea related pig viruses utilizing a multiplex PCR assay. *J. Virol. Methods* 263, 32–37. doi: 10.1016/j.jviromet.2018.10.009

Ma, Y., Zhang, Y., Liang, X., Lou, F., Oglesbee, M., Krakowka, S., et al. (2015). Origin, evolution, and virulence of porcine deltacoronaviruses in the United States. *mBio* 6:e00064. doi: 10.1128/mBio.00064-15

Pan, Z., Lu, J., Wang, N., He, W. T., Zhang, L., Zhao, W., et al. (2020). Development of a TaqMan-probe-based multiplex real-time PCR for the simultaneous detection of emerging and reemerging swine coronaviruses. *Virulence* 11, 707–718. doi: 10.1080/21505594.2020.1771980

Pettersson, E., Hestad, S., Möttus, I., Skiöldebrand, E., and Wallgren, P. (2019). Rotavirus and *Cystoisospora suis* in piglets during the suckling and early post weaning period, in systems with solid floors and age segregated rearing. *Porcine Health. Manag.* 5:7. doi: 10.1186/s40813-019-0114-0

Saeng-Chuto, K., Madapong, A., Kaeoket, K., Piñeyro, P. E., Tantituvanont, A., and Nilubol, D. (2021). Coinfection of porcine deltacoronavirus and porcine epidemic diarrhea virus increases disease severity, cell trophism and earlier upregulation of IFN-α and IL12. *Sci. Rep.* 11:3040. doi: 10.1038/s41598-021-82738-8

Shibata, I., Tsuda, T., Mori, M., Ono, M., Sueyoshi, M., and Uruno, K. (2000). Isolation of porcine epidemic diarrhea virus in porcine cell cultures and experimental infection of pigs of different ages. *Vet. Microbiol.* 72, 173–182. doi: 10.1016/S0378-1135(99)00199-6

Shu, X., Han, F., Hu, Y., Hao, C., Li, Z., Wei, Z., et al. (2022). Co-infection of porcine deltacoronavirus and porcine epidemic diarrhoea virus alters gut microbiota diversity and composition in the colon of piglets. *Virus Res.* 322:198954. doi: 10.1016/j.virusres.2022.198954

Si, F., Hu, X., Wang, C., Chen, B., Wang, R., Dong, S., et al. (2020). Porcine epidemic diarrhea virus (PEDV) ORF3 enhances viral proliferation by inhibiting apoptosis of infected cells. *Viruses* 12:214. doi: 10.3390/v12020214

Tao, R., Chang, X., Zhou, J., Zhu, X., Yang, S., Li, K., et al. (2023). Molecular epidemiological investigation of group A porcine rotavirus in East China. *Front. Vet. Sci.* 10:1138419. doi: 10.3389/fvets.2023.1138419

Vlasova, A. N., Amimo, J. O., and Saif, L. J. (2017). Porcine rotaviruses: epidemiology, immune responses and control strategies. *Viruses* 9:48. doi: 10.3390/v9030048

Wang, D., Fang, L., and Xiao, S. (2016). Porcine epidemic diarrhea in China. *Virus Res.* 226, 7–13. doi: 10.1016/j.virusres.2016.05.026

Wang, L., Byrum, B., and Zhang, Y. (2014). Porcine coronavirus HKU15 detected in 9 US states, 2014. *Emerg. Infect. Dis.* 20, 1594–1595. doi: 10.3201/eid2009.140756

Woo, P. C., Lau, S. K., Lam, C. S., Lau, C. C., Tsang, A. K., Lau, J. H., et al. (2012). Discovery of seven novel Mammalian and avian coronaviruses in the genus deltacoronavirus supports bat coronaviruses as the gene source of alphacoronavirus and betacoronavirus and avian coronaviruses as the gene source of gammacoronavirus and deltacoronavirus. *J. Virol.* 86, 3995–4008. doi: 10.1128/JVI.06540-11

Wu, X., Liu, Y., Gao, L., Yan, Z., Zhao, Q., Chen, F., et al. (2022). Development and application of a reverse-transcription recombinase-aided amplification assay for porcine epidemic diarrhea virus. *Viruses* 14:59. doi: 10.3390/v14030591

Zhang, H., Liang, Q., Li, B., Cui, X., Wei, X., Ding, Q., et al. (2019). Prevalence, phylogenetic and evolutionary analysis of porcine deltacoronavirus in Henan province, China. *Prev. Vet. Med.* 166, 8–15. doi: 10.1016/j.prevetmed.2019.02.017

frontiers | Frontiers in Microbiology

TYPE Original Research
PUBLISHED 23 April 2024
DOI 10.3389/fmicb.2024.1387309

OPEN ACCESS

EDITED BY
Jianke Wang,
Hebei Agricultural University, China

REVIEWED BY
Guo Huichen,
Lanzhou Veterinary Research Institute, Chinese Academy of Agricultural Sciences, China
Mengmeng Zhao,
Foshan University, China

*CORRESPONDENCE
Fandan Meng
✉ mengfandan@caas.cn
Tongqing An
✉ antongqing@caas.cn
Yan-Dong Tang
✉ tangyandong@caas.cn

†These authors have contributed equally to this work

RECEIVED 17 February 2024
ACCEPTED 01 April 2024
PUBLISHED 23 April 2024

CITATION
Zhou H, Sun M, Su S, Meng L, Yang W, Yang L, Shi X, Li X, Wang H, Ma H, Cai X, Tang Y-D, An T and Meng F (2024) Identification of a linear B-cell epitope on the "puff" loop of the Senecavirus A VP2 protein involved in receptor binding. *Front. Microbiol.* 15:1387309. doi: 10.3389/fmicb.2024.1387309

Identification of a linear B-cell epitope on the "puff" loop of the Senecavirus A VP2 protein involved in receptor binding

Hanrong Zhou[1†], Mingxia Sun[1†], Shibo Su[1†], Liang Meng[1], Wei Yang[2], Lan Yang[3], Xinqi Shi[1], Xin Li[1], Haiwei Wang[1], Hongwei Ma[1,3], Xuehui Cai[1,4], Yan-Dong Tang[1]*, Tongqing An[1,5]* and Fandan Meng[1]*

[1]State Key Laboratory for Animal Disease Control and Prevention, Harbin Veterinary Research Institute of Chinese Academy of Agricultural Sciences, Harbin, Heilongjiang, China, [2]College of Veterinary Medicine, Northeast Agricultural University, Harbin, China, [3]Division of Nanobiomedicine, Suzhou Institute of Nano-Tech and Nano-Bionics, Chinese Academy of Sciences, Suzhou, China, [4]Heilongjiang Research Center for Veterinary Biopharmaceutical Technology, Harbin Veterinary Research Institute, Chinese Academy of Agricultural Sciences, Harbin, China, [5]Heilongjiang Provincial Key Laboratory of Veterinary Immunology, Harbin Veterinary Research Institute, Chinese Academy of Agricultural Sciences, Harbin, China

Senecavirus A (SVA) is an important emerging swine pathogen that causes vesicular lesions in swine and acute death in newborn piglets. VP2 plays a significant role in the production of antibodies, which can be used in development of diagnostic tools and vaccines. Herein, the aim of the current study was to identify B-cell epitopes (BCEs) of SVA for generation of epitope-based SVA marker vaccine. Three monoclonal antibodies (mAbs), named 2E4, 1B8, and 2C7, against the SVA VP2 protein were obtained, and two novel linear BCEs, ^{177}SLGTYYR^{183} and ^{266}SPYFNGL^{272}, were identified by peptide scanning. The epitope ^{177}SLGTYYR^{183} was recognized by the mAb 1B8 and was fully exposed on the VP2 surface, and alanine scanning analysis revealed that it contained a high continuity of key amino acids. Importantly, we confirmed that ^{177}SLGTYYR^{183} locates on "the puff" region within the VP2 EF loop, and contains three key amino acid residues involved in receptor binding. Moreover, a single mutation, Y182A, blocked the interaction of the mutant virus with the mAb 1B8, indicating that this mutation is the pivotal point for antibody recognition. In summary, the BCEs that identified in this study could be used to develop diagnostic tools and an epitope-based SVA marker vaccine.

KEYWORDS

Senecavirus A (SVA), B-cell epitopes (BCEs), monoclonal antibodies (mAbs), VP2 protein, receptor binding

1 Introduction

Senecavirus A (SVA), previously called Seneca Valley virus (SVV), is the only member of the genus *Senecavirus* in the family *Picornaviridae* (Hales et al., 2008; Zhang et al., 2018). SVA is a single-stranded positive-sense RNA virus associated with porcine idiopathic vesicular disease (PIVD) and epidemic transient neonatal loss (ETNL) (Vannucci et al., 2015; Leme et al., 2016); it has become an important swine pathogen and has caused significant economic losses. The clinical signs in SVA-infected pigs include ulcerative

lesions on the snout and coronary bands, lameness, anorexia, lethargy, cutaneous hyperemia, and fever, affecting a high percentage of sows, finisher pigs, and neonatal piglets (Leme et al., 2017; Houston et al., 2020). The clinical manifestations and lesions of SVA are comparable to those of foot-and-mouth disease virus (FMDV), swine vesicular disease virus (SVDV), vesicular stomatitis virus (VSV), and vesicular exanthema of swine virus (VESV), which makes clinical diagnosis difficult. In 2015, SVA was first reported in China in Guangdong Province, and both adult and newborn pigs were infected during this outbreak (Wu et al., 2017). SVA began to spread rapidly among pigs in more regions and countries (Sun et al., 2018; Liu et al., 2020). In addition, co-infecting pigs with SVA and porcine reproductive and respiratory syndrome virus (PRRSV) may increase mortality (Paiva et al., 2023).

SVA is a non-enveloped RNA virus composed of an icosahedral capsid ~30 nm in diameter with a genome size of 7.2 kilobases (Hales et al., 2008). Like in other *picornaviruses*, SVA has one open reading frame (ORF) and encodes a single polyprotein precursor, which is then cleaved by protease into 12 functional proteins, including the lead protein L, structural protein P1 (VP1, VP2, VP3, VP4), nonstructural protein P2 (2A, 2B, 2C) and P3 (3A, 3B, 3C, 3D) (Houston et al., 2020). Among the SVA structural proteins, the VP1, VP2, and VP3 proteins are exposed on the virion surface and are responsible for stimulating host immune responses and binding to host receptors, while VP4 is located internally and interacts with internal nucleic acids (Strauss et al., 2018). In addition, VP2 is crucial for determining the cell tropism of SVA (Wang et al., 2023) and mediating virus binding to the cell receptor anthrax toxin receptor 1 (ANTXR1) (Miles et al., 2017). Although VP2 is the major structural protein that induces neutralizing antibodies (Dvorak et al., 2016; Maggioli et al., 2018; Wen et al., 2022), few neutralizing epitopes have been identified. Thus, identifying the epitopes of the SVA capsid protein VP2 has potential application value for analyzing the function and antigenicity of the VP2 protein.

In prior studies, several B-cell epitopes (BCEs) of SVA VP2 were identified by bioinformatics prediction (Ru et al., 2023; Zhang et al., 2023), overlapping synthesis of polypeptides (Ma et al., 2022) and monoclonal antibodies (mAbs) (Fan et al., 2020; Wen et al., 2022). It has been confirmed that ^{153}QELNEE^{158} is a conserved antigenic epitope of the VP2 protein and has virus-neutralizing activity (Wen et al., 2022). The most common antigenic epitopes in the VP2 protein secondary structure are random coils, which include the EF loop (the "puff" structure) (Jayawardena et al., 2018), and the residues D166-G179, T180, and Y182-W187 in the SVA VP2 EF loop can recognize the cell receptor ANTXR1 (Miles et al., 2017; Cao et al., 2018). Neutralizing antibodies can block SVA infection, however, whether the receptor binding region on the VP2 EF loop contains the neutralizing BCEs of SVA has not been determined. In addition, Ma et al. (2022) identified highly conserved epitope peptides located at the C-terminus of VP2, the key amino acids not precisely defined in the present study.

In this study, we obtained three mAbs against the recombinant SVA VP2 protein and characterized the antigenic epitopes with a series of synthetic peptides and truncated proteins. The mAb 1B8 was bound at ^{177}SLGTYYR^{183}, and 2C7 was bound at ^{266}SPYFNGL^{272} of VP2; the former is a novel epitope involved in the "puff" loop, while the latter corresponds to the carboxyl terminus of VP2. These two novel epitopes were identified for the first time by monoclonal antibodies. As vaccines currently remain the most effective methods for preventing SVA infection, characterization of SVA BCEs will provide novel insights into the development of diagnostic tools and the generation of a vaccine that enables the differentiation of infected individuals from vaccinated animals (DIVA).

2 Materials and methods

2.1 Cells, viruses, and plasmids

Baby hamster kidney fibroblast (BHK) 21 cells, the myeloma cell line SP2/0 and human embryonic kidney 293T cells were maintained in Dulbecco's modified Eagle's medium (DMEM; Gibco, USA) supplemented with 10% fetal bovine serum (FBS; Gibco, USA) at 37°C and 5% CO_2 in a humidified atmosphere. The Senecavirus A strain (ZS) and the EGFP-expressing recombinant SVA used in this study were preserved at the Harbin Veterinary Research Institute (CAAS) (Jia et al., 2022). For SVA propagation, BHK-21 cells were infected with SVA at a multiplicity of infection (MOI) of 0.01 in DMEM and incubated at 37°C and 5% CO_2 in a humidified atmosphere. When the cytopathic effect reached 80%, the cell supernatant was collected after being frozen and thawed 3 times. The SVA stocks were kept at −80°C. The pET-28a (+)-SUMO and pCAGGS-HA expression vectors were preserved in our laboratory. The full-length infectious cDNA clone pSVA16 was constructed previously (Li et al., 2019).

2.2 Expression and purification of the recombinant VP2 protein

Full-length SVA-VP2 was amplified, cloned and inserted into the pET-28a (+) expression vector to prepare purified SVA-VP2 proteins as an immunogen. For purification and protein solubility purposes, recombinant VP2 proteins were induced with 6 × His and SUMO tags. The pET28a-SUMO-VP2 recombinant plasmid was transformed into *E. coli* BL21 (DE3) competent cells. When the OD600 reached 0.6, the protein expression was induced by 0.1 mmol/L IPTG for 18 h at 16°C. The bacterial cells were harvested by centrifugation at 8,000 × g for 10 min and resuspended in PBS. Then, sonication was performed with an ultrasonic cell disruptor (Cole Parmer, Vernon Hills, IL, USA). Thereafter, the recombinant VP2 protein was analyzed via SDS–PAGE. The soluble recombinant VP2 protein was purified, primarily by nickel affinity chromatography and precisely by a size-exclusion chromatographic column in an automated system (AKTA, GE-Healthcare Life Sciences, USA). The concentration of purified protein was measured by a BCA protein concentration determination kit (Thermo Fisher Scientific, USA), and the proteins were stored at −80°C.

2.3 SVA purification

SVA particles were purified according to methods adapted from previously published protocols (Reddy et al., 2007; Jayawardena et al., 2018; Strauss et al., 2018). Briefly, SVA-infected BHK-21 cells were harvested for virus purification when a complete cytopathic effect was observed. After three freeze–thawing steps, the cell lysate was centrifuged at 8,000 rpm for 30 min at 4°C to remove cellular debris. Subsequently, the supernatant was transferred to 70 mL polypropylene centrifuge tubes (catalog no. 355622; Beckman Coulter) and centrifuged at 80,000 × g for 3 h in a Beckman Coulter SW 45 Ti rotor at 4°C. The virus pellet was resuspended in 1 ml of cesium chloride (CsCl) buffer (20 mM Tris-HCl, 1 mM EDTA, pH 7.8). For purification, the virus was isolated by CsCl gradient ultracentrifugation. The suspended virus was loaded on top of a CsCl gradient (concentration from top to bottom: 1 mL, 1.30 g/mL; 10 mL, 1.33 g/mL; and 1 mL, 1.40 g/mL) prepared in a 13.2 mL open-top polypropylene tube (catalog no. 331372; Beckman Coulter) and centrifuged at 61,580 × g for 18 h in a Beckman Coulter SW 41 Ti rotor at 22°C. The virus band was slowly collected for further identification via SDS–PAGE and TEM. The concentration was measured using spectrophotometry, and small aliquots of the virus were stored in sterile tubes at −80°C.

2.4 Generation of monoclonal antibodies

The animal experiments were approved by the Animal Care and Ethics Committees of Harbin Veterinary Research Institute, Chinese Academy of Agricultural Sciences. The methods were conducted in accordance with the approved animal ethics guidelines (number 210119-02). Six-week-old specific pathogen-free (SPF) female BALB/c mice were obtained from Beijing Weitong Lihua Laboratory Animal Technology. The purified recombinant VP2 protein was used as an immunogen emulsified with equal volumes of the adjuvant Montanide ISA-201 (SEPPIC, France). Mice were immunized with 50 μg of emulsified VP2 proteins three times on Days 0, 14, and 28 by intramuscular injection in the inner thigh. One week after the third vaccination, serum samples were collected, and antibody titers were detected via indirect ELISA. When the antibody titer reached more than 1:10,000, the mice were intraperitoneally injected with recombinant VP2 protein.

On the 3rd day after booster vaccination, the mice were humanely euthanized, and the spleen was aseptically extracted for spleen lymphocyte isolation. Splenocytes were fused with SP2/0 cells by 50% (w/v) PEG4000 (Sigma–Aldrich) according to the standard procedure (Galfrè and Milstein, 1981). The fused cells were cultured in medium containing HAT (Sigma–Aldrich) selection medium for 1 week, after which the medium was changed to HT medium until the 10th day. The supernatants of the hybridomas were screened by an indirect ELISA on a purified SVA precoated microplate. Positive hybridomas were subcloned at least three times by a limited dilution method to obtain a single hybridoma cell line. Ascites fluid was produced by intraperitoneal injection of positive hybridoma cells (10^5-10^6 cells/mouse) in liquid paraffin pre-treated BALB/c mice, and purified by Protein G affinity column (GenScript, Nanjing, China).

2.5 Enzyme-linked immunosorbent assay

Recombinant VP2 protein, purified virions and synthetic peptides were precoated onto microplates for indirect ELISA to determine the reactivity and epitopes of the monoclonal antibodies. Briefly, a 96-well ELISA plate was coated with 100 ng of the above antigen at 4°C overnight and then blocked with 5% (w/v) skim milk in PBS at 37°C for 2 h. A total of 100 μL of the hybridoma cell supernatant was added to each well and incubated at 37°C for 1 h. After washing with PBST, an HRP-conjugated goat anti-mouse IgG antibody (diluted 1:10,000 in PBST) was added to each well and incubated at 37°C for 1 h. The plates were washed with PBST before adding TMB Chromogen Solution (Abcam) as an enzyme substrate, and 2 M HCl was used to terminate the reaction. After color development, the optical density (OD) was measured by a microplate reader (Bio-Rad) at 450 nm. Furthermore, the antibody isotype was analyzed by the Antibody Isotyping Assay Kit (Proteintech, USA).

2.6 Indirect immunofluorescence assay

BHK-21 cells that reached 100% confluence were infected with EGFP-SVA at an MOI of 0.1 for 24 h. Then, the cells were washed with PBS, fixed with 3.7% paraformaldehyde for 20 min and permeabilized with 0.1% Triton X-100 for 20 min at room temperature. After blocking with 2% BSA for 1 h, the cells were incubated with 100 μL of hybridoma cell supernatant for 1 h. After washing three times with PBS, 100 μL of Alexa Fluor 568 dye-conjugated goat anti-mouse IgG (H + L) (red) at a dilution of 1:1,000 was added to each well for 1 h at room temperature. Finally, the cell nuclei were stained with 4′,6-diamino-2-phenylindole (DAPI; Sigma) after washing three times with PBST. The samples were then observed with a fluorescence microscope (EVOS F1, AMG, USA).

2.7 Western blot

The recombinant VP2 protein, vector protein, SVA and cell control were separated via 12% SDS–PAGE and subsequently transferred onto a PVDF membrane (Millipore, MA, USA). After blocking with 5% skim milk powder at 37°C for 2 h, the hybridoma cell supernatant was incubated with the primary antibody at 37°C for 1 h, after which the cells were washed thrice with PBST. HRP-conjugated goat anti-mouse IgG (Proteintech Group, China, 1:10,000 dilution) was added and incubated at 37°C for 1 h. After the wash step, the membranes were scanned on a near-infrared fluorescence scanning imaging system (Odyssey CLX, USA).

2.8 B-cell epitope identification via peptide mapping

To locate the recognition epitopes of the mAbs, a total of 28 overlapping peptides of the VP2 protein were manufactured by the Suzhou Epitope (Suzhou, China). There were 20 amino acids in length that overlapped each other by 10 amino acids, except for the final peptide, which was 14 amino acids in length. The short peptides were precoated (100 ng/well) in 96-well microplates, and the hybridoma cell supernatants were added as primary antibodies to test the binding activity via indirect ELISA as described above. Upon the identification of bound peptides, the peptides were further truncated into a series of peptides, which were subsequently cloned and inserted into the pCAGGS vector and expressed as HA-peptide-fused proteins in the eukaryotic expression system. Recombinant truncated proteins were expressed in HEK-293T cells and analyzed by Western blotting.

2.9 Alanine scanning

To determine which residues are crucial for mAb binding, a series of alanine mutations were generated in the indicated HA-tag fusion epitopes. The amino acids in the epitope were substituted with alanine. Therefore, 14 alanine mutants of the two epitopes were constructed. The point mutant proteins were expressed in HEK-293T cells, and the cell lysates were collected at 24 h post transfection and analyzed via Western blotting.

2.10 Generation of recombinant viruses

To further identify the amino acids that are critical for mAb 1B8 binding in virions, the infectious clone pSVA16 was used as a template for site-directed mutagenesis, and seven recombinant plasmids were constructed (pSVA-S177R, pSVA-L178A, pSVA-G179A, pSVA-T180A, pSVA-Y181A, pSVA-Y182A, and pSVA-R183A). BHK-21 cells seeded in 6-well plates were transfected with plasmids harboring pSVA16 or SVA mutants to rescue the recombinant viruses. Transfection was conducted using Lipofectamine^{TM} 3000 reagent following the manufacturer's instructions (Life Technologies, NY, USA). The cytopathic effect (CPE) was monitored daily after infection, and mutant viruses were harvested when significant CPE was observed. The recovered viruses were passaged ten times in BHK-21 cells, and the stability of the introduced mutations was confirmed by sequencing the VP2 coding region. The binding activity of the mAbs to the recombinant viruses was analyzed by IFA and Western blotting. The SVA VP1 mAb was preserved in our laboratory.

2.11 Biological information analysis

A total of thirty representative SVA strains were collected from the NCBI database for sequence comparison. The epitopes identified by the 1B8 and 2C7 mAbs were compared using BioEdit software to clarify the conserved characteristics of the epitopes among the different SVA strains. Subsequently, the SVA-VP2 amino acid sequence was submitted to the SWISS online system to predict its structural models through template searching and modeling. PyMOL software was used to construct the SVA VP2 three-dimensional (3D) structural model.

3 Results

3.1 Purification of the SVA recombinant VP2 protein and SVA virions

The SUMO-fusion recombinant VP2 protein (reVP2) cloned and inserted into the pET-28a (+) vector was successfully expressed in *E. coli* BL21 (DE3). The reVP2 protein was purified by Ni^{2+} column affinity chromatography and size-exclusion column (SEC) electrophoresis and analyzed via SDS–PAGE (Figure 1A). The molecular weight of the reVP2 protein was 55 kDa, which was consistent with the predicted recombinant protein size, and the purified reVP2 protein was detected as a single band by SDS–PAGE at a final concentration of 0.5 mg/mL. In addition, Western blot analysis was performed using SVA-positive pig sera, and the results confirmed that reVP2 could be specifically recognized by SVA antiserum, which indicated that the reVP2 protein had good reactivity with the antibody (Figure 1B). To screen for monoclonal antibodies that recognize the virus well, SVA virions were purified via CsCl gradients by ultrahigh-speed centrifugation, and the purified SVA virions were confirmed via SDS–PAGE (Figure 1C) and TEM (Figure 1D). Three specific bands were observed for high-purity virus particles by SDS–PAGE, and the protein sizes were ~39, 37, and 34 kDa, which are consistent with the known sizes of the SVA VP2, VP1, and VP3 proteins. In addition, the purified SVA was analyzed by a nanoparticle size analyzer, and the virus particles were ~ 30 nm in diameter (Figure 1E).

3.2 Characterization of mAbs against the VP2 protein

Three monoclonal antibodies against VP2 were obtained, namely, 2E4, 1B8, and 2C7. All the mAbs exhibited similar binding activity to the reVP2 protein (Figure 2A), while 2C7 exhibited increased binding activity to SVA particles (Figure 2B). In addition, the heavy-chain and light-chain isotypes of all the mAbs were IgG1 and kappa (Table 1). Western blot analysis confirmed that the three mAbs strongly reacted with the denatured reVP2 protein and SVA-infected BHK-21 cell lysates (Figure 2C). Because precursor VP0 was cleaved into VP2 and VP4 proteins to assemble into full capsids, the VP0 protein is also recognized by antibodies in cell lysates. These results suggested that these mAbs recognized mainly linear epitopes on the capsid protein VP2 of SVA. Furthermore, to confirm the specificity of the three mAbs, IFA was carried out. Briefly, EGFP-SVA-infected BHK-21 cells were incubated with the primary antibodies 2E4, 1B8, and 2C7. The results demonstrated that SVA-infected cells (green) were recognized by 2E4, 1B8, and 2C7 (red), and specific red fluorescence signals were localized to cells expressing green fluorescence, but no red fluorescence was detected in the negative control (Figure 2D). Furthermore, the

10.3389/fmicb.2024.1387309

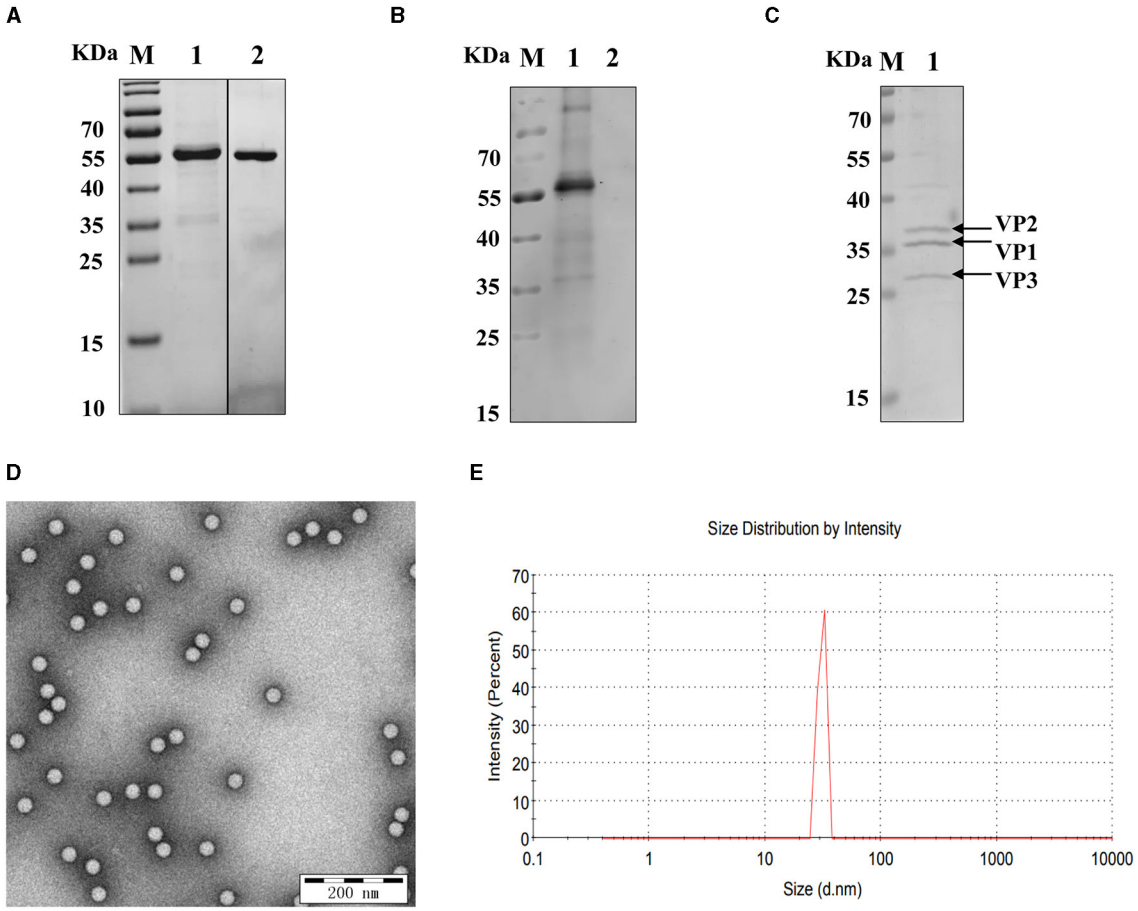

FIGURE 1
Identification of recombinant VP2 protein and SVA virions. **(A)** The purity of the SVA VP2 protein was analyzed by SDS–PAGE and visualized by Coomassie blue staining. M: protein marker; 1: reVP2 purified by Ni^{2+} column affinity chromatography; 2: reVP2 purified by size-exclusion chromatography (SEC). **(B)** Western blot analysis of the reactivity of the reVP2 protein with SVA-positive serum. 1: reVP2 protein; 2: pET-28a-SUMO protein. The purification of SVA virions was analyzed using SDS–PAGE and TEM. **(C)** SDS–PAGE. 1: Purification of SVA. **(D)** TEM image of SVA virions (×33,000), bar: 200 nm. **(E)** SVA particle size analysis via a nanoparticle size analyzer.

ascites fluid was purified by Protein G affinity column and identified by SDS-PAGE. The results showed heavy and light chains were detected in the purified ascitic fluid of all three antibodies, and the heavy chain was 55 kDa and the light chain was about 23 kDa (Figure 2E).

3.3 Epitope mapping recognized by the mAbs

To preliminarily screen the linear epitopes recognized by the three mAbs, 28 synthetic peptides (Table 2), each of which is an 20-mer with 10 overlapping residues at the ends that span the entire VP2 region, was used to screen the binding activity of the mAbs. The results demonstrated that the three mAbs recognized three different epitope peptides of VP2. 2E4 strongly bound to peptide 15 (^{141}LDVRPDGKAKSLEELNEEQW^{160}) (Figure 3A). The mAb 1B8 exhibited increased binding activity to peptide 18 (^{171}KNMPFQSLGTYYRPPNWTWG^{190}) (Figure 3B). In addition, 2C7 strongly responded to peptide 27 (^{261}SVRPTSPYFNGLRNRFTTGT^{280}) (Figure 3C).

The epitope located at peptide 15 ^{141}LDVRPDGKAKSLEELNEEQW^{160} has been reported to be a crucial neutralizing epitope (Wen et al., 2022), but mAb 2E4 showed no neutralizing activity against SVA (data not shown). Although, mAb 1B8 and 2C7 also had no neutralizing activity, the epitopes contained in peptides 18 and 27 recognized by these two mAbs have not yet been identified. Hence, we focused on precisely identifying the corresponding core epitopes of mAbs 1B8 and 2C7. The complete SVA VP2 gene was cloned and inserted into a eukaryotic expression vector with an HA tag as a template and a positive control for truncated peptides. A series of truncated peptides were transfected into HEK-293T cells, and the HA-fusion truncated peptides were identified via Western blotting.

To precisely identify the core sequence recognized by the mAb 1B8, the VP2 protein was sequentially truncated at the position of peptide 18 from the N-terminus and C-terminus. The length and position of these truncated fragments in VP2 were shown in Figure 4A. A total of 13 truncated fragments

10.3389/fmicb.2024.1387309

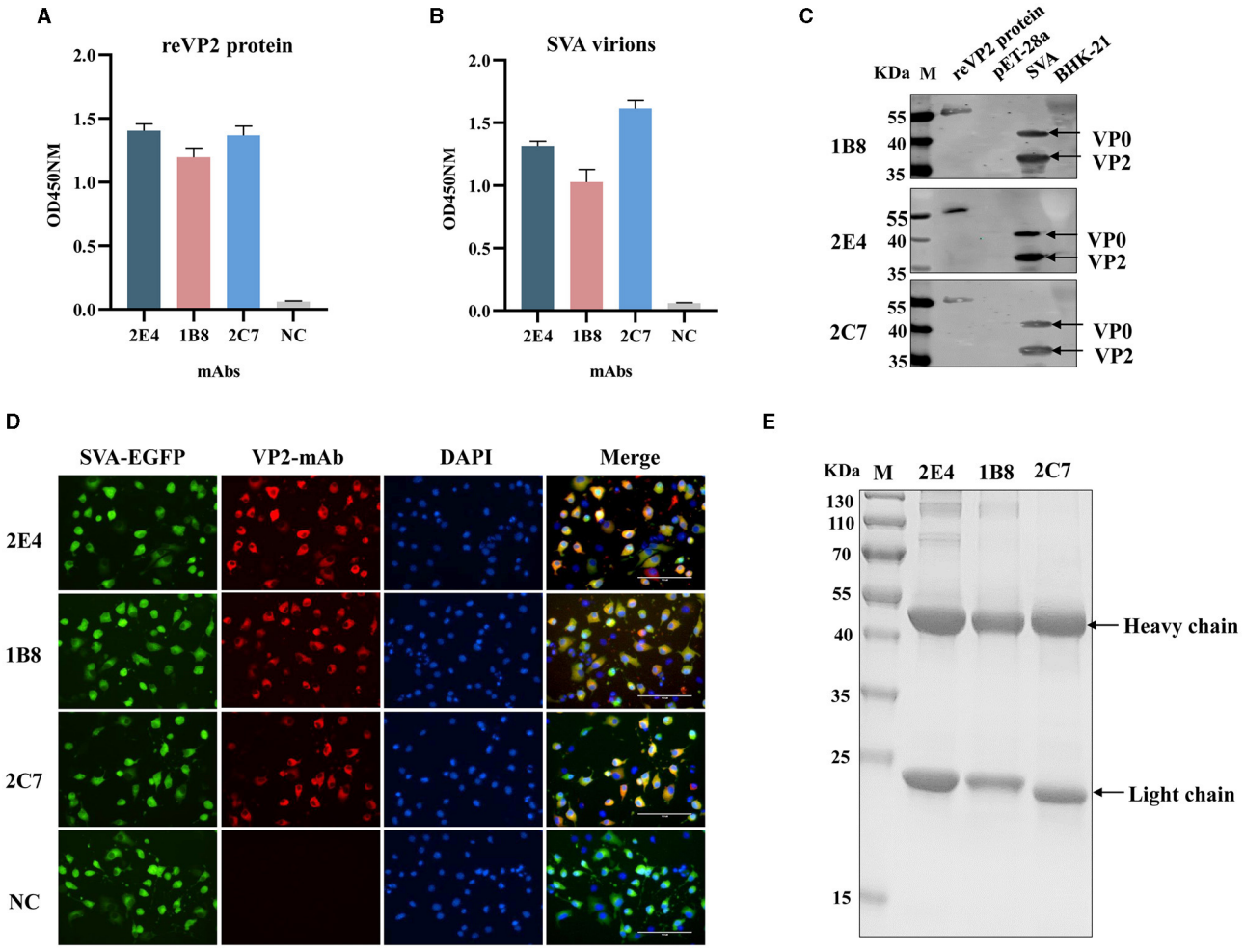

FIGURE 2
Functional analysis of monoclonal antibodies. The 2E4, 1B8, and 2C7 mAbs were used as primary antibodies in an indirect ELISA to test the reactivity with **(A)** the reVP2 protein and **(B)** the virus. NC: Negative control and SP2/0 cell supernatants were used as primary antibodies. All the experiments were repeated three times, and the error bars represent the standard deviation (SD). **(C)** The cell lysates of SVA-infected BHK-21 cells and reVP2 protein were collected for Western blotting, and the cell lysates of mock-infected BHK-21 cells and *E. coli* BL21 were used as control groups. **(D)** BHK-21 cells were infected with SVA-EGFP for 12 h. Then, the cells were fixed and incubated with the mAbs 2E4, 1B8, and 2C7 or with the supernatants of the SP2/0 cells as primary antibodies. NC: the supernatants of the SP2/0 cells. **(E)** SDS-PAGE analysis of purification of ascitic fluid produced by mAbs 2E4, 1B8, and 2C7. The two bands indicate heavy chain (55 KDa) and light chain (23 KDa) respectively.

TABLE 1 The results of monoclonal antibody isotype ELISA.

OD450	IgG 1	IgG 2a	IgG 2b	IgG 3	IgM	IgA	Kappa	Lambda
2E4	1.784	0.133	0.073	0.105	0.099	0.227	0.966	0.068
1B8	1.574	0.084	0.081	0.083	0.095	0.089	0.892	0.058
2C7	2.084	0.092	0.083	0.108	0.103	0.095	1.089	0.066

based on peptide 18 were used to investigate the binding activity to 1B8. For peptide 18, N-truncated fragments bind mAb 1B8 effectively until residue Ser^{177} is removed (P18-5), and C-truncated fragments of peptide 18 bind 1B8 strongly until residue Arg^{183} is removed (P18-8) (Figure 4B). These results indicated that the peptide ^{177}SLGTYYR^{183} was the minimal residue for binding to mAb 1B8.

To map the core sequence recognized by the mAb 2C7, 10 truncated fragments were used to determine the binding activity. Because the peptide 27 was located at the VP2 protein's C-terminus, the N-terminus of peptide 27 was subsequently truncated from full-length VP2 protein (Figure 4C). Deletion of Ser^{266} led to a decrease in the immunoreactivity of the N-truncated fragment P27-3 compared with that of P27-2 (Figure 4D). Moreover, the mAb 2C7 effectively recognized the C-truncated fragments until Leu^{272} was removed (P27-6). The results indicated that the minimal residue recognized by mAb 2C7 was ^{266}SPYFNGL^{272}.

10.3389/fmicb.2024.1387309

TABLE 2 List of synthetic peptides of VP2.

Peptide name	Position	Sequences
VP2-1	1–20	DHNTEEMENSADRVITQTAG
VP2-2	11–30	ADRVITQTAGNTAINTQSSL
VP2-3	21–40	NTAINTTQSSLGVLCAYVEDP
VP2-4	31–50	GVLCAYVEDPTKSDPPSSST
VP2-5	41–60	TKSDPPSSSTDQPTTTFTAI
VP2-6	51–70	DQPTTTFTAIDRWYTGRLNS
VP2-7	61–80	DRWYTGRLNSWTKAVKTFSF
VP2-8	71–90	WTKAVKTFSFQAVPLPGAFL
VP2-9	81–100	QAVPLPGAFLSRQGGLNGGA
VP2-10	91–110	SRQGGLNGGAFTATLHRHFL
VP2-11	101–120	FTATLHRHFLMKCGWQVQVQ
VP2-12	111–130	MKCGWQVQVQCNLTQFHQGA
VP2-13	121–140	CNLTQFHQGALLVAMVPETT
VP2-14	131–150	LLVAMVPETTLDVRPDGKAK
VP2-15	141–160	LDVRPDGKAKSLEELNEEQW
VP2-16	151–170	SLEELNEEQWVEMSDDYRTG
VP2-17	161–180	VEMSDDYRTGKNMPFQSLGT
VP2-18	171–190	KNMPFQSLGTYYRPPNWTWG
VP2-19	181–200	YYRPPNWTWGPNFINPYQVT
VP2-20	191–210	PNFINPYQVTVFPHQILNAR
VP2-21	201–220	VFPHQILNARTSTSVDISVP
VP2-22	211–230	TSTSVDISVPYIGETPTQSS
VP2-23	221–240	YIGETPTQSSETQNSWTLLV
VP2-24	231–250	ETQNSWTLLVMVLVPLVPLDYKE
VP2-25	241–260	MVLVPLVPLDYKEGATTDPEITF
VP2-26	251–270	GATTDPEITFSVRPTSPYFN
VP2-27	261–280	SVRPTSPYFNGLRNRFTTGT
VP2-28	271–290	GLRNRFTTGTDEEQ

3.4 Critical residues of the linear epitopes responsible for mAb binding

Next, the critical residues in these two novel epitopes responsible for mAb binding were analyzed. Single alanine substitution scanning of the HA-fused VP2 protein was carried out, and the protein was identified via Western blotting. The mAb 2C7-recognized epitope (^{266}SPYFNGL^{272}) was subjected to continuous alanine mutation to construct alanine mutants. The results confirmed that the protein contains a discontinuous key amino acid. The Ser^{266}, Asn^{270}, and Gly^{271} mutants reacted strongly with the mAb 2C7, and the Pro^{267} mutant reacted relatively weakly with 2C7 (Figure 5A). However, the mutants Tyr^{268}, Phe^{269}, and Leu^{272} were unable to bind to the mAb 2C7. These results indicate that the residues Tyr^{268}, Phe^{269}, and Leu^{272} are critical amino acids for recognition of the VP2 protein by mAb 2C7.

However, the ^{177}SLGTYYR^{183} epitope contains a continuous key amino acid, and the residues from Ser^{177} to Arg^{183} with alanine substitution strongly affect the reactivity of the VP2 epitope recognized by 1B8 but not by the anti-HA antibody (Figure 5B), indicating that all the residues are necessary for the binding of VP2 to mAb 1B8. These results indicate that ^{177}SLGTYYR^{183} may be a potential epitope for the development of a marker vaccine. Therefore, the reactivity of point mutant viruses located at the VP2 ^{177}SLGTYYR^{183} epitope with the mAb 1B8 was further analyzed. We successfully rescued five mutant viruses (S177R, L178A, T180A, Y182A, and R183A), but substituting arginine or alanine at residues 179 and 181 failed to afford the mutant virus, which indicates that residues Gly^{179} and Arg^{181} of VP2 are crucial for the replication of SVA. By Western blotting, we found that mAb 1B8 strongly binds to SVA-WT and much weakly binds to the T180A and R183A mutants. No binding of the mAb 1B8 to the S177R, L178A, or Y182A mutant was detected (Figure 5C). However, the expression of the VP1 protein in both SVA-WT and SVA-mutant-infected cells was detected. In comparison, the mAb 2C7 strongly reacted to the mutant viruses and SVA-WT, while the mAb 1B8 exhibited notably lower reactivity to the mutant viruses than did SVA-WT. The Y182A mutation in particular completely abrogated the ability of the mAb 1B8 to bind to the virus (Figure 5D), which suggested that the Tyr^{182} residue is involved in the interaction between SVA and the mAb 1B8. Our results suggest that the combination of the Ser^{177}, Leu^{178}, and Tyr^{182} residues may be an ideal mutation site for the generation of epitope-based SVA marker vaccines.

3.5 The identified epitopes are highly conserved in SVA VP2 proteins

In addition to the amino acid sequence, the antigenicity of the epitope is related to the spatial structure of the epitope. The structural homology model of the VP2 protein was constructed by SWISS, and the one with the highest confidence (PBD:3CJI) was selected for subsequent analysis. The spatial structure was displayed with PyMoL software. The epitope ^{177}SLGTYYR^{183} (marked in pink) formed a random coil (Figure 6A) that was fully exposed on the surface of the VP2 protein (Figure 6B). In addition, this epitope is located at the interface area of the ANTXR1-SAV binding site (Jayawardena et al., 2018) and is exposed on the surface of the capsid protomer with VP1, VP2, VP3, and VP4 (Figure 6C). In contrast to the epitope at ^{177}SLGTYYR^{183}, the epitope at ^{266}SPYFNGL^{272} (marked in blue) formed part of a β-sheet (Figure 6A). The surface of the VP2 protein was partially exposed, and the middle region was obscured by the amino acid ^{52}QPTTT^{56} (Figure 6B); this feature determines whether the position of the crucial amino acid that binds to the antibody is discontinuous.

To determine the conservation of these two epitopes, the VP2 gene of SVA from China and other countries was collected from GenBank, and the conservation of these epitopes was analyzed via BioEdit software. The epitopes ^{177}SLGTYYR^{183} and ^{266}SPYFNGL^{272} were highly conserved between SVA strains, and they exhibited 100% sequence similarity (Figure 6D). These results

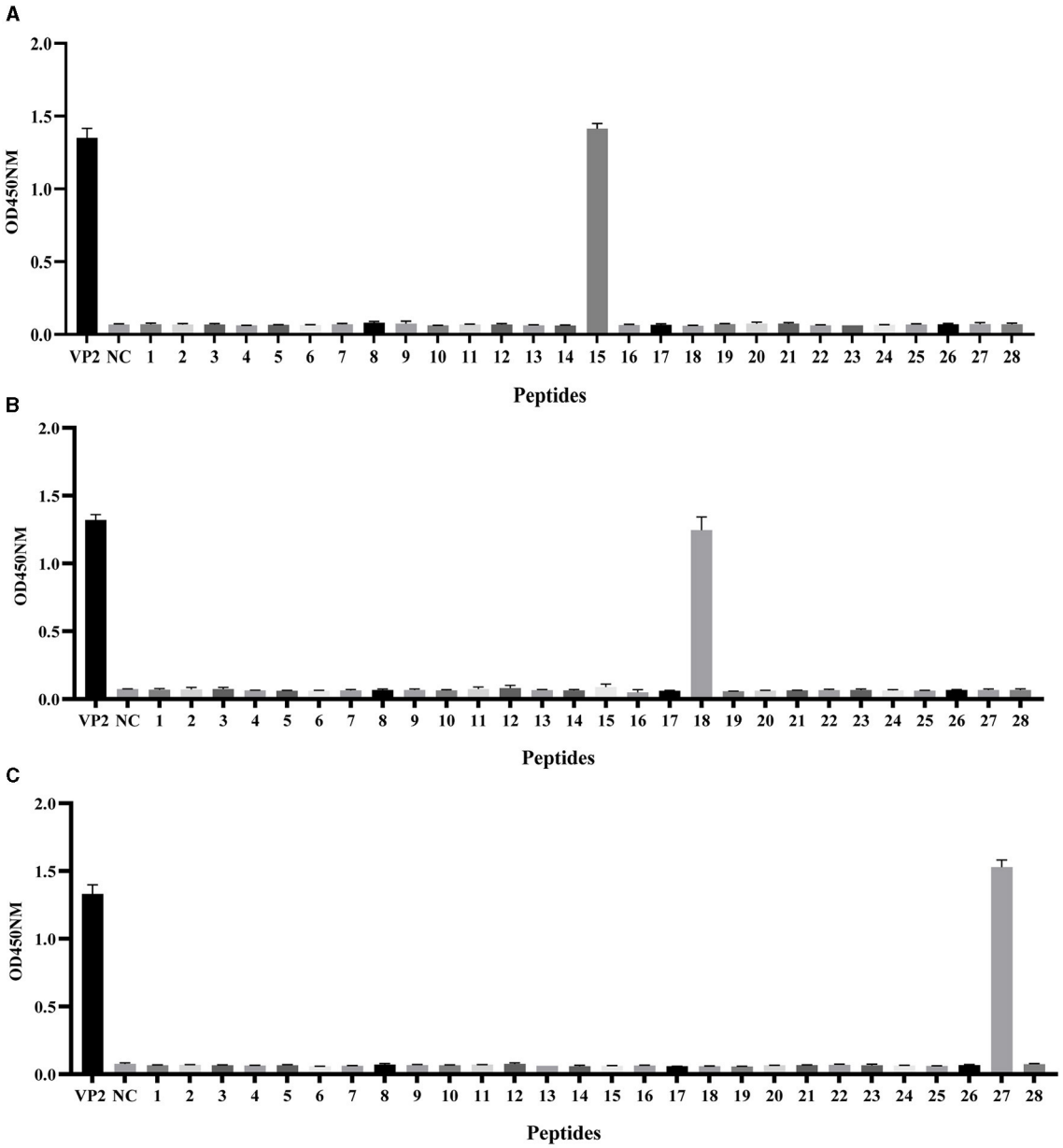

FIGURE 3
Identification of VP2 protein linear epitopes via PepScan. Reaction of the **(A)** mAb 2E4, **(B)** mAb 1B8, and **(C)** mAb 2C7 with 28 synthetic VP2 peptides. All the experiments were repeated three times, and the error bars represent the standard deviation (SD). The NC was an unrelated synthetic peptide.

suggest that these residues are important for maintaining epitope structure or function.

4 Discussion

SVA is prevalent in many countries, and SVA-associated vesicular diseases have caused economic losses to the pig industry. In this study, two novel linear epitopes of VP2 were precisely identified by mAbs. Importantly, we confirmed that the epitope ^{177}SLGTYYR^{183} is located at the VP2 "puff" loop region and contains key residues involved in receptor binding. In addition, the single mutation Y182A abolishes the interaction between the mutant virus and the mAb 1B8. Therefore, our findings could lead to the development of an epitope-based SVA marker vaccine to distinguish infected pigs from vaccinated pigs.

Monoclonal antibodies with high specificity and sensitivity are widely used in the diagnosis and treatment of diseases, such as Alzheimer's disease (AD), have produced encouraging cognitive and clinical results (Qiao et al., 2024). Besides, engineering modifications of mAbs significantly improve their therapeutic properties, which has emerged as a promising strategy to enhance tumor targeting specificity and immune cell interactions (Mathieu et al., 2024). In addition, mAbs are widely applied for the

10.3389/fmicb.2024.1387309

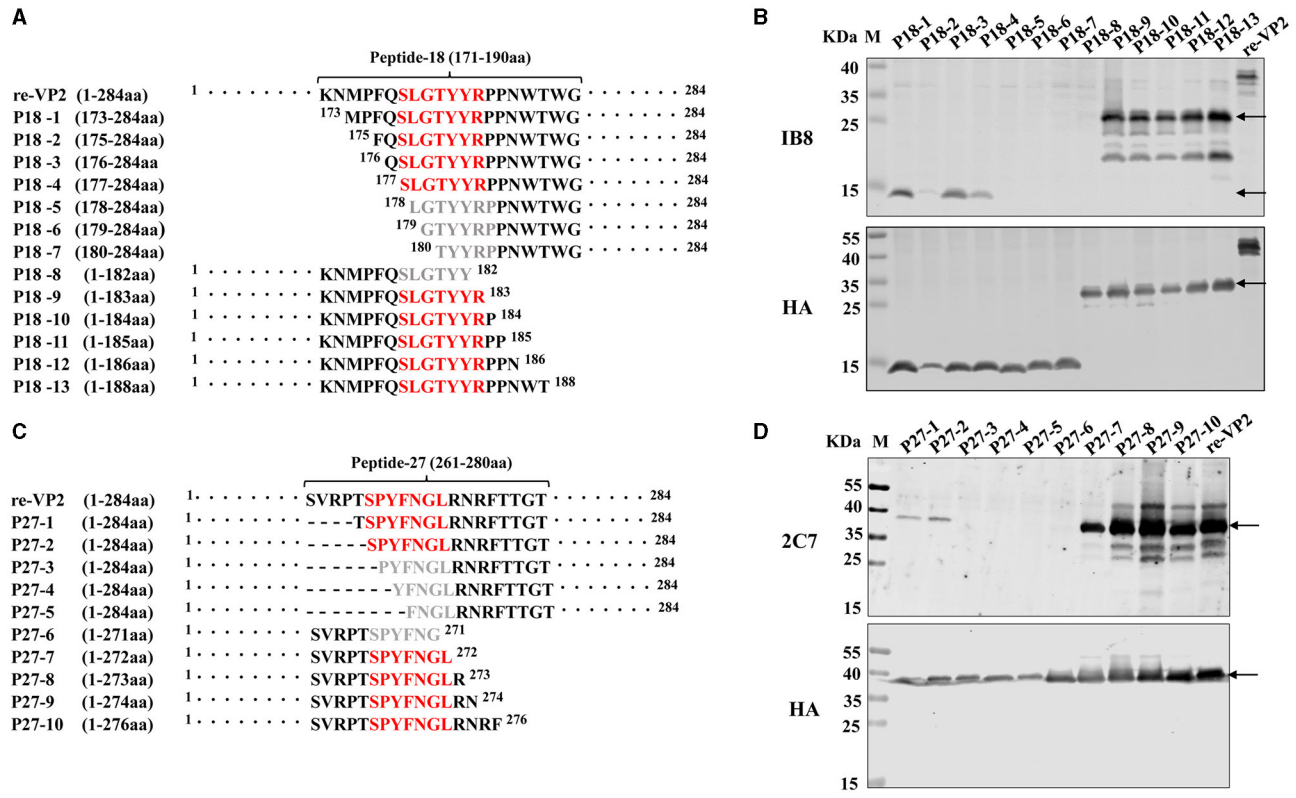

FIGURE 4
Mapping of the B-cell epitope by truncating short peptides. **(A)** Schematic diagram of peptide 18 ([171]KNMPFQSLGTYYRPPNWTWG[190]) used for epitope mapping, "·" represents the abbreviated amino acid. **(B)** HEK-293T cells were transfected with plasmids encoding thirteen truncated fragments for 24 h. The cell lysates were analyzed by Western blotting using an HA antibody and mAb 1B8. **(C)** Schematic diagram of peptide 27 ([261]SVRPTSPYFNGLRNRFTTGT[280]) used for epitope mapping. "·" represents the abbreviated amino acid and "-" represents the deleted amino acid. **(D)** HEK-293T cells were transfected with plasmids encoding five truncated fragments for 24 h. The cell lysates were analyzed by Western blotting using an HA antibody and the mAb 2C7.

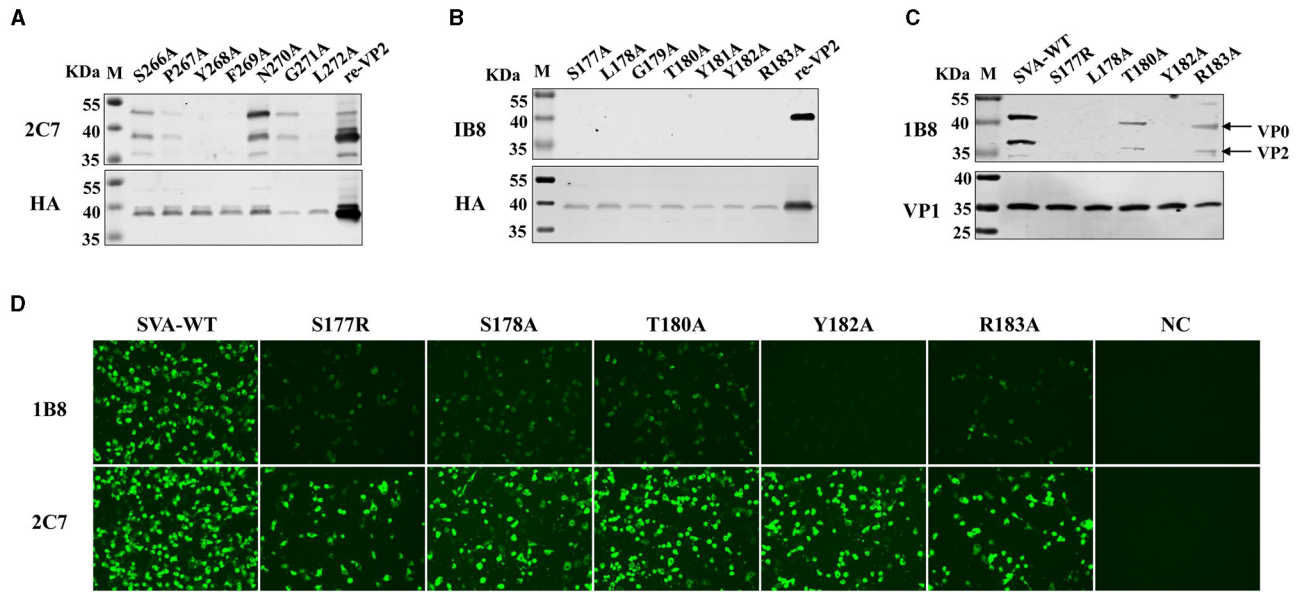

FIGURE 5
Identification of the pivotal points in the epitopes. Single alanine substitution scanning of the HA-fused VP2 protein was carried out, and the proteins were identified via Western blotting. **(A)** Binding ability of the mAb 2C7 to VP2 mutants. **(B)** Binding capacity of the mAb 1B8 to VP2 mutants. **(C, D)** BHK-21 cells were infected with SVA-WT or the SVA mutant virus at an MOI of 0.1 for 24 h, and the reactivity of the mAb 1B8 to the single-site mutation SVA was analyzed by **(C)** Western blotting and **(D)** Immunofluorescence analysis; NC: mock-infected cells.

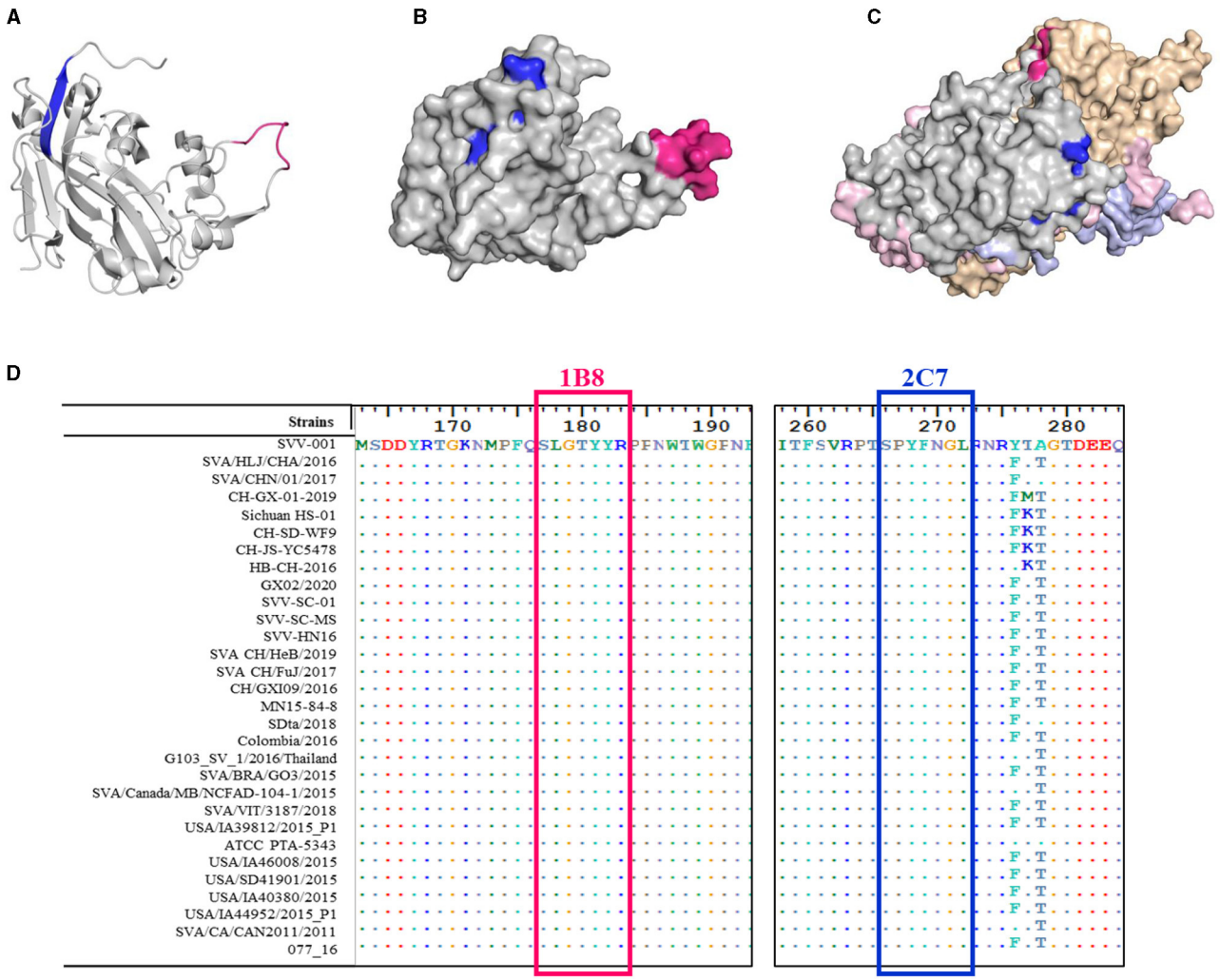

FIGURE 6
Spatial distribution and conservation of the identified epitopes. 3D model of the SVA VP2 protein. The epitope ^{177}SLGTYYR^{183} is marked in red, and the epitope ^{266}SPYFNGL^{272} is marked in blue and drawn as **(A)** a secondary structural analysis of the two epitopes on the VP2 monomer skeleton and **(B)** stereo-structures of the two epitopes in the VP2 protein monomer (gray). **(C)** Stereo-structures of the two epitopes in the capsid protomer with VP1 (light brown), VP3 (pink), and VP4 (purple). **(D)** Amino acid alignment of the VP2 protein was performed for different SVA strains. Only the different residues are shown. The red box indicates the epitope recognized by mAb 1B8, and the blue box indicates the epitope recognized by mAb 2C7.

establishment of immunological detection methods for infectious or non-infectious diseases. At the same time, mAbs as an important tool have been used in identifying antigenic epitopes. The gold standard for epitope definition is X-ray analyses of crystals of antigen-antibody complexes, however, this method requires a high degree of sophistication and expertise. Most other methods rely on monitoring the binding of the antibody to antigen fragments. The epitope identification will benefit to the study of pathogen-host interaction mechanism and the structure and function of target proteins.

To date, several antigenic epitopes of SVA VP2 have been identified through bioinformatics prediction and synthetic polypeptide therapy using mAbs or porcine serum (Fan et al., 2020; Ru et al., 2023; Zhang et al., 2023). The ^{141}LDVRPDGKAKSLEELNEEQW^{160} region is a dominant epitope region with relatively abundant epitopes in the VP2 protein (Fan et al., 2020; Wen et al., 2022; Ru et al., 2023; Zhang et al., 2023). In addition, Wen et al. obtained five neutralizing mAbs by immunizing mice with ultra-purified SVA, and the linear epitope ^{153}QELNEE^{158} recognized them. The amino acid residue Glu^{157} is the pivotal site for neutralizing SVA (Wen et al., 2022). However, Fan et al. (2020), reported that two mAbs generated by recombinant SVA VP2 protein immunization showed high affinity to peptide ^{149}AKSLQELNE^{157}, but did not have neutralizing activity. Similarly, we identified mAb 2E4, which strongly binds to ^{141}LDVRPDGKAKSLEELNEEQW^{160}, showed no neutralizing effects on SVA either. All these suggest that the antigen with conformational epitopes is more likely to induce the production of neutralizing mAb. Nevertheless, the epitope localized in ^{141}LDVRPDGKAKSLEELNEEQW^{160} is an important immunodominant epitope and provides an important detection target for epidemiological investigations.

Importantly, the protruding part of the VP2 "puff" loop responsible for ANTXR1 binding is highly conserved. Based on the structure of the SVA-ANTXR1 complex, ANTXR1 interacts with three major capsid proteins and is centered on the "puff"

loop of VP2 (Miles et al., 2017; Cao et al., 2018). Jayawardena et al. suggested that residues 178–186 contribute to the bulk of receptor interactions, and residues Leu^{178}, Thr^{180}, Tyr^{182} and Pro^{184} on the "puff" loop of VP2 form van der Waals interactions or aromatic interactions with residues on the α4 helix of ANTXR1 (Jayawardena et al., 2018). The ANTXR1 binding site can be recognized by neutralizing mAbs, which suggests that the ANTXR1 binding site on SVA capsids may partially overlap with the epitope of neutralizing antibodies. We identified a linear epitope (^{177}SLGTYYR^{183}) is located at VP2 receptor binding site, and this is the first minimal epitope on the VP2 "puff" loop identified using the mAb 1B8. However, the mAb 1B8 has no neutralizing effect on SVA. Recently, Zhao et al. (2023), confirmed that mAb 2G6 exhibits strong neutralizing activity to SVA, which recognized conformational epitope, and the mAb heavy chains bind to VP2 and knob loop of VP3, respectively. It has been suggested that most conformational epitopes are composed of several linear epitopes (Liu et al., 2017; Ferdous et al., 2019). Therefore, ^{177}SLGTYYR^{183} may constitute a segment with a conformational epitope that induces neutralizing antibody production. Investigating conformational epitopes and neutralizing antibody production in the "puff" loop of VP2 would be highly important for future work. In particular, identifying SVA mutants capable of evading neutralizing effects may benefit oncolytic virotherapy in humans (Zhao et al., 2023).

Furthermore, the C-terminal region of VP2 (^{271}GLRNRFTTGTDEEQ^{284}) was identified as a diagnostic target for testing SVA antibodies in pigs (Ma et al., 2022). In the present study, the minimal epitope ^{266}SPYFNGL^{272} of the C-terminus of VP2 was identified accurately by the mAb 2C7, and two amino acids (Gly^{271} and Leu^{272}) were found overlapping with previous study conducted by Ma et al. Recently, the epitope ^{267}PYFNGLRNRFTTGT^{280} was predicted and identified by bioinformatics-based computational prediction and the Pepscan approach (Ru et al., 2023). However, we found that residue Ser^{266} is important for maintaining the binding of ^{266}SPYFNGL^{272} to mAb 2C7. In addition, ^{266}SPYFNGL^{272} was shown to be partially exposed on the VP2 protein, and the key amino acids analysis revealed that the immunodominant residues are associated with the immunogenicity and reactivity of the epitope. Our results suggest that the epitope ^{266}SPYFNGL^{272} is an important and conserved B-cell immunodominant epitope.

In summary, two novel epitopes of SVA VP2, ^{177}SLGTYYR^{183} and ^{266}SPYFNGL^{272}, were identified using mAbs. Importantly, we found that the epitope ^{177}SLGTYYR^{183} completely exposed on the surface of the VP2 protein, and confirmed that the VP2 "puff" loop region harbors a BCE containing key amino acid residues involved in receptor binding. These results will help to elucidate the antigenic characteristics of VP2 and promote the development of diagnostic tools and DIVA vaccines for SVA.

Data availability statement

The datasets presented in this study can be found in online repositories. The names of the repository/repositories and accession number (s) can be found below: https://www.ncbi.nlm.nih.gov/genbank/, DQ641257.1; KY419132.1; MG765550.1; MT457474.1; MH588717.1; MN882360.1; MN882361.1; KX377924.1; MW117126.1; MH716015.1; MN700930.1; MF893200.1; MZ375462.1; MH490944.1; KY038016.1; KU359211.1; MN433300; KX857728.1; KY368743.1; KR063109.1; KY486156.1; MH704432.1; KU954087.1; KU954086.1; KT757282.1; KT757281.1; KT757280.1; KU954090.1; MT360257.1; MF615504.1.

Ethics statement

The animal study was approved by Animal Care and Ethics Committees of Harbin Veterinary Research Institute, Chinese Academy of Agricultural Sciences. The study was conducted in accordance with the local legislation and institutional requirements.

Author contributions

HZ: Data curation, Formal analysis, Validation, Writing – original draft. MS: Data curation, Validation, Writing – review & editing. SS: Data curation, Formal analysis, Validation, Writing – review & editing. LM: Data curation, Writing – review & editing. WY: Funding acquisition, Validation, Writing – review & editing. LY: Data curation, Methodology, Writing – review & editing. XS: Formal analysis, Writing – review & editing. XL: Data curation, Formal analysis, Writing – review & editing. HW: Formal analysis, Validation, Writing – review & editing. HM: Formal analysis, Project administration, Writing – review & editing. XC: Formal analysis, Validation, Writing – review & editing. Y-DT: Project administration, Supervision, Writing – original draft. TA: Funding acquisition, Project administration, Supervision, Writing – review & editing. FM: Funding acquisition, Supervision, Writing – original draft.

Funding

The author (s) declare that financial support was received for the research, authorship, and/or publication of this article. This study was supported by grants from the National Science Foundation of China (grant number 32002249 to FM), the Heilongjiang Provincial Natural Science Foundation of China (No. LH2023C023 to WY), the National Key Research and Development Program of China (No. 2022YFD1800300 to TA), the Foundation of the National Research Center of Engineering and Technology for Veterinary Biologicals [No. GTKF (23)008 to FM], the Natural Science Foundation of Heilongjiang Province (No. ZD2023C005 to TA), the Key Research and Development Foundation of Heilongjiang Province (No. JD22A023 to TA), and the Innovation Program of the Chinese Academy of Agricultural Sciences (CAAS-CSLPDCP-202301 to TA).

Acknowledgments

TEM analysis was performed by the Electron Microscope Center of the Harbin Veterinary Institute of the Chinese Academy of Agricultural Sciences.

Conflict of interest

FM and MS filed a patent related to this technology.

The remaining authors declare that the research was conducted in the absence of any commercial or financial relationships that could be construed as a potential conflict of interest.

The author (s) declared that they were an editorial board member of Frontiers, at the time of submission. This had no impact on the peer review process and the final decision.

Publisher's note

References

Cao, L., Zhang, R., Liu, T., Sun, Z., Hu, M., Sun, Y., et al. (2018). Seneca Valley virus attachment and uncoating mediated by its receptor anthrax toxin receptor 1. *Proc. Nat. Acad. Sci. U. S. A.* 115, 13087–13092. doi: 10.1073/pnas.1814309115

Dvorak, C. M. T., Akkutay-Yoldar, Z., Stone, S. R., Tousignant, S. J. P., Vannucci, F. A., and Murtaugh, M. P. (2016). An indirect enzyme-linked immunosorbent assay for the identification of antibodies to Senecavirus A in swine. *BMC Vet. Res.* 13, 1–6. doi: 10.1186/s12917-017-0967-x

Fan, H., Zhu, H., Li, S., Shi, M., Zhou, E., Wang, X., et al. (2020). Identification of linear B cell epitopes on VP1 and VP2 proteins of Senecavirus A (SVA) using monoclonal antibodies. *Vet. Microbiol.* 247:108753. doi: 10.1016/j.vetmic.2020.108753

Ferdous, S., Kelm, S., Baker, T. S., Shi, J., and Martin, A. C. R. (2019). B-cell epitopes: discontinuity and conformational analysis. *Mol. Immunol.* 114, 643–650. doi: 10.1016/j.molimm.2019.09.014

Galfrè, G., and Milstein, C. (1981). Preparation of monoclonal antibodies: strategies and procedures. *Methods Enzymol.* 73, 3–46. doi: 10.1016/0076-6879(81)73054-4

Hales, L. M., Knowles, N. J., Reddy, P. S., Xu, L., Hay, C., and Hallenbeck, P. L. (2008). Complete genome sequence analysis of Seneca Valley virus-001, a novel oncolytic picornavirus. *J. Gen. Virol.* 89, 1265–1275. doi: 10.1099/vir.0.83570-0

Houston, E., Temeeyasen, G., and Piñeyro, P. E. (2020). Comprehensive review on immunopathogenesis, diagnostic and epidemiology of Senecavirus A. *Virus Res.* 286:198038. doi: 10.1016/j.virusres.2020.198038

Jayawardena, N., Burga, L. N., Easingwood, R. A., Takizawa, Y., Wolf, M., and Bostina, M. (2018). Structural basis for anthrax toxin receptor 1 recognition by Seneca Valley Virus. *Proc. Natl. Acad. Sci. U. S. A.* 115, E10934–E10940. doi: 10.1073/pnas.1810664115

Jia, M., Sun, M., Tang, Y.-D., Zhang, Y.-Y., Wang, H., Cai, X., et al. (2022). Senecavirus A entry into host cells is dependent on the cholesterol-mediated endocytic pathway. *Front. Vet. Sci.* 9:840655. doi: 10.3389/fvets.2022.840655

Leme, R., Alfieri, A., and Alfieri, A. (2017). Update on senecavirus infection in pigs. *Viruses* 9 :170. doi: 10.3390/v9070170

Leme, R. A., Oliveira, T. E. S., Alcântara, B. K., Headley, S. A., Alfieri, A. F., Yang, M., et al. (2016). Clinical manifestations of Senecavirus A infection in neonatal pigs, Brazil, 2015. *Emerg. Infect. Dis.* 22, 1238–1241. doi: 10.3201/eid2207.151583

Li, C., Wang, H., Shi, J., Yang, D., Zhou, G., Chang, J., et al. (2019). Senecavirus-specific recombination assays reveal the intimate link between polymerase fidelity and RNA recombination. *J. Virol.* 93, e00576-19. doi: 10.1128/JVI.00576-19

Liu, F., Wang, Q., Huang, Y., Wang, N., and Shan, H. (2020). A 5-year review of Senecavirus A in China since its emergence in 2015. *Front. Vet. Sci.* 7 :567792. doi: 10.3389/fvets.2020.567792

Liu, W., Yang, B., Wang, M., Liang, W., Wang, H., Yang, D., et al. (2017). Identification of a conserved conformational epitope in the VP2 protein of foot-and-mouth disease virus. *Arch. Virol.* 162, 1877–1885. doi: 10.1007/s00705-017-3304-6

Ma, Z., Lv, J., Zhang, Z., and Pan, L. (2022). Development of an indirect ELISA using a novel linear epitope at the C-terminal region of the VP2 protein to specifically detect antibodies against Senecavirus A. *Virol. J.* 19:204. doi: 10.1186/s12985-022-01934-8

Maggioli, M. F., Lawson, S., de Lima, M., Joshi, L. R., Faccin, T. C., Bauermann, F. V., et al. (2018). Adaptive immune responses following Senecavirus A infection in pigs. *J. Virol.* 92:e01717. doi: 10.1128/JVI.01717-17

Mathieu, C., Ghosh, S., Draussin, J., Gasser, A., Jacquot, G., Banerjee, M., et al. (2024). Supramolecular heterodimer peptides assembly for nanoparticles functionalization. *Adv. Healthc. Mater.* 5, e2304250. doi: 10.1002/adhm.202304250

Miles, L. A., Burga, L. N., Gardner, E. E., Bostina, M., Poirier, J. T., and Rudin, C. M. (2017). Anthrax toxin receptor 1 is the cellular receptor for Seneca Valley virus. *J. Clin. Investig.* 127, 2957–2967. doi: 10.1172/JCI93472

Paiva, R. C., Moura, C. A., Thomas, P., Haberl, B., Greiner, L., Rademacher, C. J., et al. (2023). Risk factors associated with sow mortality in breeding herds under one production system in the Midwestern United States. *Prev. Vet. Med.* 213:105883. doi: 10.1016/j.prevetmed.2023.105883

Qiao, Y., Gu, J., Yu, M., Chi, Y., and Ma, Y. (2024). Comparative efficacy and safety of monoclonal antibodies for cognitive decline in patients with Alzheimer's disease: a systematic review and network meta-analysis. *CNS Drugs* 38, 169–192. doi: 10.1007/s40263-024-01067-2

Reddy, P. S., Burroughs, K. D., Hales, L. M., Ganesh, S., Jones, B. H., Idamakanti, N., et al. (2007). Seneca Valley Virus, a systemically deliverable oncolytic picornavirus, and the treatment of neuroendocrine cancers. *J. Natl. Cancer Inst.* 99, 1623–1633. doi: 10.1093/jnci/djm198

Ru, Y., Hao, R., Wu, C., Li, Y., Lu, B., Liu, H., et al. (2023). Identification of potential novel B-cell epitopes of capsid protein VP2 in Senecavirus A. *Microbiol. Spectr.* 11, e04472. doi: 10.1128/spectrum.04472-22

Strauss, M., Jayawardena, N., Sun, E., Easingwood, R. A., Burga, L. N., and Bostina, M. (2018). Cryo-electron microscopy structure of Seneca Valley Virus procapsid. *J. Virol.* 92, e01927–e01917. doi: 10.1128/JVI.01927-17

Sun, Y., Cheng, J., Wu, R.-T., Wu, Z.-X., Chen, J.-W., Luo, Y., et al. (2018). Phylogenetic and genome analysis of 17 novel Senecavirus A isolates in Guangdong Province, 2017. *Front. Vet. Sci.* 5:314. doi: 10.3389/fvets.2018.00314

Vannucci, F. A., Linhares, D. C. L., Barcellos, D. E. S. N., Lam, H. C., Collins, J., and Marthaler, D. (2015). Identification and complete genome of Seneca Valley Virus in vesicular fluid and sera of pigs affected with idiopathic vesicular disease, Brazil. *Transbound. Emerg. Dis.* 62, 589–593. doi: 10.1111/tbed.12410

Wang, Q., Meng, H., Ge, D., Shan, H., Geri, L., and Liu, F. (2023). Structural and nonstructural proteins of Senecavirus A: recent research advances, and lessons learned from those of other picornaviruses. *Virology* 585, 155–163. doi: 10.1016/j.virol.2023.06.004

Wen, W., Chen, X., Lv, Q., Chen, H., Qian, P., and Li, X. (2022). Identification of a conserved neutralizing epitope in Seneca Valley virus VP2 protein: new insight for epitope vaccine designment. *Virol. J.* 19:65. doi: 10.1186/s12985-022-01791-5

Wu, Q., Zhao, X., Bai, Y., Sun, B., Xie, Q., and Ma, J. (2017). the first identification and complete genome of Senecavirus A affecting pig with idiopathic vesicular disease in China. *Transbound. Emerg. Dis.* 64, 1633–1640. doi: 10.1111/tbed.12557

Zhang, X., Zhu, Z., Yang, F., Cao, W., Tian, H., Zhang, K., et al. (2018). Review of Seneca Valley Virus: a call for increased surveillance and research. *Front. Microbiol.* 9 :940. doi: 10.3389/fmicb.2018.00940

Zhang, Z., Yao, F., Lv, J., Ding, Y., Liu, X., Zhang, L., et al. (2023). Identification of B-cell epitopes on structural proteins VP1 and VP2 of Senecavirus A and development of a multi-epitope recombinant protein vaccine. *Virology* 582, 48–56. doi: 10.1016/j.virol.2023.03.015

Zhao, Z., Cao, L., Sun, Z., Liu, W., Li, X., Fang, K., et al. (2023). A structure-guided genetic modification strategy: developing Seneca Valley virus therapy against nonsensitive nonsmall cell lung carcinoma. *J. Virol.* 97, e00459–e00423. doi: 10.1128/jvi.00459-23

frontiers | Frontiers in Microbiology

TYPE Original Research
PUBLISHED 25 April 2024
DOI 10.3389/fmicb.2024.1324243

OPEN ACCESS

EDITED BY
Jingqiang Ren,
Wenzhou University, China

REVIEWED BY
Ahmed N. F. Neamat-Allah,
Zagazig University, Egypt
Gamil S. G. Zeedan,
National Research Centre, Egypt

*CORRESPONDENCE
Alimul Islam
✉ alimul.vmh@bau.edu.bd

†These authors have contributed equally to this work and share first authorship

RECEIVED 19 October 2023
ACCEPTED 26 March 2024
PUBLISHED 25 April 2024

CITATION
Uddin MA, Hossain MT, Rahman AKMA, Siddique MP, Kafi MA, Hossain MG, Chakraborty S, Rahman MM, Khasruzzaman AKM, Ward MP and Islam MA (2024) Characterization, histopathology and immunogenicity of the lumpy skin disease virus isolated during 2019–20 in Bangladesh.
Front. Microbiol. 15:1324243.
doi: 10.3389/fmicb.2024.1324243

Characterization, histopathology and immunogenicity of the lumpy skin disease virus isolated during 2019–20 in Bangladesh

Mohammad Asir Uddin[1†], Muhammad Tofazzal Hossain[1†], A. K. M. Anisur Rahman[2], Mahbubul Pratik Siddique[1], Md. Abdul Kafi[1], Md. Golbar Hossain[3], Sourav Chakraborty[1], Mohummad Muklesur Rahman[1], A. K. M. Khasruzzaman[1], Michael P. Ward[4] and Md. Alimul Islam[1*]

[1]Department of Microbiology and Hygiene, Bangladesh Agricultural University, Mymensingh, Bangladesh, [2]Department of Medicine, Bangladesh Agricultural University, Mymensingh, Bangladesh, [3]Department of Veterinary and Animal Sciences, University of Rajshahi, Rajshahi, Bangladesh, [4]Sydney School of Veterinary Science, The University of Sydney, Camden, NSW, Australia

Introduction: Lumpy skin disease (LSD) is a highly contagious vector-borne viral disease of cattle. LSD has emerged in Bangladesh in 2019, causing significant economic losses due to its high morbidity and mortality. This research was designed to isolate, identify, and assess the immunogenicity of LSD virus (LSDV) using nodular tissue samples obtained from affected cattle during the 2019–20 outbreak across nine districts of Bangladesh.

Methods: To determine the presence of LSDV in nodular tissues, we initially used iiPCR and PCR, followed by histopathological examination. 151 were positive via iiPCR and PCR among the 180 collected samples. The PCR positive 151 samples were then inoculated into 10-day-old embryonated chicken eggs via the CAM route to isolate LSDV, confirmed through PCR. Subsequently, partial sequencing and phylogenetic analysis of the P32 gene were performed to determine the origin of the circulating LSDV strain. The immunogenicity of selected LSDV strains was assessed through an ELISA test.

Results: The PCR results revealed a distinct positive band at 192 bp in both the nodular tissue samples and the LSDV isolated from chicken embryo inoculations. Microscopic analysis of the nodular lesions revealed thickening of the epidermis, ballooning degeneration of keratinocytes, and proliferation of follicular epithelia. Additionally, mononuclear infiltration was observed at the demarcation line between infected and healthy tissue, with necrosis of muscular tissues beneath the epidermis. The LSDV isolate from Bangladesh exhibited a close genetic relationship with LSDV strains isolated from neighboring and other regional countries including India, Myanmar, and Mongolia. This observation strongly suggests the possibility of a transboundary spread of the LSD outbreak in Bangladesh during 2019–2020. The results of the immunogenicity test showed that the serum antibody titer remained at a protective level for up to 18 months following secondary immunization with inactivated LSDV antigen. This finding suggests that the inactivated LSDV antigen could be a potential vaccine candidate to protect cattle in Bangladesh against LSDV.

Conclusion: In conclusion, our research successfully isolated, identified, and characterized LSDV in cattle nodular tissues from the 2019–20 outbreak in Bangladesh. Furthermore, it provided insights into the probable origin of the circulating strain and investigated a potential vaccine candidate to protect cattle in the region from LSDV.

KEYWORDS

embryo inoculation, P32 gene, iELISA, phylogenetic analysis, LSDV, iiPCR, PCR

Introduction

Lumpy Skin Disease (LSD) is an important transboundary viral disease of livestock with substantial economic implications. It is caused by the Lumpy Skin Disease Virus (LSDV), which belongs to the genus Capripoxvirus, subfamily Chordopoxvirniae, and family Poxviridae (Uddin et al., 2022). LSD is highly host-specific, primarily affecting cattle (both *Bos indicus* and *B. taurus*), although it can also infect water buffalo (*Bubalus bubalis*) (Yousefi et al., 2017;World Organization for Animal Health, 2023). Notably, LSDV does not infect or spread between sheep and goats (World Organization for Animal Health, 2023). The clinical presentation of LSD varies widely, ranging from asymptomatic illness to fatal outcomes (Carn and Kitching, 1995). Common clinical features of LSD include high fever, loss of appetite, generalized skin nodules, enlarged lymph nodes, sterility, skin erythema, and abortion (Uddin et al., 2022). The severity of the disease can vary depending on factors such as the LSDV strain, cattle breed, sex, age, with lower mortality typically below 2% and variable morbidity that can reach up to 100% (Sprygin et al., 2018; Badhy et al., 2021; Wilhelm and Ward, 2023). In southeast Asia during 2020–21, average estimated morbidity and mortality of 21 and 2.68%, respectively, were estimated (Wilhelm and Ward, 2023).

Originally, LSD was an endemic disease in numerous African countries, and it subsequently expanded from sub-Saharan Africa to the Middle East. It then continued to spread into Europe and Asia (Milovanović et al., 2019). The first reports of LSD outbreaks in Bangladesh and India came in July and August 2019, respectively. These outbreaks further spread to nearly all Central, South, and Southeast Asian countries (Parvin et al., 2022; Uddin et al., 2022). By 2019–20, LSD had reached virtually every district in Bangladesh, emerging as an important disease (Haque and Gofur, 2020; Sarkar et al., 2020; Badhy et al., 2021; Hasib et al., 2021; Khalil et al., 2021; Chouhan et al., 2022; Uddin et al., 2022). This widespread outbreak inflicted substantial financial losses on the livestock industry due to hide damage and a decrease in body mass. LSD has significant economic impact on the livestock industry due to its rapid spread in recent years. Its continued spread poses a global threat, evident in regions such as Africa, the Middle East, and Asia, with Western Europe and Australia now facing imminent risk. Due to its fast-expanding nature the potential for extensive losses in livestock is unavoidable (Akther et al., 2023).

Several methods to detect the LSDV genome are available worldwide, including PCR, real-time PCR, and HRM-based techniques. In Bangladesh, PCR (Giasuddin et al., 2019; Badhy et al., 2021) and real-time PCR (Parvin et al., 2022) have been utilized for the detection and phylogenetic analysis of LSDV. Parvin et al. (2022) also conducted gross and microscopic pathology examinations of skin nodules in affected cattle. However, there have been no studies on LSDV isolation in chicken embryos or cell culture in Bangladesh. A recent technique, insulated isothermal PCR (iiPCR), has been used for the detection of various veterinary viruses (Lung et al., 2016; Zhang et al., 2019; Song et al., 2022). This method induces spontaneous fluid convection in a capillary tube, ensuring efficient denaturation, annealing, and extension of the PCR process (Tsai et al., 2012). iiPCR shows sensitivity equivalent to real-time PCR and provides clear positive or negative results on the device screen after data processing. In this study we isolated LSDV using chicken embryos after initial screening of field samples using iiPCR and PCR. We also conducted pathology and phylogenetic analyses of the embryo-adapted isolate and assessed its antigenicity.

Materials and methods

Sample collection

Clinical signs of the LSD suspected cattle were skin nodules, fever, depression with anorexia, weight loss, reduced milk yield and peripheral lymphadenopathy. A total of 180 skin nodular tissues were collected from cattle suspected to be affected with LSD, all of which were under 2 years of age (see Figure 1). These cattle were located in nine different districts in Bangladesh: Brahmanbaria, Chattogram, Gaibandha, Kishoreganj, Moulvibazar, Naogaon, Narsingdi, Rangpur, and Satkhira. These districts were chosen because LSD outbreaks occurred there during the study period. The sample collection was conducted within 4–30 days of infection during the 2019–20 outbreaks (Table 1; Figure 2). All samples were collected using aseptic techniques, transported with ice carriers and then stored at −80°C for the isolation of LSDV. In addition, 18 skin nodule biopsies, with two samples collected from each of the nine districts, were obtained from the suspected cases. These biopsies were placed in plastic containers containing 10% neutral buffered formalin for subsequent histopathological analysis (Slaoui and Fiette, 2011).

Sample preparation

The nodular tissue samples were homogenized with sea sand using mortar and pestle, and subsequently 20% suspensions were prepared by adding sterile phosphate buffered saline. The suspension was then centrifuged at 3000 rpm for 10 min maintaining a temperature of 4°C (Zinnah et al., 2010). After centrifugation, the supernatant was carefully collected and stored at -20°C. A portion of this supernatant was used for the extraction of LSD viral DNA, while the remainder was treated with antibiotics (penicillin 10,000 IU/mL + streptomycin 10,000 µg/mL) for the propagation of LSD virus in chicken embryo.

LSD viral DNA extraction from nodular tissue, chicken embryo and CAM for screening and detection of LSDV by iiPCR and PCR

The genomic viral DNA was extracted from the collected nodular tissues, chicken embryo and chorioallantoic membrane (CAM) using the DNeasy Blood & Tissue kit (Qiagen, Germany) following the manufacturer's instructions for molecular studies. The elution of DNA

FIGURE 1
LSD affected cattle **(A)** and collection of skin nodular tissues from LSD affected cattle **(B)**.

was carried out using 70 µL of elution buffer, and the extracted DNA was stored at -20°C for subsequent use.

Insulated isothermal PCR (iiPCR)

To detect LSDV nucleic acids, we conducted iiPCR using the PockitTM LSDV reagent set (GeneReach Biotechnology Corp., Taiwan) (Chang et al., 2012; Tsai et al., 2012). In brief, we combined 50 µL of premix buffer with 5 µL of the extracted genomic DNA in an R-tube. After a brief centrifugation using the cubee™ mini-centrifuge (GeneReach Biotechnology Corp., Taiwan), the R-Tube was loaded onto the POCKITTM nucleic acid analyzer. The default program included a step at 50°C for 10 min followed by 95°C for 48 min. Fluorescent signals were collected, and signal-to-noise (S/N) ratios were calculated by dividing signals collected after iiPCR by those collected before iiPCR. The results were then automatically displayed on the screen as "Positive" (+), "Negative" (−), or "Unknown" (?) based on the default S/N thresholds.

PCR

All the nodular tissue from LSD suspected cattle were initially screened for the presence of LSDV genome using the forward primer 5′-TCCGAGCTCTTTCCTGATTTTTCTTACTAT-3′ and reverse primer 5′-TATGGTACCTAAATTATATACGTAAATAAC-3′. These primers amplify a 192-bp fragment of the P32 envelope protein gene (LSDV074). A total volume of 25 µL PCR mixture was prepared consisting of 12.5 µL of master mix (Bio-Rad, United States), 1 µL (10 pmol) of each forward and reverse primers, 5.5 µL of nuclease-free water, and 5 µL of template DNA. The PCR assays were carried out in a thermal cycler (T-1000, Bio-Rad, USA) with the following cycling conditions: an initial cycle at 94°C for 5 min, followed by 35 cycles at 94°C for 1 min, 50°C for 30 s, and 72°C for 1 min. This was then followed by a final cycle at 72°C for 5 min. The PCR products were subsequently analyzed by electrophoresis on a 1.5% agarose gel-containing ethidium bromide (1 µg/mL) in 1x TAE buffer.

Histopathological examination

The nodular skin tissues were fixed in 10% neutral buffered formalin, subjected to dehydration using increasing concentrations of alcohol, cleaned with xylene, and then embedded in paraffin. The paraffin embedded tissues were subsequently sectioned at a thickness of 5 µm and stained with hematoxylin and eosin.

Chicken embryo inoculation

A total of 26 PCR-positive nodular tissue samples, three samples from eight districts and two from another district, were inoculated into 10-day-old embryonated chicken eggs using the chorioallantoic membrane route (Akter et al., 2004; Hossain et al., 2005; Ahamed et al., 2015). In cases in which pock lesions were observed on the chorioallantoic membrane, allantoic fluid, the embryo, and the chorioallantoic membrane were collected and processed. Subsequently, PCR was again performed to confirm the presence of LSDV in the collected samples from dead embryos.

Amplification and sequencing of the RPO30 gene

For one isolate from Brahmanbaria district (embryo-adapted), PCR was carried out using a specific pair of primers: CpRPO30F

10.3389/fmicb.2024.1324243

TABLE 1 The distribution of nodular tissue samples that tested positive for iiPCR and PCR across different geographic areas.

	Districts									Total
	Brahmanbaria	Chattogram	Gaibandha	Kishoreganj	Moulvibazar	Naogaon	Narsingdi	Rangpur	Satkhira	
Samples tested	30	14	5	55	28	2	32	10	4	180
iiPCR and PCR positive	24	11	4	47	23	2	27	9	4	151
Detection frequency (%)	80.0	78.6	80.0	85.5	82.1	100	84.4	90	100	83.88

(forward): 5'-CAGCTGTTTGTTTACATTTGATTTTT-3′ and CpRPO30R (reverse): 5'-TCGTATAGAAACAAGCCTTTAATAGA-3′ (Gelaye et al., 2015; Badhy et al., 2021). The PCR reaction was conducted in a total volume of 25 μL, consisting of 500 nM forward primer, 500 nM reverse primer, 0.2 mM dNTPs, 1 PCR buffer (Qiagen), 2.5 U of Taq Polymerase (Qiagen), and 5 μL of template DNA. The PCR involved initial denaturation at 95°C for 4 min, followed by 40 cycles at 95°C for 30 s, 56°C for 30 s, and 72°C for 45 s, concluding with a final extension at 72°C for 7 min. The PCR products were separated by electrophoresis on a 1.5% agarose gel at 100 V for 60 min and visualized using a Gel Documentation System (Bio-Rad, United States). The PCR amplicons were purified using the Wizard SV Gel and PCR clean-up system kit (Promega) according to the manufacturer's instructions. LGC Genomics (Germany) performed the sequencing of the purified PCR amplicons. Vector NTI 11.5 software (Invitrogen, USA) was used for sequencing data analysis and assembly.

Phylogenetic analysis

The nucleotide sequences were aligned using the Muscle algorithm, and the codon option was applied using MEGA7 (Kumar et al., 2016). Subsequently, TreeAnnotator was utilized to generate the Maximum Clade Credibility (MCC) tree, with a 3% burn-in discarded. The resulting tree, along with its associated meta-data, was visualized using the ggtree package in R (Yu et al., 2017).

Immunogenicity test of the selected LSD virus antigen

The LSDV isolate was propagated in chicken embryos in large quantities. The allantoic fluid, which contained LSDV, was collected and subjected to centrifugation, filtration, and inactivation using 0.3% formalin. The inactivated LSDV was then mixed with montanide MS 130 (SEPPIC, China) for inoculation into experimental cattle. The initial immunization was inoculated into ten cattle at a rate of 1 mL subcutaneously. After 28 days from the first immunization, a booster dose was administered using the same 1 mL dose. In addition, ten cattle were vaccinated once with goat pox vaccine, while another five cattle were used as control subjects. Blood samples were collected for sera at intervals of 1, 2, 9, and 18 months after immunization. The detection of antibodies through ELISA was conducted using the ID Screen® Capripox double antigen Multi-species ELISA kit from ID.Vet® (Grabels, France), following the manufacturer's instructions.

Results

Detection of LSDV in field samples

Of the 180 nodular tissue samples (Table 1), 151 were confirmed positive for LSDV via both iiPCR (Figure 3A) and PCR (Figure 3B). A positive band at 192 bp was consistently observed for all positive cases, indicating the presence of LSDV (Figure 3B). The overall isolation frequency was 83.9%.

Histopathological analysis

Grossly, nodular skin lesions were up to 2–5 cm in diameter and were elevated above the skin surface. Microscopically, the nodular lesions consisted of epidermal thickening, ballooning degeneration of the keratinocytes, and proliferation of follicular epithelia (Figure 4). The degenerated keratinocytes often contained intracytoplasmic eosinophilic inclusion bodies. Additionally, there were mononuclear inflammatory infiltrates observed at the demarcation line between the lesion and the adjacent healthy tissue. Moreover, the muscular tissues situated beneath the epidermis showed signs of necrosis.

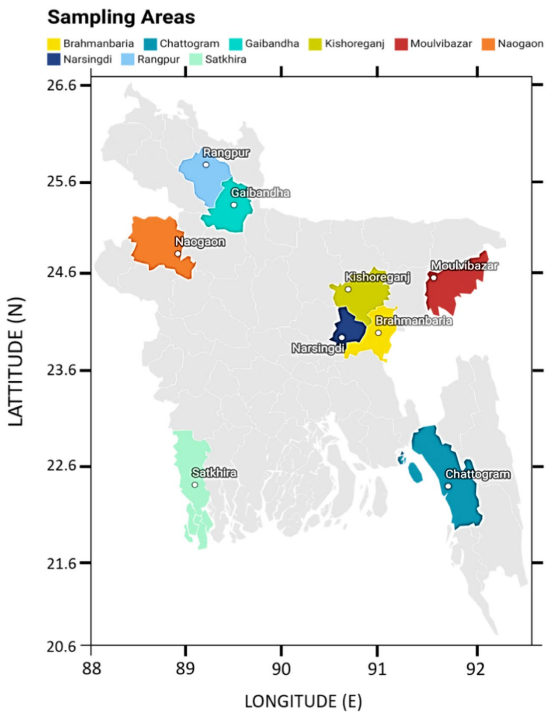

FIGURE 2
Map of Bangladesh showing the sampling areas, Brahmanbaria (24.1585° N, 89.4481° E), Chattogram (22.3350° N, 91.8325° E), Gaibandha (25.3290° N, 89.5415° E), Kishoreganj (24.4331° N, 90.7866° E), Moulvibazar (24.4808° N, 91.7644° E), Naogaon (24.8000° N, 88.9333° E), Narsingdi (23.9167 ° N, 90.7167° E), Rangpur (25.7500° N, 89.2444° E), and Satkhira (22.7185° N, 89.0705° E).

Isolation of LSDV using chicken embryo and reconfirmation by PCR

The isolation of LSDV resulted in the characteristic pock lesions on the Chorioallantoic Membrane (CAM) of embryonated chicken eggs (ECE). Notably, embryo mortality was evident as early as the first passage, along with the generation of pock lesions. By the third passage, observations included a hemorrhagic membrane, congestion, clotted blood within blood vessels, and pock lesions appearing as stretched white lines. These pock lesions became even more prominent 5 days after inoculation during the third passage. The dead embryos showed hemorrhagic and edematous characteristics, along with an enlarged and bloody liver, and clots of blood within the core (Figure 5). It is worth noting that all PCR-positive samples inoculated into ECE consistently produced a 192 bp PCR product after amplification of P32 gene.

Nucleotide sequencing and phylogenetic analysis

We successfully amplified and sequenced fragments of the RPO30 gene of LSDV. NCBI blast results revealed that the Alim_LSD_100 isolate shares a 100% nucleotide sequence similarity with all Bangladeshi LSDV isolates, as well as those from neighboring countries such as India and Myanmar. A phylogenetic analysis of LSDV was constructed based on the RPO30 gene, and it was observed that our isolate is closely related to LSDV strains from Bangladesh, India, Mongolia, and Myanmar. Importantly, it is distinctly different from LSDV strains found in Russia and China (Figure 6).

Immunogenicity test of the selected LSD virus antigen

In cattle immunized with LSD antigen, serum antibody titers were measured at 7929.53, 18807.99, 12425.76, and 8317.54 after 1, 2, 9, and

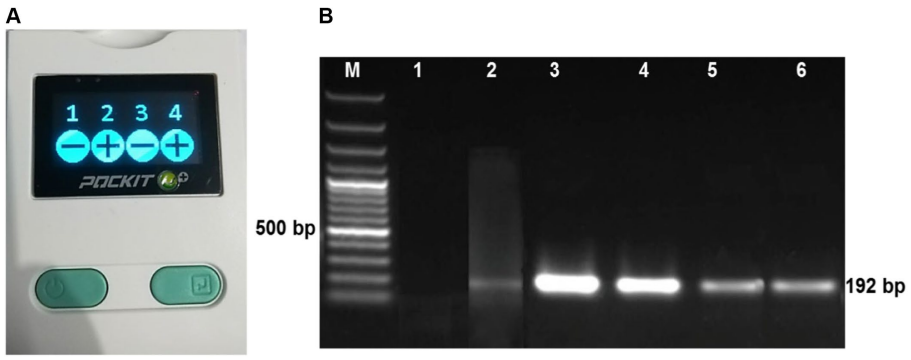

FIGURE 3
LSDV screening from field sample by iiPCR **(A)** and PCR **(B)**. 1 & 3: LSD Negative sample, 2 & 4: LSD positive samples **(A)** and M: 100 bp DNA marker, Lane 1: negative control, Lane 2: positive control, Lane 3 to 6: the fresh nodules/lumps showed positive band at 192 bp **(B)**.

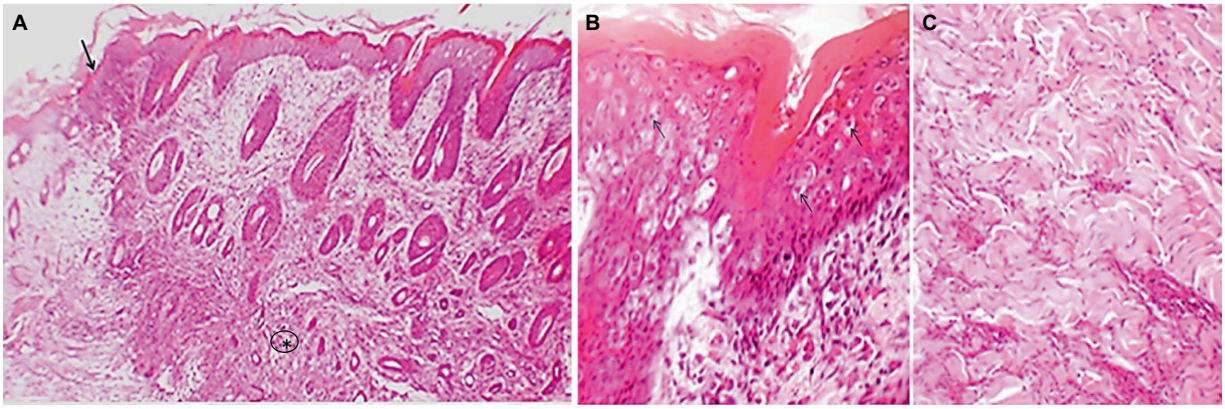

FIGURE 4
Representative image showing microscopic lesions of lumpy skin disease in cattle. The epidermis is thickened with ballooning degeneration of keratinocytes, proliferation of follicular epithelia and thickening and degeneration of subcutaneous muscular tissue (asterisk), the dermis is infiltrated with foci of inflammatory cells (arrow) mainly involving mononuclear cells at the junction between healthy and nodular tissue **(A)**. The degenerated cells of the epidermis often contain intracytoplasmic inclusion body (**B**, arrows). The muscular tissue in the dermis is degenerated **(C)**. Hematoxylin and eosin stain.

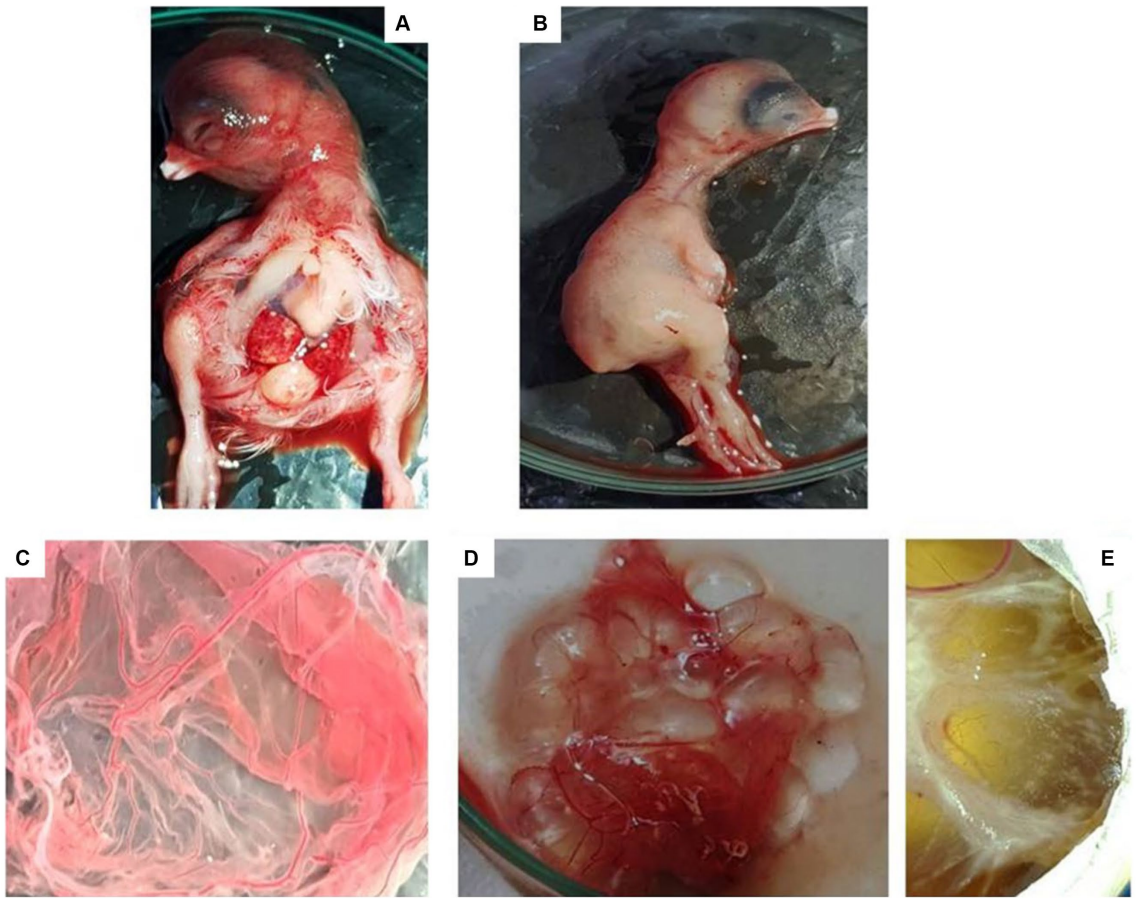

FIGURE 5
Embryo and Chorioallantoic membrane of EGEs after three passages by LSDV. Hemorrhegic and edematous embryo **(A)**, a hemorrhagic CAM with congestion and pock lesion infected by LSDV **(D–E)**. Control embryo and CAM **(B,C)**.

18 months of immunization, respectively. In contrast, in the goat pox vaccinated group, the antibody titers were 4825.79, 2070.60, 699.00, and 11099.00 after 1, 2, 9, and 18 months of immunization, respectively. For the non-immunized cattle, the antibody titer was nearly 700. The highest antibody titer was observed in the LSD-immunized group after 2 months of immunization (Figure 7).

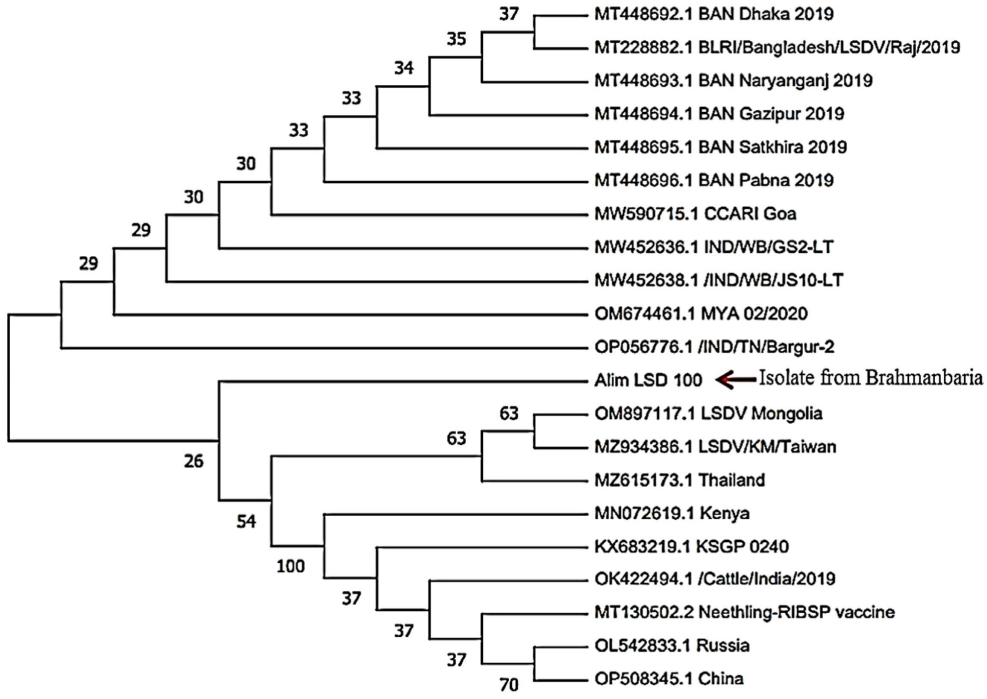

FIGURE 6
Phylogenetic analysis of the nt sequences gene of LSDV isolates of Bangladesh with the nt sequences of RPO30 gene of other countries including Bangladesh.

Discussion

We employed a novel PCR technique for the screening of nodular tissue samples to detect LSDV. Subsequently, we successfully cultivated large quantities of LSDV in chicken embryos, and we also assessed the immunogenicity of the inactivated LSDV. Our molecular evidence strongly suggests a transboundary spread of the LSD outbreak in Bangladesh during 2019–2020. Moreover, our LSDV isolates show a potential vaccine candidate to combat LSD in Bangladesh.

The iiPCR technique offers a distinct advantage in rapidly completing the denaturation, annealing, and extension steps within a capillary tube, achieving high amplification efficiency over a short time period. This feature makes it particularly suitable for swift and efficient screening of field virus infections (Song et al., 2022). In our study, iiPCR was employed to screen the nodular tissue samples for LSDV. Importantly, all iiPCR-positive samples were subsequently confirmed as PCR-positive, with a specific 192 bp band appearing for the P32 gene, a well-established marker for LSDV detection. This demonstrates the superiority of iiPCR in enabling the rapid and accurate screening of LSDV. Giasuddin et al. (2019) and Sudhakar et al. (2020) also used the P32 gene as a specific marker for detecting LSDV via PCR.

Lumpy skin disease affects the skin of cattle and water buffalo, leading to the development of nodular lesions that may rupture in advanced stages of the disease (Sanz-Bernardo et al., 2021). Microscopically, these lesions exhibit characteristic features, including acanthosis (thickening of the epidermis), ballooning degeneration of epidermal cells, and the presence of intracytoplasmic inclusion bodies (Ali et al., 2021). Notably, the presence of intracytoplasmic inclusion bodies is considered a hallmark of lumpy skin disease (Gharban et al., 2019; Neamat-Allah and Mahmoud, 2019). The skin lesions are typically demarcated from nearby healthy tissue by the presence of inflammatory infiltrates, which consist of lymphocytes and macrophage cells. Additionally, the disease leads to thickening and coagulation necrosis of subcutaneous muscle tissue (Neamat-Allah, 2015; Sanz-Bernardo et al., 2020; Parvin et al., 2022). In the present study, LSDV was successfully isolated from nodular tissues collected from the skin of naturally infected cattle through inoculation on the Chorioallantoic Membrane (CAM) of embryonated chicken eggs (ECE). During the third passage, the embryos exhibited hemorrhagic and edematous characteristics, a finding consistent with the observations made by van Rooyen et al. (1969). Characteristic pock lesions were initially observed after the first passage and became more pronounced after the third passage. This method of LSDV isolation on the CAM of ECE, along with the detection of characteristic pock lesions, has been successfully employed by several authors (House et al., 1990; Hassan et al., 1992; Tamam, 2006; El-Nahas et al., 2011; El-Tholoth and El-Kenawy, 2016). Importantly, all LSDV isolates obtained from the infected CAM were confirmed through PCR analysis. El-Nahas et al. (2011) also employed PCR to detect LSDV in infected CAM.

The RPO30 gene has consistently demonstrated its suitability as a prime candidate for the phylogenetic differentiation of field strains of LSDV, as evidenced by prior studies (Gelaye et al., 2015; Agianniotaki et al., 2017; Sudhakar et al., 2020). In our study, we utilized the partial sequence of the RPO30 gene for phylogenetic analysis. The selected LSDV isolate from Brahmanbaria district (highlighted by the red arrow in Figure 6) exhibited genetic similarities with LSDV isolates from Bangladesh and neighboring countries such as India and Myanmar. This genetic relationship highlights the critical need for regional collaboration and coordinated efforts in disease surveillance, early detection, and response mechanisms. Effective control and

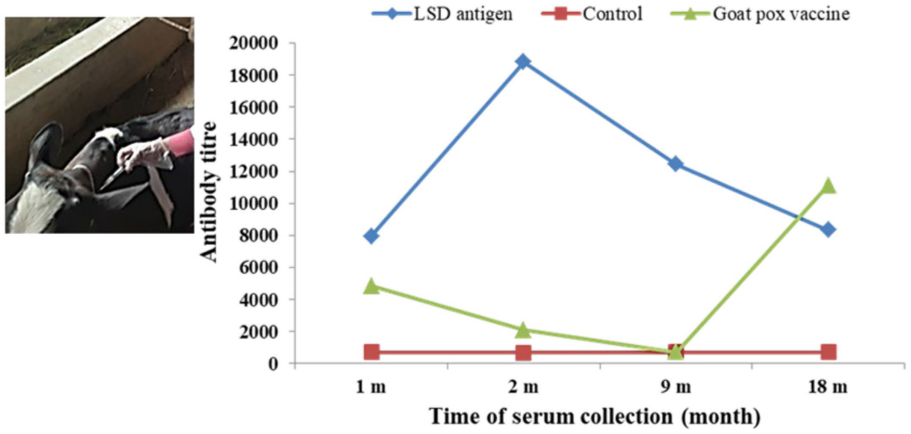

FIGURE 7
Subcutaneous immunization of cattle with the killed LSDV antigen and serum antibody titre after immunization.

prevention of LSDV necessitate cross-border cooperation among neighboring countries. While the observed genetic similarities strongly suggest the possibility of transboundary transmission of LSD in Bangladesh during 2019–2020, it is crucial to note that confirmation of such spread requires the availability of whole-genome sequences, encompassing a combination of LSDV target genes.

The immune response elicited in cattle by the inactivated LSDV antigen was compared with that in goat pox-vaccinated cattle and the control group. Notably, a stronger immune response was observed in the cattle immunized with the inactivated LSDV antigen compared to the other two groups. However, it is important to highlight that LSDV infection was observed in both the goat pox-vaccinated group and the control group. The antibody titre was sharply increased in goat pox vaccinated cattle after 9 months due to the sudden outbreak of LSD 5 months after immunization. This increase in antibody titer was attributed to the recovery of the cattle from LSD infection. In contrast, there were no reports of LSDV infection recorded in the cattle immunized with the LSDV antigen.

Our study focuses on developing and evaluating an inactivated LSDV vaccine candidate. Current LSD vaccines typically use strains like Neethling or KSGP O-240 and O-180, requiring extensive passages in cell cultures and in the chorioallantoic membrane of embryonated chicken eggs (Kitching, 2003; Wallace and Viljoen, 2005). The Neethling strain vaccination can lead to adverse reactions like skin nodules and reduced milk yield (Wallace and Viljoen, 2005). Inactivated vaccines offer a shorter immunity duration but are free from adverse effects, making them favorable in disease-free, at-risk regions (Tuppurainen et al., 2021). Our study contributes to this field by exploring the potential of an inactivated LSDV vaccine candidate, offering an alternative approach with its own set of benefits and limitations.

In conclusion, this study represents a significant advancement in our understanding of LSDV in Bangladesh. We introduced an innovative PCR technique for the rapid and efficient screening of nodular tissue samples, enabling the detection of LSDV with high accuracy. Furthermore, we successfully cultivated substantial quantities of LSDV using chicken embryos. One of the most notable findings of this study is the strong molecular evidence indicating potential transboundary spread of the LSD outbreak in Bangladesh during the period 2019–2020. This highlights the interconnectedness of the region and the potential for diseases like LSDV to cross borders, emphasizing the importance of vigilance and cooperation in disease management and control efforts. Additionally, our LSDV isolates hold promise as potential vaccine candidates to combat LSD in Bangladesh. Further investigation into the effectiveness of the inactivated LSDV antigen as a vaccine candidate, as well as the development of surveillance strategies to monitor LSDV circulation in the region, is recommended.

Data availability statement

The data presented in the study are deposited in the GenBank, accession number OP948135.

Ethics statement

The animal studies were approved by Animal Welfare and Experimentation Ethics Committee at Bangladesh Agricultural University, Mymensingh. The studies were conducted in accordance with the local legislation and institutional requirements. Written informed consent was obtained from the owners for the participation of their animals in this study. Written informed consent was obtained from the individual(s) for the publication of any potentially identifiable images or data included in this article.

Author contributions

MAU: Investigation, Methodology, Writing – original draft. MTH: Conceptualization, Data curation, Methodology, Supervision, Writing – original draft, Writing – review & editing. AKMAR: Data curation, Formal analysis, Writing – review & editing. MPS: Formal analysis, Writing – review & editing. MAK: Writing – review & editing. MGH: Methodology, Writing – review & editing. SC: Writing – original draft. MMR: Writing – review & editing. AKMK: Writing – review & editing. MPW: Writing – review & editing. MAI: Conceptualization, Data curation, Formal analysis, Funding acquisition, Investigation, Methodology, Supervision, Writing – review & editing.

Funding

The author(s) declare that financial support was received for the research, authorship, and/or publication of this article. This research was partially funded by the Livestock and Dairy Development Project (LDDP), Department of Livestock Services, Bangladesh, 2023.

Acknowledgments

The authors express their sincere gratitude to the cattle owners who generously permitted the collection of samples from their LSD-affected animals during the study.

Conflict of interest

The authors extend their heartfelt thanks to the Managing Director of FnF Pharmaceuticals Ltd., Bangladesh, for providing financial support that enabled the execution of this research. The funder was not involved in the study design, collection, analysis, interpretation of data, the writing of this article, or the decision to submit it for publication.

The author(s) declared that they were an editorial board member of Frontiers, at the time of submission. This had no impact on the peer review process and the final decision.

Publisher's note

All claims expressed in this article are solely those of the authors and do not necessarily represent those of their affiliated organizations, or those of the publisher, the editors and the reviewers. Any product that may be evaluated in this article, or claim that may be made by its manufacturer, is not guaranteed or endorsed by the publisher.

References

Agianniotaki, E. I., Tasioudi, K. E., Chaintoutis, S. C., Iliadou, P., Mangana-Vougiouka, O., Kirtzalidou, A., et al. (2017). Lumpy skin disease outbreaks in Greece during 2015–16, implementation of emergency immunization and genetic differentiation between field isolates and vaccine virus strains. *Vet. Microbiol.* 201, 78–84. doi: 10.1016/j.vetmic.2016.12.037

Ahamed, M. M., Hossain, M. T., Rahman, M., Nazir, K. H. M. N. H., Khan, M. F. R., Parvej, M. S., et al. (2015). Molecular characterization of duck plague virus isolated from Bangladesh. *J. Adv. Vet. Anim. Res.* 2, 296–303. doi: 10.5455/javar.2015.b90

Akter, S., Islam, M. A., Hossain, M. T., Amin, M. M., Begum, M. I. A., and Sadekuzzaman, M. (2004). Characterization and pathogenicity of duck plague virus isolated from natural outbreaks in ducks of Bangladesh. *Bangladesh J. Vet. Med.* 2, 107–111. doi: 10.3329/bjvm.v2i2.2540

Akther, M., Akter, S. H., Sarker, S., Aleri, J. W., Annandale, H., Abraham, S., et al. (2023). Global burden of lumpy skin disease, outbreaks, and future challenges. *Viruses* 15:1861. doi: 10.3390/v15091861

Ali, A. A., Neamat-Allah, A. N. F., Sheire, H. A. E.-m., and Mohamed, R. I. (2021). Prevalence, intensity, and impacts of non-cutaneous lesions of lumpy skin disease among some infected cattle flocks in Nile Delta governorates, Egypt. *Comp. Clin. Pathol.* 30, 693–700. doi: 10.1007/s00580-021-03264-7

Badhy, S. C., Chowdhury, M. G., Settypalli, T. B., Cattoli, G., Lamien, C. E., Fakir, M. A., et al. (2021). Molecular characterization of lumpy skin disease virus (LSDV) emerged in Bangladesh reveals unique genetic features compared to contemporary field strains. *BMC Vet. Res.* 17:61. doi: 10.1186/s12917-021-02751-x

Carn, V. M., and Kitching, R. P. (1995). An investigation of possible routes of transmission of lumpy skin disease virus (Neethling). *Epidemiol. Infect.* 114, 219–226. doi: 10.1017/s0950268800052067

Chang, H. F., Tsai, Y. L., Tsai, C. F., Lin, C. K., Lee, P. Y., Teng, P. H., et al. (2012). A thermally baffled device for highly stabilized convective PCR. *Biotechnol. J.* 7, 662–666. doi: 10.1002/biot.201100453

Chouhan, C. S., Parvin, M. S., Ali, M. Y., Sadekuzzaman, M., Chowdhury, M. G. A., Ehsan, M. A., et al. (2022). Epidemiology and economic impact of lumpy skin disease of cattle in Mymensingh and Gaibandha districts of Bangladesh. *Transbound. Emerg. Dis.* 69, 3405–3418. doi: 10.1111/tbed.14697

El-Nahas, E. M., El-Habbaa, A. S., El-bagoury, G. F., and Radwan, M. E. I. (2011). Isolation and identification of lumpy skin disease virus from naturally infected buffaloes at Kaluobia. Egypt. *Glob. Vet.* 7, 234–237.

El-Tholoth, M., and El-Kenawy, A. A. (2016). G-protein-coupled chemokine receptor gene in lumpy skin disease virus isolates from cattle and water Buffalo (*Bubalus bubalis*) in Egypt. *Transbound. Emerg. Dis.* 63, e288–e295. doi: 10.1111/tbed.12344

Gelaye, E., Belay, A., Ayelet, G., Jenberie, S., Yami, M., Loitsch, A., et al. (2015). Capripox disease in Ethiopia: genetic differences between field isolates and vaccine strain, and implications for vaccination failure. *Antivir. Res.* 119, 28–35. doi: 10.1016/j.antiviral.2015.04.008

Gharban, H. A. J., Al-Shaeli, S. J. J., Al-Fattli, H. H. H., and Altaee, M. N. K. (2019). Molecular and histopathological confirmation of clinically diagnosed lumpy skin disease in cattle, Baghdad Province of Iraq. *Vet. World* 12, 1826–1832. doi: 10.14202/vetworld.2019.1826-1832

Giasuddin, M., Yousuf, M., Hasan, M., Rahman, M., Hassan, M., and Ali, M. (2019). Isolation and molecular identification of lumpy skin disease (LSD) virus from infected cattle in Bangladesh. *Bangladesh J. Livestock Res.* 26, 15–20. doi: 10.3329/bjlr.v26i1-2.49933

Haque, M. N., and Gofur, M. R. (2020). Investigation of lumpy skin disease outbreak in cattle in Naogaon, Bangladesh. *Bangladesh J. Agric. Life Sci.* 1, 89–93.

Hasib, F. M. Y., Islam, M. S., Das, T., Rana, E. A., Uddin, M. H., Bayzid, M., et al. (2021). Lumpy skin disease outbreak in cattle population of Chattogram, Bangladesh. *Vet. Med. Sci.* 7, 1616–1624. doi: 10.1002/vms3.524

Hassan, H. B., Ebied, M. H., El-Din, A., El-Attar, H., Mousa, S., Yassin, S., et al. (1992). Some virological, serological and hematological studies on LSD in Egypt. *Proc. 5th Sci. Cong. Fac. Vet. Med.* 8, 61–65.

Hossain, M. T., Islam, M. A., Amin, M. M., and Islam, M. A. (2005). Comparative efficacy of the conventional and experimentally developed duck plague vaccine. *Int. J. Poult. Sci.* 4, 369–371. doi: 10.3923/ijps.2005.369.371

House, J. A., Wilson, T. M., el Nakashly, S., Karim, I. A., Ismail, I., el Danaf, N., et al. (1990). The isolation of lumpy skin disease virus and bovine herpesvirus-4 from cattle in Egypt. *J. Vet. Diagn. Invest.* 2, 111–115. doi: 10.1177/104063879000200205

Khalil, M. I., Sarker, M. F. R., Hasib, F. Y., and Chowdhury, S. (2021). Outbreak investigation of lumpy skin disease in dairy farms at Barishal, Bangladesh. *Turkish J. Agric. Food Sci. Technol.* 9, 205–209. doi: 10.24925/turjaf.v9i1.205-209.3827

Kitching, R. P. (2003). Vaccines for lumpy skin disease, sheep pox and goat pox. *Dev. Biol.* 114, 161–167.

Kumar, S., Stecher, G., and Tamura, K. (2016). MEGA7: molecular evolutionary genetics analysis version 7.0 for bigger datasets. *Mol. Biol. Evol.* 33, 1870–1874. doi: 10.1093/molbev/msw054

Lung, O., Pasick, J., Fisher, M., Buchanan, C., Erickson, A., and Ambagala, A. (2016). Insulated isothermal reverse transcriptase PCR (iiRT-PCR) for rapid and sensitive detection of classical swine fever virus. *Transbound. Emerg. Dis.* 63, e395–e402. doi: 10.1111/tbed.12318

Milovanović, M., Dietze, K., Milićević, V., Radojičić, S., Valčić, M., Moritz, T., et al. (2019). Humoral immune response to repeated lumpy skin disease virus vaccination and performance of serological tests. *BMC Vet. Res.* 15:80. doi: 10.1186/s12917-019-1831-y

Neamat-Allah, A. N. F. (2015). Immunological, hematological, biochemical, and histopathological studies on cows naturally infected with lumpy skin disease. *Vet. World* 8, 1131–1136. doi: 10.14202/vetworld.2015.1131-1136

Neamat-Allah, A. N. F., and Mahmoud, E. A. (2019). Assessing the possible causes of hemolytic anemia associated with lumpy skin disease naturally infected buffaloes. *Comp. Clin. Pathol.* 28, 747–753. doi: 10.1007/s00580-019-02952-9

Parvin, R., Chowdhury, E. H., Islam, M. T., Begum, J. A., Nooruzzaman, M., Globig, A., et al. (2022). Clinical epidemiology, pathology, and molecular investigation of lumpy skin disease outbreaks in Bangladesh during 2020–2021 indicate the re-emergence of an old African strain. *Viruses* 14:2529. doi: 10.3390/v14112529

Sanz-Bernardo, B., Haga, I. R., Wijesiriwardana, N., Basu, S., Larner, W., Diaz, A. V., et al. (2021). Quantifying and modeling the acquisition and retention of lumpy skin disease virus by Hematophagus insects reveals clinically but not subclinically affected cattle are promoters of viral transmission and key targets for control of disease outbreaks. *J. Virol.* 95, e02239–e02220. doi: 10.1128/JVI.02239-20

Sanz-Bernardo, B., Haga, I. R., Wijesiriwardana, N., Hawes, P. C., Simpson, J., Morrison, L. R., et al. (2020). Lumpy skin disease is characterized by severe multifocal dermatitis with necrotizing fibrinoid vasculitis following experimental infection. *Vet. Pathol.* 57, 388–396. doi: 10.1177/0300985820913268

Sarkar, S., Meher, M. M., Parvez, M. M. M., and Akther, M. (2020). Occurrences of lumpy skin disease (LSD) in cattle in Dinajpur sadar of Bangladesh. *Res. Agric. Livestock Fisheries* 7, 445–455. doi: 10.3329/ralf.v7i3.51364

Slaoui, M., and Fiette, L. (2011). Histopathology Procedures: From Tissue Sampling to Histopathological Evaluation. *Methods in Mol. Biol.* 691, 69–82. doi: 10.1007/978-1-60761-849-2_4

Song, R., Liu, P., Yang, Y., Lee, H. S., Chen, C., Wu, X., et al. (2022). Development of a duplex insulated isothermal PCR assay for rapid on-site detection and differentiation of genotypes 1 and 2 of African swine fever virus. *Front. Cell. Infect. Microbiol.* 12:948771. doi: 10.3389/fcimb.2022.948771

Sprygin, A., Artyuchova, E., Babin, Y., Prutnikov, P., Kostrova, E., Byadovskaya, O., et al. (2018). Epidemiological characterization of lumpy skin disease outbreaks in Russia in 2016. *Transbound. Emerg. Dis.* 65, 1514–1521. doi: 10.1111/tbed.12889

Sudhakar, S. B., Mishra, N., Kalaiyarasu, S., Jhade, S. K., Hemadri, D., Sood, R., et al. (2020). Lumpy skin disease (LSD) outbreaks in cattle in Odisha state, India in august 2019: epidemiological features and molecular studies. *Transbound. Emerg. Dis.* 67, 2408–2422. doi: 10.1111/tbed.13579

Tamam, S. M. (2006). Isolation of lumpy skin disease virus form naturally infected cattle previously vaccinated with live attenuated sheep poxvirus vaccine. *J. Vet. Med. Res.* 16, 27–31. doi: 10.21608/jvmr.2006.77916

Tsai, Y. L., Wang, H. T., Chang, H. F., Tsai, C. F., Lin, C. K., Teng, P. H., et al. (2012). Development of TaqMan probe-based insulated isothermal PCR (iiPCR) for sensitive and specific on-site pathogen detection. *PLoS One* 7:e45278. doi: 10.1371/journal.pone.0045278

Tuppurainen, E., Dietze, K., Wolff, J., Bergmann, H., Beltran-Alcrudo, D., Fahrion, A., et al. (2021). Vaccines and vaccination against lumpy skin disease. *Vaccine* 9:1136. doi: 10.3390/vaccines9101136

Uddin, M. A., Islam, M. A., Rahman, A. K. M. A., Rahman, M. M., Khasruzzaman, A. K. M., Ward, M. P., et al. (2022). Epidemiological investigation of lumpy skin disease outbreaks in Bangladeshi cattle during 2019–2020. *Transbound. Emerg. Dis.* 69, 3397–3404. doi: 10.1111/tbed.14696

van Rooyen, P. J., Munz, E. K., and Weiss, K. E. (1969). The optimal conditions for the multiplication of Neethling-type lumpy skin disease virus in embryonated eggs. *Onderstepoort J. Vet. Res.* 36, 165–174.

Wallace, D. B., and Viljoen, G. J. (2005). Immune responses to recombinants of the south African vaccine strain of lumpy skin disease virus generated by using thymidine kinase gene insertion. *Vaccine* 23, 3061–3067. doi: 10.1016/j.vaccine.2004.10.006

Wilhelm, L., and Ward, M. P. (2023). The spread of lumpy skin disease virus across Southeast Asia: insights from surveillance. *Transbound. Emerg. Dis.* 2023, 1–9. doi: 10.1155/2023/3972359

World Organization for Animal Health (2023). *Lumpy Skin Disease, Chapter 3.4.12* WOAH Terrestrial Manual, 1–12.

Yousefi, P. S., Mardani, K., Dalir-Naghadeh, B., and Jalilzadeh-Amin, G. (2017). Epidemiological study of lumpy skin disease outbreaks in North-Western Iran. *Transbound. Emerg. Dis.* 64, 1782–1789. doi: 10.1111/tbed.12565

Yu, G., Smith, D. K., Zhu, H., Guan, Y., and Lam, T. T.-Y. (2017). Ggtree: an r package for visualization and annotation of phylogenetic trees with their covariates and other associated data. *Methods Ecol. Evol.* 8, 28–36. doi: 10.1111/2041-210x.12628

Zhang, J., Nfon, C., Tsai, C. F., Lee, C. H., Fredericks, L., Chen, Q., et al. (2019). Development and evaluation of a real-time RT-PCR and a field-deployable RT-insulated isothermal PCR for the detection of Seneca Valley virus. *BMC Vet. Res.* 15:168. doi: 10.1186/s12917-019-1927-4

Zinnah, M. A., Islam, M. T., Rahman, M. M., Hossain, M. T., Zinnah, M. A., Bari, M. R., et al. (2010). Standardization of multiplex reverse transcription-polymerase chain reaction and typing of foot-and-mouth disease virus prevalent in Bangladesh. *Bangladesh J. Vet. Med.* 8, 149–155. doi: 10.3329/bjvm.v8i2.11199

Frontiers in Microbiology

Explores the habitable world and the potential of microbial life

The largest and most cited microbiology journal which advances our understanding of the role microbes play in addressing global challenges such as healthcare, food security, and climate change.

Discover the latest Research Topics

See more →

Frontiers

Avenue du Tribunal-Fédéral 34
1005 Lausanne, Switzerland
frontiersin.org

Contact us

+41 (0)21 510 17 00
frontiersin.org/about/contact